

Extraction of Urban Environmental Quality Indicators using LiDAR-Based Digital Surface Models

THÈSE N° 5050 (2011)

PRÉSENTÉE LE 17 JUIN 2011

À LA FACULTÉ ENVIRONNEMENT NATUREL, ARCHITECTURAL ET CONSTRUIT
LABORATOIRE DE SYSTÈMES D'INFORMATION GÉOGRAPHIQUE
PROGRAMME DOCTORAL EN ENVIRONNEMENT

ÉCOLE POLYTECHNIQUE FÉDÉRALE DE LAUSANNE

POUR L'OBTENTION DU GRADE DE DOCTEUR ÈS SCIENCES

PAR

Claudio MAGALHAES CARNEIRO

acceptée sur proposition du jury:

Prof. B. Merminod, président du jury
Prof. F. Golay, directeur de thèse
Prof. C. Borrego, rapporteur
Prof. T. Kolbe, rapporteur
Prof. J.-L. Scartezzini, rapporteur



ÉCOLE POLYTECHNIQUE
FÉDÉRALE DE LAUSANNE

Suisse
2011

Science is a way of thinking much more than it is a body of knowledge.

Carl Sagan

ABSTRACT

The visualization of specific 3-D urban scenes can be done calling upon different techniques, from those more traditional, such as photogrammetry, to the most advanced ones, such as laser scanning that uses different techniques and algorithms of selection and modelling of 3-D point clouds. The use and utility of this kind of data for the study of urban development remain however debatable. Indeed, indicators for urban development and durability are highly necessary and the best methodology to build them is largely open.

This thesis anticipates the use of 2-D and 3-D models and data for the environmental analysis of cities, aiming to provide useful tools for urban planning and design. According to end-users requirements, the extraction of urban environmental quality (UEQ) indicators from 2-D and 3-D information using innovative methods is proposed and implemented, which is based on recent research on computational algorithms for the analysis, evaluation, management and design of the urban space. Moreover, results that can be obtained with different data sources and aggregation methods are compared. In particular, the main advantages of urban models generated from LiDAR data are highlighted.

In consequence, an iterative process is proposed, involving professionals of various fields, aiming at improving the utility of those indicators for the support of applied decision activities related to the sustainable development of cities. This process is sub-divided in three correlated steps:

(1) - A preliminary inquiry concerning the user requirements for the implementation of a 3-D project of the State/City of Geneva was launched. Based on the obtained replies, several potential applications related to both the definition and extraction of urban indicators were identified, and also, end-users were classified into 6 different domains: 1- architecture, urbanism and territory planning; 2 - urban traffic (motor vehicles, trains and airplanes); 3 - environment and energy; 4 - pedestrian and cyclist mobility; 5 - security and emergency situations management; 6 - underground information;

(2) - Based on point (1) and according to the assessment of the specific needs among each of these domains, several interviews were carried out in which 25 end-users decided to focus on UEQ indicators considering three main stakes: 1 - assessment of the morphological properties of the urban texture; 2 – exploration of the solar potential on the urban fabric; 3 – estimation of the energy demand on the urban fabric. Many empirical case-studies are emphasized, mostly for the city of Geneva, and also for the cities of Lausanne and Florence. These indicators are extracted from the segmentation of planar roof areas using classified LiDAR point clouds and the use of image processing techniques based on Digital Elevation Models (DEM) and Digital Height Models (DHM), defined in this thesis as 2.5-Digital Urban Surface Models (2.5-DUSM) and normalized 2.5-Digital Urban Surface Models (n2.5-DUSM) respectively. These models are constructed in a step by step basis, using LiDAR and 2-D and 3-D vector data, thus applying different methods of interpolation and enhancement, whose accuracy is also evaluated on a statistical basis;

(3) - Finally, an inquiry on how the same group of 25 end-users mentioned in point (1) perceives and interprets the different exploratory 2-D and 3-D geo-visualizations proposed for some of the UEQ indicators is undertaken, evaluating their utility according to the requirements previously defined.

Key-words: Light Detection And Ranging (LiDAR), Digital Elevation Models (DEM), Urban environmental quality (UEQ), Indicator, Visualization, Utility.

La représentation de scènes 3D en milieu urbain peut faire appel à différentes techniques, des plus classiques, comme la photogrammétrie (à partir d'images aériennes), jusqu'aux plus récentes, comme les systèmes laser aéroportés (airborne LiDAR - « Light Detection And Ranging »), qui utilisent différentes techniques et différents algorithmes de sélection et de modélisation d'un nuage de points 3D. L'utilité et utilisabilité de ces données pour l'étude du développement urbain restent cependant discutables.

Cette thèse étudie l'utilisation de données et modèles 2-D et 3-D pour l'analyse environnementale des villes. Elle vise à fournir des outils pertinents pour l'aménagement du territoire et l'urbanisme. Conformément à une analyse des besoins auprès d'utilisateurs métier, des indicateurs liés à la qualité environnementale urbaine sont extraits des différentes sources de données et modèles 2-D et 3-D. Dans cette perspective, des méthodes et des algorithmes informatiques innovants ont été élaborés pour l'analyse, l'évaluation, la conception et la gestion de l'espace urbain. On compare en outre les résultats qui peuvent être obtenus avec différentes sources de données et différentes méthodes d'agrégation, permettant de souligner les apports des données LiDAR pour l'extraction d'indicateurs spatiaux à trois dimensions en milieu urbain.

La thèse met en œuvre une démarche itérative. Elle fait appel à des professionnels de divers champs, visant à améliorer l'utilité de ces indicateurs comme appui à des activités liées au développement durable en milieu urbain. Ce processus est subdivisé en trois étapes interdépendantes:

(1) - Une enquête préliminaire concernant les besoins d'utilisateurs métier pour l'exécution d'un projet à trois dimensions à l'état/ville de Genève a été réalisée. Sur la base des réponses obtenues, plusieurs champs d'application potentiels liés à la définition et à l'extraction d'indicateurs urbains ont été identifiés. Dans ce cadre, chaque utilisateur métier a été classifié dans 6 domaines différents : 1 - architecture, urbanisme et aménagement du territoire ; 2 - trafic urbain (véhicules à moteur, trains et avions) ; 3 - environnement et énergie ; 4 - mobilité piétonnière et cyclable ; 5 - gestion de sécurité et de situations d'urgence ; 6 - information souterraine ;

(2) - Sur la base du point (1) et selon une évaluation préliminaire de besoins spécifiques inhérente à chaque utilisateur métier, plusieurs entrevues ont été effectuées, au cours desquelles 25 utilisateurs métier ont fait émerger un jeu d'indicateurs liés à la qualité environnementale en milieu urbain. La structuration et modélisation de ces indicateurs est fondée sur trois enjeux principaux : 1 - évaluation des propriétés morphologiques de la texture urbaine ; 2 - exploration du potentiel solaire sur le tissu urbain ; 3 - estimation de la demande énergétique sur le tissu urbain. Plusieurs études de cas empiriques ont été réalisées, la plupart d'entre elles pour la ville de Genève, mais aussi pour les villes de Lausanne et de Florence. En utilisant des techniques de traitement d'image, ces indicateurs sont principalement extraits à partir de modèles numériques d'altitude (MNA) - définis dans cette thèse en tant que modèles urbains digitaux de surface -, mais aussi par une procédure de segmentation basée sur des données LiDAR. Les modèles urbains digitaux de surface sont construits étape-par-étape, en utilisant des données LiDAR et des données 2-D et 3-D en mode vecteur et en appliquant différentes méthodes d'interpolation et de correction. L'exactitude de ces modèles est également évaluée sur une base statistique ;

(3) - Finalement, une enquête est entreprise sur la façon dont le même groupe de 25 utilisateurs mentionnés au point (1) perçoit et interprète les différentes interfaces exploratoires 2-D et 3-D construits pour des géo-visualisations à trois dimensions de certains des indicateurs liés à la qualité environnementale en milieu urbain. Cette étape vise à évaluer l'utilité de ces indicateurs selon les conditions préalablement définies.

Mots-clé : Systèmes Laser Aéroportés (LiDAR), Modèles Numériques d'Altitude (MNA), Qualité Environnementale Urbaine, Indicateur, Visualisation, Utilité.

ACKNOWLEDGMENTS

First and foremost I would like to deeply thank my supervisor, François Golay, for having accepted me as a PhD student at the GIS laboratory (LaSIG), EPFL, Lausanne, Switzerland. Beyond his irreplaceable assistance and opinions, he granted me with the necessary independence to conduct my research thinking and follow my own ideas.

I am grateful to all the colleagues I met and had the pleasure to work with at the LaSIG: Régis Caloz, Stéphane Joost, Abram Pointet, Gilles Gachet, Jens Ingensand, Michael Kalbermatten, Matthieu Noucher, Nicolas Lachance-Bernard, Elena Andrey, Véronique Boillat Kireev, Sylvie Stucki, Eduardo Camacho-Hübner, Mathieu Kientga, Thirry Bussien, Timothée Produit and Kevin Lempoeel.

A very special thanks to Eugenio Morello, from the Polytechnic of Milano, Italy, and to Gilles Desthieux, from HEPIA, HES-Geneva, Switzerland, for their intense collaboration in MATLAB programming, clever thinking, fruitful teamwork and critical reviewing of this thesis.

I am also definitely indebted to Vítor Silva and Corinne Plazanet, from the Urban, Rural, and Architectural Projects Laboratory, EPFL, Yue M. Lu and Mina Karzand from the Audiovisual Communications Laboratory, EPFL, Carla Balocco and Virginia Gori, from the Department of Energy Engineering "Sergio Stecco" of the University Florence, Italy, Thomas Vögtle, from the University of Karlsruhe, Germany, and Jorge Gustavo Rocha, from the University of Minho, Portugal, for their essential collaboration, and also to my brother Gustavo for reviewing my English writing.

I would like to acknowledge Peter Gallinelli, from HEPIA, HES-Geneva, and André Mermoud, from the University of Geneva, for their support, and Laurent Niggeler, from the "Direction Cantonale de la Mensuration Officielle" of the State of Geneva and Adrien Vieira de Mello, from the "Service de l'Organisation et des Systèmes d'Information" of the State of Geneva, for their vast contribution to this project.

I am also thankful to Thomas Pettersson, leader of the General Infrastructure Services Department of the European Organization for Nuclear Research (CERN), for allowing me to finalize my thesis in optimal conditions and to "Fundação para a Ciência e Tecnologia", Portugal, for its financial support.

I am very thankful to all members of my thesis committee: Jean-Louis Scartezzini, from EPFL, Carlos Borrego, from the University of Aveiro, Portugal, and Thomas Kolbe, from the Technical University of Berlin, Germany, for their constructive review and helpful remarks.

And last but not at least, I want to thank my family: my wife Paula, for giving me the space I needed to finish my thesis, and my two beautiful daughters, Inês and Sofia, for giving me the positive energy that sometimes I thought was lost. I also would like to thank my father Alberto, my mother Ana and my sister Ariana, for their wonderful heart and encouraging thoughts.

TABLE OF CONTENTS

<i>Abastract</i>	<i>I</i>
<i>Résumé</i>	<i>III</i>
<i>Acknowledgments</i>	<i>V</i>
<i>Abbreviations</i>	<i>XIII</i>
<i>Chapter 1. Introduction</i>	<i>1</i>
1.1 Context	1
1.2 Problematic	1
1.3 Research goals and methods	3
1.4 Empirical research process	5
1.5 Thesis outline	8
<i>PART I – Theoretical knowledge</i>	<i>11</i>
<i>Chapter 2. 2-D and 3-D spatial data for urban modelling</i>	<i>13</i>
2.1 Introduction	13
2.2 Classes of 3-D object representations	14
2.3 Geographical information systems, digital elevation models (DEM) and digital height models (DHM)	16
2.4 Image processing of digital elevation models (DEM) and digital height models (DHM)	20
2.4.1 Overview	20
2.4.2 Definition of a digital image	20
2.4.3 Digital image processing	21
Geometric transformation	25
2.5 Airborne laser scanning systems	26
2.5.1 Introduction	26
2.5.2 Historical overview	27
2.5.3 Airborne laser scanning technological components	27
2.5.4 Filtering and classification of airborne laser scanning	29
2.5.5 Airborne laser scanning: measuring different echoes	31
2.5.6 Airborne laser scanning data formats	32
2.5.7 Accuracy of airborne laser scanning	34
2.6 Gridding interpolation of digital elevation models (DEM) and digital height models (DHM) using LiDAR data	35
2.7 3-D data extraction and acquisition	37
2.8 3-D city models	38
2.9 Conclusions and chapter synthesis	38

Chapter 3. Urban indicators	39
3.1 Introduction	39
3.2 Roles of indicators	39
3.3 Properties of indicators	40
3.3.1 Overview	40
3.3.2 Geographical dimension	40
3.3.3 Level of measure and scale of analysis	41
3.3.4 Comparison aptitude	44
3.4 Methods and conceptual models for the definition of indicators	44
3.5 Elementary indicators, complex indicators and indexes	45
3.6 Visualization of indicators	46
3.6.1 Overview	46
3.6.2 Visualization taxonomy	46
3.6.2.1 Dynamic versus static view	47
3.6.2.2 Level of interactivity	47
3.6.2.3 Dimensionality	47
3.6.2.4 Levels of realism	47
3.6.2.5 Single versus multiple representations	48
3.6.3 3-D visualization of urban indicators	49
3.6.3.1 Presentation	49
3.6.3.2 Three-dimensionality of visualization	49
3.6.3.3 Levels of detail for 3-D visualization	50
3.7 Conclusions and chapter synthesis	52
PART II - Methodological framework	53
Chapter 4. User requirements analysis	55
4.1 Introduction	57
4.2 Pilot project: state of Geneva	58
4.2.1 Presentation	58
4.2.2 Preliminary inquiry	59
4.2.3 Identification and classification of the existing users in different fields	59
4.2.4 Interviews	60
4.2.5 Principles of indicators and indexes	60
4.2.6 Selection of indicators and indexes	63
4.2.6.1 Presentation	63
4.2.6.2 Assessment of the morphological properties of the urban texture	66
4.2.6.3 Exploration of the solar potential on the urban fabric	67
4.2.6.4 Estimation of the energy demand on the urban fabric	71
4.2.7 Visualization of indicators	72
4.3 Conclusions and chapter synthesis	75
Chapter 5. Data sources used and models constructed	77
5.1 Introduction	79
5.2 Context, assumptions and different scenarios	79
5.3 Geo-referenced data sources available	84

5.4	Selected indicators: geo-referenced data sources used and definition of the models to be constructed	86
5.5	Construction of the different 2.5-DUSM used	87
5.5.1	Construction of the 2.5-DUSM without vegetation	87
5.5.2	Construction of the normalized 2.5-DUSM of vegetation	90
5.5.3	Construction of the 2.5-DUSM of roof lines and the 2.5-DUSM of building outlines with vegetation	91
5.6	Creation of masks for the enhancement of the 2.5-DUSM used	92
5.7	Segmentation of planar roof areas	96
5.8	Punch case: assessing the accuracy of the constructed and enhanced 2.5-DUSM of roof lines	97
5.8.1	Presentation	97
5.8.2	Method applied	98
5.8.3	Significance statistical validation and analysis of results	100
5.8.4	Conclusions	102
5.9	Punch-case: assessing a sensor network by verifying shadows derived from a 2.5-DUSM of building outlines	102
5.9.1	Presentation	102
5.9.2	SensorScope project	103
5.9.3	Method applied	104
5.9.4	Analysis of results	107
5.9.5	Conclusions	109
5.10	Conclusions and chapter synthesis	109
PART III - Practical implementation: empirical case-studies		111
Chapter 6. Assessment of the morphological properties of the urban texture		113
6.1	Introduction	115
6.2	Background and related work	115
6.3	Case-study: Digital urban morphometrics - automatic extraction and assessment of morphological properties of buildings	117
6.3.1	Presentation	117
6.3.2	Dataflow process	117
6.3.3	Data sources used and normalized 2.5-DUSM constructed	118
6.3.4	Creation of masks for the application of morphological operations on each building	120
6.3.5	The calculation of the morphological indicators: volume of buildings, area of roofs and area of facades	121
6.3.5.1	Volume of buildings	121
6.3.5.2	Area of facades	122
6.3.5.3	Area of roofs	127
6.3.6	Performed validations	128
6.3.7	Significance statistical analysis of the proposed method	130
6.3.7.1	Significance statistical analysis related to the calculation of volume	131
6.3.7.2	Significance statistical analysis related to the calculation of area of facades	132
6.3.7.3	Significance statistical analysis related to the calculation of area of roofs	133
6.3.8	Conclusions	134

6.4	Case-study: incorporation of morphological properties of buildings computed from GIS and LiDAR data on an urban multi-agent vector based geo-simulator	136
6.4.1	Presentation	136
6.4.2	Data sources used and normalized 2.5-DUSM constructed	137
6.4.3	The calculation of the morphological indicators and indexes	138
6.4.3.1	Volume and envelope area	138
6.4.3.2	Type of roof	139
6.4.3.3	Average height	142
6.4.3.4	Number of faces	143
6.4.3.5	Indexes	145
6.4.4	Brief description of the multi-agent vector based geo-simulator	146
6.4.5	Analysis of results	149
6.4.6	Conclusions	151
6.5	Conclusions and chapter synthesis	151
Chapter 7. Exploration of the solar potential on the urban fabric		153
7.1	Introduction	155
7.2	Background and related work	157
7.2.1	Basic irradiative parameters	157
7.2.2	Direct and diffuse components of radiation	158
7.2.3	State of the art	158
7.3	Solar irradiation analysis over the urban fabric	159
7.3.1	Method applied	159
7.3.2	Meteorological data sources	167
7.3.3	Choice of the suitable anisotropic sky model	167
7.3.4	Conclusion	169
7.4	Case-studies	170
7.4.1	Overview	170
7.4.2	Data sources used and 2.5-DUSM constructed	171
7.4.3	Geo-referenced raster information produced	171
7.4.4	Case-study: analysis of solar irradiation over building roofs	172
7.4.4.1	Presentation	172
7.4.4.2	Synoptic view of the process	173
7.4.4.3	Calculation of solar irradiation on building roofs	174
7.4.4.4	Extraction of indicators and analysis of results	178
7.4.4.5	Conclusions	183
7.4.5	Case-study: impact of vegetation on the solar irradiation over the urban fabric	183
7.4.5.1	Presentation	183
7.4.5.2	Synoptic view of the process	184
7.4.5.3	Extraction of indicators and analysis of results	185
7.4.5.4	Conclusions	187
7.4.6	Case-study: Comparison of solar irradiation over building roofs on two case-study areas presenting different building textures	187
7.4.6.1	Presentation	187
7.4.6.2	Synoptic view of the process	189
7.4.6.3	Extraction of indicators and analysis of results	190
7.4.6.4	Conclusions	194
7.4.7	Case-study: analysis of solar irradiation over building facades	194
7.4.7.1	Presentation	194
7.4.7.2	Synoptic view of the process	194

7.4.7.3	Calculation of solar irradiation on building facades _____	195
7.4.7.4	Extraction of indicators and analysis of results _____	198
7.4.7.5	Conclusions _____	202
7.4.8	Case-study: potential for active solar technology _____	202
7.4.8.1	Presentation _____	202
7.4.8.2	Synoptic view of the process _____	203
7.4.8.3	Extraction of indicators and analysis of results _____	205
7.4.8.4	Conclusions _____	208
7.5	Conclusions and chapter synthesis _____	209
Chapter 8.	<i>Estimation of the energy demand on the urban fabric _____</i>	211
8.1	Introduction _____	213
8.2	Background and related work _____	214
8.3	Case-study: evaluation of solar energy potential and energy needs for heating and lighting using 2.5-DUSM constructed from LiDAR data _____	215
8.3.1	Presentation _____	215
8.3.2	Synoptic view of the process _____	216
8.3.3	Available information about buildings _____	217
8.3.4	Energy analysis and scenarios _____	218
8.3.5	Heating needs evaluation _____	218
8.3.6	Artificial lighting needs evaluation _____	220
8.3.7	Exploration of the solar potential _____	222
8.3.8	Analysis of results _____	224
8.3.8.1	Direct outputs _____	224
8.3.8.2	Different energy scenarios _____	227
8.4	Validation and usefulness _____	229
8.5	Conclusions and chapter synthesis _____	229
Chapter 9.	<i>Utility of the 3-D geo-visualizations for urban environmental quality indicators _____</i>	231
9.1	Introduction _____	231
9.2	Background and related work _____	231
9.3	Geo-visualizations for urban environmental quality indicators _____	233
9.3.1	Indicators related to the assessment of the morphological properties on the urban texture _____	233
9.3.2	Indicators related to the exploration of the solar potential on the urban fabric _____	234
9.3.3	Indicators related to the estimation of the energy demand on the urban fabric _____	239
9.4	Evaluating the utility of the proposed 2-D and 3-D geo-visualizations _____	242
9.4.1	Presentation of the survey conducted _____	242
9.4.2	Analysis of results _____	243
9.5	Conclusions and chapter synthesis _____	245
Chapter 10.	<i>Conclusions and perspectives _____</i>	247
10.1	General overview _____	247
10.2	Review of the research goals _____	247

10.3	Final outcome	251
10.4	Perspectives	252
10.4.1	Research perspectives	252
10.4.2	Application perspectives	254
10.4.3	Commercial perspectives	255
	<i>Bibliography</i>	257
	<i>Appendix A. Inquiry about 3-D needs for the State of Geneva</i>	271
	<i>Appendix B. Morphological properties of buildings: statistical analysis</i>	277
	<i>Appendix C. Calculation of yearly and monthly irradiation values (2.5-D visualization) using the isotropic model</i>	287
	<i>Appendix D. Heating analysis: assumptions made for the buildings of Florence and CERN</i>	295
	<i>Curriculum Vitae</i>	297

ABBREVIATIONS

- ALS** – Airborne Laser Scanning
- AVL** – Automatic Vehicle Location
- CAD** – Computer Aided Design
- CEN** – Comité Européen de Normalization
- CERN** – Centre Européen pour la Recherche Nucléaire
- CSG** – Constructive Solid Geometry
- DEM** – Digital Elevation Model
- DGPS** – Differential Global Positioning System
- DHM** – Digital Height Model
- DHW** – Domestic Hot Water
- DIP** – Digital Image Processing
- DSM** – Digital Terrain Model
- DTM** – Digital Terrain Model
- 2.5 DUSM** – 2.5 Digital Urban Surface Model
- EPFL** – Ecole Polytechnique Fédérale de Lausanne
- FAR** – Floor Area Ratio
- GIS** – Geographical Information System
- GML** – Geography Markup Language
- GPS** – Global Positioning System
- GR** – Glazing Ratio
- IDW** – Inverse Distance Weighted
- INS** – Inertial Navigation System
- ISO** – International Organization for Standardization
- LASER** – Light Amplification by Stimulated Emission of Radiation
- LiDAR** – Light Detection and Ranging
- LoD** – Level of Detail
- MDL** – Minimum Description Length
- n2.5-DUSM** – Normalized 2.5 Digital Urban Surface Model
- POS** – Positioning Unit System
- PPS** – Pulse per Second
- prENV** – European Pre-Standard

Abbreviations

PV - Photovoltaic

RGB – Red, Green and Blue

RMSE – Root Mean Square Error

SVF – Sky View Factor

TIN – Triangulated Irregular Network

UEQ – Urban Environmental Quality

UNI – International Standard

WGS – World Geodetic System

CHAPTER 1. INTRODUCTION

1.1 Context

During the last decades, with rural exodus, the world is rapidly changing, particularly around and within metropolis. Indeed, urban planning became extremely complex, considering both conceptual and technological points of view, thus demanding different actions and new qualifications. Moreover, with the growth of developing countries this is a problem of global dimension. During the decades to come, in order to absorb the growth of world's urban population, cities with more than one million inhabitants will increase considerably. According to United Nations, in 2009, the number of cities with more than 10 million inhabitants was already higher than 20. Moreover, considering that around 65% of the world's urban population lives in developing countries, where sustainable policies are greatly lacking, how is it possible to control their energy consumption? Knowing how important this topic is, the indicators extracted by the means of empirical studies in this thesis respect urban environmental quality (UEQ) – for this reason, a main focus is given to urban morphology, the analysis of solar potential and energy demand on the urban fabric.

Although the topics presented in this study, as well as the proposed methods, always focus on universal phenomena related to urban environments, results presented have a strong connection with the requirements about 3-D geo-referenced information that was undertaken with potential end-users of the State of Geneva. In October 2005, the State of Geneva acquired a new LiDAR dataset. An inquiry to several potential end-users showed a strong interest for the integration of the third dimension in the available GIS data of the State of Geneva, mainly by the integration of new layers of information (in this thesis defined as 3-D urban indicators). Such specific and novel demand can only be achieved when using 3-D geo-referenced information (for instance, LiDAR data). As this was an ambitious and innovative research aspect related to geo-information sciences, it was chosen as a valid case-study environment, as presented in detail within this thesis. Moreover, different geo-referenced data of excellent quality, such as 2-D cadastral data, aerial images and a 3-D vector model of the State of Geneva, is also available and was also used for this study. These different data sources contributed to enrich and complement the LiDAR data source already available by a process of a more empirical nature. The 3-D vector model of the State of Geneva is also used in this study to statistically validate some of the extracted indicators, such as the morphological properties of buildings highlighted in chapter 6.

Finally, it is worth mentioning that this thesis intends to be a valid input for the European Action TU0801. The main goal of this action is to semantically enrich 3-D models with urban knowledge and models, so as to spread their utility, functionality and usability in a perception of sustainability.

1.2 Problematic

According to Roncayolo (1988), the concept of city implies an organization of spaces and objects within the framework of a complex and collective organization. In the last decades, analysis related to the urban evolution of the city has been done in a 2-D perspective, mostly by aggregating and presenting information as a set of indicators. During the decade of 1990, with the appearance of laser altimetry, or LiDAR (Light Detection And Ranging), a new revolution was started in the world of geo-information. Indeed, since then, the production of very high-resolution

tri-dimensional numerical data became much easier and, thus, it allowed to quickly improve the knowledge of territory. Due to its precision, as well as their mode of fast acquisition, LiDAR altimetric models arise as a serious alternative in various fields, such as urban planning and, intrinsically, its application for the extraction of indicators at different scales of the city. In such a context, altimetric LiDAR models allow the development of new and adapted models, methods and tools, leading to innovative original solutions. This study will demonstrate that LiDAR can significantly both improve and simplify the description and analysis of cities.

Among multiple questions inherent to the extraction of 3-D urban indicators - mainly related to its use, which includes visualization aspects - some problems can be easily identified:

Problem 1 - Which groups of end-users present real needs concerning the definition and extraction of 3-D urban indicators?

In order to improve the real utility of these numerical urban models, this thesis intends to develop novel processes of acquisition, aggregation and presentation of indicators of the urban evolution in a three-dimensional perception of the city, according to end-users requirements. A special attention is given to the relevance of the selected indicators, allowing specific end-users and decision-makers to be informed about the quality of cities, being a valid input for urban design and development processes. Moreover, these indicators enable the understanding of specific urban phenomena, being a reliable input for decision-making. Indeed, requirements concerning 3-D urban indicators and the application of reliable methods to build them are nowadays still largely ignored. More specifically, effective and efficient acquisition methods for the extraction of urban indicators are still lacking. Finally, it is important to show and represent these indicators using distinct levels of detail (LoD), according to user requirements and applications, allowing the apprehension of the nature, scale and impacts of the observed phenomena.

Problem 2 - Using several input geo-referenced data, which 3-D urban models should be constructed for each of the 3-D urban indicators to be extracted? Furthermore, how to define reliable methods based on these 3-D models for each of the 3-D urban indicators to be extracted?

Nowadays, the main use of 3-D urban models is still focused on the visualization of urban texture. Indeed, numerical models and 3-D visualization are still subjugated by the technological offer, which implies that the representation of objects is the most important aim of modelling. However, little attention is given to the best way to articulate these graphical interfaces with other data and more abstract models intended for spatial analysis and simulation. Usually, users can navigate through these 3-D environments, but can seldom reach relevant information, effectively aggregated for a problem that must be solved. Thus, 3-D urban modelling challenges are especially related to the utility and relevance of these models for the evaluation of urban development - also the improvement of processes inherent to an effective acquisition and aggregation of data, defined in this thesis as geo-referenced indicators, are highly necessary.

Finally, it is worth mentioning that an effective problem is that current 3-D models - for instance, a Digital Elevation Model (DEM), which is commonly interpolated from LiDAR data - usually used for the extraction of urban indicators are not sufficiently precise (if specific end-users' requirements are taken into consideration).

Problem 3. Do the extracted 3-D urban indicators have to be always visualized? If so, which type of visualization must be chosen? Moreover, for 3-D visualization and according to the CityGML standard (Kolbe et al., 2005), which level of detail (LoD) must be retained for each of these indicators?

Awaited information of 3-D urban models must be specified, such as the functions necessary to their aggregation and further significance to the decision-making processes – quite often it is under the form of geo-referenced indicators that this information can be effectively presented to

1.3 Research goals and methods

specialized and concerned end-users and decision-makers. The proposed indicators must be relevant considering the point of view of an evaluation and, consequently, must clearly indicate a tendency: what is expected to be evaluated and measured - according to cardinal (quantitative information) and ordinal (hierarchy or qualitative state) scales - using different data and models for the definition and extraction of these indicators? Can those indicators be visualized in different environments and considering different levels of detail (LoD)?

1.3 Research goals and methods

The research method of this thesis presents both an exploratory and an empirical nature. The methodological framework is connected to the theory and to the empirical case-studies undertaken in this thesis. Indeed, the methodological framework is conceptually built from theory drawn from bibliography and is ripened through the design and exploration of specific empirical case-studies that translate end-user needs into a set of specific 3-D urban indicators. The retained choice of these indicators emphasizes particular concerns from a point of view of sustainable development, defined in the form of three essential stakes: (1) assessment of the morphological properties of the urban texture, (2) exploration of the solar potential on the urban fabric, and (3) estimation of the energy demand on the urban fabric. Such is mainly done in case-studies areas belonging to the city of Geneva, but also on the cities of Lausanne and Florence.

Thus, this study is continuously improved using both theoretical knowledge and the practical implementation and validation of those empirical case-studies (Figure 1.1).

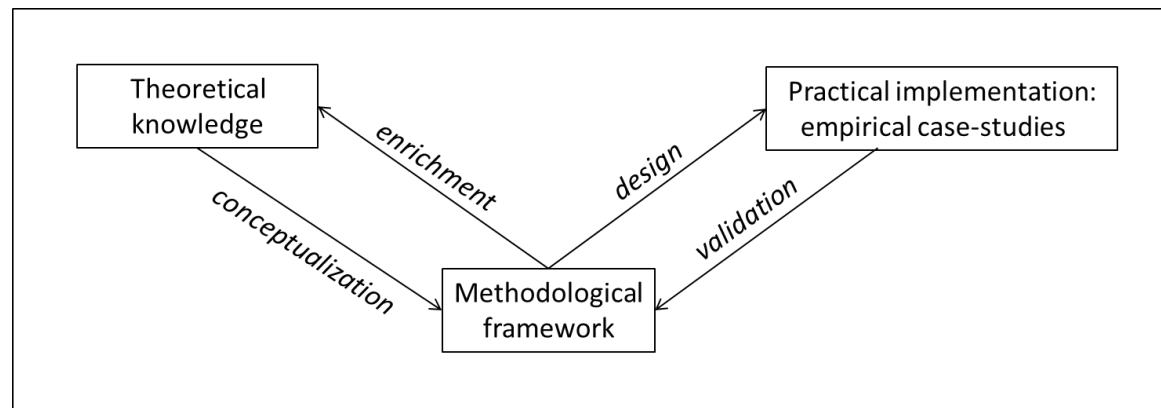


Figure 1.1. The research method of this thesis, which is based on a continuous improvement of the methodological framework using the theoretical knowledge and the empirical case-studies.

Considering the three main problems exposed in section 1.2, three main research goals and methods of this study can be summarized as follows (Figure 1.2):

Goal and method defined according to the first problem exposed in section 1.2

- *goal*: to define a list of pertinent 3-D urban indicators based on a user-requirements analysis, providing a wide-ranging assessment of the analytical capabilities and tools required by potential end-users;
- *method*: this goal is implemented for the city of Geneva by selecting a specific group of end-users interested on this topic. The proposed and extracted indicators are directly related to the field of UEQ, and are defined according to three main stakes presented in the first paragraph of this section.

Goals and methods defined according to the second problem exposed in section 1.2

- *goal*: to design new methods and tools using different data and models in order to extract relevant UEQ indicators presenting a 3-D dimension and to produce trustworthy results. The potential of LiDAR technology, as much as its limits, used for the extraction of this type of indicators, is especially highlighted;
- *method*: this goal is set up from the use of: (1) Digital Elevation Models (DEM) and Digital Height Models (DHM), in this thesis called 2.5-Digital Urban Surface Models (2.5-DUSM) and normalized 2.5-Digital Urban Surface Models (n2.5-DUSM) respectively, (2) a segmentation procedure directly applied on LiDAR data, and (3) specific algorithms that are developed and implemented in a raster-basis over the data and models presented in points (1) and (2). A main focus is given to an enhancement of the different 2.5-DUSM and n2.5-DUSM constructed, allowing to improve its truthfulness. Indeed, these models are less consistent along zones (edges) of discontinuity, such as external building facades, when compared to traditional 3-D CAD models.

Goal defined according to the third problem exposed in section 1.2:

- *goal*: to evaluate the utility of the different exploratory 2-D, 2.5-D and 3-D geo-visualizations proposed for the UEQ indicators extracted in this thesis;
- *method*: in order to fulfil this goal, an analysis about how end-users perceive and interpret these geo-visualizations is undertaken.

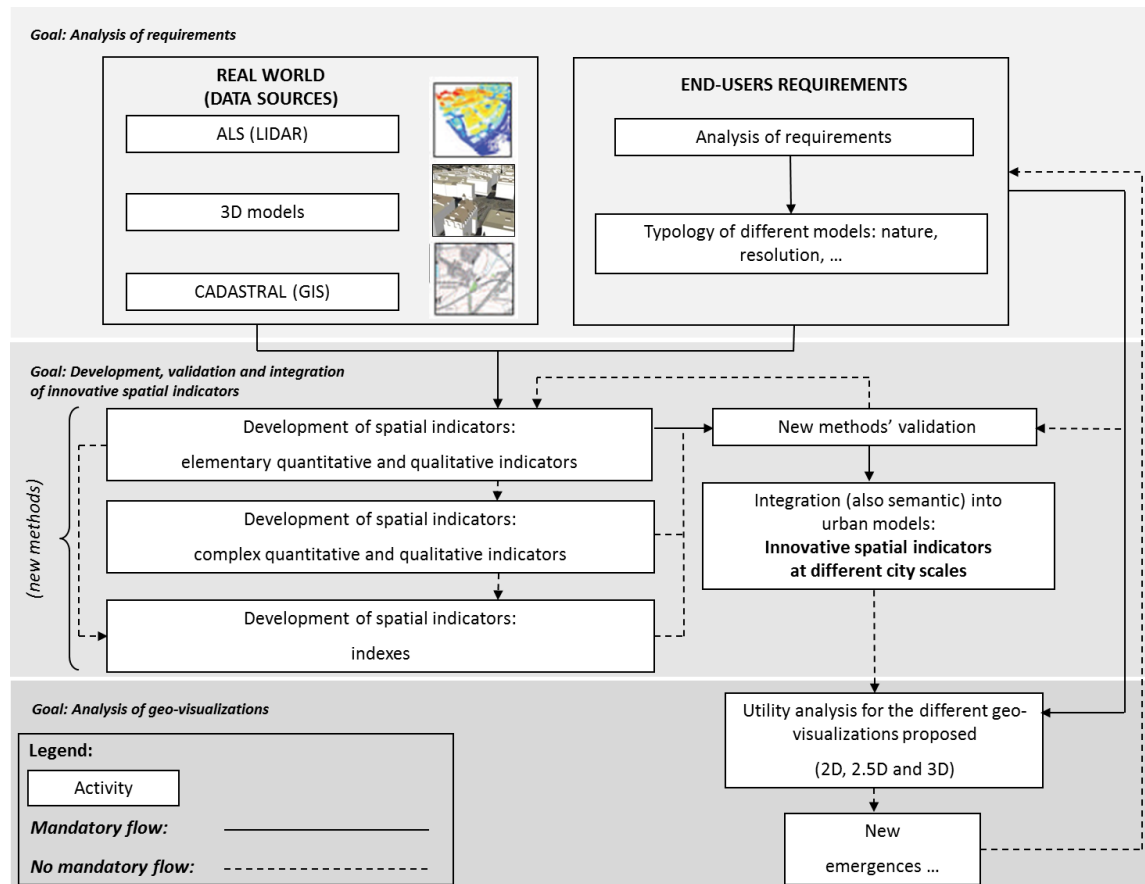


Figure 1.2. Synoptic view describing the integrated research process of this thesis.

1.4 Empirical research process

The methodological framework of this thesis follows the conceptualization method proposed by Maystre and Bollinger (1999), which follows a *top-down* and *bottom-up* processes: the description of a set of pertinent UEQ indicators based on a user-requirements analysis (also briefly defined as “demand” process) and the selection and organization of data, models and tools in order to extract these indicators (also briefly defined as “offer” process) respectively. This double process represents the starting point of the empirical research process, allowing to define a set of case-studies that are developed and emphasized in this thesis (Figure 1.3). Those are related to one of the three main stakes previously presented in section 1.3 (Table 1.1), and are classified according to two main approaches: (1) a technical and statistical assessment and validation of indicators related to the morphological properties of buildings, and (2) a technical and relevant demonstration among the end-users engaged in this study of several UEQ indicators. In anticipation to the empirical case-studies, two punch-cases are also mobilized to make the usefulness of the constructed 2.5-DUSM emerge. The main goal of a punch-case is to raise new ideas and methods, which are relevant considering the purposes of this thesis.

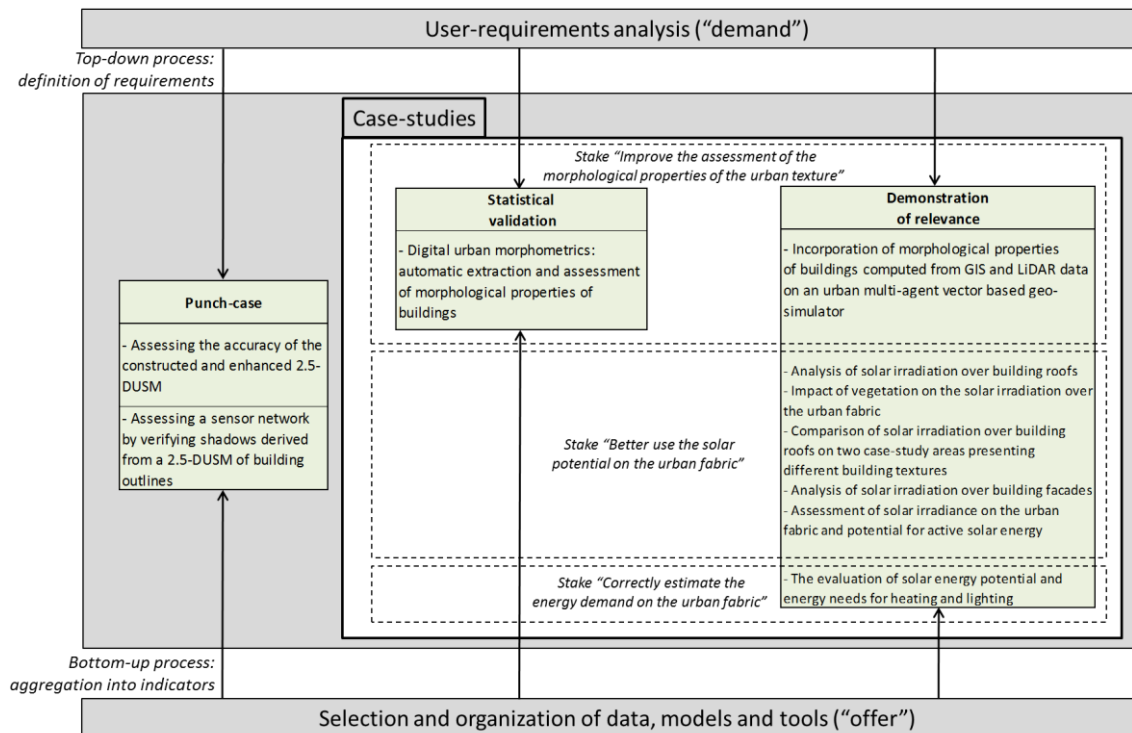


Figure 1.3. Synoptic view of the top-down and bottom-up processes adopted for the definition of a set of pertinent case-studies and punch-cases.

Stake	Input data	Example of urban environmental quality (UEQ) indicator extracted	Visualization
Assessment of the morphological properties of the urban texture	2-D, 3-D	Area of building roofs Area of building facades Volume of buildings	No visualization
Exploration of the solar potential on the urban fabric	2-D, 3-D	Solar forecast on roofs Solar forecast on facades	2-D, 3-D
Estimation of the energy demand on the urban fabric	2-D, 3-D	Heating analysis Lighting analysis	2-D, 3-D 2-D, 3-D

Table 1.1. Example of UEQ indicators extracted for the specific stakes analysed in this study.

The process applied for the extraction of each of the UEQ indicators is shown in the synoptic view of Figure 1.4, which is based in three main operations:

1. The *initial operations*, which are defined upstream of all the other processes, are concerned with the optimal preparation of all the initial data used. It refers in particular to the classification and filtering of raw LiDAR data used for the different 2.5-DUSM and n2.5-DUSM constructed (raster-based), and the segmentation of planar roof areas using classified point clouds (vector-based);
2. The *analysis operations* allow the extraction of a set of UEQ indicators for each of the proposed stakes. These operations may require several sectors and competences that include urban design and morphology, geography, environment, energy, programming and image processing. These indicators are mainly exploitable by specialized end-users - in some cases they can be also used for wider public diffusion;
3. The *validation operations* are applied in order to control the reliability of the extracted UEQ indicators. Those are validated at the end of the process shown in Figure 1.4 with the specialized end-users engaged in this study and according to its requirements. Nevertheless, in some cases - for instance concerning the accuracy of the novel method proposed for the extraction of indicators related to the morphological analysis of buildings (volume, area of facades and area of roofs) -, the validation process of these indicators is complemented by a statistical assessment, allowing to improve its trustworthiness.

1.4 Empirical research process

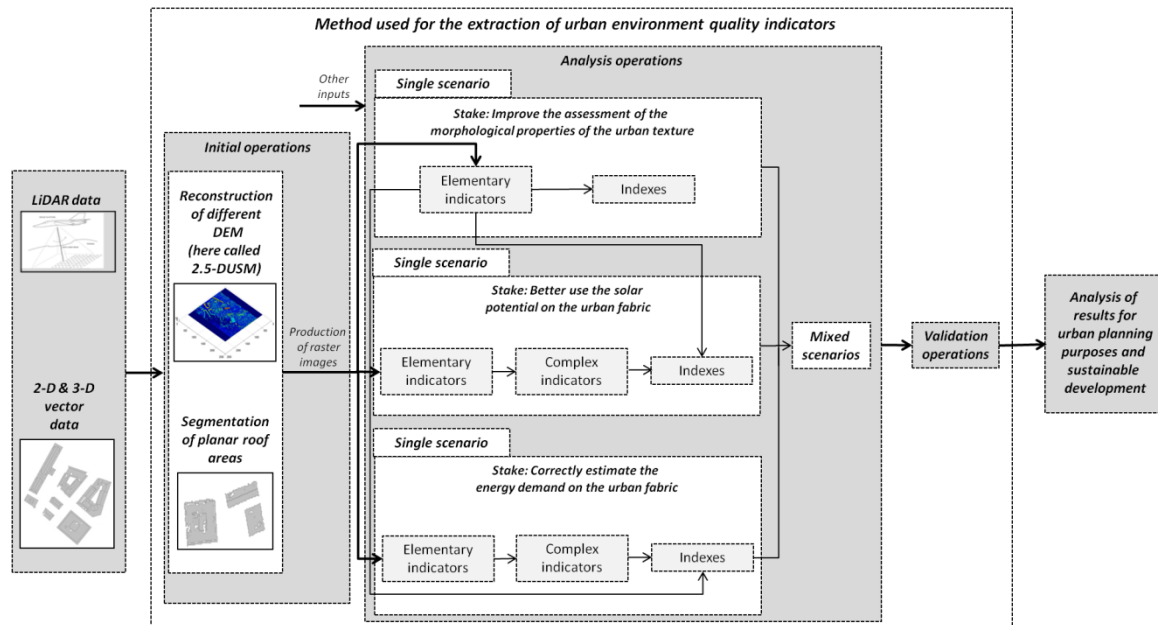


Figure 1.4. Synoptic view of the methods used for the extraction of UEQ indicators.

UEQ indicators corresponding to different stakes may be used together, defined as mixed scenarios, in order to extract aggregated UEQ indicators or UEQ indexes - some examples of mixed approaches are further emphasized in chapters 7 and 8. In these cases, morphological properties of buildings, such as the area of roofs or the area of storey, are used together with other indicators related to solar potential or energy demand on the urban fabric in order to refine the analysis presented for each of these subjects. The construction of mixed scenarios highlighted in this thesis is also a novel work.

The core of the method proposed in this study for the extraction of the UEQ indicators is based on the *analysis operations* method – in this case, three different classes of indicators can be distinguished (Figure 1.4):

- an *elementary indicator* is directly derived from the different analysed data used, by applying digital image processing algorithms and techniques. Commonly it is represented using 2-D or 3-D (includes 2.5-D) visualizations. Indeed, even if input data used for the extraction of this type of indicators is always 3-D based, sometimes its representation is considered to be more pertinent using a 2-D display (chapter 9 of this thesis focus on this specific point, related to the utility of innovative 3-D visualizations);
- a *complex indicator* results from the use of several elementary indicators, eventually complemented by the different analysed data used - in most of the cases these indicators are directly derived through pioneering digital image processing algorithms and techniques and the use of other input data not geo-referenced, e.g., statistical meteorological data used for the assessment of solar potential on the urban fabric. Commonly it is also represented using 2-D or 3-D (includes 2.5-D) visualizations;
- an *index* represents an indicator with a higher level of abstraction, with minimal loss of information, being represented as relative values that can be very useful on generalization and comparison procedures. In this thesis, all highlighted indexes refer to an aggregation resulting from the ratio of two elementary or complex indicators.

These indicators and indexes are extracted using image processing techniques based on different 2.5-DUSM and n2.5-DUSM. These models replicate the geometry of the urban fabric and are created by regularly spaced matrices of altitude (in the case of 2.5-DUSM) or height from terrain

(in the case of n2.5-DUSM) values, which contain 3-D information on 2-D digital support. Indeed, by implementing image processing algorithms on the 2.5-DUSM and n2.5-DUSM it is conceivable to develop proficient tools for the analysis and planning of the sustainable urban form, measuring geometric parameters and assessing the solar potential on the urban fabric, among others. Moreover, most of the methods proposed for the extraction of the UEQ indicators can be automatically implemented and the results achieved are extremely fast and accurate for an analysis aimed at neighbourhood or city scales, as exposed in this study. All the algorithmic implementations needed are made with Matlab software. The conduction of this type of analysis on Matlab requires a basic understanding of mathematical programming, fundamentals of image processing and a good level of confidence with computer aided design (CAD) in two and three dimensions. In conclusion, the classification of raw LiDAR data and the construction of the different 2.5-DUSM and n2.5-DUSM used are based on CAD and GIS software.

1.5 Thesis outline

Following this introduction, which focuses on the problematic, context, goals and method of the present thesis, the next chapters are structured as follows:

Part I - Theoretical knowledge

Chapter 2: 2-D and 3-D spatial data for urban modelling

In this chapter, different concepts related to data sources used and techniques applied throughout this study are presented, with a main focus given to LiDAR data and its properties. The different classes of 3-D objects representations, gridding and image processing of digital elevations models and 3-D data modelling are also briefly described.

Chapter 3: Urban indicators

This chapter emphasis the roles, properties and related methods of indicators - special attention is given to the definition and visualization - including 3-D visualization - of geographical indicators at urban scales.

Part II - Methodological framework

Chapter 4: User requirements analysis

This chapter highlights the use of 2-D and 3-D urban models and data for the extraction of urban indicators, considering different kinds of applications related to end-user's needs of the State of Geneva. The purpose of the use cases highlighted in this chapter is to define the application of this type of information from an end-user's perspective and to create the basis of a valid conceptual model.

Chapter 5: Data sources used and models constructed

Based on the user requirements analysis presented in chapter 4, this chapter illustrates how the use of one or more sources of geo-referenced information allows to construct different 2.5-DUSM and n2.5-DUSM or to apply a segmentation of planar roof areas - both techniques are used for the extraction of the UEQ indicators emphasized in this study. A special focus is given to the enhancement of the 2.5-DUSM and n2.5-DUSM constructed, by applying specific techniques along the zones of discontinuity of the models.

Two punch-cases are presented:

- *Assessing the accuracy of the constructed and enhanced 2.5-DUSM of roof lines;*
- *Assessing a sensor network by verifying shadows derived from a 2.5-DUSM of building outlines.*

Part III - Practical implementation: empirical case-studies

Chapter 6: Assessment of the morphological properties of the urban texture

This chapter focus on the extraction of morphological properties of buildings using different n2.5-DUSM: volume and total area, which includes the area of the ground, facades and roofs.

Two case-studies are presented:

- *Digital urban morphometrics: automatic extraction and assessment of morphological properties of buildings,* highlighting an innovative method used for the extraction of areas of facades and roofs using digital image processing techniques based on normalized 2.5-DUSM and segmentation of planar roof areas, which are transformed from vector to raster format;
- *Incorporation of morphological properties of buildings computed from GIS and LiDAR data on an urban multi-agent vector based geo-simulator:* in this study, the intention is to go a step further, presenting the implementation of morphological properties of buildings, which allows the evaluation of new planned architectural programs.

Chapter 7: Exploration of the solar potential on the urban fabric

This chapter focus on the assessment of the solar potential over the urban fabric using different 2.5-DUSM and n2.5-DUSM.

Five different case-studies are presented:

- *analysis of solar irradiation over building roofs:* a tool that estimates the solar irradiation over building roofs considering different periods of time;
- *impact of vegetation on the solar irradiation over the urban fabric:* in this study the main goal is to analyse the impact of vegetation on the solar irradiation over the urban fabric;
- *comparison of solar irradiation over building roofs on two case-study areas presenting different building textures:* a tool that estimates and compares the solar irradiation over building roofs on two case-study areas;
- *analysis of solar irradiation over building facades:* a tool that estimates the solar irradiation over building facades considering different periods of time;

Chapter 1. Introduction

- *potential for active solar technology*: in order to assess the potential implementation of renewable energies at the scale of the city, a general understanding of the solar admittance and solar gains incident on the urban fabric is applied in this study.

Chapter 8: Estimation of the energy demand on the urban fabric

This chapter focus on the assessment of the energy demand over the urban fabric using different 2.5-DUSM and n2.5-DUSM.

A case-study is presented:

- *The evaluation of solar energy potential and energy needs for heating and lighting*: a tool that estimates heating and lighting demand at the district level.

Chapter 9: Utility of 3-D geo-visualizations for urban environmental quality indicators

This chapter presents an analysis of the utility of the 3-D geo-visualizations built for the UEQ indicators extracted from chapters 6 to 8. This analysis is undertaken with the same of group of end-users presented in chapter 4 of this thesis.

Final of Part III

Chapter 10: Conclusions and perspectives

This chapter concludes the study by reviewing all the goals expressed in section 1.3, as well as providing some perspectives regarding the methodological framework proposed and further work related to the extraction of UEQ indicators.

PART I
THEORETICAL KNOWLEDGE

CHAPTER 2. 2-D AND 3-D SPATIAL DATA FOR URBAN MODELLING

2.1 Introduction

In the geoinformation field, two-dimensional (2-D) and three-dimensional (3-D) spatial data is commonly obtainable and frequently used for spatial analysis, even though 2-D data remains as the most commonly used. The main reasons for this are attributable to the difficulties in 3-D data structuring, particularly in a correct definition of requirements for 3-D topology (Ellul and Haklay, 2006). These problems need to be further investigated so that the feasibility of having a system capable of handling both 2-D and 3-D data types for different end-users needs and GIS applications can be considered. According to Abdul-Rahman and Pilouk (2008), a large overview of 3-D application areas in GIS include:

- Ecological studies - for instance, the study of malaria vectors around the world;
- Environment and energy- for instance, monitoring of soil and groundwater quality;
- Geological analysis - for instance, the geologic hazard assessment;
- Civil engineering - for instance, to provide the tools for creating, managing, analysing and visualizing the data associated with developing and managing infrastructure;
- Mining exploration - for instance, by using basic geological maps, hyper-spectral airborne and multispectral satellite imagery to search for mineral deposits. GIS allows geoscientists to bring these datasets together and accurately calculate economic potential;
- Oceanography - for instance, to apply methods for the mapping and measurement of major ocean processes;
- Automatic vehicle navigation and location - for instance, by combining Automatic Vehicle Location (AVL) technology, GIS, and analytical models it is possible to improve the emergency response operations in the electric utility industry;
- Archaeology - for instance, GIS can be used as a database management for archaeological records, with the additional advantage of being capable to create 2-D and 3-D maps;
- Landscape planning - for instance, GIS can be used to compare a great number of area-related data describing the affected natural resources;
- Defence and intelligence - for instance, GIS can be used as a support for military planning and operations;
- Command and control - for instance, GIS allows to display the location and status of all command and control assets on a topographical map, allowing for complete management of all information systems using one single interface;
- 3-D urban mapping - for instance, in urban noise mapping;
- Architecture and urban planning - for instance, in the areas of urban design, community planning, and the site selection process.

The main applications hereby presented in chapters 6, 7 and 8 are related to the fields of environment and energy, 3-D urban mapping and planning and architecture and urban planning: assessment of the morphological properties of the urban texture, analysis of the solar potential on the urban fabric and estimation of the energy demand on the urban fabric respectively.

In the next sections of this chapter most relevant concepts related to the technical framework of this thesis are presented: (2.2) classes of 3-D object representations, (2.3) geographical information systems, digital elevation models (DEM) and digital height models (DHM), (2.4) image processing of digital elevation models (DEM) and digital height models (DHM), (2.5) Airborne laser scanning systems, (2.6) gridding interpolation of digital elevation models (DEM) and digital height models (DHM) using LiDAR data, (2-7) 3-D data modelling, and (2.8) conclusions and chapter synthesis.

2.2 Classes of 3-D object representations

Geo-information data may be defined as two distinct forms: vector and raster. In the case of objects being represented by one of the basic discrete entities such as points, lines or areas, which are spatially represented by a Cartesian coordinate system, they are said to be in vector form (Burrough and McDonnell, 1998). Raster models use map layers composed of an array or grid of square cells with a specific resolution, each of which has assigned a value, such as the elevation of the terrain or the height of a building. Thus, each cell represents a square parcel of the real world. Cells are arranged on 2-D Cartesian planes and identified by a row and a column coordinate usually attached to real world coordinate systems such as UTM, among others. Hence, each cell can basically be considered a pixel; in this case, map layers are equivalent to digital images.

The representation of objects in vector or raster forms has both advantages and disadvantages. Vector form offers better accuracy, being represented by exact coordinates in space. On the other hand, in some cases (for instance, the analysis of solar irradiation on building roofs), the use of raster form as a mean for data processing of complex algorithms for the extraction of spatial indicators is incomparably more efficient than vector form. Moreover, topology information (in terms of positions of object entities) is implicitly defined (Peucker, 1978).

During the last decade, the advancement of sensor technologies has also opened many new avenues for acquiring 3-D data (Tao, 2006). For mapping applications, one of the main progresses has been the direct geo-referencing technology, as used by airborne laser scanning (ALS) systems, also called light detection and ranging (LiDAR). Direct geo-referencing offers both position and orientation information of ALS systems using integrated inertial devices and positioning systems without ground controls. The use of direct geo-referencing technology on ALS systems has also improved the system workflow for 3-D data collection (in the form of point clouds having x , y and z coordinates) and data processing for different type of applications, such as the extraction of urban indicators.

A general overview of the different classes of 3-D object geometry/topology commonly used is presented in this chapter. According to Li (1994) 3-D object geometry/topology may be described as follows:

- *surface-based*: the object is represented only by surface primitives, including grid, shape model, facet model and boundary representation (B-rep);
- *volume-based*: the object's interior is described by solid information, including 3-D array, octree, constructive solid geometry (CSG) and 3-D triangulated irregular network (TIN).

2.2. Classes of 3-D object representations

Surface-based representations are presented as follows (Figure 2.1):

- *Grid*: commonly used method for surface representation in GIS, such as for digital terrain models (DTM) and digital elevation models (DEM). In this case it is a structure that specifies altitude or height values at regular locations;
- *Shape model*: describes an object surface by using surface derivatives (e.g. slopes) of surface points;
- *Facet model*: defines an object's surface by planar surface cells which can have different shapes and sizes. A widely used representation of a facet model that uses triangle facets is a Triangulated Irregular Network (TIN);
- *Boundary representation (B-rep)*: represents an object by a grouping of predefined primitives of point, edge, face and volume. B-rep is also a method for the description of volumes. Surfaces are used to represent the closed shell of a volume. The three previously mentioned surface representations can be used to describe the shell of a B-rep.

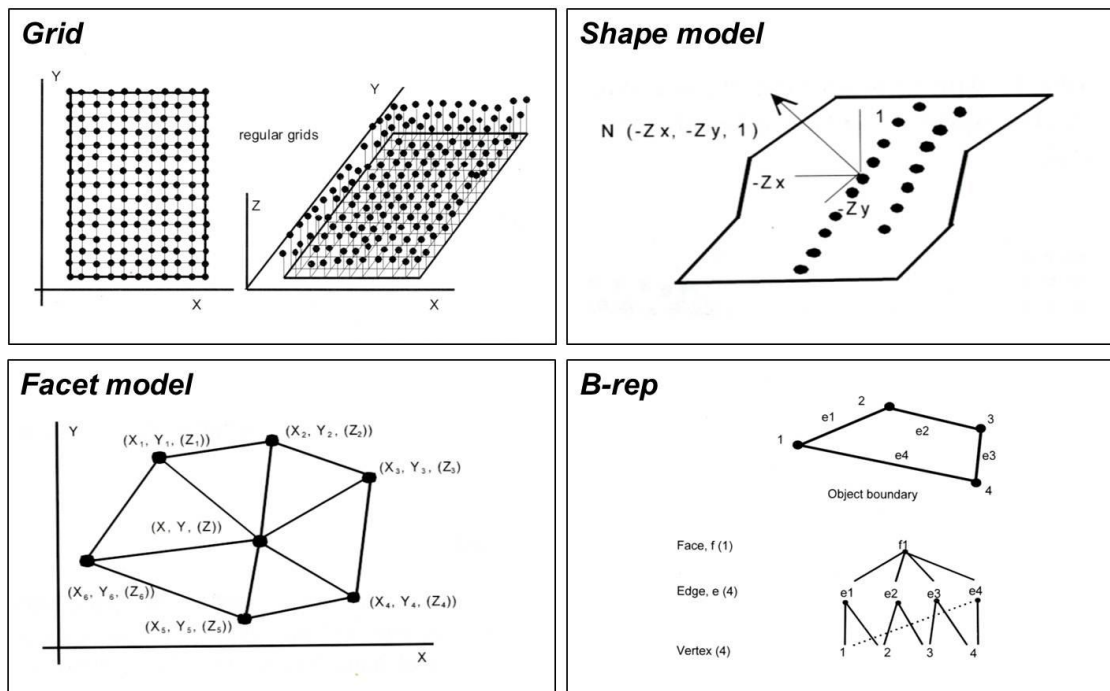


Figure 2.1. Surface-based 3-D representations.

Volume-based representations are presented as follows (Figure 2.2):

- *3-D array (also called voxels)*: it is considered the most simple data structure in the 3-D domain. Three dimensional arrays are basically multiple two dimensional arrays layered on top of each other. This type of representation consumes vast computer resources and this is one of the reasons why it is rarely used in practice (Dong, 1996);
- *Octree*: concerns a hierarchical data structure that defines the occupancy of cubic regions of the object space. This type of representation is widely used in image processing and computer graphics (Samet, 1990);
- *Constructive solid geometry (CSG)*: represents an object by a mix of predefined simple primitives defined as geometric primitives. The latter are regularly shaped volumetric

instances that can be combined by using geometric transformation, such as translation, rotation and scaling, and boolean operations, such as union, intersection and subtraction;

- *3-D TIN (Tetrahedral network, TEN)*: basically 3-D TIN is an extension of 2-D TIN, also called TEN (for a tetrahedral network). As for 2-D TIN, TEN also offers many advantages for manipulation, display and analysis purposes, and is very suitable for earth sciences applications. A TEN possesses four vertices, six edges and four faces.

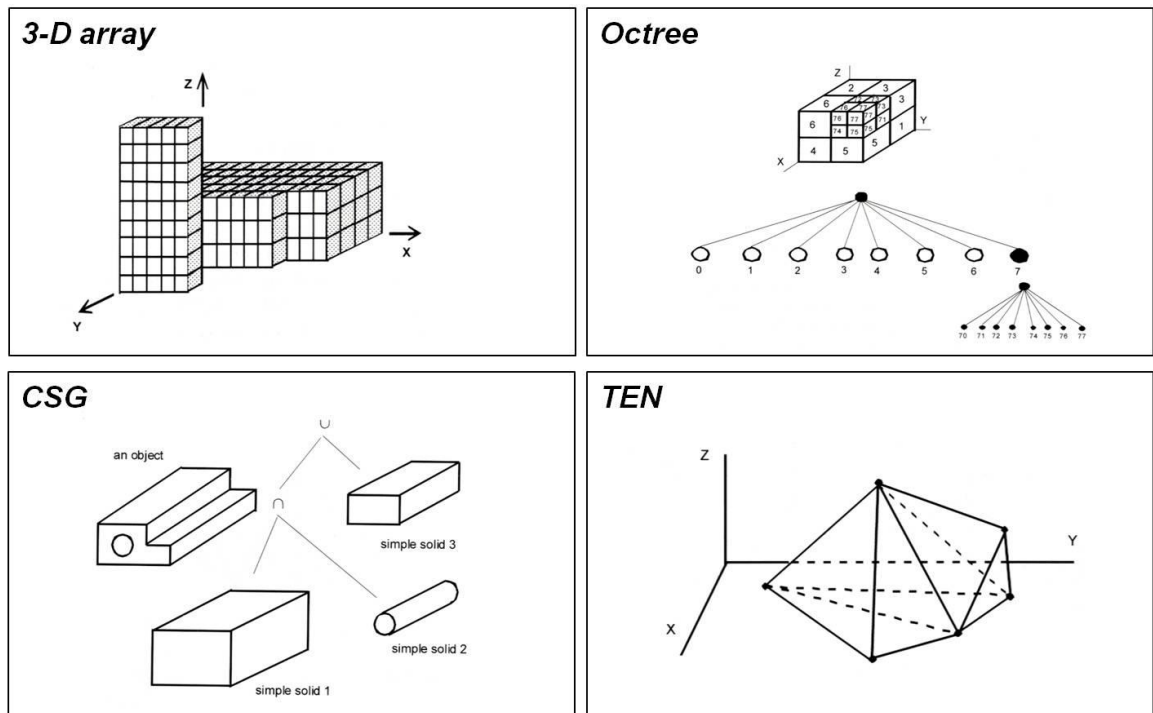


Figure 2.2. Volume-based 3-D representations.

More details about 3-D object representations are presented in Abdul-Rahman and Pitoul (2008).

In this thesis the main focus is given to grids, which are used for the implementation of specific algorithms that allow the analysis of the urban form and the extraction of inherent urban indicators. Boundary representation (B-rep) is used for the extraction of 3-D roof lines and for the 3-D visualization of the proposed indicators.

2.3 Geographical information systems, digital elevation models (DEM) and digital height models (DHM)

Since the emergence of GIS software many procedures have been developed in the environment of raster techniques in order to analyse map layers, including those which store elevation information in the form of Digital Elevation Models (DEM). In the early 1980's spatial mathematics evolved within the domain of GIS, and was subsequently defined as *Map Algebra*. It is a general framework that mathematically describes map operations and was defined by its developer Tomlin (1983) as “a starting point for the co-ordination of the development of digital overlay mapping techniques”. The configuration of map algebra is composed of a set of map layers, primitive operations on and between different map layers, and sequences of these operations. It is similar to conventional algebra where entire maps represent the variables (Tomlin, 1990).

2.3. Geographical information systems, digital elevation models (DEM) and digital height models (DHM)

Map algebra has been influenced by ideas and techniques derived from image processing. It adopts a common definition of operations: for instance, as presented in section 2.4, zonal operations are the equivalent of neighbourhood operations and local operations are similar to point operations. The main focus in map algebra, however, is to analyse multiple layers simultaneously, such as elevation, slope, among others.

Some examples of simple attributes and their respective fields of application (extraction of pertinent indicators) that can be derived from DEM using map algebra were initially proposed by Burrough and McDonnell (1998), such as presented in Table 2.1.

Attribute	Definition	Applications
Elevation	Height above mean sea level or local reference	Potential energy determination; climatic variables
Slope	Rate of change of elevation	Steepness of terrain; overland and sub-surface flow, land capability classification
Aspect	Compass direction of steepest downhill slope	Solar irradiance; evapotranspiration
Viewshed	Zone of inter-visibility	Stationing of microwave transmission towers; fire watch towers; visual impact of a new building
Irradiance	Amount of solar energy	Vegetation and soil studies; Location of energy saving buildings

Table 2.1. Example of attributes that can be computed from DEM and their applications. Adapted from Burrough and McDonnell (1998).

The first Digital Elevation Models (DEMs) used in GIS were interpolated using cartographic contours or computed through parallax measures in aerial photography interpretation (Moore *et al.*, 1991) and its origins are related to physical terrain model (Li *et al.*, 2005). Synthetic aperture radars (SAR), interferometry, and radargrammetry, appeared through the evolution of space technology, e.g. the shuttle radar topography mission (SRTM) of the National Aeronautics and Space Administration (NASA). Although these new technologies have enabled the acquisition of global terrestrial coverage, the DEM resolutions remained in the range of 15 to 90 meters. Only terrestrial methods, like levelling, GPS measures and, in some cases, aerial photography and interferometry can result in high resolution DEMs (1 to 5 m). Airborne laser scanning (ALS) emerged approximately 15 years ago for DEM acquisition purposes (Baltsavias, 1999b).

The following techniques are or have been used for DEM data acquisition (Li *et al.*, 2005):

- *Aerial photography*: through two stereo photographs an image matching is fulfilled; coordinates (x, y and z) can therefore be measured;
- *Radargrammetry and SAR interferometry*: space techniques in which the interferometry of phase is measured. This is an active system using microwaves. Such as carrier phase tracking with a GPS, coordinates can therefore be derived from the phase differences;

- *Cartographic interpolation*: for example, the Swiss national DEM (25 meter resolution) was created using a cubic interpolation from cartographic contour data;
- *Manual terrestrial acquisition*: using GPS or levelling techniques, on site coordinates are measured and interpolated;
- *Light detection and ranging (LiDAR)*: the data used in this study is issued from Airborne Laser Scanning (ALS), also called LiDAR.

The DEM used in this study are constructed from LiDAR data. For this reason, from now on, this thesis will focus on the description and use of this type of data. For an overview of LiDAR data systems and technology please consult section 2.5.

Since the appearance of numerical technologies, DEM has been widely accepted as the term for the characterization of elevation grids. For clarification, a short definition of each term used in this study is given:

- *DEM - Digital Elevation Model*: DEM is the term generically used for the description of the general properties and process of matrix elevation data. Generally refers to a representation of the earth's surface (or subset of this), including features such as vegetation, buildings, bridges, among others;
- *2.5-Digital Urban Surface Model (2.5-DUSM) of building outlines and 2.5-DUSM of roof lines*: this is also image-based geo-referenced information. Both these models are similar to DEM and are constructed using a hybrid approach that integrates raw LiDAR data with 2-D vector digital maps;
- *DTM - Digital Terrain Model*: DTM is the part of elevation data that represents the terrain;
- *DSM - Digital Surface Model*: DSM is the model of surface, namely all elements independently of their kind (natural or human infrastructures), including vegetation (trees) or buildings. In the case of a model that contains none of these objects, the DSM is equivalent to the DTM;
- *DHM - Digital Height Model (in this thesis called normalized 2.5-DUSM of building outlines or normalized 2.5-DUSM of roof lines)*: it is not a representation of elevation, but rather a representation of height. By computing the difference between the 2.5-DUSM of building outlines or the 2.5-DUSM of roof lines and the DTM, a DHM containing the differences of surface and terrain is generated. An example of the application of this type of model is the estimation of tree heights (Gachet, 2009). An illustration (3-D view) of a normalized 2.5-DUSM of building outlines located in a neighbourhood of the city of Geneva is presented in Figure 2.3.

2.3. Geographical information systems, digital elevation models (DEM) and digital height models (DHM)

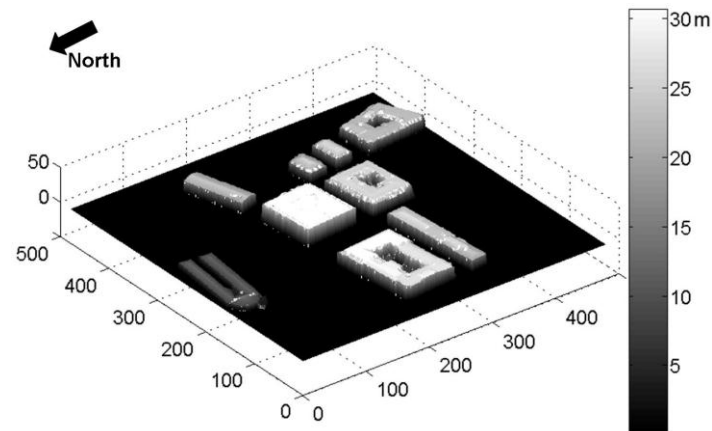


Figure 2.3. 3-D view of a normalized 2.5-DUSM of building outlines of a neighbourhood of Geneva's city.

In this study, the terms DEM, DTM, DSM, 2.5-DUSM of building outlines, 2.5-DUSM of roof lines, normalized 2.5-DUSM of building outlines, and normalized 2.5-DUSM of roof lines will always refer to the urban models adapted in the form of a regular grid.

As already mentioned in this chapter, a grid is a structure that specifies height values at regular locations, also called cells. Moreover, geo-referencing of each cell is assured by both its location and the definition of the grid sampling size and orientation. Throughout this study new information for these cells will be computed, and hence, it is important to specify the following basic properties of DEM or DHM:

- *Resolution (r)*: size of a usually square grid cell, which corresponds to two non-diagonal adjacent nodes of the DEM or DHM;
- *Width (m)*: number of columns of the grid, which defines the east-west extend of the DEM or DHM;
- *Height (n)*: number of lines of the grid, which defines the north-south extend of the DEM or DHM;
- *Minimum (min)*: the lowest pixel value, which defines the minimum elevation of the DEM or DHM at a specific location;
- *Maximum (max)*: the highest pixel value, which defines the maximum elevation of the DEM or DHM at a specific location;
- *Range (R)*: the range of elevations is defined as $max - min$. The range gives an indication of discontinuity zones of the of the DEM or DHM, such as borders of roofs.

The three last statistical properties shown above are totally dependent on the spatial extension of the DEM or DHM, being therefore implicitly related to the width, height and resolution of the used grid.

According to Li *et al.* (2005), a DTM, a DEM or a DHM can also contain non-topographical information, such as the intensity signal of LiDAR point clouds. However, in this study, only topographical information of DEM will be deeply explored and analysed.

2.4 Image processing of digital elevation models (DEM) and digital height models (DHM)

2.4.1 Overview

A digital image is a data file or structure representing in general a rectangular grid of pixels, or points of colour, on a computer monitor, paper, or other display device. The colour of each pixel is individually defined. Images in the RGB colour space, for instance, frequently consist of coloured pixels defined by three bytes: one byte each for red, green and blue. Less colourful images have need of not as much of information per pixel. An image with only black and white pixels only requires a single bit for each pixel.

An urban DEM or DHM, such as presented in section 2.3, is a rectangular array of numbers which represents the elevation or height of the city surface respectively, usually concerning the terrain, buildings and vegetation at regularly spaced intervals, called cells. As such, DEM or DHM can be considered a simple digital image, called raster image, and, thus, may be analysed using digital image processing techniques.

2.4.2 Definition of a digital image

This section presents an overview of some basic concepts related to digital image processing, that are applied throughout this thesis. More detailed information may be found in Jähne (2005) and Liu and Mason (2009), while a description of digital treatment of images may be found in Gonzalez *et al.* (2004).

A digital image is a set of picture elements, or pixels, often arranged in a rectangular array. A pixel is the smallest graphic unit of the image and it is not further divisible, except if the resolution of the image is changed. Moreover, each pixel of an image has one assigned numerical value, such as its colour, brightness, etc.

The horizontal and vertical position of each pixel in the image is respectively given by its x and y co-ordinates. An example of pixel co-ordinates such as (0,0) representing the upper left corner of the image is shown in Figure 2.4.

2.4. Image processing of digital elevation models (DEM) and digital height models (DHM)

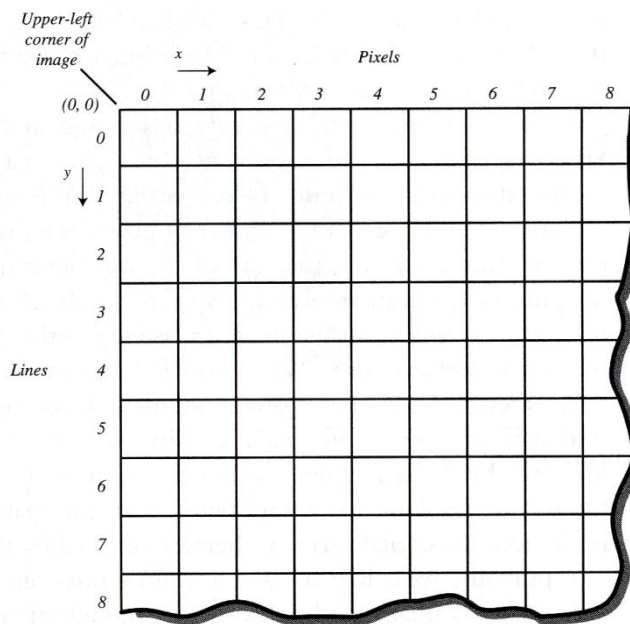


Figure 2.4. The pixel numbering convention. Diagram from Baxes (2004).

The different classes of images that exist are based on the numerical values associated with pixels: binary, grey-scale, colour, etc. In binary (or *bitmap*) images, each pixel contains just one bit of information, which can therefore represent 0 and 1, respectively white and black values. In grey-scale images, each pixel embraces generally 8 bits of information, which correspond to 256 possible values. Finally, in full colour images the number of channels is tripled: three images of 8 bits per pixel are used, defining the amount of Red, Green and Blue contained within each pixel. These images are called *RGB* and can accurately represent real colours, allowing for over 16 million colours, which correspond to $256 \times 256 \times 256$ combinations of red, green and blue.

Another important parameter of an image is its resolution. This is not an absolute parameter, but it is defined considering the way in which the image was constructed: for instance, a small 1x1 inch photograph can be converted into a digital image of either 100x100 or 1000x1000 pixels. The number of pixels per inch defines the image resolution and is measured in *dpi* (dots per inch). This is a crucial parameter as it characterizes the digitization process, defined as the process by which an analogue signal in a 2-D continuous space is converted into a 2-D discrete space using a sampling procedure. In fact, the higher the resolution and the number of pixels used, the better the quality of the image.

2.4.3 Digital image processing

Nowadays digital image processing is applied in a range of diverse fields, such as biology, remote sensing, and medicine, among others. According to Baxes (1994) words “*this dynamic field truly touches us all, playing an important role in our world ... Digital image processing techniques are used to do everything from reading your checks at the bank to automatically inspecting the fill-level of your pop bottle*”.

Through the use of image processing numerical techniques, the form or appearance of an image can be changed. Since 1970 different methods have been developed: while one of them may

improve the quality of an image, another may automatically extract information from it. Both methods are applied throughout this thesis.

Furthermore, the same steps are followed: a digital technique is applied to an input image and a digital result, such as a new image or a list of extracted data, is produced as an output (Figure 2.5).

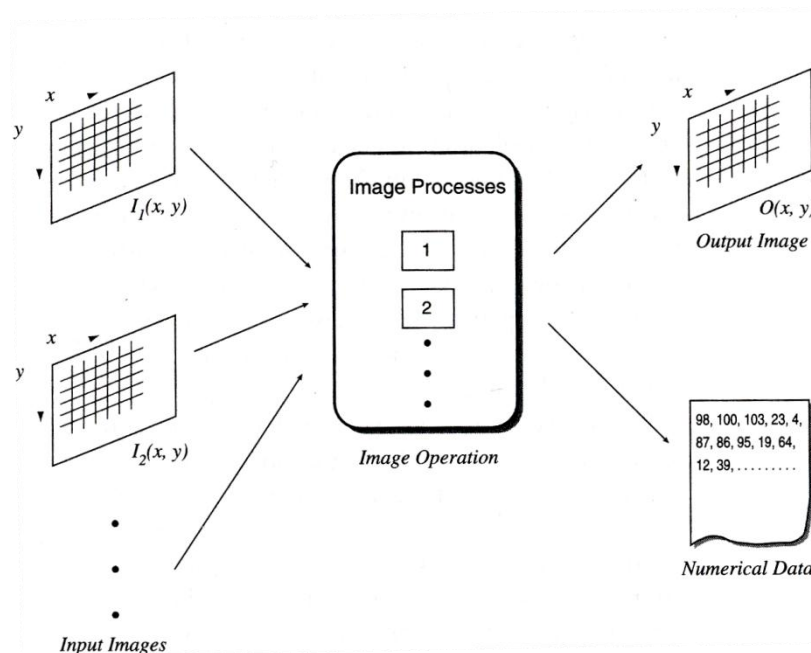


Figure 2.5. A general digital image processing operation. Diagram from Baxes (1994).

According to Gonzalez *et al.* (2004), an accepted classification for image processing operations is presented as follows (Figure 2.6):

- *Point operations*: the output value at a specific co-ordinate pixel is only dependent on the input value at that same co-ordinate pixel;
- *Neighbourhood operations*: the output value at a specific co-ordinate pixel is dependent on the input values in the neighbourhood of that co-ordinate pixel;
- *Global operations*: the output value at a specific co-ordinate pixel is dependent on all the values of the input image under analysis.

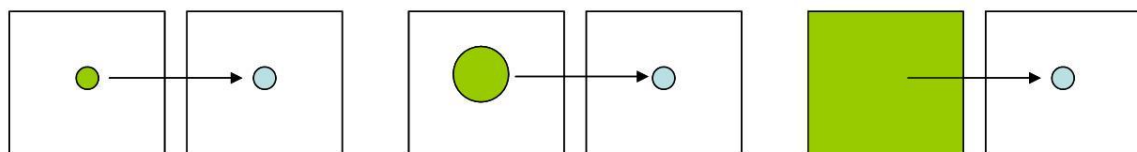


Figure 2.6. Diagram showing (from left to right) point, local and global operations in digital image processing.

A brief review of point, local and global operations, a general overview of mathematical morphology and geometric transformation processing in digital image processing are presented as follows.

Point operations

Point operations are the most simple, yet crucial operations in image processing. The output value at a particular co-ordinate pixel is only dependent on the input value of that same co-ordinate pixel. Such is expressed by the following formula:

$$O(x_0, y_0) = f(I(x_0, y_0)) \quad (2.1)$$

where $O(x_0, y_0)$ and $I(x_0, y_0)$ are, respectively, the values of the output and input images at pixel (x_0, y_0) .

In fact, important point operations include contrast stretching, threshold, intensity level slicing and histogram modification. Moreover, point operations can collect multiple images as inputs. In this case, each output at a given co-ordinate pixel is a function of the input at that same co-ordinate pixel, through the input of several pixel information located on different images, which are combined using mathematical operators, such as $+$, $-$, $/$, $*$, among others, and logical operators, such as *AND*, *OR*, *NOT*, among others. The concept of map algebra presented in section 2.3 uses point operations between different images.

Neighbourhood operations

Neighbourhood operations (also called focal functions) calculate the output value at a given co-ordinate pixel as a function of the input values in the neighbourhood of that co-ordinate pixel. These operations are also applied to a group of pixels enclosing the centre pixel of the image, which supply valuable information on the whole area being analysed and processed. Such may be expressed by the formula:

$$O(x_0, y_0) = f(I(N(x_0, y_0))) \quad (2.2)$$

where $O(x_0, y_0)$ is the value of the output image at point (x_0, y_0) , also called *origin pixel*, and $I(N(x_0, y_0))$ corresponds to the set of values of the neighbourhood of (x_0, y_0) in the input image. The most common neighbourhoods have 3×3 pixels wide dimensions, and are centred around (x_0, y_0) ; it can also be either 4-connected (also called *star* or *diamond*) or 8-connected neighbourhoods, as shown in Figure 2.7.

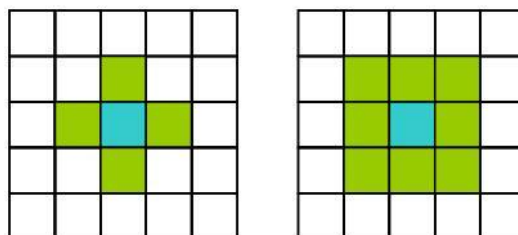


Figure 2.7. Four-connected (green pixels) and eight-connected (green pixels) neighbourhoods around the pixel under analysis (blue pixel).

Most filters implemented in digital image processing use a straightforward neighbourhood operation called Convolution Kernel: indicates the neighbourhood size, while its elements define the weights which need to be applied to each pixel in the neighbourhood before they are all summed up. It is called linear, as it involves the summation of elements multiplied by constant values, called convolution kernel coefficients. Filters differ from one another due to the different kernels they use, even though all of them apply the same sequence of operations. Some examples of Convolution Kernel filters are given as follows:

- *Low-pass filters*: it lets low frequencies of the image pass while high frequencies are removed, resulting in a smoothing or blurring effect;
- *Edge detectors*: this kind of filters emphasizes pixels belonging to discontinuity zones of the image. An example is the Sobel edge detectors that highlight variations in the x and y directions of the image respectively, by creating a finite difference between pixels two positions apart;
- *Non-linear spatial filters*: this type of filters uses other techniques rather than linearly summing pixel values multiplied by constant weights. The *median filter* for example, is used to remove noise from images by replacing each pixel value by the median value in the neighbourhood under analysis.

There exists however, many other filters based on different methods. For a detailed review please consult Gonzalez *et al.* (2004).

Global operations

A global operation on a digital image consists of assigning all pixels of the input image into an output pixel value $O(x_0, y_0)$. It can be expressed by the formula:

$$O(x_0, y_0) = f(I(x_0, y_0)), \quad \text{for all } x, y \quad (2.3)$$

where $O(x_0, y_0)$ represents the value of the output image at point (x_0, y_0) , being a function of the input image $I(x_0, y_0)$ for every (x, y) .

An example of global operation is the *Fourier transformation*, which analyses a signal in the time domain for its frequency content. The transform works by first translating a function in the time domain into a function in the frequency domain. The signal can then be analysed for its frequency content because the Fourier coefficients of the transformed function represent the contribution of each sine and cosine function at each frequency.

Mathematical morphology

These operators belong to the class of local operations. However, they have been classified as an independent position within image processing literature (Serra, 1968). They are very similar to Convolution Kernel filters, as they operate on pixels in a given neighbourhood using a set of theory operations, such as AND, OR, NOT, in order to combine pixels logically into a resulting pixel value. In other words, at each location, the pixel and its neighbours are logically compared against a structuring element (also called a morphological mask). In this process, the image is transformed and reduced to a more revealing shape (Figure 2.8).

2.4. Image processing of digital elevation models (DEM) and digital height models (DHM)

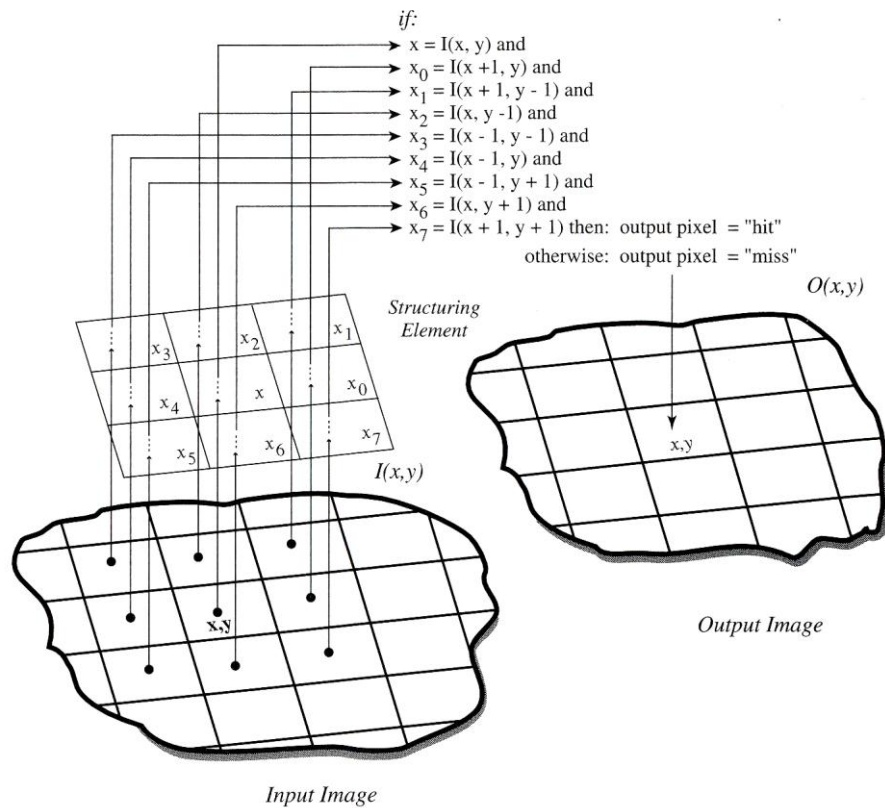


Figure 2.8. Applying a morphological structuring element to the input image $I_{(x,y)}$ to obtain the output image $O_{(x,y)}$. Diagram from Baxes (1994).

An example of a mathematical morphology operator is the *binary erosion* which homogeneously reduces the size of objects (blobs of white pixels valued 1) in relation to their background (black pixels valued 0). Thus, each pixel of the output image is compared with the input image; if an absolute conformity occurs, i.e. if the input image in the neighbourhood of that location has all pixels valued 1, then the output is fixed to 1. On the contrary, if at least one pixel in the neighbourhood is valued 0 (which corresponds to an edge pixel), the output is fixed to 0. Hence, the erosion structuring element removes all white pixels which have a black pixel amongst their 3x3 neighbours.

Both erosion and its complementary mathematical morphology operation, called *dilation*, are frequently used in image processing. Using both techniques, firstly erosion, and then dilation, allows to delete small-image object features of the image, such as noise (Gonzalez *et al.*, 2004).

Geometric transformation

The geometric transformation operators enable the reposition of pixels within an image. Each of them is translated from its initial position (x_0, y_0) in the input image into a final position (x'_0, y'_0) in the output image. Such may be expressed by the following formula:

$$I(x', y') \rightarrow O(x, y) \quad (2.4)$$

where I and O are the input and output images respectively. Geometric transformations include translation, rotation, scaling and a number of non-linear operations (Gonzalez *et al.*, 2004). An example of geometric transformation is presented in Figure 2.9.

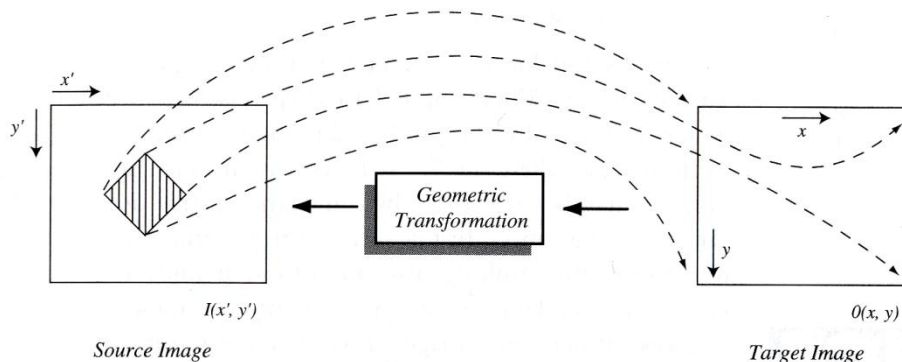


Figure 2.9. Geometric transformations on digital images sequence, pixel by pixel, through the output pixel locations and fetches transformed input pixel locations to fill them. Diagram from Baxes (1994).

2.5 Airborne laser scanning systems

2.5.1 Introduction

The construction of the 3-D urban models employed in this thesis is mainly based on exploitation of airborne laser scanning (ALS) technology and resulting data. Thus, this section presents a general overview of the theoretical knowledge and state of the art of this technology.

Airborne laser scanning (ALS) systems (or LiDAR) offer the possibility to measure a finite distance based on laser technology. Two types of LiDAR systems are available: the *pulsed* LiDAR systems use the time of flight to measure the length between the transmitter, usually mounted on an airplane or on a helicopter, and the target, located on the earth surface; the *continuous wave* LiDAR systems measure the phase shift between the emitted and the received signal. Nowadays, *pulsed* LiDAR systems are more often used for applications at urban scale. This type of LiDAR system can still be sub-divided into two main categories according to the registering mode of energy signal returned: *discrete return* LiDAR systems, which are based on an algorithm that detects and registers in real time the amplitude rise of each returned pulse, for which XYZ coordinates are associated; *full waveform or waveform digitization* LiDAR systems measure the amplitude of energy continuously returned to the sensor over a period of time and allowing therefore the recording of detailed information about the geometric and physical properties of the backscattering objects (Reitberger *et al.* 2008). Even though *full waveform or waveform digitization* LiDAR systems are now more commonly used in many diverse fields, such as ecological and forestry applications (Chauve *et al.*, 2007), its exploitation is still currently restricted to specific research purposes and for that reason it was not applied to the operational processes and methods inherent to the empirical studies highlighted in this thesis. Thus, the detailed description of LiDAR systems presented in this section is restricted to the discrete return LiDAR systems.

The present section focuses on LiDAR technology information, presenting the advantages and limitations of its application for urban analysis. Following a short historical overview, the different components of LiDAR systems and acquisition principles are presented. Moreover, a special interest is given to the mechanisms that allow the registering of an echo, the classification methods used, and finally the available data formats.

2.5.2 Historical overview

One major advantage of LiDAR technology when compared to more common photogrammetric techniques is that, using different echoes, LiDAR is also able to "see" between different objects such as roofs covered by trees, where photogrammetric technicians have difficulty interpreting the elevation of the ground. Thus, LiDAR technology presents a fast, accurate, and direct (not inferential) method for generating 3-dimensional data, and hence became a very attractive mapping since the mid 1990's.

The demand for more dense LiDAR point data sets accelerated rapidly, however, CAD and GIS software in the early 2000's was not able to process such volumes of data. In the early 2000's fast advances in data processing systems and in the support of IT architecture required the handling of terabytes of data being produced by state-of-the-art LiDAR scanners. As the demand for LiDAR data grew steadily, so did the need for guidelines, technical specifications, and accuracy standards. US government entities, namely FEMA, the US Army Corps of Engineers (USACE), USGS, and the Federal Geographic Data Committee (FGDC) developed standards for quality assurance and accuracy reporting. Likewise, professional associations, such as the International and American Societies for Photogrammetry and Remote Sensing (ISPRS and ASPRS) provided places for the swift exchange of science and application-based research in the use of LiDAR data in many domains. Although there are no public standards yet available for LiDAR data or derived products, the ASPRS has developed the LiDAR Archive Standard (LAS¹) for binary data exchange of LiDAR data, which has been broadly accepted by sensor manufacturers, software developers, and end-users community. Currently, there are more than 200 LiDAR systems operating around the world. State-of-the-art systems can reach 250,000 pulses per second, and manage multiple pulses in the air at any given moment, therefore capturing multiple returns from individual pulses, or even digitizing the entire return waveform. Data collection can be customized to meet specific application requirements, and end-users are supported by reliable quality assurance methods and large data storage capacity. In the last few years many applications were developed in order to process LiDAR data in different fields such as forestry (Gachet, 2009), geomorphology (Theler and Reynard, 2008), urban planning (Morello, 2006) and 3-D urban reconstruction (Eelberink, 2010).

2.5.3 Airborne laser scanning technological components

The combination of LiDAR and Positioning Unit Systems (POS) defines an airborne laser scanning (ALS), as shown in Figure 2.10.

¹ http://www.asprs.org/society/committees/standards/lidar_exchange_format.html

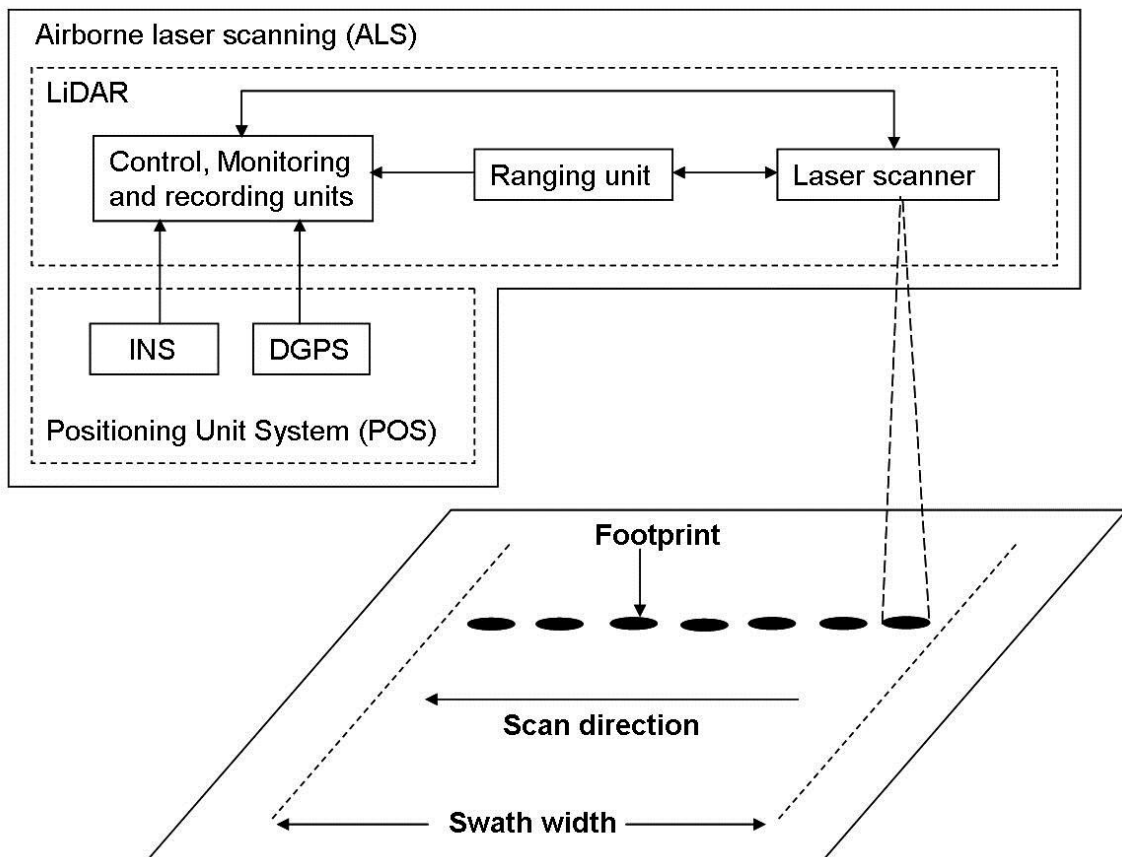


Figure 2.10. ALS system. Adapted from Wehr and Lohr (1999).

The LiDAR unit is composed by the laser unit and the computational unit, which together allow the calculation of the distance covered by the laser beam and the position of the aircraft for each scanned LiDAR point. The high measuring rate of ALS is of extremely importance. Nowadays, measuring rates of LiDAR telemeter lie in the range of thousands of Hz to 200 kHz . The transceivers are able to measure the emittance – reflectance time. Using mirrors to excite light at a specific frequency highly increases its concentration. Finally, this one is discharged and forms a laser beam. The diameter of the beam on the ground depends on the flying height of the aircraft due to the propagation divergence. Usually, the diameter ranges between 15 and 30 centimetres. The sampling densities on the ground vary from approximately 1 point per m^2 to 40 points per m^2 and depend on the system and the balance between the flying speed, pulse rate, scan angle and flying height. For the great majority of ALS available in the market, a new laser pulse will only be emitted after reception by the detection system of precedent emitted pulse².

The POS unit quantifies the absolute position using a differential global positioning system (DGPS) and an inertial navigation system (INS), presented as follows:

- **DGPS:** in order to accurately measure the position of the aircraft, two receivers using two independent frequencies, called L1 and L2, are applied. The DGPS system assesses the x , y and z differential positioning coordinates of the aircraft in the global WGS84 coordinate system with a range accuracy of about 10 centimetres. The GPS used is defined as

² A new multipulse generation of LiDAR systems was launched in the market, such as the Optech ALTM Gemini.

2.5. Airborne laser scanning systems

“differential” because a ground GPS control station is used to correct the GPS measures made inside the aircraft.

- *INS*: the use of this system allows the measurement (frequency between 100 *Hz* and 400 *Hz*) of both the acceleration and the behaviour of the three possible axis of rotation of the aircraft: rolling, pitch and yaw, as shown in Figure 2.11. However, and contrary to DGPS, this measure is deteriorated with time, which reduces the accuracy of the aircraft comportment and consequently also its position.

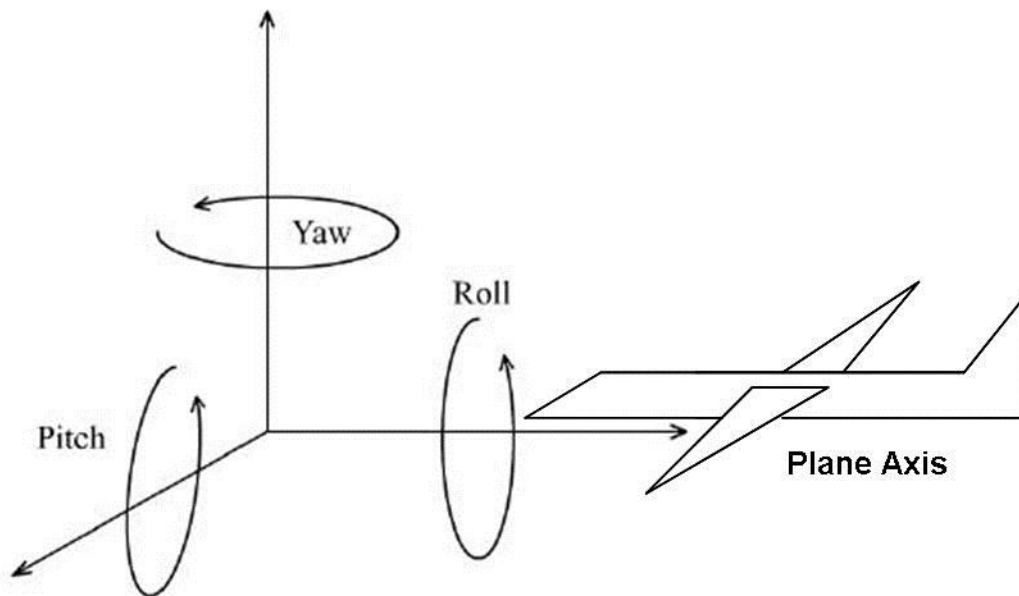


Figure 2.11. Aircraft attitude. Adapted from Kalbermatten (2010).

Since the ALS achieves a range accuracy lower than 10 centimetres, POS should therefore guarantee at least the same level of accuracy. Such accuracy can be only accomplished by combining GPS and INS, so that the errors inherent to both systems are attenuated. Geocoding of laser scanner measurements demand exact synchronization of all systems used: LiDAR, INS and DGPS. Moreover, POS data and LiDAR data is stored in different devices, e.g., different computer hard disks. Hence, two independent times should be considered: the GPS time to which POS data is connected and the internal time of the computer hard disk to which LiDAR data is related. Hence, the synchronization based on pulse per second (PPS) intervals allows for the correction of eventual time errors between the extremely accurate GPS time and the less accurate time of the computer (Morin, 2002).

2.5.4 Filtering and classification of airborne laser scanning

Some information in the original 3-D point clouds is lost if data is straightforward interpolated into a regular grid, i.e., a DSM. In urban areas, the loss of information can be important, especially if multiple echoes are registered above building roofs covered by trees, since points with similar *xy*-coordinates but at different elevation are impossible to characterize in a regular grid. Thus, as considered for this study, original data should be used in the filtering and classification process until an object representation and generalization can be applied.

The classification of LiDAR data aims to provide thematic information to raw points. As a first step, ground echoes are classified independently from other echoes, such as buildings or trees, resulting in two distinct models: the digital terrain model (DTM) and the digital surface model (DSM). The DSM is usually built from LiDAR points already filtered. The number and definition of supplementary classes needed depends on the type of application to be developed. The most common classes are: (1) – ground; (2) – buildings; (3) – vegetation; (4) – electrical lines, and other elements. Finally, the final step of the classification process is to filter and remove unwanted measurements, which can be characterized as noise, outliers or gross errors. These may be LiDAR points touching birds or the ALS platform itself. It is also important to note that temporary objects or moving objects, such as cars, should be also removed (Luethy and Stengele, 2005).

The LiDAR point clouds data used in this study was classified using algorithms based on the Minimum Description Length (MDL) criterion (Axelsson, 1999). A general overview of these algorithms for the classification of ground, building and vegetation LiDAR points is presented as follows:

- *ground points*: here, a classification tool is developed where a surface is linked from below to the point cloud. This surface is permitted to fluctuate within certain values, which are controlled by the MDL models, constrained spline functions, active contour models like snakes or geometrical thresholds for elevation differences;
- *building and vegetation points*: here, a classification tool is implemented that classify surface objects into two classes, buildings and vegetation respectively. The capacity of the laser to pierce vegetation and thus giving echo from several heights makes it conceivable to differentiate raw LiDAR points between these two classes. The classification method is based on an employment of the MDL criterion for robust estimation (Rissanen, 1983; Axelsson, 1992). Hence, a cost function is formulated for the classes building and vegetation, which is based on second derivatives of the elevation differences. The model considers that buildings consist of connected planar surfaces and vegetation as points with randomly distributed second derivatives.

An example of the classification undertaken for a pilot zone of the centre of Geneva is shown in Figure 2.12.

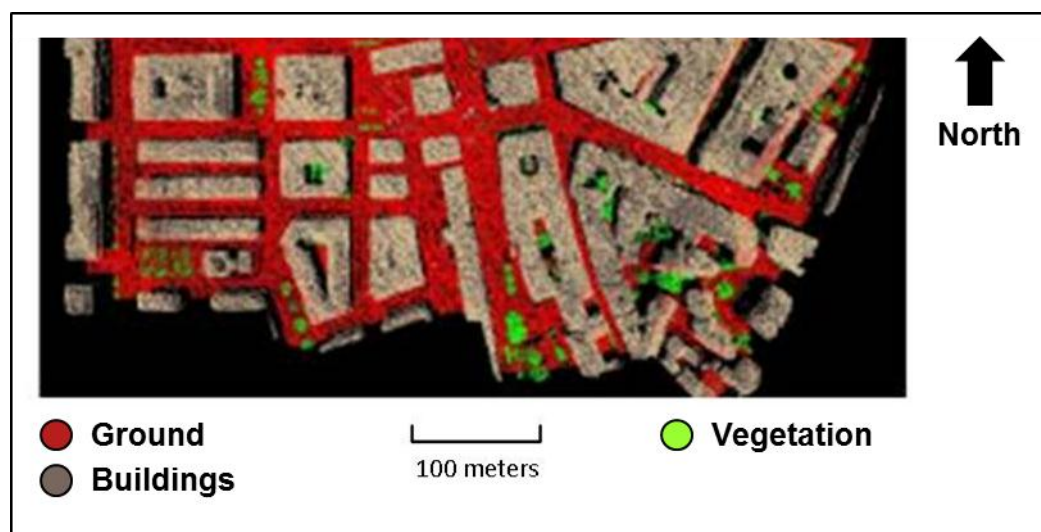


Figure 2.12. Classification of raw LiDAR points belonging to a neighbourhood of Geneva's city.

2.5. Airborne laser scanning systems

Other researchers have made important studies related to the classification of LiDAR data: (1) - morphological filtering (Kilian *et al.*, 1996); (2) – slope based filtering (Vosselmann, 2000); (3) – multiple pass filtering (Bretar, 2006). An interesting comparison between 8 classification methods, which includes the methods used in this study was made by Sithole and Vosselmann (2003). The main conclusion is that considering all the filtering techniques evaluated none gives perfect results. In fact, although all algorithms produce very reliable results in open landscape areas with low slopes, they all produce errors in urban areas and in sloped landscape areas, especially when covered by dense vegetation.

Finally, it is important to mention the concept of data reduction of the input, which allows to decrease the amount of raw data used for the construction of DEM (Anderson *et al.*, 2005; Liu *et al.*, 2007). The main goal of data reduction is to accomplish an ideal balance between density of sampling and volume of data, hence optimizing price of data assemblage (Robinson, 1994). Moreover, it allows the reduction of laser data at an early stage of the process, hence resulting in the flexible use of large datasets. This is particularly important when processing LiDAR data. Although high point density LiDAR data is relevant for a trustworthy classification of buildings, trees, among other urban objects, it is known that for higher urban areas the point density can become hard to manage, disabling its use for a proficient processing of DEM.

2.5.5 Airborne laser scanning: measuring different echoes

The LiDAR system is also able to measure more than only one echo. The classification of scanned points into different echo classes results from the penetration potential of laser beam. Some surfaces, such as streets and building roofs, produce only a single echo, but others, such as trees or roof limits, generate more than one echo – in this case, if we consider for example the penetration of laser beam into trees, the first measured distance (first echo) is the tree foliage and the last distance (last echo) is the ground (Figure 2.13).

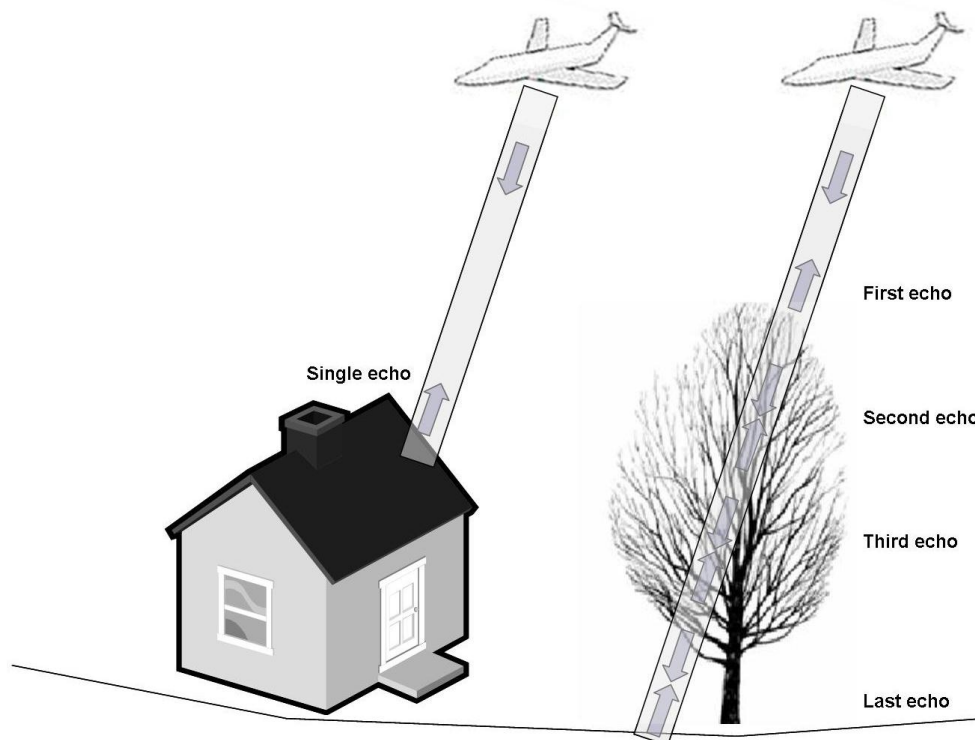


Figure 2.13. Different laser echoes.

Some LiDAR systems are also able to register laser pulse intensity information. Hence, it is then possible to produce a monochromatic image from which is possible to extract complementary information. An experiment by Clode *et al.* (2004) demonstrated although the valid use of laser pulse intensity information in order to extract existing outlines between roads and several terrain objects. The classification applied is based on intensity information of laser points close to terrain surface. Despite its preciously shown interest, the application of this field of research was considered to be not required for this study.

2.5.6 Airborne laser scanning data formats

Raw LiDAR points can be easily geo-referenced as each point is uniquely identified by x,y,z coordinates in the WGS84 coordinate system, and eventually complemented with other attributes, such as the laser pulse intensity information. Using available GIS software, the original text files can be easily transformed into a vector format, allowing the visualization of this data as sets of point clouds. An example of this type of data with a density point of 4 points per square meter for a pilot zone in the centre of Geneva is presented in Figure 2.14: elevation values are visualized from blues (lower) to reds (higher).

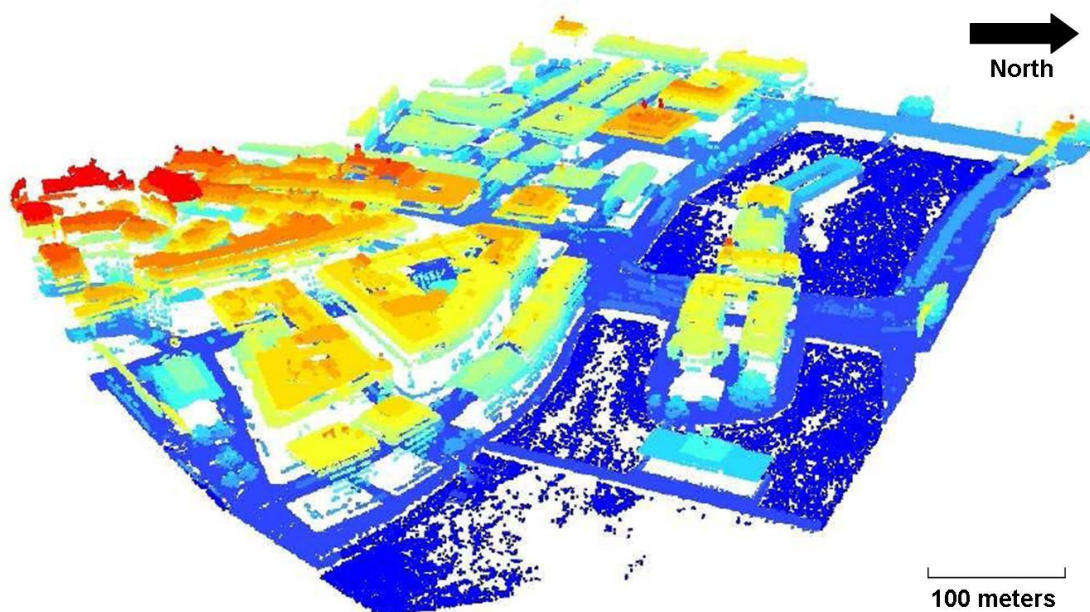


Figure 2.14. Raw LiDAR points belonging to a neighbourhood of Geneva's city.

Another option is to produce a digital elevation model (DEM) in the form of a regular grid by interpolation of raw LiDAR points. An example of a DEM of the EPFL campus, interpolated (applying a TIN technique) from a set of point clouds with a density of 1 point per square meter is presented in the right-hand side image of Figure 2.15.

The sampling resolution of the grid is chosen by considering the density of the raw LiDAR points. This allows the control of the uncertainty affecting the estimated altitudes (Smith *et al.*, 2004).

2.5. Airborne laser scanning systems

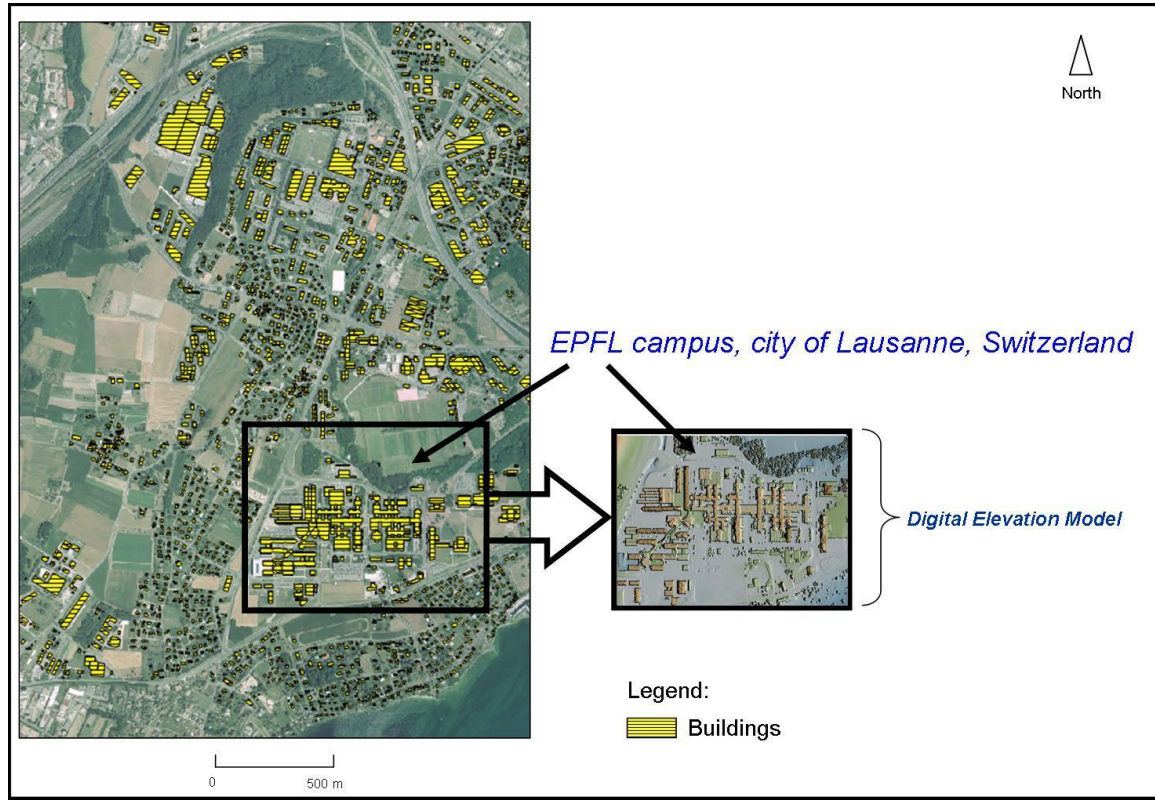


Figure 2.15. DEM of the EPFL campus considering terrain, buildings and vegetation higher than 3 meters (trees).

Moreover, these altitudes are also highly dependent on the interpolation method used. According to Behan (2000), an empirical relation between the sampling resolution of the grid (S_r) and the density of raw LiDAR point (D_p) may be defined by the following equation:

$$D_p = 1 / (S_r)^2 \quad (2.5)$$

Some examples of the sampling resolutions of the more commonly adapted grids are presented as follows (Table 2.2):

S_r (m)	D_p (points per m^2)
1	1
0.5	4
0.25	16

Table 2.2. Relation between the sampling resolution of grids (S_r) and the density of raw LiDAR points (D_p).

The choice between vector or grid format depends not only on the use needed for original LiDAR data but also on the available resources and informatics tools available. Each format has its own advantages and limitations (Table 2.3):

	Vector format	Raster format
Advantages	Allows the exploration of all measures with higher precision because x,y,z coordinates are directly used	Very easy to manipulate. The application of mathematical algorithms using image digital processing techniques is reliable
Limitations	For high volumes of data its manipulation can be very heavy and not easy to manage. Moreover the application of mathematical algorithms is commonly highly complex	The interpolation of LiDAR points into a grid format decreases the accuracy of the constructed models when compared to 3-D vector format. Loss of original information

Table 2.3. Advantages and limitations of vector and raster formats.

In this study both formats are applied, however in order to extract urban environmental quality (UEQ) indicators by applying innovative methods based on digital image processing (DIP) techniques, the use of raster format is the natural choice and for that reason its weight on this thesis is considerable.

2.5.7 Accuracy of airborne laser scanning

According to Baltsavias (1999a), the accuracy of x,y,z coordinates depends on the following factors: (1) – range; (2) – position of the laser beam; (3) – direction of the laser beam. Since the original raw LiDAR data is usually in the WGS84 coordinate system, the final results are also highly dependent on the accuracy of the transformation from WGS84 to the local coordinate system, including adjustments for the geoid undulations, which can be significant with regards to the accuracy capacity of ALS. Furthermore, since the range, position and beam direction are measured by independent sensors, errors inherent to inaccurate registration will also negatively influence the results.

The range accuracy of pulse lasers is essentially dependent on the following aspects:

- ability to select the same relative position both for the transmitted and received pulse in order to measure the time interval;
- the accuracy with which fixed time delays in the system are known, e.g., counter (frequency) instability can lead to drift systematic errors;
- the accuracy of the time interval counter.

The planimetric error is highly dependent on the topography of the terrain and the incidence angle of the measured pulses. According to Baltsavias (1999b), the planimetric error is 2 to 5 times more important than the altimetric error. Such as the planimetric error, the altimetric error also considerably increases when the incidence angle of pulse, the height of flight and the local slope of the terrain rise.

The correlation between planimetric and altimetric errors (considering slope, i) is shown in Figure 2.16, being given by the following equation:

2.6. Gridding interpolation of digital elevation models (DEM) and digital height models (DHM) using LiDAR data

$$\Delta Z = \Delta XY \times \tan(i) \quad (2.6)$$

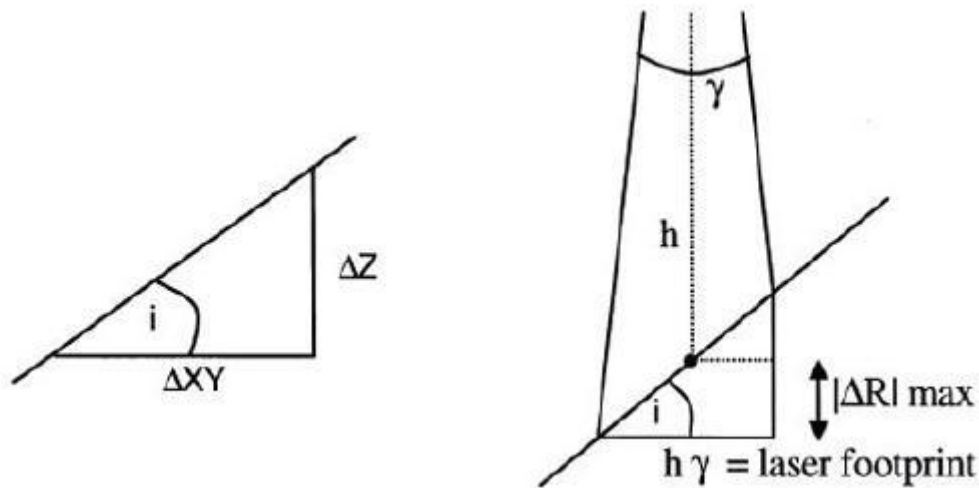


Figure 2.16. Influence of the slope in the precision of the measure. Diagram from Baltsavias (1999b).

Common accuracy for LiDAR systems are usually announced by constructors as being lower than 15 centimetres in altimetry and lower than 40 centimetres in planimetry. According to Alharthy *et al.* (2004) the altimetric uncertainty for flat terrains is around 15 centimetres, while the planimetric uncertainty can vary between 30 to 60 centimetres. An original study that rigorously analysed the errors related to the geo-referencing equation in order to evaluate the planimetric and altimetric accuracy of different LiDAR systems (terrestrial and aerial) was undertaken by Glennie (2007). An interesting conclusion of this study is that the planimetric error is substantially influenced (60% to 75% according to the height of flight) by the combination of errors in relation with the INS and the attitude errors of the aircraft.

2.6 Gridding interpolation of digital elevation models (DEM) and digital height models (DHM) using LiDAR data

The goal of gridding interpolation techniques is to generate, through spatial interpolation, a rectangular array of z values derived from irregularly spaced x,y,z data points. Many spatial interpolation methods are available and can be classified, including:

- *Global*: each interpolated value, defined as a cell node of the gridded DSM, is influenced by all the data points, in this case raw LiDAR data in the form of x,y,z point clouds;
- *Local*: each interpolated value is only influenced by the values at pre-defined nearby points of the x,y,z point clouds;
- *Exact*: creates a surface that passes through all of the x,y,z point clouds;
- *Approximate*: produces a surface that follows only an overall tendency in the x,y,z point clouds, it implies a certain degree of error;
- *Stochastic*: incorporates geo-statistic theory in order to produce surfaces with particular levels of error.

Quite often the inverse distance weighting technique is used for interpolation of irregularly spaced points. LiDAR point clouds are weighted during interpolation in order to decrease the influence of one point relative to another with distance from the grid node under analysis (Shepard, 1968). The main concept inherent to this technique is that nearby points have similar height values, while the heights at distant points are classified as being independent (Figure 2.17). Moreover, a weighting power that controls how the weighting factor drops off as distance from a grid node increases is usually assigned to the data. The generation of *bull's-eyes* surrounding the position of observations within the gridded area occurs after applying inverse distance weighting interpolation. Thus, a smoothing parameter can be applied during the interpolation process in order to reduce the *bull's-eye* output by smoothing the interpolated grid.

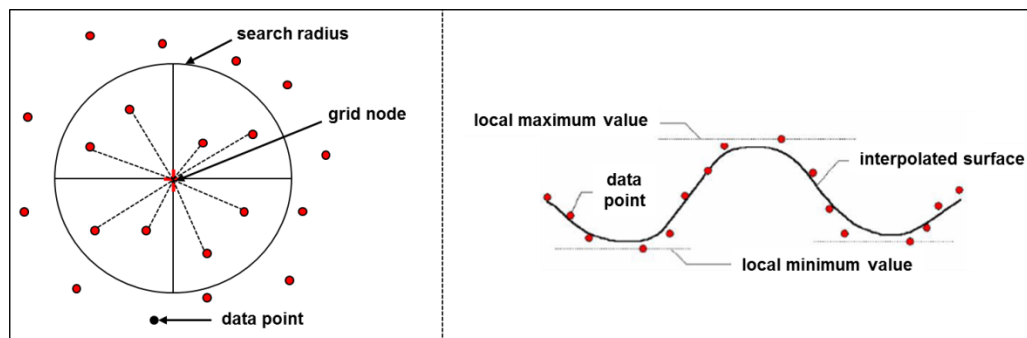


Figure 2.17. Inverse distance weighted (IDW) technique; left hand-side picture: principal of the distance balance in the search radius; right hand-side picture: principal adapted for the generation of a surface.

Kriging is a geo-statistical interpolation technique similar to the IDW technique. It allows us to estimate the heights at the grid nodes as a weighted average of the measured heights at the reference points (LiDAR point clouds). It is usually applied in two steps: weight determination and estimation of the height values using a weighted average. A procedure called variogram modelling, which describes the spatial variability between the height values of the reference points, is used for the determination of weights (Cressie, 1993).

For the creation of a triangulated irregular network (TIN) an algorithm that creates a structure from the LiDAR points using a Delaunay Triangulation routine is applied in order to maximize the minimum angle of all the angles of the triangles (Figure 2.18). The original points are connected in such a way that no triangle edges are intersected by other triangles. A sequential search allows for the set-up of a triangle in which each grid node is enclosed. The gradients of the chosen triangle enable the interpolation of a value for the grid node (Franklin, 1973).

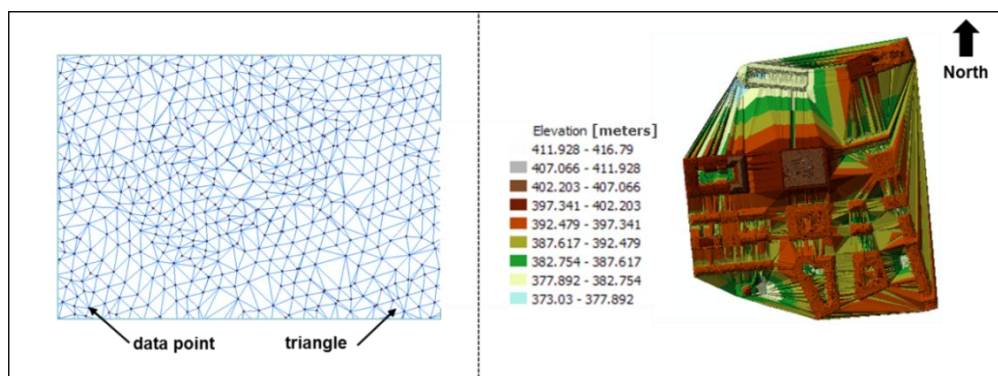


Figure 2.18. Triangulated Irregular Network (TIN) interpolation; left hand-side image: principal adapted for the generation of a surface; right hand-side image: example of TIN interpolation for a neighbourhood of the city of Geneva.

2.7. 3-D data extraction and acquisition

The diversity of accessible interpolation methods led to questions about which is most suitable in different circumstances and motivated numerous comparative studies of relative accuracy (Zimmerman *et al.*, 1999). To test the ability of some commonly-used interpolation methods, a variety of empirical work has been conducted to assess the effects of different methods of interpolation on DEM accuracy (Chaplot *et al.*, 2006; Kyriakidis and Goodchild, 2006; Lloyd and Atkinson, 2006). Indeed, there seems to be no single interpolation method that is the most accurate for the interpolation of terrain data (Fisher and Tate, 2006). Moreover, none of the interpolation methods currently available is universal for all kinds of data sources, terrain configurations or applications (Liu, 2008).

According to Gonçalves (2006), with good density of LiDAR points, such as in the great majority of the case-study areas emphasized in this study, where LiDAR points were acquired with a density of 4 to 6 points per square meter, there is no great difference among some of the existing gridding interpolation methods that can be employed in urban areas: inverse distance weighting, kriging and triangulation with linear interpolation. Hence, for its generalised use by the scientific community for DTM interpolation, the TIN interpolation was chosen.

Finally it is also important to mention that innovative or altered interpolation methods are still being developed, trying to improve the interpolation methods currently available (Shi and Tian, 2006).

2.7 3-D data extraction and acquisition

From an information processing perspective, there are three primary approaches to collecting 3-D objects, namely image-based, point cloud-based, and the hybrid approach (Tao, 2006):

- *Image-based 3-D data acquisition*: use of images, such as close-range, aerial photographs or satellite images in order to assemble information about 3-D objects, often buildings. Applying this approach from imagery enables to derive 3-D structural and dimensional information. Some examples of this type of 3-D data acquisition were proposed in the last years. Zlatanova *et al.* (1998) presented an innovative method for the 3-D object reconstruction from aerial stereo images. A fully automatic reconstruction from aerial images was proposed by Jaynes *et al.* (2003). Brenner (2004) described in a theoretical manner a mix of model and data-driven approach, by using weak primitives. In fact, weak primitives have a primordial interest because they allow to vary constraints without losing weak primitives;
- *Point cloud-based 3-D data acquisition*: originally this technique was developed for the acquisition of 3-D data in order to establish digital terrain models (DTM). During the last decade, this type of data started to be used in order to add a third dimension to Geographical Information Systems (GIS) and also for a larger domain of applications, such as 3-D urban modelling. Either airborne and ground-based laser scanning, or a combination of the two, can produce very dense and accurate 3-D point clouds that can be easily automated for the extraction of height information. However, textures from point clouds are most of the times weak. Vosselmann (1999) presented an approach that allows the detection and outlining of planar faces from dense height data. These planar faces were detected by Hough-based plane extraction. In Rottensteiner and Briese (2002, 2003) an analysis of roof segments, looking for an intersection, a step edge, or both an intersection and a step edge, were presented. Also geometric constraints on the reliability of buildings were studied, by achieving an overall adjustment comprising available sensor information, parameters of the planes and vertices;

- *Hybrid approaches*: as a technological trend of the last years, it combines optical images, point cloud data, and other data sources, such as maps or GIS/CAD databases. These approaches are in general more consistent, but require complementary data sources. The French partnership between MATIS (IGN) and INFRA has shown a deep research background in the reconstruction of 3-D buildings using a hybrid approach that combines aerial images and DEM, such as presented by Durupt and Taillandier (2006), or aerial images and LiDAR point clouds (Bretar, 2006).

It is important to note that though broad research has been done in the area in the last decade, algorithms are still limited to image type and resolution. Development of reliable and operational algorithms, with a focus on the implementation of hybrid approaches, is still under research.

With regards to the studies presented in this thesis, 3-D models (mainly buildings) were primarily used for visualization purposes, but they have also served for the extraction of 3-D roof lines. This source of information also allows the construction of a more accurate 2.5-DUSM of roof lines, such as presented in chapter 5 of this thesis.

Finally, it is worth mentioning that some commercial systems are already available for the semantic extraction of 3-D building models using both LiDAR and building footprint data, which includes the reconstruction and classification of different roof types.

2.8 3-D city models

A 3-D city model is a three dimensional digital representation of a urban environment or city, by means of data derived from manifold sources, such as stereo aerial images, airborne LiDAR data and high resolution satellite data. It holds a large number of objects belonging to different classes and diverse data models and structures. A 3-D city models can be an important tool used in various fields such as urban planning and territory planning, or car-navigation systems, as well as for 3-D visual representation of the urban environment in the form of textured images. An example of an information model for the representation of 3-D urban objects is the CityGML standard (Kolbe *et al.*, 2004). It defines the classes and relations for the objects with respect to their geometrical, topological, semantical and appearance properties.

2.9 Conclusions and chapter synthesis

This chapter presents the theoretical knowledge and state of the art of the 2-D and 3-D spatial data available for urban modelling. A main focus was given to airborne laser scanning technology (also called LiDAR), which allows the acquisition of very high-resolution altimetry data in a fast way. Moreover, the high planimetric and altimetric degree of accuracy of this type of data shows high potential of application for different urban studies. The potential of using LiDAR data on vector and raster formats is also an important point that will be further developed in this thesis.

The extraction of relevant urban indicators highlighted in this thesis is based on the image processing of 2.5-Digital Urban Surface Models (2.5-DUSM), which are constructed by applying innovative methods using LiDAR data. An important point related to the construction of these models is the gridding interpolation method chosen. From a longer list, three main techniques for interpolation were selected for analysis in this study: Inverse Distance Weighted (IDW), Kriging and Triangulated Irregular Network (TIN). An analysis of the accuracy of each of these interpolation methods is emphasized in chapter 5.

CHAPTER 3. URBAN INDICATORS

3.1 Introduction

The benefit of using urban indicators to measure spatial phenomena is the fact that they can communicate in a simple way, allowing to identify and quantify variations and monitoring tendencies. They can also be used to highlight areas of action and strategy intervention, and furthermore to simplify complex, and frequently abstract phenomena into quantifiable measures. According to Adriaanse (1997), indicators have three functions: to simplify, to quantify, and to communicate. An indicator can be defined as a set of rules for collecting and organizing data in order to consign a meaning - like a portion of research, prioritizing some aspects of a situation at the cost of others. Moreover, it allows observers to “see” the world through a certain lens (Innes, 1990). This concept undoubtedly reinforces the significance of choosing a set of indicators considering beforehand what types of singularities and problems are expected to be extracted and communicated.

In the next sections of this chapter the following concepts are briefly presented: (3.2) roles of indicators, (3.3) properties of indicators, (3.4) methods and conceptual models for the definition of indicators, (3.5) elementary indicators, complex indicators and indexes, (3.6) visualization of indicators, and (3.7) conclusions and chapter synthesis.

3.2 Roles of indicators

With the emergence of the “sustainable development” concept that took place during the last two decades, the concept of “territorial management” has significantly changed: projects are no longer only individually evaluated; instead, other elements such as the influence on the surrounding environment are also considered (Repetti and Desthieux, 2006). Hence, the role of urban indicators became essential for the sustainable development at different scales. Below follows a list of some of the most relevant agents in the process of the on-going definition of urban indicators”:

- *international*: one of the international agencies that helped to define the role of indicators, and urban indicators in particular, is UN-HABITAT. This agency considers that urban indicators should be clearly connected to urban policy objectives and capable of being changed by the use of strategy instruments. Some of the criteria for selecting indicators, according to UN-HABITAT, are their relevance to policy making, their ease of interpretation, and the fact that they should be able to be collected in a profitable way and on a systematic basis (UNCHS, 1995);
- *national*: the Swiss *Monet* project (OFS *et al.*, 2003) launched in 2003 proposes a system for the sustainable development of Switzerland;
- *regional or local*: these are usually participative processes undertaken by different groups of actors, enabling the definition of a set of pertinent indicators. The *Pastille* project launched in 2002 joining together four European cities of wide-ranging size (Lyon, Vienna, Winterthur, Southwark) is a good example of a sustainable development project for this scale of analysis (Pastille, 2002). The main goal was to produce, for each city, specific indicators of durability, according to participative methods implying several researchers, as well as the political actors of the municipalities. This same scale of

analysis is applied in this thesis for the extraction of urban indicators using different 2-D and 3-D data sources as well as different models considering specific end-user needs.

An indicator is defined as an indirect and empirical interpretation of reality, but not as reality on itself, being the result of a pertinent selection and aggregation of data (Von Stokar *et al.*, 2001). The aggregation of information allows a better understanding of complex phenomena and its use by different groups of users with specific needs.

Authors as Gallopin (1997), Blanchet and November (1998), Both *et al.* (2003) suggest different roles for indicators:

- *to give a description*: describes the state of a system, a phenomena or its dynamic by comparing its situation at different moments;
- *to be explicative*: establishes an understanding regarding the relationships between different phenomena, by means of measuring correlations between phenomena;
- *to allow normalization*: allows to evaluate the state of a system, or a phenomenon, regarding certain goals;
- *to bring simplification*: permits to take back to first principles the complexity of a system or phenomenon under analysis;
- *to create communication*: makes possible to diffuse pertinent information for a larger public, usually by the means of qualitative indicators.

Gallopin (1997) made an inventory about the nature of indicators. For different situations they can be considered as a parameter, a variable, a measure, a value, a fraction, information, a sub-index, a quantity, a sign or even an empirical model. According to Maby (2004) the etymological nature of an indicator is “to indicate”, “to show” a phenomenon that has an incidence over an object, a system, such as the territory for the case of a geographical indicator. For Gallopin (1997), an indicator can be also defined as a variable representing an attribute, which means a characteristic, a property, a quality of a phenomenon associated to an object. As a variable, it represents the information not only of the state, but also of the temporal and space evolution of the phenomenon under analysis. Finally, an indicator can be distinguished from other variables due to its relevant pragmatism (Both *et al.*, 2003).

3.3 Properties of indicators

3.3.1 Overview

Before describing the main properties of indicators it is important to mention that they must be sufficiently representative and reliable of the phenomenon under analysis - it depends in particular on the availability of data, which often limits the relevance of the extracted indicators, and also on the capacity of the algorithms and methods applied in order to extract them.

3.3.2 Geographical dimension

According to Maby (2004), when an indicator focuses on phenomena that have an incidence in the territory, in this thesis defined for an urban environment, it is called *geographical indicator*. This type of indicator connects a spatial object to an observation metaphor of the space - spatial objects are geo-referenced to the surface of earth. Furthermore, it is important to analyse and represent the spatial heterogeneity and variability of urban phenomena according to an adapted scale (Bell and Morse, 2000). In this context, the use of GIS is also extremely relevant as it

3.3. Properties of indicators

facilitates the storage and spatial analysis of raw data, allowing to implement and represent pertinent geographical indicators.

The development of geographical indicators can be done by combining thematic and spatial indicators (Desthieux, 2005). A thematic indicator can be linked to a geographic object. For instance, for building roofs, many themes can be evaluated, such as the average yearly solar irradiation or the average sky view factor (SVF). Some useful examples that can be applied for the construction of geographical indicators are presented as follows (Malcwski, 1999):

- *overlay*: through arithmetical operations a new layer of attributes is created from two or more attributes: addition, subtraction, multiplication, division and average, among others;
- *(re)classification*: this operator allows to group object attributes into new classes defined by comparison analysis: *equal to*, *higher than* and *lower than*, among others.

Some examples of overlay and (re)classification operators applied to geographical indicators are presented in the third part of this thesis.

A spatial indicator gives information about the position, the form and the organization of an object in the space (Maby, 2004). In this specific case, only relations between a position and an attribute are considered, which means relations between attributes are no longer considered. Thus, the indicator is represented by a variable depending on space. Among some of the existing spatial operators, the main focus is given to two types (Joerin, 1998; Malcwski, 1999):

- *distance analysis operators*: an example of an algorithm applied in this thesis is the interpolation method applied for the construction of a 2.5-DUSM, which is based in a TIN interpolation;
- *neighbourhood operators*: an example of an algorithm applied in this thesis is the use of a square window (e.g., 3 by 3) in order to calculate the slope of a 2.5-DUSM pixel, which is based on the altitude values of its neighbourhoods.

3.3.3 Level of measure and scale of analysis

According to Stevens (1946), all measurements in science are conducted using four different types of levels of measurement: (1) Nominal, (2) Ordinal, (3) Interval, and finally (4) Ratio. Another issue related to the level of measure was derived from Chrisman (1998) in which he introduces for the GIS field an extended list of levels of measurement to account for various measurements that do not inevitably fit with the traditional notion of levels of measurement: (1) Nominal, (2) Graded membership, (3) Ordinal, (4) Interval, (5) Log-Interval, (6) Extensive Ratio, (7) Cyclical Ratio, (8) Derived Ratio, (9) Counts, and finally (10) Absolute.

As an indicator must indicate a direction or tendency, a simplification was introduced by Desthieux (2005) by considering only two levels of measurements: cardinal or ordinal, representing quantitative and qualitative information respectively. Indeed, nominal scales are not useful and pertinent for the definition of indicators as they do not take into account a direction considering a finality of evaluation.

According to Mesev (2010), the spatial scale of analysis on urban studies related to remote sensing and GIS should be defined considering five different levels, going from micro to macro scales: (1) building, (2) sub-street, (3) street, (4) neighbourhood and finally (5) city. For this study, considering that the complexity of the phenomenon under evaluation is for most of the cases related to building analysis, a simplification is made by considering only three of these five scales: (1) building, (2) neighbourhood and finally (3) city (Figure 3.1).

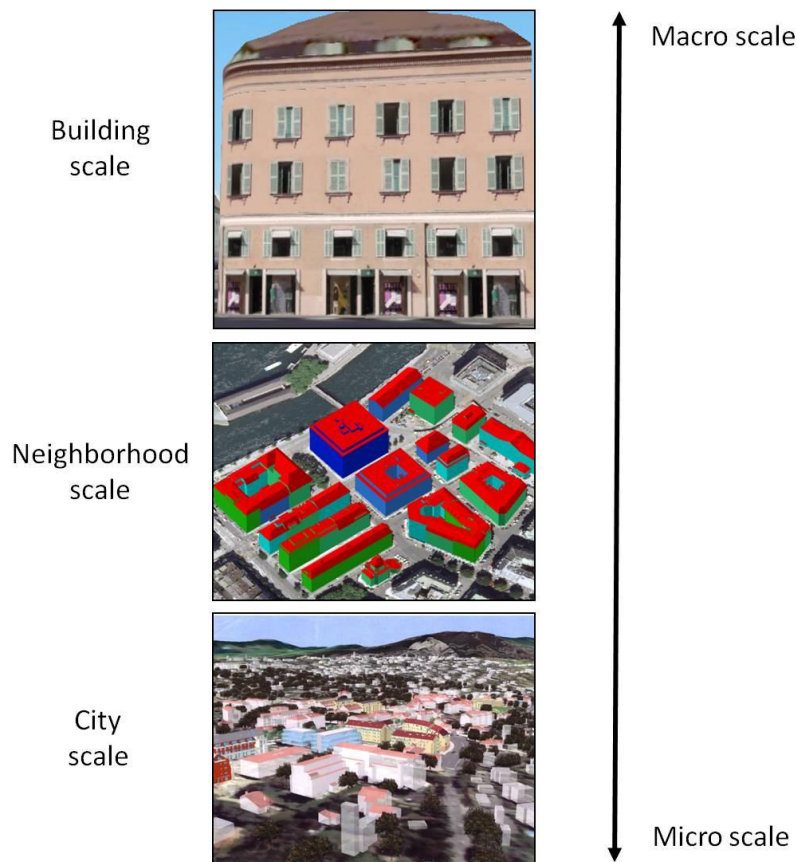


Figure 3.1. Scales adopted for analysis.

Thus, the level of measure is an important concept that should be considered for each indicator under analysis in this study. Indeed, it is very important to scrutinize the right modalities in order to present results: quantitative indicators (cardinal level of measurement) are more relevant when used for comparative studies (technical and operational) among different design schemes for specialized end-users; qualitative indicators (ordinal level of measurement) are an easier approach when used for strategic communication with common end-users and the general public. Regarding the qualitative indicators extracted in this study, it is important to mention that they are considered “pseudo-qualitative” because they directly result from quantitative information, as the example shown on Figure 3.2. Thus, behind any quantitative information there is also a qualitative component in the manner of selecting, incorporating and representing data.

Figure 3.2 shows an example of 2-D visualization for an indicator illustrating the meaning of both quantitative and qualitative indicators of roofs covered by trees for the district of Moillesulaz, State of Geneva:

- picture above: quantitative indicator (cardinal values are aggregated into different intervals) showing, for each roof, the percentage in terms of trees' coverage, considering a single LiDAR dataset measurement made in 2004;
- picture below: pseudo-qualitative indicator based on the pre-specifications defined by end-users, showing, for each roof, the quality in terms of trees' coverage. The ranking of this pseudo-qualitative indicator results from the aggregation of the cardinal values (quantitative indicator) shown in the picture above into different ordinal classes.

3.3. Properties of indicators

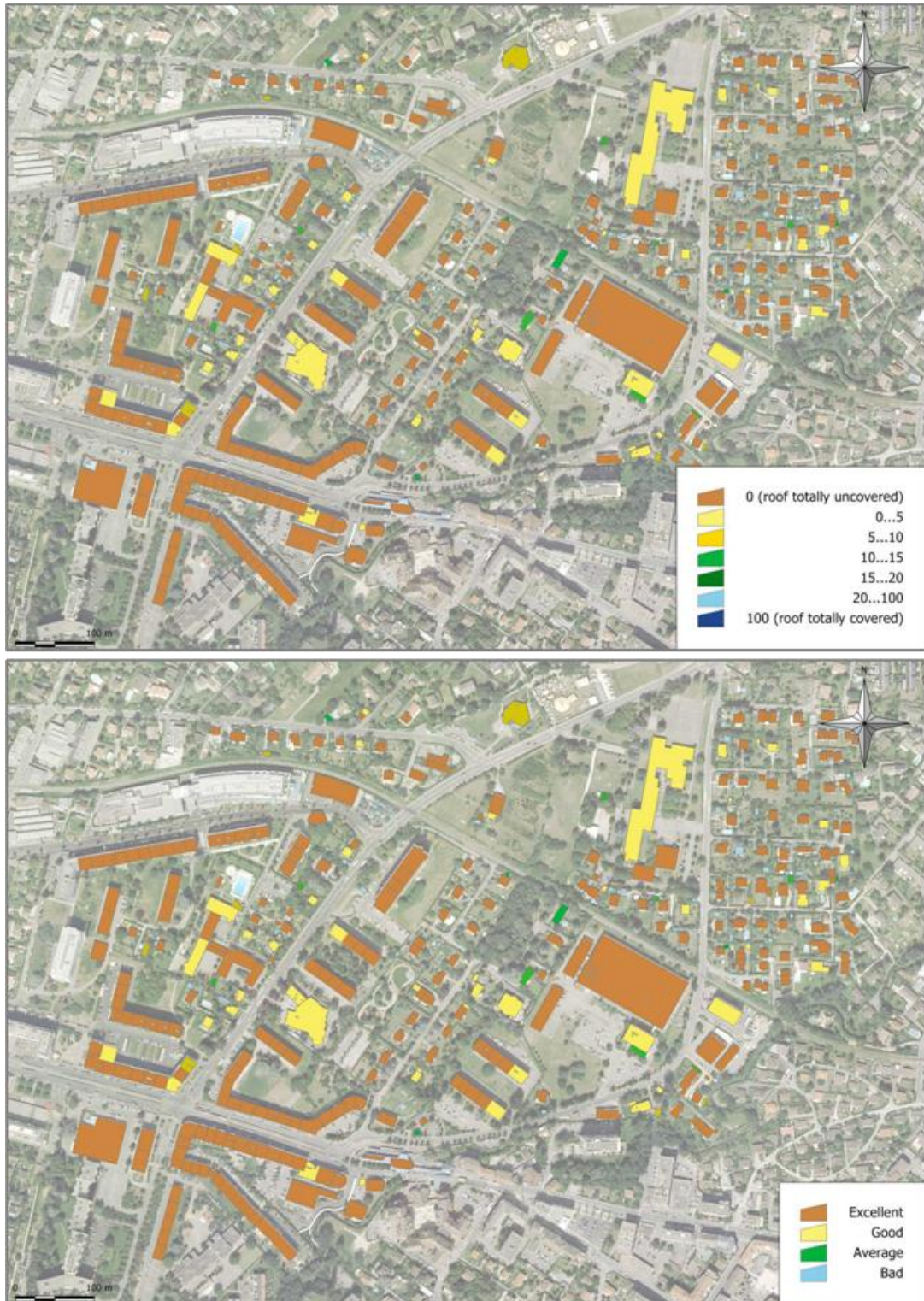


Figure 3.2. Picture above, quantitative indicator showing, for each roof, its percentage in terms of trees' coverage; picture below, pseudo-qualitative indicator showing, for each roof, its quality in terms of trees' coverage.

3.3.4 Comparison aptitude

Finally, the proposed indicators must allow at least one of the three types of comparisons presented as follows (Joerin *et al.*, 2005):

- *comparison between the considered phenomenon and an objective or norm*: considered as a *controlling* indicator. If the result of this indicator is not satisfactory further measures must be undertaken. A very simple example for urban areas is the comparison between the height of a building and the maximum height allowed by law;
- *comparison between different entities*: considered as a *benchmarking* indicator. The significance of this type of indicator is given by comparing different entities. An example for urban areas is the energetic performance of a city, which even though may have low significance when evaluated on its own, it does acquire a higher relevance when compared to the performance of other cities (Ratti and Richens, 2004);
- *comparison between different periods of time*: considered as a *monitoring* indicator. This type of indicator is achieved by following the evolution of a territory along the time. An example for urban areas is the monthly evaluation of solar irradiation over building roofs, such as emphasized in chapter 7 of this thesis.

3.4 Methods and conceptual models for the definition of indicators

The concept of indicator's *utility* is strongly related to its relevance (Desthieux, 2005). The implementation of an indicator system to support visualization and decision making should be done following a double process, called *top-down* and *bottom-up* (Maystre and Bollinger, 1999). The *top-down* process starts from the decision-makers' worldview which is generally based on qualitative or quantitative evaluations. The main question to answer is: *what has to be measured or valuated and according to which goals?* From this worldview, one goes down until descriptive or predictive models of experts that select and organize data and progressively aggregate them into indicators, defined as the *bottom-up* process. Or in other words, the construction of an indicator system consists, in one hand, of selecting relevant indicators according to issues and goals expressed by users; and on the other hand, the proposal of methods, grouping new models and tools, to aggregate data and, thus, to build these indicators. The organization of chapters 4 and 5 of this thesis follows the *top-down* and *bottom-up* approaches respectively.

In the context of sustainable development, some conceptual methods were proposed in the past, such as the pressure-state-response model (OCDE, 1997) and the stock-flux model (Prélaz-Droux, 2001). The conceptual model presented in this study is similar to the Swiss MONET project (OFS *et al.*, 2003), where indicators are organized and structured in two dimensions:

- *thematic (top-down approach)*: what do we need to measure according to specific end-user needs?
- *methodological (bottom-up approach)*: how can we measure specific phenomena and thus build this type of indicators?

According to Gallopin (1997), the use of conceptual models for the organization and structuring of a set of indicators is extremely relevant - some advantages related to the application of conceptual methods are presented as follows:

- guides the collecting process of data and information among the involved groups of end-users;
- puts in evidence the most pertinent information;

3.5. Elementary indicators, complex indicators and indexes

- helps in the process of logical aggregation of indicators, which simplifies its interpretation and integration;
- identifies important problems for which pertinent information is lacking.

3.5 Elementary indicators, complex indicators and indexes

For some cases, the purpose of building indicators is to produce and communicate synthetic information by means of aggregation of data or other indicators of a lower hierarchical level (Figure 3.3). Some distinctions are presented as follows:

- an *elementary indicator* directly results from the analysed data and the application of specific methods. An *elementary indicator* can be used to create a complex indicator or can be aggregated into an index;
- a *complex indicator* results from the combination of two or more indicators (generally elementary, but sometimes also complex), eventually the use of analysed data and the application of specific methods. Usually, a *complex indicator* demonstrates high relevance on the scientific and technical domains, being very useful for specialized end-users. A *complex indicator* can be used to create an indicator of the same type or can be aggregated into an index;
- an *index* can be distinguished from other types of information by its level of aggregation within a hierarchy of indicators (Bauler and Zaccai, 2004). An *index* has a high level of abstraction, but with minimal loss of information, defined from two or more indicators (Rotmans and de Vries, 1997). A synthetic and aggregated indicator is indeed more representative of global phenomena, thus producing a simplified vision and a new significance of it. The use of *indexes*, instead of indicators, allows therefore to more easily communicate with the general public. However, if too simplified, it can become unrealistic, and lose its meaning.

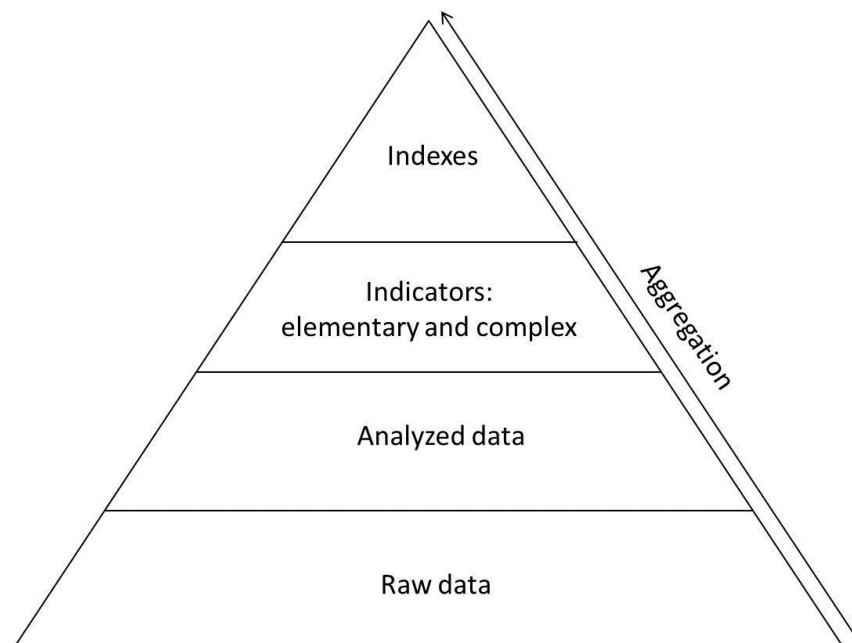


Figure 3.3. Aggregation triangle for the construction of indicators and indexes from raw data. Adapted from Bauler and Zaccai, 2004.

The conceptual model used for the construction of the urban indicators highlighted in chapter 4 follows this method, hence aggregating data from a lower hierarchical level (indicators) to a higher hierarchical level (indexes).

3.6 Visualization of indicators

3.6.1 Overview

Due to our ancestral past of drawing pictures of our environment and the significant objects within it, usually we do not normally question the *Why do we need to visualize?* On the other hand, the development of technology capabilities has provided new methods and techniques for visualization, and most importantly, for the use of visualization according to different needs. A few key points on this matter are worth mentioning (Bishop and Lange, 2005):

- through the ability to share this experience and potential for exploration, visualization may help communities (of whatever side) to build consensus and make decisions about their future;
- the relationship of people with their environment is a key contributor to environmental decisions and hence visualization may help us to learn more about that relationship.

Nowadays, for landscape designers and urban planners, it is extremely important to visually represent the existing world and its eventual changes. This process allows them to show and transmit specific and different views of the world. Historically, 2-D maps and plans were mostly used for the visualization of the territory, but these representations have often been particularly abstract. For this reason, the use of alternative ways of visualization (mainly 3-D), also for urban indicators, is significant in order to communicate targeting to the general public and specialized end-users. More than ever before, we have the ability to create more information-rich, interactive, realistic and dynamic visualization processes using 3-D (Wood *et al.*, 2005).

3.6.2 Visualization taxonomy

Linking both the concepts of seeing and understanding the term “visualization” was firstly defined by McCormick *et al.* (1987):

Visualization is a method of computing. It transforms the symbolic into the geometric, enabling the researchers to observe their simulations and computations. Visualization offers a method for seeing the unseen. It enriches the process of scientific discovery and fosters profound and unexpected insights. In many fields it is already revolutionizing the way scientists do science.

Despite its dating, the definition above is still very relevant. According to Bishop and Lange (2005), moving beyond the cartographic framework, other important distinctions can be made within visualization concept and in relation with the outline of this thesis:

- dynamic versus static views;
- level of interactivity;
- dimensionality;
- levels of realism;
- single versus multiple representations.

For each of these concepts follows a brief explanation.

3.6. Visualization of indicators

3.6.2.1 Dynamic versus static view

The difference between dynamic and static views is that dynamic refers to displays changing continuously, either with or without user intervention (Slocum *et al.*, 2003). Two types of dynamic views should be considered:

- *animated maps*: the display changes uninterruptedly without any interference of the user and most commonly it is a temporal phenomenon that is shown dynamically. A good example of a dynamically display intrinsic to this study could be the daily, weekly or monthly solar irradiation on building roofs during a year (chapter 7);
- *direct manipulation*: in this case, the user explores the data and interacts with mapped displays. Nowadays, a user interacting with the system can easily control the displays using functions such as map zoom and pan, changes of colour, projections, among many others.

3.6.2.2 Level of interactivity

This point is highly relevant because it allows both communication and discovery of the displayed information (Andrienko and Andrienko, 2003 and 2007). The user can change views according to a different number of input categories and, considering its needs, may also zoom the maps produced interactively. The degree of interactivity in visualization mainly depends on the characteristics of the existing user interface's controls. Another important subject is real-time performance, which represents the capacity of computer systems to redraw images almost instantly, being a good basis for exploratory approaches with users.

3.6.2.3 Dimensionality

The great majority of maps produced use 2-D and 3-D representations. According to Wood *et al.* (2005), conventional 2-D maps use two spatial dimensions of a dataset onto two location dimensions of the cartographic "page". This convention is appropriately general and hence it is assumed by the reader of the map that further non-spatial aspects of a dataset can be represented including additional visual variables. On the other hand, 3-D representation in a 2-D display builds on this convention by projecting three location coordinates onto a 2-D plane. By doing this, a new cartographic "degree of freedom" is added to visual representation, only possible due to the experience and practice of human beings in reconstructing 3-D views from 2-D retinal projections. The level of abstraction is much higher in 2-D maps while 3-D maps always present some zones of occlusion. Another dimensionality that can be used for visualization is the 2.5-D (two and a half dimensions) view: this definition is based on the fact that height is modelled by storing a *z* value for each *x,y* pair in the dataset, which is *raster* based.

3.6.2.4 Levels of realism

The aim is to define the degree of realism necessary for the natural perception of a landscape and changing environments, including urban displays. According to Lange (1998), a more meticulous modelling increases the impression of realism and makes the resulting visualization more trustworthy. For urban environments such visualizations can be used in order to present and communicate different type of information with high levels of realism to decision makers and specialized end-users: (1) plans of flood risk, (2) traffic volumes, (3) visual pollution levels, and (4) other factors influenced by environmental management. On the other hand, there are clearly

environmental management impacts which cannot be represented realistically, such as non-visual pollution, regions of influence, among others (Bishop and Lange, 2005).

In this context it is of great importance that the level of realism adapted for an explicit visualization is coherent and truthful. Moreover, the fact that fine looking visualizations with high levels of realism can gloss over reality implies a responsible use of these simulations. Therefore, the visualizations adopted for urban environments have to be considered *realistic* only at times when it both looks visually reliable and represents a correct situation in the geo-sciences domain, such as the 2-D, 2.5-D and 3-D representations of the urban indicators highlighted in this thesis. Related to this subject it is important to mention that on the opening day of 2010 *Imagina* conference, a “3-D Ethics Charter” was signed. This charter deals with territorial models created by public bodies and represents an important innovation for land management and public information.

3.6.2.5 Single versus multiple representations

For urban analysis and design, specialized end-users should have the possibility to interact with any of the representations, as they relate to different aspects of the design process from global financial outcomes to aesthetics (Batara *et al.*, 2001). Another important point, that is not always simple to solve, is the real time streaming between all views. In fact, when a change is applied to one view, all other views must be updated through a common database.

To emphasize the concept of multiple data views, three different visual representations were suggested by Verbree *et al.* (1999), which include three simple views of user’s natural and artificial surroundings (Figure 3.4):

- *plan view* and ordinary 2-D colour map for initial orientation;
- *model view*, a simple 3-D map for professional analysis;
- *world view*, a detailed photorealistic map in 3-D for public presentations.

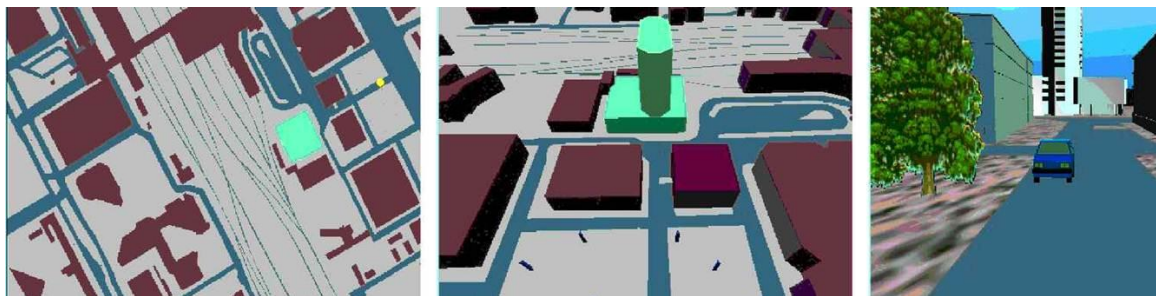


Figure 3.4. Multiple data views proposed by Verbree (1999). Left to right images: *plan view*, *model view* and *world view*.

Another aspect that is not negligible when working in a collaborative environment is which of the views is available for interaction – in some cases should it be given priority to a particular view? An example in the GIS field is that the user may view maps, tables, charts and 2.5-D perspectives but can only edit the data through the map (most of the times a complex process) or the attribute tables (Bishop and Lange, 2005).

Since this study is developed and proposed for professional end-users, the focus on representation of multiple data views is given to plan and enhanced model views.

3.6.3 3-D visualization of urban indicators

3.6.3.1 Presentation

Commonly used planning tools applied during the last decades, such as 2-D maps, diagrams, tables or texts frequently fail to communicate the results to unprofessional users (Appleton and Lovett, 2005). Compared to these tools, 3-D visualizations (commonly GIS-based) demonstrate an extraordinary potential for contributing to a better understanding of the information (Heißenhuber *et al.*, 2004). Moreover, 3-D technology reinforces the application of dynamism in visualization. Hence, the capability to modify 3-D viewpoint in real-time is essential to generate a sense of virtual reality, which is impossible by means of 2-D visualization.

By integrating indicators, 3-D visualizations give the chance to connect all the visual and non-visual fragments of the urban landscape and its artificial objects, and may even offer innovative planning tools (Bishop and Lange, 2005). However, few studies exist that suggest possible designs of integrating indicators in visualization tools (Hehl-Lange, 2001; Wissen *et al.*, 2005). Furthermore, none of these studies deals with urban indicators, which implies that research applications are still lacking for this specific topic.

3.6.3.2 Three-dimensionality of visualization

Using 3-D in visualization can take benefit of refined policies for 3-D visual mapping and also, it reinforces the application of dynamism in visualization. Nevertheless, there is still little knowledge about when it is suitable to use 3-D visualization and how it can be used most proficiently. There are multiple implications of 3-D in visualizations with respect to expressiveness, effectiveness and appropriateness (Wood *et al.*, 2005).

To elucidate the term “3-D”, the well-known “visualization pipeline” (Figure 3.5) initially proposed by Haber and McNabb (1990) and later modified to “3-D visualization” by Wood *et al.* (2005), was adapted for the purpose of this study.

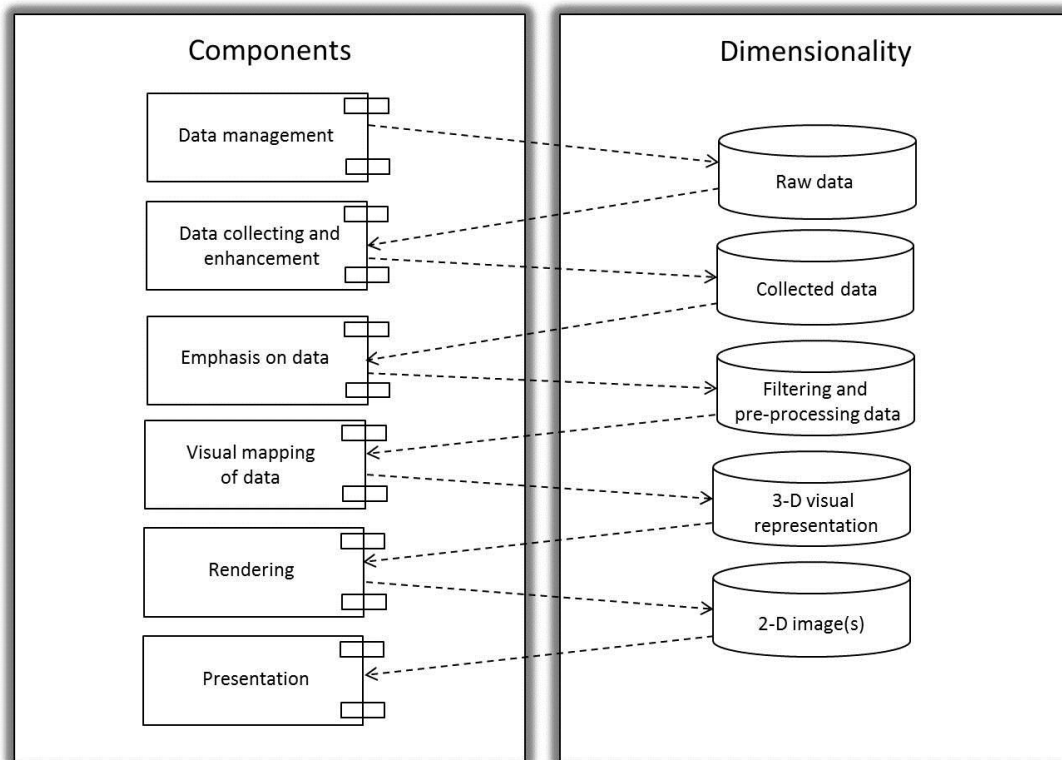


Figure 3.5. The “visualization pipeline” for 3-D visualization with six components and five dimensions. Adapted from Haber and McNabb (1990) and Wood et al. (2005).

All the steps presented in the workflow of Figure 3.5 are briefly described below:

- *data management*: organizing, managing and giving access to raw data;
- *data collection and enhancement*: composing, aggregating, associating and enhancing collected data for the goal of visualization;
- *emphasis on data*: filtering and pre-processing data to be visualized;
- *visual mapping of data*: transforming collected data by means of 3-D graphics, generating a 3-D visual representation of data, based on 3-D geometries such as polygons meshes, 3-D lines and 3-D points;
- *rendering*: production of 2-D image(s) by means of one or more created images of views of a 3-D visual representation;
- *presentation*: using output media such as 2-D monitors or displays to present images (information).

3.6.3.3 Levels of detail for 3-D visualization

Conventionally, the main reason for representing different levels of detail (LoD) is efficient visualization mainly due to cognitive and perceptive reasons (Guthe and Klein, 2003; Reichenbacher and Swienty, 2007). Well-organized analysis is another important cause for using LoD in optimal 3-D visualization displays. For example, counting the number of buildings in a city can be accomplished most proficiently by considering the buildings on a lower LoD. Beside efficiency, one other reason for managing different LoD is the availability of high quality 3-D

3.6. Visualization of indicators

data sets. Frequently, highly detailed data only exists for some landmarks of the city, whereas less detailed data covers the entire zone of interest. In such cases, a process accomplishing an analysis should use the coarser data only where detailed data is not available (Kolbe and Gröger, 2004).

Hence, for the study highlighted in this thesis, the CityGML standard was chosen, which is a common information model for the representation of both complex and geo-referenced 3-D vector data along with the associated semantics. This standard also includes a well-defined method for the visualization of different LoD (Figure 3.6), which was initially proposed by Kolbe *et al.* (2005):

- *LoD0*: 2.5-D visualization;
- *LoD1*: very generic 3-D model. Usually, buildings are represented without any roof structures, which means all roofs are flat. The representation of a building under this concept is called “block model”;
- *LoD2*: differentiated roof structures and facade textures of buildings are represented. Starting from this LoD, other urban objects, such as trees and urban furniture, can be also included for visualization;
- *LoD3*: detailed architectural model including all the details of the roofs, such as chimneys;
- *LoD4*: “walkable” architectural model. In this case, all objects belonging to the interior of buildings, such as stairs, can be also represented.

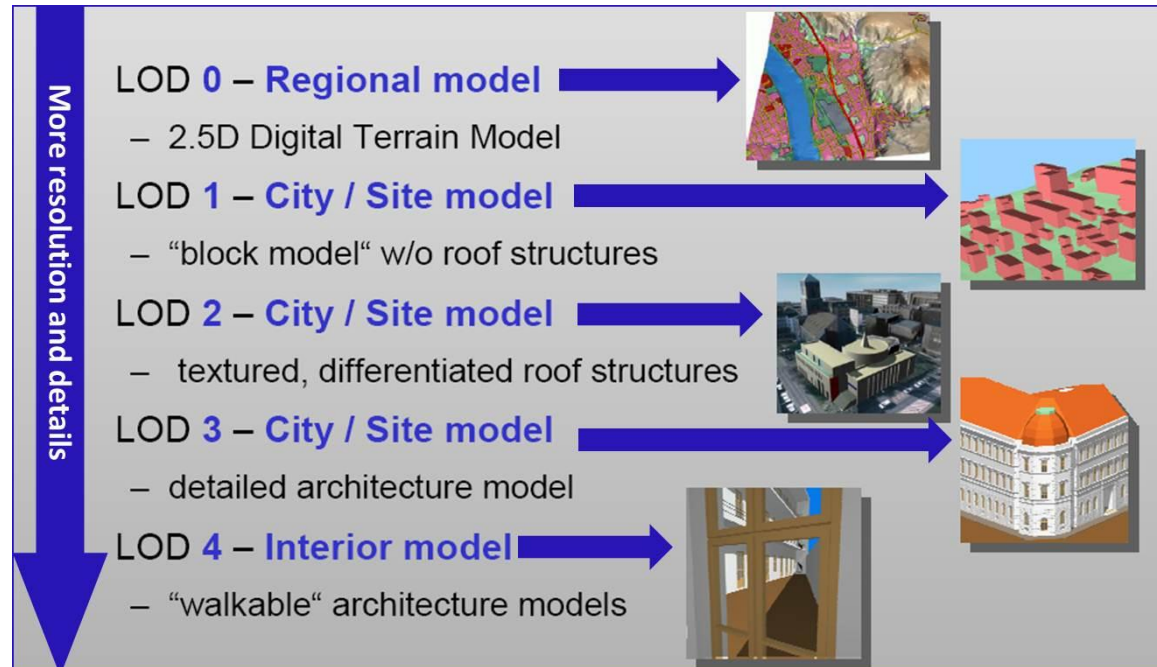


Figure 3.6. Levels of Detail (LoD) according to CityGML standard. Adapted from Kolbe *et al.* (2004).

An essential aspect when managing different LoD is to guarantee that for each object – although it is represented at different LoD – only one of those levels is considered when accomplishing an analysis or visualization of data. The set of representations of objects which can be analysed or visualized together is defined as a *view*. It is important to mention that a view may include objects from different LoD, but it must never contain the same object or the same portion of space more

than once, otherwise, an erroneous visualization is produced because the same building is displayed twice.

The LoD classification method proposed inside the CityGML standard is perfectly appropriate for this study because it deals mainly with representation and detailed aspects of buildings. Indeed, most of the proposed indicators highlighted and extracted (third part of this thesis) are intrinsic to this type of urban objects.

3.7 Conclusions and chapter synthesis

This chapter presents the main properties of indicators in order to distinguish them from common information:

- an indicator must be relevant considering some precise issues as well as indicate a tendency from the point of view of a finality of evaluation;
- an indicator must be measured according to an ordinal (qualitative) or cardinal (quantitative) scale;
- an indicator must allow at least one of three comparisons: between the considered phenomenon and an objective or norm, between different entities, between different periods of time;
- the extraction of an indicator can either be directly based on the selection of relevant data, or result from the aggregation of two or more data sources (indicators) of a lower abstract level;
- an index can be distinguished from other types of indicators by its level of aggregation within a hierarchy of indicators, represented in this thesis as a ratio;
- an indicator must be sufficiently representative of the measured phenomenon, which depends on the availability of the data, often limiting its relevance.

The actual situation and development of an urban system are normally evaluated by a set of indicators which are positioned on the interface between the information system and the decision system. Presently, several methodological approaches can be applied in order to extract a set of indicators meeting specific aims of use. The organization of a set of indicators results from the projection of a list of indicators within a theoretical framework, which is materialized in the form of a conceptual model of a given reality, as highlighted in chapter 4. This kind of approach allows a clear and easy communication, and thus it meets one of the main objectives of this thesis, which is to propose a system of indicators based on a preliminary knowledge of reality. Furthermore, as emphasized in the following chapters of this thesis, it is also convenient to associate the actors (end-users) with the development and implementation of these indicators under the context of a participative process.

Finally, the representation of urban indicators, mainly the way in which 3-D visualization environments based on the CityGML standard can be both used and adapted for the visualisation of these geographical urban indicators, is of importance. This specific topic is specifically targeted and analysed in the chapter 9 of this thesis.

This chapter closes the first part of this thesis, related to the theoretical knowledge used in order to fulfil its research requirements. In the next part of this thesis, the methodological framework of this thesis is emphasized. It is based on the conceptualization method proposed by Maystre and Bollinger (1999), which follows a *top-down* and *bottom-up* processes.

PART II
METHODOLOGICAL FRAMEWORK

CHAPTER 4. USER REQUIREMENTS ANALYSIS¹

¹ The main concepts of this chapter were published in:

Carneiro, C. (2008) Communication and visualization of 3-D urban spatial data according to user requirements: case study of Geneva. *The International Archives of the Photogrammetry, Remote Sensing and Spatial Information Sciences*, Vol. 37, Part B2, pp. 631-636.

4.1 Introduction

This chapter studies the use of 2-D and 3-D urban models and data for the extraction of urban indicators, considering different kinds of applications related to needs of the end-users. The aim of the cases-studies highlighted in this thesis is to describe the application of this type of information from a user's point of view. The purpose of describing the end-user's perspectives and needs is to create a valid conceptual model, relating it to the empirical studies described in the third part of this thesis. As emphasized in the third chapter of this thesis, the selection of relevant indicators according to issues and goals expressed by end-users follows a *top-down* process (Maystre and Bollinger, 1999). The user requirement analysis presented in this chapter was organized and documented at the start of this PhD thesis.

An advantage of using 3-D data as an alternative to 2-D data is that 3-D better represents the as-is situation, allowing end-users to accomplish their activities in a larger domain (Elberink, 2010). For example, architects and civil engineers are able to calculate the morphological properties of buildings, such as the total area of facades or the volume, which would be otherwise impossible if only 2-D data was used. Indeed, for some end-users the use of 3-D data and the emergence of new applications can be the first contact with geo-referenced information. Nevertheless, it is important to note that for a considerable number of applications, representing in 2-D is still the most suitable way to reach the proposed objectives – an example is the management and assessment of the cadastral parcels of the territory.

The empirical studies highlighted in the third part of this thesis are in an explorative stage and have a data-driven character, defined in this thesis as the *bottom-up* process. Hence, in a first phase users look at what type of applications can be proposed with the existing 2-D and 3-D data. Secondly, with the implementation of these applications and the extraction of the selected urban indicators, the initial requirements will become more demand-driven. This fact allows for a better in-depth elucidation of what the specifications of 2-D and 3-D data should be concerning end-users' needs, which eventually includes the visualization purposes and the semantic enrichment of 3-D models. Figure 4.1 shows an *iterative process* describing this approach.

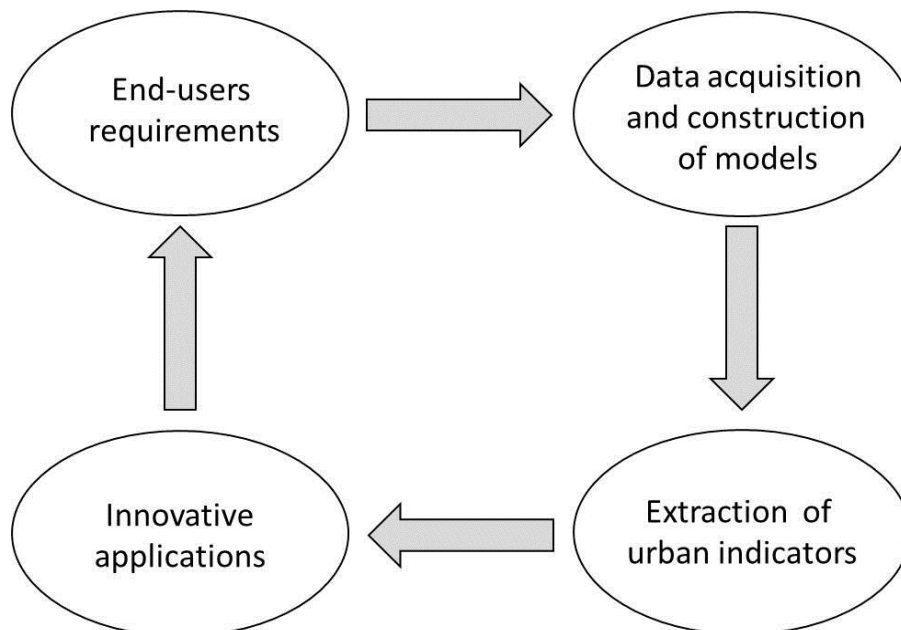


Figure 4.1. Iterative process inherent to the extraction of urban indicators, connecting user requirements, data, models and applications.

Complementing the generic *iterative process* shown in Figure 4.1 it is also important to evaluate the utility of the proposed innovative applications, which takes into account different scales of visualization (2-D and 3-D, including 2.5-D) throughout the design and development phases by:

- getting users to review the design;
- having users walk through the implementation process;
- asking users about their satisfaction;
- conducting utility tests with users.

Finally, it is important to note that user requirements on 3-D urban models and data are still under development, mainly due to the following reasons:

- the number of users and applications is rapidly and continuously growing;
- during the last years, technical improvements (mainly concerning geometric and radiometric resolution) of airborne imagery and laser altimetry have been quite relevant and are still continuously progressing.

Hence, with the increasing offer of more accurate data, the user requirements have become more exhaustive and the appeal for new type of information (including urban indicators) has grown. Furthermore, research projects that demonstrate the interest of reusing 3-D data for the extraction of pertinent information and not only for the display of both 3-D urban models and gadgets, are essential for end-users in order to justify the acquisition of this type of data.

However, with regards to the analysis of user requirements for 3-D urban modelling and geo-visualization of spatial indicators a few large studies have been undertaken to date - some examples are presented as follows:

- Zlatanova and Brandova (1998) presented a user-requirements analysis focusing on real objects of interest and frequent spatial and thematic analysis as their importance for the third dimension;
- Nielsen (2005) inquired a group of end-users about visual representations, usability and urban planning in real-time 3-D geo-visualization at the University of Aalborg;
- Elberink (2007) presented a study about re-using laser scanner data in applications for different groups of end-users on 3-D topography.

This chapter tries to overlap this gap by giving a contribution on the utility and possible applications of 3-D data, which are related to the needs of end-users of the State of Geneva.

The following sections will introduce information about: (4.2) pilot project: state of Geneva, and (4.3) conclusions and chapter synthesis.

4.2 Pilot project: state of Geneva

4.2.1 Presentation

In October 2005, the GIS department of the state of Geneva purchased a new set of LiDAR data with a planimetric accuracy of 15 centimetres and an altimetric accuracy of 20 centimetres. A simple bibliographical research about different projects on 3-D modelling revealed that the richness of the data gathered by this method is seldom exploited. In 2006, a national inquiry made in Switzerland among some potential end-users of this type of information showed a strong interest for the integration and use of the third dimension in the available geographical data. Subsequently, the state of Geneva launched a pilot project for the incorporation of the third

4.2. Pilot project: state of Geneva

dimension, including the definition and extraction of novel urban indicators that could be useful for end-user needs and applications (Vieira de Mello, 2006). This study allowed to evaluate the potential of using LiDAR data for the integration of the *3-D dimension* into the cadastral and GIS data of the state of Geneva – it was done by considering successive stages, according to specific user's needs, as presented in the next sections of this chapter, and following the method proposed by Dumas and Redish (1999).

For the definition and extraction of the indicators highlighted in this thesis for the state of Geneva a diverse number of data sources are available: 2-D vector data, 2.5-D raster data, alphanumerical data containing altimetric information about buildings heights, LiDAR and terrestrial laser data, orthophotos and terrestrial photos.

4.2.2 Preliminary inquiry

A preliminary inquiry concerning the user requirements and the relevance of 3-D urban information (*utility study*) was launched to all potential users. In this first evaluation, some generic questions concerning the construction of a 3-D urban model were placed:

- Interest and utility for users' activities?
- First idea about the desired level of detail (LoD)?
- Urban objects to be visualized?

This first inquiry, which was answered by more than 30 users, highlighted that more than 90% of the replies consider that there exists in fact a real need to construct and visualize 3-D urban spatial data and indicators. Finally, a group of 25 end-users was selected for further interviews. The final results (in French) of this inquiry, made with the collaboration of Laurent Nigeller and Adrien Vieira de Mello of the GIS department of the state of Geneva, can be consulted in appendix A.

4.2.3 Identification and classification of the existing users in different fields

Based on the answers obtained among the selected 25 potential end-users of 3-D urban data and models, and in order to better organize and comprehend the existing user requirements, the results of the first inquiry were classified into 6 distinct domains:

- Architecture, urbanism and territory planning: 9 users;
- Urban traffic (motor vehicles, trains and airplanes: 4 users;
- Environment and energy: 4 users;
- Pedestrian and cyclist mobility: 3 users;
- Security and emergency situations management: 3 users;
- Underground information: 2 users.

Hence, in order to clarify and look further into the specific user requirements, several interviews were led with pre-defined and selected users of each one of these six classified fields, presented as follows.

4.2.4 Interviews

Based on the users' classification presented in section 4.2.3, interview sessions were organized between researchers, owners and users of 3-D geo-information of the state of Geneva, focusing on two main axes:

- the definition of 3-D urban applications and its intrinsic indicators and indexes considered to be pertinent. This point is presented in sections 4.2.5 and 4.2.6;
- a preliminary analysis of the different possibilities of visualization (2-D and 3-D) for the indicators and indexes to be extracted was undertaken. The CityGML standard presented in section 3.6.3.3 was considered for 3-D thematic visualization purposes, by relating the computed UEQ indicators to the city objects. This point is presented in section 4.2.7.

During these interviews some important rules were followed:

- users were interviewed about their work;
- users lead conversation;
- look to expand and challenge the background of assumptions one brings to each interview.

4.2.5 Principles of indicators and indexes

An important point is to correctly set quantitative utility goals: *how can we be sure that the proposed data is pertinent if we do not know the projects under evaluation? The relevance is defined according to some objectives; if these objectives are not identified, how can we reasonably evaluate its pertinence?* Thus, many of the utility goals come from task analysis. A task analysis leads to a list of significant and pertinent information, in this thesis represented as indicators and indexes, which is selected and organized according to the goal of use of 3-D urban information.

All the raw information collected during the interviews with the six groups of end-users allowed to define a list of indicators and indexes. In order to better communicate with these stakeholders and also to help structuring further work, an easily understandable and user-oriented conceptual model was implemented. The method applied is organized according to four steps, in a pyramidal structure, as shown in Figure 4.2.

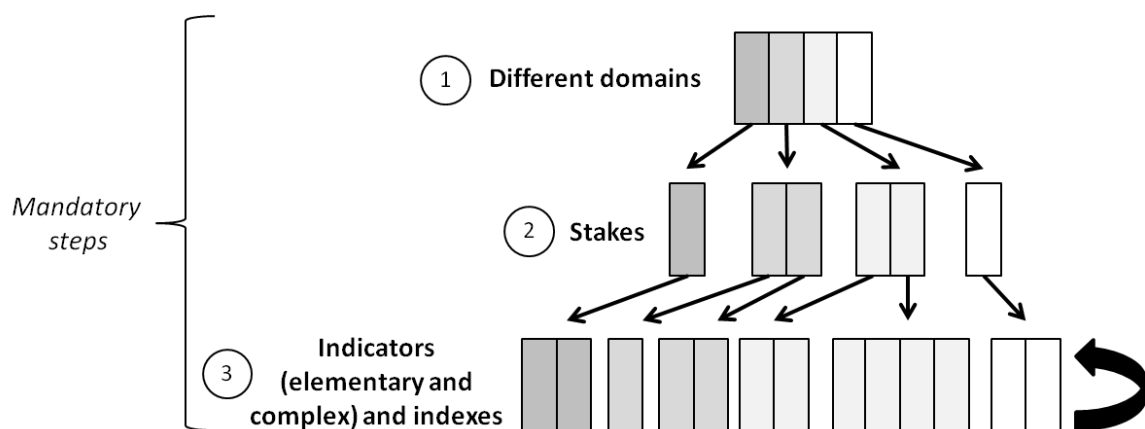


Figure 4.2. The pyramidal process used for integrating the selected indicators and indexes.

4.2. Pilot project: state of Geneva

In this study, the list of domains where the 3-D dimension may be of concern is referred to as “3-D applications”. Those are structured into the six domains presented in section 4.2.3, and grouped into different stakes. According to Desthieux (2005), a stake is defined as a general objective representing an expected evolution or a tendency for a given problem. Thus, for each stake, one or more geographical indicators (elementary or complex) considered as sufficiently representative and pertinent are mandatorily defined, whilst the creation of indexes, according to end-users’ needs, is not obligatory. It is important to mention that, for most of the cases, complex indicators are derived from elementary indicators, but for some specific cases a complex indicator can be also constructed from an indicator of the same type. As presented in section 3.5, an index has a higher level of abstraction, with minimal loss of information, being represented as relative values that can be very useful on generalization and comparison procedures. In this thesis, as already mentioned in the introduction, all presented indexes refer to an aggregation resulting from the ratio of two elementary or complex indicators.

Hence, the definition of stakes can be classified into five distinct cases:

- The stake is represented by a *single indicator*, which is judged significant for the stake under analysis. This is the most common situation. Some examples of single indicators, which were evaluated and defined by the six groups of end-users of the state of Geneva, are shown in Figure 4.3.

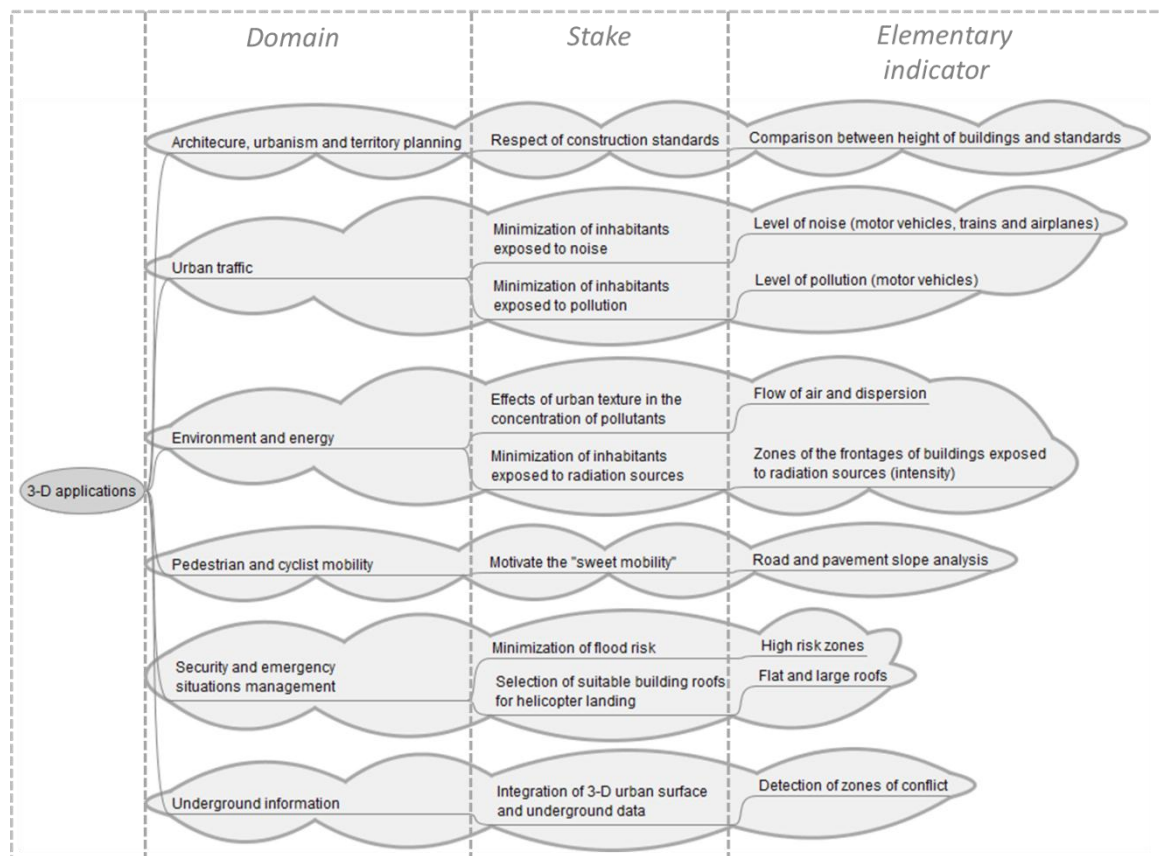


Figure 4.3. Some examples of stakes represented by elementary indicators.

- The stake is represented and evaluated by a *complex indicator*, which is calculated from two or more elementary indicators.

$$\text{Stake} = \text{Indicator}_{\text{Complex}} = f(\text{Indicator}_A, \text{Indicator}_B, \text{Indicator}_C, \dots) \quad (4.2)$$

One example of this type of complex indicator, which was evaluated and defined by the six groups of end-users of the state of Geneva, is shown in Figure 4.4.

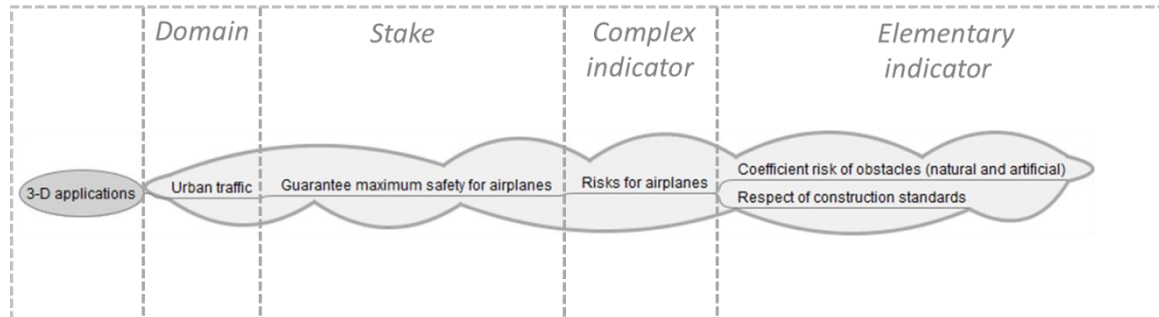


Figure 4.4. One example of a stake (“guarantee maximum safety for airplanes”) represented by a complex indicator.

- The stake is represented and evaluated by one or more *indicators* (these can be elementary or complex) and one or more *indexes*. In this case, the characteristics of indicators and indexes can be analysed separately:

$$\text{Stake} = \langle \text{Indicator}_A, \text{Indicator}_B, \text{Indicator}_C, \dots, \text{Index}_A, \text{Index}_B, \text{Index}_C, \dots \rangle \quad (4.3)$$

One example of a stake, which was evaluated and defined by the six groups of end-users of the state of Geneva, represented by two elementary indicators and its respective index (calculated by dividing the first and second elementary indicators), is shown in Figure 4.5.

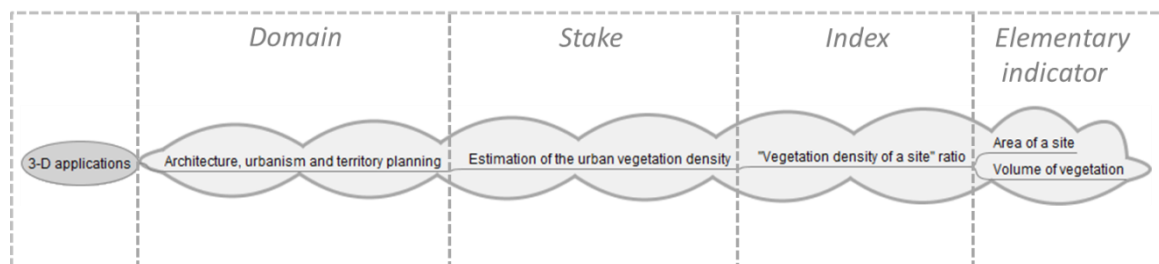


Figure 4.5. One example of a stake (“estimation of the urban vegetation density”) represented by two elementary indicators and one index.

- The stake is represented and evaluated by one or more *indexes*. In this case, the characteristics of these indexes can be analysed separately. An example of a stake representing a simplified version of the analysis of the urban texture and energy consumption, represented by two indexes, which was evaluated and defined with the six groups of end-users of the state of Geneva, is shown in Figure 4.6:
- ⇒ *index 1* - an index representing the “Surface to volume ratio” of buildings, which is calculated by dividing the addition of the elementary indicators “Area of ground”, “Area of facades” and “Area of roofs” by the elementary indicator “Volume”;

4.2. Pilot project: state of Geneva

⇒ *index 2* - an index representing the “Passive and no passive ratio” of buildings, which is calculated from the elementary indicator “Passive and no passive areas analysis” (Ratti *et al.*, 2005).

$$\text{Stake} = \langle \text{Index}_A, \text{Index}_B, \text{Index}_C, \dots \rangle \quad (4.4)$$

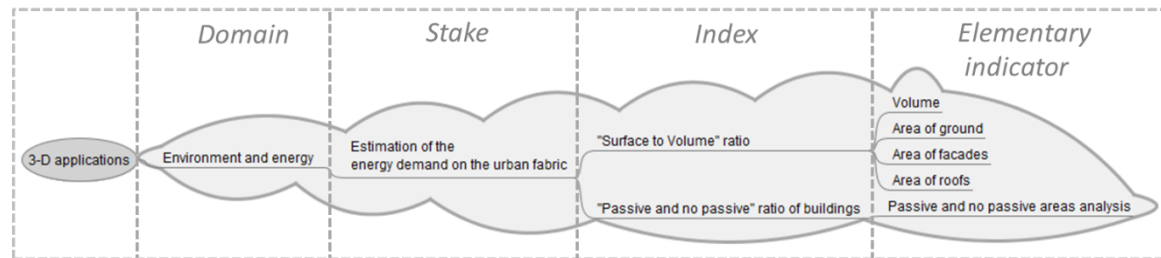


Figure 4.6. One example of a stake (“estimation of the energy demand on the urban fabric”) represented by two indexes.

4.2.6 Selection of indicators and indexes

4.2.6.1 Presentation

The stakes and the intrinsic extraction of spatial indicators using 2-D and 3-D urban models and data presented in the previous section (4.2.5) have already been deeply studied, such as:

- urban air flows (Ratti *et al.*, 2006);
- sound propagation to manage noise pollution and other parameters (Biswas and Lohani, 2008);
- traffic air pollution in urban areas (Borrego *et al.*, 2006);
- estimation of vegetation density (Lim, 2007; Gachet, 2009).

The points presented above fall beyond the scope of research related to this thesis. Moreover, some commercial software already exists in these domains, which can help users to find solutions for its problems. Thus, this section presents a list of three priority stakes as evidenced during the interviews (Table 4.1).

Priority stakes	Important stakes
<ul style="list-style-type: none"> - Assessment of the morphological properties of the urban texture (13 users: 9 users from the field “Architecture, urbanism and territory planning” and 4 users from the field “Environment and energy”) - Exploration of the solar potential on the urban fabric (4 users from the field “Environment and energy”) - Estimation of the energy demand on the urban fabric (4 users from the field “Environment and energy”) 	<ul style="list-style-type: none"> - Respect of construction standards (9 users from the field “Architecture, urbanism and territory planning”) - Minimization of inhabitants exposed to noise (4 users from the field “Urban traffic”) - Minimization of inhabitants exposed to pollution (4 users from the field “Urban traffic”) - Minimization of the concentration of pollutants in the urban texture (4 users from the field “Environment and energy”) - Minimization of inhabitants exposed to radiation sources (4 users from the field “Environment and energy”) - Motivate the sweet mobility (3 users from the field “Pedestrian and cyclist mobility”) - Minimization of flood risk (3 users from the field “Security and emergency situations management”) - Selection of suitable building roofs for helicopter landing (3 users from the field “Security and emergency situations management”) - Integration of 3-D urban surface and underground data (2 users from the field “Underground information”)

Table 4.1. Priority and important stakes according to end-users’ needs and innovative research domains.

Indeed, nowadays, researchers in urban studies are growingly more concerned about the improvement of the quality of life in cities, where more than half of the world’s population resides. Hence, the potential use of geo-referenced 2-D and 3-D data and models, typically for the assessment of the Urban Environmental Quality (UEQ) in the city, district or neighbourhood scale, such as the estimation of the potential deployment of renewable energies in the built environment and the determination and monitoring of several urban indicators, has become a very important topic. According to Morello (2006), environmental quality is not assessed just by the computation of energy consumption, also resulting from considerations on urban metabolism and density; besides such quantitative factors, the qualitative aspects affecting human well-being also play a major role: hence, variables like visual perception, the openness to skylight and the psychological comfort can be computed in an effort to translate them into measurable indicators. Thus, there is a direct and logical relation between UEQ and the three priority stakes shown in Table 4.1, matching end-users’ needs and innovative research domains, considered priority for this study.

These multi-disciplinary stakes are particularly related to the professional activities of architects, urbanism and territory planners, and energy and environment specialists, among others. For this reason, the extracted UEQ indicators have the clear potential of being used through different domains and stakes.

4.2. Pilot project: state of Geneva

An overview of the UEQ indicators and indexes selected by end-users is shown in Table 4.2 and Table 4.3: the indicators shown in bold and italic are those that were researched and extracted under this study, as shown in the third part of this thesis. More detailed information is given in the form of *mind maps*. These last follow a structure of domain, stake and indicators, which may also include indexes (sections 4.2.6.2 to 4.2.6.4).

Domain	Stake	Indicator
Architecture, urbanism and territory planning	Respect of construction standards	Comparison between height of buildings and standards
	Maximize the quality of the built environment	Visibility analysis Sunshine analysis
	<i>Estimation of the urban vegetation density</i>	<i>Area of a site</i> <i>Volume of vegetation</i>
Environment and energy	Effects of urban texture in the concentration of pollutants	Flow of air and dispersion
	Minimization of inhabitants exposed to radiation sources	Zones of the frontages of buildings exposed to radiation sources (intensity)
	<i>Exploration of the solar irradiation on building roofs</i>	<i>Radiation collected by roofs</i>
	<i>Exploration of the solar irradiation on building facades</i>	<i>Radiation collected by facades</i>
	<i>Potential for active solar energy</i>	<i>Photovoltaic energy production on building roofs</i>
	<i>Potential for active solar energy</i>	<i>Thermal energy production on building roofs</i>
	<i>Estimation of the heating demand on the urban fabric</i>	<i>Seasonal thermal energy requirements</i>
		<i>Seasonal heat losses</i>
<i>Seasonal gains</i> <i>Seasonal thermal energy needs</i>		
<i>Estimation of the lighting demand on the urban fabric</i>	<i>Lighting demand analysis</i>	
Architecture, urbanism and territory planning + environment and energy	<i>Assessment of the morphological properties of the urban texture</i>	<i>Volume (building)</i>
		<i>Area of site</i>
		<i>Area of roofs (building)</i>
		<i>Area of facades (building)</i>
		<i>Area of storey (building)</i>
		<i>Area of ground (building)</i>
		<i>Number of faces (building)</i>
		<i>Average height (building)</i>
<i>Type of roof</i>		
Urban traffic	Minimization of inhabitants exposed to noise	Level of noise (motor vehicles, trains and airplanes)
	Minimization of inhabitants exposed to pollution	Level of pollution (motor vehicles)
	Guarantee maximum safety for airplanes	Risks for airplanes
Pedestrian and cyclist mobility	Motivate the "sweet mobility"	Road and pavement slope analysis
Security and emergency situations management	Minimization of flood risk	High risk zones
	Selection of suitable building roofs for helicopter landing	Flat and large roofs
Underground information	Integration of 3-D urban surface and underground data	Detection of zones of conflict

Table 4.2. List of indicators considered pertinent by end-users (considering each specific domain and stake).

Domain	Stake	Index
Architecture, urbanism and territory planning	Estimation of the urban vegetation density	"Vegetation density of a site" ratio
Environment and energy	Estimation of the coverage and impact of vegetation on roofs	"Vegetation impact" ratio
Architecture, urbanism and territory planning + environment and energy	Estimation of the energy demand on the urban fabric	"Passive and no passive" ratio (buildings) "Surface to volume" ratio (buildings)
	Assessment of the morphological properties of the urban texture	"Envelope area to ground area" ratio (buildings)
		"Urban built density" ratio (buildings)
		"Volume to number of faces" ratio (buildings)
		"Floor area" ratio (buildings)
	Estimation of the coverage and impact of vegetation on roofs	"Vegetation coverage" ratio
	Estimation of the influence of shadowing and SVF on the urban texture	"Influence of shadowing and SVF" ratio

Table 4.3. List of indexes considered pertinent by end-users (considering each specific domain and stake).

4.2.6.2 Assessment of the morphological properties of the urban texture

- The stake is represented and evaluated by a set of eight *elementary indicators* (Figure 4.7) and five *indexes* (Figure 4.8):

⇒ *elementary indicators*: composed of eight elementary indicators:

1. volume;
2. area of site;
3. area of roofs;
4. area of facades;
5. area of ground;
6. number of faces;
7. average height;
8. type of roof.

⇒ *index 1* - represents the "Surface to volume" ratio of buildings, which is calculated by dividing the addition of the indicators "Area of ground", "Area of facades" and "Area of roofs" by the indicator "Volume";

⇒ *index 2* - represents the "Envelope area to ground area" ratio of buildings, which is calculated by dividing the addition of the indicators "Area of facades" and "Area of roofs" by the single indicator "Area of ground";

4.2. Pilot project: state of Geneva

- ⇒ *index 3* - represents the “Volume to number of faces” ratio of buildings, which is calculated by dividing the addition of the indicator “Volume” by the single indicator “Number of faces”;
- ⇒ *index 4* - represents the “Floor area” ratio of buildings, which is calculated by multiplying the addition of the indicator “Volume” by the single indicator “Average height” divided by 3, which corresponds to the average height of a building’s storey;
- ⇒ *index 5* - represents the “Urban built density” ratio, which is calculated by dividing the indicator “Volume” by the indicator “Area of site”.

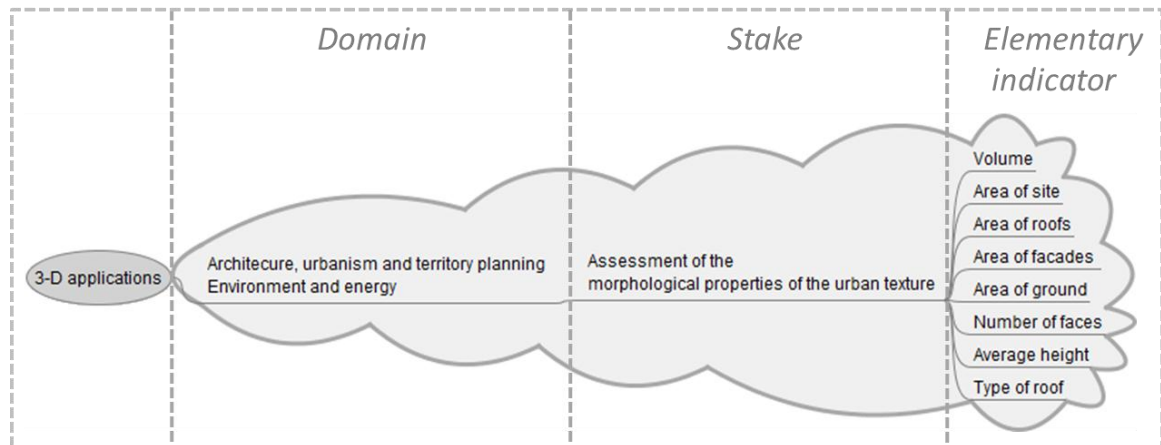


Figure 4.7. The stake “assessment of the morphological properties of the urban texture” and its inherent eight elementary indicators.

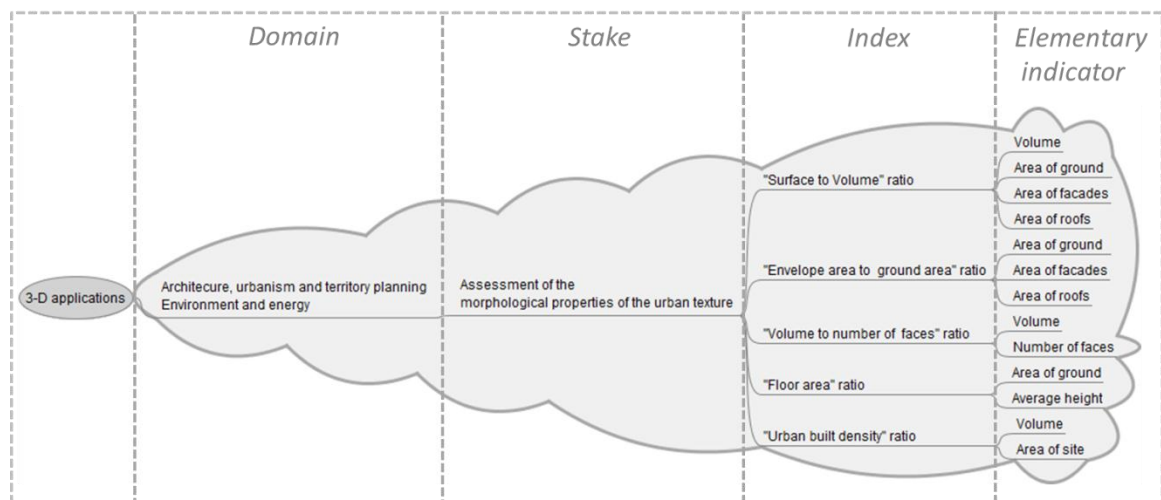


Figure 4.8. The stake “assessment of the morphological properties of the urban texture” and its inherent five indexes.

4.2.6.3 Exploration of the solar potential on the urban fabric

According to the interviews made with the end-users and considering a better organization of the requirements presented, in this case the stake “exploration of the solar potential on the urban fabric” can be divided into five sub-stakes:

- Exploration of the solar irradiation on building roofs;
- Estimation of the coverage and impact of vegetation on roofs;
- Estimation of the influence of shadowing and Sky View Factor (SVF) on the urban texture;
- Exploration of the solar irradiation on building facades;
- Potential for active solar energy.

These five stakes are presented as follows.

Exploration of the solar irradiation on building roofs

- The stake is represented and evaluated by one complex indicator (Figure 4.9):
 ⇒ *complex indicator* – represents the “Radiation collected by roofs”, which is calculated using four elementary indicators (“Shadowing”, “SVF”, “Slope” and “Orientation”);

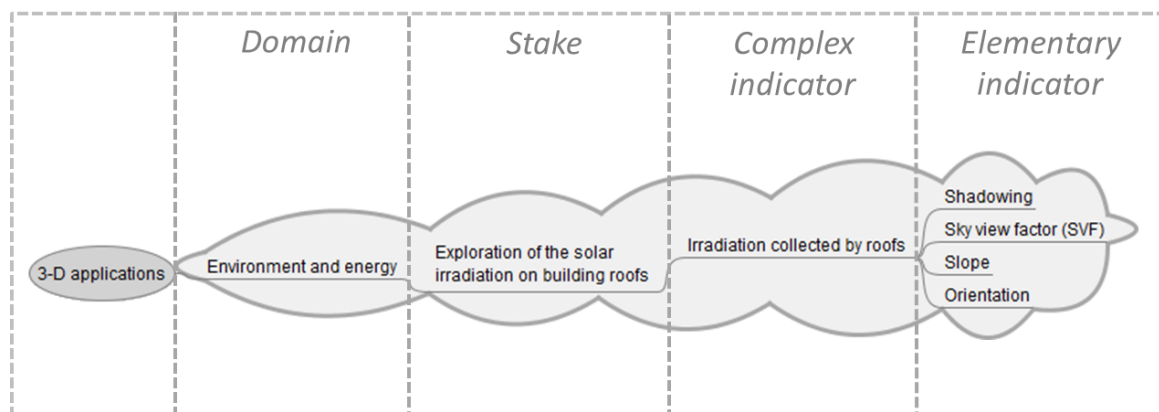


Figure 4.9. The stake “exploration of the solar irradiation on building roofs” and its inherent complex indicator.

Estimation of the coverage and impact of vegetation on roofs

- The stake is represented and evaluated by two indexes:
 ⇒ *index 1* – represents the “Vegetation coverage” ratio (expressed in percentage), which is calculated by dividing the 2.5-DUSM that includes urban vegetation and the one purged from this information, as shown in Figure 4.10.

4.2. Pilot project: state of Geneva

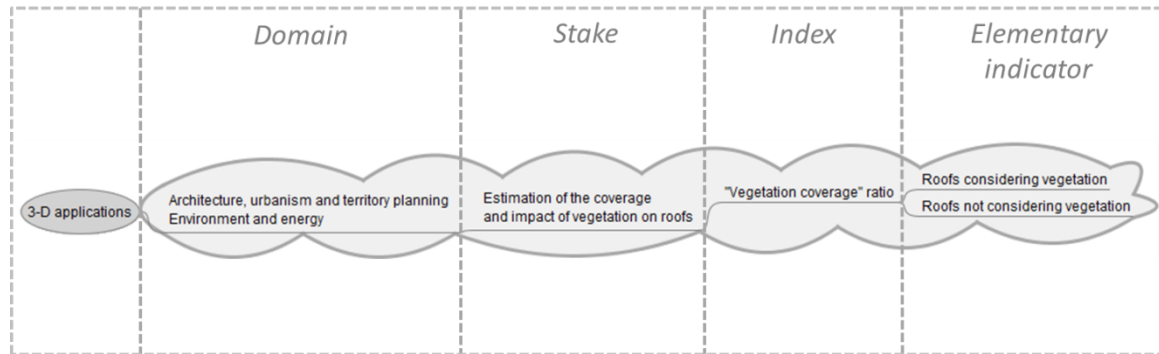


Figure 4.10. The stake “estimation of the coverage and impact of vegetation coverage on roofs” and its inherent index n°1.

⇒ index 2 – represents the “Vegetation impact” ratio (expressed in percentage), which is calculated by dividing the aggregated complex “Radiation collected by roofs considering existing urban vegetation” and the complex indicator “Radiation collected by roofs not considering existing urban vegetation”, as shown in Figure 4.11. The process used to derive both complex indicators is similar to the one shown in Figure 4.9, differing solely on the data used.

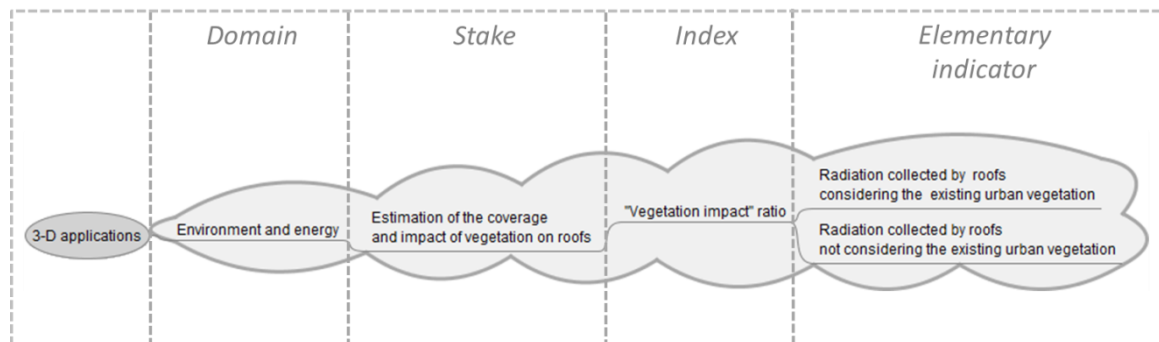


Figure 4.11. The stake “estimation of the coverage and impact of vegetation coverage on roofs” and its inherent index n°2.

Estimation of the influence of shadowing and SVF on the urban texture

- The stake is represented and evaluated by the index “Influence of shadowing and SVF”, which is calculated by dividing the complex indicator “Radiation over the urban texture considering shadowing and SVF” and the complex indicator “Radiation over the urban texture not considering shadowing and SVF”, as shown in Figure 4.12. The process used to derive both complex indicators is similar to the one shown in Figure 4.9. The only difference comes from the fact that for the complex indicator “Radiation over the urban texture not considering shadowing and SVF” the elementary indicators, “Shadowing” and “SVF”, are not contemplated for analysis.

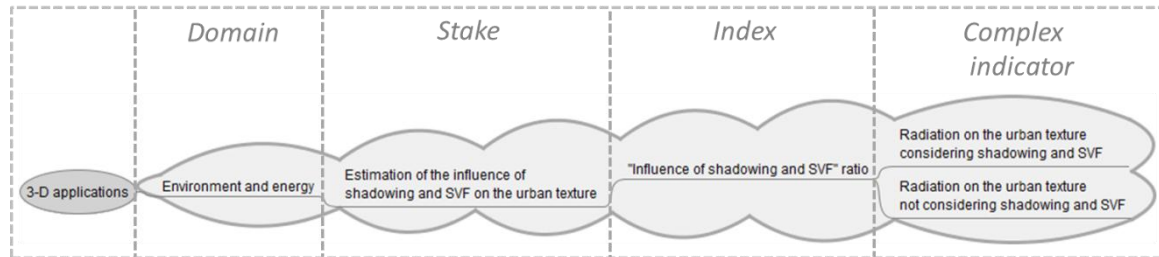


Figure 4.12. The stake “estimation of the influence of shadowing and SVF on the urban texture” and its inherent index.

Exploration of the solar irradiation on building facades

- The stake is represented and evaluated by one complex indicator (Figure 4.13):
 ⇒ *complex indicator* – represents the “Radiation collected by facades”, which is calculated using three elementary indicators (“Shadowing”, “SVF” and “Orientation”);

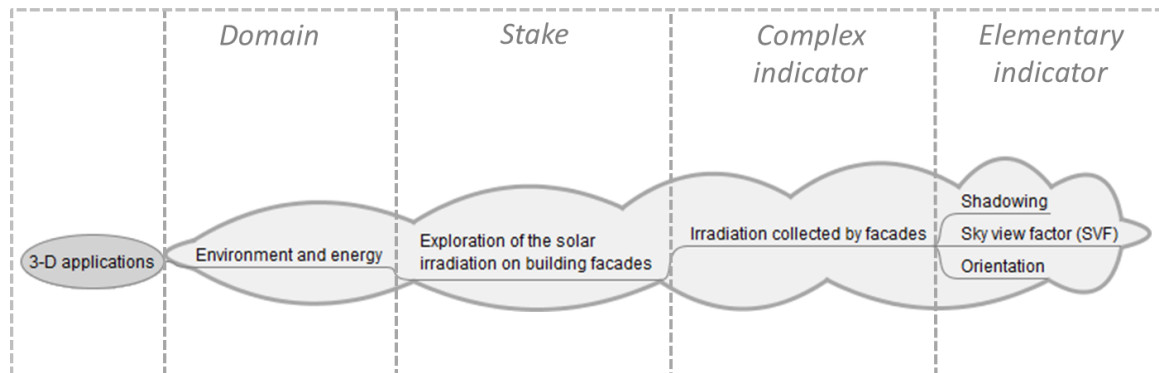


Figure 4.13. The stake “exploration of the solar irradiation on building facades” and its inherent complex indicator “irradiation collected by facades”.

Potential for active solar energy

- The stake is represented and evaluated by the complex indicators “Photovoltaic energy production on building roofs” and “Thermal energy production on building roofs, which are calculated using four elementary indicators (“Shadowing”, “SVF”, “Slope” and “Orientation”), as shown in Figure 4.14.

4.2. Pilot project: state of Geneva

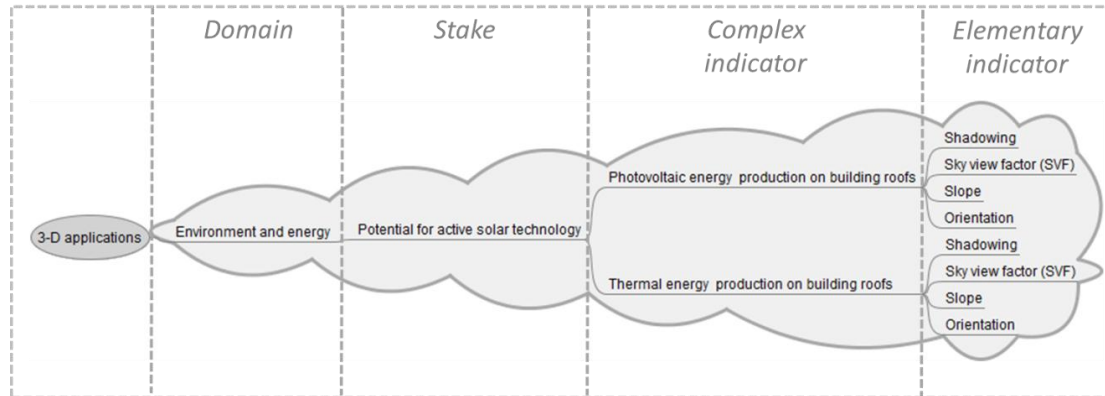


Figure 4.14. The stake “potential for active solar energy” and its inherent complex indicators.

4.2.6.4 Estimation of the energy demand on the urban fabric

According to the interviews made with the end-users and considering a better organization of the requirements presented, in this case the stake “estimation of the energy demand on the urban fabric” can be divided into two sub-stakes:

- Estimation of the heating demand on the urban fabric;
- Estimation of the lighting demand on the urban fabric.

These two stakes are presented as follows.

Estimation of the heating demand on the urban fabric

- The stake is represented and evaluated by the complex indicators “Seasonal heat losses”, “Seasonal thermal energy requirements”, “Seasonal gains” and “Seasonal thermal energy needs”, which are calculated using several elementary and complex indicators, as shown in Figure 4.15.

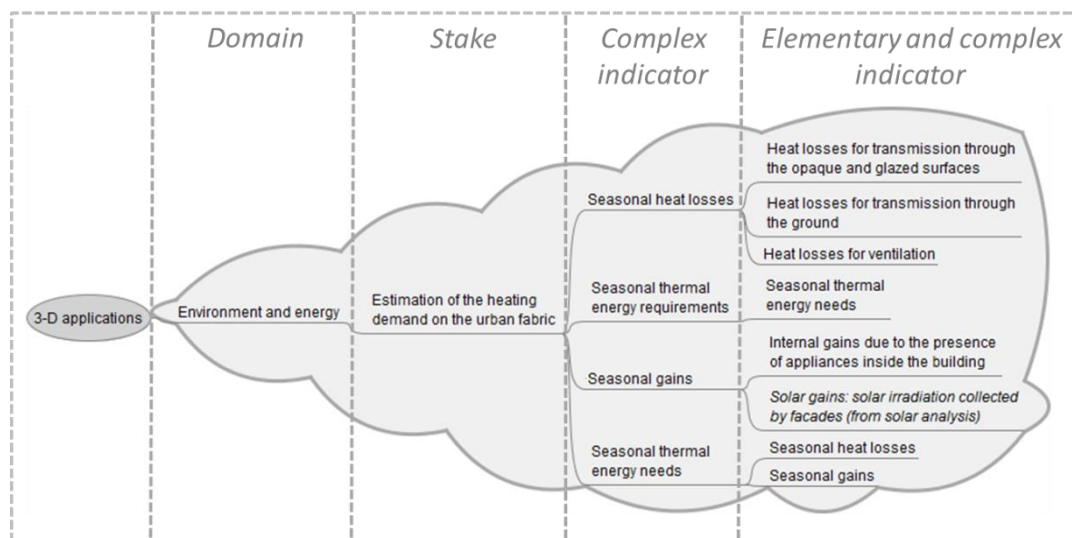


Figure 4.15. The stake “estimation of the heating demand on the urban fabric” and its inherent complex indicators.

Estimation of the lighting demand on the urban fabric

- The stake is represented and evaluated by the complex indicator “Lighting demand analysis”, which is calculated using the elementary indicator “Passive and no passive areas analysis” and the complex indicator “Radiation collected by facades”, as shown in Figure 4.16.

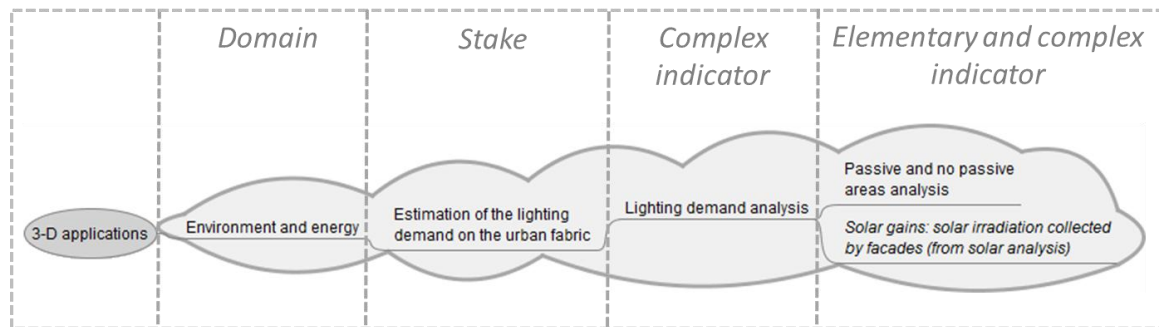


Figure 4.16. The stake “estimation of the lighting demand on the urban fabric” and its inherent complex indicator.

4.2.7 Visualization of indicators

In the field of 3-D, the *utility* expectations of users about the proposed visualizations of urban indicators have not yet gained much attention within the world of research. Thus, it is essential to propose visualization displays that are in conformity with user’s needs. For this reason, the questionnaires undertaken with the six groups of end-users of the city of Geneva also included a preliminary evaluation about the different possibilities of visualization for the indicators and indexes shown in sections 4.2.5 and 4.2.6. The results of the interviews were compared for each of the existing six groups of end-users.

This classification allows for a preliminary definition about visualization regarding the following questions:

- The indicator or index should be visualized?
- For the indicators and indexes that should be visualized which type(s) of representation (2-D, 3-D, or both) should be used?

Results of the two questions above are shown in Table 4.4 and Table 4.5. In the latter, the indicators shown in bold and italic are those that due to its innovative characteristics were researched and extracted under this study, as shown in the third part of this thesis.

4.2. Pilot project: state of Geneva

Domain	Stake	Indicator	To be visualized?	Type of visualization
Architecture, urbanism and territory planning	Respect of construction standards	Comparison between height of buildings and standards	No	---
	Maximize the quality of the built environment <i>Estimation of the urban vegetation density</i>	Visibility analysis	Yes	2-D and 3-D
		Sunshine analysis	Yes	2-D and 3-D
		<i>Area of a site</i> <i>Volume of vegetation</i>	No No	--- ---
Environment and energy	Minimization of the concentration of pollutants in the urban texture	Flow and air dispersion	Yes	3-D
	Minimization of inhabitants exposed to radiation sources	Zones of the frontages of buildings exposed to radiation sources	Yes	3-D
	<i>Estimation of the solar irradiation on building roofs</i>	<i>Radiation collected by roofs</i>	Yes	2-D and 3-D
	<i>Exploration of the solar irradiation on building facades</i>	<i>Radiation collected by facades</i>	Yes	2-D and 3-D
	<i>Potential for active solar energy</i>	<i>Photovoltaic energy production on building roofs</i>	Yes	2-D
	<i>Potential for active solar energy</i>	<i>Thermal energy production on building roofs</i>	Yes	2-D
	<i>Estimation of the heating demand on the urban fabric</i>	<i>Seasonal thermal energy requirements</i>	Yes	2-D and 3-D
		<i>Seasonal heat losses</i>	Yes	2-D and 3-D
		<i>Seasonal gains</i>	Yes	2-D and 3-D
<i>Estimation of the lighting demand on the urban fabric</i>	<i>Lighting demand analysis</i>	Yes	2-D and 3-D	
Architecture, urbanism and territory planning + environment and energy	<i>Assessment of the morphological properties of the urban texture</i>	<i>Volume (building)</i>	No	---
		<i>Area of site</i>	No	---
		<i>Area of ground (building)</i>	No	---
		<i>Area of storey (building)</i>	No	---
		<i>Area of facades (building)</i>	No	---
		<i>Area of roofs (building)</i>	No	---
		<i>Number of faces (building)</i>	No	---
		<i>Average height (building)</i>	Yes	3-D
<i>Type of roof</i>	Yes	3-D		
Urban traffic	Minimization of inhabitants exposed to noise	Level of noise	Yes	2-D and 3-D
	Minimization of inhabitants exposed to pollution	Level of pollution	Yes	2-D and 3-D
	Guarantee maximum safety for airplanes	Risks for airplanes	Yes	3-D
Pedestrian and cyclist mobility	Motivate the "sweet mobility"	Road and pavement slope analysis	Yes	3-D
Security and emergency situations management	Minimization of flood risk	High risk zones	Yes	2-D and 3-D
	Selection of suitable building roofs for helicopter landing	Flat and large roofs	Yes	3-D
Underground information	Integration of 3-D urban surface and underground data	Detection of zones of conflict	Yes	2-D and 3-D

Table 4.4. Type of visualization considered for each indicator.

Chapter 4. User requirements analysis

Domain	Stake	Index	To be visualized?	Type of visualization
Architecture, urbanism and territory planning	<i>Estimation of the urban vegetation density</i>	"Vegetation density of a site" ratio	No	---
Environment and energy	<i>Estimation of the coverage and impact of vegetation on roofs</i>	"Vegetation impact" ratio	No	---
Architecture, urbanism and territory planning + environment and energy	<i>Estimation of the energy demand on the urban fabric</i>	"Passive and no passive" ratio (buildings)	Yes	3-D
		"Surface to volume" ratio (buildings)	Yes	3-D
	<i>Assessment of the morphological properties of the urban texture</i>	"Envelope are to ground area" ratio (buildings)	No	---
		"Urban built density" ratio (buildings)	No	---
		"Volume to number of faces" ratio (buildings)	No	---
		"Floor area" ratio (buildings)	No	---
	<i>Estimation of the coverage and impact of vegetation on roofs</i>	"Vegetation coverage" ratio	Yes	2-D
<i>Estimation of the influence of shadowing and SVF on the urban texture</i>	"Influence of shadowing and SVF" ratio	No	---	

Table 4.5. Type of visualization considered for each index.

Finally, for the cases where 3-D visualization should be used and according to the CityGML standard shown in section 3.8.3, two final questions were placed:

- which scales of 3-D visualization should be used?
- which level of detail (LoD) should be used for each scale of representation?

Results of the two questions above are shown in Table 4.6 and Table 4.7. In the latter, the indicators shown in bold and italic are those that due to its innovative characteristics were researched and extracted under this study, as emphasized in the third part of this thesis.

4.3. Conclusions and chapter synthesis

Domain	Stake	Indicator	Scale of 3-D visualization	Level of Detail (LOD)
Architecture, urbanism and territory planning	Maximize the quality of the built environment	Visibility analysis	City	LOD0
		Sunshine analysis	Neighborhood	LOD0
			Building	LOD1
Environment and energy	Minimization of the concentration of pollutants in the urban texture	Flow and air dispersion	City	LOD0
	Minimization of inhabitants exposed to radiation sources	Zones of the frontages of buildings exposed to radiation sources	Neighborhood	LOD2 (it may include other urban objects)
			Building	LOD1
	<i>Exploration of the solar irradiation on building roofs</i>	<i>Radiation collected by roofs</i>	City	LOD0
			Neighborhood	LOD1 / LOD2 (without other urban objects)
	<i>Exploration of the solar irradiation on building facades</i>	<i>Radiation collected by facades</i>	City	LOD0
			Neighborhood	LOD1 / LOD2 (without other urban objects)
	<i>Estimation of the heating demand on the urban fabric</i>	<i>Seasonal thermal energy requirements</i>	City	LOD0
			Neighborhood	LOD1 / LOD2 (without other urban objects)
			City	LOD0
			Neighborhood	LOD1 / LOD2 (without other urban objects)
			City	LOD0
			Neighborhood	LOD1 / LOD2 (without other urban objects)
	<i>Estimation of the lighting demand on the urban fabric</i>	<i>Lighting demand analysis</i>	City	LOD0
Neighborhood			LOD1 / LOD2 (without other urban objects)	
Architecture, urbanism and territory planning + environment and energy	<i>Assessment of the morphological properties of the urban texture</i>	<i>Average height (building)</i>	City	LOD1
			Neighborhood	LOD1
		<i>Type of roof</i>	City	LOD2 (it may include other urban objects)
			Building	LOD3 (it may include other urban objects)
Urban traffic	Minimization of inhabitants exposed to noise	Level of noise	City	LOD0
			Neighborhood	LOD1
			Building	LOD2 (it may include other urban objects)
	Minimization of inhabitants exposed to pollution	Level of pollution	City	LOD0
			Neighborhood	LOD1
			Building	LOD2 (it may include other urban objects)
Guarantee maximum safety for airplanes	Risks for airplanes	City	LOD2 (it may include other urban objects)	
		Neighborhood	LOD2 (it may include other urban objects)	
Pedestrian and cyclist mobility	Motivate the "sweet mobility"	Road and pavement slope analysis	City	LOD0
Security and emergency situations management	Minimization of flood risk	High risk zones	City	LOD0
			Neighborhood	LOD2 (it may include other urban objects)
	Selection of suitable building roofs for helicopter landing	Flat and large roofs	City	LOD2 (it may include other urban objects)
			Building	LOD2 (it may include other urban objects)
Underground information	Integration of 3-D urban surface and underground data	Detection of zones of conflict	Neighborhood	LOD2 (it has to include other urban objects)
			Building	LOD2 (it has to include other urban objects)

Table 4.6. Scales of 3-D visualization and Levels of Detail (LoD) to be used for the representation of the urban indicators.

Domain	Stake	Index	Scale of 3-D visualization	Level of Detail (LOD)
Architecture, urbanism and territory planning + environment and energy	<i>Estimation of the energy demand on the urban fabric</i>	<i>"Passive and no passive" ratio (buildings)</i>	City	LOD0
			Neighborhood	LOD0
		<i>"Surface to volume" ratio (buildings)</i>	City	LOD1
			Neighborhood	LOD1

Table 4.7. Scales of 3-D visualization and Levels of Detail (LoD) to be used for the representation of the urban indexes.

The results of these first questionnaires and interviews were not used for statistical analysis. Instead, they were only used to initially define, for the extracted indicators of this study that should be visualized, a correct representation according to end-users' needs. For the cases where 2-D and 3-D visualizations should be considered, a comparison between the *utility* of different 2-D and 3-D displays of these indicators is also undertaken as the final step of this study - for more details please consult chapter 9.

4.3 Conclusions and chapter synthesis

This chapter presents the definition of the indicator system related to the needs on 3-D urban indicators of the end-users of the State of Geneva, based on the top-down process proposed by Maystre and Bollinger (1999) – it is implemented in the form of a specific conceptual model inherent to this case-study, organized in four main steps:

- Domains;

Chapter 4. User requirements analysis

- Stakes;
- Indicators: elementary and complex;
- Indexes.

The three main stakes adopted for this study were defined according to thematic end-user needs, the organization of the indicators to be extracted and innovative aspects of the research to be implemented:

- Assessment of the morphological properties of the urban texture;
- Exploration of the solar potential on the urban fabric;
- Estimation of the energy demand on the urban fabric.

The very detailed and objective organization proposed for the set of indicators and indexes defined was only possible due to the participation of the different groups of end-users interested in this study. Indeed, end-users have a full understanding of reality, hence knowing very precisely which type of requirements should be defined. Thus, the top-down process presented in this thesis aimed to be as much objective and concise as possible. Indeed, without the convenient participation of the associated end-users such goal would have been impossible.

The definition of whether the indicators and indexes extracted in this study should be visualized is also important. In fact, this evaluation allows to the understanding of how displays of these indicators should be created. Moreover, the CityGML standard was adopted for the representation of indicators requiring 3-D visualization. An evaluation of the level of details (LoD) that should be used for the scales of analysis adopted for this study was also considered: city, neighbourhood and building. Thus, this preliminary inquiry showed that very detailed urban models, on its own, do not offer an effective solution for geo-visualization of the majority of the 3-D UEQ indicators defined as being relevant.

According to the methodology proposed by Maystre and Bollinger (1999), next chapter will focus on the *bottom-up* process. Thus, different methods related to the use of 2-D and 3-D data applied to the construction of the adapted models will be proposed. In the third part of this thesis, using novel methods based on image processing techniques, such models will be used for the extraction of the UEQ indicators defined in this chapter.

CHAPTER 5. DATA SOURCES USED AND MODELS CONSTRUCTED¹

¹ The main concepts of this chapter were published in:

Carneiro, C., Karzand, M., Golay, F., Lu, Y. M., Vetterli, M. (2009) Assessing Digital Surface Models by Verifying Shadows: A Sensor Network Approach. In: Devillers, R., Goodchild, H. (Eds.), *Spatial Data Quality: From Process to Decisions*. CRC Press, Boca Raton, Florida, USA, pp. 147-61.

Carneiro, C., Morello, E., Desthieux, G., Golay, F. (2010) Urban environmental quality indicators: application to solar radiation and morphological analysis on built area. *Proceedings of the 3rd WSEAS Conference: Advances in Visualization, Imaging and Simulation*, 3rd and 4th November, Faro, Portugal, pp. 141-148. ISBN: 978-960-474-246-2. (Best student paper award).

5.1 Introduction

This chapter proposes innovative methods, grouping new models and tools, in order to aggregate different 2-D and 3-D data sources. Thus, the urban environmental quality (UEQ) indicators can be accurately extracted, complementing and concluding the conceptual model proposed for this study, by adding the *bottom-up* process proposed by Maystre and Bollinger (1999). It follows the *top-down* process presented in the previous chapter, where relevant indicators were defined according to issues and goals expressed by end-users.

The following sections introduce information about: (5.2) – context, assumptions and different scenarios, (5.3) – geo-referenced data sources available, (5.4) - selected indicators: geo-referenced data sources used and definition of the models to be constructed, (5.5) – construction of the different 2.5-DUSM used, (5.6) – creation of masks for the enhancement of the 2.5-DUSM used, and (5.7) – segmentation of planar roof areas.

Finally, two *punch-cases* are highlighted by the end of this section: (5.8) – *punch-case*: assessing the accuracy of the constructed and enhanced 2.5-DUSM, and (5.9) – *punch-case*: assessing a sensor network by verifying shadows derived from a 2.5-DUSM of building outlines. The first *punch-case* (5.8) aim to statistically validate the use of the innovative methods that allow to construct the different models (mainly 2.5-DUSM) proposed and used in this thesis for the extraction of the UEQ indicators emphasized in the next chapters of this thesis. The second *punch-case* (5.9) introduces a novel study related to the use of a 2.5-DUSM of building outlines in order to validate solar irradiation measurements of a wireless sensor network. Finally, section (5.10) presents conclusions and chapter synthesis.

5.2 Context, assumptions and different scenarios

The availability of urban digital 3-D data and models has tremendously increased in the recent years. The World Wide Web, as well as geo-environments such as Google Earth, Microsoft Live and Geographic Information Systems (GIS) are rapidly changing the way urban information is acquired. Moreover, the evolution of information and communication technology (ICT) along with the increased power and storage capabilities of computers currently allow the management and processing of huge quantities of data. Therefore, a variety of tools and software aimed to permit the analysis of this type of data has been developed in the last decade (Teller and Azar, 2001; Takase *et al.*, 2003; Molines *et al.*, 2006). The accessibility of this data opens up various possibilities to extract rich information about cities. However today, the range of tools that offer useful applications at the city scale are lacking to a certain extent. Therefore, 3-D GIS seem to be the natural container for most of the proposed applications and the opportunity for new research and developments.

Before presenting the different scenarios that were considered for the construction of the different digital elevation models (DEM) and digital height models (DHM) constructed, defined in this study as 2.5-digital urban surface models (2.5-DUSM) and normalized 2.5-digital urban surface models (n2.5-DUSM) respectively, it is important to mention some assumptions about the geo-referenced data used for this study:

- All data sources used, as well as the geometric positioning accuracy between different data sources used are free of systematic errors;
- Only objects that are visible from an airborne point of view are taken into consideration for this study. This means that, for example, detailed structures on building facades and underground objects are not measured although they may represent a very interesting source of information for other kind of 3-D studies and applications;

- The only altimetric information used in this study is derived from LiDAR data, which means that the integration of other sources, such as imagery, was voluntarily put aside;
- The spatial distribution of LiDAR points is anisotropic, which means it does not have the same properties in all directions and the spacing of points is not always rigorously uniform;
- the construction of the different 2.5-DUSM proposed in section 5.5 for the extraction of the UEQ indicators was done without applying any kind of filter reduction on raw LiDAR data. Indeed, the construction of different 2.5-DUSM used did not cause problems on the management of LiDAR point clouds.

As presented in this chapter, by using one or more sources of geo-referenced information, the urban model can be constructed and the UEQ indicators can be derived at the neighbourhood and city scales. For instance, in the field of solar radiation, a significant amount of accurate software has been developed in the last decades at the scale of architecture for the analysis and simulation of the performance of small objects, such as buildings (Miguet and Groleau, 2002; Compagnon, 2004). However, those tools demonstrate to be inappropriate if larger parts of the urban fabric ought to be evaluated and, even with powerful means, the degree of accuracy would be too high for the purposes of analysis at the neighbourhood and city scales. Furthermore, the end users of the proposed tools are professionals in urban design and decision makers for environmental policies at the city scale. Batty *et al.* (1999) stressed the need to couple such CAD tools with 3-D GIS, so as to include data processing and spatial analysis, and to provide automated analysis on urban area. Thus, under this context, the capabilities of 2.5-DUSM for this type of analysis are explored in this thesis. As already mentioned in section 2.4, these models are in fact 2-D arrays whereby the intensity value of each element contains the elevation of the element itself. This simplification allows the model to be processed as a raster image, as a mathematical matrix, as highlighted in the next chapters of this thesis.

The different data sources available and selected aggregation processes used for the construction of the 3-D models applied in this thesis are shown in Figure 5.1. Those are based on different data sources, used for the construction of the six 2.5-DUSM used in this. Also the segmentation procedure based on LiDAR data applied in this thesis is shown in Figure 5.1.

5.2 Context, assumptions and different scenarios

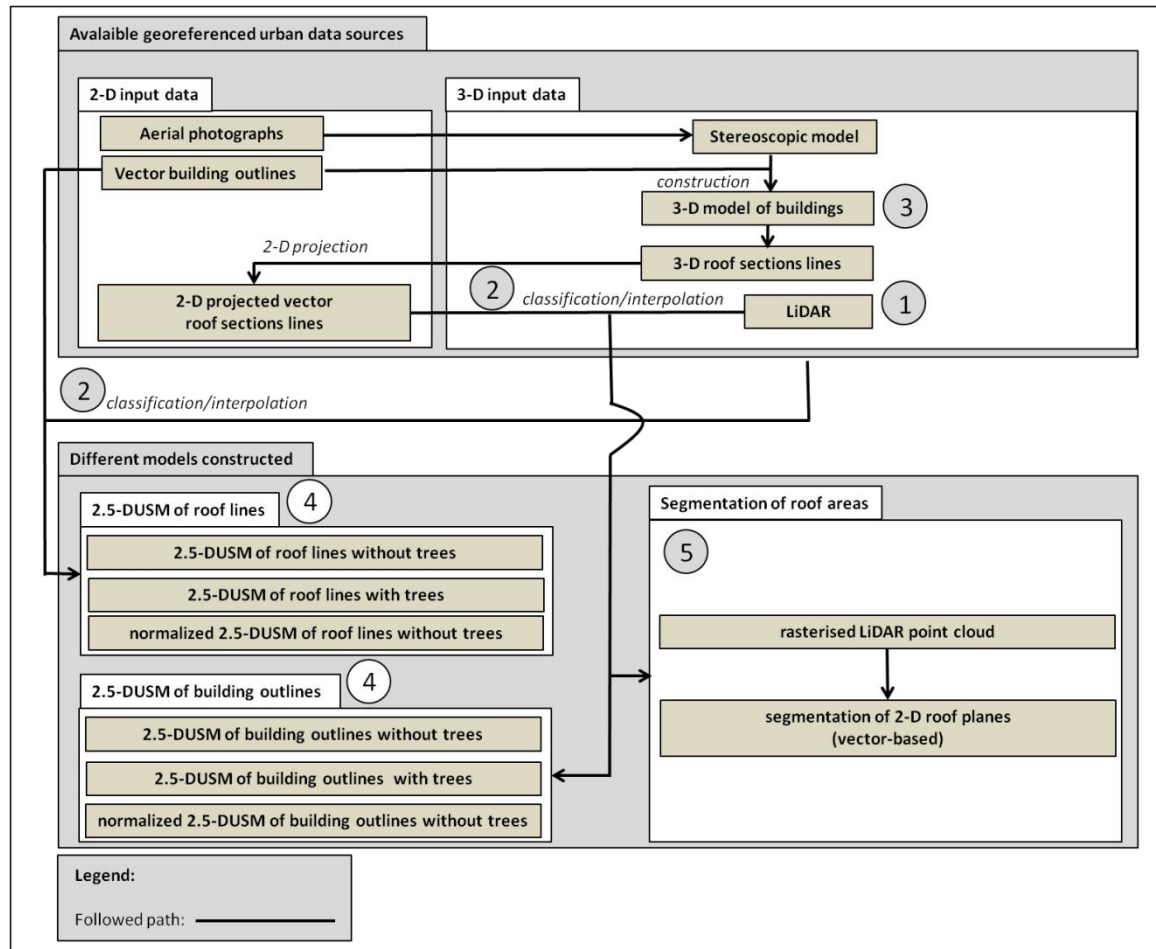


Figure 5.1. Different data sources available and selected aggregation processes used for the construction of the different 2.5-DUSM and the segmentation of roof areas.

According to the numbering (1 to 5) shown in Figure 5.1 some explanations are presented as follows:

- 1) LiDAR data allows a rapid and continuous predicting of urban form and phenomena, offering the possibility of constructing fast and automatic 2.5-DUSM. Thus, there is no need to refer to the construction of complex 3-D models (mainly LoD3 and LoD4) of the urban geometry. Nevertheless, if those are available the computation of most of the indicators presented in this thesis is also feasible;
- 2) the construction of different 2.5-DUSM is made on a step-by-step basis (Figure 5.2): LiDAR points corresponding to terrain, buildings and vegetation are independently analysed and interpolated. It is done using a hybrid approach combining: (1) LiDAR data and 2-D cadastral vector data of building outlines or (2) LiDAR data and the 2-D projection of 3-D vector data of roof lines (LoD2), that improves its final quality and reliability (Hofmann, 2004; Schwalbe *et al.*, 2005). Moreover, nowadays, 3-D building models up to LoD2 can be fully automatically extracted (Haala and Kada, 2010). Thus, no direct interpolation techniques, such as Kriging or Inverse Distance Weighting (IDW) are applied in this thesis for the construction of the 2.5-DUSM proposed. The reason to use a 2.5-DUSM instead of a DEM directly interpolated from LiDAR data is that along zones (edges) of discontinuity common DEM directly interpolated from LiDAR data are not reliable. Indeed, this is an important and innovative aspect that should be researched in

this thesis, otherwise some of the extracted UEQ indicators, mainly related to building's morphology, for instance the calculation of the area of external facades, wouldn't be trustworthy;

- 3) 3-D vector data corresponding to building roofs is used for the construction of a specific 2.5-DUSM of roof lines based on LiDAR data because in many cases building outlines do necessarily represent the outline of the building roof. This is particularly important when analysing solar irradiation on building roofs. Nevertheless, for this type of analysis in urban areas, when 3-D vector data corresponding to building roofs is not available, 2-D vector building outlines should be alternatively used for the construction of the 2.5-DUSM based on LiDAR data;
- 4) The distinction of two main independent 2.5-DUSM is important because, as already mentioned in point 3, in many cases the building outlines do not necessarily represent the outline of the building roof. Furthermore, it enables to save time for computation and avoids the generation of superfluous information that will be discarded regardless - normally, the construction of the city model is the result of numerous contributions that follow the same template. Hence, the importance of both accuracy of the reported objects and the adaptation (maintenance and evolution) of such models through time are not irrelevant issues. The normalized 2.5-DUSM is used to compute the morphological properties of buildings, such as the area of facades, because in this specific case pixel stores information about heights values and not altitude values. Logically, this last information is not useful for the morphological analysis of buildings. Moreover, normalized 2.5-DUSM are also used to slice the models into different storeys, for instance this procedure is used in the analysis of solar irradiation on building facades and presents a novel aspect of this research. The distinction between 2.5-DUSM with and without vegetation is applied for the extraction of UEQ indicators related to solar radiation, especially if the impact of vegetation on the solar irradiation collected by the urban texture needs to be assessed;
- 5) Finally, a segmentation of planar roof areas using raw LiDAR data is also considered, implemented and analysed. This procedure allows to determine important features, such as slope and orientation of roofs, and to classify the type of roof of each building according to three main primitives: flat, classic or complex. For instance, as described in chapter 4, this type of information is used as an elementary indicator for the calculation of the complex indicator "irradiation collected by roofs".

5.2 Context, assumptions and different scenarios

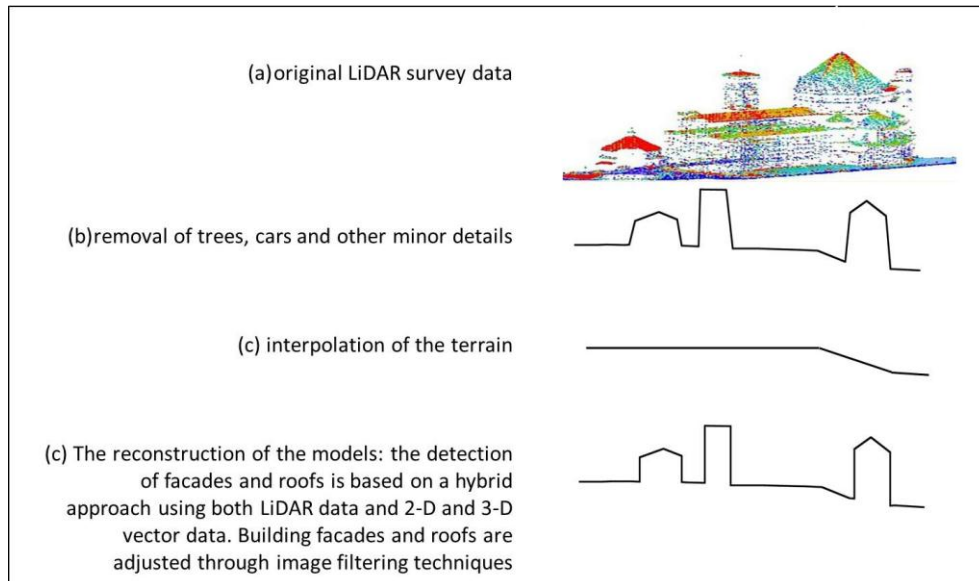


Figure 5.2. General overview of the process of construction of the 2.5-DUSM used in this study.

Besides these available data sources and selected aggregation processes, other possibilities could be also taken into account for the construction of the 3-D models applied in this thesis (Figure 5.3).

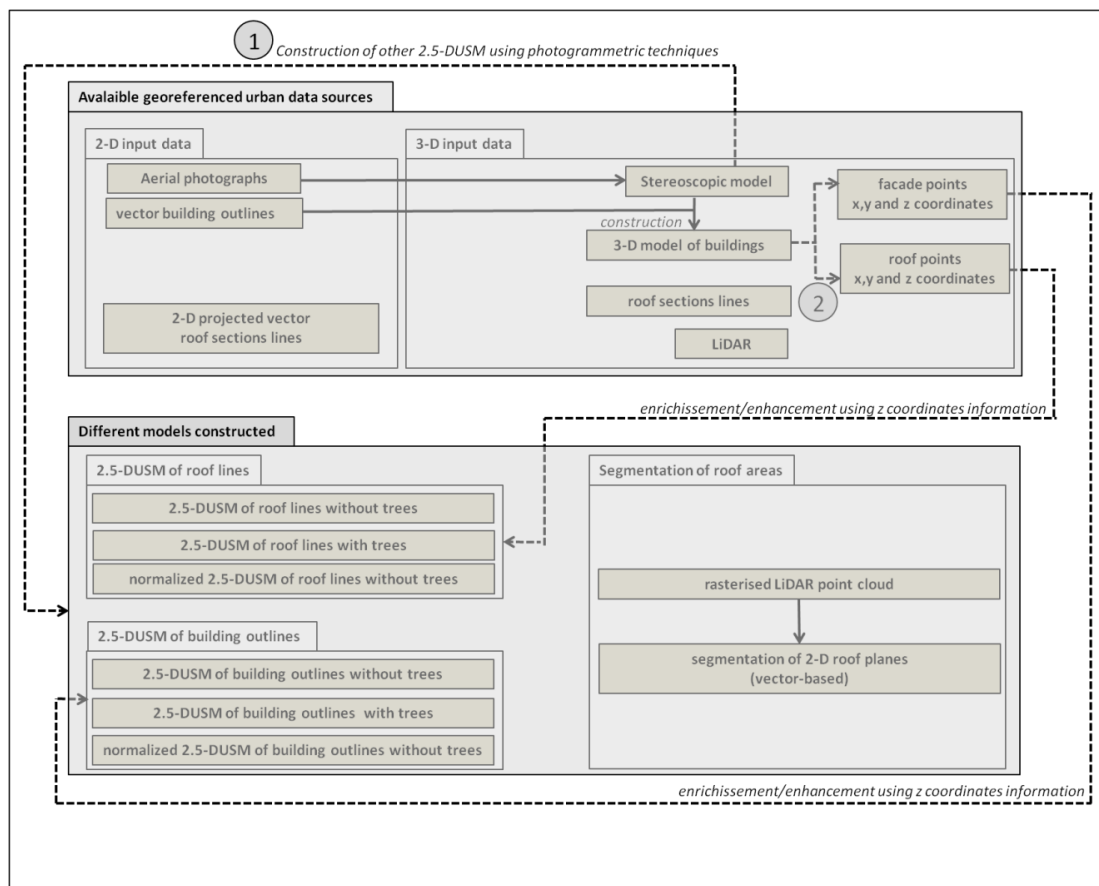


Figure 5.3. Alternative data aggregation processes not used for the construction of the different 2.5-DUSM.

According to the numbering (1 to 2) shown in Figure 5.3 some explanations are presented as follows:

- 1) compared with photogrammetry, LiDAR technology is able to penetrate vegetation (using different echoes), specially tree canopy. Thus, DEM (or 2.5-DUSM) generation from LiDAR data overcomes the limitations of photogrammetry for DEM generation in urban areas covered by vegetation, especially along building roofs (Liu, 2008). After an analysis of the end-users' requirements of the city of Geneva, this is an important topic that should be taken into account. For this reason, the construction of other 2.5-DUSM directly using photogrammetric techniques was not considered, even if such technique could have been also applied;
- 2) the possibility of integrating information about x , y and z coordinates of buildings facades and roofs stored in the available 3-D model of the state of Geneva in order to enrich and enhance the 2.5-DUSM only constructed from LiDAR data was not considered. Indeed, the main purpose of this research work was given to an analysis of the potential and limitation of LiDAR data for a fully automatic extraction of UEQ indicators. For instance, if 3-D vector roof models are available, x , y , z coordinates of roof edges can be used to interpolate information about roofs in a raster basis, followed by the construction of a 2.5-DUSM of roof lines. After, the UEQ indicator "exploration of the solar potential on building roofs" can be also computed;

5.3 Geo-referenced data sources available

Considering the assumptions and different scenarios presented in the previous section (5.2), the construction of 2.5-DUSM used for the extraction of the UEQ indicators is based on different data:

- *LiDAR data*: for the case-studies presented for the State of Geneva, the LiDAR data used has a density of 4 points/m², a planimetric accuracy of 20 centimetres RMSE and an altimetric accuracy of 15 centimetres RMSE (Vieira de Mello, 2006). For the case-studies presented for the cities of Lausanne and Florence the LiDAR data used has a density of 1 point/m², a planimetric accuracy of 20 centimetres RMSE and an altimetric accuracy of 15 centimetres RMSE. This information concerning the quality of LiDAR data used for the State of Lausanne and the city of Florence was given by them GIS departments. For more details about LiDAR technology please consult section 2.5.
- *2-D GIS building outlines*: the cadastral data stored in a 2-D GIS database can be used to extract vector information about building outlines, which is used to construct a more accurate 2.5-DUSM of building outlines. Usually, this type of data has an accuracy range of 5 to 10 centimetres RMSE. An example of 2-D GIS building outlines of a neighbourhood of the city of Geneva is presented in Figure 5.4.

5.3 Geo-referenced data sources available



Figure 5.4. 2-D GIS building outlines of a neighbourhood of the city of Geneva, Switzerland.

- ⇒ *2-D projection of 3-D roof lines*: The 3-D city model of the State of Geneva is used to extract the 2-D projection of 3-D vector data of roof lines. In this case, information about building roofs is also used to construct a more accurate 2.5-DUSM of roof lines. For the case-studies highlighted in this study, this type of data is only available in the State of Geneva. It is constructed by using a 3-D stereoscopic model based on aerial images, offering an accuracy of 25 centimetres RMSE (Vieira de Mello, 2006). The existing 3-D stereoscopic model offers a resolution of 16 centimetres RMSE, taken with a Vexcel camera, which is used for the semi-automatic digitalization of 3-D vector building outlines. Figure 5.5 shows a set of 3-D buildings belonging to a neighbourhood of the city of Geneva.



Figure 5.5. Set of 3-D buildings belonging to a neighbourhood of the city of Geneva, Switzerland.

An example of the 2-D projection of 3-D vector data of roof lines of a neighbourhood of the city of Geneva is presented in Figure 5.6.

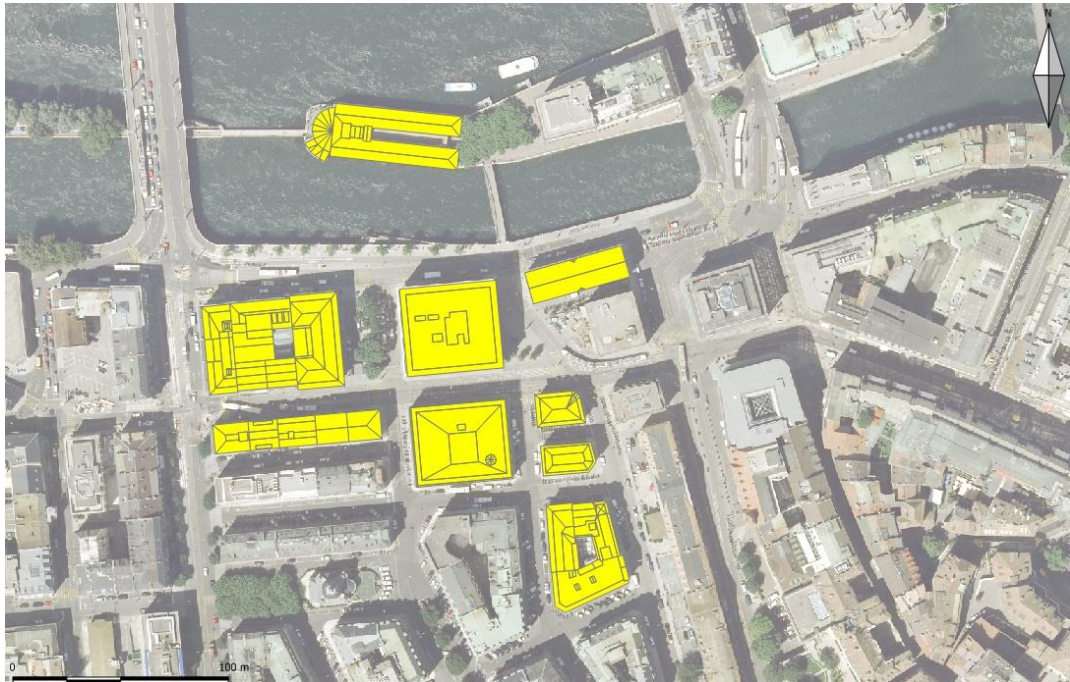


Figure 5.6. 2-D projection of 3-D roof lines of a neighbourhood of the city of Geneva, Switzerland.

⇒ *alphanumerical information about the volume, areas of façades and areas of roofs, which are compared with the same type of outputs resulting from the morphological analysis emphasized in chapter 6.*

5.4 Selected indicators: geo-referenced data sources used and definition of the models to be constructed

According to the list of indicators and indexes selected for this study (section 4.2.6), Table 5.1 presents both the geo-referenced data sources used and the definition of the models to be constructed for the extraction of each of these indicators.

5.5 Construction of the different 2.5-DUSM used

Data sources used	Models constructed	Indicator
- LiDAR data	- Normalized 2.5-DUSM of vegetation	- <i>Volume of vegetation</i>
- 2-D projection of 3-D vector roof lines - LiDAR data	- 2.5-DUSM of roof lines without vegetation or 2.5-DUSM of roof lines with vegetation (it can include segmentation of planar roof areas, converted into a raster format)	- <i>Shadowing of roofs</i> - <i>Sky view factor (SVF) of roofs</i> - <i>Slope of roofs</i> - <i>Orientation of roofs</i> - <i>Radiation collected by roofs</i> - <i>Roofs considering vegetation</i> - <i>Roofs not considering vegetation</i> - <i>Photovoltaic energy production on building roofs</i> - <i>Thermal energy production on building roofs</i>
- 2-D vector building outlines - LiDAR data	- 2.5-DUSM of building outlines without vegetation or 2.5-DUSM of building outlines with vegetation	- <i>Shadowing of building facades</i> - <i>Sky view factor (SVF) of building facades</i> - <i>Orientation of building facades</i> - <i>Radiation collected by facades</i> - <i>Lighting demand analysis</i>
- 2-D vector building outlines - LiDAR data	- Normalized 2.5-DUSM of building outlines	- <i>Volume (building)</i> - <i>Area of ground (building)</i> - <i>Area of facades (building)</i> - <i>Area of storey (building)</i> - <i>Passive and no passive areas analysis</i> - <i>Thermal demand analysis: 4 indicators</i>
- 2-D projection of 3-D vector roof lines - LiDAR data	- Normalized 2.5-DUSM of roof lines (it can include segmentation of planar roof areas, converted into a raster format)	- <i>Area of roofs</i>
- LiDAR data	- Digital Terrain Model (DTM)	- <i>Area of site</i>
- 2-D projection of 3-D vector roof lines - LiDAR data	- Segmentation of planar roof areas (for roof faces) - 2-D vector building outlines (for facade faces)	- <i>Number of faces (building)</i>
- 2-D vector building outlines - LiDAR data	- Normalized 2.5-DUSM of building outlines - 2-D vector building outlines (for transferring heights of pixels)	- <i>Average height (building)</i>
- 2-D projection of 3-D vector roof lines - LiDAR data	- Segmentation of planar roof areas	- <i>Type of roof</i>

Table 5.1. Data sources used and models constructed in order to extract the selected indicators.

In the following sections the different type of models constructed are presented, as well as the creation of masks and the digital image processing techniques applied in order to enhance the 2.5-DUSM used.

5.5 Construction of the different 2.5-DUSM used

5.5.1 Construction of the 2.5-DUSM without vegetation

In this case, four different cases of interpolating and constructing a 2.5-DUSM without vegetation are considered:

1. normalized³ 2.5-DUSM (n2.5-DUSM) of roof lines without vegetation;
2. 2.5-DUSM of roof lines without vegetation;
3. n2.5-DUSM of building outlines without vegetation;
4. 2.5-DUSM of building outlines without vegetation.

A synoptic view presenting the method applied for the construction of each of the four 2.5-DUSM without vegetation considered is shown in Figure 5.7.

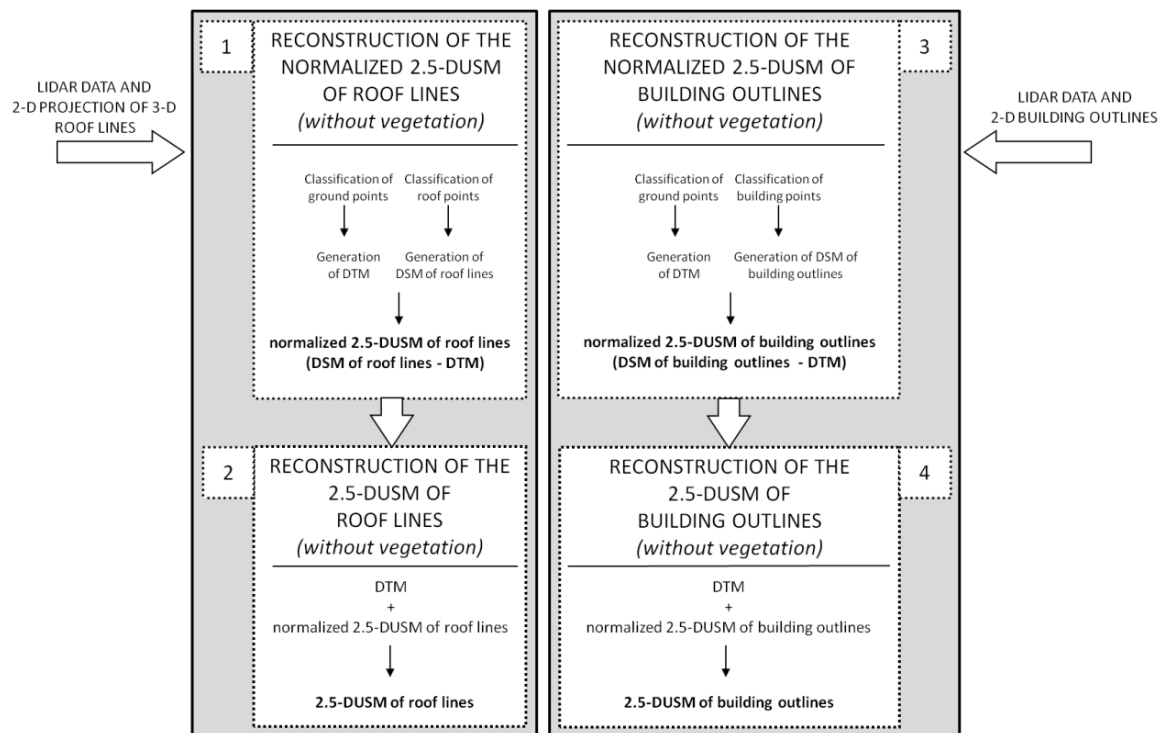


Figure 5.7. Synoptic view presenting the method applied for the construction of the four 2.5-DUSM without vegetation considered.

More detailed explanations related to the interpolation and construction of each of these four models is presented as follows.

Normalized 2.5-DUSM of roof lines without vegetation (case 1) and 2.5-DUSM of roof lines without vegetation (case 2)

As presented in Table 5.1, the interpolation and construction of the 2.5-DUSM of roof lines without vegetation includes the altitude values of all the roofs (not only at the roof edges) and terrain and is based on two data sources:

- raw LiDAR data;

³ As already mentioned in section 2.3 “normalized” refers not to a representation of elevation, but rather a representation of height.

5.5 Construction of the different 2.5-DUSM used

- 2-D projection of 3-D vector data of roof lines derived from a 3-D city model.

Firstly, a digital terrain model (DTM) is interpolated by classifying the LiDAR points according to the following sequential operations:

- Using a GIS software, LiDAR points contained within building polygons (outlines) and in the 1 meter buffer generated from building polygons are eliminated.
- Using the algorithms⁴ initially presented by Axelsson (1999) and available in TerraScan *software*, LiDAR points for which the elevation value varies significantly from surrounding points are considered to be points indicating features such as aerial points (for example, if the laser beam touches a bird), vegetation higher than 3 meters (trees) and vehicles, and are therefore removed.

Following the elimination of the points indicating all these features, a DTM can be interpolated only from ground points. Indeed, there is no significant difference among some of the existing gridding interpolation methods, such as the nearest neighbour binning, inverse distance weighting, triangulation with linear interpolation, minimum curvature, kriging and radial basis functions, that can be employed (using LiDAR data with a density of at least 1 point per m², such as in the case-study areas highlighted in this study) to generate a DSM (Gonçalves, 2006). All these interpolation methods are accessible in common GIS software available on the market. Due to its generalised use by the scientific community for DTM interpolation, the triangular interpolation was chosen.

Secondly, a value for each pixel of the DSM of roof lines, corresponding to a roof value for all the existing buildings on the areas of study, is interpolated (using only the LiDAR points classified as being contained within vector roof lines). Thus, a triangulation with linear interpolation is also applied to each of the roofs of the buildings. For each building, and more specifically for each pixel contained within, its roof height is taken to be the value of subtraction of the terrain elevation (calculated in the DTM interpolated) from the roof elevation of the DSM of roof lines.

Lastly, each roof is added to the DTM as a column (the borders are defined from the vector roof lines), using the roof height found previously for each pixel contained within, as described in last paragraph. The final result allows the construction of a 2.5-Digital Urban Surface Model (2.5-DUSM) of roof lines, which is composed only of information on terrain and roof altitudes.

Data sources needed for generating the 2.5-DUSM of roof lines are shown in Figure 5.8.

⁴ Already summarized in section 2.5.4.

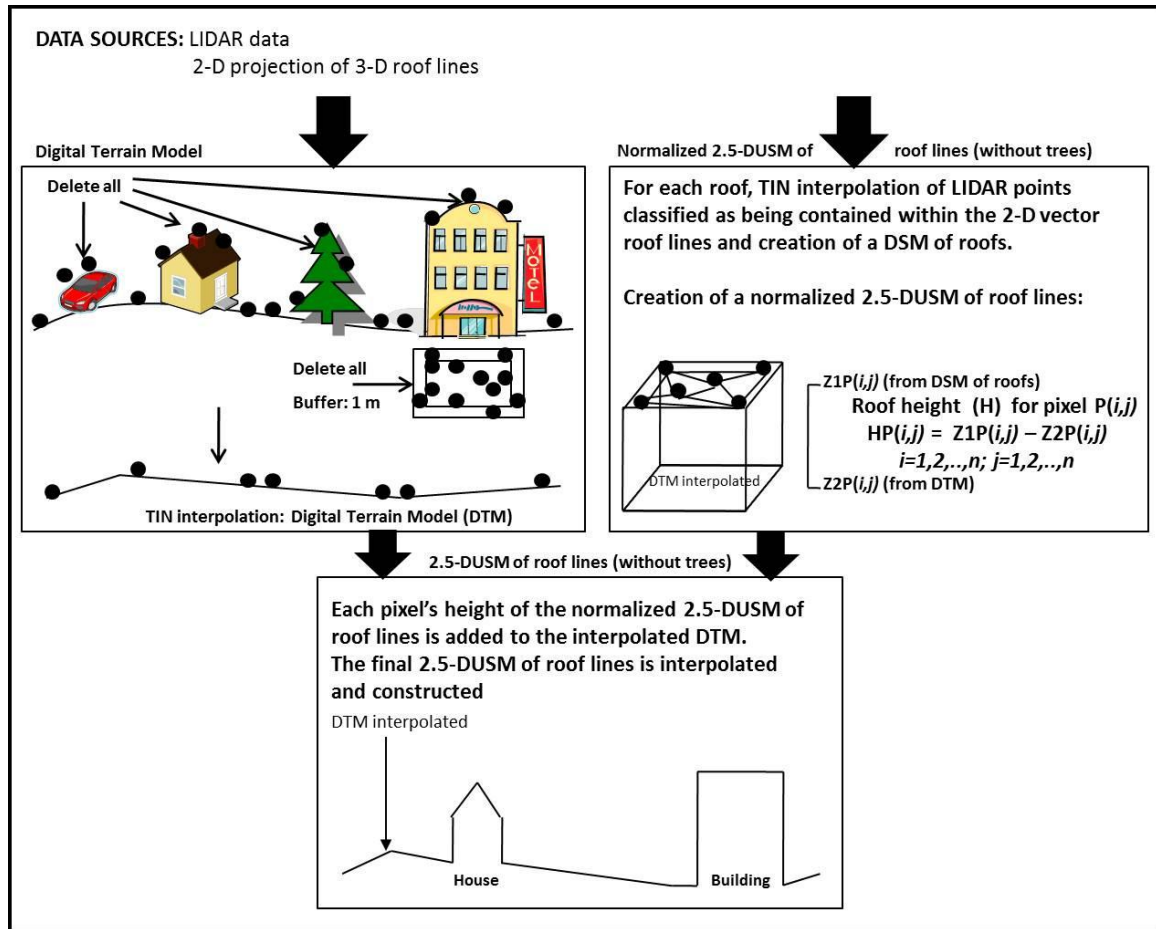


Figure 5.8. Interpolation and construction of the 2.5-D Urban Surface Model (2.5-DUSM) without vegetation.

2.5-DUSM of building outlines without vegetation (case 3) and normalized 2.5-DUSM of building outlines without vegetation (case 4)

As presented in Table 5.1, the interpolation and construction of the 2.5-DUSM of building outlines (also called building footprints) without vegetation is based on two data sources:

- raw LiDAR data;
- 2-D vector data of building outlines stored in a GIS database.

The interpolation and construction of these models is similar to the one presented for the n2.5-DUSM of roof lines, such as presented in Figure 5.8. The only difference is concerned with the vector data used, that in the present case refers to the building outlines and not the roof lines.

5.5.2 Construction of the normalized 2.5-DUSM of vegetation

Such as presented in Figure 5.9, the construction of the 2.5-DUSM of vegetation is rather simple and is based on two main steps:

5.5 Construction of the different 2.5-DUSM used

- according to the algorithm initially proposed by Axelsson (1999) and available in *TerraScan software*, LiDAR points considered to be vegetation higher than three meters (trees) are classified;
- for each pixel considered to be a vegetation, its height is taken to be the value of the difference between vegetation elevations (using only first echoes of raw LiDAR data) and the 2.5-DUSM of roof lines without vegetation. At the final of this step the normalized 2.5-DUSM of vegetation is constructed.

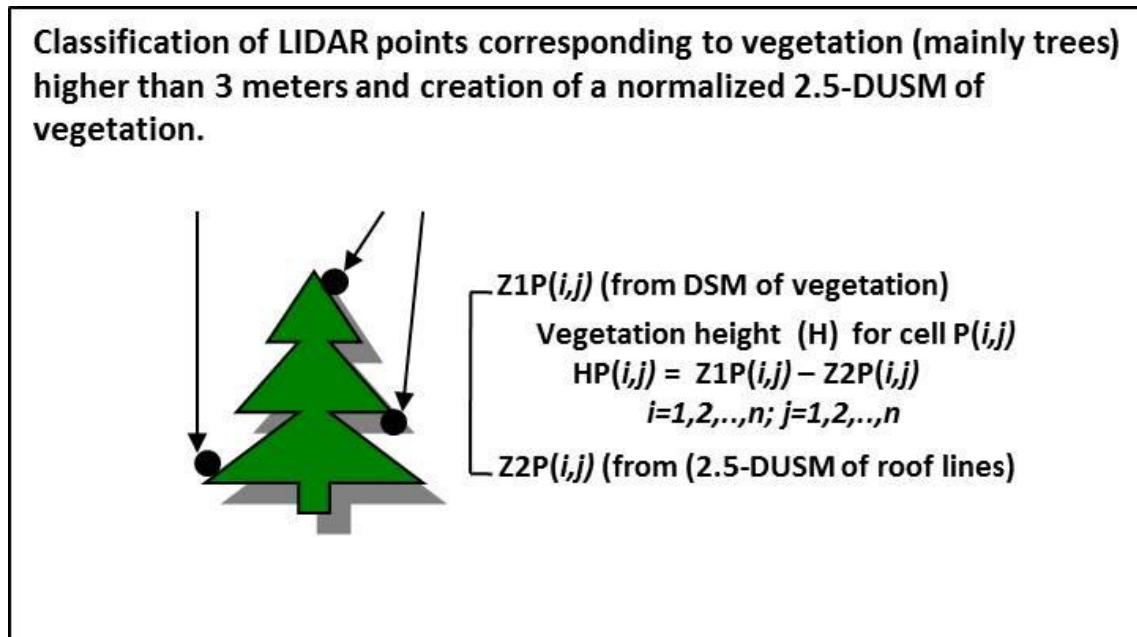


Figure 5.9. Method applied for the construction of the 2.5-DUSM of vegetation.

5.5.3 Construction of the 2.5-DUSM of roof lines and the 2.5-DUSM of building outlines with vegetation

The construction of both the 2.5-DUSM of roof lines with vegetation and the 2.5-DUSM of building outlines with vegetation is very similar to the one presented in section 5.5.1, which does not consider vegetation. In this case, the main difference is that the normalized 2.5-DUSM of vegetation must be added to the 2.5-DUSM without vegetation, as shown in Figure 5.10.

Thus, in order to construct the 2.5-DUSM of roof lines with vegetation, each tree is added to the 2.5-DUSM of roof lines without vegetation, using the height found previously for each pixel considered as vegetation, as described in section 5.5.3.

The construction of the 2.5-DUSM of building outlines with vegetation is similar to the one presented for the 2.5-DUSM of roof lines with vegetation. The only difference is concerned with the vector data used, that in the present case refers to the building outlines and not the roof lines.

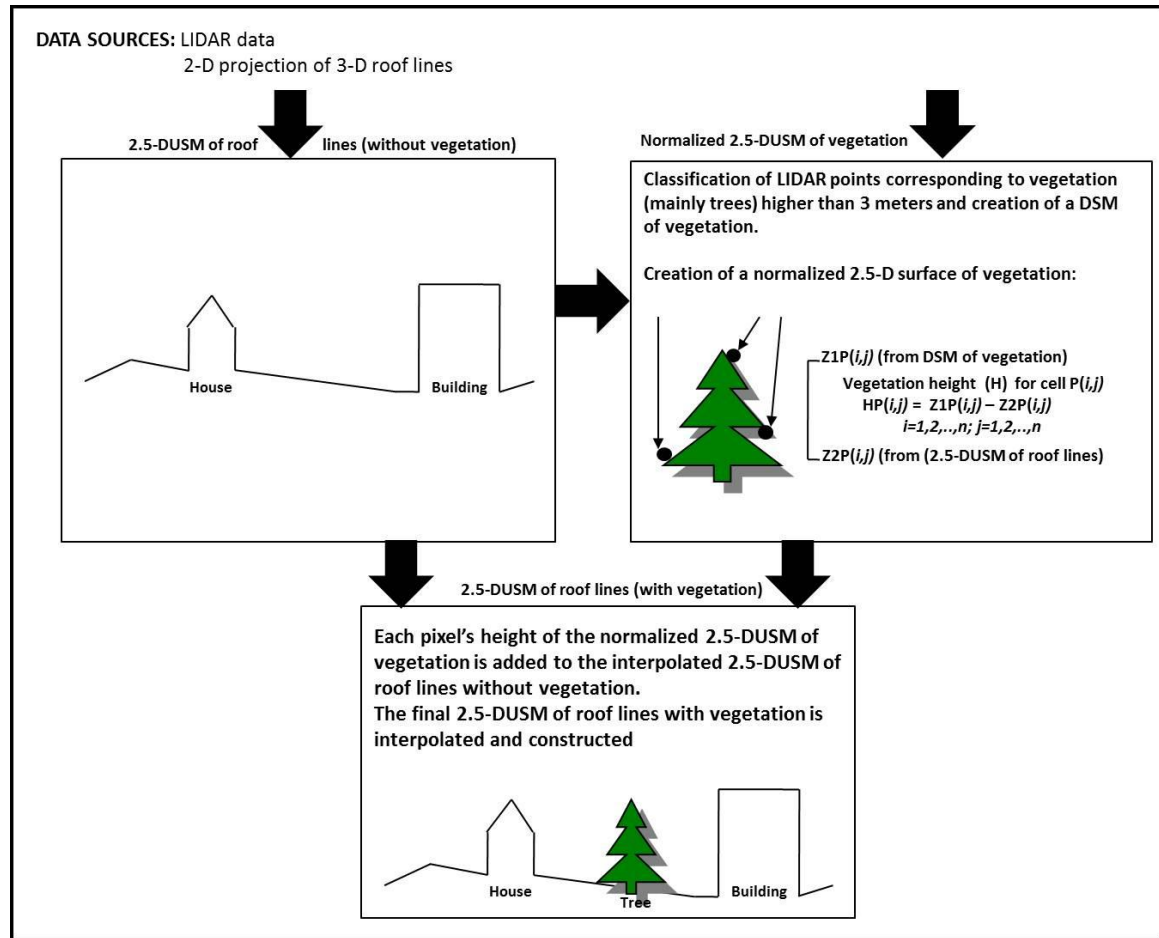


Figure 5.10. Interpolation and construction of the 2.5-D Urban Surface Model (2.5-DUSM) with vegetation.

5.6 Creation of masks for the enhancement of the 2.5-DUSM used

Depending on the 2.5-DUSM models used, the LiDAR points along edges of building roofs for which the elevation value varies significantly from surrounding points are considered to be points indicating features such as low points and should therefore be removed. Indeed, the wrong interpolation of these low points may result in higher noise at the pixels belonging to these zones of discontinuity of building roofs. In order to refine these models, a first attempt was made in order to classify and delete these low points directly using raw LiDAR data and applying the algorithm initially proposed by Axelsson (1999) available in *TerraScan* software. Nevertheless, results were not satisfying due to the difficulty in the classification of these points, especially along internal edges of building roofs that present higher complexity. For this reason, an alternative method is proposed inside the framework of this thesis:

- for each roof line, a single mask of each building outline is created using the transformation of the 2-D projection of 3-D roof lines vector data into a raster format. This mask is multiplied with the 2.5-DUSM of roof lines in order to create a mask corresponding the 2.5-DUSM of roof lines and after enhance it in a roof-by-roof basis. Figure 5.11 shows the procedure applied for the enhancement of the 2.5-DUSM of roof lines;

5.6 Creation of masks for the enhancement of the 2.5-DUSM used

- for each building outline, a single mask is created using the transformation of 2-D building footprints vector data into a raster format. This mask is multiplied by the 2.5-DUSM of building outlines in order to create a mask corresponding the 2.5-DUSM of building outlines and after enhance it in a building-by-building basis;
- in order to detect all the pixels belonging to each roof lines or building outline that need to be reclassified the central pixel of the 3 by 3 window filtering is selected by adding the condition of having at least four neighbour pixels that are higher (under a certain limit, usually one or two meters) than the pixel under analysis. The central pixel is corrected considering the four neighbour pixels that are at least one (or two) meters higher than the pixel under analysis and taking into account four different criteria of all its neighbour pixels: minimum, mean, median and maximum;
- at the end of the process, the enhanced 2.5-DUSM is constructed by replacing the pixels of roof lines or building outlines that changed in the not enhanced (original) 2.5-DUSM of roof lines or the not enhanced (original) 2.5-DUSM of building outlines respectively.

Finally, it is worth mentioning that two options were independently tested for the enhancement: (1) the reclassification is made to all pixels of the building, which means the enhancement is applied to all external and internal zones of discontinuity existing in a roof, and (2) the reclassification is only made to all pixels belonging to the external zones of discontinuity of the building.

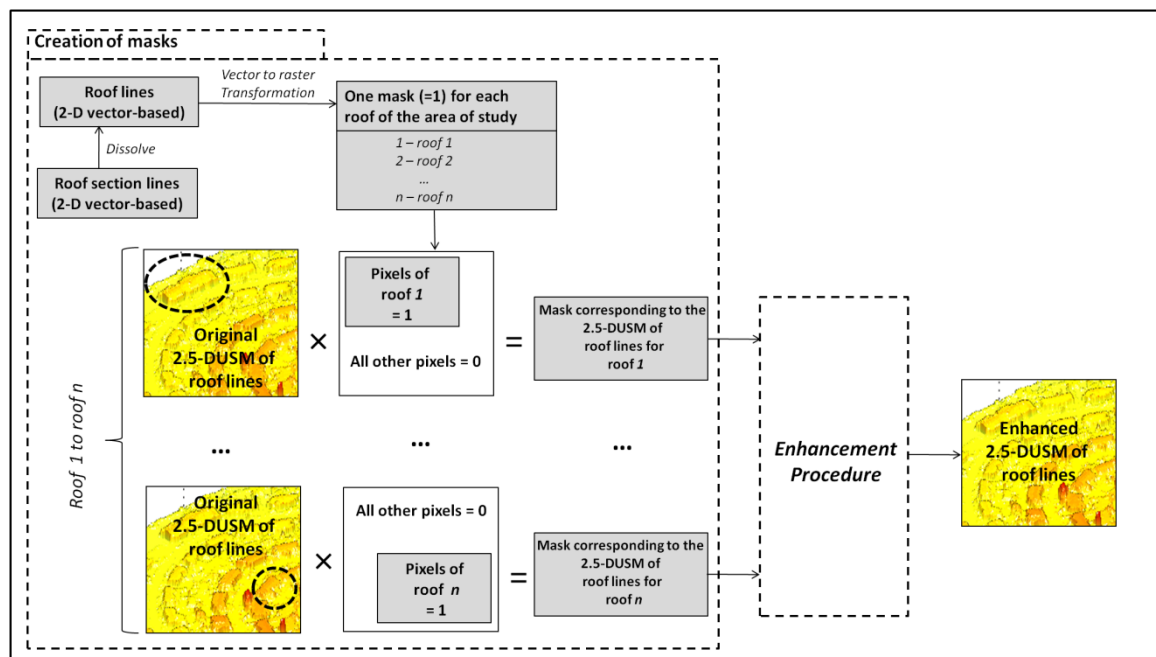


Figure 5.11. Method applied for the construction of masks (roof-by-roof basis) and the application of the enhancement procedure using the 2.5-DUSM of roof lines.

Figure 5.12 shows a theoretical example of the process applied for the enhancement of the 2.5-DUSM of roof lines using the maximum criteria. In this case the considered limit is equal to one meter.

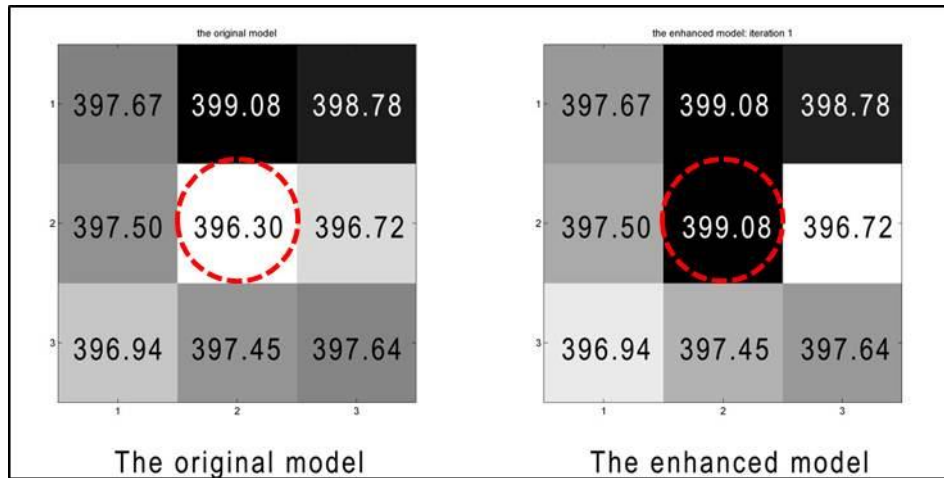


Figure 5.12. Theoretical example of the process applied for the enhancement of the normalized 2.5-DUSM of roof lines using the maximum criteria.

Figure 5.13 shows an example of the enhancement of a building roof belonging to a normalized 2.5-DUSM of roof lines. Figure 5.14 shows an example of the enhancement of some building outlines, from raw LiDAR data to the result of the enhancement on the normalized 2.5-DUSM of building outlines (without vegetation). Finally, the pixels enhanced after application of the enhancement procedure (considering only external facades) on a 2.5-DUSM of building outlines, for 36 buildings of a neighbourhood of the city of Geneva, are shown in Figure 5.15. In this last case it is interesting to note that only north, east and north-east pixels are corrected – this phenomenon is mainly caused by the timing quantization error of LiDAR speed-measurements devices (Fisher and Pyhtila, 2000).

5.6 Creation of masks for the enhancement of the 2.5-DUSM used

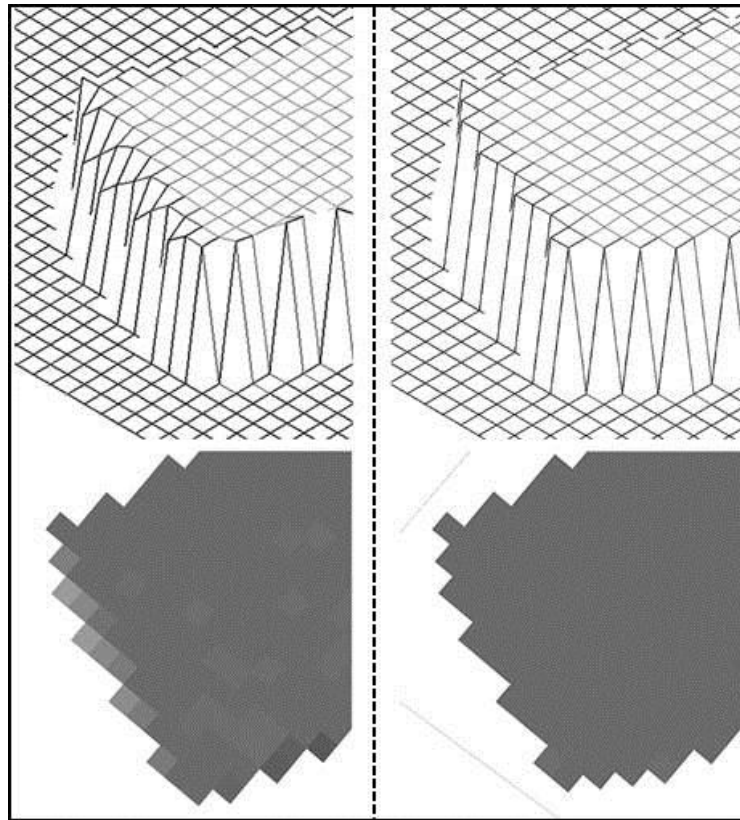


Figure 5.13. Example of the enhancement of a building roof belonging to a 2.5-DUSM of roof lines without vegetation. Left hand-side images: the normalized 2.5-DUSM of roof lines represented as an isometric view (above) and as a top view (below); right hand-side images: the result of the enhancement on the 2.5-DUSM of roof lines without vegetation represented as an isometric view (above) and as a top view (below), characterised by sharper edges after reclassification of pixels.

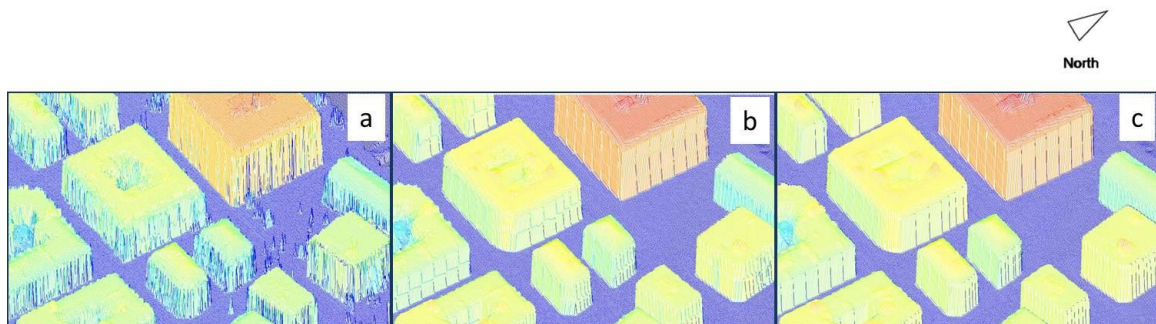


Figure 5.14. The enhancement of some building facades belonging to a 2.5-DUSM of building outlines. From the left hand-side image: (a) the raw LiDAR data, (b) the normalized 2.5-DUSM of building outlines, (c) result of the enhancement on the normalized 2.5-DUSM of building outlines.

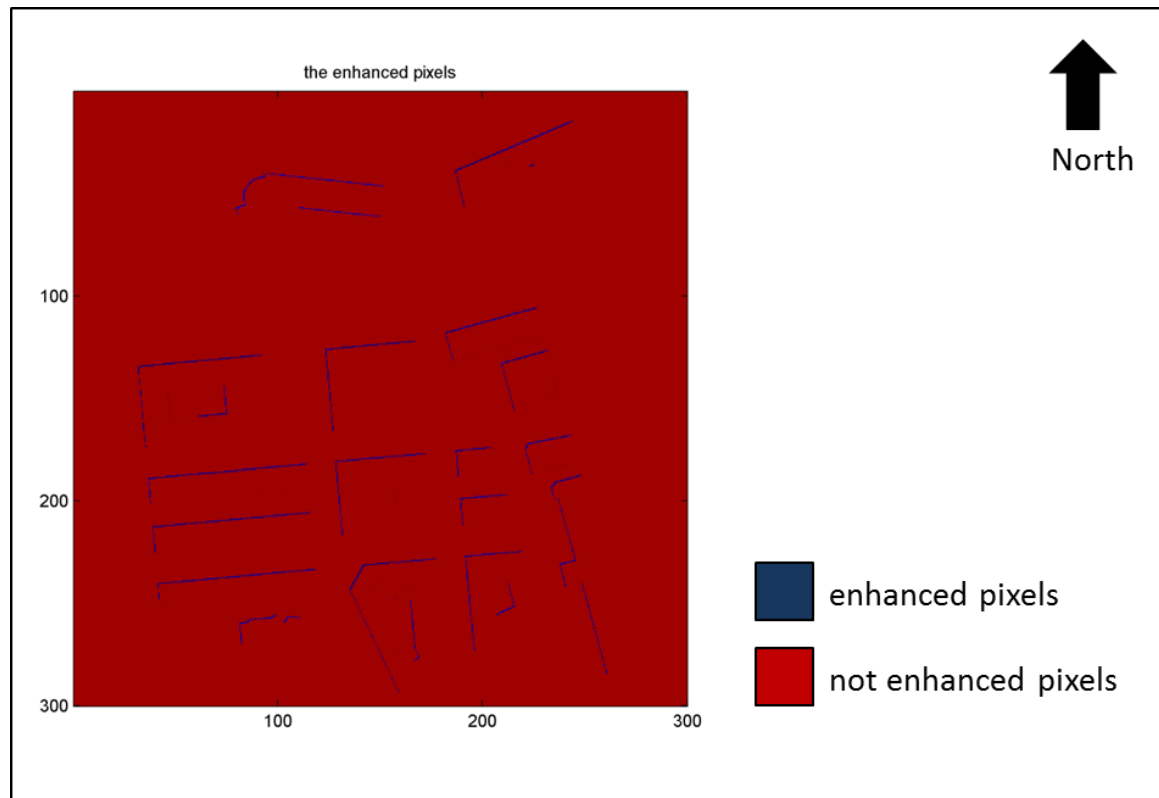


Figure 5.15. Pixels enhanced after application of the enhancement procedure (considering only external facades) on the 2.5-DUSM of building outlines, for 36 buildings of a neighbourhood of the city of Geneva.

5.7 Segmentation of planar roof areas

The segmentation of roof planes can, in principle, be performed directly on the laser point cloud, but the latter is firstly rasterised by a region growing algorithm for easier and faster determination. It starts at the so called seed area, a local neighbourhood of a point (e.g. 3 pixels by 3 pixels) where the laser points fulfil user defined conditions. In this case all points of the seed area must lie within the same plane (initial plane) with small acceptable deviations (e.g. due to data noise), i.e. the point coordinates must fulfil the mathematical equation of a plane.

After determination of the initial plane the region growing algorithm iteratively analyses the adjacent points. A point is added to this plane if it fulfils the so called *homogeneity condition*, by means of the orthogonal distance of the point to the current plane. The point is accepted and integrated if this distance is small enough to fulfil a probability condition, and the plane parameters are recalculated by an adjustment procedure. If no new adjacent points can be found, the region growing stops, and the plane area (and its parameters) is stored and subsequently masked out. The algorithm will therefore search for a new seed area and start segmenting a new plane until no new planes can be found in the data set.

This procedure was initially described by Quint and Landes (1996) and later enhanced for application on LiDAR data by Vögtle and Steinle (2000). As proposed by Lemp and Weidner (2005), the algorithm was also applied in this thesis using only last pulse laser data, however results were not satisfactory, especially along roof edges. Many other authors have studied the segmentation procedure for LiDAR data. For example, Vosselmann and Dijkman (2001) used 3-D Hough Transform to detect planes in LiDAR data, and Hofmann *et al.* (2003) made a comparison between 2-D and 3-D Hough Transform in order to detect building planes in LiDAR

5.8 Punch case: assessing the accuracy of the constructed and enhanced 2.5-DUSM of roof lines

data. An algorithm for the automated delineation of roof planes from LiDAR data was proposed by Rottensteiner *et al.* (2005).

According to the procedure proposed by Vögtle and Steinle (2000), Figure 5.16 shows an example of the result of the segmentation of roof planes for an area of the CERN campus using LiDAR data.

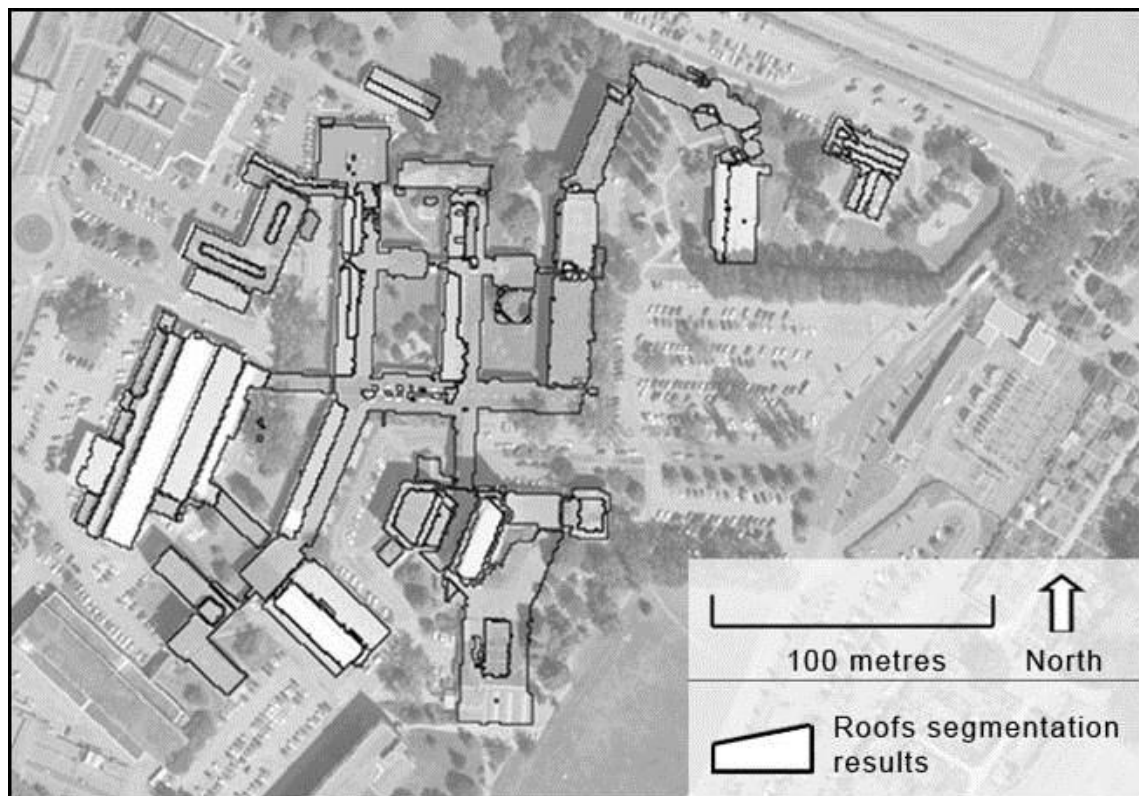


Figure 5.16. According to the procedure proposed by Vögtle and Steinle (2000), example of the segmentation of planar roof areas in CERN's case-study area.

The results of this extraction process are used to determine slope and orientation features of the roof planes. Subsequently, these features are used as input data for the extraction of some UEQ indicators (such as the “irradiation collected by building roofs”) in image mode by applying DIP techniques.

5.8 Punch case: assessing the accuracy of the constructed and enhanced 2.5-DUSM of roof lines

5.8.1 Presentation

This *punch-case* intends to assess the quality and accuracy of the constructed and enhanced 2.5-DUSM of roof lines highlighted and used in this study. This is done by applying a significance statistical analysis between a reference 2.5-DUSM of roof lines and the constructed and enhanced 2.5-DUSM of roof lines (Figure 5.17). The reference 2.5-DUSM of roof lines was obtained by an automatic correlation of the optical aerial images (photogrammetric techniques), and presents an accuracy of 16 centimetres RMSE in the case-study area, located in a neighbourhood of the city of Geneva - 36 buildings with different roofs typologies were used for the analysis. The density

of LiDAR raw data is 4 points/m². According to Gonçalves (2006), this reference 2.5-DUSM has a better RMSE accuracy than traditional DSM interpolated from LiDAR data and for that reason can be used for the assessment and statistical validation of the latter.



Figure 5.17. Reference 2.5-DUSM of roof lines, for 36 buildings of a neighbourhood of the city of Geneva, obtained by an automatic correlation of the optical aerial images (photogrammetric techniques) with an accuracy of 16 centimetres RMSE.

5.8.2 Method applied

In order to estimate, quantitatively, the quality of the interpolated surface models, a correlation coefficient between the reference 2.5-DUSM of roof lines (X) and the constructed or enhanced surface model (Y), called 2.5-DUSM of roof lines, is used:

$$\rho = \frac{\sum_{i=1}^N \sum_{j=1}^M (X_{ij} - \bar{X})(Y_{ij} - \bar{Y})}{\sqrt{\sum_{i=1}^N \sum_{j=1}^M (X_{ij} - \bar{X})^2 \sum_{i=1}^N \sum_{j=1}^M (Y_{ij} - \bar{Y})^2}} \quad (5.1)$$

Where:

- N, M are the number of rows and columns in the reference 2.5-DUSM and the enhanced 2.5-DUSM of roof lines respectively;
- X_{ij} and Y_{ij} are the heights at the pixel (i, j) ,
- \bar{X} and \bar{Y} are the mean heights of the reference 2.5-DUSM of roof lines and the enhanced 2.5-DUSM of roof lines respectively.

Thus, the closer the correlation coefficient (ρ) is to the positive unit, the more the reference 2.5-DUSM of roof lines and the constructed or enhanced 2.5-DUSM of roof lines will be similar.

5.8 Punch case: assessing the accuracy of the constructed and enhanced 2.5-DUSM of roof lines

For comparison with the reference 2.5-DUSM of roof lines the following six interpolated surface models were used:

- *Case 1: 2.5-DUSM of roof lines without vegetation not enhanced;*
- *Case 2: 2.5-DUSM of roof lines (without vegetation), enhanced only for external zones of discontinuity of the roof (considering “minimum”, “maximum”, “mean” and “median” criteria)*
 - o *Limit for the detection of low pixels: case a: 1 meter; case b: 2 meters;*
- *Case 3: 2.5-DUSM of roof lines (without vegetation), enhanced for external and internal zones of discontinuity of the roof (considering “minimum”, “maximum”, “mean” and “median” criteria)*
 - o *Limit for the detection of low pixels: case a: 1 meter; case b: 2 meters;*
- *Case 4: Inverse Distance Weighted (IDW)*
 - o *weighting power = 2;*
 - o *search radius = 0.5 (meters);*
 - o *minimum number of points: 2;*
- *Case 5: Kriging (ordinary)*
 - o *neighbours to include = 4;*
 - o *neighbours to include (at least) = 2;*
- *Case 6: Triangular Irregular Network (TIN), which was converted into a raster format.*

An overview of the results, considering for cases 2 and 3 a limit of 1 meter for the detection of low pixels, is presented in Table 5.2. The limit of 1 meter is selected because the correlation presents slightly better results.

	<i>case 1: 2.5-DUSM constructed</i>	<i>case 2: 2.5-DUSM of roof lines, enhanced only for external zones of discontinuity of the roof</i>				<i>case 3: 2.5-DUSM of roof lines, enhanced for external and internal zones of discontinuity of the roof</i>				<i>case 4: DSM (IDW)</i>	<i>case 5: DSM (Krig)</i>	<i>case 6: DSM (TIN)</i>
		<i>minimum</i>	<i>maximum</i>	<i>median</i>	<i>mean</i>	<i>minimum</i>	<i>maximum</i>	<i>median</i>	<i>mean</i>			
Correlation between reference 2.5-DUSM and different 2.5-DUSM/DSM	0.762	0.765	0.767	0.764	0.764	0.765	0.770	0.766	0.766	0.734	0.566	0.475

Table 5.2. Different correlations between the reference 2.5-DUSM of roof lines and the 12 interpolated 2.5-DUSM of roof lines under analysis

From the analysis of Table 5.2 the following points can be concluded:

- The constructed and not enhanced 2.5-DUSM of roof lines presents better results than direct interpolation techniques: IDW, Kriging or TIN;
- All the constructed and enhanced 2.5-DUSM of roof lines (cases 2 and 3) present better results than direct interpolation techniques: IDW, Kriging or TIN and slightly better results than the constructed and not enhanced 2.5-DUSM of roof lines;
- Among the four criteria analysed for the enhancement of the 2.5-DUSM of roof lines considering only external zones of discontinuity of the roof (case 2) or all zones of discontinuity of the roof (case 3), the “maximum” reclassification method for case 3 presents the preminent results.

5.8.3 Significance statistical validation and analysis of results

In this case a comparison between two sets of measurements to evaluate whether their population means differ is applied. In statistics, this is most commonly called as a paired difference test. Explicit methods for carrying out paired difference tests are the paired t-test and the paired z-test. Thus, the two-tailed “t-test” statistical analysis was applied in order to evaluate whether the improvement of results can be considered significant. The reason for applying a two-tailed “t-test” and not a simpler one-tailed “t-test” is that, for the two-tailed “t-test” the differences between each pair of buildings can be positive or negative, guaranteeing therefore a more strict significance statistical test. The significance level (α) is set to 0.05, which means that H_0 is rejected in favour of H_1 when α is lower than 0.05. Thus, in order to evaluate the improvement of accuracy between two surface models, the null hypothesis H_0 is tested as shown in Table 5.3, and applied for the following cases:

- *Test 1*: significance statistical analysis of the constructed and not enhanced 2.5-DUSM of roof lines when compared to direct interpolation techniques: IDW, Kriging or TIN (Table 5.4);
- *Test 2*: significance statistical analysis of the constructed and enhanced 2.5-DUSM of roof lines considering only external zones of discontinuity of the roof (case 2) and the “maximum” criteria, when compared to the constructed and not enhanced 2.5-DUSM and to direct interpolation techniques: IDW, Kriging or TIN (Table 5.5);
- *Test 3*: significance statistical analysis of the constructed and enhanced 2.5-DUSM of roof lines considering external and internal zones of discontinuity of the roof (case 2) and the “maximum” criteria, when compared to the constructed and not enhanced 2.5-DUSM of roof lines and to direct interpolation techniques: IDW, Kriging or TIN (Table 5.6);

	Significance statistical analysis (t test; level of significance: 0.05)	
	Null hypothesis (H ₀)	Hypothesis 1 (H ₁)
<i>Test:</i> <i>improvement of accuracy between two surface models</i>	No significant improvement is reached	A significant improvement is reached

Table 5.3. Hypothesis related to the significance on the improvement of accuracy between the reference 2.5-DUSM of roof lines and the constructed and enhanced 2.5-DUSM of roof lines.

5.8 Punch case: assessing the accuracy of the constructed and enhanced 2.5-DUSM of roof lines

Test 1: significance statistical analysis (t test; level of significance: 0.05)		
2.5-DUSM of roof lines not enhanced vs. IDW	2.5-DUSM of roof lines not enhanced vs. Krig	2.5-DUSM of roof lines not enhanced vs. TIN
0.033 (significant)	3.35E-08 (significant)	2.27E-11 (significant)

Table 5.4. Significance statistical analysis of the constructed and not enhanced 2.5-DUSM of roof lines when compared to direct interpolation techniques: IDW, Kriging or TIN.

Test 2: significance statistical analysis (t test; level of significance: 0.05)			
2.5-DUSM of roof lines enhanced considering only external zones of discontinuity of the roof vs. 2.5-DUSM of roof lines not enhanced	2.5-DUSM of roof lines enhanced considering only external zones of discontinuity of the roof vs. IDW	2.5-DUSM of roof lines enhanced considering only external zones of discontinuity of the roof vs. Krig	2.5-DUSM of roof lines enhanced considering only external zones of discontinuity of the roof vs. TIN
0.060 (not significant)	0.013 (significant)	1.83E-08 (significant)	1.20E-11 (significant)

Table 5.5. Significance statistical analysis of the constructed and enhanced 2.5-DUSM of roof lines considering only external zones of discontinuity of the roof (case 2) and the “maximum” criteria, when compared to the constructed and not enhanced 2.5-DUSM of roof lines and to direct interpolation techniques: IDW, Kriging or TIN.

Test 3: significance statistical analysis (t test; level of significance: 0.05)			
2.5-DUSM of roof lines enhanced considering external and internal zones of discontinuity of the roof vs. 2.5-DUSM of roof lines not enhanced	2.5-DUSM of roof lines enhanced considering external and internal zones of discontinuity of the roof vs. IDW	2.5-DUSM of roof lines enhanced considering external and internal zones of discontinuity of the roof vs. Krig	2.5-DUSM of roof lines enhanced considering external and internal zones of discontinuity of the roof vs. TIN
0.005 (significant)	0.006 (significant)	9.46E-09 (significant)	7.51E-12 (significant)

Table 5.6. Significance statistical analysis of the constructed and enhanced 2.5-DUSM of roof lines considering external and internal zones of discontinuity of the roof (case 2) and the “maximum” criteria, when compared to the constructed and not enhanced 2.5-DUSM of roof lines and to direct interpolation techniques: IDW, Kriging or TIN.

The significance statistical analysis shown in tables 5.4 to 5.6 shows that for a level of significance of 0.05 the constructed and enhanced 2.5-DUSM of roof lines, considering external and internal zones of discontinuity of the roof (case 2) and the “maximum” criteria, presents the

most significant improvements when compared to all other interpolation techniques. Hence, all the interpolated and constructed 2.5-DUSM of roof lines (also the 2.5-DUSM of building outlines, the normalized 2.5-DUSM of roof lines and the normalized 2.5-DUSM of building outlines) further emphasized in this thesis are based on this method. These improvements are particularly important for the calculation of the morphological properties of buildings, which is rather sensitive to existing inaccuracies on the normalized 2.5-DUSM used.

5.8.4 Conclusions

This study refers to an area of the State of Geneva, where LiDAR data was acquired with a density of 4 points/m², resulting in a sampling size of the interpolated grids of 0.5 meters. No relevant geometrical inaccuracies in the matching between different geo-referenced datasets were noticed. For other cities, where available geo-referenced datasets are different, it could be pertinent to test the robustness of the interpolation methods presented by evaluating its sensitivity, both to the variation of the sample LiDAR point density and to the variation of the grid size of the interpolated and constructed 2.5-DUSM.

5.9 Punch-case: assessing a sensor network by verifying shadows derived from a 2.5-DUSM of building outlines

5.9.1 Presentation

The present innovative *punch-case* aims to assess the accuracy of real solar irradiation measurements directly derived from sensor network data (available at the EPFL Campus, Lausanne, Switzerland) by comparing its outputs with shadowing analysis derived from a 2.5-DUSM of building outlines of the same Campus. The average error between the transition time derived from the solar irradiation measurements and that from shadowiness analysis using the 2.5-DUSM of building outlines is computed in order to validate - especially to detect sensor fuzzy measurements - the solar irradiation outputs derived from the wireless sensor network. The density of LiDAR points available at the EPFL Campus is equal to one point per square meter. According to Behan (2000), the most accurate surfaces are created using a grid with a sampling size that relates as close as possible to the LiDAR point density during the acquisition phase. Thus, the 2.5-DUSM of building outlines interpolated has a sampling size of 1 meter. An example of a 2.5-DUSM of building outlines of the EPFL Campus is shown in Figure 5.18.

5.9 Punch-case: assessing a sensor network by verifying shadows derived from a 2.5-DUSM of building outlines

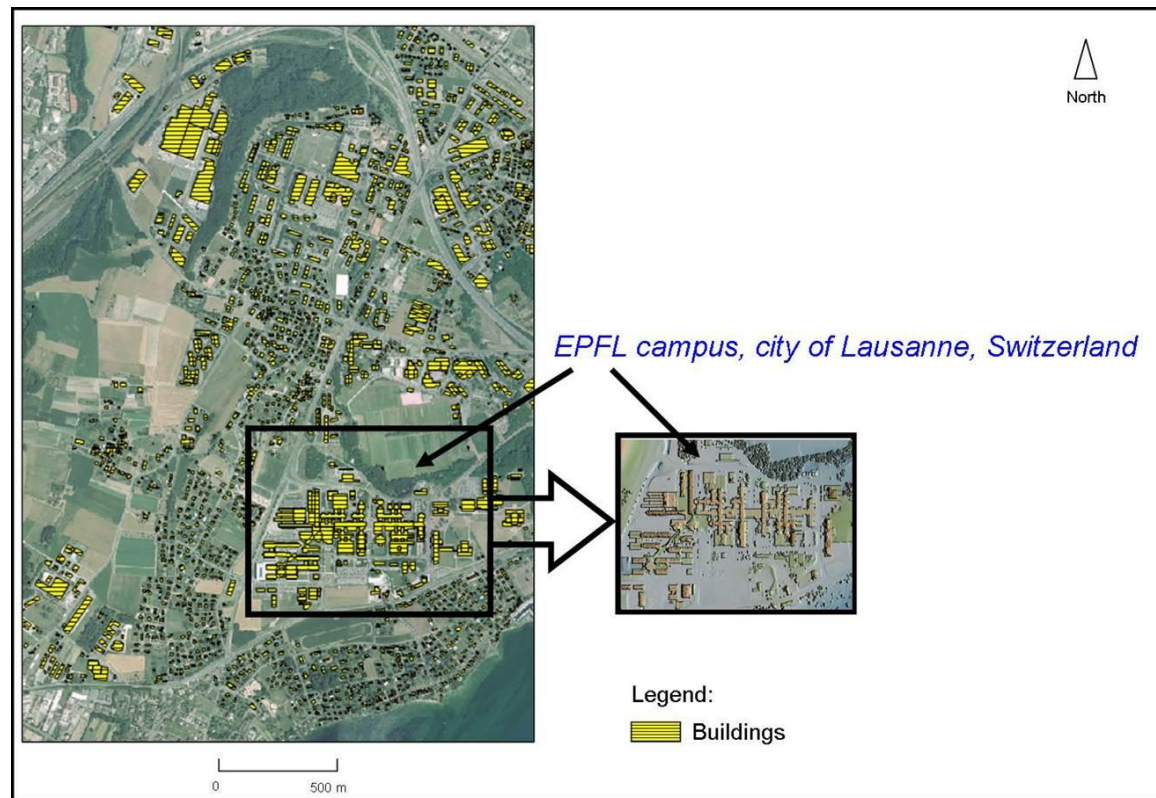


Figure 5.18. Picture on the left-hand side: 2-D GIS building outlines and aerial pictures of the district of Chavannes and EPFL campus, city of Lausanne, Switzerland; picture on the right-hand side: 2.5-DUSM of building outlines of the EPFL campus, city of Lausanne, Switzerland, with a cell resolution of 1 meter; black rectangle: case study (pilot zone), within the EPFL campus, city of Lausanne, Switzerland.

5.9.2 SensorScope project

As presented by Barrenetxea *et al.* (2008), SensorScope is a joint project between network, signal processing, and environmental researchers that aims to provide a cheap and out-of-the-box environmental monitoring system based on a wireless sensor network. It has been successfully used in a number of deployments in order to gather hundreds of megabytes of environmental data. The geographical position of the wireless sensor network of the EPFL campus was originally defined in WGS84 coordinates (GPS measurements) and later transformed into New Swiss Grid (CH-1903 datum) coordinates. The location and labelling (identification) of each sensor of the EPFL campus wireless sensor network is shown in Figure 5.19.

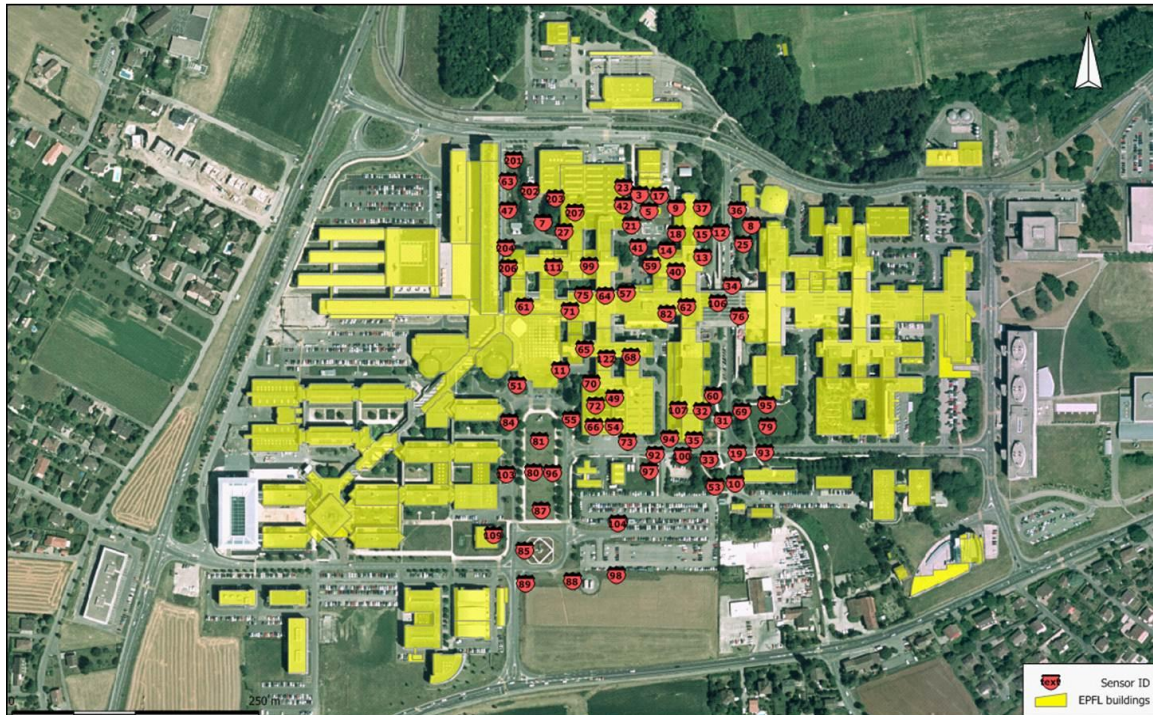


Figure 5.19. Position and identification of the wireless sensors network at the EPFL campus, city of Lausanne, Switzerland.

5.9.3 Method applied

The method applied is based on the comparison between real measurements of solar irradiation made by sensors and shadowing predictions derived from a 2.5-DUSM of building outlines. The solar irradiation parameter greatly depends on the amount of existing clouds during the day: on cloudy or rainy days the density of clouds covering the sun determines how much solar irradiation is received by the sensor. Therefore, as a result of the disordered nature of the water drops in clouds, the measured solar irradiation is a very chaotic signal. On the contrary, on sunny days, measured solar irradiation is a piece-wise smooth signal which increases from morning to noon and decreases from noon to evening. The only irregularity present in this signal is confined to a variation (jumps and drops) - sudden increase or decrease in the level of signal over a very short time interval - in the level of the measured solar irradiation. The reason for the latter observation is a shadowing phenomenon, i.e., whenever a sensor gets out of shadow, the solar irradiation measured by it increases a lot in a short amount of time, and whenever it goes into the shadow, the measured solar irradiation drops suddenly. Thus, in order to predict the exact times of changing of shadowing for each sensor position, the main idea of the project was to use the observed jumps and drops of a sensor measurement and compare it with the shadowing forecasts resulting from the 2.5-DUSM of building outlines (Figure 5.20).

5.9 Punch-case: assessing a sensor network by verifying shadows derived from a 2.5-DUSM of building outlines

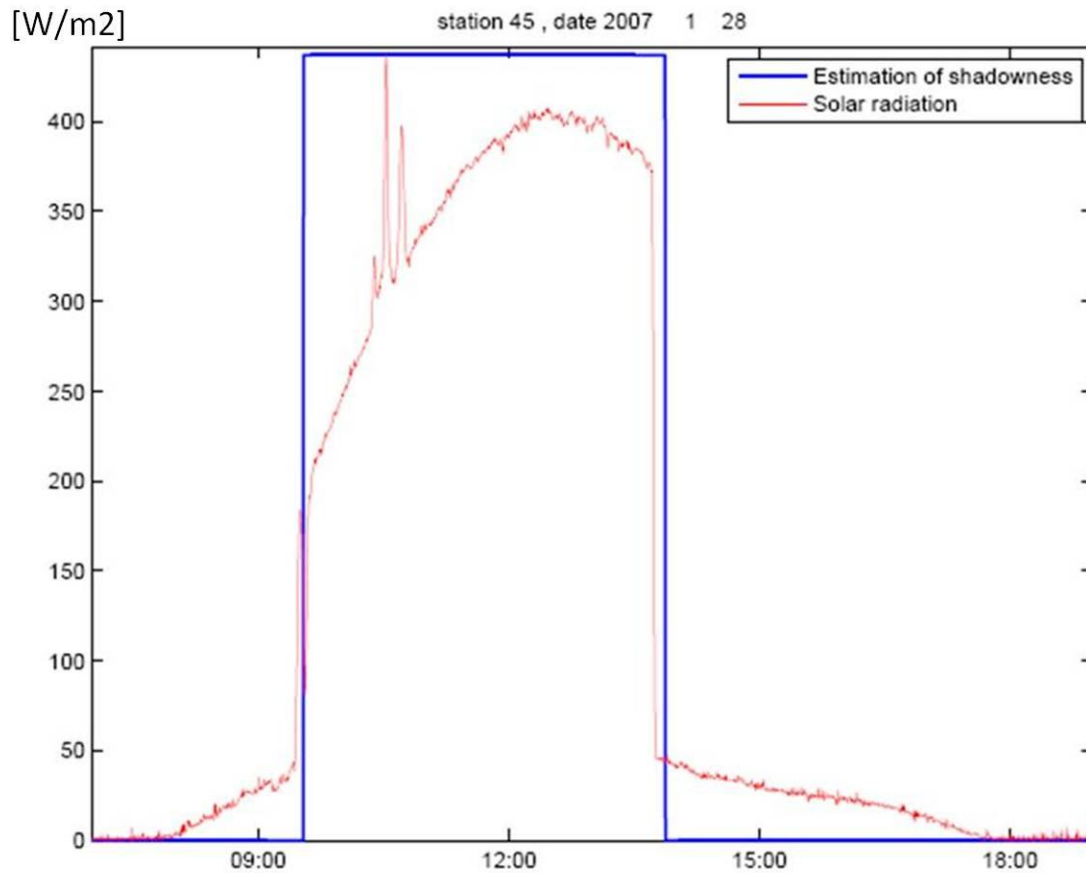


Figure 5.20. Comparison, on a sunny day, between the solar irradiation information collected by a sensor and the estimated shadowiness derived from a 2.5-DUSM of building outlines.

As shown in Figure 5.20, there is no perfect match between the two independent parameters: the estimation of shadowiness for a sensor position (x,y,z coordinates) using a 2.5-DUSM of building outlines and the solar irradiation measured by sensors. A back tracing algorithm proposed by karzand (2009) was used to estimate the shadow-state of each sensor at each time instant. Based on the day of the year and the latitude and longitude of the city of Lausanne, the algorithm calculates the exact direction of the Sun for each sensor at each moment and back-traces the ray of light from the sensor toward the Sun. Subsequently, the height of this ray of light is compared to the curve derived from the 2.5-DUSM of building outlines, which shows the elevation along the line in the same direction, as shown in Figure 5.21. In the case of an intersection where the ray of light is below the elevation according to the 2.5-DUSM of building outlines, the point of that intersection will cast a shadow on the corresponding sensor at that moment.

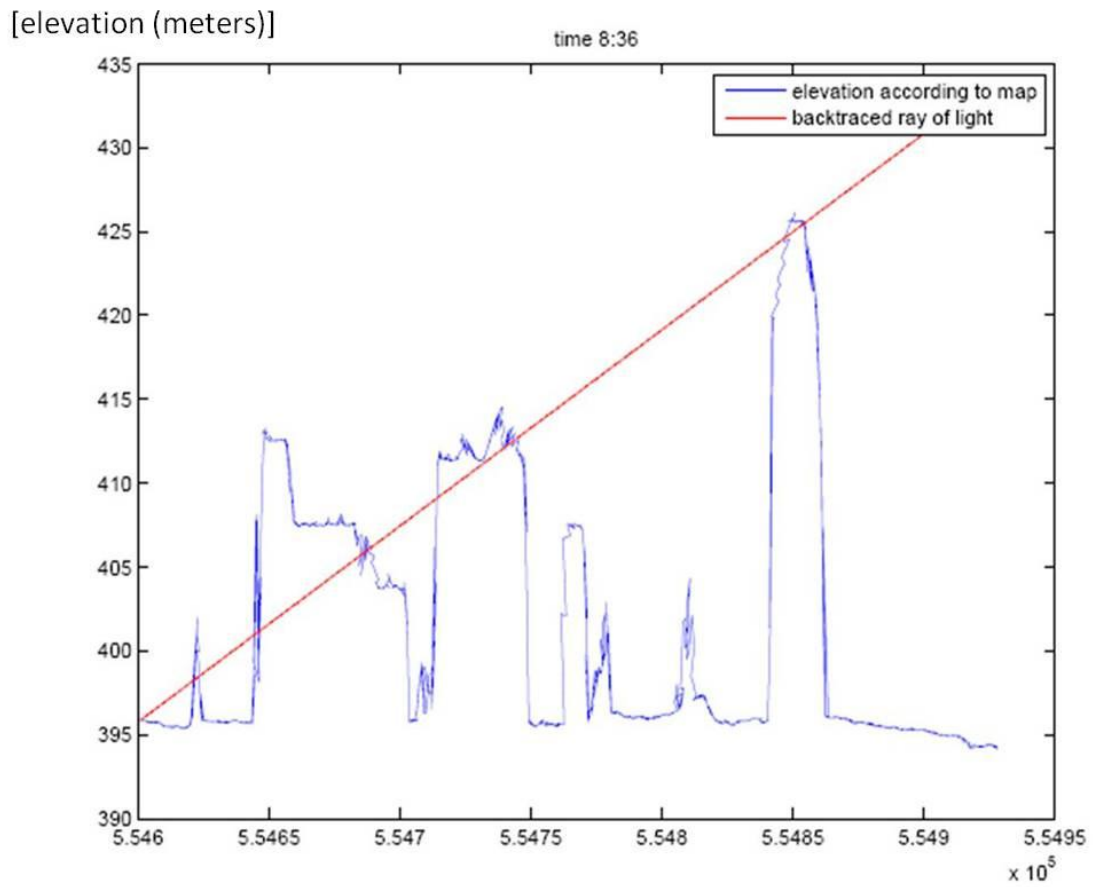


Figure 5.21. Comparison between the height of the ray of light, which is back-traced towards the Sun, and the elevation values of the 2.5-DUSM of building outlines.

An illustrative representation of a theoretical shadow-map of the EPFL campus at one time instant is presented in Figure 5.22. The direction of light coming from the sun is also shown in this figure.

5.9 *Punch-case: assessing a sensor network by verifying shadows derived from a 2.5-DUSM of building outlines*

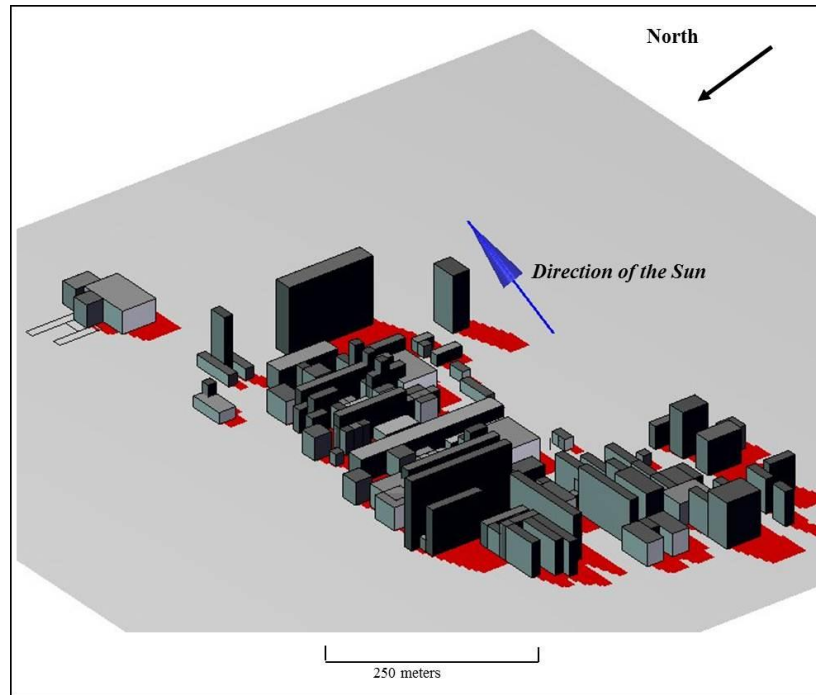


Figure 5.22. For one time instant and the direction of sun, illustrative presentation of the theoretical shadow-map in the EPFL campus.

5.9.4 Analysis of results

The prediction of shadowiness is undertaken according to the 2.5-DUSM of building outlines, and the measurements of solar irradiation for each sensor are distributed throughout the year. Besides the detection of sensors with fuzzy performances (Figure 5.23), a deviation parameter is introduced as a measure of accuracy between the application of 2.5-DUSM of building outlines for the shadowiness analysis and a sensor position (x,y,z coordinates) for eight sunny days, using both image processing techniques and the solar irradiation information of sensors:

- *Average deviation error (in minutes)* for those jumps that could be predicted for a threshold of 30 minutes. The error is defined as the difference of time between jumps in solar irradiation and boundaries of shadowiness which are predicted according to the 2.5-DUSM of building outlines.

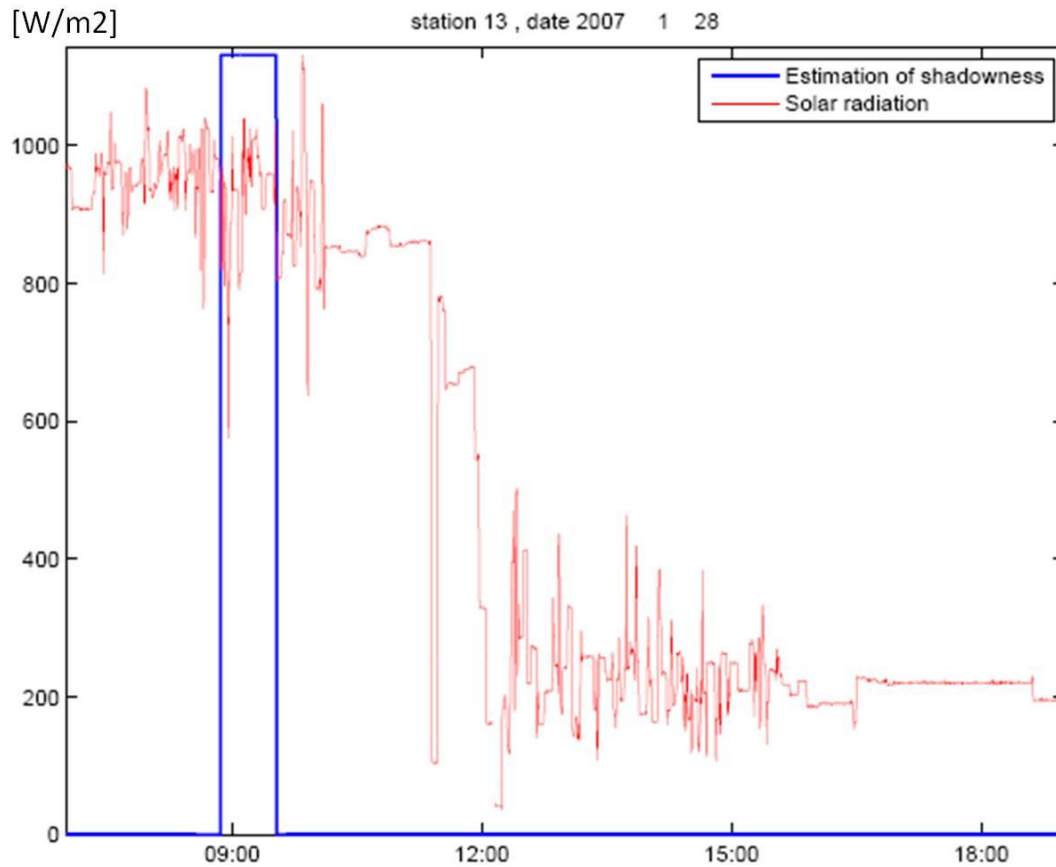


Figure 5.23. Example of a sensor with a fuzzy performance: solar irradiation line.

The simulation results of the average deviation error (in minutes), for the 2.5-DUSM of building outlines under analysis is presented in Table 5.7.

	AvDE (minutes)
2.5D USM (1m of resolution)	4.57

Table 5.7. Average Deviation Error: defined as the difference of time between jumps in solar irradiation and boundaries of shadowiness which are predicted according to the 2.5-DUSM of building outlines.

From the analysis of Table 5.7 it can be observed that the average deviation error between the sensor network irradiation measurements and the 2.5-DUSM of building outlines used is less than 5 minutes. This difference can have many reasons, but one is certainly caused by the fact that the density of LiDAR points used for this classification is equal to one point per square meter. The use of modern LiDAR datasets with higher density of points per square meter and different signal pulses will certainly achieve better results. Thus, it will be possible to improve both the classification and construction of the 2.5-DUSM of building outlines used in this study, especially a higher sampling size, such as 0.5 meters.

5.9.5 Conclusions

This study demonstrates how 2.5-DUSM of building outlines can be applied in an innovative way. This last proved to be usefulness for the validation of outputs from other research fields, also related to urban applications. In this case, it allows to detect fuzzy sensor irradiation measurements that should not be taken into consideration for further environmental analysis. Moreover, the application of this method can be easily and automatically done to very large datasets of sensor measurements.

5.10 Conclusions and chapter synthesis

This chapter presents an overview of the main data sources used and the models constructed in order to extract the UEQ indicators presented in the previous chapter. Thus, in order to construct reliable and enhanced 2.5-DUSM that are further used for the application of digital image processing techniques, different possibilities of data sources were considered for this study: (1) LiDAR data, (2) 2-D and 3-D vector data, and (3) orthophotos. As already explained in detail in section 5.2, the main focus is given to a hybrid approach that uses a double and independent approach: (1) 2-D vector data related to building outlines and LiDAR data, and (2) the 2-D projection of 3-D vector data of roof lines and LiDAR data, used for the construction of different and enhanced 2.5-DUSM or building outlines and 2.5-DUSM of roof lines respectively. All these 2.5-DUSM are specifically applied for the extraction of each of the UEQ indicators (simple and complex) researched in this thesis. This “indicator-model” oriented method, implemented with the participation of end-users of the State of Geneva, allows to efficiently extract each of the indicators, hence significantly improving the final results presented in the next chapters.

The different possibilities of enhancement to be applied on the 2.5-DUSM constructed represent an innovative research aspect of this chapter. Indeed it allows to improve the trustworthiness of the 2.5-DUSM used, especially along its zones of discontinuity. As proposed and implemented in the next chapters of this thesis, this is particularly important for the extraction of some of the indicators studied, particularly those related to phenomena occurring on building facades. The *punch-case* presented for the enhancement of the 2.5-DUSM of roof lines when compared to the original 2.5-DUSM of roof lines or other interpolation techniques (TIN, Kriging and Inverse Distance Weighting) was complemented by an assessment of the accuracy on a statistical basis, which includes a significance t-test.

Another point on this chapter is the use of 2.5-DUSM of building outlines in order to assess the quality of the wireless sensor network used for the measurement of solar irradiation in the urban fabric. This *punch-case* reveals that other possibilities of application of this type of models in multi-disciplinary fields are emerging. Furthermore, it also highlights the urge of enhancing the different 2.5-DUSM used in order to increase its consistency and innovative potential of applicability.

This chapter closes the second part of this thesis (methodological framework), which is mainly related to a correct definition of the top-down (last chapter) and the bottom-up (this chapter) approaches proposed by Maystre and Bollinger (1999). The third and last part of this thesis, which presents several case-studies related to the extraction of the UEQ indicators studied (according to three main stakes), is based on the main concepts emphasized in this part (chapters 4 and 5).

PART III
PRACTICAL IMPLEMENTATION:
EMPIRICAL CASE-STUDIES

CHAPTER 6. ASSESSMENT OF THE MORPHOLOGICAL PROPERTIES OF THE URBAN TEXTURE¹

¹ The main concepts of this chapter were published in:

Carneiro, C., Silva, V., Golay, F. (2009) Incorporation of Morphological Properties of Buildings' Descriptors Computed from GIS and LiDAR Data on an Urban Multi - agent Vector Based Geo - simulator. In: Gervasi, O., Taniar, D., Murgante, B. (Eds.), *Lecture Notes in Computer Science: Computational Science and its Applications*, Berlin, Springer Vol. 5592/2009, pp. 205-220.

Carneiro, C., Morello, E., Voegtle, T., Golay, F. (2010) Digital urban morphometrics: automatic extraction and assessment of morphological properties of buildings. *Transactions in GIS*, Vol. 14, Issue 4, pp. 497-531.

6.1 Introduction

As highlighted in the end-user requirement analysis (section 4.2.6), this first chapter related to the empirical studies undertaken in this research emphasizes on the extraction of a set of indicators and indexes belonging to the stake “assessment of the morphological properties of the urban texture”. Indeed, researchers in urban studies are growingly more concerned with the improvement of the quality of life of cities, where more than half of the world’s population resides. Towards a better understanding of the urban environmental quality (UEQ), several indicators and measurements have been proposed in the last years in order to analyse and compare built-up areas worldwide, involving cross-disciplinary competences in urban design and planning, health, ecology and transportation, among others. One set of those indicators directly deals with the measurement of the urban form, defined as the morphological properties of buildings, aiming at quantifying the role of the built fabric in assessing the environmental performance of cities and revealing structural features of different built-up areas.

According to Baker and Steemers (2000), despite the evident relationship between urban geometry, which can include the calculation of the morphological properties of a set of buildings belonging to a whole city or a neighbourhood, and energy consumption, this link is generally neglected, hence remaining partially studied and extremely debatable. A possible cause is the complexity of the environmental processes involved. Thus, this thesis tries to overcome this problem in two ways: firstly, by proposing novel methods based on the use of LiDAR data for the extraction of morphological properties of the urban texture, which are emphasized in this chapter; secondly, by making the connection between these results about urban geometry and other applications related to solar analysis and energy consumption, which are later highlighted in chapters 8 and 9. Inside this chapter and under this topic of urban geometry, a main focus is given to the morphological analysis of buildings, where only the parameters related to its urban form (the volume, the area of facades and area of roofs) are taken into account. These indicators are extracted under the two case-studies further presented in this chapter.

The following sections will introduce information about: (6.2) – background and related work, (6.3) – case-study: digital urban morphometrics - automatic extraction and assessment of morphological properties of buildings, (6.4) – case-study: incorporation of morphological properties of buildings computed from GIS and LiDAR data on an urban multi-agent vector based geo-simulator, and (6.5) – conclusions and chapter synthesis.

6.2 Background and related work

The new potentialities of urban morphology in the environmental studies were discovered and implemented by environmental and urban designers rather than by pure morphologists (Morello, 2006). The research at the Martin Centre (Department of Architecture, Cambridge University) deals with the environmental design starting from the theories about the correct land uses for urbanization and the morpho-typological solutions that optimize the environmental quality. The research on the optimization of land uses has a long tradition at the University of Cambridge and was first investigated during the 1960’s at the Centre for Land Use and Built Form Studies (Martin and March, 1972). This research has been successfully carried out until the present and represents the common basis in the field of environmental design for the urban form (Knowles, 1978 and 1985; Baker and Steemers, 2000; Ratti and Richens, 2004; Morello and Ratti, 2009a and 2009b).

Urban geometry is a very wide topic. One of the main points when evaluating this topic is the assessment of the availability of sunlight or daylight on building facades: highly-obstructed urban

areas are deprived from useful daylight and solar gains, thus generally requiring higher energy inputs (Morello *et al.*, 2009). There are also indirect effects as urban geometry affects urban microclimate, such as the outdoor temperature, wind speed and solar radiation to which an individual building is exposed. Indeed, it is not caused by a regional “synoptic” climate, but instead by the local microclimate as modified by the “structure” of the city, mainly of the neighbourhood where the building is located (Givoni, 1998). These changes in the urban environment result in modified energy consumption. Also, air pollution and noise are dependent on urban form, and hence affect the potential for natural ventilation via a behavioural mechanism (Ratti, 2002). According to Morello and Ratti (2007) and Montavon (2010), the question is whether – and in what measure – the correct arrangement and the shape of the urban fabric alone might improve the environmental behaviour of the city. As a result, many design tools can be developed, aiming to evaluate novel potentialities related to the form of human settlements. For instance, the energy-based urban morphogenesis of the built environment could be proposed as the initial step towards the enhancement of the sustainability of cities with no supplementary cost due to the application of complex technologies.

As related work it is worth mentioning Yoshida and Omae (2005) who derived the morphological properties of city blocks using an urban landscape model constructed from a large LiDAR dataset. Also Koomen and Bação (2005) presented a new method, based on different topographical data, describing the density of urban systems and quantifying the urban volume of cities.

Finally, before embarking on the derivation of the morphological properties of buildings presented in this chapter, it is useful to review some basic terminology. “Morphology” is defined as “the history of variation in form” (from The Oxford English Dictionary). A complementary and interesting definition was proposed by Batty and Longley (1994, p. 43): “Morphology is [...] the study of form and process, growth and form, form and function”. According to Larkham and Jones (1991, p. 55), if the main focus is given to “urban morphology”, this definition is re-adapted for the specific case of the city, intended as the “study of the physical (or built) fabric of urban form, and the people and processes shaping it”. As mentioned by Larkham (2002), the term “urban morphology” is frequently distorted as authors use “morphology” in place of “form”, confusing the object with the process of study. Indeed, the recent introduction of the term of “sustainability” into the discipline of the “urban morphology” shows the lack of research in this field (Stanilov, 2003). The gap between descriptive and prescriptive theories in this field remains and few design solutions have been proposed yet (Morello, 2006). Many growth strategies have been explored during the last century in order to tackle the problematic increment of urbanization throughout the world’s largest cities, however no coherent answer has been found. Moreover, demographers predict that by the year 2020 nearly 60 per cent of the world’s population will inhabit urban areas (Hall and Pfeiffer, 2000). Policies of superficial “infilling” and “gentrification” were often applied in the name of sustainability, with little understanding of the historical process of growth at a local sphere. Urban morphology, as invoked by Stanilov (2003), must propose feasible solutions to environmental issues, and cannot limit its field of action in purely descriptive analyses (Morello, 2006). Finally, the term “urban morphometrics” was deliberately transferred from other disciplines. In fact, morphometrics studies the variation and change in the form of objects, and is widely diffused in biology, zoology and medicine, whereby different methods of extracting data from shapes are investigated.

6.3 Case-study: Digital urban morphometrics - automatic extraction and assessment of morphological properties of buildings

6.3.1 Presentation

The aim of this case-study is to present a new method to calculate the morphological properties (volumes, area of roofs and areas of facades) of the built environment using LiDAR data, 2-D GIS vector data and the 2-D projection of 3-D vector building roofs (stored in a 3-D city model). A hybrid approach that takes into account different types of inputs and consequently evaluates the accuracy of each type of data used is presented. The method is tested in two case-study areas of the State of Geneva, Switzerland.

It is worth mentioning that when a 3-D vector model is available, the calculation of the area of facades, areas of roofs and volumes can be more easily and precisely done than traditional computation on a raster basis. Indeed, even if the 3-D model of the city of Geneva was available, the main purpose of this study was to show how LiDAR data and derived products (such as the n2.5-DUSM of building outlines) can be explored in order to extract the morphological indicators of buildings in a reliable way. Moreover, the construction of a n2.5-DUSM of roof lines based on a hybrid approach that uses LiDAR data and the 2-D projection of 3-D roof lines stored in a 3-D vector model is mandatory because it allows to correctly apply the statistical validation further presented for both case-studies: the areas of roofs calculated using the n2.5-DUSM of roof lines are compared to those directly extracted from the 3-D buildings (LoD2) stored in the 3-D vector model.

6.3.2 Dataflow process

The process for structuring the proposed method is based on three major steps, as shown in the dataflow of Figure 6.1: (1) the construction of the homogeneous roof slopes, the normalized 2.5 Digital Urban Surface Model (n2.5-DUSM) of building outlines and the n2.5-DUSM of roof lines (section 5.5); (2) the creation of the different raster images used, defined in this thesis as grid masks; (3) the calculation of the output results using digital image processing (DIP) techniques. All steps above mentioned will be further detailed and analysed in the next three sections of this paper.

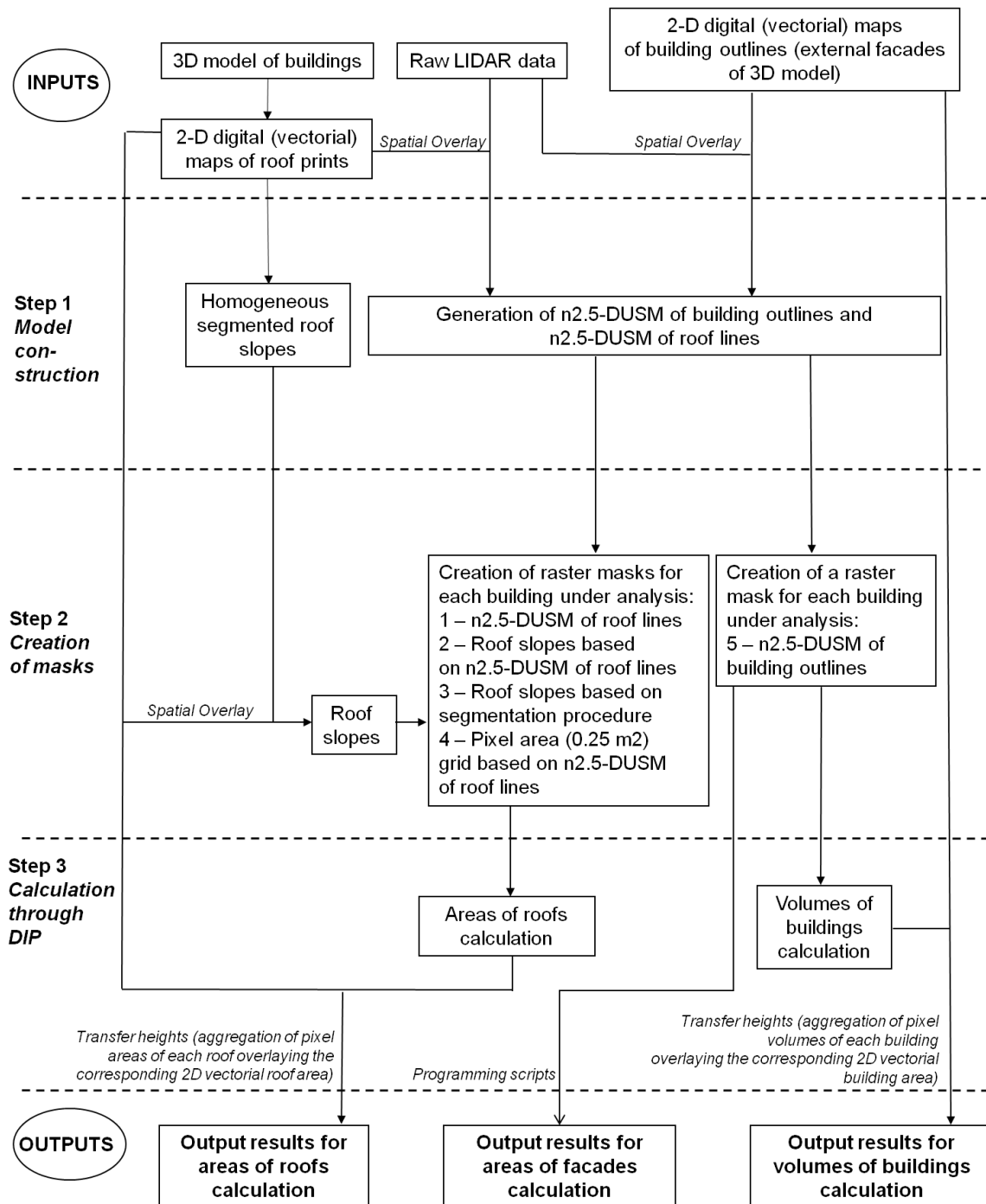


Figure 6.1. The dataflow process describing the method implemented to produce and analyse the n2.5-DUSM of building outlines and the n2.5-DUSM of roof lines.

6.3.3 Data sources used and normalized 2.5-DUSM constructed

Two case-study areas are used to test this method. The first site (Figure 6.2, left hand-side image) is a selection of 18 buildings inside the campus of the European Organization for Nuclear Research (CERN), more precisely in the eastern area within the Swiss boundary. This

6.3 Case-study: Digital urban morphometrics - automatic extraction and assessment of morphological properties of buildings

organization showed a strong interest on this research project because they are currently implementing an urban master plan. Thus, the morphological properties of buildings and its applications to environmental and energetic studies were considered a very valuable input. For that reason this pilot-zone was considered for this research project. At CERN, most of the buildings are characterized by simple geometry but present different heights and footprints; only a few require particular attention in the computation because they present very complex shapes, having multiple faces. The second site selected for the analysis is a square area near the Rhone River in the old town of Geneva, in Switzerland. This area was selected due to the morphological characteristics of the buildings available. As shown in the right hand-side image of Figure 6.2, 44 different buildings with an average height of 18.5 metres are located at this site, where the urban fabric is quite compact and densely built. Moreover, these buildings present many super-structures on roofs that are sufficiently separated from each other and do not present particular problems caused by the presence of vegetation (for example trees touching the facades or roofs).

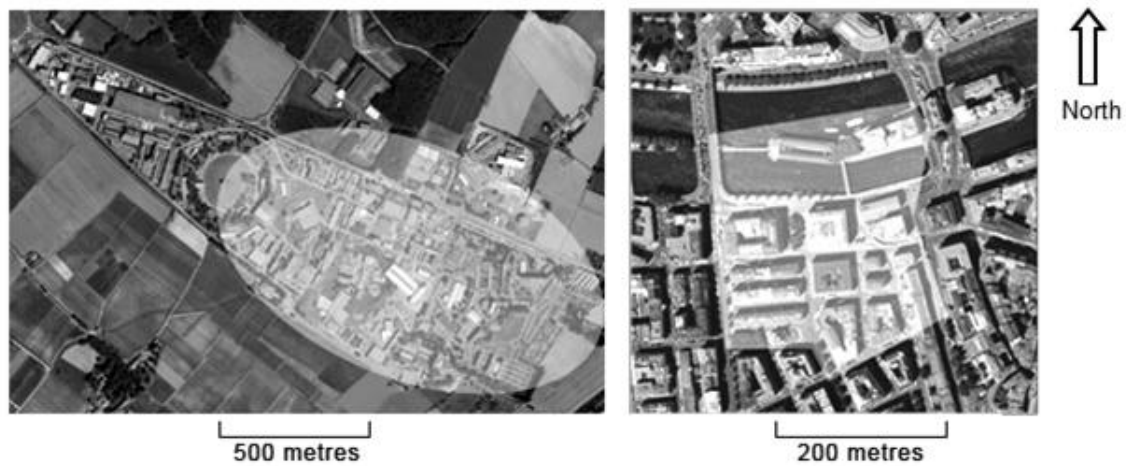


Figure 6.2. The orthophotos of the 2 case-study areas. Left hand-side image: the CERN campus; right hand-side image: the site in the old town of Geneva, close to the Rhone River.

The following data was used: (1) 2-D GIS building outlines, (2) 2-D projection of 3-D roof lines, (3) LiDAR data, and (4) 3-D vector city model. For more details about the data sources used please consult section 5.3.

For more details about the method used for the construction of the n2.5-DUSM of building outlines and the n2.5-DUSM of roof lines used in this case-study please consult section 5.5. As an example, the n2.5-DUSM of building outlines of the centre of Geneva case-study area is represented in Figure 6.3.

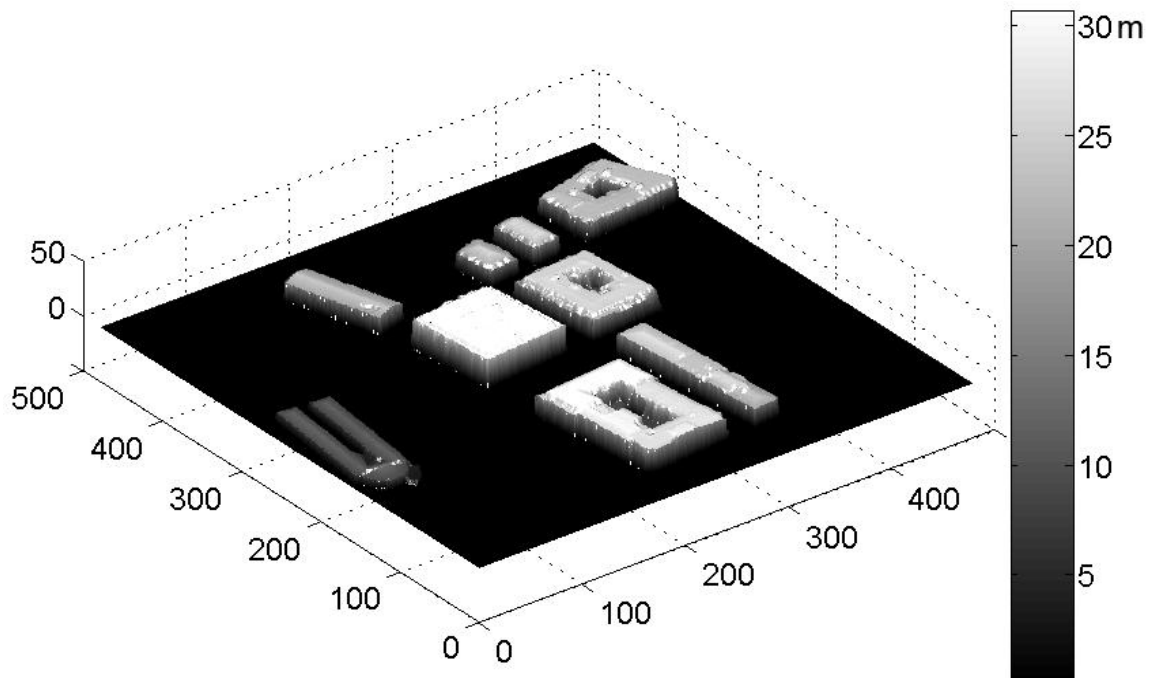


Figure 6.3. The n2.5-DUSM of building outlines of the centre of Geneva case-study area.

6.3.4 Creation of masks for the application of morphological operations on each building

Once each of the three considered models (homogeneous segmented roof slopes, n2.5-DUSM of building outlines and n2.5-DUSM of roof lines) are constructed, image processing operations are performed inside each of these models on a pixel basis. In order to apply such operations, each building (extracted from the n2.5-DUSM of building outlines) or roof section (extracted from the n2.5-DUSM of roof lines) is imported as a single image, defined as a mask, i.e. a 2-D array where the z value of each pixel corresponds to the height of the pixel in metres. On each pixel belonging to the edges of the building or the roof sections, a series of morphological operations are then performed (Figure 6.4). This process enables the calculation of the morphological properties of each building under analysis:

- using the n2.5-DUSM of building outlines, creation of one mask for each building and calculation of the volume and area of facades of each building;
- using the homogeneous segmented roof slopes and the slopes derived from the n2.5-DUSM of roof lines, creation of one mask for each roof section, calculation of the area of roofs of each building and aggregation of the area of each roof section by building roof.

6.3 Case-study: Digital urban morphometrics - automatic extraction and assessment of morphological properties of buildings

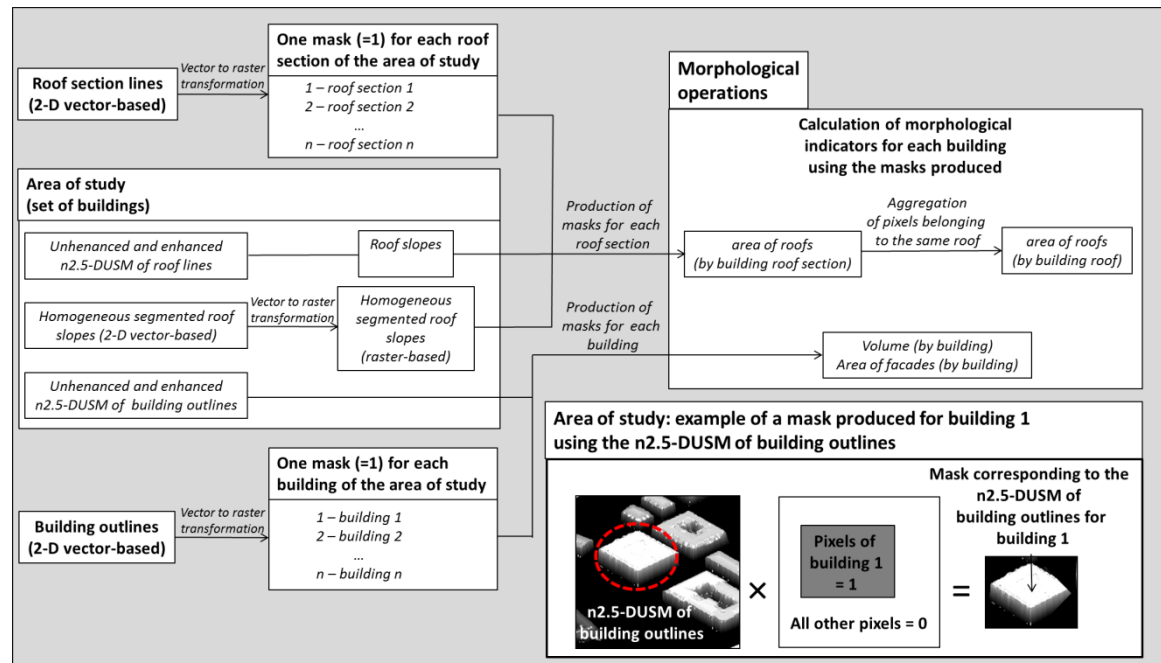


Figure 6.4. Method applied for the creation of masks for each analysed building.

6.3.5 The calculation of the morphological indicators: volume of buildings, area of roofs and area of facades

6.3.5.1 Volume of buildings

The volume is built from each pixel within each building's mask corresponding to the n2.5-DUSM of building outlines, having a sampling size of 0.5 metres. It is obtained by multiplying the unit square of the pixel itself by the height derived from the corresponding value on the n2.5-DUSM of building outlines, as shown in Figure 6.5. Thus, in order to derive the volume of each building, pixel volumes⁵ overlaying the corresponding 2-D digital (vector) building area are aggregated and summed.

⁵ The total volume built for each building comes straightforwardly by adding the elementary volumes of its pixels.

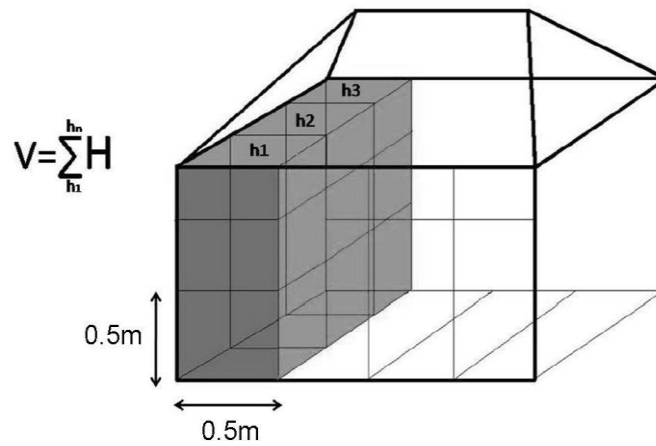


Figure 6.5. Extraction of the volume of a building using the n2.5-DUSM of building outlines (enhanced and unenhanced models).

6.3.5.2 Area of facades

For each building, a mask corresponding to the n2.5-DUSM of building outlines is created in order to compute the areas of the vertical surfaces. Firstly, its edges must be detected; secondly, two separate procedures allow to determine the height and length of each pixel (Figure 6.6). Both procedures require the application of filters with the aim of both detecting the edges of the object and assigning the proper values to them. Different types of operations are used in this work as follows: reclassification of pixels in the zones of discontinuity of the object, which corresponds to its enhancement, as presented in section 5.6; the Canny filter⁶ (Canny 1986) and other operations in order to average the value of the pixels considering various types of structuring elements (Figure 6.7).

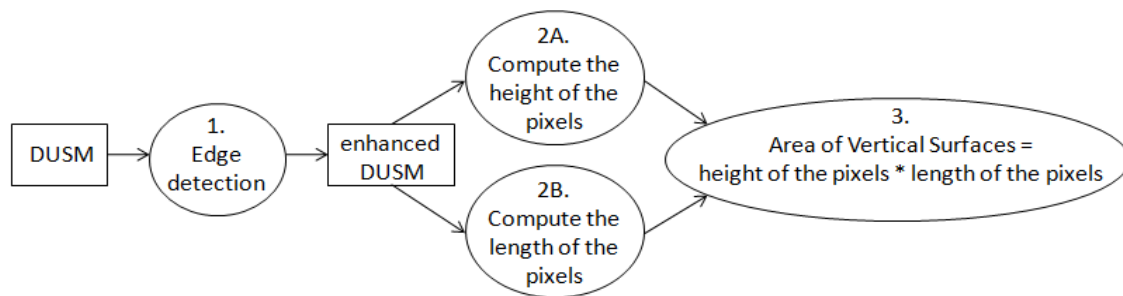


Figure 6.6. Structure of the procedure related to the calculation of vertical areas of facades.

⁶ The Canny filter is considered as the most powerful edge detection method. It identifies strong and weak edges and its peculiarity is that it takes weak edges only into consideration when they are connected to strong ones. This allows the reduction of noise in the image.

6.3 Case-study: Digital urban morphometrics - automatic extraction and assessment of morphological properties of buildings

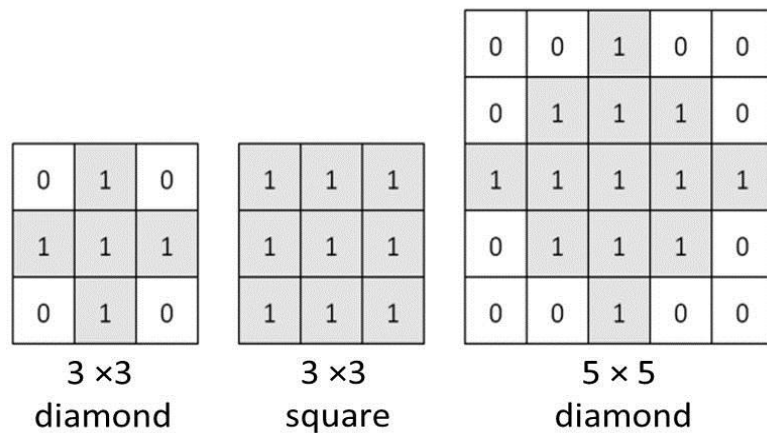


Figure 6.7. Details of structuring elements used to enhance the model and calculate the area of facades.

Flat structuring elements can vary according to their size (neighbourhood) and their shape. The neighbourhood is a matrix containing 1's (the so named neighbours) and 0's. As shown in Figure 6.7 the location of the 1's defines the neighbourhood selected pixels for the morphological operation. In the routine the neighbourhood is centred on those pixels on which we want to apply the image enhancement (in this case the pixels on the perimeter of the object). Beside the definition of the neighbourhood as the size of the filter, it is also important to establish the shape of the filter itself, in other words where the 1's inside the neighbourhood are available.

Out of this basic procedure, eight different variations are created for each building's mask corresponding to the n2.5-DUSM of building outlines, as shown in Figure 6.8 and explained in Table 6.1. Several morphological operations on pixels are scrutinised by applying specific structuring elements (Figure 6.7) and a decision about how to proceed with the fastest techniques is made, applying small changes in the used parameters. In fact, slight changes in the definition of the parameters of the morphological operations (size and shape of the neighbourhood, filters used in the edge detection) can dramatically affect the results. The use of more sensitive edge detectors allows the identification of the edges of internal surfaces in the case of complex geometries. For instance, the main issue with morphological indicators is related to the variation of the vertical section of the object. As a sample, please refer to Figure 6.9, where the tower does not correspond to the footprint of the basement. These complex shapes are difficult to analyse because the external perimeter does not include the edges of the tower. Hence, many edge detectors do not recognize the internal perimeters.

Concerning the proposed eight variations in particular shown in Figure 6.8, the external edges of objects can be detected using different neighbourhoods for the variations number 1 and 2. In addition, the use of more sensitive edge detectors allows the identification of the boundaries of internal surfaces in the case of complex geometries (variations 3, 5 and 7). Finally, three optimized variations (variations 4, 6 and 8) are proposed combining the computation of external edges of case 2 with the computation of internal edges of case 3, 5 and 7.

Chapter 6. Assessment of the morphological properties of the urban texture

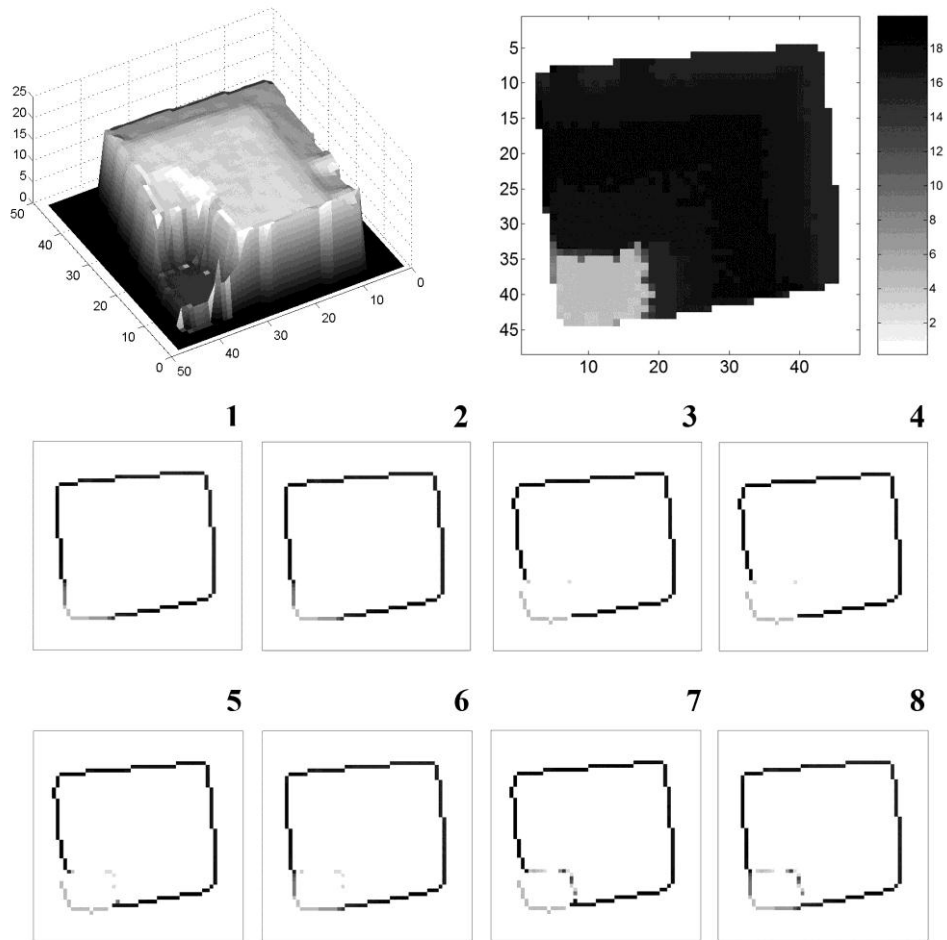


Figure 6.8. An example of an analysed object and the detection of edges with 8 variations on the procedure.

6.3 Case-study: Digital urban morphometrics - automatic extraction and assessment of morphological properties of buildings

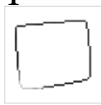
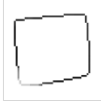
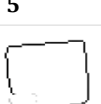
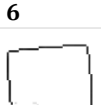
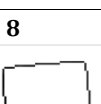
Case ID	1 Enhancement on the original DUSM	2 Morphological operation to contract and dilate the perimeter of the object + application of the Canny filter			3 Morphological operation on the enhanced model (point 1) to detect edges applying a diamond filter				Short description of the procedure
		Description of the applied neighbourhood			Description of the applied neighbourhood			Detection of internal edges (if complex geometry)	
		Size	Shape	# of neighbours	Size	Shape	# of neighbours		
1 	no	3x3	diamond	5					
2 	No	5x5	diamond	13					
3 	Yes	5x5	diamond	13	3x3	diamond	5	yes	
4 	only for internal facades							yes	Selecting detected external edges from case 2 and internal ones from case 3
5 	yes	5x5	diamond	13	3x3	square	9	yes	
6 	only for internal facades							yes	Selecting detected external edges from case 2 and internal ones from case 5
7 	yes	5x5	diamond	13	5x5	diamond	13	yes	
8 	only for internal facades							yes	Selecting detected external edges from case 2 and internal ones from case 7

Table 6.1. Eight variations on the morphological operations used to enhance the edges of vertical surfaces.

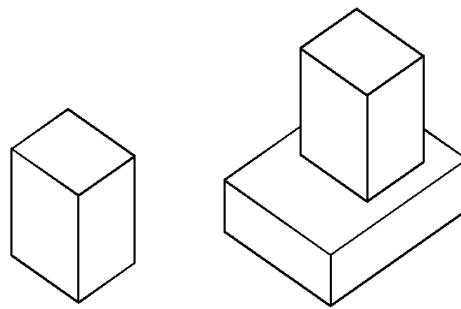


Figure 6.9. From simple (left) to complex (right) geometry: the tower on a basement.

Once the external and the internal edges are detected, the height of the analysed pixel can be straightforwardly derived by subtracting the maximum height value by the minimum height value of the selected neighbourhood pixels.

With regards to determining the length of pixels, it is important to precisely locate those pixels belonging to the diagonal segments on the perimeter and assign a longer linear extension. It is not a straightforward task to define the correct method to calculate the perimeter of an object based on a pixel structure. In order to reduce the error during the computation, it was decided to distinguish only between two lengths to assign to each edge pixel: pixels of value $1*u$ and “diagonal” pixels with value $\sqrt{2}*u$ (where u represents the original unit of the pixel-grid defined on the n2.5-DUSM of building outlines used). This method is a good compromise for a quick and accurate computation; for instance, methods that use more fine-grained pixel-lengths require the application of larger neighbourhoods to detect the inclination of the pixel, and this operation often leads to computational mistakes. Hence, it was decided to apply an analysis performed on the sequence of the perimeter segment and simply assigning the $\sqrt{2}*u$ value every time the pixels in the series are only 8-connected but not 4-connected⁷ (refer to Figure 6.10).

Finally, for all selected pixels, by multiplying the height of each pixel by its length, the area of each facade segment can be obtained.

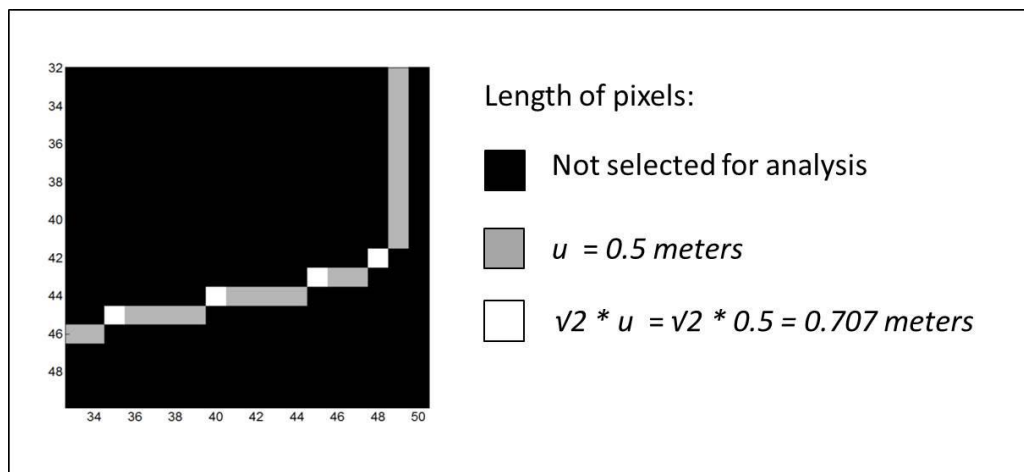


Figure 6.10. A detail of the edge of an object showing the lengths assigned to each pixel. The unit u of the grid is 0.5 metres: pixels have values of $1*u$ and $\sqrt{2}*u$.

⁷ The term of “adjacency” is used in image processing to define “connected components”, also referred as “objects”. Pixels can be primarily 4-connected or 8-connected, depending on the definition of adjacency. Generally, 4-connected pixels do not count diagonal neighbours, whereas 8-connected do. (Gonzalez et al., 2004).

6.3 Case-study: Digital urban morphometrics - automatic extraction and assessment of morphological properties of buildings

A validation process was applied to the calculation of the length of pixels belonging to the external facades of each of the 44 buildings of the square area near the Rhone River, in the old town of Geneva: firstly, for each building, 2-D vector GIS data corresponding to a building footprint was transformed into a raster layer (mask), which means 44 masks with a sampling size of 0.5 meters were produced; secondly, for each of these masks, the length of pixels equivalent to the external facades of a building was compared to the length of the corresponding building outlines calculated from the 2-D vector GIS data. Results related to this validation process are presented as follows:

- each building deviation varies from -3% to 5%;
- the average building's deviation is 0.9%, for a standard deviation of 2.4%;
- the average building's absolute deviation is 1.9%, for a standard deviation of 1.6%.

Note that these results are highly dependent on: (1) the sampling size of the raster layers used, and (2) the way vector data is transformed into a raster format (in this case a common GIS software was used). Nevertheless, considering end-user needs and applications of this type of information, results were considered more than satisfactory.

6.3.5.3 Area of roofs

The main interest of this study is focused on the oblique surfaces (real areas of roofs) and not the projected ones. Thus, a slightly different procedure is applied in this case:

- a mask corresponding to the n2.5-DUSM of roof lines is created for each building roof in order to compute the slope area of each pixel. Hence, the oblique area of each pixel can be calculated by applying simple trigonometric formulae:

$$Real\ Area_{pixel(i,j)} = \frac{Projected\ Area_{pixel(i,j)}}{\cos(Slope_{pixel(i,j)})} \quad (6.1)$$

For instance, the areas of pixels may vary depending on the inclination. The surface of the pixels can easily be calculated. In this work, six classes of slopes are distinguished (each class was characterised in steps of 15 degrees, from 0 to 75 degrees), which are latter used for statistical analysis purposes. In order to eliminate the parts that can represent the contours of buildings (the vertical surfaces) a reclassification of the slopes of the pixels can be undertaken. In Figure 6.11 the reclassification of the slopes on a pixel basis is shown: on the left, the slopes are represented on a pixel basis, whereas on the right slopes higher than 60 degrees are set to 0. Moreover, using different structuring elements (3 pixels by 3 pixels or 13 diamond pixel filter sizes), slopes higher than 45° or 60° are also reclassified by selecting the mean value of the neighbourhood pixels of the reclassified pixel;

- the segmentation procedure for laser scanning data is independently implemented to search for homogeneous vector planar faces, allowing to calculate a slope value for each of these planar faces. After, for each case-study area, all vector planar faces slopes are firstly transformed into a raster format (sampling size of 0.5 meters), producing information about slopes; secondly, for each building and using this new mask derived from the segmentation procedure on LiDAR data, an additional mask with information about slopes is created.

Finally, in order to derive the area of each roof, pixel areas⁸ overlaying the corresponding 2-D projection of 3-D digital (vector) roof areas are aggregated and summed.

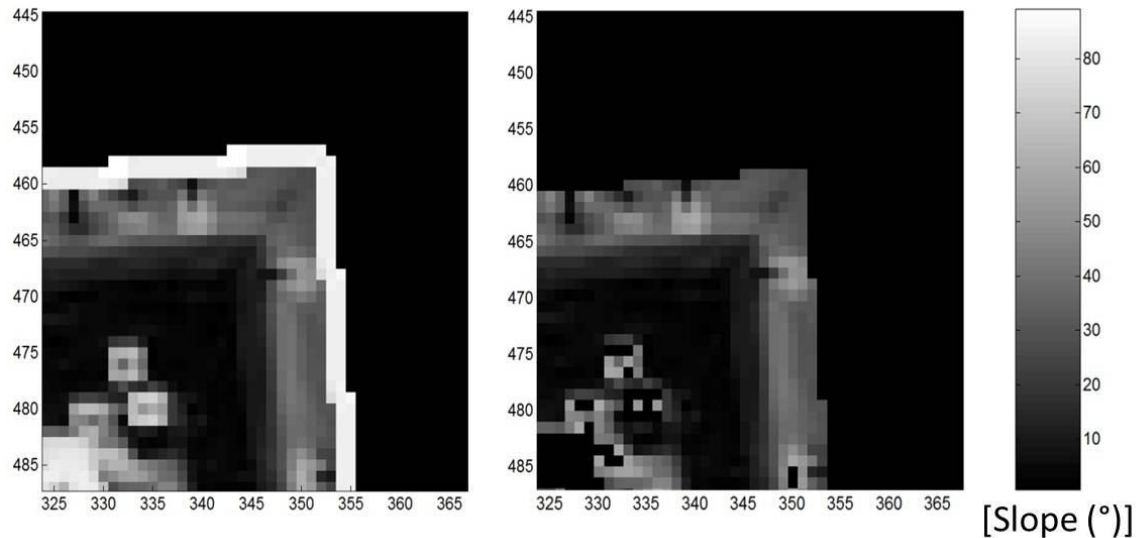


Figure 6.11. The reclassification of the slopes of the roof pixels. Left hand-side image: the slopes on a pixel basis; right hand-side image: the slopes higher than 60 degrees are set to 0. In fact, brighter pixels on the edges of the object and features do not appear on the image on the right.

6.3.6 Performed validations

According to Aalders (2002) and Devillers *et al.* (2005), spatial data quality (SDQ) can be described using five to eleven elements. One of such is the description of spatial/positional accuracy of a given dataset. Hence, for each building, a statistical analysis that compares the results of the computation (volume, area of facades and area of roofs) with the same type of information stored as attributes in a 3-D vector model of the built environment is used to validate the results. It is important to mention that even if the main focus of this thesis is related to different environmental analysis at the scales of the neighbourhood or the city, in this specific case, the statistical analysis of the extracted morphological properties of buildings is done by comparing building by building values. Anyway, the goal of the research is to evaluate the reliability of this method considering different typologies of buildings, from simple to complex. In this case, also a set of building has to be considered, which is more related to a “neighbourhood analysis” concept. Moreover, as highlighted in the next chapters of this thesis, the application of the morphological properties of buildings (for instance, the area of roofs) on environmental studies is never individually done, but instead considering a set of buildings, eventually all the buildings belonging to a same neighbourhood.

The analysis is grouped into two different parts, corresponding to the 2 case-study areas (please refer to Table 6.2). In order to organize the statistical analysis, 3 possible geometric primitives are considered, which describe both roofs and facades. These categories represented in Figure 6.12 are mainly:

1. The flat roofs and simple facades: both are defined by flat planes without interruptions (e.g. flat roofs);

⁸ The total area of each roof comes straightforwardly by adding the elementary areas of its pixels.

6.3 Case-study: Digital urban morphometrics - automatic extraction and assessment of morphological properties of buildings

2. The classic roofs and the intermediate facades: these are defined by multiple surfaces but do not include jumps among its faces (typically continuous pitched roofs);
3. The complex roofs and the multifaceted facades, whereby different planes determine discontinuities among the surfaces (typically shaded roofs or facades in terraced buildings).

	<i>Number of analysed buildings</i>
1 – Case study at CERN	
1.A - Analysis of normalized 2.5-D DUSM derived from building outlines and LiDAR data for volume calculation	10
1.B - Analysis of the 2.5-D nDUSM derived from the 2-D projection of the 3-D model of roofs lines and LiDAR data for areas of roofs calculation	10
1.C - Analysis of the 2.5-D nDUSM derived from building outlines (also external facades of the 3-D model of buildings) and LiDAR data for areas of facades calculation	18
2 – Case study in the Centre of Geneva	
2.A - Analysis of the 2.5-D nDUSM derived from building outlines and LiDAR data for volume calculation	34
2.B - Analysis of the 2.5-D nDUSM derived from the 2-D projection of the 3-D model of roofs lines and LiDAR data for areas of roofs calculation	17
2.C - Analysis of the 2.5-D nDUSM derived from building outlines (also external facades of the 3-D model of buildings) and LiDAR data for areas of facades calculation	44

Table 6.2. The set of analyses conducted on the 2 case-study areas using different source information.

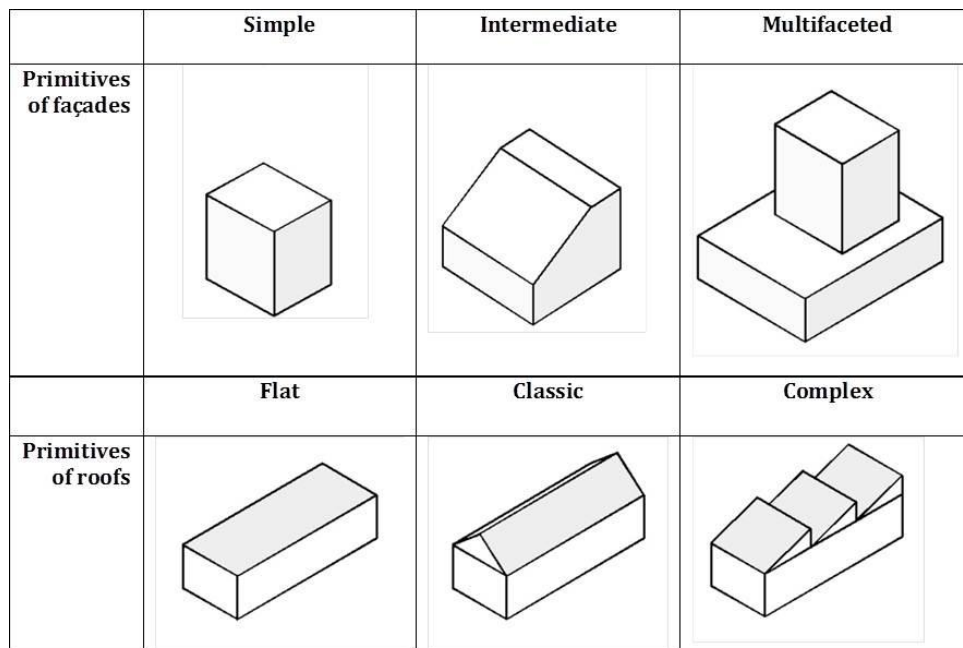


Figure 6.12. Different primitives considered for façades and roofs.

In this case, the classification (only used for statistical validation) of each roof into the three different types of roof primitives was done manually, using aerial photos of the case-study areas. This is particularly important in the case that aerial photos of the analysed zones are not available or if aerial photos are available but the number of building roofs is too large for a visual classification. As proposed by Chen *et al.* (2009), using object-oriented classification of very high resolution imagery and LiDAR data could also be readapted and tested in order to classify each roof into different types of roof primitives, however this specific topic fall beyond the main focus of research of this study.

The results, which are summarized in the tables B.1 to B.10 of the appendix B, are grouped by morphological property, distinguishing between: (a) the global (all buildings) and the building by building analysis; (b) the use of the unenhanced n2.5-DUSM, enhanced n2.5-DUSM, optimized n2.5-DUSM and the segmentation procedure; (c) the level of complexity of building and roof types. Moreover, the “global deviation error” (percentage: %) is defined as the relation of the global (all buildings) calculated morphological indicator derived from LiDAR data and the theoretical known value stored as an attribute in the 3-D vector model, whereas the “absolute building deviation error” (percentage: %) for each building represents the absolute relation of the calculated morphological indicator derived from LiDAR data and the theoretical known value stored as an attribute in the 3-D model.

6.3.7 Significance statistical analysis of the proposed method

Once again (as described in section 5.8.3), a two-tailed “t-test” significance statistical analysis is applied to each of the morphological properties of buildings calculated using the: (1) unenhanced n2.5-DUSM, (2) the enhanced n2.5-DUSM, (3) optimized n2.5-DUSM, and (4) segmentation procedure. This test allows the interpretation of the probability related to the decrease of the absolute deviation error between each pair of buildings of the following cases: (a) the unenhanced and the enhanced n2.5-DUSM; (b) the unenhanced n2.5-DUSM and the segmentation procedure; (c) the unenhanced n2.5-DUSM and the optimized n2.5-DUSM. As already described in section 5.8.3, the reason to have applied a two-tailed “t-test” and not a simpler one-tailed “t-test” is that the differences between each pair of buildings can be positive or negative (calculated values can be higher or lower than the theoretical known value stored as an attribute in the 3-D vector model), which ensures a more strict significance statistical test. Thus, for each of the three morphological properties of the evaluated buildings, the null hypothesis H_0 is tested, as shown in Table 6.3.

6.3 Case-study: Digital urban morphometrics - automatic extraction and assessment of morphological properties of buildings

Significance statistical analysis (<i>t</i> test; level of significance: 0.05)		
	Null Hypothesis (H_0)	Hypothesis 1 (H_1)
Test 1 For volumes, areas of roofs and areas of façades	No significant improvement between the use of the unenhanced and the enhanced models for the calculation of volumes, areas of roofs and areas of façades	Significant improvement between the use of the unenhanced and the enhanced models for the calculation of volumes, areas of roofs and areas of façades
Test 2 Only for areas of façades	No significant improvement between the use of the unenhanced and the optimized models for the calculation of areas of façades	Significant improvement between the use of the unenhanced and the optimized models for the calculation of areas of façades
Test 3 Only for areas of roofs	No significant improvement between the use of the unenhanced model and the segmentation technique for the calculation of areas of roofs	Significant improvement between the use of the unenhanced model and the segmentation technique for the calculation of areas of roofs

Table 6.3. Hypothesis related to the significance tests conducted in this study.

The significance level (α) is set to 0.05, which means that H_0 is rejected in favour of H_1 when α is lower than 0.05.

6.3.7.1 Significance statistical analysis related to the calculation of volume

In general, it is fairly easy to derive volumes using DIP techniques and such work does not propose significant improvements to the traditional pixel based computation. In particular, the conducted analysis summarized in tables B.1 and B.2 of the appendix B shows that no major improvement can be reached using the enhanced n2.5-DUSM in order to reduce the global deviation error, even if at the building's scale (table B.2 of the appendix B) some minor improvement not significant was noticed for the absolute building deviation error. This is so because in the process of enhancement on the perimeter the distribution of height values inside the neighbourhood is averaged, thus reducing the effects of LiDAR interpolation and obtaining more defined edges; this enhancement does not really affect the overall volume calculation, but it has a significant effect on the calculation of the facade areas. Moreover, results of deviation demonstrate that volumes are always slightly overestimated for both the enhanced and the unenhanced models.

The significance statistical analysis that tests the improvement of using the unenhanced model versus the enhanced model for the calculation of volumes is shown in Table 6.4, confirming that no significant improvements were achieved for the different types of considered buildings.

CERN + Centre of Geneva			
Volumes of roofs			
Significance statistical analysis (<i>t</i> test; level of significance: 0.05)			
<i>Volumes of 44 buildings (complex, classic and flat roofs)</i>	Test 1 Enhanced Model	<i>Volumes of 21 buildings (classic only)</i>	Test 1 Enhanced Model
Unenhanced Model	0.14 <i>Significance of improvement: No</i>	Unenhanced Model	0.13 <i>Significance of improvement: No</i>
<i>Volumes of 10 buildings (complex only)</i>	Test 1 Enhanced Model	<i>Volumes of 13 buildings (flat only)</i>	Test 1 Enhanced Model
Unenhanced Model	0.49 <i>Significance of improvement: No</i>	Unenhanced Model	0.59 <i>Significance of improvement: No</i>

Table 6.4. Significance statistical analysis on volumes to test the improvement of the proposed calculation, referring to different types of considered buildings in the enhanced and unenhanced models.

6.3.7.2 Significance statistical analysis related to the calculation of area of facades

The assessment of the accuracy of the eight proposed variations (see for instance Table 6.1) for the calculation of the areas of facades is shown in tables B.3 and B.4 of the appendix B. Referring to the validation of the computation of the areas of the facades, it can be observed that among the proposed variations of the procedure to enhance the model the variation number 7 gives the best results at a global level. However, if the precision is analysed at the building level, variation number 8 performs better. The reason is that, for these particular routines, larger neighbourhoods were used to enhance the edges of the object, thus enabling to detect more internal vertical surfaces, mainly in the case of multifaceted buildings, such as towers on the basement, as shown in Figure 6.9.

The significance statistical analysis that tests the improvement of using the unenhanced model versus the enhanced model (case 7) or versus the optimized model (case 8) shows a significant improvement for the calculation of areas of facades of multifaceted buildings in both cases. Moreover, the significance statistical analysis shows that the optimized model (case 8) also presents a significant improvement when evaluating all three types of buildings in a single dataset (Table 6.5).

6.3 Case-study: Digital urban morphometrics - automatic extraction and assessment of morphological properties of buildings

CERN + Centre of Geneva		
Areas of facades		
Significance statistical analysis (<i>t</i> test; level of significance: 0.05)		
<i>Areas of facades of 62 buildings (multifaceted, intermediate and simple buildings)</i>	Test 1 Enhanced Model (case 7)	Test 2 Optimized Model (case 8)
Unenhanced Model (case 1)	0.095 <i>Significance of improvement: No</i>	1E-3 <i>Significance of improvement: Yes</i>
<i>Areas of facades of 18 multifaceted buildings</i>	Test 1 Enhanced Model (case 7)	Test 2 Optimized Model (case 8)
Unenhanced Model (case 1)	3E-04 <i>Significance of improvement: Yes</i>	1E-3 <i>Significance of improvement: Yes</i>
<i>Areas of facades of 30 intermediate buildings</i>	Test 1 Enhanced Model (case 7)	Test 2 Optimized Model (case 8)
Unenhanced Model (case 1)	0.14 <i>Significance of improvement: No</i>	0.47 <i>Significance of improvement: No</i>
<i>Areas of facades of 14 simple buildings</i>	Test 1 Enhanced Model (case 7)	Test 2 Optimized Model (case 8)
Unenhanced Model (case 1)	0.54 <i>Significance of improvement: No</i>	0.25 <i>Significance of improvement: No</i>

Table 6.5. Significance statistical analysis on the areas of facades to test the improvement of the proposed calculation, referring to different types of considered buildings in the enhanced (case 7) and optimized models (case 8).

6.3.7.3 Significance statistical analysis related to the calculation of area of roofs

In this set of analysis for the assessment of the areas of roofs calculated (tables B.4 to B.10 of the appendix B), DIP techniques are processed on the unenhanced and enhanced 2.5-DUSM of roof lines. With regards to the segmentation procedure applied for areas of roofs calculation, it is important to notice that many super-structures on roofs – especially in the Geneva city centre case-study area – are not easy to detect, namely buildings with classic and complex geometries having many super-structures on roofs caused lower accuracies and higher standard deviations. The reclassification with DIP techniques of those pixels having slopes higher than 45 or 60 degrees proved to be a good alternative for the segmentation procedure.

The significance statistical analysis that tests the improvement of using: (1) the unenhanced model versus the enhanced model by reclassifying slopes $> 45^\circ$ to 0° , (2) the unenhanced model versus the enhanced model with reclassification of slopes $> 45^\circ$ by selecting the mean value of the neighbourhood pixels of the reclassified pixel inside a 13 size diamond mask, and (3) the

unenanced model versus the segmentation procedure, shows a significant improvement for all cases, as presented in Table 6.6.

CERN + Centre of Geneva			
Areas of roofs			
Significance statistical analysis (<i>t</i> test; level of significance: 0.05)			
<i>Areas of all roofs</i> (27 buildings)	Test 1 Enhanced Model (reclassification of slopes > 45° to 0°)	Test 1 Enhanced Model (reclassification of slopes > 45°) by applying a 13 size diamond mask	Test 3 Segmentation procedure
Unenhanced Model (not reclassified)	1E-05 <i>Significance of improvement: Yes</i>	1E-05 <i>Significance of improvement: Yes</i>	2E-05 <i>Significance of improvement: Yes</i>
<i>Areas of complex roofs</i> (15 buildings)	Test 1 Enhanced Model (reclassification of slopes > 45° to 0°)	Test 1 Enhanced Model (reclassification of slopes > 45°) by applying a 13 size diamond mask	Test 3 Segmentation procedure
Unenhanced Model (not reclassified)	1E-03 <i>Significance of improvement: Yes</i>	1E-03 <i>Significance of improvement: Yes</i>	9E-04 <i>Significance of improvement: Yes</i>
<i>Areas of classic roofs</i> (6 buildings)	Test 1 Enhanced Model (reclassification of slopes > 45° to 0°)	Test 1 Enhanced Model (reclassification of slopes > 45°) by applying a 13 size diamond mask	Test 3 Segmentation procedure
Unenhanced Model (not reclassified)	0.041 <i>Significance of improvement: Yes</i>	0.045 <i>Significance of improvement: Yes</i>	0.040 <i>Significance of improvement: Yes</i>
<i>Areas of flat roofs</i> (6 buildings)	Test 1 Enhanced Model (reclassification of slopes > 45° to 0°)	Test 1 Enhanced Model (reclassification of slopes > 45°) by applying a 13 size diamond mask	Test 3 Segmentation procedure
Unenhanced Model (not reclassified)	0.037 <i>Significance of improvement: Yes</i>	0.039 <i>Significance of improvement: Yes</i>	0.034 <i>Significance of improvement: Yes</i>

Table 6.6. Significance statistical analysis on roof areas to test the improvement of the proposed calculation, referring to different types of considered buildings in the enhanced and unenhanced models and the segmentation procedure.

6.3.8 Conclusions

Outcomes shown in the tables B.1 and B.10 of the appendix B, complemented by the significance statistical analysis presented in section 6.3.7, demonstrate that the proposed method to derive morphological properties can obtain high levels of accuracy, thus enhancing the potential uses of LiDAR data for numerous applications, typically for the assessment of the UEQ at the city and neighbourhood scales, such as the estimation of the potential deployment of renewable energies in the built environment and the determination and monitoring of several urban indicators. The best results achieved from all the techniques and models used are summarized in Table 6.7.

6.3 Case-study: Digital urban morphometrics - automatic extraction and assessment of morphological properties of buildings

CERN + Centre of Geneva Volumes			
	Global Analysis (Unenhanced Model)	Building by Building analysis (Enhanced Model)	
Type of building	Global deviation error	Absolute building deviation error	Standard deviation
Total	2.30%	4.09%	3.26%
Simple	3.82%	4.15%	3.30%
Intermediate	0.99%	4.25%	2.93%
Multifaceted	0.90%	5.49%	4.40%

CERN + Centre of Geneva Areas of facades			
	Global Analysis (Enhanced Model: case 7)	Building by Building analysis (Optimized Model: case 8)	
Type of building	Global deviation error	Absolute building deviation error	Standard deviation
Total	-3.45%	6.78%	6.77%
Simple	-5.03%	5.04%	2.80%
Intermediate	3.53%	4.07%	4.15%
Multifaceted	-9.78%	10.92%	7.32%

CERN + Centre of Geneva Areas of roofs			
	Global Analysis (Segmentation Technique)	Building by building analysis (Segmentation Technique)	
Type of building	Global deviation error	Absolute building deviation error	Standard deviation
Total	1.19%	3.47%	4.09%
Simple	-1.57%	1.19%	0.59%
Intermediate	-0.95%	2.79%	3.43%
Multifaceted	1.74%	4.45%	4.71%

Table 6.7. Review of best results achieved by applying the proposed methods.

A few general remarks to the results achieved considering the significance statistical analysis applied are presented as follows:

- For the analysis of volumes, the use of the enhanced model is not justified. In fact, the global analysis with the unenhanced model performs better since the procedure of enhancement tends to overweight the height values of pixels, even if results are very similar;
- The enhanced model is particularly suitable to improve results for the calculation of facade and roof areas;
- The segmentation procedure performs better for the analysis of roof areas, even if the use of DIP for reclassification of slopes higher of 45° by selecting the mean value of the neighbourhood pixels of the reclassified pixel inside a 13 size diamond mask shows to be a good alternative when segmentation procedure is not applied to raw LiDAR data;

- The optimized model shows to be a good option for the calculation of facade areas, especially for zones characterised by low density built-up areas with simple buildings;
- The significance statistical analysis applied in this case-study gives more sense to the significance statistical analysis presented in the precedent chapter, thus highlighting the importance of constructing and using both enhanced 2.5-DUSM of building outlines and 2.5-DUSM of roof lines.

Finally, it is important to note that the influence of the density of raw LiDAR points in the method developed and implemented for this case-study is certainly not negligible - in this case, the density of raw LiDAR points is around 4 point/m². Although it is not the main purpose of this research, it would be certainly interesting and a focus for further research to analyse what could be the impact of using lower or higher density of raw LiDAR points on the accuracy of the results achieved.

6.4 Case-study: incorporation of morphological properties of buildings computed from GIS and LiDAR data on an urban multi-agent vector based geo-simulator

6.4.1 Presentation

This case-study highlights the relevance of incorporating the morphological properties of buildings as an effective input into another research process.

The framework of this research refers to the dynamics of cities, understood as complex auto-organized urban systems (Berger and Nouhaud, 2004). Nowadays, contemporary cities are considered to be a complex and unstable system – in fact, it has become extremely difficult to understand and control its evolution and form. Modern metropolises are somehow governed by laws of morphogenesis⁹, going from local to global scales. Moreover, actual urban planning methods are no longer adapted to the fast and intricate growth of modern cities. The main idea is to provide an efficient analysis support, in the form of a new software simulation platform, which should enable to evaluate scenarios of dynamic impacts induced by new planned architectural programs.

The proposed method is quite innovative as it is based upon multi-scale vector multi-agent modelling of buildings - their physical neighbourhood, spatial and topological relationships, and states and behaviours according to modelled dynamic laws of urban morphogenesis from micro level (surfaces in buildings, buildings and programs) to macro level (metropolis), as presented by Silva (2010). The laws used in this model refer to general architecture knowledge of city morphogenesis, mainly formulated by Alexander (2005). Visibility and sunshine analysis are some of the morphogenetic laws that can be considered, and are both involved in the perception computation of an agent building geo-simulator, as it was presented in a previous work of the author (Carneiro *et al.*, 2008).

In this case-study, the intention is to go a step further, presenting the implementation of morphological properties of buildings on this same computation. Considering a building's morphology under analysis, its properties are extracted following the method proposed in the previous section (6.3), which is complemented by additional processes, presented as follows. Once again, it is based on a 2-D GIS vector database and a normalized n2.5-DUSM of building

⁹ In architecture and urbanism domain, morphogenesis designs the growing of the city's form, allowing to create material objects, such as buildings, roads, etc. (Silva, 2010)

6.4 Case-study: incorporation of morphological properties of buildings computed from GIS and LiDAR data on an urban multi-agent vector based geo-simulator

outlines, with a resolution grid of 1 by 1 meter, constructed from a hybrid approach that uses GIS and LiDAR data, or a segmentation procedure for LiDAR data. The case-study for application is the district of Chavannes, in Lausanne, where GIS and LiDAR data are available.

As described in section 4.2.6, this type of indicators is part of a larger group of indicators included in the set of indicators and indexes belonging to the stake “assessment of the morphological properties of the urban texture”.

The morphological indicators of buildings studied are presented as follows:

- volume;
- envelope area = area of ground + area of facades + area of roofs;
- type of roof;
- average height;
- number of faces.

The indexes derived from these indicators are presented as follows:

- envelope area-to-area of ground ratio;
- envelope area-to-total volume ratio;
- volume-to-number of faces ratio.

These indicators and indexes provide wide capabilities for spatial analysis, better representation of urban area features and can become the essential basis for advanced architectural and urban planning design work. Additionally, the results presented confirm both the potential and limitations of LiDAR data with respect to these tasks.

For details about related work on the subject of urban geo-simulation, cellular agents and fractal cities please consult Silva (2010).

6.4.2 Data sources used and normalized 2.5-DUSM constructed

The case-study area is located in the district of Chavannes, city of Lausanne, as shown in the left hand-side image of Figure 6.13. In the right hand-side image of Figure 6.13 an illustrative example of the 2.5-DUSM of building outlines without vegetation constructed for the same case study area is shown.

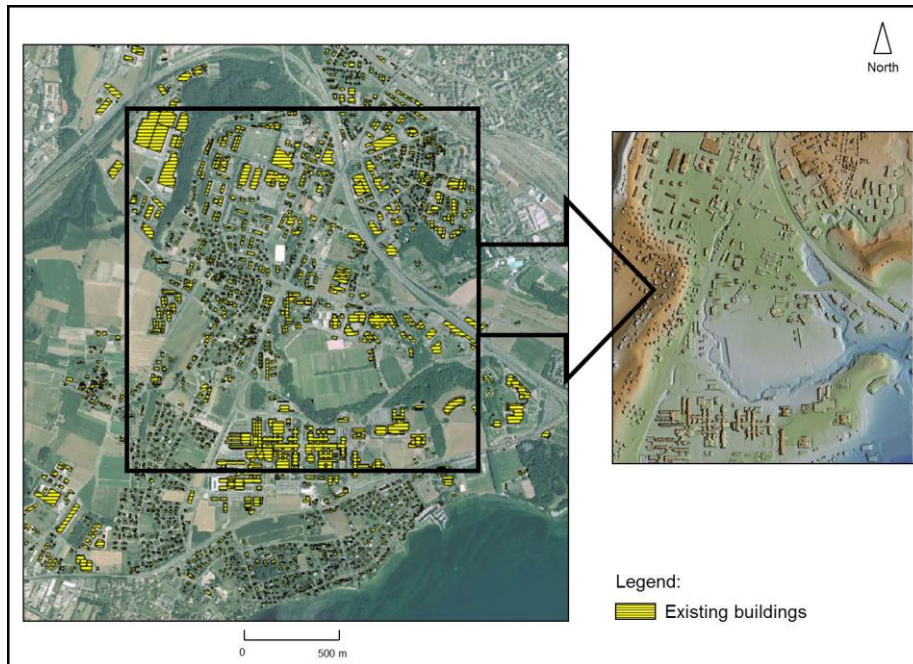


Figure 6.13. Left hand-side image: 2-D GIS building outlines and aerial pictures of the case study area, within an area of 2.000×2.000 meters district of Chavannes, city of Lausanne; right hand-side image: illustrative example of the 2.5-DUSM of building outlines without vegetation of the same case study area.

The following data was used: (1) 2-D GIS building outlines and (2) LiDAR data. The LiDAR data used for the construction of the n2.5-DUSM of building outlines of the district of Chavannes, city of Lausanne, has a density of 1 points/m², a planimetric accuracy RMSE of 20 centimetres and an altimetric accuracy of 15 RMSE centimetres. For more details about the method used for the construction of the n2.5-DUSM of building outlines used in this case-study please consult section 5.5. The results of the segmentation process on LiDAR data described in section 5.7 are used to determine the slope feature of the roof planes, and to classify each roof into three possible geometric primitives: flat, classic or complex.

Finally, it is worth mentioning that the 2-D projection of 3-D vector roof lines is not available in this case-study area of Lausanne. Indeed, it is not possible to construct a n2.5-DUSM of roof lines or apply the segmentation procedure to a selection of pre-classified LiDAR points being within the roof lines. Thus, in order to extract all the morphological indicators and indexes presented in this case-study, only the n2.5-DUSM of building outlines is constructed and the segmentation procedure applied is based on a selection of pre-classified LiDAR points being within the building outlines (2-D vector maps).

6.4.3 The calculation of the morphological indicators and indexes

6.4.3.1 Volume and envelope area

The calculation of the volume and the envelope area of each building follow the procedure described in section 6.3.5.1. The only element that needs to be added for the calculation of the envelope area is the real area of ground, which is straightforwardly obtained from the geometry of type surface stored in the 2-D GIS cadastral database. A theoretical and very simple example is shown in Figure 6.14.

6.4 Case-study: incorporation of morphological properties of buildings computed from GIS and LiDAR data on an urban multi-agent vector based geo-simulator

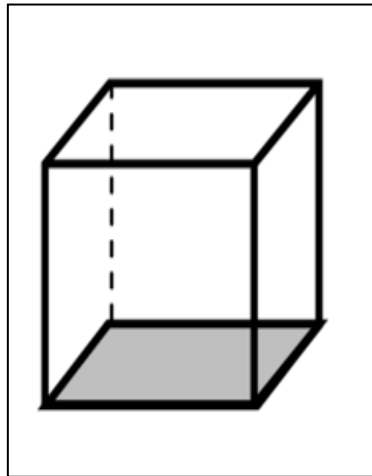


Figure 6.14. Ground surface (in grey)

6.4.3.2 Type of roof

The classification of each type of roof is based on the segmentation procedure for LiDAR data presented in section 5.7. The segmentation of roofs for this case-study (district of Chavannes, Lausanne, Switzerland) is shown in Figure 6.15.

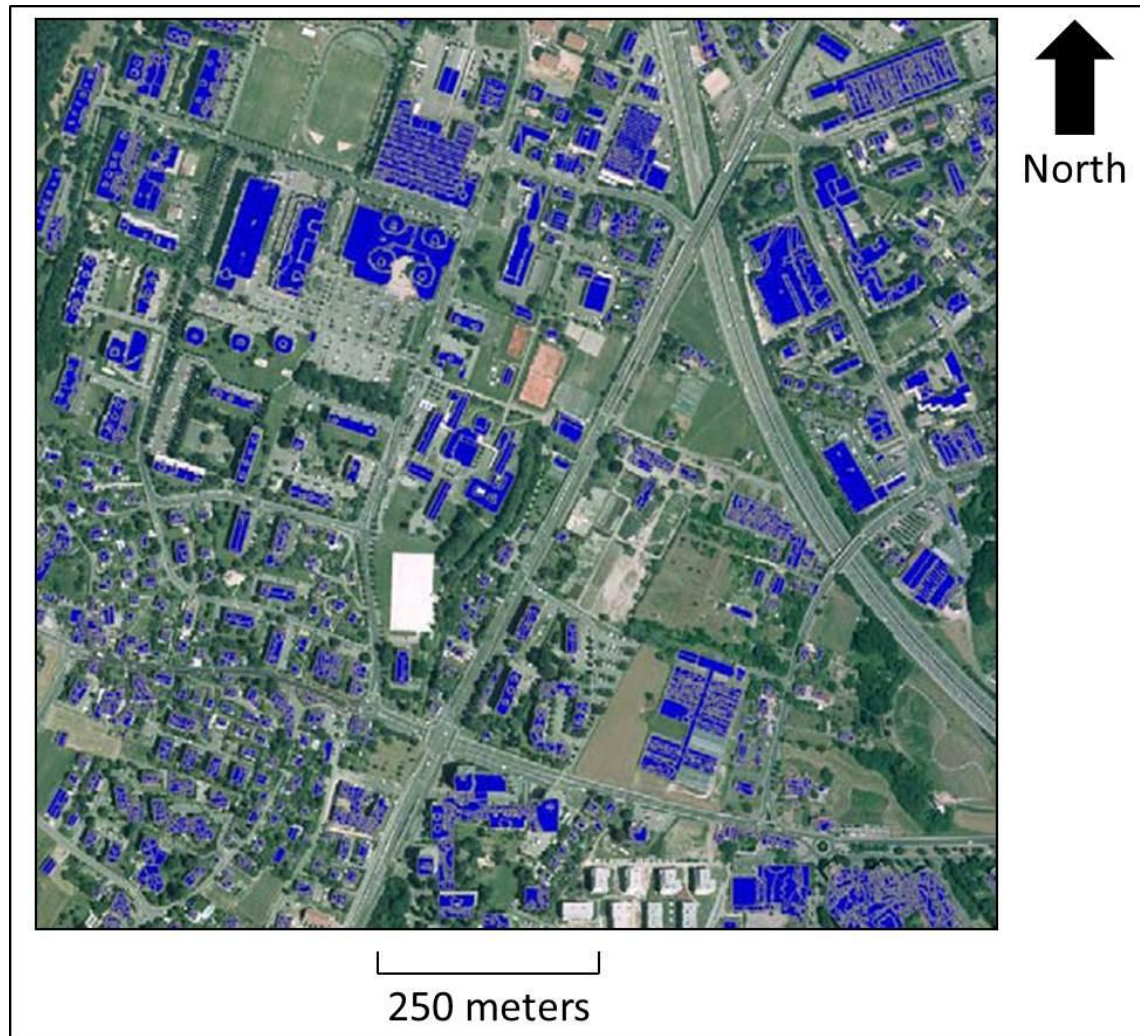


Figure 6.15. Result of the roof segmentation procedure for LiDAR data for this case-study (district of Chavannes, Lausanne, Switzerland).

Each roof is classified into specific roof primitives, as already described in section 6.3.6: flat roof, classic roof and complex roof (Figure 6.12). It is important to note that a classic roof includes primitives of type hip, gable and desk (Figure 6.16). The hip roof is the most common roof in housing settlements for single-family homes. It is rather distinguishable due to its characteristic shape. In some cases though, faces of this type of roofs present different slopes. The gable roof is characteristic of housing estates, as well as industrial buildings. Usually, it contains two faces with the same slope, which means both faces are distributed symmetrically. The desk roof is characterized by a single face presenting a slope different than zero (non-flat). Usually it corresponds to a garage of a residential building.

6.4 Case-study: incorporation of morphological properties of buildings computed from GIS and LiDAR data on an urban multi-agent vector based geo-simulator

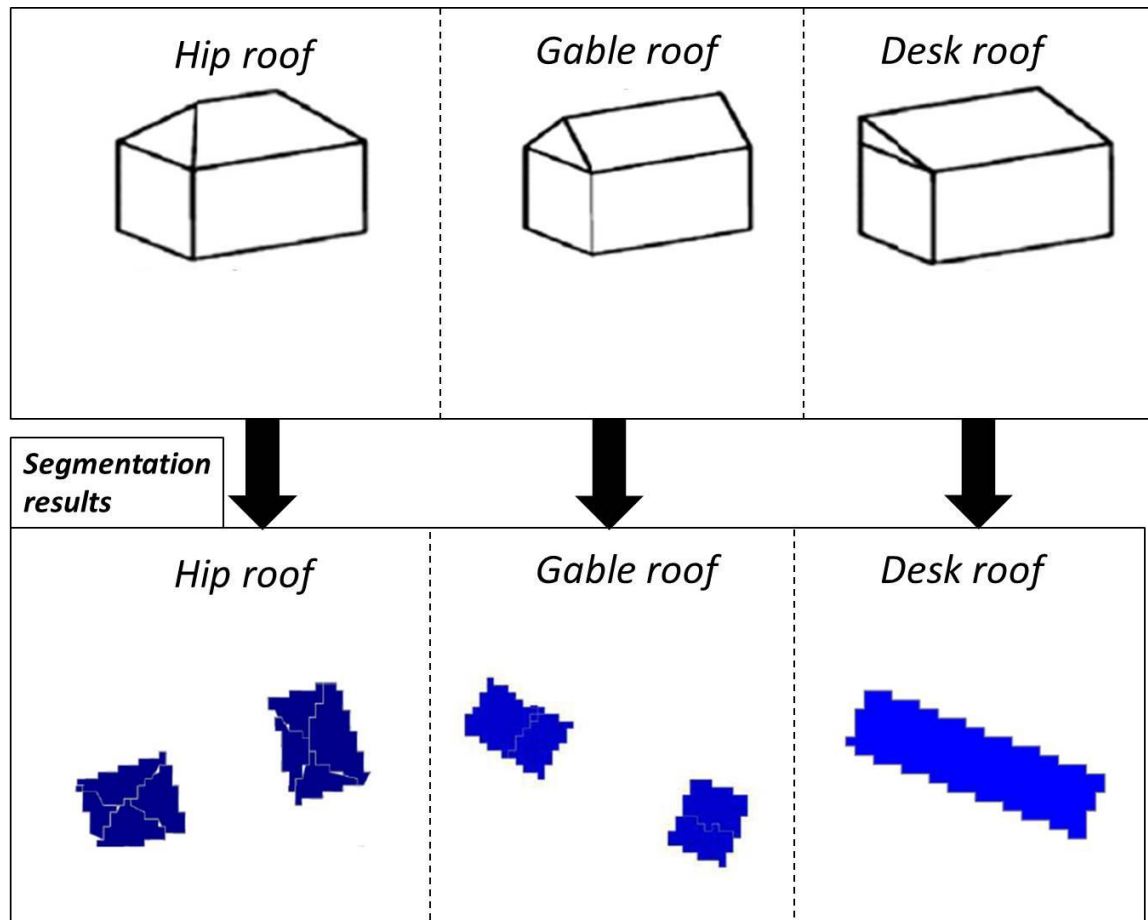


Figure 6.16. Primitives used for the classification of classic roofs (includes hip, gable and desk roofs) and some examples of segmentation results for these same primitives.

The type of roof classification is made by assigning one of the three classes of primitives considered, according to three parameters:

- 1) - the number of faces derived from the segmentation procedure for LiDAR data;
- 2) - the slope of each roof face derived from the segmentation procedure for LiDAR data;
- 3) - the evaluation of the zones of discontinuity of the n2.5-DUSM of building outlines.: firstly, using a mask for each building (using the method proposed in section 6.3.4), the internal edges of the object (applying a Canny edge detector, as presented in section 6.3.5.2) are detected; secondly, the difference of heights between these zones of discontinuity is analysed. This process is performed by considering a limit value (in this case-study 2 meters) between contiguous pixels belonging to the zones of discontinuity of the n2.5-DUSM of building outlines. This point enabled to evaluate the distribution of the building volume in the space: an example is shown in Figure 6.17.

The workflow summarizing the method applied for the classification of each roof into one of the three classes of primitives considered is shown in Figure 6.18.

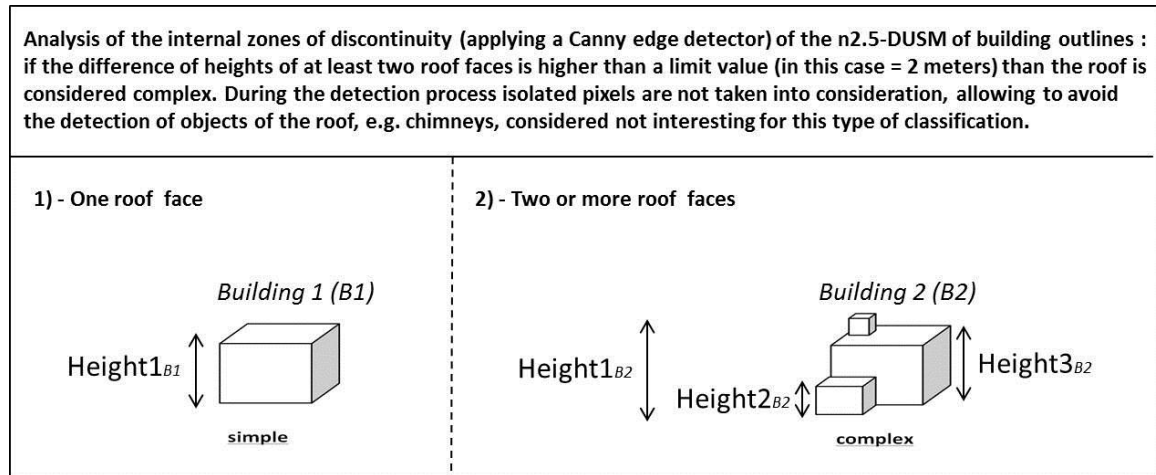


Figure 6.17. Roof with low complexity (left) and roof with high complexity (right).

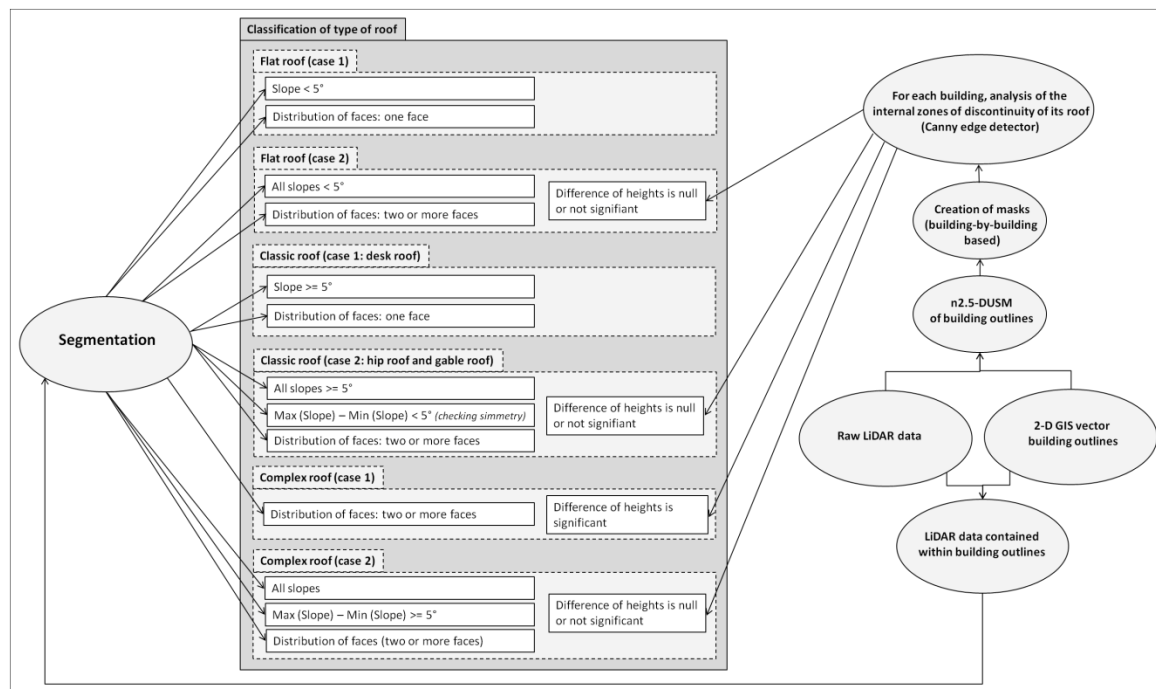


Figure 6.18. Workflow showing the method applied for the classification of each roof into one of the three classes of primitives considered.

Finally, it is important to note that this method of classifying each type of roof was statistically validated for a set of 50 buildings belonging to this case-study area of the district of Chavannes, city of Lausanne, Switzerland, and reached an accuracy of around 90% (Zwolak, 2008).

6.4.3.3 Average height

By grouping all pixels of the n2.5-DUSM of building outlines belonging to each GIS cadastral building's outline it is possible to calculate its mean building height, as shown in the workflow of Figure 6.19.

6.4 Case-study: incorporation of morphological properties of buildings computed from GIS and LiDAR data on an urban multi-agent vector based geo-simulator

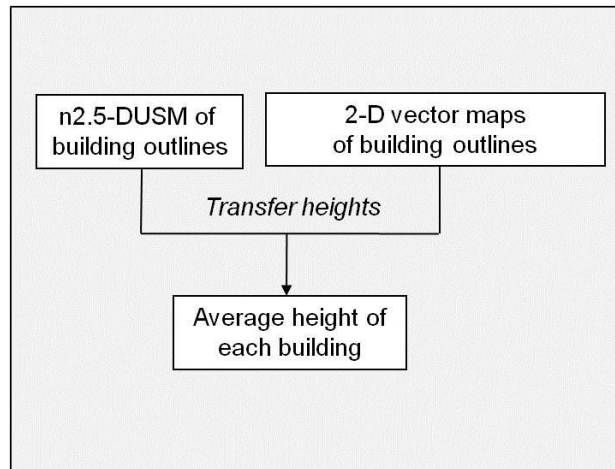


Figure 6.19. Workflow showing the method applied for the calculation of the average height of each building.

6.4.3.4 Number of faces

The number of faces of a building is calculated by adding the number of vertical faces of buildings and the number of faces belonging to roofs, as shown in the workflow of Figure 6.20. In order to calculate the number of vertical faces, the geometry of the type line stored on the 2-D GIS layer of buildings is directly used. Thus, each line belonging to the same building corresponds to one facade. By adding them the total number of external facades can be determined, as shown in Figure 6.21. The number of faces of non-vertical faces of the roof is directly calculated by adding all of its planar faces which is computed from the segmentation procedure for LiDAR data, as shown in Figure 6.22.

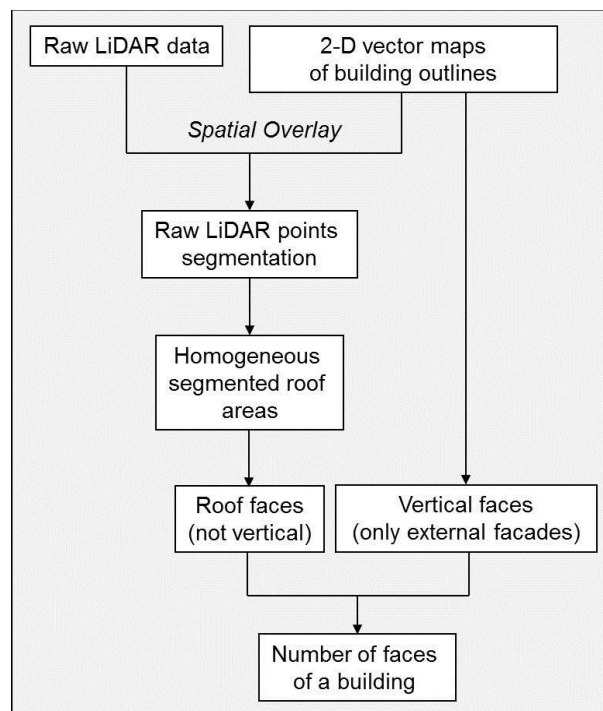


Figure 6.20. Workflow showing the method applied for the calculation of the number of faces of each building.



Figure 6.21. Example of geometry (points and lines) of some buildings belonging to the case-study area, stored in the 2-D GIS cadastral database.



Figure 6.22. Example of segmentation for LiDAR data of two buildings belonging to the case-study area.

Finally, it is important to note that, considering the initial user requirements presented by architects and urban planners, a simplification was applied to the geometry of buildings presenting complex roofs, therefore internal vertical faces of buildings were not considered.

6.4 Case-study: incorporation of morphological properties of buildings computed from GIS and LiDAR data on an urban multi-agent vector based geo-simulator

Moreover, in order to detect the internal walls a method similar to the one presented in section 6.3.5 (applying a Canny edge detector on the n2.5-DUSM of building outlines) could be also taken into analysis.

6.4.3.5 Indexes

A building's complexity is undertaken by calculating three different indexes that are independently computed from the available indicators previously presented in this section. These indexes are further reported in the analysis of the results:

- envelope area-to-area of ground ratio = envelope area/ area of ground: ratio between the whole area of the building (ground area + area of facades + area of roofs) and the area of ground of the building;
- envelope area-to-total volume ratio = envelope area/ volume: ratio between the whole area of the building (ground area + area of facades + area of roofs) and the whole volume of the building;
- volume-to-number of faces ratio = volume / number of faces = ratio between the whole volume of the building and the number of faces composing the envelope of the building.

An example of the indicators and indexes extracted for two buildings belonging to the case-study area of the District of Chavannes, city of Lausanne, Switzerland, and stored in a GIS database, is shown in Figure 6.23.

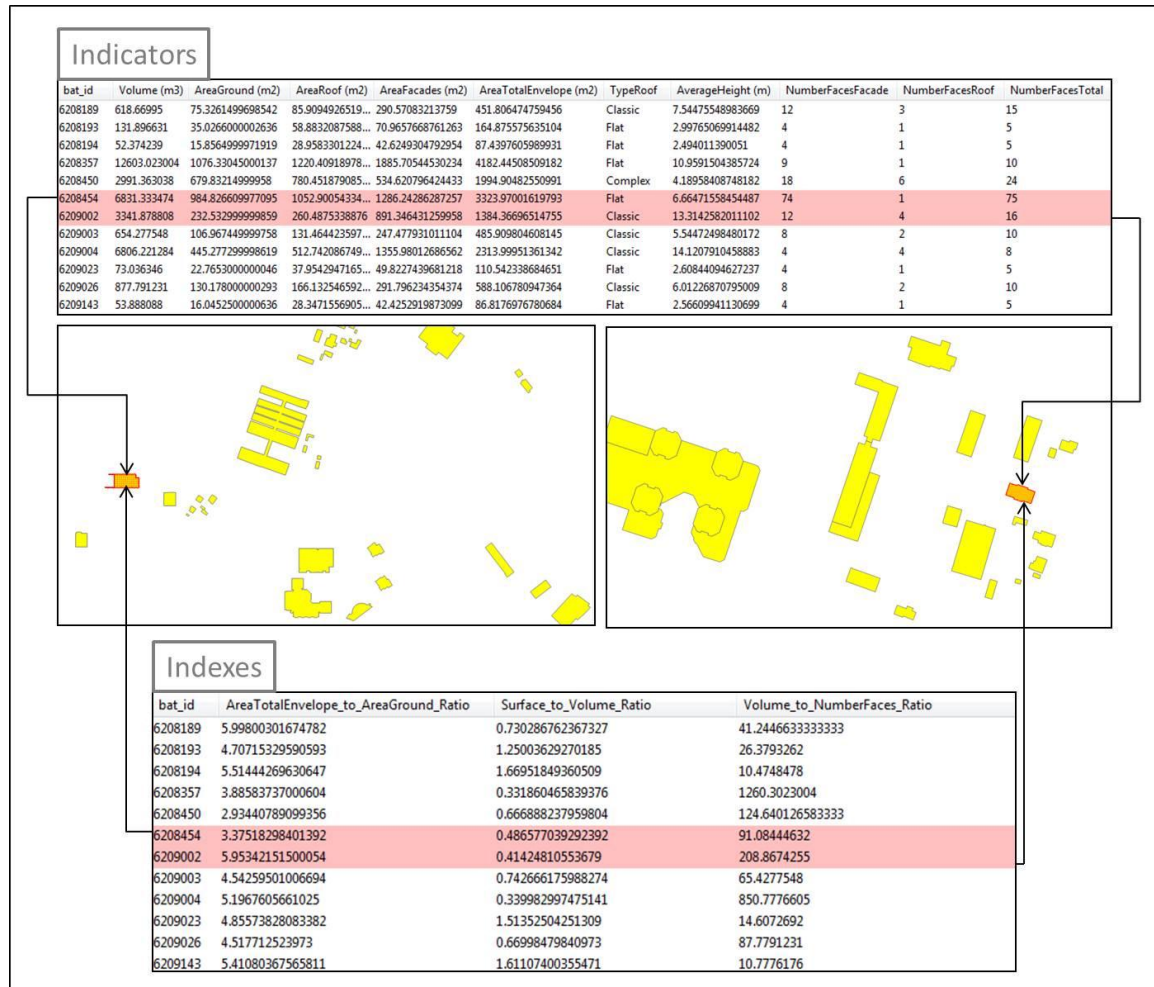


Figure 6.23. Example of the indicators and indexes extracted for two buildings belonging to the case-study area of District of Chavannes, city of Lausanne, Switzerland, and stored in the GIS database.

6.4.4 Brief description of the multi-agent vector based geo-simulator

The geo-simulator used is based on both multi-agent systems and a vector modelling approach. For more details please consult Silva (2010).

The main objectives of its conception are related to the simulation of the urban morphogenesis, and the computing language used is Java. The main class representing the agents in the system is the class *building*, as shown in Figure 6.24. Thus, in order to detect these groups a *link* class is added to the conceptual data model enabling therefore to determine the group classes.

The simulator computes the building's creation following a formula called *Satisfaction Degree*.

6.4 Case-study: incorporation of morphological properties of buildings computed from GIS and LiDAR data on an urban multi-agent vector based geo-simulator

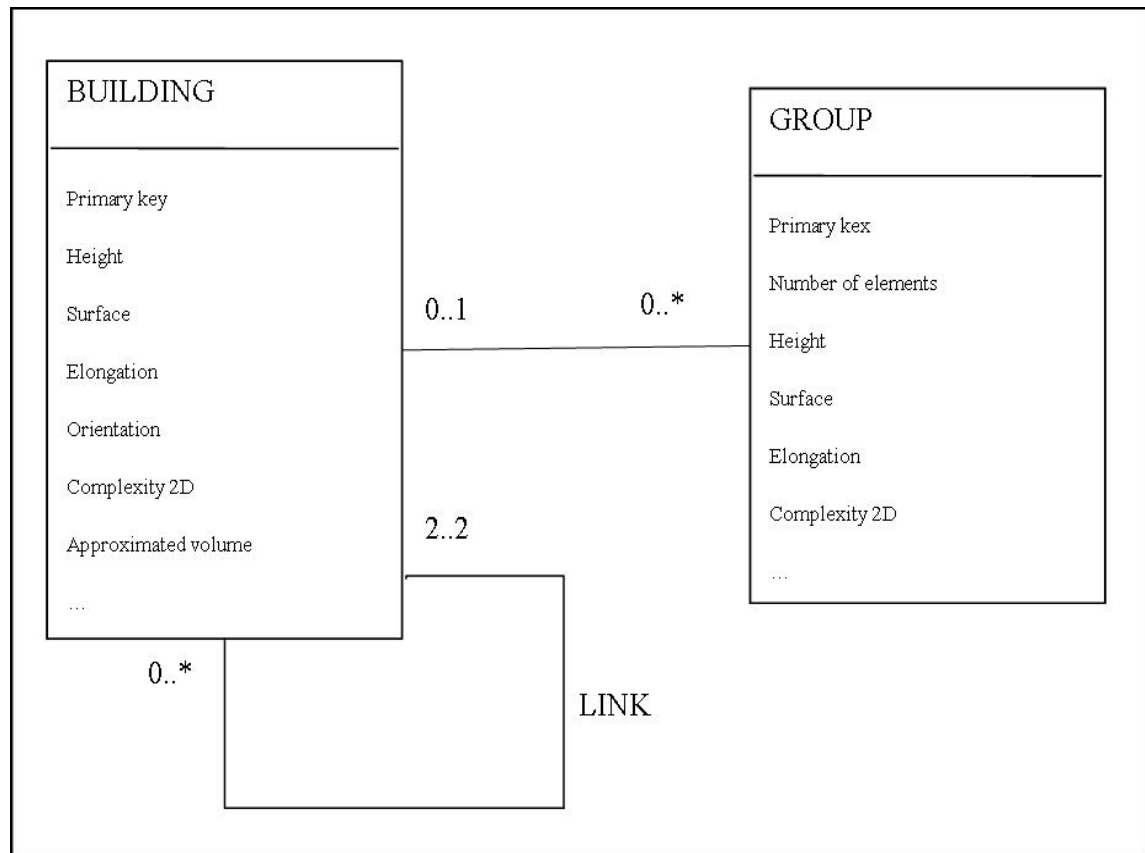


Figure 6.24. UML model with the group class and the link association class. Diagram from Silva (2010).

Urban groups

The presence of organized structures in urban housing is detectable: in fact, they represent regular geometric figures called *groups* as they reflect building's regrouping following some criteria (same geometric pattern, complexity, etc.). These regroupings can be found at several scales.

Groups' detection using the morphological descriptors

Firstly, a selection of the buildings with the same function (the numbers representing functions are a code used in the model developed for this study) is applied:

- 113: housing with mean density;
- 191: housing + garage.

Secondly, a detection of links between buildings is carried out, presented as follows:

- Computation of the gravity centre of each building considering its 2-D geometry;
- Research of the gravity centre of each building in a buffer whose diameter depends on the height of the building and the urban density of the city over in which it is situated, as shown in Figure 6.25.

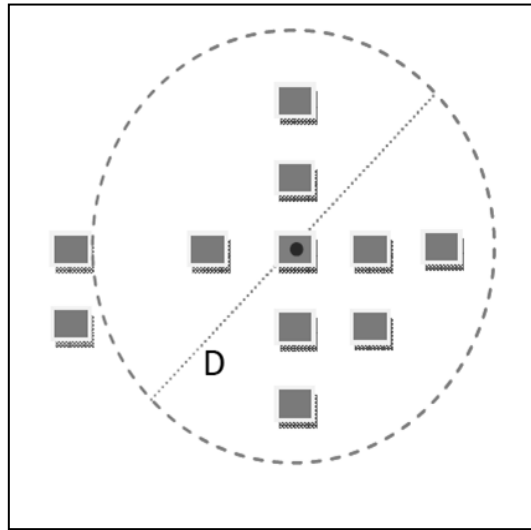


Figure 6.25. Research of gravity centres. Diagram from Silva (2010.)

$D = p * (1 - d) * h$, where:

- D: buffer's diameter;
- P: parameter depending on the building's height and fixed to 10;
- d: density of the district.

For each gravity centre found in the buffer we verify similarity with each building following morphological descriptors, as shown in Figure 6.26.

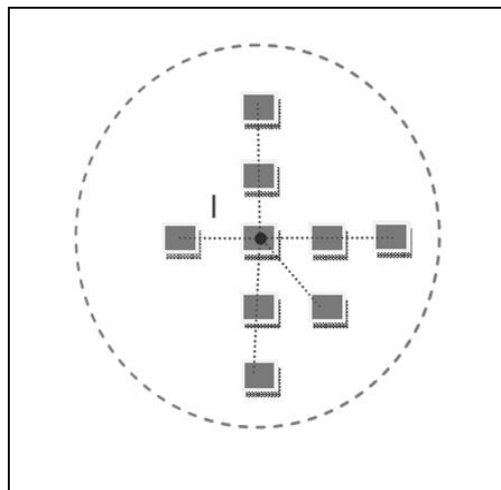


Figure 6.26. Verification of building's similarity. Diagram from Silva (2010).

For each link (the values presented below are empirically determined by architects working on the project and represent the degree of similarity between the indicators):

- the difference of indicator "average height" must be less than 7 meters (which represents a difference of 2 storey);
- the indicator "area of ground" ratio (represents the ratio between the ground surfaces of the buildings) must be less than 0.5;

6.4 Case-study: incorporation of morphological properties of buildings computed from GIS and LiDAR data on an urban multi-agent vector based geo-simulator

- the indicator “volume” ratio (represents the ratio between the total volume of the buildings) must be less than 0.5;
- the indicator “type of roof” must be the same;
- one of the 3 indexes of complexity ratio (represents the ratio between the complexities of the buildings) must be less than 0.5.

The links are stored in the table of links, as shown in Figure 6.24.

Finally, the creation of the groups with the detected links is applied:

- groups are stored in the table *group*;
- groups are deleted if a building composing the group already belongs to a group;
- the number of elements of each group is updated;
- the geometry of each group that corresponds to the barycentre of the whole barycentre of the buildings composing the group is computed.

6.4.5 Analysis of results

The groups in Chavannes area are detected by applying the morphological indicators and indexes described in section 6.4.3. Table 6.8 shows the results of the detection with the three types of indexes analysed. The detection is made for both cases of taking and not taking into account the indicator “type of roof”. Function 113 represents “housings with mean density” and function 191 “housings with garage”. More explanations about how the indexes “envelope area-to-area of ground ratio”, “envelope area-to-total volume ratio” and “volume-to-number of faces ratio” are derived can be consulted in section 4.2.

Index	Type of roof	Function	Nb of links	Nb of groups
envelope area-to -area of ground ratio	No	113	138	34
	Yes	113	129	31
	No	191	15	13
	Yes	191	12	11
envelope area-to -total volume ratio	No	113	138	34
	Yes	113	129	31
	No	191	15	13
	Yes	191	12	11
volume-to- number of faces ratio	No	113	114	33
	Yes	113	109	30
	No	191	15	13
	Yes	191	12	11

Table 6.8. Results for the three types of indexes in analysis.

A visual result is shown in Figure 6.27 for the case considering both the index “envelope area-to-area of ground ratio” and the descriptor type of roof. It shows a zoom of a precise area where four buildings form a group composed of three links. For more visual results related to this case-study please consult Silva (2010).

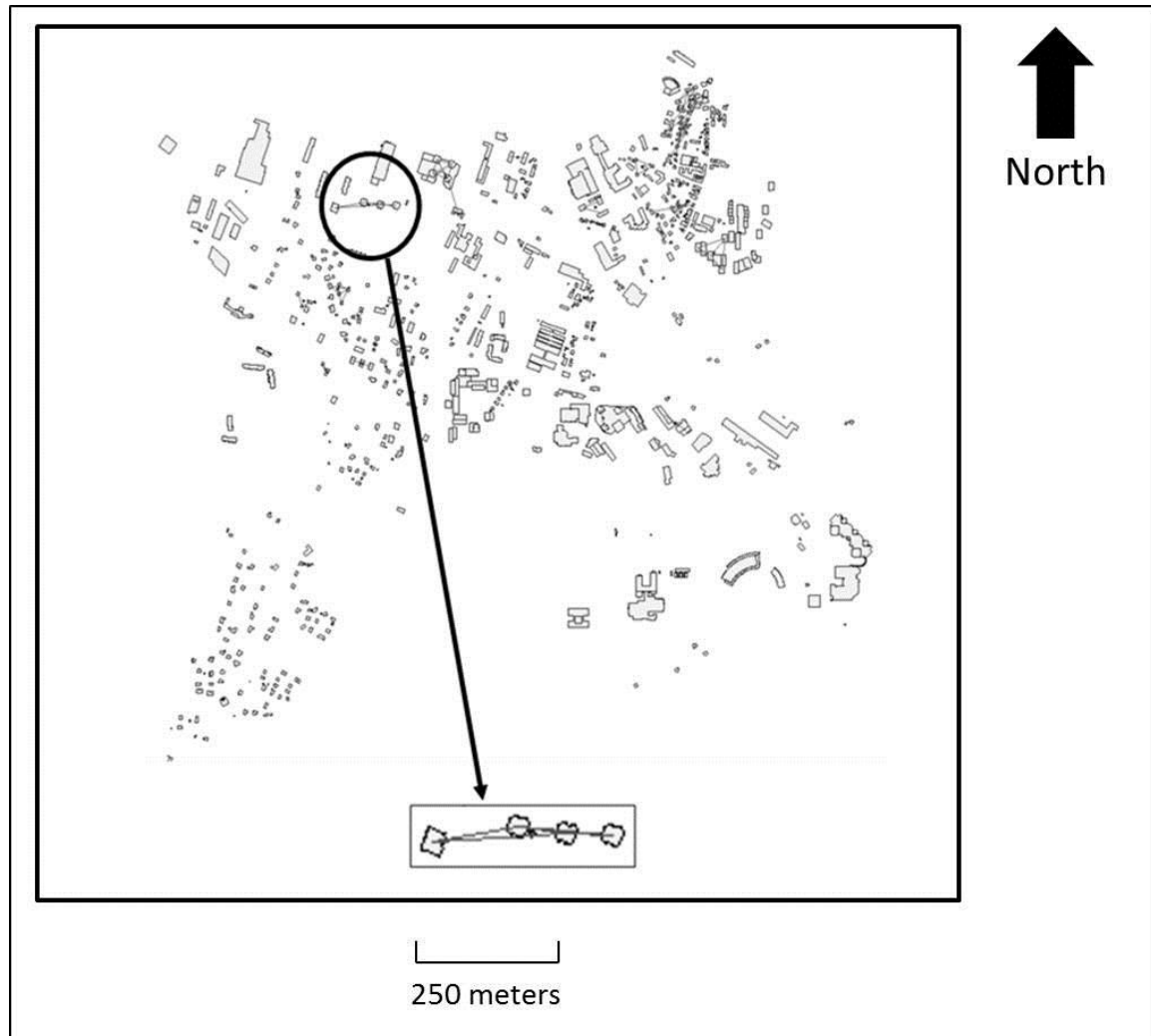


Figure 6.27. Results of the detection in Chavannes area with zoom on a group.

It is also worth mentioning the following observations: there is no significant difference in the detection between indexes “envelope area-to-area of ground ratio” and “envelope area-to-total volume ratio”. Such may imply that these indexes are describing the same type of complexity as they allow the same type of regrouping. On the other hand, the index “volume-to-number of faces ratio” may represent a different complexity with regards to function “113” (“housings with mean density”) but not with regards to function “191” (“housings with garage”). Hence, function “191” seems to show great regularity from the point of view of the three indexes of complexity. It is also interesting to note that the definition of complexity varies with the type of building. Moreover, the indicator “type of roof” has an impact on all detection approaches and on all types of buildings, which confirms that it is an important and significant indicator.

Therefore, detection results demonstrate that it is important to thoroughly choose and define indicators and indexes for groups’ detection of a building of a given type. Furthermore, the precision of these indicators and indexes is important to ensure detection reliability. As it is mentioned above, some indicators and indexes are more influent than others, but such quality must be correlated to its properties, and not to an imprecision of the input data. In fact, input data obtained with LiDAR data allowed to ensure a good precision and enabled to obtain very relevant descriptors for this type of analysis.

6.4.6 Conclusions

According to the user requirements presented by architects and urban planners, this method highlights the relevance of indicators and indexes for groups' detection. In fact, with relevant indicators and indexes the chosen urban groups could be correctly detected.

As highlighted in this case-study and already mentioned in this thesis, existing 2-D vector digital maps (GIS data) can be used if 3-D city models are not available, but the 2-D outlines of building outlines do not have to necessarily represent the outline of the building roof, especially in residential areas. This is a constraint related to this case-study area that could not be avoided.

Although it is not the main purpose of this research, the accuracy of the method described in this thesis for the classification of each roof into a class of roof primitives (flat, classic or complex) could certainly increase by exploring the following points:

- an advanced study on which segmentation method could be the most appropriate. As mentioned before in this thesis, the segmentation procedure for LiDAR data used in this case-study was chosen for its easiness of use and for practical reasons, but other segmentation methods that have been researched in the last years could eventually demonstrate better results for this type of classification. For more details please consult Sithole and Vosselmann (2003);
- the influence of the density of raw LiDAR points in the segmentation procedure is certainly not negligible. For this case-study area, the density of raw LiDAR points is around 1 point/m². It would be important to analyse if a higher density of raw LiDAR points could result in a better segmentation on LiDAR data and, thus, also a better classification of each roof into the correct class of roof primitives.

Finally, the same process could be used in order to detect urban systems, which consist in bigger urban groupings showing some similar organization properties. These abstracted spatial structures are complex to identify and the results presented open interesting perspectives for the use of high resolution LiDAR data in order to construct more accurate 2.5-DUSM of building outlines and to improve the segmentation procedure within the frame of this type of detection.

6.5 Conclusions and chapter synthesis

Considering the analysis of the user-requirements collected from the end-users of the State of Geneva, this chapter presented innovative methods based on LiDAR data as well as different models that are used for the extraction of indicators related to the stake "assessment of the morphological properties of the urban texture". Indeed, this stake is considered a priority for this research because the morphological properties of the urban texture (mainly buildings) are commonly used as input for the extraction and evaluation of other indicators requiring therefore a reliable dimensioning of the urban surfaces. Some examples of the application of the morphological properties of the urban texture as a complementary input to the other two¹⁰ main stakes researched in this thesis are emphasized in chapters 7 and 8.

The developed procedure is intended to fill the gap in this sector, thus enabling the use of LiDAR data for numerous applications at the level of the urban fabric. Afterwards, the outputs presented were statistically validated through a comparison of the same type of attributes stored in a 3-D vector city model. The conducted analysis on the two case-study areas, characterized by very

¹⁰ (1) exploration of the solar potential on the urban fabric, and (2) estimation of the energy demand on the urban fabric.

different geometries of buildings, allows to state that the methods can be extended to other cases. For instance, the calculation procedure could be chosen according to the complexity of the urban fabric.

Furthermore, once the areas of the surfaces and the built volumes are assessed, other minor indicators can be easily derived using DIP techniques (pixel analysis):

- General morphological indicators: the total built floor area considering all storeys (mean storey height is assumed to be 3m); the mean height of buildings on the site.
- Derived indicators of density: urban density, as follows: the built volume on the considered urban area (m^3/m^2); the ground occupation index, i.e. the covered area to the urban area ratio (m^2/m^2); the floor area ratio (FAR) (m^2/m^2).

This short list of derived indicators demonstrates how significant it is to accurately compute the urban surfaces when this type of information has to be used for helpful applications in urban studies.

In order to improve the method, future work should focus on the following aspects:

- automation of the process in order to directly calculate the morphological properties from the raw LiDAR data. This step requires the implementation of new software;
- the improvement of some minor issues concerning complex buildings, for example refining the computation of super-structures on roofs.
- to carefully consider the parts of the built environment that are strongly limited by vegetation (e.g. big portions of trees covering the roofs) during the phase of construction of the different 2.5-DUSM used.
- to test the robustness of the methods presented by evaluating their sensitivity to the variation of grid size and to the discrepancy of sampling density of raw LiDAR point datasets.

CHAPTER 7. EXPLORATION OF THE SOLAR POTENTIAL ON THE URBAN FABRIC¹

¹ The main concepts of this chapter were published in:

Carneiro, C., Morello, E., Ratti, C., Golay, F. (2008) Solar radiation over the urban texture: LiDAR data and image processing techniques for environmental analysis at city scale. *Lecture notes in geo-information and cartography. 3-D Geo-Information Sciences*, In: Zlatanova, S., Lee, J. (Eds.), Part II, pp. 319-340.

Carneiro, C., Morello, E., Desthieux, G. (2009) Assessment of solar irradiance on the urban fabric for the production of renewable energy using LiDAR data and image processing techniques. *Advances in GIScience*, In: Sester, M., Bernard, L., Paelke, V. (Eds.), Springer, Berlin, pp. 83-120.

Desthieux, G., Carneiro, C., Morello, E., Gallinelli, P., Camponovo, R. (2009) GIS-based assessment of solar irradiance on the urban fabric and potential for active solar technology. *Proceedings of the International Conference CISBAT: Renewables in a Changing Climate: from Nano to Urban Scale*, 2nd-3rd September, Lausanne, Switzerland, pp. 525-530.

Morello, E., Carneiro, C., Desthieux, G. (2010) The use of digital 3-D information to assess urban environmental quality indicators. *Proceedings of the 28th ECAADE Conference: Future Cities*, 15th-18th September, Zurich, Switzerland, pp. 499-505.

7.1 Introduction

As highlighted in the end-user requirement analysis (section 4.2.6), this second chapter related to the empirical studies undertaken in this thesis emphasizes on the extraction of complex indicators and indexes belonging to the stake “exploration of the solar potential on the urban fabric”. These indicators are extracted under five sub-stake categories, each of them analysed inside a specific case-study:

- stake “exploration of the solar irradiation on building roofs”: case-studies “analysis of solar irradiation over building roofs” and “comparison of solar irradiation over building roofs on two case-study areas”;
- stake “estimation of the coverage and impact of vegetation on roofs”: case-study “impact of vegetation on the solar irradiation over the urban fabric”;
- stake “estimation of the influence of shadowing and SVF on the urban texture”: case-study “analysis of solar irradiation over building roofs”;
- stake “exploration of the solar irradiation on building facades”: case-study “analysis of solar irradiation over building facades”;
- stake “potential for active solar technology”: case-study “potential for active solar technology”.

The recently increasing attention given to environmental issues in urban studies has opened up many questions about the way territory planners should manage the design process. In fact, numerous authors and architects are convinced that cities play a leading role in controlling sustainability: strategies for redefining more efficient cities in terms of energy performance and environmental quality were the centre of attention in seminal work by Richard Rogers in defining policies for UK cities (Rogers, 1997; Urban Task Force, 1999) and supported the debate around the promotion of more compact cities (Jenks *et al.*, 1996, 2000). Nowadays, the stress on the use and control of solar radiation on the urban fabric has become extremely relevant due to the increasing prominence of the resulting energy-saving repercussions: solar energy in its various forms will be more and more important in the buildings of tomorrow (Littlefair *et al.*, 2000). In fact, an increasing significance is given to public policies related to the exploitation of renewable energy through solar thermal panels or photovoltaic (PV). In April 2009, an agreement was reached by the European Union Renewable Energy Directive that could pave the way for the economic union to accomplish its plans for a 20% contribution of renewables to the whole of the energy demand and a 20% cut in greenhouse gas emissions by 2020, the denominated 20:20:20 plan. The agreement, reached among the European Parliament, the French Presidency, on behalf of the Council, and the European Commission, means that more than one third of EU electricity must derive from renewables by 2020.

Today’s availability of 3-D information about cities offers the possibility to analyse the urban fabric in a very innovative way. In fact, even if LiDAR data permits to derive precious and precise information about the physical layout of cities, still very few applications have been implemented in order to process this data with the purpose of environmental analysis or in order to get a quick understanding of the performance of the urban form. For instance, the increasing interest in the quantification of energy-based indicators at the city scale, strongly suggests the integration of 3-D geography and urban studies in order to provide useful applications for the urban planning. In particular, a novel cross-disciplinary approach that covers the whole procedure from data acquisition from Airborne Laser Scanning (ALS) to the environmental analysis through the image processing of digital urban models is introduced.

The investigation of solar radiation environmental analysis is not new and there are several tools that allow the calculation of radiation performance of buildings very accurately. Nevertheless, even though these tools are very useful at the micro-scale of architecture (environmental performance software) or at the macro-scale of landscape and regional geography (GIS tools), the focus on the urban district and tools for automatically calculating irradiation on a whole urban site are mostly lacking. Indeed, this type of tool is considered to be very relevant for planning activities of local authorities and urban developers. For this reason, Batty *et al.* (1999) stressed the need to couple such CAD tools with 3-D GIS so as to include data processing and spatial analysis systems and to provide automatic or systematic analysis on urban area. In this perspective of integrated approach, Rylatt *et al.* (2001) developed a solar energy planning system on urban scale using GIS-based decision support. A lot of these tools are based on Computer Aided-Design (CAD) in architectural domain and consist on simulating solar access: RADIANCE lighting simulation model (Compagnon, 2004), TOWNSCOPE II (Teller and Azar, 2001), SOLENE (Miguet and Groleau, 2002) and other works presented by Ward (1994) and Robinson and Stone (2005). However, those tools demonstrate to be prohibitive if we have to undergo larger parts of the urban fabric and, even with powerful means, the degree of accuracy would be nevertheless too high and superfluous for the purposes of analysis at larger scales of the city. Furthermore, common end-users of the proposed tools are professionals in urban design and decision makers for environmental policies at the city scale. , a comprehensive and reliable toolkit for sustainable urban design is lacking among practicing professionals. Hence, the methods emphasized in this thesis can be intended just as one tile of a larger mosaic aiming at the quantification of environmental parameters at the urban scale. Using the capability of LiDAR data in order to construct an accurate 2.5-DUSM, different tools for calculating solar radiation incident on the urban fabric are implemented, as shown in the five case-studies highlighted in this chapter. The results presented in this chapter provide a preliminary insight into the interrelationship between urban texture and radiation.

The following sections will introduce information about:

(7.2) – background and related work;

(7.3) – solar irradiation analysis over the urban fabric;

(7.4) – case-studies:

- analysis of solar irradiation over building roofs;
- impact of vegetation on the solar irradiation over the urban fabric;
- comparison of solar irradiation over building roofs on two case-study areas;
- analysis of solar irradiation over building facades;
- potential for active solar technology;

(7.5) – conclusions and chapter synthesis.

7.2 Background and related work

7.2.1 Basic irradiative parameters

Prior to describing the irradiative parameters in urban areas, it is important to review some simple concepts:

- Radiant flux is the power emitted, transmitted or received by the means of electromagnetic radiation, which unit is Watts (W);
- Radiance, for a given direction, at a given point of a real or imaginary surface, is the radiant flux in a given direction per unit solid angle, per unit area perpendicular to that direction (Figure 7.1). It is defined by the formula:

$$L = \frac{d\phi}{dx \cos\theta d\omega} \quad (7.1)$$

where $d\phi$ is the radiant flux transmitted by an elementary beam passing through the given point and propagating in the solid angle $d\omega$, containing the given direction; dx is the area of a section of that beam containing the given point; θ is the angle between the normal to that section and the direction of the beam;

- Irradiance, for a given point of a surface, is the quotient of the radiant flux $d\phi$ incident on an element of the surface containing the point, by the area of that element, which unit is W/m^2 ;
- Irradiation is the product of irradiance and time, i.e. surface density of the radiant energy received, which unit is Ws/m^2 .

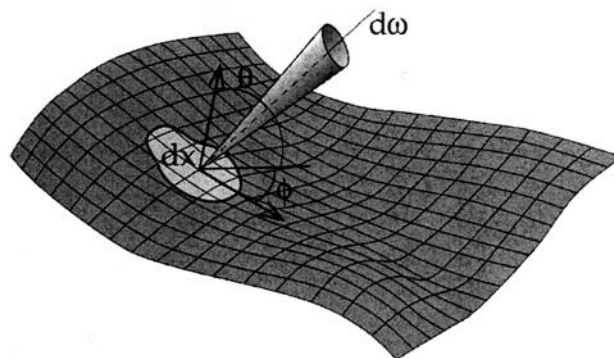


Figure 7.1. Symbols used in the definition of radiance. Image from Sillion and Puech (1994).

The standard units for assessing the distribution of solar energy in urban areas are irradiance and illuminance, which are used with regards to the emphasis of the analysis, solar energy or lighting respectively. Illuminance is defined as the total luminous flux incident on a surface, per unit area. It represents a quantity of the intensity of the incident light, which is wavelength-weighted by the luminosity function to correlate with human brightness sensitivity. Both irradiance and illuminance may be divided into two axes: the direct component, coming straightforward from the sun, and the diffuse component, received from the whole sky hemisphere. In this chapter the main focus is given to irradiance analysis on the urban fabric.

7.2.2 Direct and diffuse components of radiation

The calculation of direct component of radiation is directly linked to the analysis of the shadowing in the urban areas under study. Hence, it corresponds to zero on all shadowed surfaces, and is calculated by the means of the angle of incidence on all lit surfaces. Indeed, all lit surfaces, at any specific time of the day, receive the same amount of incident solar radiation, calculated per unit area perpendicular to the radiation beam. During the last years, many GIS systems have included shadow casting subroutines to model the self-shading of topography. This is usually done by calculating on each pixel the horizon angle in a given direction, and by comparing it with the actual sun altitude (Kumar *et al.*, 1997). According to Ratti (2002), due to the discontinuous nature of urban 2.5-DUSM, a simple transposition of common GIS algorithms to urban areas is not a reliable option. Indeed, it is harder to collect solar energy in built areas than on flat open terrain due to the effects of overshadowing and the varying distribution of radiation in space and time. This is directly caused by the complex patterns created by urban geometry. For this reason, the calculation of shadowing on urban areas presented in this work is based on the algorithm proposed by Ratti (2002), which was specifically developed for urban areas.

As described in section 7.1, a serious limitation of all computer tools based on Computer Aided-Design (CAD) in simulating solar access is the requirement of a full 3-D urban model in vector form, which can be extremely costly and very time-consuming to build, and moreover it may present difficulties of performing simulations on extensive urban areas (Compagnon, 1999). According to the same author, another relevant limitation is that such tools lack a consistent capacity to assess the diffuse radiation component received from the whole sky-vault. Thus, in the past years, a considerable progress was achieved in this domain with the development of the RADIANCE lighting simulation program (Compagnon, 2004). This tool allows the computation of solar irradiation values obtained through the anisotropic model proposed by Perez *et al.* (1990), by applying numerical simulations based on statistical observations. These numerical simulation programs offer the basis for representing a truthful sky luminance distribution, as well as the sun and the effects of the manifold reflections (both diffuse and specular) from urban obstructions of subjective complexity (Robinson *et al.*, 2005).

7.2.3 State of the art

With regards to related work presented in the last years it is important to mention a new method presented by Vögtle *et al.* (2005) that uses ALS data to automatically select suitable areas for the installation of solar panels. In this case, the extraction of the roof planes and the determination of the necessary features, such as size, aspect and slope, are performed directly on a DSM. Another tool that masks ALS data by the outlines of buildings, in order to obtain information about the roof of the building, followed by a raster interpolation of the remaining points to analyse the roofs according to aspect, slope and shaded areas was proposed by Kassner *et al.* (2008). A method for the automatic roof plane detection and analysis directly calculated from airborne LiDAR point clouds (with no need of use of digital image processing techniques) for solar potential assessment was proposed by Jochem *et al.* (2009). Finally, Gadsen *et al.* (2003) described a new methodology oriented for energy advisers and urban planners based on GIS in order to predict the urban solar fraction. This chapter also highlights some comparative results on different urban textures (case-study presented in section 7.4.6), providing an initial vision into the interrelationship between urban texture and solar radiation. Also related to this specific topic, Kämpf *et al.* (2009) coupled a multi-objective optimization algorithm using the program RADIANCE for the optimization of buildings' solar irradiation availability. The focus of this

7.3 Solar irradiation analysis over the urban fabric

work is on the design of new urban forms, but can be also used to examine the relative efficiency of existing urban settlements.

Indeed, 2.5-DUSM may present very useful results in this domain. An important question to ask in this chapter is: could the use of innovative and mixed segmentation and image processing techniques on 2.5-DUSM presented as well as the use of meteorological data sources contribute to a more reliable analysis and measurement of solar irradiation in cities and to enrich the exiting tools and methods already available? Moreover, it is important to note that most of the results obtained in past studies (presented in the last paragraph) related to solar analysis in urban areas are represented using a 2-D GIS environment. In this thesis it is intended to move further by presenting this type of results in a 3-D GIS environment, as underlined in some of the case-studies presented in sections 7.4.4 to 7.4.7.

7.3 Solar irradiation analysis over the urban fabric

7.3.1 Method applied

The technique used is based on the image processing of the 2.5-DUSM that is interpreted as raster images and the use of statistical meteorological data. These images result from the transformation of all the information attributes needed for the irradiation calculation into layers, such as the height values, slope, orientation, roof lines and building labels, among others. Numerical data of the solar irradiation is thus collected pixel by pixel.

A synoptic view showing the integration of the calculation of solar irradiation (point 4) highlighted in this thesis, applying digital image processing techniques and meteorological data, into the dataflow process (points 1 to 3 and 5) intrinsic to the extraction of this type of indicators, is shown in Figure 7.2.

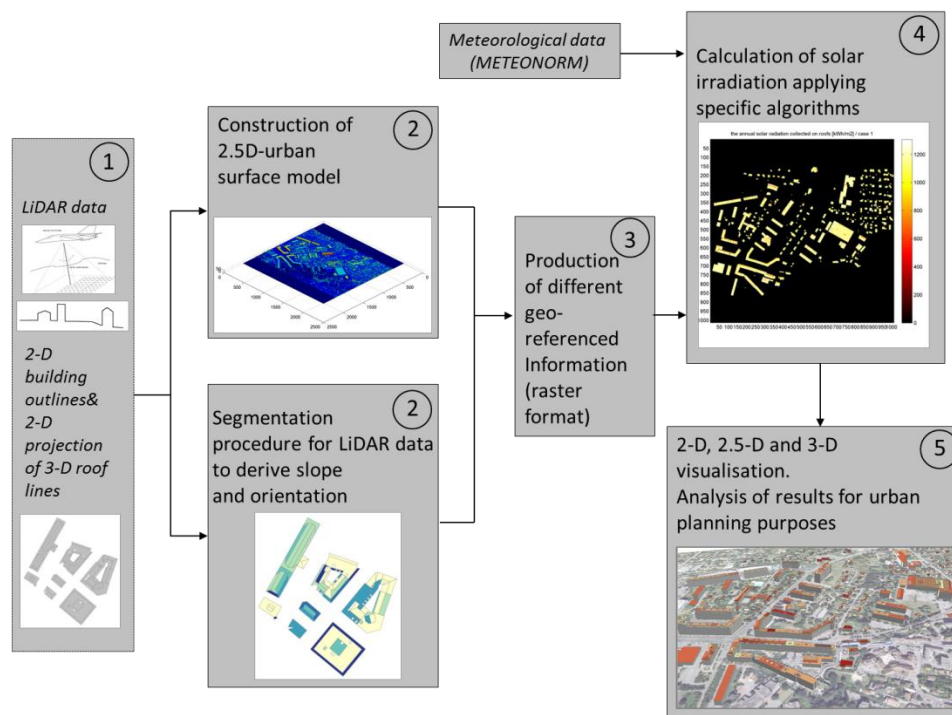


Figure 7.2. Synoptic view of the method used for the calculation of solar irradiation indicator applying digital image processing techniques (specific algorithms).

Calculating solar radiation incident on the built environment involves describing interactions between the sky model, solar geometry and 3-D buildings models (Compagnon, 2004). Solar geometry formulae proposed by different authors allow the duration of the beam, diffuse and ground reflected components of hourly radiations for every orientation and inclination of surface starting from the previous mentioned inputs (Iqbal, 1983). For the beam component, by combining the 2.5-DUSM of urban area and geometric position of the sun hour per hour, it is possible to calculate the shaded surface area during a given hour (Glenn and Watson, 1984; Incropera and DeWitt, 1960).

The model of diffuse component on inclined surface should be selected very carefully so as to take into account the simplified isotropic sky model or the more wide-ranging anisotropic model of the phenomenon. Contrasting to direct irradiance, rigorous calculation of the diffuse irradiance on a sloped surface is challenging and most of the times implicate some degree of approximation. Overall it is a function including mathematical formulae related to solar geometry, pressure (related to elevation), and specific properties of the atmosphere. Moreover, two other factors must be considered: the anisotropy in the diffuse irradiance field and the amount of sky visible at a point, which corresponds to its sky view factor (SVF). It evaluates the reduction of the sky visibility from a point of view due to obstacles in the surrounding environment; it is thus not time-dependent. According to Teller and Azar (2001) the diffuse radiation incident can be obtained through the product of SVF (%) by available diffuse radiation on unobstructed horizontal surfaces. An example of calculating SVF with 3-D GIS is proposed by Souza *et al.* (2003) through their 3-D SkyView tool.

Hence, in this study, both of the main components of the global irradiation – direct and diffuse – for isotropic and anisotropic models are multiplied by a shadowing factor according to formulae 7.2.

$$I_{g\ h} = I_{dir\ h} * S_{dir\ h} + I_{diff\ h} * S_{diff} + I_{r\ h} \quad (7.2)$$

Where:

- I_g : global irradiation on inclined surface at a given hour h [Wh/m²];
- I_{dir} : direct irradiation on inclined surface at a given hour h ;
- I_{diff} : diffuse irradiation on inclined surface at a given hour h ;
- I_r : ground reflected irradiation on inclined surface at a given hour h ;
- S_{dir} : shadowing factor on direct radiation at a given hour h {0, 1};
- S_{diff} : shadowing factor (SVF) on diffuse radiation [0, 1].

It is important to note that an assumption is made for the anisotropic models used (Hay, 1979; Perez *et al.*, 1990), by multiplying the diffuse radiation by the SVF. Indeed, according to Dubayah and Rich (1996), a SVF that gives the ratio of diffuse sky irradiance at a point on an unobstructed horizontal surface can be calculated. In theory the diffuse flux should be calculated by multiplying the view factor in a particular direction by the amount of diffuse irradiance in that sector of the sky, and integrating it over the hemisphere of sky directions. However, it is computationally complex to implement and storage intensive because it requires the calculation of SVF and diffuse irradiance for each sky sector and for each grid point. Therefore, the multiplication of hourly diffuse irradiation by a unique SVF integrated on the whole hemisphere constitutes a very good approach for taking into account shadowing on this component.

The shadow casting routine first introduced by Ratti (2002) is applied to the input raster images at a specific day of year and hour of day and is used to detect which pixels are in shadow (cast from buildings or trees in the surrounding environment) and which collect direct sunlight, allowing to calculate the S_{dir} shadowing factor used in formula 7.2.

7.3 Solar irradiation analysis over the urban fabric

The procedure used for calculating shadows from the sun for any given latitude, time of year, and time of day, using the usual astronomical formulae, specifically developed for urban environments was first introduced by Ratti (2002). The approach is based on the computation of “shadow volumes”, that is, the upper surface of the volume of air that is in shadow over a given urban DEM, in this thesis called 2.5-Digital Urban Surface Model (2.5-DUSM). This can be done by repeatedly shifting the 2.5-DUSM and reducing its height. This algorithm is very simple and impressively fast (it allows processing acres of city at a time, something unthinkable with traditional 3-D geometric models). This allows the possibility of performing simulations for a whole day or number of days. Results are shown for instance in Figure 7.3, which represents the patterns of shadows in the district of Moillesulaz, State of Geneva, on September 15th, at 16h00, 17h00 and 18h00.

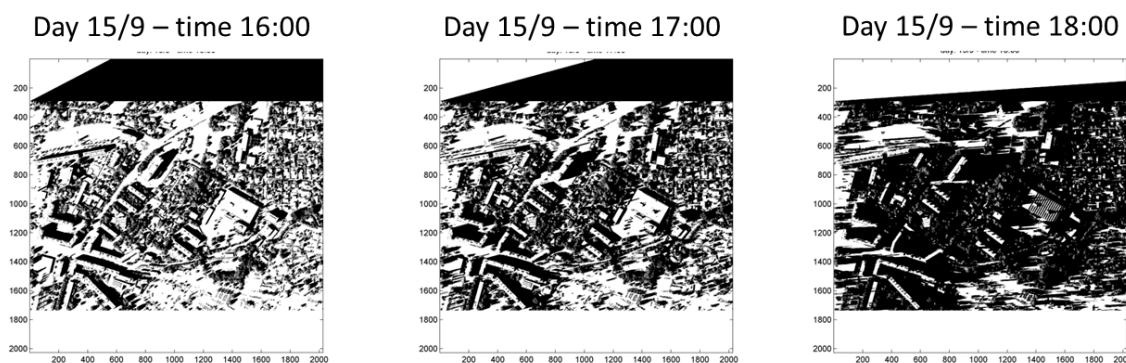


Figure 7.3. Example of patterns of shadows in the district of Moillesulaz, State of Geneva, on September 15th, at 16h00, 17h00 and 18h00.

The job of transforming latitude, time of the year, and time of the day into altitude and azimuth of the sun has been carried out in this case by a subroutine. However, this subroutine is not innovative, as it codes well-known astronomical data. For more information about the formulas used please consult Muneer (1997).

From these images, simple quantitative parameters are defined by the analysis of all the hourly frames of a single day (Steemers and Ratti, 1999). Summing all black and white shadowing images, each made of 0s and 1s, it is possible to obtain grey scale images which have values in the range 0..n, where n is the number of sun positions considered for the day, which are equivalent to the number of hours of sun. The resulting image portrays in an elementary way the number of hours of shadow for each pixel (this value is simply given by the resulting value of that pixel). Thus, considering the formula 7.2, for each pixel under analysis on the 2.5-DUSM, the global irradiation on inclined surface at a given hour h ($I_{dir h}$) is multiplied by the result ($S_{dir h}$) of the shadow casting routine, which is only equivalent to 0 or 1.

As initial assumption for the shadow-casting implemented during a whole day (applied in the case-studies emphasized in this chapter) it is just considered the hours of sun chosen for all altitudes higher than 5 degrees above the horizon, i.e. 7 hours for winter solstice, 11 for the equinoxes, and 15 for the summer solstice.

The calculation of the SVF on the 2.5-DUSM - also first introduced by Ratti (2002) -, used in this study as shadowing factor on diffuse (S_{diff} in equation 7.2), evaluates the reduction of the sky visibility from a point of view due to obstacles in the surrounding environment. It is thus not time-dependent.

Obstructions in the diffuse radiation and in the sky's visibility can be analysed through the SVF; it expresses the relationship between the visible area of the sky and the portion of the sky covered

by surrounding buildings and other obstacles viewed from a specific point of observation (Souza *et al.*, 2003). The SVF encompasses reduction of visibility due to the slope of an inclined plane and obstacles in the surrounding built environment.

The method used can achieve remarkable applications, such as determining the amount of sky that is visible from a given pixel. This process can be presented as follows: spread a number of sun positions in the sky-vault, cast shadows each time in the 2.5-DUSM and count the number of “whites” and “blacks” on each pixel. If the positions of the sun are scattered uniformly along the sky-vault, the count of “whites” on a given pixel divided by the total number of sun positions taken into analysis gives the solid angle of view of the sky by applying a proportionality factor of 2π .

By means of a trivial refinement of this algorithm the SVF can be determined. This parameter is analogous to the solid angle of view of the sky, even if two weighting coefficients are applied in order to weight diverse parts of the sky-vault in different ways. The SVF ($F_{dA_i \rightarrow sky}$) can be expressed by the formula :

$$F_{dA_i \rightarrow sky} = \int_{sky} \frac{\cos\theta_i \cos\theta_j}{\pi R^2} dA_j \quad (7.3)$$

The integration is accomplished onto all elemental surfaces dA_j which compose the sky-vault; dA_i is a basic surface of the city, θ_i and θ_j are the angles between the vectors normal to dA_i and dA_j and the line connecting them, whose length is R (Figure 7.4).

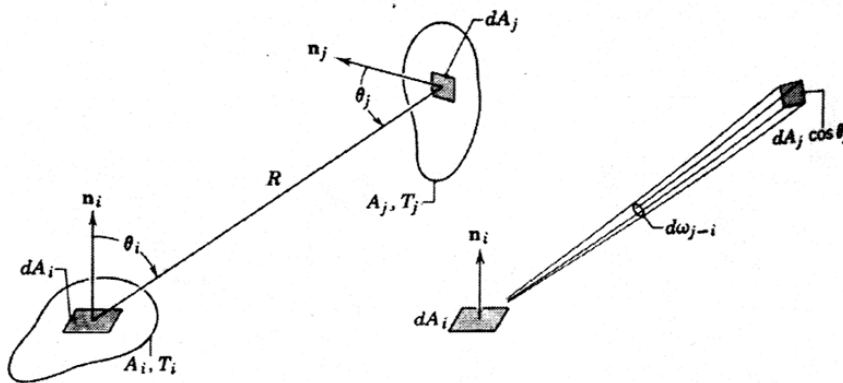


Figure 7.4. Symbols used in the sky factor formulas. Diagram from Incropera and De Witt (1990).

Indeed, the SVF is just the sum of the cosine of the weighted elemental solid angles on a whole hemisphere. The reason for this weighting derives from heat transfer theory, where the view factor was initially described to model irradiative exchange between different surfaces. More details concerning this specific subject can be found in scientific books of heat transfer theory, such as in Incropera and DeWitt (1990).

It is rather relevant to focus on the use of 2.5-DUSM for the calculation of SVF. As explained in the last paragraphs, the algorithm is based on the continual application of the shadow algorithm: shadows are computed for a large number of light sources, randomly dispersed over the sky, and for each pixel count the number of times they receive light. For instance, if 1000 samples are used, any pixel whose count is 1000 represent one that can see all the sky and has a SVF equal to

7.3 Solar irradiation analysis over the urban fabric

1, while a count of 0 represents one that cannot see the sky at all and has a SVF equal to 0. Two examples inherent to the calculation of the SVF for two case-study areas analysed, belonging to the city centre and the district of Collonges of the State of Geneva, are shown in Figure 7.5.

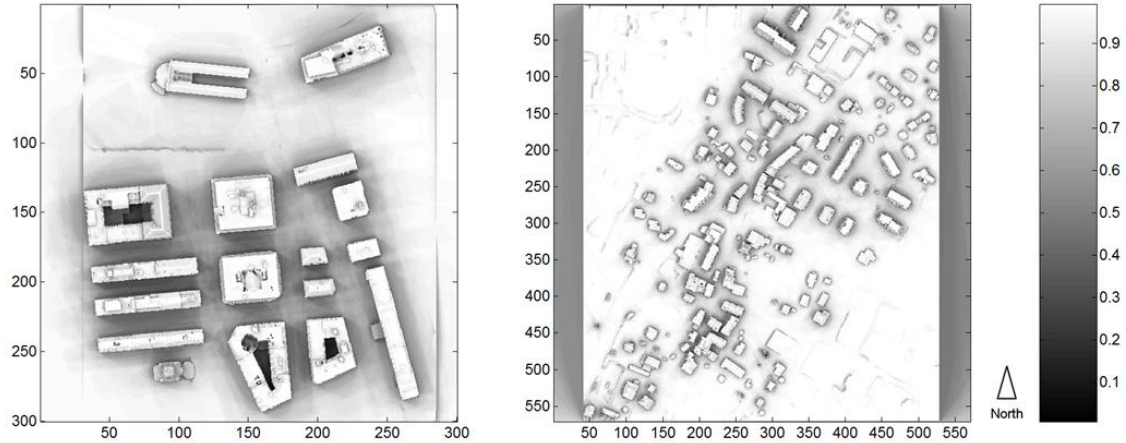


Figure 7.5. Example of the calculation of the SVF for two case-study areas of the State of Geneva: city centre (left hand-side image) and Collonges (right hand-side image).

In order to get significant results, according to the above definition of view factor, it is indispensable to distribute the sample points over the sky properly. If a uniform distribution is used, then what is measured is not the view factor but the solid-angle of the sky visible from each point. In order to consider the cosine correction, the density of samples must be higher at the zenith than near the horizon. The correct distribution aimed to calculate the view factor from the urban area to the sky can be obtained by scattering points evenly over a unit circle in the horizontal plane, and then projecting it up to a unit hemisphere. Finally, as the number of points is very large, it is conceivable to choose a uniform and random distribution of points belonging to the circle. This last procedure helps to avoid the emergence of patterns of interference, a common problem in image processing. For more details about the technique applied (iteration process) for spreading points over a unit circle please consult Ratti (2002).

According to the isotropic diffuse sky model, solar radiation incident on a tilted surface is considered to include three components: direct beam, isotropic diffuse and diffusely reflected from the ground (Hottel and Woertz, 1942; Liu and Jordan, 1963). Hence, at locations where the hourly global and diffuse radiation on horizontal surfaces are measured and known, the global radiation on an inclined surface can be written as:

$$I_{\beta\gamma} = I_{b\beta\gamma} + I_r + I_s \quad (7.4)$$

where:

- $I_{\beta\gamma}$: hourly *global* radiation incident on an inclined plane at an angle β and with an azimuth angle γ ;
- $I_{b\beta\gamma}$: hourly *beam* radiation incident on an inclined plane;
- I_r : hourly *ground-reflected* radiation incident on an inclined plane;
- I_s : hourly *sky diffuse* radiation incident on an inclined plane.

Such a formula is valid for the particular case where the roof section of interest is not shaded by any obstruction in its surrounding environment. Thus, each component of the global irradiation and the effect of shaded conditions are considered.

The hourly beam radiation incident on an inclined plane can be expressed, by referring to Iqbal (1983, p. 306), as:

$$I_{b\beta\gamma} = I_b r_b = I_b (\cos\theta / \cos\theta_z) \quad (7.5)$$

where:

- I_b : hourly beam radiation on horizontal surface, that is equal to $I - I_d$, where I is the global and I_d the diffuse, both known;
- r_b : conversion factor for beam irradiance, that is ratio of the radiation incident on an inclined surface to that on a horizontal surface;
- θ_z : zenith angle of the sun;
- θ : angle of incidence of the sun for an oriented surface.

The components $\cos\theta_z$ and $\cos\theta$ are derived from the traditional solar geometry formulae and in particular from the trigonometric relations between the sun and a horizontal, respectively inclined, surface. $\cos\theta_z$ is a function of the hour angle, the geographic latitude of the surface of interest, the solar azimuth and the angular position of the sun (declination). $\cos\theta$ is a function of θ_z , β , γ and the solar azimuth. For more details about this subject please consult Duffie and Beckman (1991). The angles under consideration and some other angles describing position of the sun and the surface considered are shown in Figure 7.6.

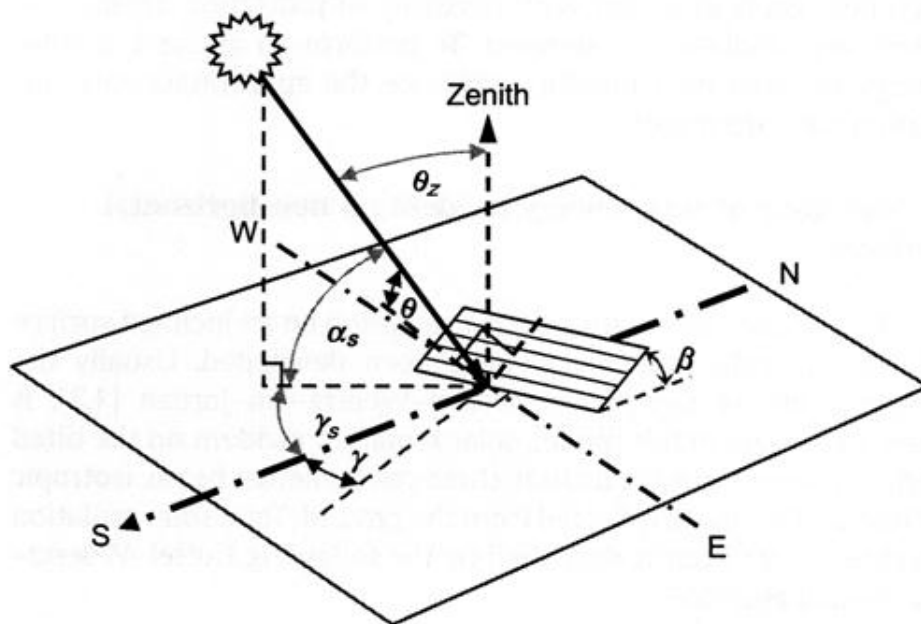


Figure 7.6. The geometric relationship between a tilted plane of any orientation relative to the earth and the beam radiation from the sun. Diagram from Chwieduk (2009).

Under realistic sky conditions, the sky diffuse radiation and its intensity are not uniform over the sky hemisphere centred on the inclined roof surface. For an accurate assessment of radiation incident on the inclined surface, detailed information on the intensity distribution of the sky diffuse radiation is required, as recommends Iqbal (1983). However, such information is generally not measured and available in meteorological databases, like the one used in this study.

Therefore, the isotropic model is applied providing a good approximation of the sky diffuse radiation incident, in spite of its underestimation on south-facing slopes in clear sky condition.

7.3 Solar irradiation analysis over the urban fabric

Following this model, the sky diffuse radiation incident is expressed, by referring to Iqbal (1983, p. 314), as:

$$I_s = \frac{1}{2} I_d (1 + \cos\beta) \quad (7.6)$$

where:

- I_s : Sky diffuse radiation incident on a inclined plane;
- I_d : Sky diffuse radiation incident on a horizontal surface (measured);
- β : angle of the inclined plane.

When a roof surface of interest is inclined, it receives additional solar radiation reflected from the surrounding ground environment, which corresponds to neighbour roof sections in our context. The incident energy may involve beam and/or diffuse radiation. The nature of the reflected energy strongly depends upon the surface properties that characterize the *albedo*¹¹ ρ of the surface.

As Iqbal (1983) asserts, isotropic reflection usually occurs when the ground cover is a perfectly diffuse reflector, such as a concrete floor and roof materials in particular. Moreover, for such a type of surface it is assumed that the reflectance (albedo) to beam and diffuse radiation are identical. Under such conditions the hourly ground-reflected irradiation can be expressed, by referring to Iqbal (1983, p. 308), as:

$$I_r = \frac{1}{2} I_d \rho (1 - \cos\beta) \quad (7.7)$$

where:

- β : angle of the inclined plane;
- ρ : reflectance or albedo factor.

In this context, an albedo of 0.13 is considered as a good average value for the albedo ρ factor of roof materials according to the literature (see Iqbal, 1983, p. 290).

Calculations of solar radiation incident on an inclined surface can be also performed using the anisotropic sky model. In this model diffuse radiation is composed of three parts: isotropic, circumsolar diffuse, which is concentrated in the sky near the sun, and horizon brightening, which is concentrated in the sky near the horizon, as shown in Figure 7.7.

¹¹ According to Montavon (2010), the albedo of an object is the extent to which it diffusely reflects light from the Sun. It is therefore a more specific form of the term reflectivity. Albedo is defined as the ratio of diffusely reflected to incident electromagnetic radiation. It is a unit less measure indicative of a surface's or body's diffuse reflectivity.

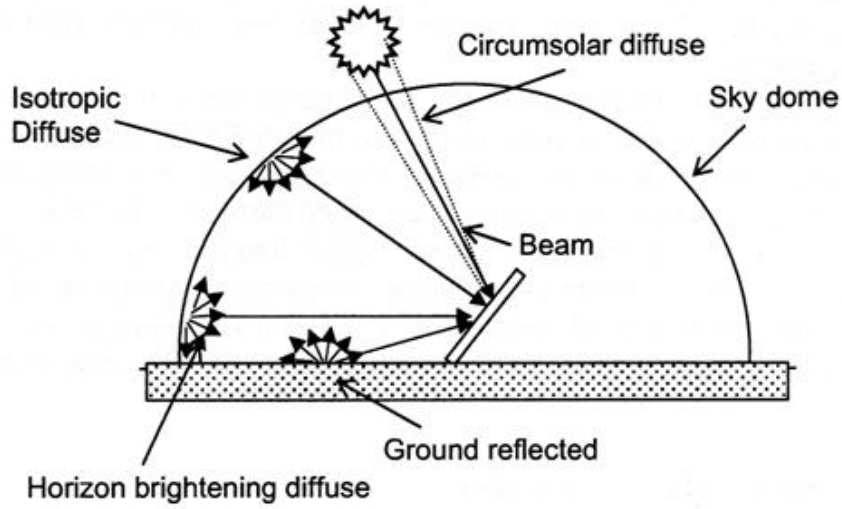


Figure 7.7. Schematic view of the distribution of solar radiation on a tilted surface according to anisotropic sky model. Diagram from Chwieduk (2009).

Among the numerous anisotropic models, two of the most common are chosen, according to the following generic properties:

- a simpler model, proposed by Hay (1979), assumes linearity of the isotropic and circumsolar contributions to the diffuse radiation on a tilted plane:

$$\psi_H(I_b) = Fr_b + (1 - F)\cos^2\left(\frac{\beta}{2}\right) \quad (7.8)$$

where F is Hay's sky-clarity factor and is defined as:

$$F = \left(\frac{I_b}{I_0}\right) \quad (7.9)$$

and r_b is the beam radiation conversion factor given by $r_b = \max\left[0, \left(\frac{\cos\theta}{\sin\alpha}\right)\right]$

- a more complex and rich model, proposed by Perez *et al.* (1986; 1987; 1990), based on the three parts of the sky-diffuse radiation mentioned above, geometrical representation of the sky dome, a parametric representation of the radiation conditions and a statistical component linking the two:

$$\psi_R(I_d, I_b) = (1 - F_1)\cos^2\left(\frac{\beta}{2}\right) + F_1r'_b + F_2\sin\beta \quad (7.10)$$

where r'_b is the modified beam radiation conversion factor given by: $r'_b = \frac{\max[0, \cos\theta]}{\max[85^\circ, \sin\alpha]}$

F_1 and F_2 are Perez's circumsolar and horizon brightness coefficients, which are function of the zenith angle, sky clearness and brightness.

For more details about other anisotropic models please consult Evseev and Avraham (2009).

7.3.2 Meteorological data sources

The solar irradiation data used was sourced from METENORM® that is a meteorological reference incorporating a catalogue of meteorological data and calculation procedures at several locations in the world. This database offers, among other features, average data on global and diffuse radiation incident on horizontal surface, for a given time period and scale. By subtraction, beam irradiation can be deduced. From the monthly values (station data), METENORM calculates hourly values of all these parameters using a stochastic model. The resulting time series correspond to "typical years".

The used version, (6.1¹²), provides statistical data of a typical year that corresponds to the period 1980-2000 for a location corresponding to the case-study areas highlighted in this study. Such data allows the calculation of a yearly balance of irradiation for a given area. However, calculating irradiation for each hour of a typical year and for each pixel of a high resolution 2.5-DUSM model would result in several days of computer time simulation. Consequently, solar irradiation dataset is reduced by averaging hourly values for each month. The yearly dataset contains thus 288 (24 hours x 12 months) hourly values instead of 8'760. The solar geometry taken into account corresponds to the day considered to be the mostly representative of each month, which is usually close to the day 15th (Duffie and Beckman, 1991). It is important to note that using METENORM® solar irradiation data allows to calculate results in a hourly, daily, monthly or yearly basis, showing great flexibility according to end-user's needs.

7.3.3 Choice of the suitable anisotropic sky model

As previously presented in section 7.3.1, the diffuse radiation is of anisotropic nature. Several models attempting to account for diffuse radiation anisotropy have demonstrated to be better than the isotropic model in many instances. The most successful and common models are those proposed by Perez *et al.* (1986; 1987; 1990), and Hay (1979). In a comparative study of several models, Perez *et al.* (1986) showed that the Perez model achieves the most reliable results with regards to the measured diffuse radiation in different parts of the world.

However, as explained above, the solar model implemented in this thesis uses a reduced solar irradiation dataset by averaging hourly values for each month. Given that the reference anisotropic model of Perez is particularly addressed for very accurate time scale (strictly minute or hour), it should be verified whether the Perez model holds its reliability if using average hourly values per month.

Therefore, the anisotropic models of Perez and Hay are compared in order to find which diffuse radiation model is the most suitable when using average hourly irradiation values¹³. This study is based on the METENORM statistics for Geneva that provide hourly irradiation values on horizontal surface for a typical year. For each model, the global irradiation on titled surface for different orientations and slopes is calculated, using both strictly hourly irradiation inputs through formulae implemented to Excel and average hourly values with our Matlab solar model. As a reference purpose, the global irradiation for the isotropic diffuse model is also computed. The results of these calculations and the differences between them using strictly and average hourly values can be achieved by the following equation.

¹² The most recent version 6.1 (2008) offers radiation data for the time period 1980-2000

¹³ This comparative study was done in the framework of the solar radiation analysis for the pilot zone of Moillesulaz in Geneva (Desthieux, Carneiro and Morello, 2010 : "Analyse de la radiation solaire sur les toits de bâtiment. Zone pilote de Moillesulaz. Présentation ppt de la démarche et des résultats")

For each model analysed, the difference is calculated as following:

$$D = (1 - a / b) * 100 \text{ [\%]} \quad (7.11)$$

where:

- a: global irradiation using average hourly inputs, for a given diffuse model, orientation and slope;
- b: global irradiation using strictly hourly inputs, for a given diffuse model, orientation and slope.

On the basis of these results, presented in Table 7.1, the following remarks can be noted:

- a) The isotropic model is almost not sensitive to the type of solar dataset (strictly or average hourly inputs);
- b) For all models, the gap increases with the slope: the difference between using the two solar datasets is low for the slope of 15° and is a bit higher for the slope of 45°;
- c) For the Hay model, the gap tends to increase and to be positive in the orientations close to North, whereas it is lower and negative in the near-south orientations;
- d) For the Perez model, the gap is higher and negative in the near-south orientations and positive and lower in the near-north orientations;
- e) The gaps are globally lower when using the Hay model relatively to the Perez model: the maximal gaps occur for the orientation of 45° and are 3.6 % for Perez (near-south orientations) and 2.1 % for Hay (near-north orientations). Moreover, when using average hourly inputs and for slope = 30° /orientation = 0° (South), the Perez model gives an yearly irradiation value (1404 kWh/m²) which is far from the usual expected yearly irradiation value in Geneva (1340 kWh/m²), while the yearly irradiation value obtained with Hay is more realistic (1367 kWh/m²).

Finally, using both the solar model implemented and the average hourly inputs, it may be concluded that the Hay model is more suitable as the gaps are lower than those of Perez, particularly for the near-south orientations that are the most significant for the solar energy use (PV collectors).

7.3 Solar irradiation analysis over the urban fabric

Slope 15 °									
Orientation	Isotropic			Perez			Hay		
	Average	Hourly	% Diff	Average	Hourly	% Diff	Average	Hourly	% Diff
180	1071	1071	0.0	1037	1042	0.5	1044	1048	0.4
135	1108	1108	0.0	1088	1088	0.0	1089	1092	0.2
90	1188	1187	0.0	1199	1190	-0.8	1186	1186	0.0
45	1261	1260	-0.1	1302	1285	-1.3	1276	1274	-0.2
0	1288	1289	0.0	1342	1322	-1.5	1310	1308	-0.2
-45	1256	1256	0.0	1298	1281	-1.3	1272	1269	-0.2
-90	1181	1180	-0.1	1192	1184	-0.7	1179	1179	0.0
-135	1102	1102	0.0	1083	1084	0.1	1083	1086	0.2

Slope 30 °									
Orientation	Isotropic			Perez			Hay		
	Average	Hourly	% Diff	Average	Hourly	% Diff	Average	Hourly	% Diff
180	904	904	0.0	838	849	1.3	851	860	1.0
135	981	980	-0.1	942	943	0.1	945	950	0.6
90	1136	1134	-0.2	1158	1140	-1.6	1133	1134	0.1
45	1263	1262	-0.1	1338	1306	-2.5	1290	1286	-0.3
0	1308	1308	0.0	1404	1367	-2.7	1346	1341	-0.4
-45	1255	1254	-0.1	1330	1300	-2.4	1282	1277	-0.4
-90	1122	1120	-0.2	1144	1129	-1.4	1120	1120	0.0
-135	967	967	0.0	928	931	0.3	930	936	0.7

Slope 45 °									
Orientation	Isotropic			Perez			Hay		
	Average	Hourly	% Diff	Average	Hourly	% Diff	Average	Hourly	% Diff
180	736	737	0.2	645	661	2.4	663	678	2.1
135	852	851	-0.2	802	802	0.0	804	812	1.0
90	1061	1059	-0.2	1093	1067	-2.4	1059	1060	0.1
45	1215	1214	-0.1	1314	1271	-3.4	1249	1246	-0.3
0	1268	1268	0.0	1391	1343	-3.6	1315	1309	-0.4
-45	1205	1203	-0.2	1304	1263	-3.3	1239	1235	-0.4
-90	1044	1040	-0.3	1076	1053	-2.2	1041	1041	0.0
-135	832	831	-0.2	781	783	0.3	782	791	1.1

Table 7.1. Analysis and comparison of the isotropic model and the anisotropic models of Perez and Hay to find which diffuse radiation model is the most suitable one.

7.3.4 Conclusion

Finally, subsequently to determining for every pixel its shadowing condition, its SVF, its orientation, and its inclination, the global incident solar irradiation, calculated in W or J /m², can be assigned for various times scales (hour, aggregation to month, year). An example of a simplified synoptic view of the pixel based solar irradiation calculation map (considering an isotropic sky condition) - considering both direct and diffuse components - on December 15th, 4 PM (MJ/m²) for a case-study area of Lisbon (District of Chão de Loureiro) is shown in Figure 7.8.

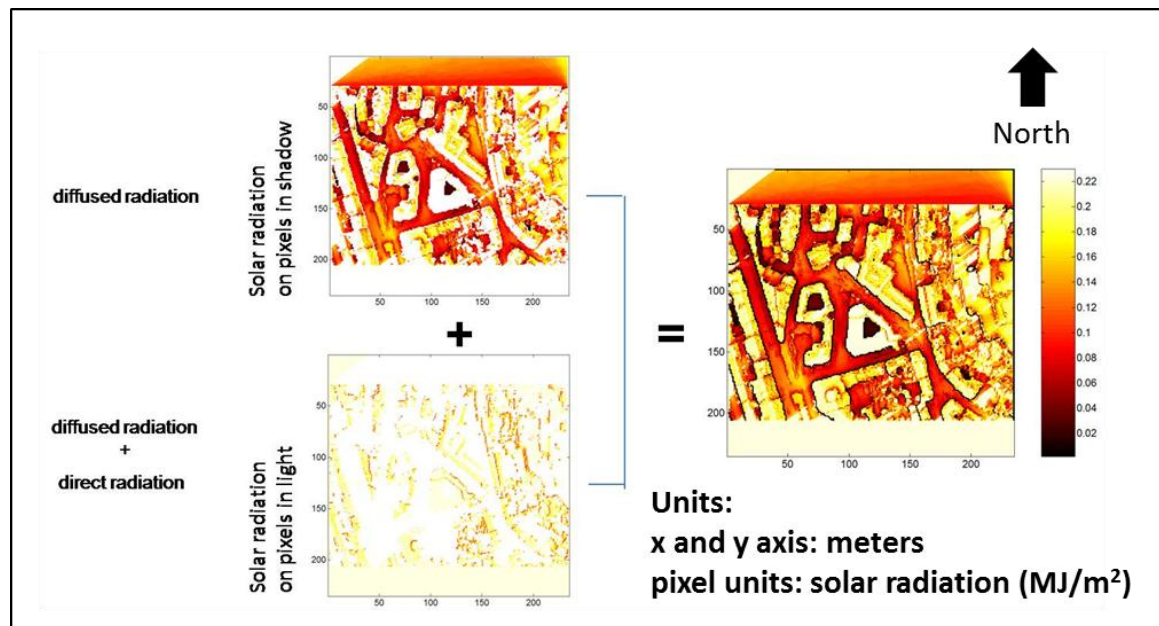


Figure 7.8. Simplified synoptic view of the pixel based solar irradiation calculation map (in this case, applying an isotropic sky condition) on December 15th, 4 PM [MJ/m²] for a case-study area of Lisbon (District of Chão de Loureiro).

7.4 Case-studies

7.4.1 Overview

As already mentioned in the introduction (section 7.1) of this chapter the empirical studies highlighted in this thesis are related to the extraction of complex indicators and indexes belonging to the stake “exploration of the solar potential on the urban fabric”, each of them presented inside a specific case-study:

- *analysis of solar irradiation over building roofs*, by analysing the solar and shadowing conditions on a specific built-area considering different periods of time (daily, monthly and yearly conditions);
- *impact of vegetation on the solar irradiation over the urban fabric*, by analysing and comparing two different scenarios of the same pilot-zone, which is performed by constructing a 2.5-DUSM of roof lines including vegetation and a 2.5-DUSM of roof lines without vegetation respectively;
- *comparison of solar irradiation over building roofs on two case-study areas*, by analysing and comparing two different pilot-zones generically presenting different building textures;
- *analysis of solar irradiation over building facades*, by analysing solar and shadowing conditions on a specific built-area considering different periods of time;
- *potential for active solar technology*, to assess the potential implementation of renewable energies at the scale of the city.

Each of these five case-studies is presented in detail from sections 7.4.4 to 7.4.8.

7.4.2 Data sources used and 2.5-DUSM constructed

Since all five case-studies highlighted represent different geographical areas of the State of Geneva, the data used (which presents the same properties) for the analysis was supplied by the same organisation¹⁴, described as follows (for more details about the data sources used please consult section 5.2):

- *2-D projection of 3-D roof lines.* The 2-D projection of 3-D roof lines is used to extract vector information of building roofs that are used to construct a more accurate 2.5-DUSM of roof lines;
- *LiDAR data.* The LiDAR used for the construction of the different 2.5-DUSM used in these case-studies has a density of 4 points/m², a planimetric accuracy of 20 centimetres and an altimetric accuracy of 15 centimetres;
- *3-D city model.* An accurate 20 to 25 centimetres 3-D vector city model is used in this chapter only for visualization purposes.

For more information about the method used for the construction of the different 2.5-DUSM and n2.5-DUSM used in these case-studies please consult chapter 5.

7.4.3 Geo-referenced raster information produced

Considering the five different case-studies presented as follows nine different raster sets can be produced and used for each of them in order to run the model. These are the following:

1. The 2.5-DUSM layer (2.5-DUSM of roof lines or 2.5-DUSM of building outlines), whereby intensity values of pixels represent the height above the sea level. This input image is the main 2.5-D information to run the script;
2. The layer of shadowing of each pixel belonging to the 2.5-DUSM layer, calculated from the use of the 2.5-DUSM of roof lines or the 2.5-DUSM of building outlines, depending on the type of analysis undertaken, and considering hourly solar irradiation values (statistical values extracted from METEONORM).
3. The layers representing the SVF of each pixel of the 2.5-DUSM, calculated from the use of the 2.5-DUSM of roof lines or the 2.5-DUSM of building outlines, depending on the type of analysis undertaken;
4. The layers for describing slope of each pixel, calculated from the use of the 2.5-DUSM of roof lines, the 2.5-DUSM of building outlines or the segmentation procedure on LiDAR data, depending on the type of analysis undertaken;
5. The layers for describing orientation of each pixel, calculated from the use of the 2.5-DUSM of roof lines, the 2.5-DUSM of building outlines or the segmentation procedure on LiDAR data, depending on the type of analysis undertaken;
6. The layers including labels of buildings, calculated from the 2-D GIS cadastral data. Hence it is possible to determine the exact identification of each building;
7. The layers including labels of roofs or roof sections, calculated from the 2-D projection of the 3-D vector model of roof lines. Hence it is possible to determine the exact identification of each roof or roof section;
8. The n2.5-DUSM of building outlines, whereby intensity values of each pixel represent the height above the terrain;
9. The n2.5-DUSM of vegetation higher than 3 meters.

¹⁴ DCMO : Direction Cantonale de la Mensuration Officielle de Genève.

For each of the five case-studies highlighted a synoptic view showing the different layers created and implemented is presented. The numbering format shown in each of these dataflow for the layers used strictly respects the numbering order of layers shown in this section.

7.4.4 Case-study: analysis of solar irradiation over building roofs

7.4.4.1 Presentation

A general understanding of the solar admittance and solar gains incident on the urban fabric is very useful in order to assess the potential implementation of renewable energies at the scale of the city, especially over building roofs.

In this case, the area selected for the analysis is a square of 1000 by 1000 meters in the District of Moillesulaz in the city of Geneva, as presented in the shadowed white zone of Figure 7.9. The urban texture presents low density urbanization (420 buildings counted on site) with mixed typologies, mainly residential and some tall buildings. The constructed 2.5-DUSM of roof lines considering vegetation is shown in Figure 7.10.



Figure 7.9. Case-study area (shadowed white zone) in the District of Moillesulaz, city of Geneva.

7.4 Case-studies

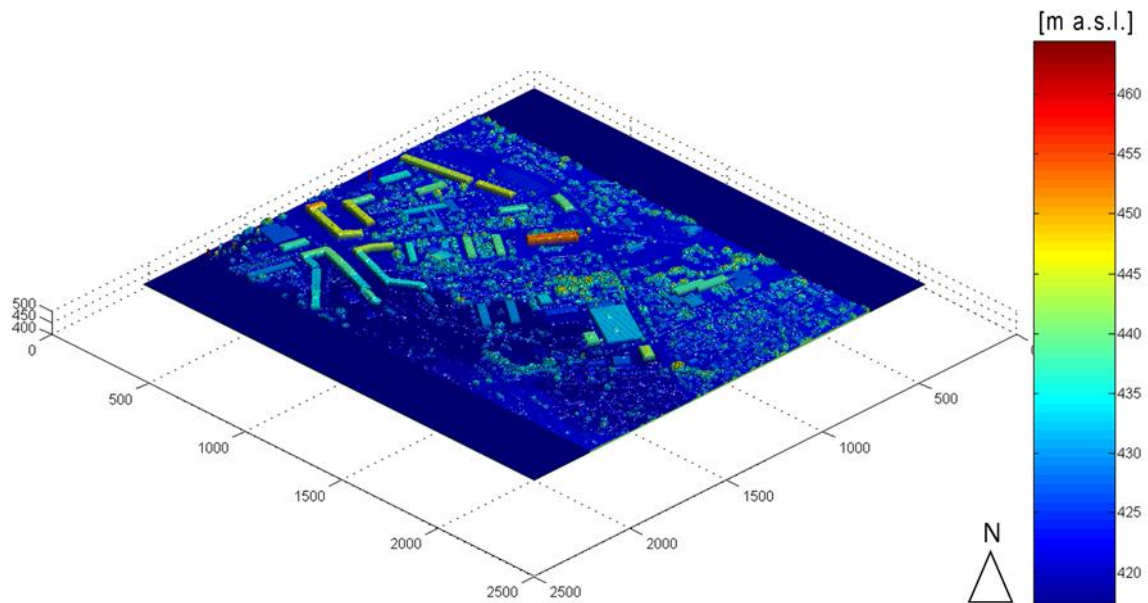


Figure 7.10. Example of 2.5-DUSM with terrain, buildings and vegetation higher than 3 meters (trees) for the neighbourhood of Moillesulaz, city of Geneva.

7.4.4.2 Synoptic view of the process

The process of structuring the proposed methodology is based on five major steps, as represented in the synoptic view of Figure 7.11: (1) the classification of LiDAR data used, (2) the creation of the 2.5-DUSM of roof lines including vegetation (3) the creation of layers used, (4) the solar irradiation and morphological analysis on building roofs through the image processing of 2.5-DUSM, which may include the selection of roof section surface areas taking into account slope derived from morphological analysis (5) the visualizations of results.

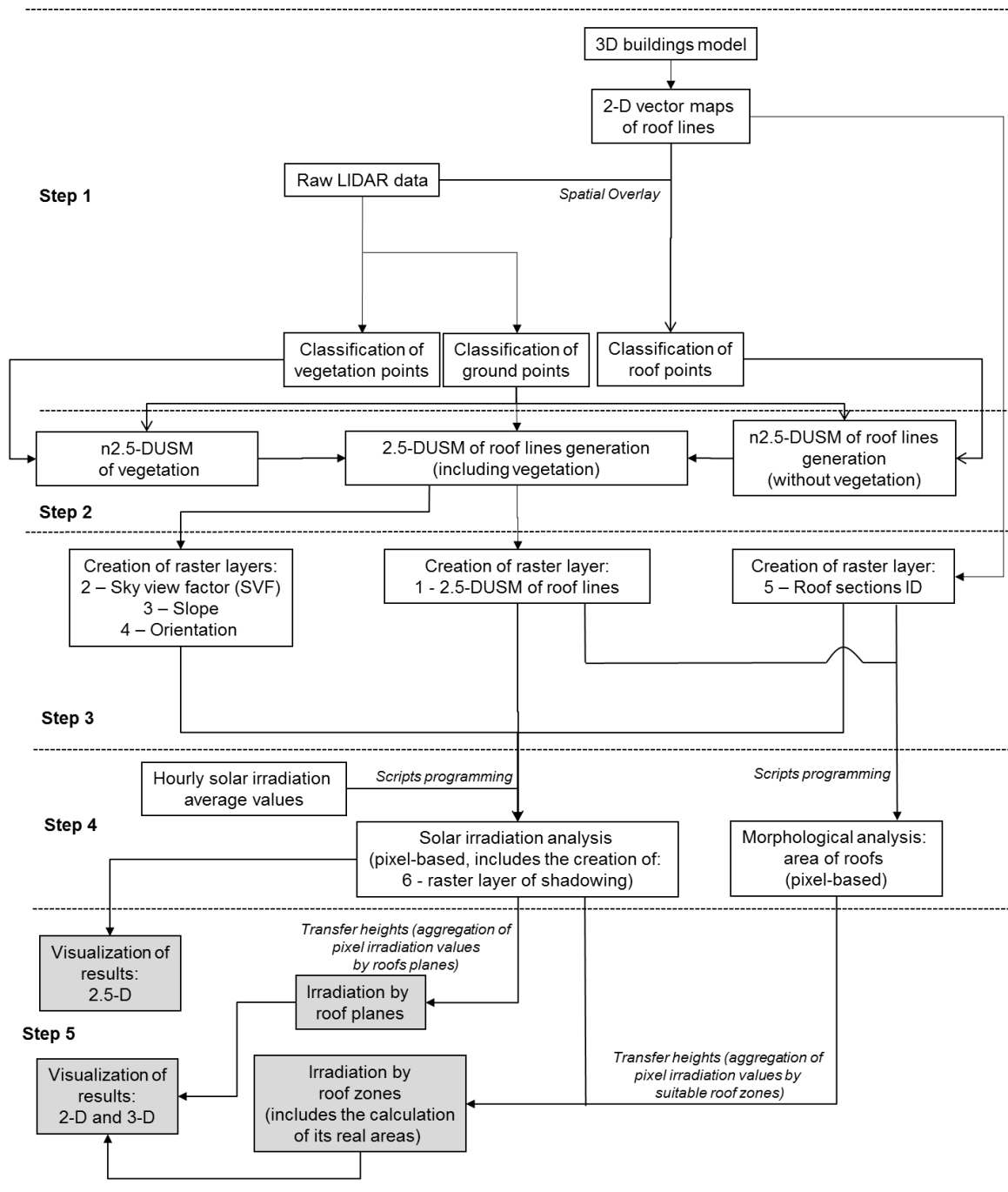


Figure 7.11. Synoptic view summarizing the process used to calculate solar irradiation on roof planes (sections) and suitable roof zones.

7.4.4.3 Calculation of solar irradiation on building roofs

As presented in the first sections of this chapter, in the case where it is possible to determine for every pixel its shadowing condition, its SVF, its orientation, its inclination and its linear extension, the incident solar irradiance, calculated in Watt per square meter, can be assigned to each roof section.

7.4 Case-studies

As introduced in section 7.3.1 this method allows the calculation of the values of solar irradiation that are based on different isotropic and anisotropic models. Moreover, the method can be also applied considering, or not, shadowing and SVF conditions. In this case, four different conditions were analysed:

- Case 1: isotropic model without shadowing and SVF;
- Case 2: anisotropic model of Hay without shadowing and SVF;
- Case 3: isotropic model considering shadowing and SVF;
- Case 4: anisotropic model of Hay considering shadowing and SVF.

An example of 2.5-D visualization of the yearly solar irradiation values (KWh/m^2) representing the difference between two outputs for this case-study area is shown in Figure 7.12: the anisotropic model of Hay considering shadowing and SVF (case 4) minus the isotropic model considering shadowing and SVF (case 3). As shown in Figure 7.12, the isotropic model can considerably overweight the yearly irradiation values of north-oriented and sloped roof sections when compared to the anisotropic model of Hay.

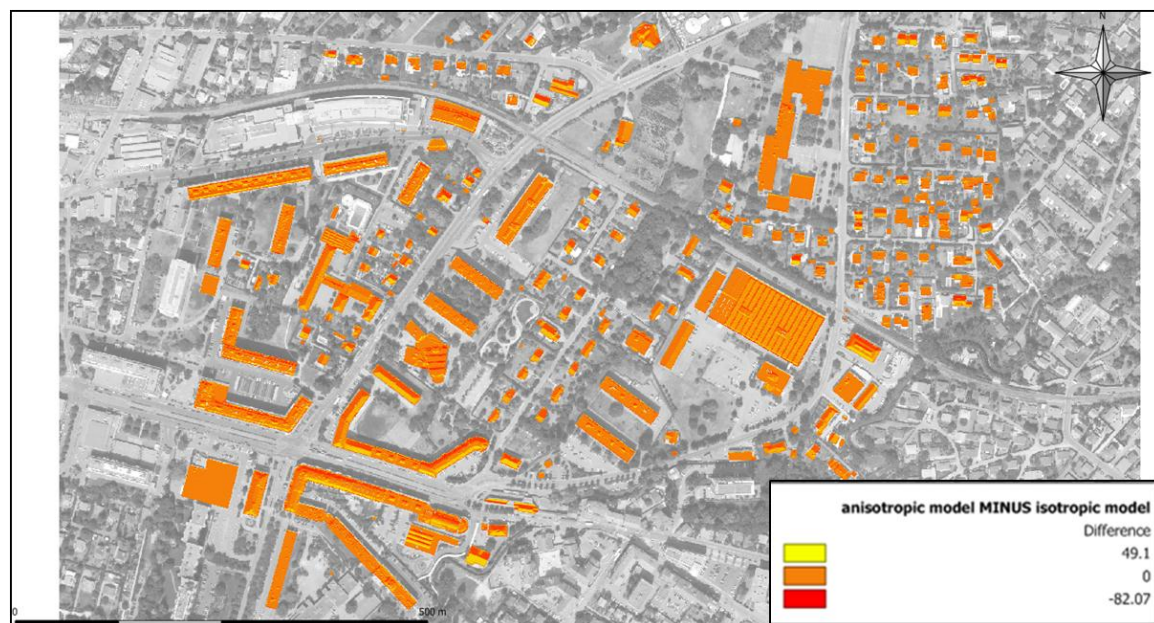


Figure 7.12. An example of 2.5-visualization of the yearly solar irradiation values (KWh/m^2) representing the difference between two outputs for the case-study area of Moillesulaz, city of Geneva: the anisotropic model of Hay considering shadowing and SVF (case 4) minus the isotropic model considering shadowing and SVF (case 3).

According to Chwieduk (2009), the anisotropic sky model should be preferentially used for calculation and evaluation of the energy balance of buildings regardless of its type or size. The reason for having chosen the anisotropic model of Hay, when compared to the model of Perez, for all the examples shown in this section is explained in section 7.3.3.

Therefore, as for final result, a set of irradiation values is stored in dedicated arrays. Firstly all irradiation maps in a 4-D matrix (length of the site x width of the site x 24 hours of the typical day of the month x 12 months) are accumulated and can be aggregated in different periods of time: daily, monthly and yearly, such as presented in Figure 7.14 to Figure 7.15 respectively.

Chapter 7. Exploration of the solar potential on the urban fabric

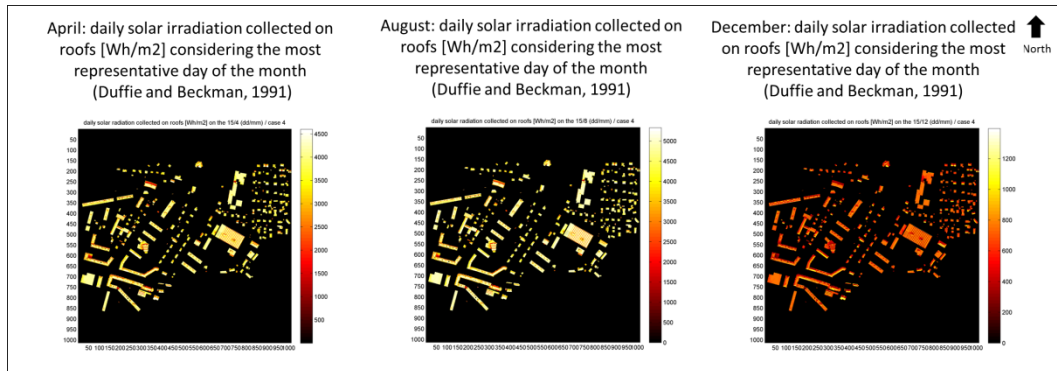


Figure 7.13. Calculation of the daily irradiation values (Wh/m²) considering the most representative day of the month (Duffie and Beckman, 1991), applying the model of Hay for the case-study area of Moillesulaz, city of Geneva. From left to right images: calculation for the months of April, August and December.

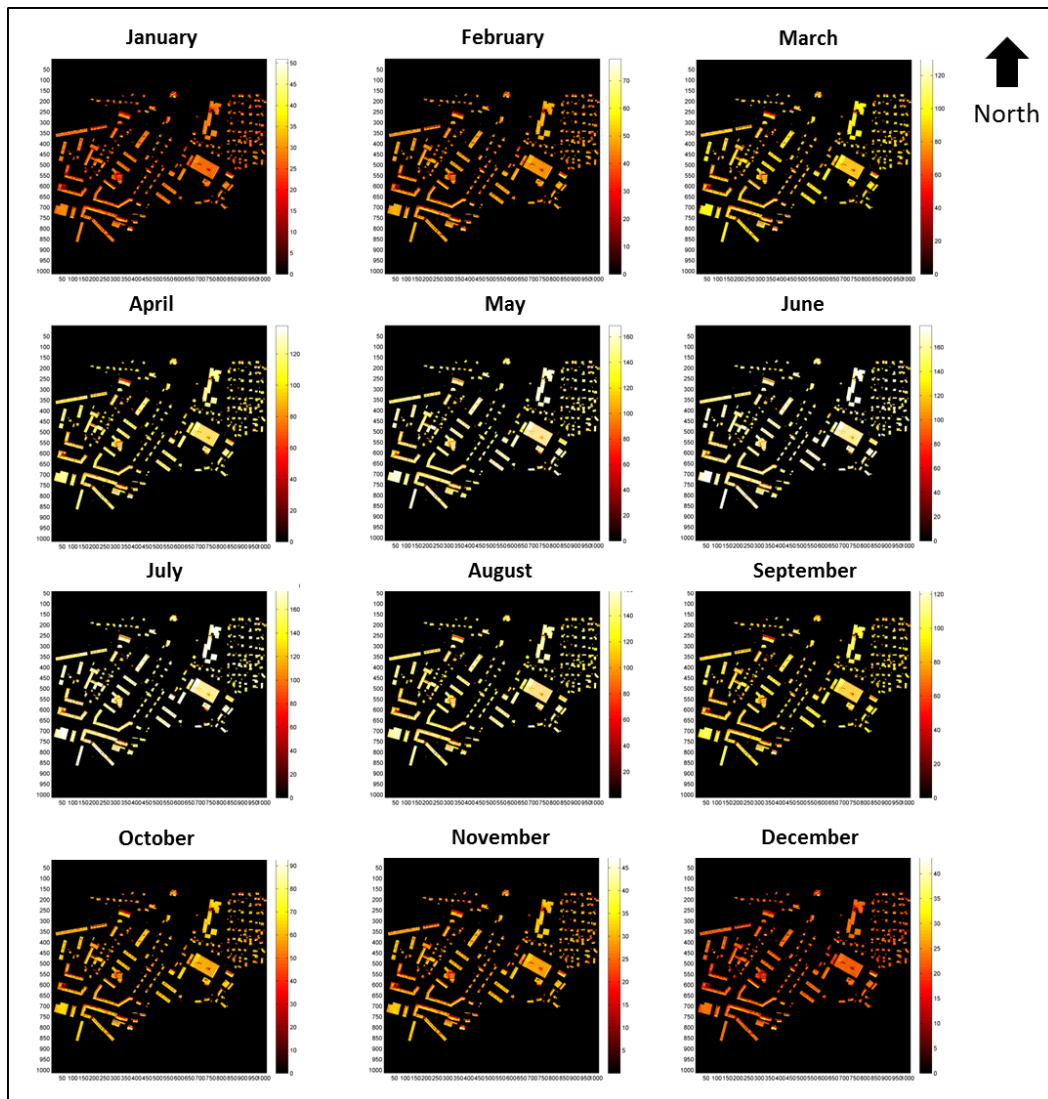


Figure 7.14. Calculation of the monthly irradiation values (KWh/m²) applying the model of Hay for the case-study area of Moillesulaz, city of Geneva. From top-left to right-bottom images: January to December.

7.4 Case-studies

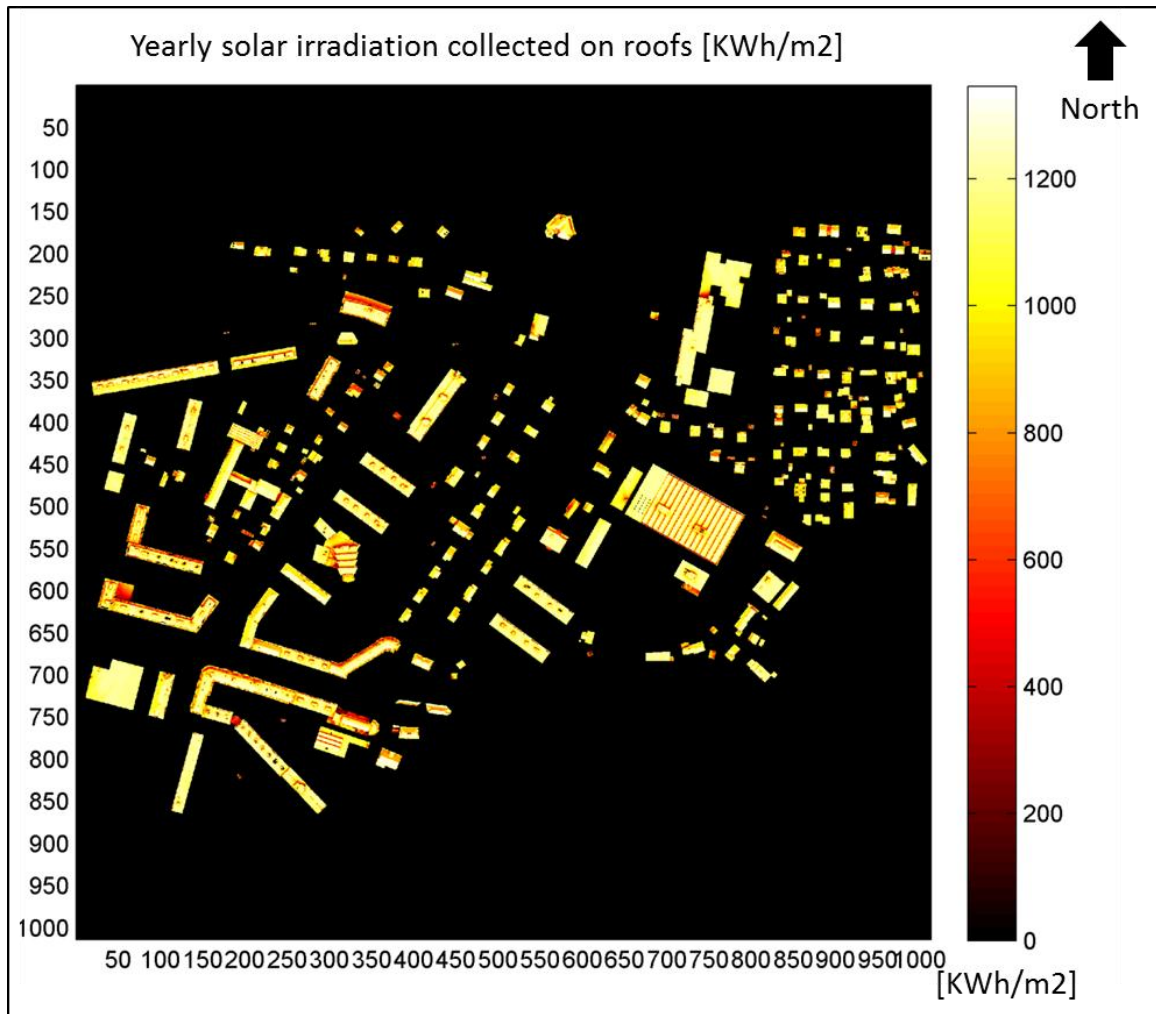


Figure 7.15. Calculation of the yearly irradiation values (KWh/m²) applying the model of Hay for the case-study area of Moillesulaz, city of Geneva.

A set of yearly and daily irradiation values (2.5-D visualization) calculated using the isotropic model is shown in Appendix C.

7.4.4.4 Extraction of indicators and analysis of results

The production and visualization of pertinent indicators for different end-users can be done using different representations: 2-D, 2.5-D and 3-D. Thus, some examples of visual displays are presented in the following figures of this section.

The calculation of irradiation values on a pixel-basis (as shown in section 7.4.4.3) can be transferred and aggregated into a vector format representing all the roof sections of the buildings under analysis in the district of Moillesulaz, as explained in the synoptic view of Figure 7.11. An example of the yearly irradiation values calculated can be represented in 2-D and 3-D views, as shown in Figure 7.16 and Figure 7.17 respectively.



Figure 7.16. 3-D visualization of the yearly irradiation values (KWh/m²) by roof sections, applying the model of Hay for the case-study area of Moillesulaz, city of Geneva.

7.4 Case-studies



Figure 7.17. 2-D visualization of the yearly irradiation values (KWh/m²) by roof sections, applying the model of Hay for the case-study area of Moillesulaz, city of Geneva.

A more detailed analysis concerning the most suitable zones of roofs, for instance, for the installation of PV, can be also applied. According to Montavon (2010), appropriate roofs for the installation of PV must present a yearly annual irradiation higher than 1000 KWh/m². Moreover, by integrating the information derived from the morphological analysis of the areas of roofs, it is also possible to derive the real area of each of the selected zones of roofs. The method applied is based on a mix approach combining raster and vector formats, as shown in the dataflow of Figure 7.18. Visual results (2-D representation), complemented with an example of the real area of four selected suitable zones of roofs derived from morphological analysis, are shown in Figure 7.19.

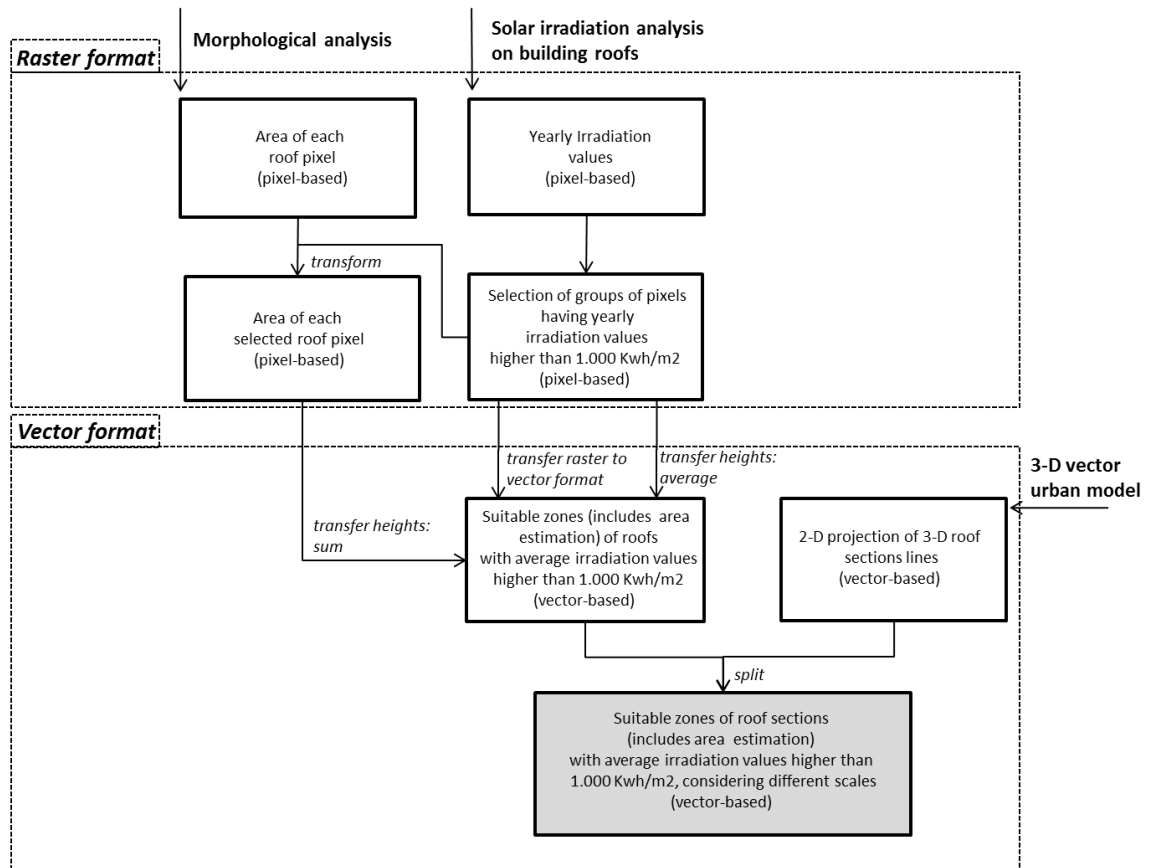


Figure 7.18. Dataflow describing the method applied for the extraction of the most suitable zones of roofs.



Figure 7.19. 2-D visualization of the suitable areas of roof sections with yearly irradiation values higher than 1.000 KWh/m², applying the model of Hay for a zone of the case-study area of Moillesluz, city of Geneva.

7.4 Case-studies

An indicator concerning the yearly percentage of shadowing can also be calculated. It allows the clearly differentiation of which parts of the solar radiation concerns the direct or diffusing components. This indicator is considered to be very useful for the analysis of shadowing along roofs: in one hand, PV technology is very sensitive to diffuse radiation and, on the other hand, PV mono-crystalline is very sensitive to direct radiation. This indicator can be calculated by applying the following formula:

$$R = 1 - (A/B) \times 100 \text{ [%]} \quad (7.12)$$

This percentage represents the ratio (R) between the calculation of irradiation taking into account a factor A, for case 2 (anisotropic model of Hay without shadowing and SVF), and a factor B, for case 4 (anisotropic model of Hay considering shadowing and SVF), as shown in the dataflow of Figure 7.20. Visual results (2-D representation) are shown in Figure 7.21.

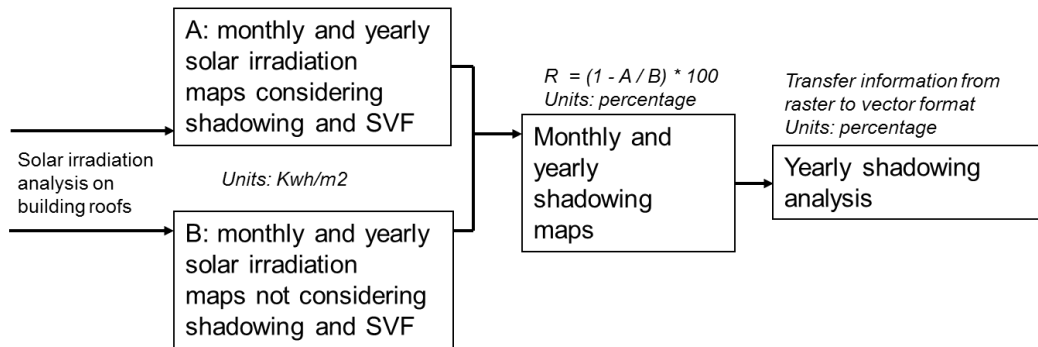


Figure 7.20. Dataflow summarizing the method applied for the calculation of shadowing analysis.



Figure 7.21. Shadowing analysis (applying the model of Hay) for a specific zone of the case-study area of Moillesulaz, city of Geneva.

A statistical analysis of the results from the raster images produced concerning the yearly solar irradiation on roofs can be undertaken. Hence, starting from 0, for each 100 Kwh/m², until the maximum value found of 1358Kwh/m², real roof areas can be calculated, as shown in Figure 7.22.

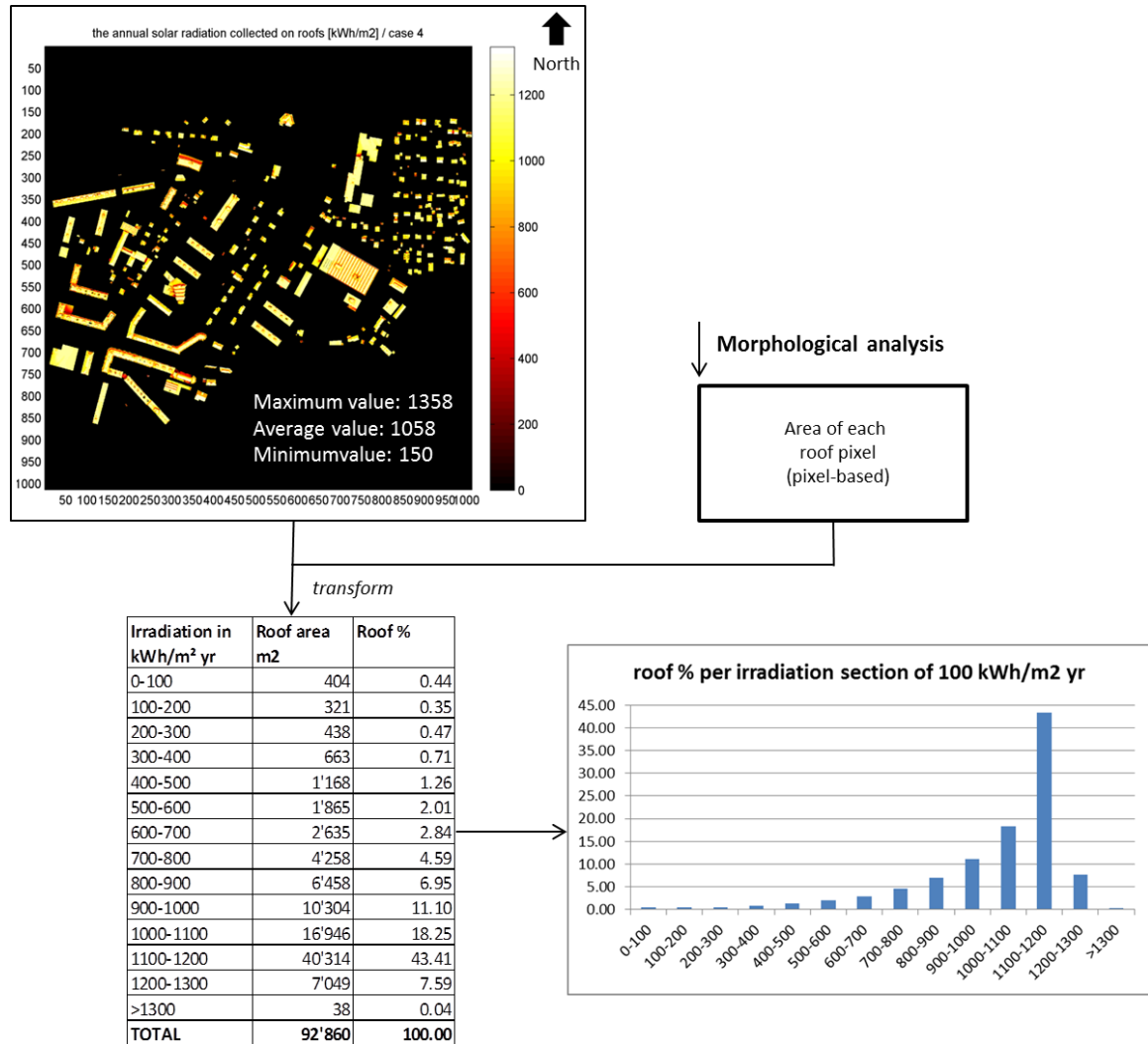


Figure 7.22. Roof area (every 100 Kwh/m²) for the case-study area of Moillesulaz, city of Geneva.

Considering the results presented in Figure 7.22 it is worth mentioning that more than 2/3 (around 69%) of the roofs under analysis present good conditions for the installation of PV because they have a yearly irradiation higher than 1000 Kwh/m². In fact, with a low site and vegetation density and buildings of relatively few storeys - most of them presenting flat and classic roofs -, solar access and, thus, the annual irradiation are relatively high. Furthermore, according to the statistical data used (from METEONORM) for these calculation outputs, the maximum value of 1358 Kwh/m² found for a pixel belonging to a south oriented roof with a slope of around 30° is similar (positive deviation of 0.9%) to the theoretical maximum value (1346 Kwh/m²) admitted for a slope of 30° using the Model of Hay, as shown in Table 7.1.

7.4.4.5 Conclusions

In this case-study, a complete process going from the extraction of LiDAR data to the analysis of solar admittance over 2.5-DUSM of roof lines considering vegetation and the visualization of several indicators is presented. It aims to analyse two sub-stakes defined as priority by the end-users of the State of Geneva: (1) “exploration of the solar irradiation on building roofs”, (2) “estimation of the influence of shadowing and SVF on the urban texture”.

Applications of this methodology in urban design and planning are very promising. In this case-study, the analysis is limited to the physical built environment, but it could be extended to assess the impact of new buildings in the city and for improving design schemes based on an evaluation of quantitative indicators before and after changes are introduced. If applied to more urban typologies in the case that LiDAR data are available, the morphological analysis could lead to interesting indicators that may be used by urban planners for predicting the environmental behaviour of different urban textures. In fact, guidelines that refer to comprehensive environmental indicators are still missing in the urban design literature.

Besides urban planning strategies, environmental policies could be promoted if a comprehensive mapping of solar irradiances on buildings is provided. In fact, a database of solar admittances on buildings is important for two main reasons: first, it could affect the real estate market by providing the values within the urban fabric according to its energetic performance; second, the community could program interventions and define specific incentives in order to consider the real potential energy production strategies of each building.

7.4.5 Case-study: impact of vegetation on the solar irradiation over the urban fabric

7.4.5.1 Presentation

In this work the impact of the urban vegetation on the solar radiation over the urban fabric is highlighted. It highlights the advantages of the use of LiDAR data as the source information for the construction of the different 2.5-DUSM used. In this case-study, the anisotropic model of Hay was used in order to calculate the results presented.

Particularly, the scope of the following analysis is twofold: firstly, it gives back some general urban morphology indicators related to the relation of green areas versus built areas; secondly, it investigates whether and how vegetation could limit the solar accessibility of urban roofs by computing the solar analysis over the entire year. The analysis is conducted by comparing the 2.5-DUSM of roof lines with vegetation and the one purged from this information. For this vegetation corresponds to plants with a volumetric relevance, such as trees and bushes (lawns are excluded) higher than 3 meters. The map of Figure 7.23 shows the percentage of roof coverage by vegetation. For each roof, it is obtained by dividing the number of pixels that are considered to be vegetation (according to the classification applied on LiDAR data) by the total number of pixels of the roof, multiplied by 100.

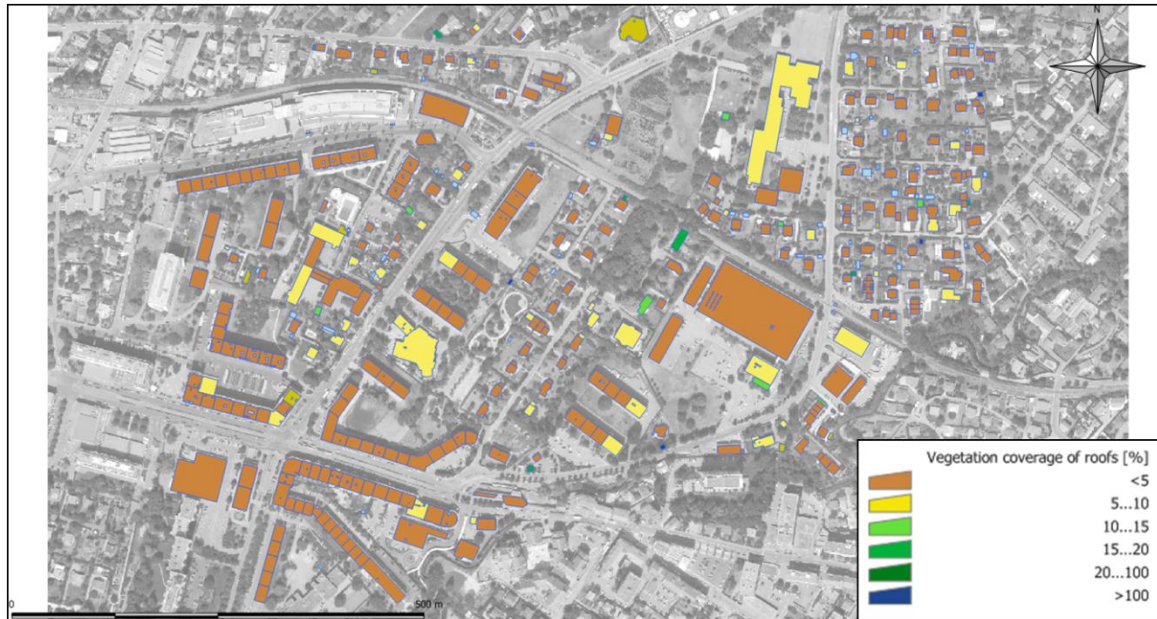


Figure 7.23. The percentage of vegetation coverage of urban roofs for the case-study area of Moillesulaz, city of Geneva.

7.4.5.2 Synoptic view of the process

The process of structuring the proposed methodology is based on five major steps as represented in the synoptic view of Figure 7.24: (1) the classification of the LiDAR data used, (2) the creation of the 2.5-DUSM of roof lines with vegetation, the 2.5-DUSM of roof lines without vegetation and the n2.5-DUSM of vegetation, (3) the creation of layers used, (4) the solar irradiation and morphological analysis on building roofs through the image processing of urban models, (5) the production of output results: 2.5-D visualizations and statistical analysis.

7.4 Case-studies

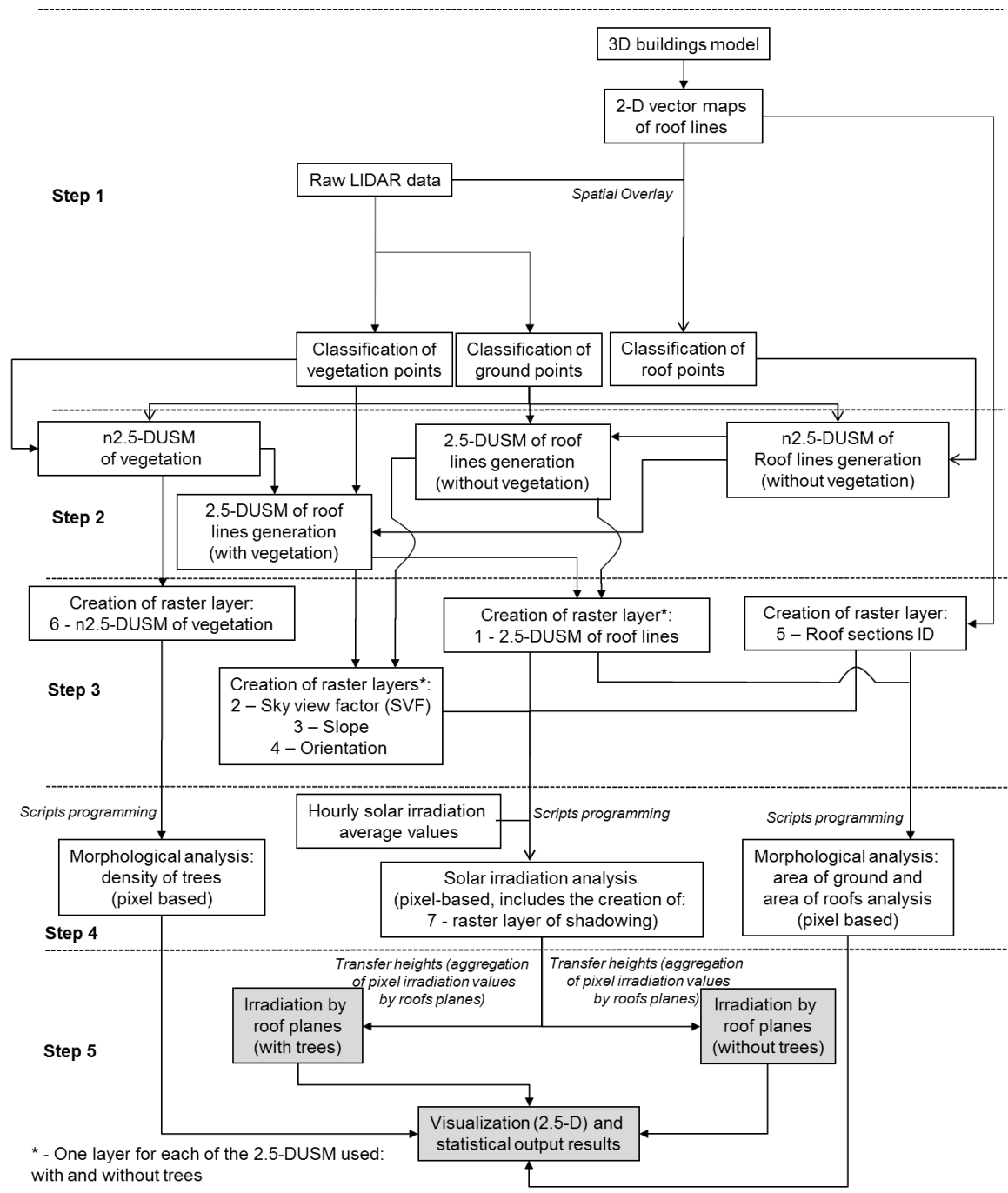


Figure 7.24. Synoptic view summarizing the process used to calculate the influence of vegetation related to the solar admittance on built-up area.

7.4.5.3 Extraction of indicators and analysis of results

Results of this comparative study (Figure 7.25) show that even with the presence of vegetation (about 1m^3 of vegetation per m^2 of area) no significant passive energy losses are reported on roofs. In fact, with a vegetation coverage ratio of 15% on the whole area of analysis, the solar irradiance on roofs is reduced by about 2.97%. In particular, the percentage of roofs directly

covered by vegetation is only 0.36% (trees are in general lower than buildings), but the overall reduction of the SVF on roofs due to the obstructions by trees reaches 2.91%.

For instance, a set of environmental and morphological indicators could inform urban designers about the distribution of vegetation inside the urban fabric in order to contribute to decision making processes. In general, numerical and visual outcomes can be used in comparative studies thus questioning the different performances of analogous urban textures. For instance, with the same availability of urban vegetation, different arrangements of built and natural features are possible, hence determining the supply of passive energy for electricity or hot water production.

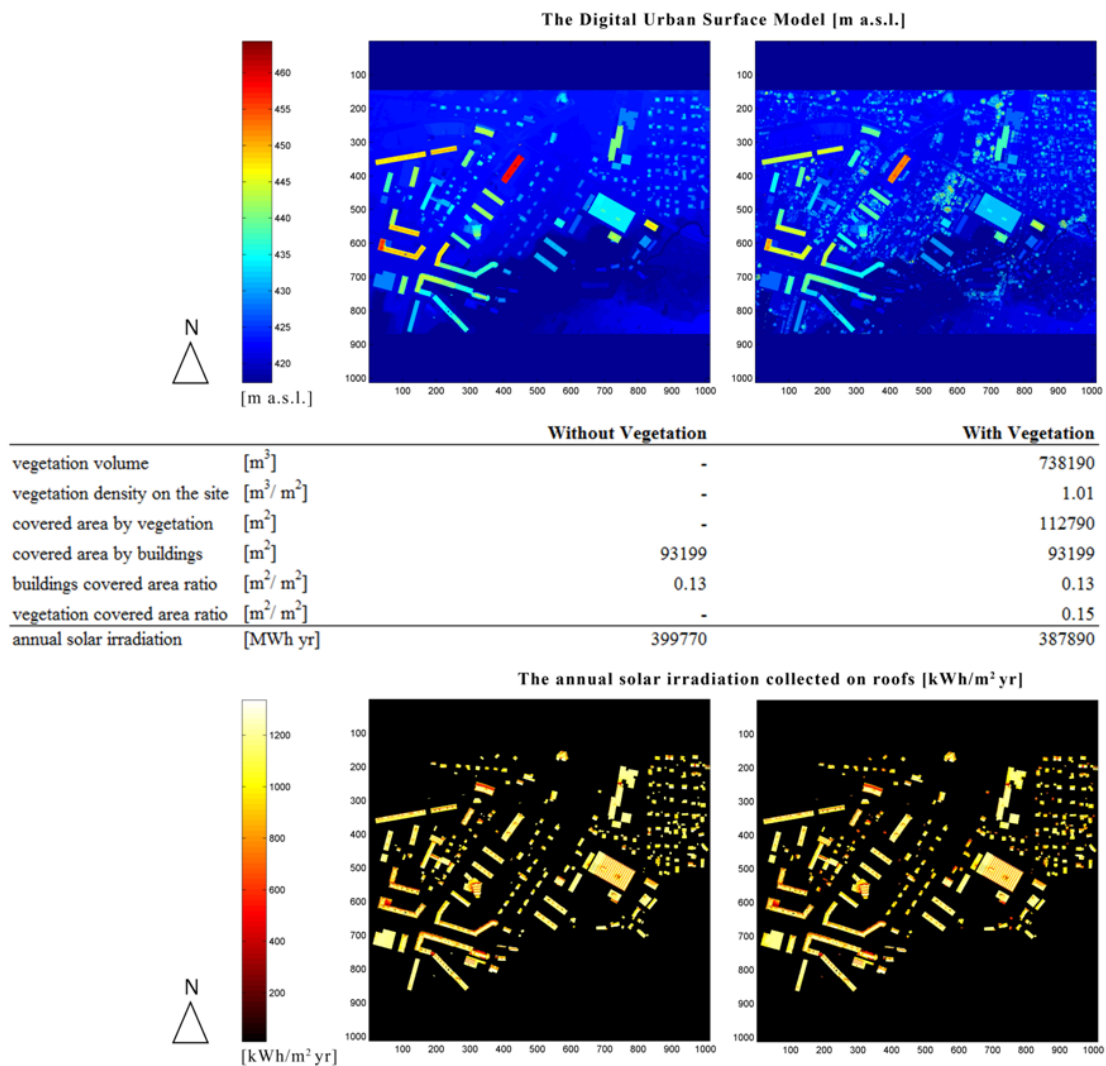


Figure 7.25. Above: The comparison of the 2.5-DUSM with (left-hand side image) and without the presence of vegetation (right hand-side image). Below: the comparison of the annual irradiation maps collected on roofs with (left hand-side image) and without the presence of vegetation (right hand-side image). Some numerical indicators are presented for comparison.

7.4.5.4 Conclusions

The need to implement more innovative tools that are suitable for urban planning and design tasks, especially with today's increasing concerns over environmental issues in cities, has become a priority. The sub-stake "estimation of the coverage and impact of vegetation on roofs" represents a paradigmatic example defined by the end-users of the State of Geneva. For this reason it was considered a priority and, thus, it was studied in this thesis chapter. Thus, aiming to achieve pertinent outputs, a complete process going from the extraction of LiDAR data to the analysis of solar admittance using different 2.5-DUSM is presented, followed by the visualization of indicators and the assessment of results on a statistical basis.

7.4.6 Case-study: Comparison of solar irradiation over building roofs on two case-study areas presenting different building textures

7.4.6.1 Presentation

This analysis aims to reveal the behaviour of solar admittance in two different case-study areas that differ in terms of size and land occupation. In order to produce a significant comparative study, it is fundamental to derive useful urban indicators that allow end-users to correlate the incident solar radiation in an objective manner. To achieve this goal, this case-study proposes a morphological study to normalize specific constraints due to the diverse urban contexts. In this case-study, the isotropic model was used in order to calculate the results presented.

In this case, the two areas selected for the analysis present very different characteristics in terms of extension and building typologies. The first pilot zone (left hand-side image of Figure 7.26) is a 300 meters sided square near the Rhone River and the old town of Geneva, in Switzerland, densely built and already described in section 6.3.3. The second pilot zone (right hand-side image of Figure 7.26) is a 600 metres sided square near the lake of Geneva, located within a residential area, as presented in the shadowed white zone of the right-hand side image of Figure 7.26. The urban texture presents a low density urbanization characterized by two storey's tall buildings (294 were counted on site) on average and by generous open areas. The 2.5-DUSM of roof lines without vegetation constructed for each of these two case-study areas is shown in Figure 7.27.



Figure 7.26. Two pre-defined areas (pilot zones) of the case study in Geneva's city; left hand-side image: dense built area near the Rhone River and the old town; right hand-side image: residential area near the lake of Geneva.

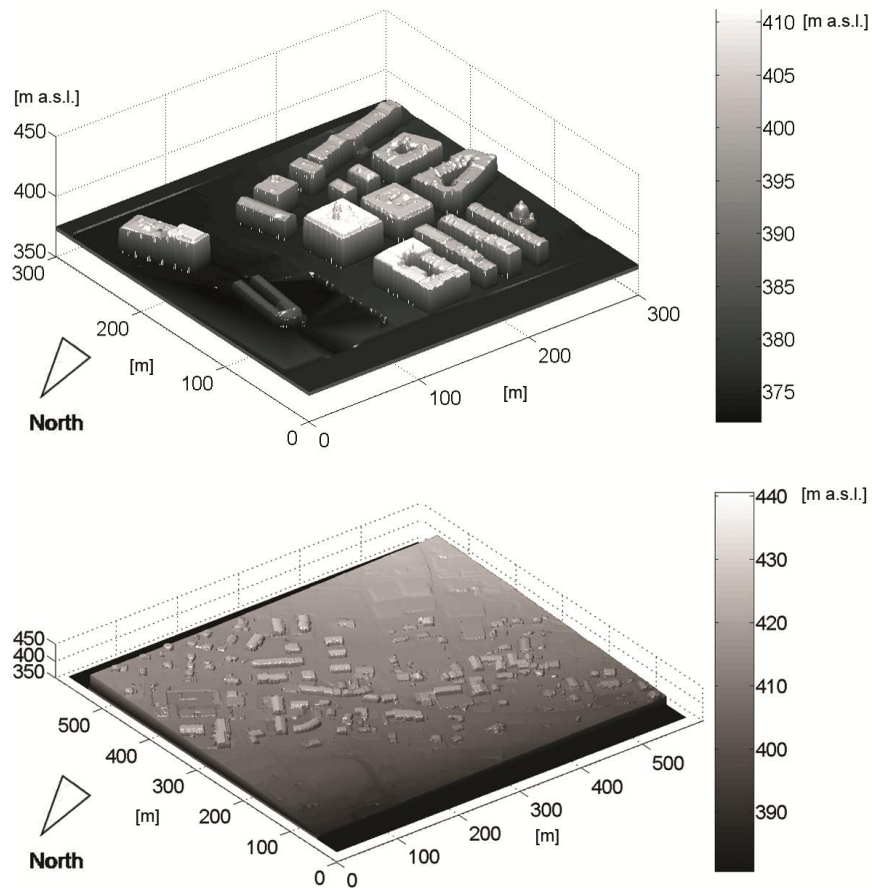


Figure 7.27. The 2.5-DUSM of roof lines without vegetation visualized on Matlab for the first (image above) and second (image below) pilot zones. Heights are expressed in meters above sea level.

7.4 Case-studies

As presented in section 5.7, a segmentation procedure for laser scanning data is also implemented in order to search for planar faces so to produce the layers of orientation and slopes of both case-study areas. Figure 7.28 shows the results of the algorithm for an area of the second pilot zone using all pulse laser scanning data.



Figure 7.28. Example of segmentation procedure (areas in black) for laser scanning data on part of the second pilot zone.

7.4.6.2 Synoptic view of the process

The process of structuring the proposed methodology is based on five major steps as represented in the synoptic view of Figure 7.29: (1) the classification of the LiDAR data used, (2) the segmentation procedure for laser scanning data (section 5.7) to derive slopes and orientations of roofs and the creation of the 2.5-DUSM of roof lines without vegetation (3) the creation of the layers used, (4) the solar irradiation and morphological analysis on building roofs through the image processing of urban models, (5) the visualizations of results.

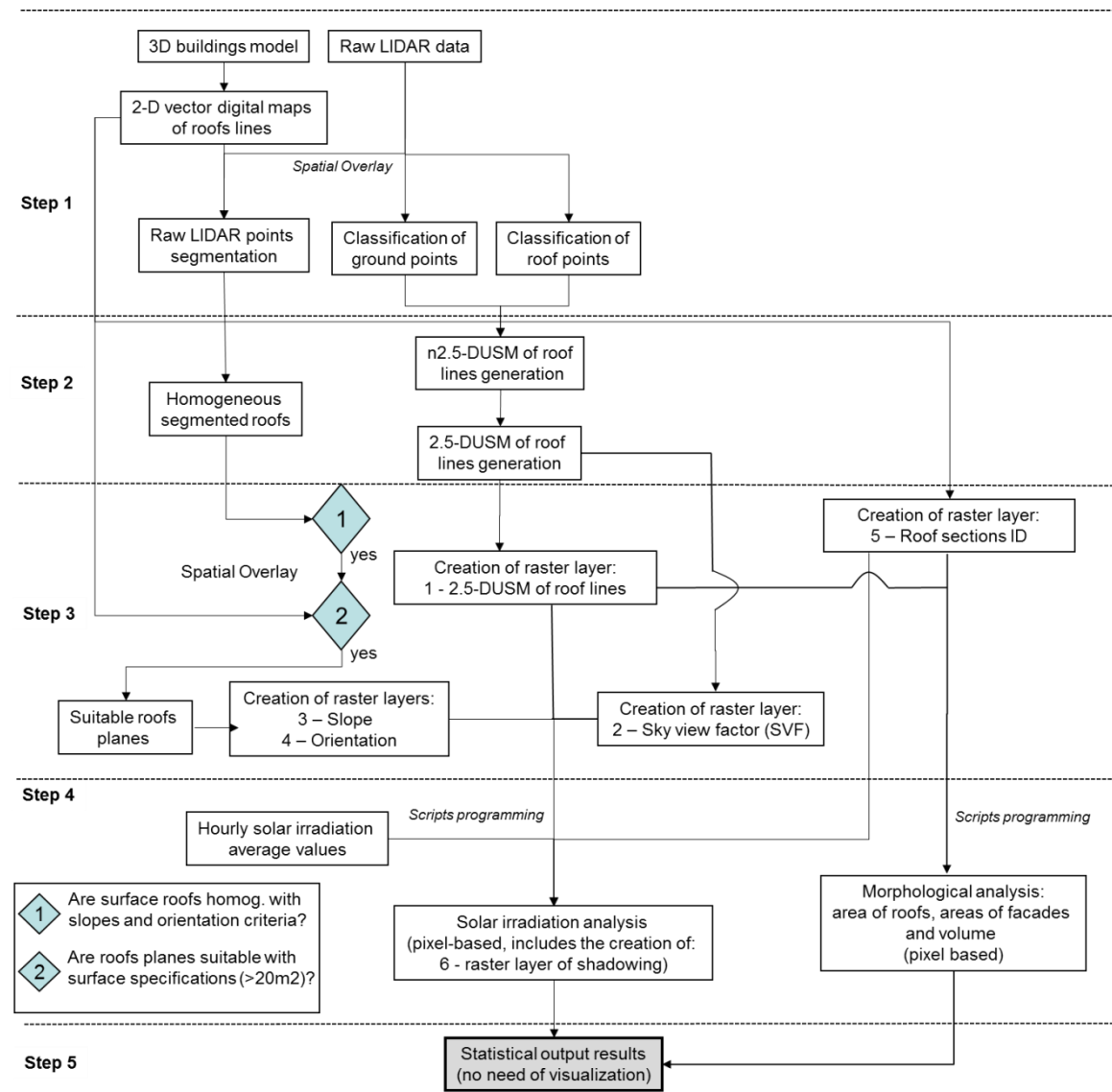


Figure 7.29. Synoptic view summarizing the process to extract statistical output results regarding the analysis of solar irradiation on building roofs.

7.4.6.3 Extraction of indicators and analysis of results

The objective of the morphological study is to better understand how different urban models behave in terms of renewable energy production, in this case solar energy. Since the two sites that are investigated present very different characteristics in terms of extension and building typologies, it is very important to find indicators to may conduct a morphological comparative study. The first pilot zone is a more central urban area with a dense fabric, tall buildings and few open spaces. On the contrary, the second zone presents a low density urbanization characterized by two storeys tall buildings on average and by generous open areas. In order to calculate plausible and comparable measures of urban density non-urban land (agricultural areas, big parks, and rivers) is discarded, and the area considered is defined by the grey contour shown in the two images of Table 7.2.

7.4 Case-studies

Beside more traditional urban morphological indicators (urban land, covered area, built volume, estimation of floor area, mean built height, theoretical population) and urban density measures (urban built density, ground coverage index), the surface to volume ratio is also assessed as an indicator of compactness. In fact, the first pilot zone is more compact than the second (S/V ratios are respectively 0.20 and 0.30). Indeed, it is possible to calculate this parameter using the morphological analysis highlighted in chapter 6. Moreover, for PV technology, roof surface areas must at least be equal to 20m² to meet the requirement of minimum installed power capacity (2kW) for cost-effectiveness.

A set of parameters that address the solar admittance of the urban fabric is also defined. These parameters are: (a) the area of roofs suitable for installing PV modules; (b) the irradiance density, i.e. the incident energy per m²; (c) an urban irradiance density, defined as the total net incident irradiance on urban roofs divided by the population. This last parameter does not represent a measure that can be converted into useful energy and for that reason is not shown in Table 7.2.

From the analysis of the total incident radiation on the different two areas, interesting considerations emerge (as shown in Figure 7.30 and Table 7.2). In fact, if the data is normalized considering the total areas of roofs (Figure 7.30, graphic below) the irradiance on the second area is slightly higher than on the first one. Hence, results are very similar regardless of how much different the two urban morphologies are. Therefore, in terms of solar admittance, compact urban areas can perform as well as less dense urban areas.

Results of this analysis reveal that the production of solar energy on low density areas is easier due to two main parameters: urban obstructions and population density. Urban obstructions have a higher impact on the compact urban area (the mean SVF computed on roofs is 0.82 in the first pilot zone versus a value of 0.86 in the second one), and the building typologies in the second case-study area allow the attainment of a higher degree of “potential solar roof” area per person. In fact, referring to the theoretical population of the two areas (derived as a standard value from the built volume), the second one presents better results (Figure 7.30, graphic above). This is due to the lower densities and consequently larger amount of roof areas available *per capite*. For instance, considering the population hosted in both sites, the mean irradiance per person in the second pilot zone is almost three times as much as for the first one (see Table 7.2). Mean irradiance per person is defined as the “urban irradiance density” (kWh/person) and intends to assign to each person the average solar irradiance incident on the roof during the entire year. It is worth observing that this irradiance density takes into account the total incident solar radiation and not the fraction that can be converted into useful energy alone. Further research emphasized in chapter 8 describes the conversion of this value into electrical energy production.

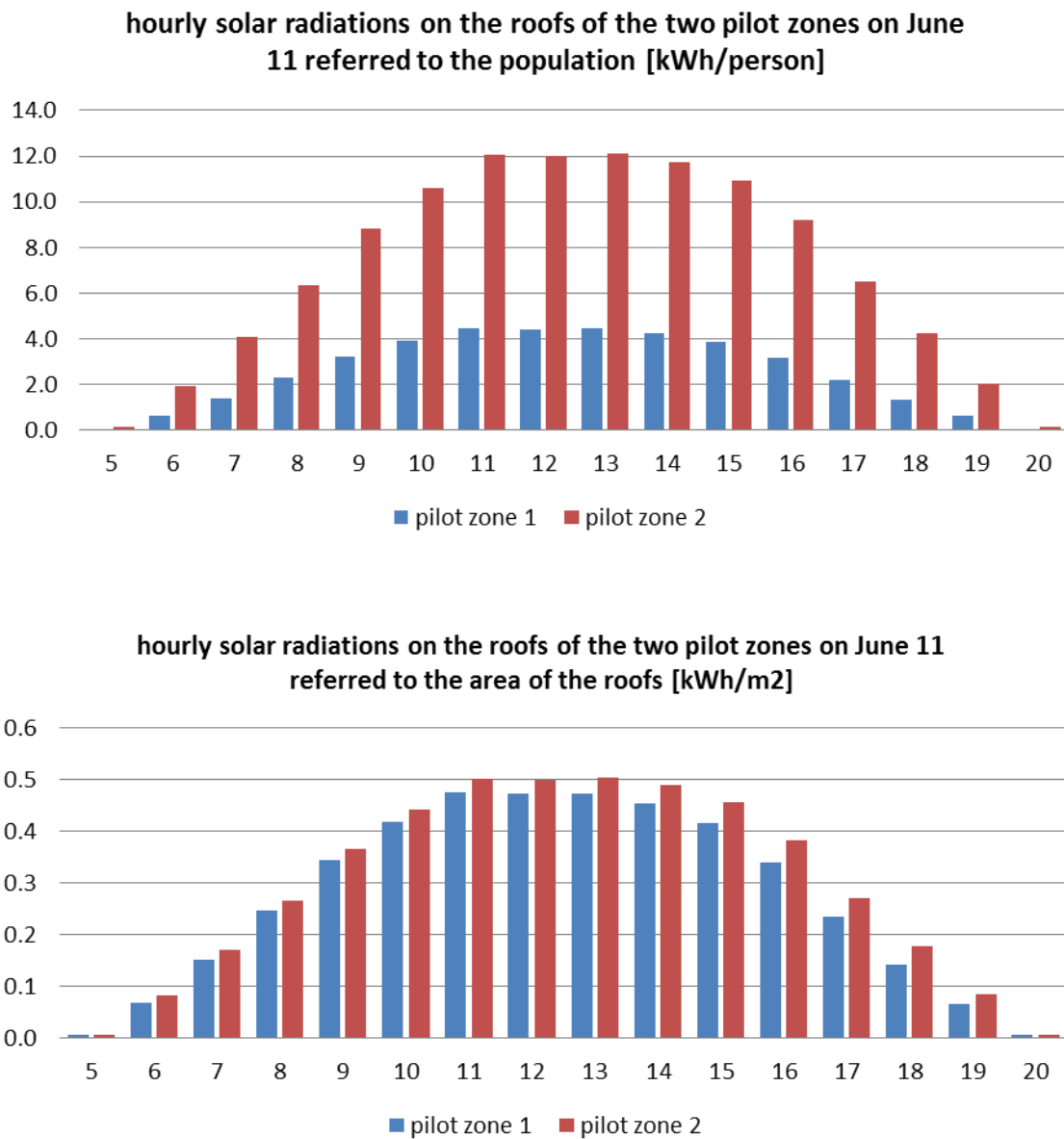


Figure 7.30. Comparison of solar irradiance (kWh) collected on the 15th of June from 6 AM to 8 PM on the two case-study areas. Above the values weighted by the population (kWh/person) and below the irradiances referred to the areas of the roofs (kWh/m2).

7.4 Case-studies

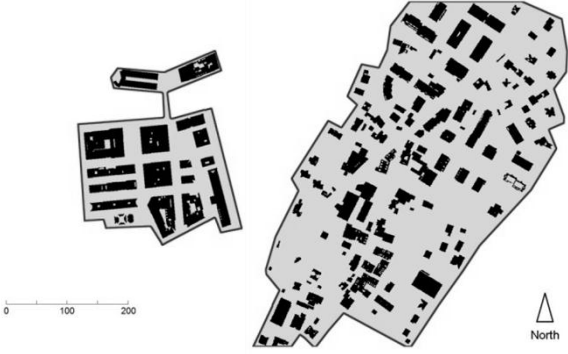
	PILOTE ZONE 1	PILOTE ZONE 2
		
<i>MORPHOLOGICAL INDICATORS</i>		
urban land [m ²] (red boundary)	42711.00	150670.00
covered area [m ²] (black footprint)	17903.00	34592.00
built volume [m ³]	331520.00	244600.00
estimation of floor area [m ²]	110510.00	81535.00
Mean height [m]	18.52	7.07
population [person]	2210.13	1630.67
area of roofs [m ²]	20660.44	39109.46
area of facades [m ²]	46535.00	34751.00
surface to volume ratio [1/m]	0.20	0.30
<i>POTENTIAL AREAS FOR INSTALLING "SOLAR ROOFS"</i>		
suitable areas of roofs for the installation of PV panels [m ²]	11438.05	20757.35
percentage of roofs suitable for the installation of PV panels [%]	55.36	53.08
<i>DENSITY MEASURES</i>		
urban built density [m ³ /m ²]	7.76	1.62
ground coverage index [m ² /m ²]	0.42	0.23
Total irradiance per year [MWh/year]	19015	37809
gross irradiance density on the urban land [MWh/m ² /year]	0.45	0.25
net irradiance density computed on roofs [MWh/m ² /year]	0.92	0.97
mean irradiance density per person [MWh/person/year]	8.60	23.19

Table 7.2. Morphological indicators computed on the two case-study areas.

7.4.6.4 Conclusions

In this case-study, a complete process going from the extraction of LiDAR data to the analysis of solar admittance of 2.5-DUSM of roof lines without vegetation is presented, followed by the description of the segmentation procedure on LiDAR data that allows to calculate slope and orientation of roof planes, and a comparison between two case-study areas presenting different building typologies. The goal was to analyse one sub-stake defined as priority by the end-users of the State of Geneva and studied in this chapter: “exploration of the solar irradiation on building roofs”.

As a general conclusion, it should be outlined that this study does not intend by any means to promote low density as an urban model. According to the literature and trends in sustainable urban design practice (Burchell *et al.*, 2005; Jenks *et al.*, 1996, 2000; Urban Task Force, 1999), the compact city model is rather preferable since it permits synergies and green policies that require minimum population densities. However, in the case that the performance of different urban textures, in terms of solar admittances, must be analyzed, the actual city model does not optimize its performance. For the same urban density, a better design should take into account the orientation of roofs and facades, as well as the slopes of pitched roofs and mutual obstructions between buildings.

7.4.7 Case-study: analysis of solar irradiation over building facades

7.4.7.1 Presentation

The aim of the proposed application is firstly to determine the rate of accessibility of urban surfaces to direct solar radiation and secondly to exactly quantify the solar irradiance (direct and diffuse) on building facades. The outputs of the tool are irradiation values that are stored in a table containing radiations computed for every storey and also for every facade of each building. Finally, beside this quantitative content, visualizations of results on the physical map are provided.

The area selected for the analysis is a square 300 metres wide near the Rhone River and the old town of Geneva, in Switzerland, already shown and applied on the case-study presented in section 7.4.6. In this case-study, the isotropic model was used to calculate the results presented.

7.4.7.2 Synoptic view of the process

The process of structuring the proposed methodology is based on five major steps as represented in the synoptic view of Figure 7.31: (1) the classification of LiDAR data used, (2) the creation of the 2.5-DUSM of building outlines without vegetation (3) the creation of layers used, (4) the solar irradiation and morphological analysis on building facades through the image processing of urban models, (5) the visualization of results.

7.4 Case-studies

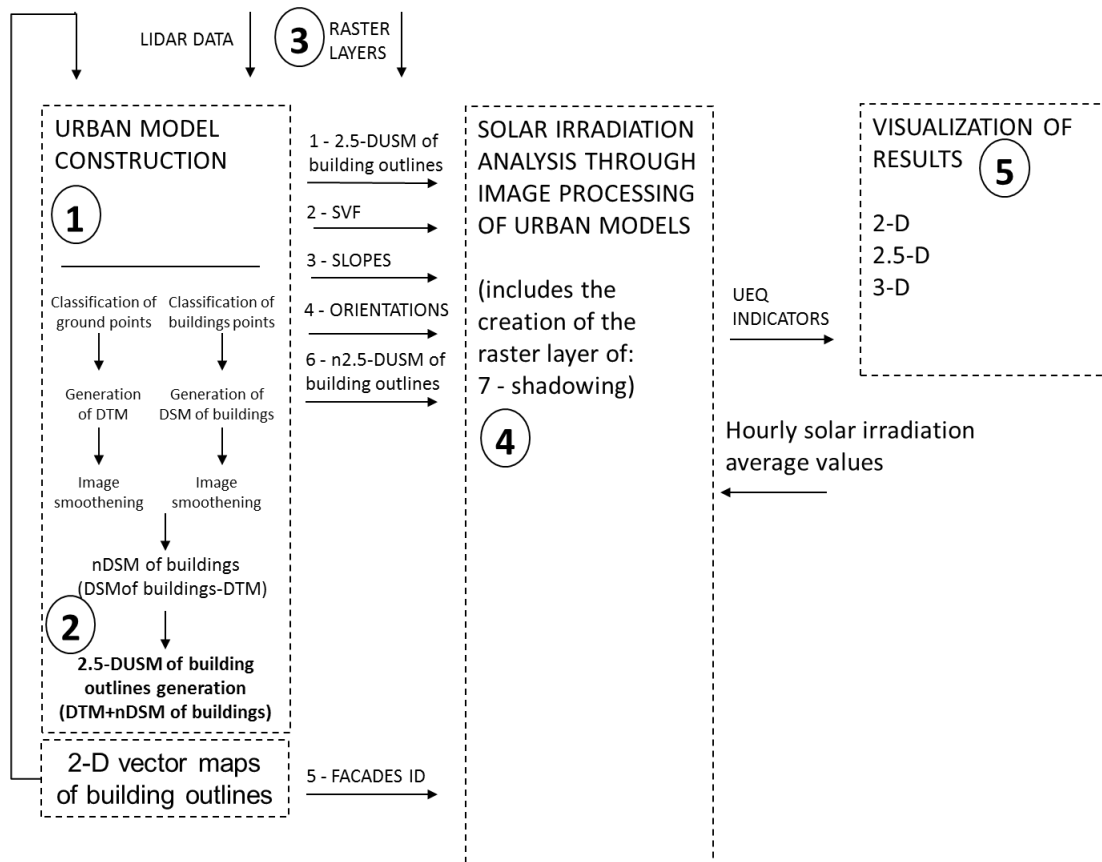


Figure 7.31. Synoptic view summarizing the process used to calculate the solar irradiation on building facades.

It is also worth mentioning that the layer corresponding to the normalized 2.5-DUSM of building outlines containing the absolute height of each building is rather useful in the process of slicing the 2.5-DUSM in several storeys, which is done from the ground to the top of the facade of each building. A new layer including labels of building facades is also produced which allows to both determine the exact identification of each building's facade and to produce shadowing and SVF maps for each storey of the building facades under analysis.

7.4.7.3 Calculation of solar irradiation on building facades

A set of possible radiations is stored in dedicated arrays that will be useful later when applied to the physical context. In particular, the typical array is a 3-D matrix (24x12x9) where the columns represent the 12 months of the year, the rows are 24 hourly intervals and the 9 z-layers are the computed values for 8 different orientations: S, SE, E, NE, N, NW, W, SW (Ratti and Richens, 2004). This typical array is computed for vertical surfaces at intervals of 15 degrees between 0 and 90.

Once the irradiance arrays are calculated and the input images are defined, the core of the computation can run. The shadow casting routine first introduced by Ratti (2002) is applied at a specific hour of the day and is used in order to detect which pixels on the facades are in shadow and which collect direct sunlight. The script computes the shadow casting routine slicing the urban model at every storey (3 metres is assumed to be the average storey height) of each building. Since the technique uses 2.5-D models, slicing each building at different heights is

necessary in order to compute the real irradiance condition in the vertical direction. In other words, the proper and reciprocal overshadowing of buildings can affect only part of the facade since this method allows distinguishing at which height vertical aligned pixels on the facade start to be irradiated (Figure 7.32 and Figure 7.33); otherwise, with simple shadow casting routine applied to the entire model, facades that were shaded at the basement would appear totally shaded until the roof. An example of visualization of this method applied for the calculation of shadowing over facades of a single building belonging to this case-study area is shown in Figure 7.34. The method for calculating SVF of each building facade is similar to the one presented in Figure 7.33.

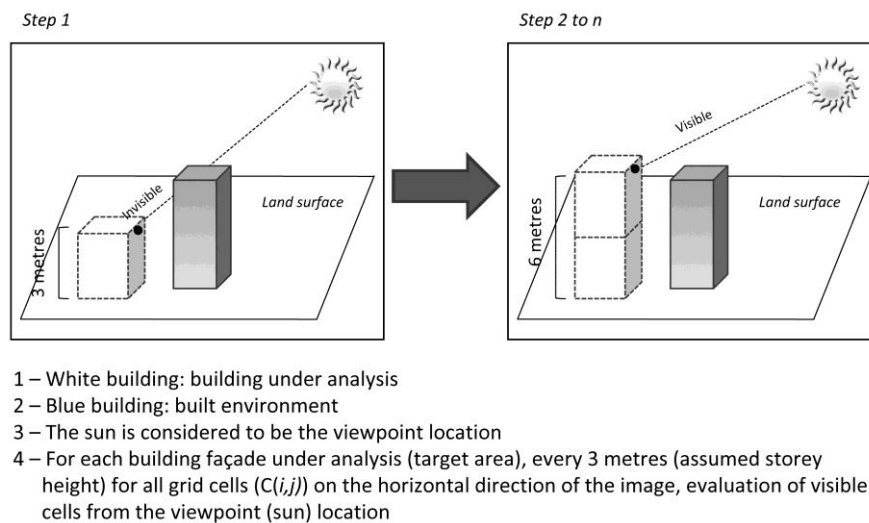


Figure 7.32. General overview of the method used (using a 2.5-DUSM) for the calculation of the solar irradiation along each building facade at a specific date of the year. Slicing the model at different heights allows taking into consideration pixels in shadow or in light.

7.4 Case-studies

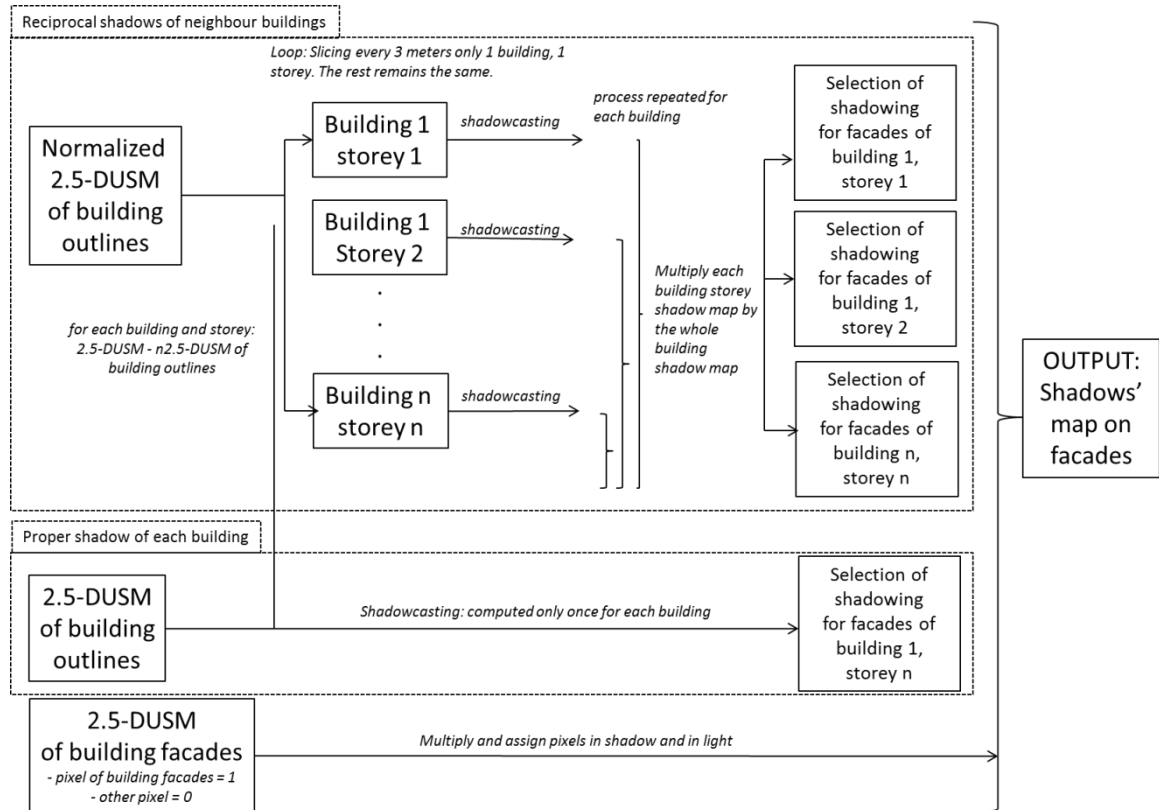


Figure 7.33. Dataflow summarizing the method used for shadowing analysis over building facades, considering different storey and proper and reciprocal overshadowing of buildings.

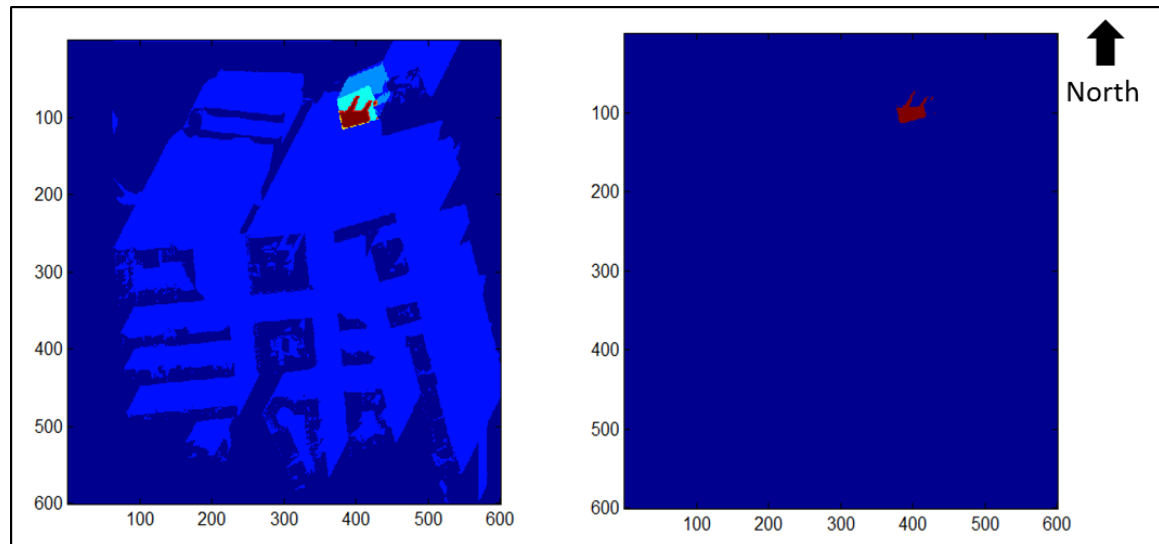


Figure 7.34. Calculation of shadowing for each building storey (in this example, the 2nd storey is considered) under analysis: left hand-side image: raster image that superimposes reciprocal (in red, calculated for each building storey) and proper (in blue, calculated only once for all building storeys) shadows of the building under analysis; right hand-side image: reciprocal shadow (in red, calculated for each building storey).

Moreover, it is mandatory to define the linear length of pixels on the perimeter of buildings: depending on their inclination, pixels can assume values between $1 \times u$ and $\sqrt{2} \times u$, where u corresponds to the pixel resolution. This can be easily calculated by applying the filter presented in section 6.3.4.

Hence, in the case where it is possible to determine for every facade at every storey whether each perimetral pixel is under shadow or light and what is its orientation and linear extension, the incident solar irradiance, calculated in Watt per square metre, can be assigned. The case-study presented is simplified because SVF is not considered.

Finally, irradiance values need to be stored in a convenient way depending on the results considered pertinent. Therefore, results are stored listing all pixels by facade identification and by orientation.

7.4.7.4 Extraction of indicators and analysis of results

Two examples of the representations of maps indicating the performance of facades on a 2-D-plot are displayed in Figure 7.35 and Figure 7.36: the first example accounts for the total irradiance (expressed in Watt per square metre) falling on vertical surfaces with increasing heights of buildings; the second example plots the percentage of facades subjected to direct solar radiation with increasing heights of buildings.

These synthetic maps provide an omni-comprehensive understanding of the irradiation conditions on the entire site. Results shown in Figure 7.37 display a 3-D visualization of the average irradiance (expressed in Watt per square metre) falling on each building. Irradiance values collected on the facades of each building were divided by the total area of vertical surfaces, whereby facades that do not receive irradiation at all were discarded (mostly separation walls between two buildings). Results present a significant uniformity due to the operation of averaging of the irradiation values on all facades, regardless of being lit or shaded.

7.4 Case-studies

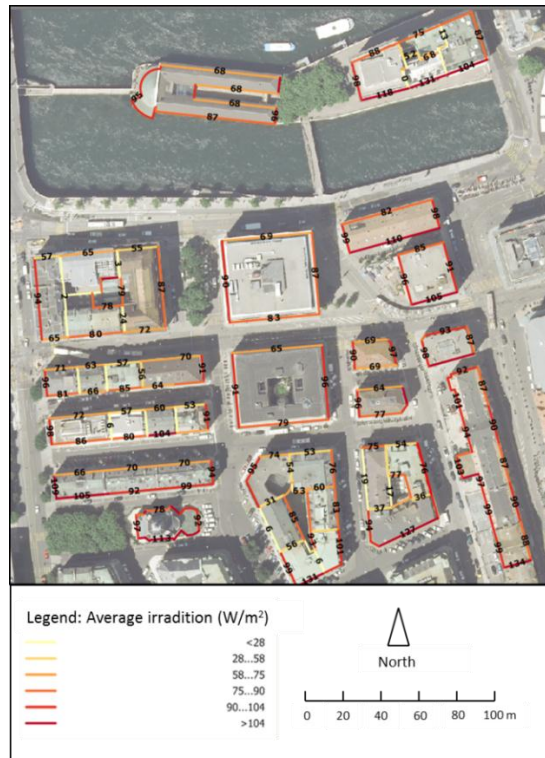


Figure 7.35. The mean solar irradiance collected by each facade on the second storey on December 10 at 12 PM, considering both beam and diffuse contributions.

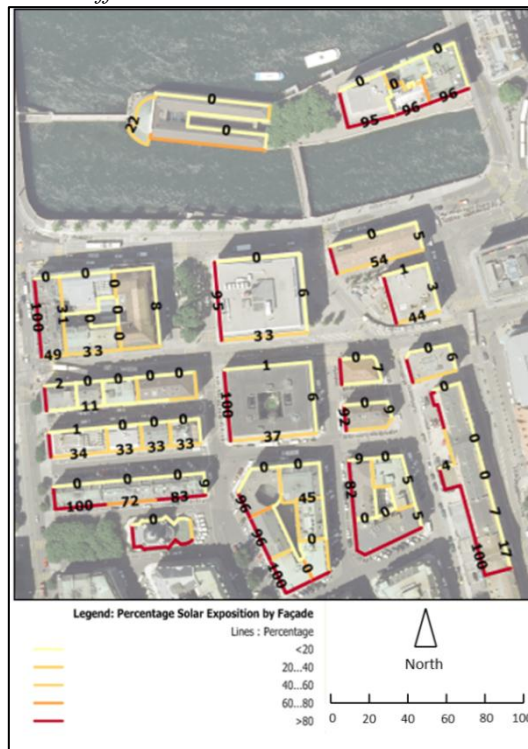


Figure 7.36. On each facade on the second storey, the percentage of surface touched by direct solar radiation on December 10 at 12 PM is displayed.

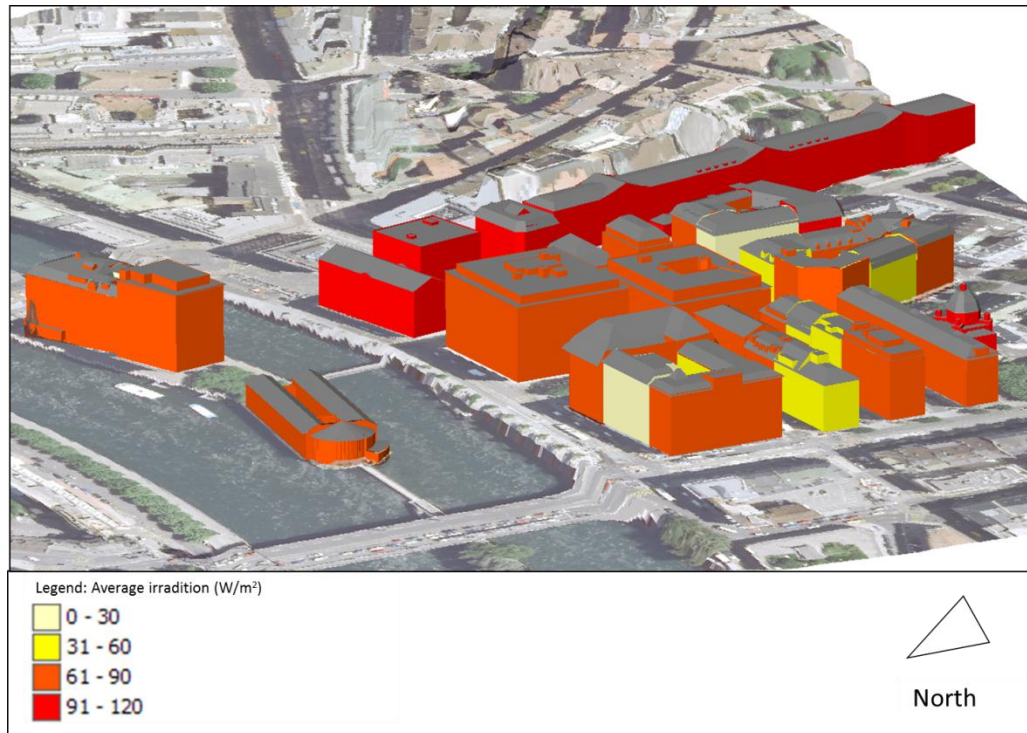


Figure 7.37. 3-D visualization of average irradiance values per building (expressed in W/m²) on December 10 at 12 AM.

A general overview of the energetic performance of vertical surfaces in an urban site is rather useful in case different fabrics need to be compared, or if an assessment of the impact of new buildings inside the city needs to be evaluated.

It can be observed that the absolute irradiance values slightly decrease with height (image above on Figure 7.38) and such is mostly caused by the parallel decrement of the amount of vertical surfaces towards upper storeys. Also, if results are normalized with respect to the areas of related vertical surfaces, the average irradiation per square metre clearly increases with height (middle image of Figure 7.38). This phenomenon partly occurs with the analysis of direct solar irradiation, whereas for the upper storeys the percentage of surfaces under direct radiation increases due to the lower reciprocal overshadowing by buildings (image below on Figure 7.38). Moreover, polar plots of solar irradiance on vertical surfaces computed for this case-study area underline the contributions of beam and diffuse irradiance on the site, as shown in Figure 7.39.

7.4 Case-studies

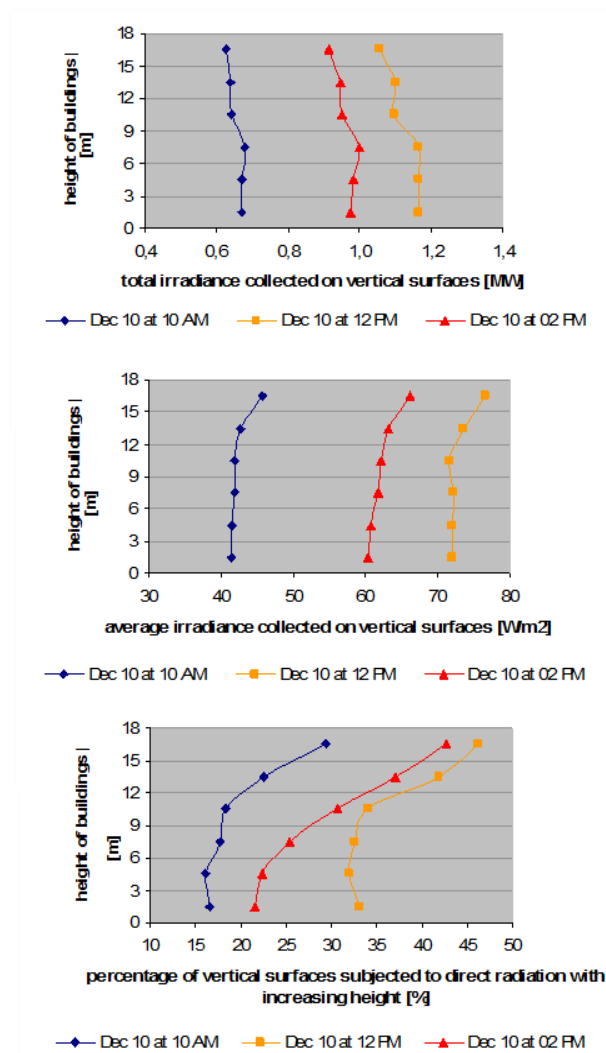


Figure 7.38. Total irradiance falling on vertical surfaces for the case-study area on the average day of December at 10 AM, 12 PM and 2 PM with increasing heights of buildings; from the top: (a) absolute irradiances in MW; (b) mean irradiances in W/m²; (c) percentages of vertical surfaces subjected to direct radiation.

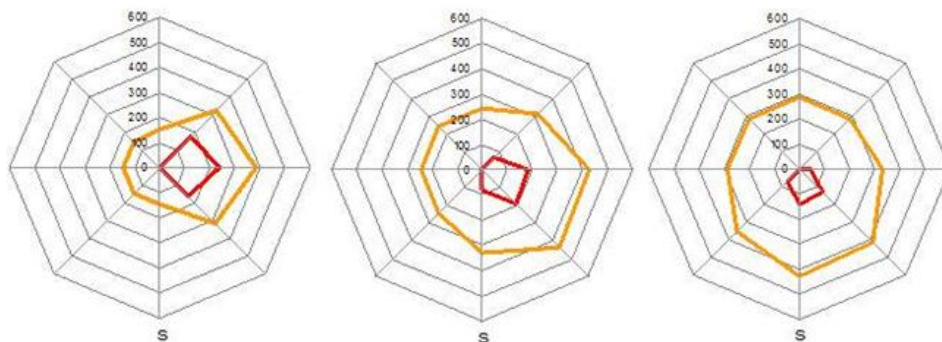


Figure 7.39. Polar plots of solar irradiances on vertical surfaces for Geneva on the average day of June; in red beam radiation, in orange diffuse radiation (values are expressed in W/m²). From left: irradiances at (a) 8 AM, (b) 10 AM, (c) 12 PM.

7.4.7.5 Conclusions

In this case-study, a complete methodology going from the extraction of LiDAR data to the analysis of solar admittance on building facades (using the 2.5-DUSM of building outlines without vegetation) is presented, followed by the visualization of results. The goal was to analyse one sub-stake defined as priority by the end-users of the State of Geneva and studied in this chapter: “exploration of the solar irradiation on building facades”.

It is worth mentioning that a large fraction of the solar irradiation collected by vertical urban surfaces corresponds to diffuse irradiance since the sky is not always clear. In terms of energy performance, increasing the direct solar contribution on vertical surfaces does present a subsequent improvement of energy collection. Indeed, more compact urban spaces can build and delegate roofs in order to collect beam radiation for the production of electric energy and/or hot water. Nevertheless, in terms of environmental quality in general, assuring a minimum amount of direct solar radiation on each building is recommended for perceived comfort inside buildings. Still, if the aim is to provide sufficient light for living conditions inside indoor spaces, the constant diffuse radiation is in most cases satisfactory. Concerning this specific case study-area as well as the irradiations at such latitude, the layout of buildings already guarantees good solar radiation.

7.4.8 Case-study: potential for active solar technology

7.4.8.1 Presentation

The aim of this work is to establish a conceptual method to calculate hourly input of irradiation on building roofs so as to estimate the potential of buildings for the production of energy from the sun through solar collectors (PV and thermal). Once again, the proposed process investigates the use of 2.5-DUSM integrating cross-disciplinary competences, like remote sensing, GIS, image processing and urban and environmental studies. In this case-study, the anisotropic model of Hay was used in order to calculate the results presented.

This method is applied, on purpose, to 31 buildings belonging to an urban area located in the CERN campus, Switzerland (shadowed white zone of Figure 7.40). As already mentioned in section 6.3.3, this organization demonstrated a strong interest on this research project because they are currently implementing an urban master plan. Thus, all applications related to environmental and energetic studies were considered a very valuable input. For this reason this pilot-zone was considered for this case-study analysis.

7.4 Case-studies

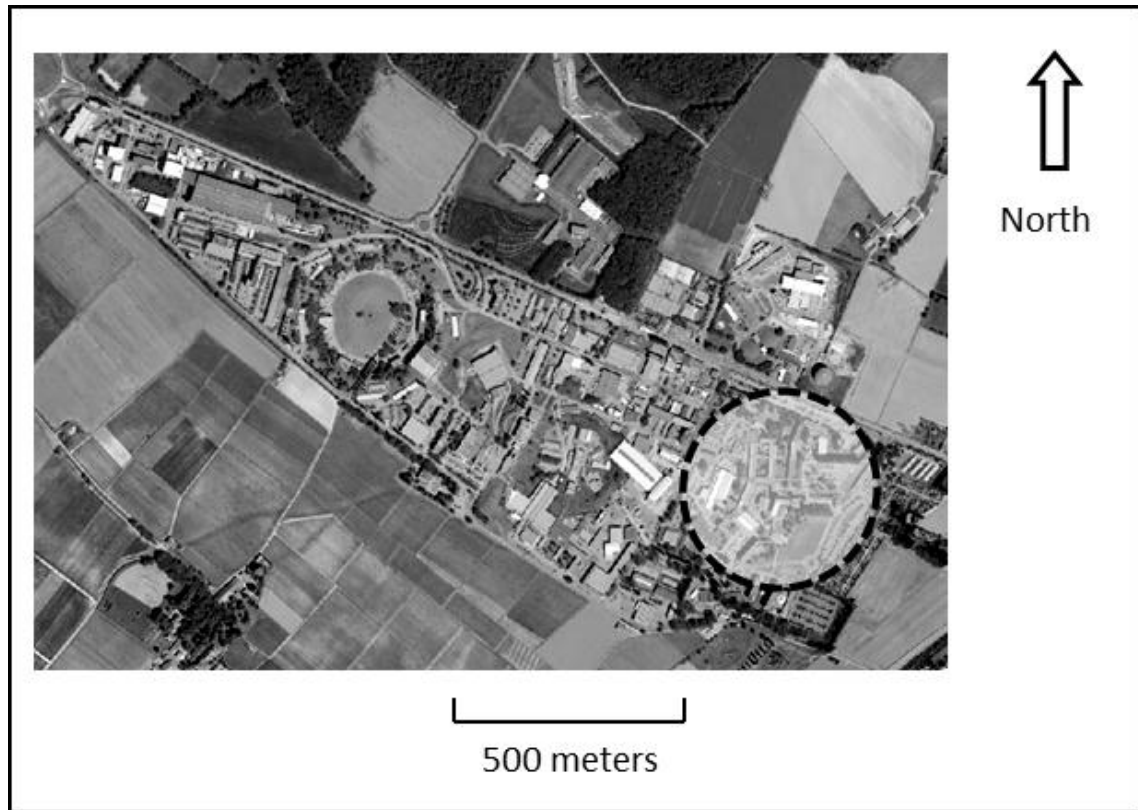


Figure 7.40. Case-study area of CERN (inside the white dashed circle).

7.4.8.2 Synoptic view of the process

The process for structuring the proposed methodology is based on five steps (Figure 7.41): (1) the classification of LiDAR data used, (2) the creation of the 2.5-DUSM of roof lines with vegetation, (3) the creation of layers used, (4) the calculation of outputs (solar irradiation on building roofs and potential for electrical and thermal energy) through the image processing of urban models, which includes the selection of roof section surface areas taking into account slope derived from morphological analysis (5) the visualizations of results by transferring and aggregating output raster data (calculated in point 4) by building.

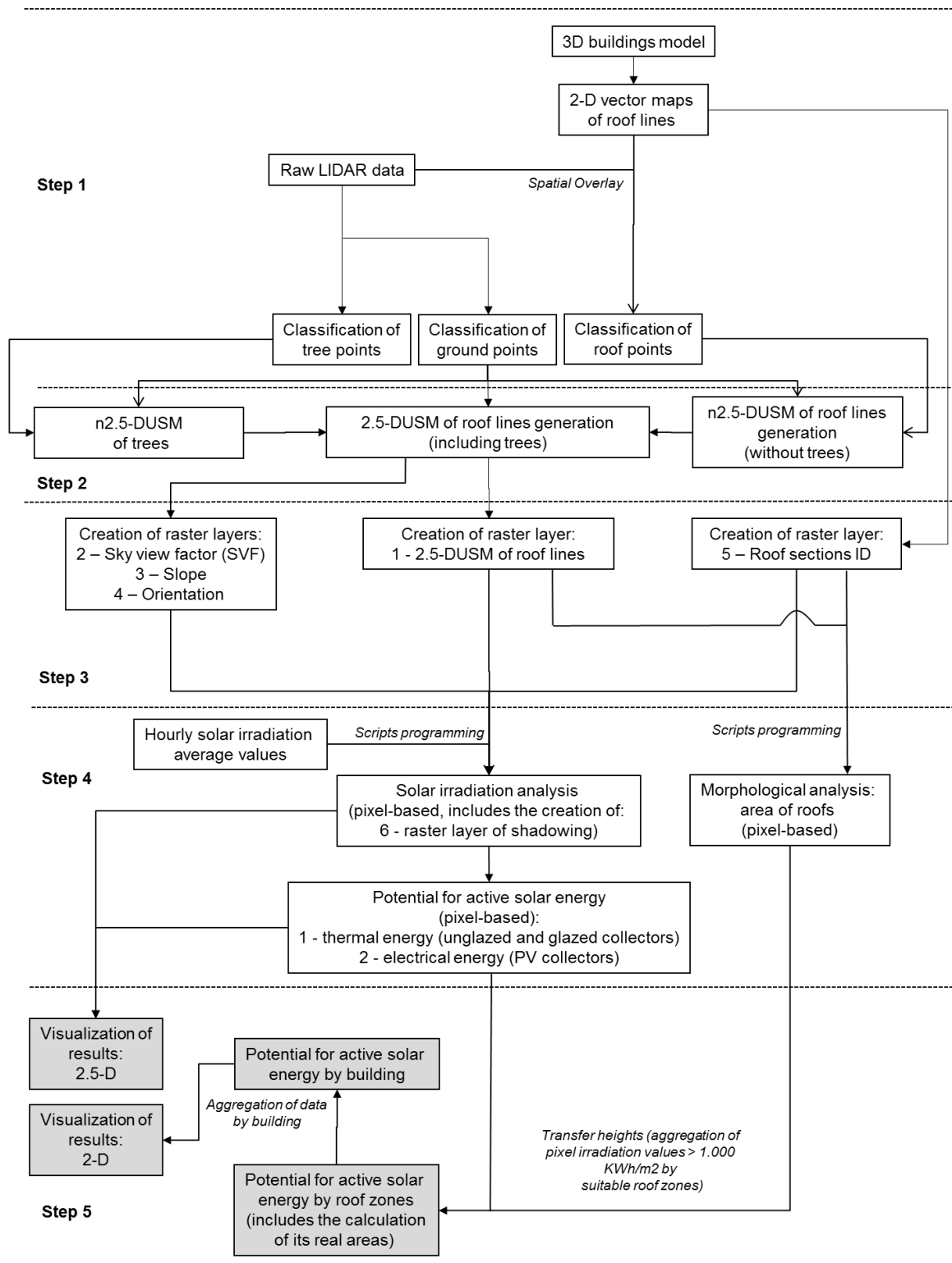


Figure 7.41. Synoptic view summarizing the process used to assess each building's solar potential for active technology.

7.4 Case-studies

As already mentioned in section 7.4.6, for PV technology, roof surface areas must at least be equal to 20m² to meet the requirement of minimum installed power capacity (2kW) for cost-effectiveness. For thermal technology, the minimum area depends on the users requirements. But, in general, it is conceivable to consider that below an area of 4 m² any installation would be unrealistic. The calculation of inclined roof surface area should consider slope (classic trigonometric formulae); slope is obtained by transferring heights information from LiDAR to each section. For flat roofs, additional slope is provided to panels to increase their efficiency, which results in decreasing the part of the roof area being used.

The technique used is based on the image processing of the 2.5-DUSM of roof lines with vegetation that is interpreted as raster images. These images result from the transformation of all the information attributes needed for the irradiation calculation into layers: height values, slope, orientation, roofs with area >20m² (PV) or 4m² (thermal), roof labels. As already highlighted in previous case-studies of this chapter, after determining for every pixel its shadowing condition, its SVF, its orientation, and its inclination, it is possible to assign the global incident solar irradiation calculated in W or J /m² for various times scales (hour, aggregation to month, year). From the irradiation value it is then possible to calculate the electrical and thermal energy production for pixels having a yearly irradiation value higher than 1000 KWh/m².

The electrical energy produced [kWh] is obtained by multiplying the global irradiation incident on a given roof section by the installed power of a given PV panel and a performance ratio. If an installed power of 120 [kWp/kW/m²] is basically considered, which corresponds to an average value among the common technologies of poly-crystalline and mono-crystalline and a PR of 75%, an electrical production equivalent to 9% of the global irradiation is obtained.

For the calculation of thermal production for heating and domestic hot water (DHW) the formulae used in the software EnerCAD were implemented in the scripts programmed. The formulae result from a simulation model that computes the energy production of typical (flat-plate) collectors from meteorological data (Lachal, 2000). The model is based on daily Input/Output functions. The formulae differ depending on the type of use (heating or DHW) and the type of collector (glazed or unglazed). For the heating production, the main parameters in addition of the irradiation are: the supply temperature, inside/outside temperature, and the surface area of the panels to be installed. The calculation of energy production for DHW depends on the number of users and total heated area of the building (available in GIS databases), on building energy requirement and surface area/resident available in common norms. For this case-study analysis, the calculation is only made for the hours when average outside temperature of the city of Geneva is below 16°C (heating cut off).

7.4.8.3 Extraction of indicators and analysis of results

The analysis aims to reveal the potential to solar admittance on the case-study area. Figure 7.42 shows an example of possible outputs (2.5-D visualization) for the case-study area of CERN under analysis: the left-hand side image shows the yearly solar irradiation collected on roofs [KWh/m²]; the right hand-side image shows the yearly solar irradiation collected if all pixels belonging to roofs are considered to be unglazed surfaces [KWh/m²].

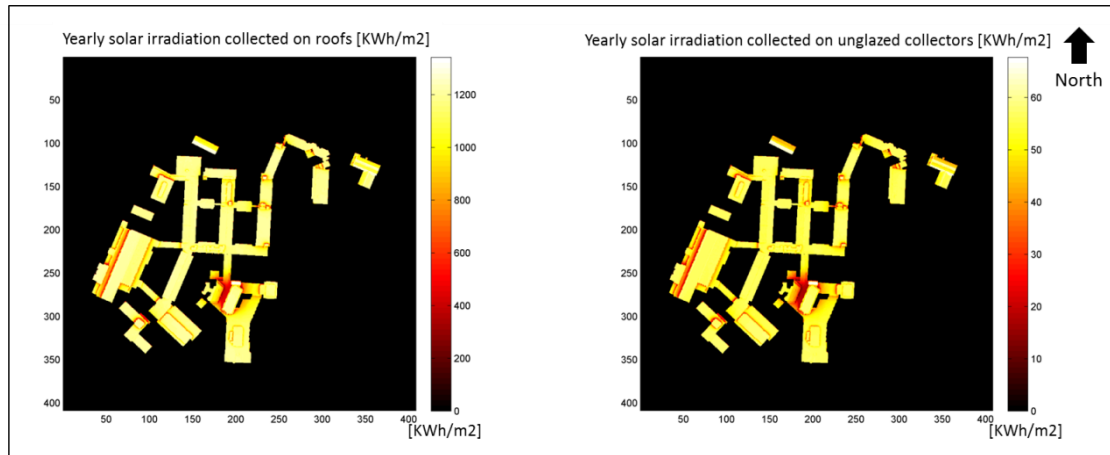


Figure 7.42. Example of possible outputs (2.5-D visualization) for the case-study area of CERN: left-hand side image: the yearly solar irradiation collected on roofs [KWh/m2]; right hand-side image: the yearly solar irradiation collected on unglazed surfaces [KWh/m2].

Moreover, the potential end-user would be interested in assessing which buildings would be suitable or not for solar panels installation. Grid pixel representation is not really appropriate for this purpose. Therefore, it is important to mention that from the global irradiation and on the pieces of building roofs where irradiation is sufficient (defined as $> 1.000 \text{ kWh/m}^2 \text{ yr}$) and the real area (using morphological analysis, as presented in chapter 6) is significant ($>$ for 4 m^2 for thermal technology and $> 20 \text{ m}^2$ for PV technology), it is possible to calculate electrical and thermal energy production from sun collectors. An example of the percentage of the solar potential of roofs (for the installation of PV technology) of the case-study area of CERN respecting these rules is shown in Figure 7.43.



Figure 7.43. Example of solar potential of roofs (for the installation of PV technology) for the case-study area of CERN.

7.4 Case-studies

For this case-study area of CERN most of the buildings present an excellent potential for the installation of solar panels: (1) most of the buildings present similar heights, which decreases the overshadowing between different buildings; (2) vegetation is not dense and the height of existing trees is lower than the height of most of the buildings. For instance, considering the specific case of electrical energy, where building roof sections used for the installation of PV collectors must have a minimum surface of 20m^2 and the yearly irradiation belonging to these areas has to be higher than 1.000 KWh/m^2 , in average 86% of the areas of building roofs can be selected for this purpose.

From the raster outputs produced with this procedure (for instance, as shown in the right-hand side image of Figure 7.42 for the specific case of unglazed collectors), pixel values are calculated and aggregated on each roof section. Finally, all values of roof sections belonging to a same building are aggregated. This procedure allows to highlight in a synthetic 2-D visualization the potential for installing solar collectors (unglazed, glazed and PV) on each building (Figure 7.44 to Figure 7.46).

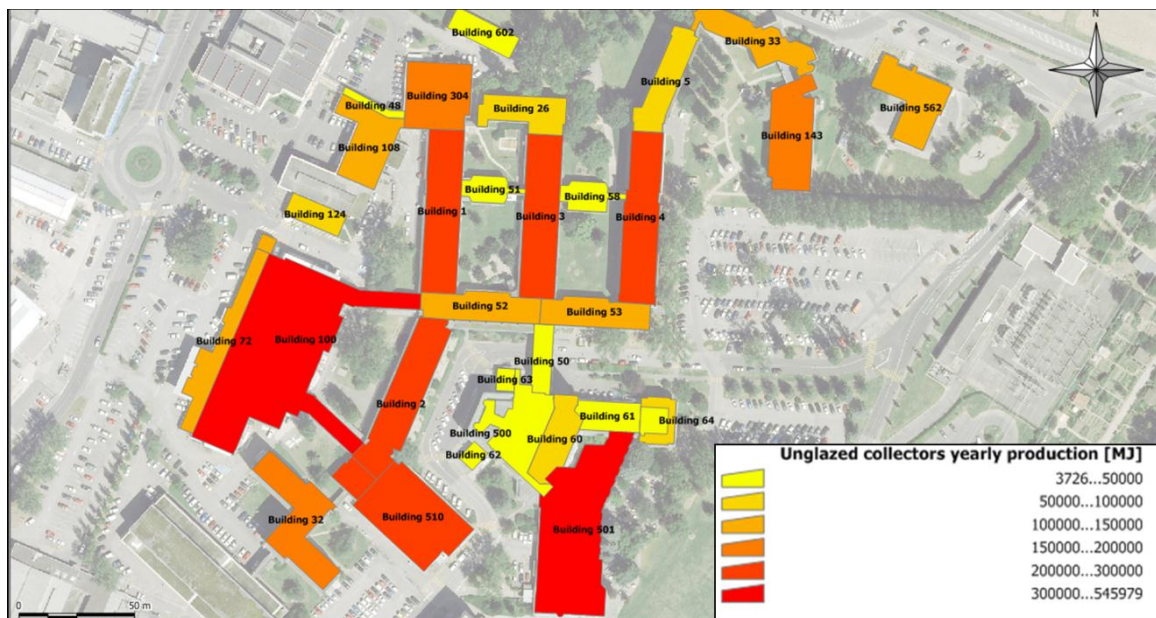


Figure 7.44. 2-D visualization of the yearly energy production [MJ] for heating with thermal unglazed collectors for the case-study area of CERN.



Figure 7.45. 2-D visualization of the yearly energy production [MJ] for heating with thermal glazed collectors for the case-study area of CERN.



Figure 7.46. 2-D visualization of the yearly energy production [MJ] for lighting with electric PV collectors for the case-study area of CERN.

Finally, for this case-study area of CERN, glazed collectors present a yearly production in average 1.426 better than unglazed collectors.

7.4.8.4 Conclusions

In this case-study, a complete methodology going from the extraction of LiDAR data to the analysis of buildings for active solar energy (using the 2.5-DUSM of roof lines considering

7.5 Conclusions and chapter synthesis

vegetation) is presented and followed by the visualization of results. The goal was to analyse one sub-stake defined as priority by the end-users of the State of Geneva and studied in this chapter: “potential for active solar technology”.

Such database of potential of buildings for active solar energy could be useful for various actors and purposes. In terms of energy urban planning, a municipality or energy company could be interested in identifying which buildings are suitable for installing centralized or decentralized PV modules, allowing for program interventions and specific incentives with regards to the real potential energy production strategies of the urban fabric. Similarly, state-owned companies or building owners would certainly be interested in knowing which of their buildings would be suitable to be equipped and what would be their value according to their energetic potentials.

7.5 Conclusions and chapter synthesis

Considering the analysis of the requirements made by the end-users of the State of Geneva, this chapter presents five case-studies that illustrate innovative methods for the extraction of urban environmental quality (UEQ) indicators related to the stake “exploration of the solar potential on the urban fabric”, more specifically five sub-stakes considered as being priority: (1) “exploration of the solar irradiation on building roofs”, (2) “estimation of the coverage and impact of vegetation on roofs”, (3) “estimation of the influence of shadowing and SVF on the urban texture”, (4) “exploration of the solar irradiation on building facades”, and (5) “potential for active solar technology”.

The processes implemented are based on the use of different 2-D and 3-D data sources (mainly LiDAR) and 3-D urban models: 2.5-DUSM and a segmentation procedure on LiDAR data that allows to calculate the slope and orientation of roof planes. Combining different interfaces and datasets reveals constraints of today’s applicability of LiDAR data for the environmental prediction of the urban form. Hence, a first result is to bring 3-D geography and urban studies together in a process that goes from data acquisition and processing to urban planning and urban design application.

The output indicators and results highlighted in this chapter were validated by the group of end-users of the State of Geneva according to the requirements initially defined. Moreover, the integration of the morphological analysis (for instance, calculating the real area instead of the projected area of roofs) in order to refine the results presented was considered a relevant added-value for the methods proposed.

In comparison to other types of software this method uses LiDAR data as input, which is easily available and gradually becoming cheaper. This type of data provides very rich information, is fast to process with the methodology presented, and is easily exported to other tools (e.g. RADIANCE) for accurate calculation of solar admittance at building scale (Compagnon, 2004; Montavon, 2010).

The case-studies proposed and designed in this chapter are limited to the physical built environment, however they could be extended to the research and assessment of the impact of new buildings in the city or refurbished buildings. This technique could also be used to improve design schemes based on an evaluation of quantitative indicators before and after changes are introduced. In the case of a refurbishment of a block of buildings or an entire district, this tool could help to evaluate whether solar technology (in particular thermal) is a good alternative of renewable energy supply with regards to the user requirements.

CHAPTER 8. ESTIMATION OF THE ENERGY DEMAND ON THE URBAN FABRIC¹

¹ The main concepts of this chapter will be published in:

Gori, V., Balocco, C., Carneiro, C., Desthieux, G., Morello, E. (2011) The evaluation of solar energy potential and energy needs for heating and lighting using LiDAR data. *Proceedings of the 27th International Conference on Passive and Low Energy Architecture (PLEA)*, 13th-15th July, Louvain-la-Neuve, Belgium. (accepted, to publish).

8.1 Introduction

As highlighted in the end-user requirement analysis (section 4.2.6), this third and last chapter related to the empirical studies undertaken in this research emphasizes on the extraction of a group of complex indicators for heating and lighting analysis belonging to the stake “estimation of the energy demand on the urban fabric”. These indicators are extracted under the case-study “evaluation of solar energy potential and energy needs for heating and lighting using 2.5-DUSM constructed from LiDAR data”, further emphasized in this chapter - the proposed method was developed and implemented in collaboration with the Energy Department “S. Stecco” of the University of Florence (Gori, 2010).

The general apprehension over climate alterations has significantly increased in the last decades, and, therefore the studies related to energy conservation became extremely relevant and to a certain degree a priority for the future of humanity. Nowadays, it is commonly accepted that the combustion of fossil fuels and the subsequent emission of greenhouse gases into the atmosphere is changing long well-known climate patterns. As noted by the American Physical Society, adopted by its council on November 18th, 2007, *“emissions of greenhouse gases from human activities are changing the atmosphere in ways that affect the Earth's climate. Greenhouse gases include carbon dioxide as well as methane, nitrous oxide and other gases. They are emitted from fossil fuel combustion and a range of industrial and agricultural processes. The evidence is incontrovertible: global warming is occurring. If no mitigating actions are taken, significant disruptions in the Earth's physical and ecological systems, social systems, security and human health are likely to occur. We must reduce emissions of greenhouse gases beginning now.”*

The entire world's economic community is under pressure to reduce energy demands. According to statistics of 2010 of the U.S. Energy Information and Administration, the building sector - comprising residential and commercial consumers - accounts for approximately one-fifth of the world's total delivered energy consumption. The latter stresses that an improvement on the energy performance of buildings and the simulation of their behaviour is highly needed. Several energy models and techniques have been developed for this purpose in recent years – a description of some of these simulation tools can be found in the website of the U.S. Department of Energy¹⁵. However, these models usually adopt the perspective of the building designer considering buildings as self-defined entities, thus neglecting the importance of phenomena that occur at the urban scale (Ratti *et al.*, 2005).

Hence, the assessment of the energy demand on the urban fabric is an essential parameter that deserves further study. Following the method highlighted in this thesis, a tool based on the use of different 2.5-DUSM constructed from LiDAR data is presented. Moreover, this chapter shows the integration of different types of morphological and solar irradiation indicators emphasized and calculated in chapters 6 and 7 respectively. This procedure allows the construction of different energy scenarios in order to develop a more integrated and sustainable vision of the city (Figure 8.1).

15

http://apps1.eere.energy.gov/buildings/tools_directory/subjects.cfm/pagename=subjects/pagename_menu=whole_building_analysis/pagename_submenu=load_calculation

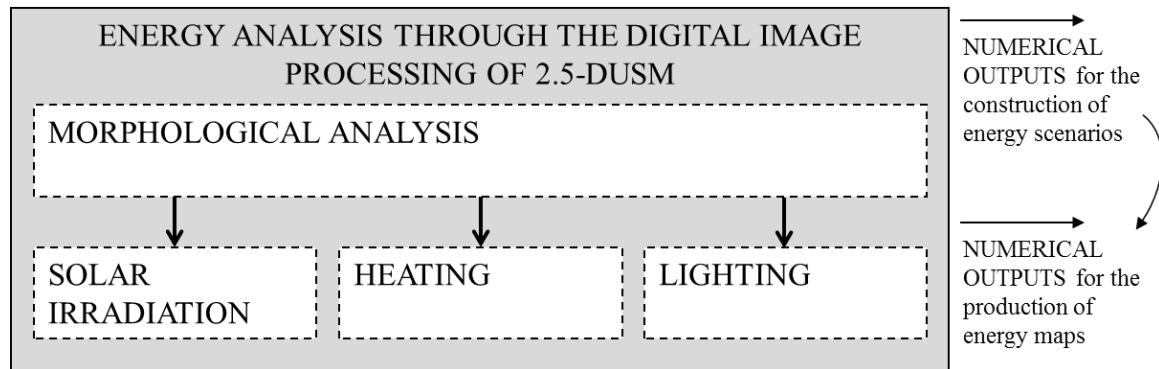


Figure 8.1. The construction of energy scenarios through the digital image processing of 2.5-DUSM and the use of different input indicators.

The following sections introduce information about:

- 8.2) – background and related work;
- 8.3) - case-study: evaluation of solar energy potential and energy needs for heating and lighting using 2.5-DUSM constructed from LiDAR data;
- 8.4) - conclusions and chapter synthesis.

8.2 Background and related work

Currently numerous tools for the assessment of the energy demand, based on time consuming and dynamic calculations, are implemented at the building scale. In fact, most of the times, for territory planners, urban designers and decision-makers, this level of detail is superfluous if neighbourhood and city scales must be considered for analysis (Batty *et al.*, 1999). Thus, in order to present an overview of the energy consumptions considering these scales of analysis, a simplified and innovative tool is lacking and expected – an example is highlighted in this chapter. The method proposed is based on the integration of several and different sectors and competences that include urban design and building morphology, energetic of urban systems, programming, and image processing techniques.

According to Baker and Steemers (2000), despite the evident relationship between urban geometry - which can include the calculation of the morphological properties of a building or a set of buildings belonging to a whole city or a neighbourhood - and energy consumption, this link is generally neglected, resulting in deficient study and debate.

Using the innovative morphological analysis of buildings proposed in chapter 6, this chapter focuses on the integration of urban geometry, which includes shadowing conditions and leaning effect, into a tool that is capable of estimating heating and lighting demands at the district level. Moreover it computes the potential energy supply through solar and PV panels. The aim of this study is to provide useful guidelines to end-users, mainly territory planners, urban designers and decision-makers, in order to both evaluate different energy scenarios and to promote integrated energy strategies to be tailored according to the specific urban form. An initial approach of integrating airborne laser scanning and GIS data at the city and neighbourhood scales for the calculation of the heat demand, based on the calculation of: (1) the volume of buildings, and (2) the specific heat coefficient of buildings, derived from a classification of different building typologies, was proposed by Neidhart and Sester (2006). In this case-study, also by focusing on urban geometry implications, a method that allows the calculation of energy needs is presented.

8.3 Case-study: evaluation of solar energy potential and energy needs for heating and lighting using 2.5-DUSM constructed from LiDAR data

In particular, heating demand is calculated according to the current European Regulations, whereas for lighting demand a simplified method based on the Daylight Autonomy concept is suggested. Finally, solar irradiation is computed for all building roofs and the potential of solar energy uses and applications is derived.

The goals of this study are:

- To provide useful information and guidelines to end-users, such as territory planners, urban designers and decision-makers, in order to promote integrated energy strategies to be tailored according to the specific urban form. In fact, depending on the availability and the arrangement of the urban surfaces, different solutions may be proposed. For example, incentives for the installation of PV panels on a very fine-grained basis, i.e. only where these are really effective;
- To set up an innovative tool that is capable of investigating energy problems at the scale of the neighbourhood and city rather than at the scale of the building. A new method that uses different data sources and different data bases for evaluating energy needs at the urban scale without complex or time consuming calculations is proposed;
- To provide a simple tool that considers a set of relevant variables at the urban scale: for instance, overshadowing by buildings and leaning effect (buildings touching each other's thus reducing thermal dispersant surfaces).

8.3 Case-study: evaluation of solar energy potential and energy needs for heating and lighting using 2.5-DUSM constructed from LiDAR data

8.3.1 Presentation

The rational use of energy resources is mandatory in order to reduce the environmental impact of human activities. Cities can be modelled as thermodynamic systems that must be organized by relating variable energy demand as to minimize entropy production. The aim of this case-study is to provide a tool that estimates the heating and lighting energy needs at the district level and simultaneously computes the potential energy supply through solar and PV panels, allowing the construction of different energy scenarios. Moreover, the estimation of different indicators related to the morphological analysis of buildings (part of the urban form of the city) is also integrated as a valid input into the method proposed.

This method is purposely applied to two different urban areas located in the centre of Florence, Italy (Figure 8.2) and part (31 buildings) of the Meyrin CERN campus, Switzerland, already described in section 7.4.8.1 (Figure 7.40). The two sites differ in terms of spatial arrangements and configurations of buildings, typologies and materials of construction. In addition, the climatic data of the two locations is rather relevant in terms of latitude, solar radiation, external air temperature and humidity, and wind velocity and direction. The case-study area of Florence was chosen due to the interest shown by its municipality on this project. For this specific case-study area it is worth mentioning that the original raw LiDAR data has a density of 1 point/m², which implies 2.5-DUSM with a sampling size of 1 meter (Behan, 2000). As already mentioned in section 6.3.3 the international organization CERN also demonstrated a strong interest on this research project because they are currently implementing an urban master plan. Thus, all applications related to environmental and energetic studies were considered a very valuable input. For this reason this pilot-zone was considered for this case-study analysis.

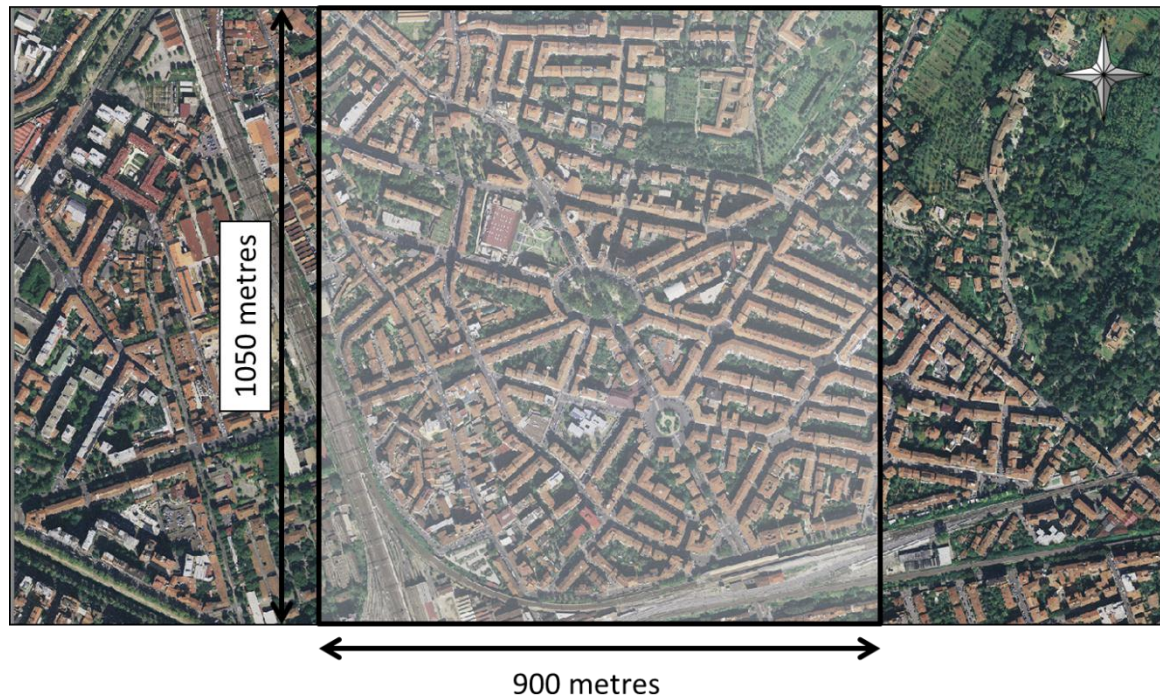


Figure 8.2. Case-study area of Florence.

8.3.2 Synoptic view of the process

The method is organized in a sequence of steps that cover different technical competences (Figure 8.3):

1. The selection of the geo-referenced input information used;
2. The production of different raster images used;
3. The energy analysis of built up-areas based on the use of DIP techniques implemented, considering different assumptions and environmental data;
4. The construction of energy scenarios using heating, lighting and solar energy outputs;
5. The 2-D, 2.5-D and 3-D visualization of results through maps.

8.3 Case-study: evaluation of solar energy potential and energy needs for heating and lighting using 2.5-DUSM constructed from LiDAR data

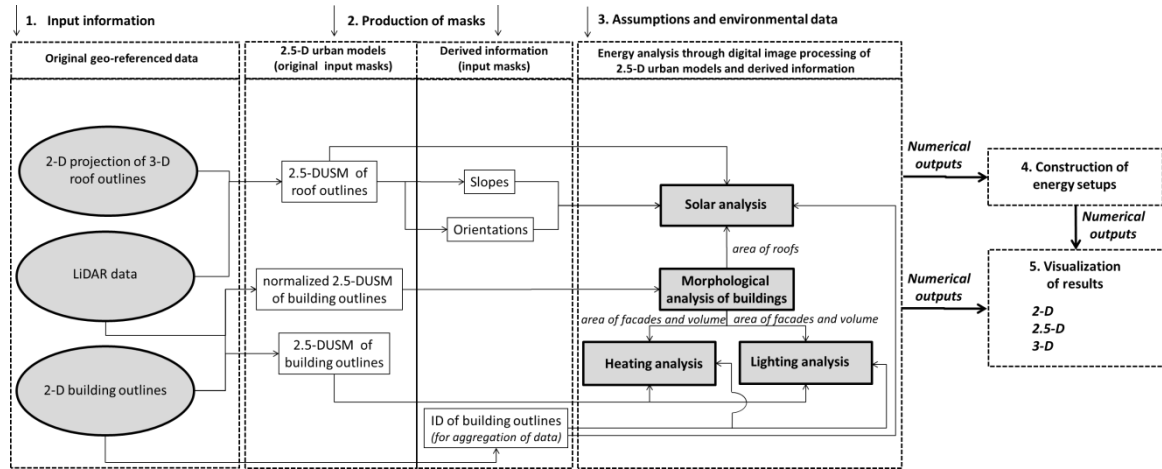


Figure 8.3. Synoptic view of the process.

8.3.3 Available information about buildings

In order to run the proposed simulations, important information about the buildings included in the two case study areas is inferred by two different databases. For the area of Florence a structured GIS database provides basic data on XIX century buildings. This database, originally compiled for the Municipality Environmental Energy Programming (“Piano Energetico Ambientale Comunale”: PEAC), included building energy need evaluations on GIS using spatial analysis techniques to connect descriptive data of different plant typologies to the relevant buildings. Such permitted to obtain the thermo-physical parameters of the buildings and hence, the thermal maps and energy savings scenarios for the whole urban area. A statistical method was used in order to evaluate the energy needs of the urban building system. The method utilizes a numerical map to extend to the universe the evaluation obtained from a probability stratified simple random sampling design with the optimum allocation of sample buildings to the strata. The strata considered refer to the age of construction of buildings. This statistical approach to the energy analysis of the urban system required the primary definition of the energy characteristics of the universe of buildings. Such was necessary in order to avoid a systematic error in both the calculation method of the sample size and the techniques used to select the elements of sample units. An equal probability selection method of stratification by age classes was used, referring to existing information and data, cartography and historical series maps. Disproportionate stratification utilization was due to the allocation of sufficient sample size to certain strata identified with the age classes of construction of buildings in order to identify estimates of sufficient precision. Under such conditions sample estimates are required not only for the total population but also for the various sub-populations which are termed as domains of study. The energy balance of a building provided variables that are connected to its thermo-physical parameter and therefore, its energy consumption was evaluated using a correlation between dimensionless numbers. Dimensional number correlation was extended to each building of the universe of buildings because the sample used has a statistical meaning. Using both spatial analysis techniques and GIS, the energy consumption maps of the population of buildings were obtained (Balocco *et al.*, 2008). CERN possesses a very rich GIS database providing information about the year of construction, type of wall, type of roof, function and number of storey for each building under analysis, and such, the latter were used as valid inputs for this case-study.

8.3.4 Energy analysis and scenarios

The energy analysis is presented in three parts: firstly, the estimation of energy needs for heating. Secondly, the artificial lighting and the electrical and thermal energy production from sun collectors. The third part, which is related to solar analysis assessment, was described in section 7.3.8. As shown in Figure 8.3, the inputs for this analysis are both the models and a series of layers obtained from LiDAR data and GIS datasets, energy assumptions for building types according to the building class of age and environmental data referred to the locations. In both case studies different classes of age were established according to the information stored in the two databases (for more details please consult appendix D). The outputs of the analysis are the visual maps and the numerical data to be used in order to provide energy scenarios, which can include the analysis of specific questions:

- Which goals must be achieved on the area of analysis?
- Which sustainability targets towards a more self-sufficient built environment?

Hence, using the outputs provided by the three parts of energy analysis leads to two main comparisons (Figure 8.4):

- artificial lighting versus electrical energy production from sun collectors (energy scenario 1);
- heating versus thermal energy production from sun collectors (energy scenario 2).

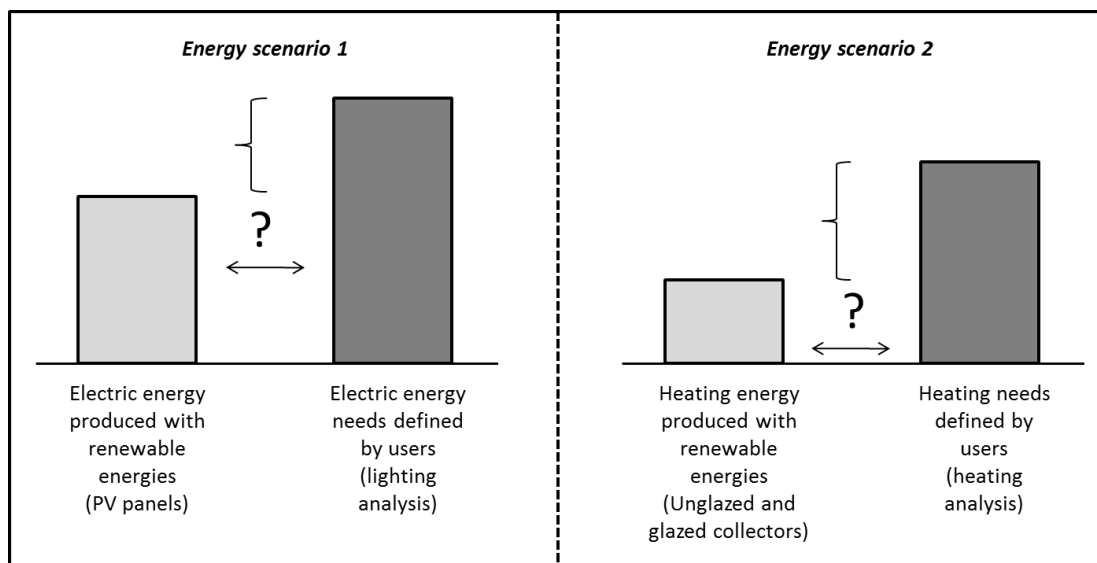


Figure 8.4. Energy scenarios using heating, lighting and solar energy outputs.

8.3.5 Heating needs evaluation

The model computes the monthly energy requirement building by building for the heating period, taking into account the effects of mutual shadowing by the urban fabric, represented by the 2.5-DUSM of building outlines, using the method (storey-by-storey analysis) proposed in section 7.4.7.3. The heating demand is obtained by implementing the current European Regulation for the calculation of energy use for space heating and cooling (UNI-EN ISO 13790:2008) and in particular its Italian version (UNI-TS 11300-1:2008). Results are stored in a data structure: building storey-by-storey organization of data. Indeed, buildings are sliced at 3 meters intervals in order to consider each building storey. This subdivision allows the assignment of different uses to spaces. In this study, only residential use is considered. The core function calculates thermal

8.3 Case-study: evaluation of solar energy potential and energy needs for heating and lighting using 2.5-DUSM constructed from LiDAR data

losses and gains through the building envelope of each thermal zone corresponding to each storey. This function is repeated for every slice of every building. The heating period is provided by climatic data of the location. Two different internal climatic conditions for the heating period are set in order to simulate the intermittent regime of the heater during the day. As suggested in CEN standards for indoor air quality (EN prENV 1752: 1996), the temperatures are set as follows: 20°C temperature and 50% relative humidity for the time span between 7 AM and 11 PM; 18.5°C and 50% relative humidity for the remaining hours. The input data from the two databases are the following: (1) thermal parameters of different materials according to the class of age of buildings (the transmittances of horizontal and vertical opaque and glazed surfaces, the transmittance of the ground floor, the conductivity of the ground, the solar transfer coefficient of the window glasses, the thermal capacity of the wall), and (2) some constructive characteristics of the buildings (glazing ratios, external wall thickness). For the case where accurate data is not available, the minimum values are set according to the standards. In particular, morphological building properties are provided by the normalized 2.5-DUSM of building outlines. Indeed, for each building, it is possible to derive the floor area for each storey (every 3 meters), the volume, and the area of each building facade using the method highlighted in section 6.3.

The thermal gains and losses through the side-facades, the ground floor or the roof floor are computed. Heat losses through external surfaces are caused by transmission and ventilation, while thermal gains are due to internal and solar gains. Internal gains are computed referring to table 9 in UNI/TS 11300-1:2008 Standard (UNI-TS 11300-1: 2008) taking into account different time intervals connected to building zones utilization. Solar gains, related to both opaque and glazed surfaces, depend on the solar irradiation intercepted by the external building envelope both on the surfaces orientation and inclination and on the presence of surrounding buildings (section 7.4.7.3).

Finally, monthly and seasonal energy balance for all the buildings is carried out. For each building and each storey, thermal needs are computed taking into account the intermittency and the efficiency of the heating system as well as the utilization factor of total heat gains. The synoptic view showing the heating calculation structure is presented in Figure 8.5.

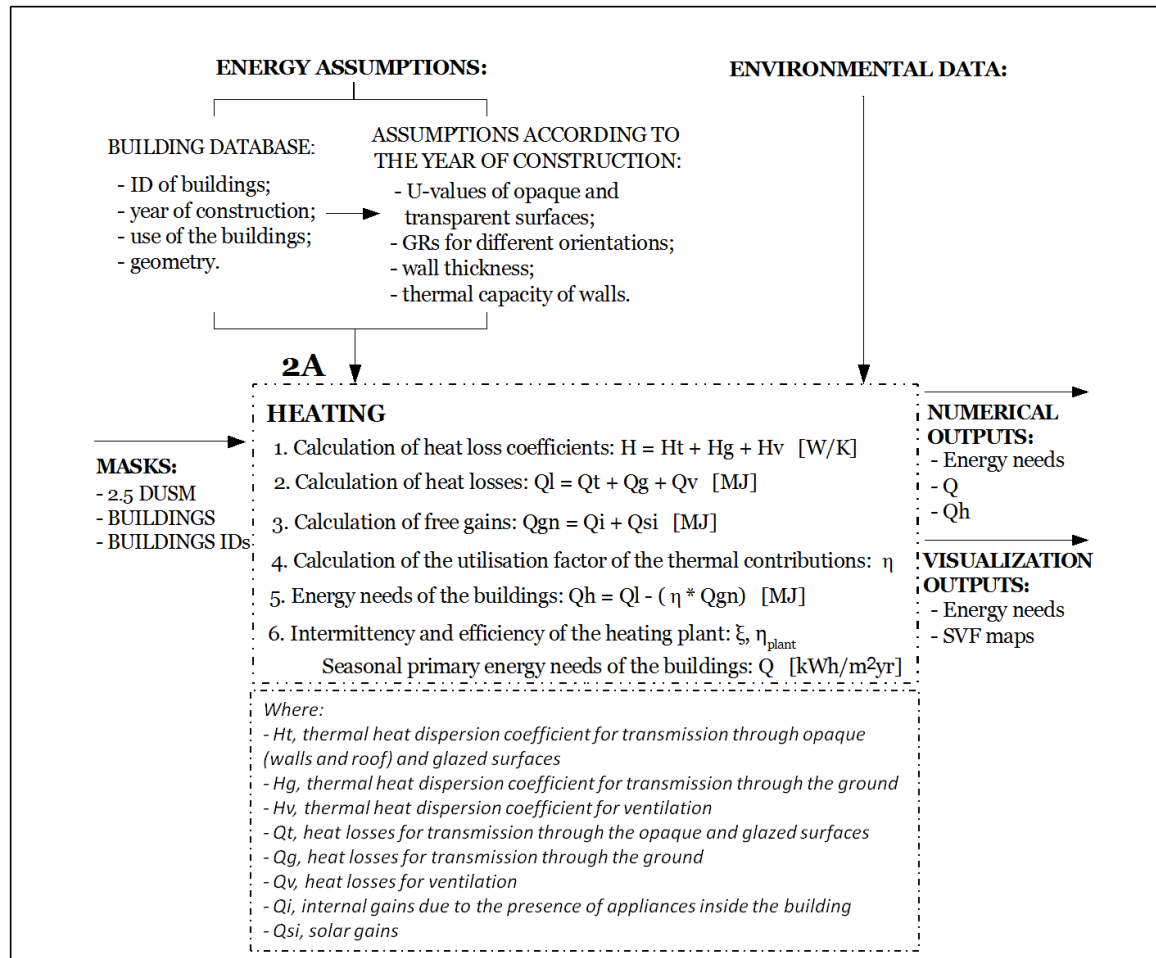


Figure 8.5. Heating calculation structure.

8.3.6 Artificial lighting needs evaluation

The simulation runs during the winter season and takes into account a time span from 9 AM to 5 PM as to compute useful day-lighting contributions. For the remaining hours of usage, an estimation of consumptions was obtained taking into account the typical space utilisation patterns and occupancy rates during the day.

The model used in this study is presented in Morello *et al.* (2009), summarized as follows. It is based on the computation of solar irradiances (W/m²) intercepted on vertical urban surfaces (section 7.4.7). The contribution of beam and diffuse irradiation at each point is derived using the shadow casting routine presented in section 7.3.3, which allows the differentiation among lit and shadowed pixels on the facades of the urban model. In particular, for lit pixels, the beam contribution of irradiance is summed to the diffuse. Moreover, the model is sliced at every storey (once again 3 meters intervals are used) in order to account for the solar admittance variations of the vertically aligned pixels. Irradiances are subsequently converted into illuminance values (lx). Illuminance spread out inside the building whereby the model considers a constant Glazing Ratio (GR) for the areas of windows, applied to all orientations, with openings running uninterruptedly along all the perimeter of the buildings. Hence, referring to the total flux method proposed by Szokolay (2004), the luminous flux ϕ_l (lm) entering the room can be calculated. The day-lighting level dramatically drops with the increase of distance from the openings. The derivation of the

8.3 Case-study: evaluation of solar energy potential and energy needs for heating and lighting using 2.5-DUSM constructed from LiDAR data

simplified daylight factor's profiles in indoor spaces, assuming these identical over all orientations, follows the method proposed by Krarti *et al.* (2004). In order to calculate internal illuminance profiles, only passive zones are considered (Ratti *et al.*, 2005). In this case, for each floor, passive zones are defined as the area within a distance to the external perimeter that is twice the height of the ceiling, hence e.g. 6 meters. An example of the calculation for the case-study area of CERN is shown in Figure 8.6.

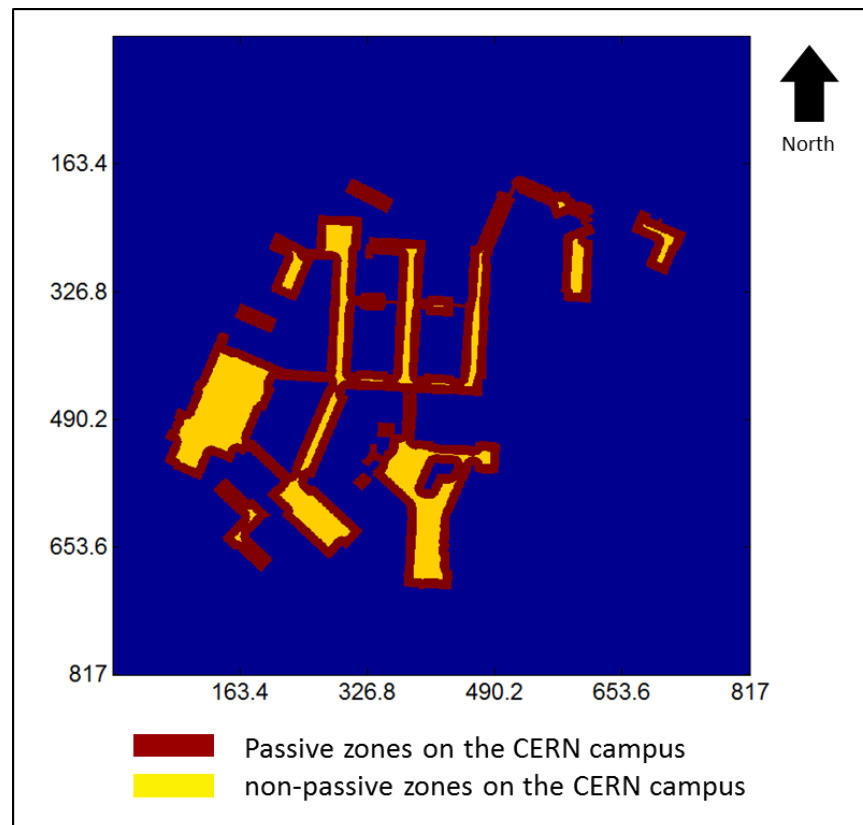


Figure 8.6. Passive and non-passive zones for the buildings' first floor of CERN case-study area.

Once the patterns of indoor illuminance levels are mapped, the integration of natural and artificial lighting can be assessed. The model computes the average hourly energy consumption in Wh/m^2 over the passive zones required by the integration of artificial lighting. It assumes 5 W/m^2 as the general electrical consumption for artificial lighting in the non-passive zones where full electric lighting system is always provided - this value is calculated considering a 100 W lamp that covers an area of about 20 m^2 whereby also unlit floor areas occupied by furniture or facilities are included in this estimation. A threshold of minimum illuminance over the work plane must be guaranteed; otherwise artificial lighting needs to be provided. It is assumed 100 lux as the minimum illuminance that must be reached at every point of space (Morello *et al.*, 2009a). Even though such threshold does not represent a high level of illuminance and is usually provided in spaces that do not require specific visual tasks, it constitutes a good average limitation if it is spread out over all points of the building. The synoptic view showing the lighting calculation structure is presented in Figure 8.7.

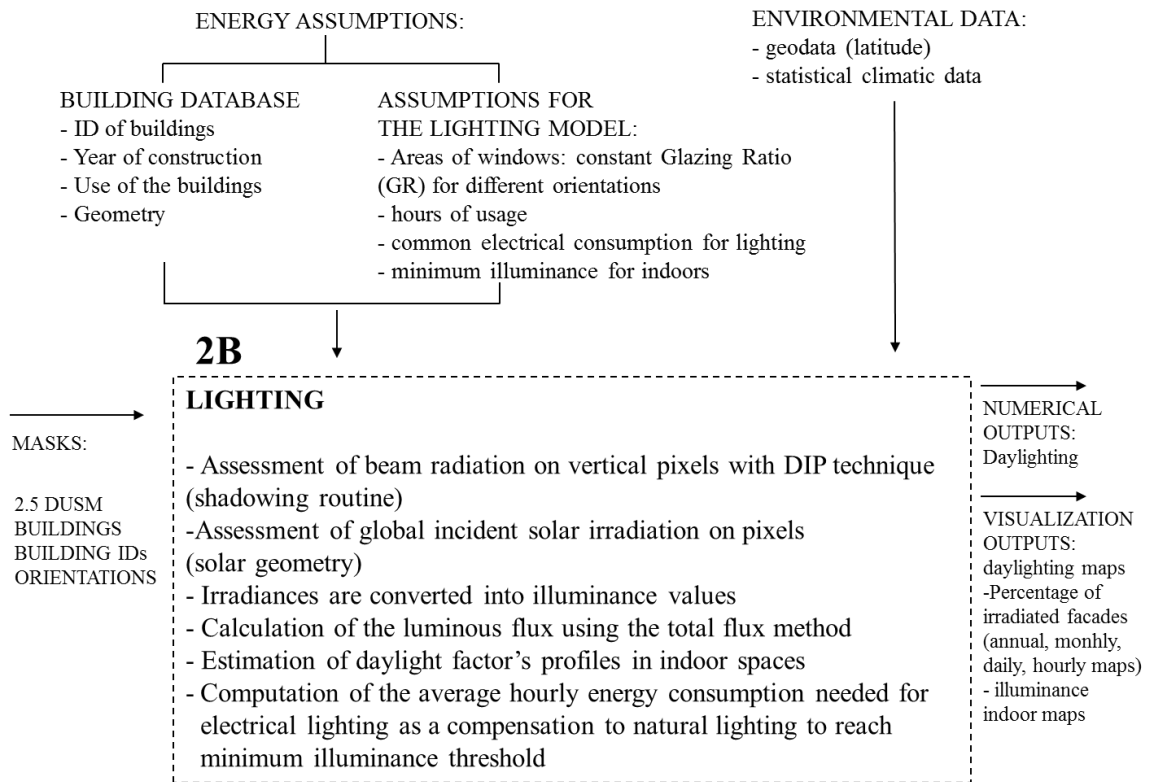


Figure 8.7. Artificial lighting calculation structure.

8.3.7 Exploration of the solar potential

The exploration of the solar potential of building roofs follows the method proposed in section 7.4.4.

The electrical and thermal energy production from sun collectors is calculated applying the method proposed in section 7.4.8. It is worth mentioning that, this computation, obtained from the global irradiation outputs, is conducted only on the pieces (roof sections) of building roofs where solar irradiation is considered to be sufficient (defined as $> 1.000 \text{ kWh/m}^2 \text{ yr}$), and the real area is significant ($>$ for 4 m^2 for thermal technology and $> 20 \text{ m}^2$ for PV technology). The roof area is computed using the morphological analysis presented in section 6.3.

For heating analysis, the calculation is performed for the hours when outside temperature is below 16°C (heating cut off). The synoptic view showing the solar radiation calculation structure is presented in Figure 8.10.

8.3 Case-study: evaluation of solar energy potential and energy needs for heating and lighting using 2.5-DUSM constructed from LiDAR data

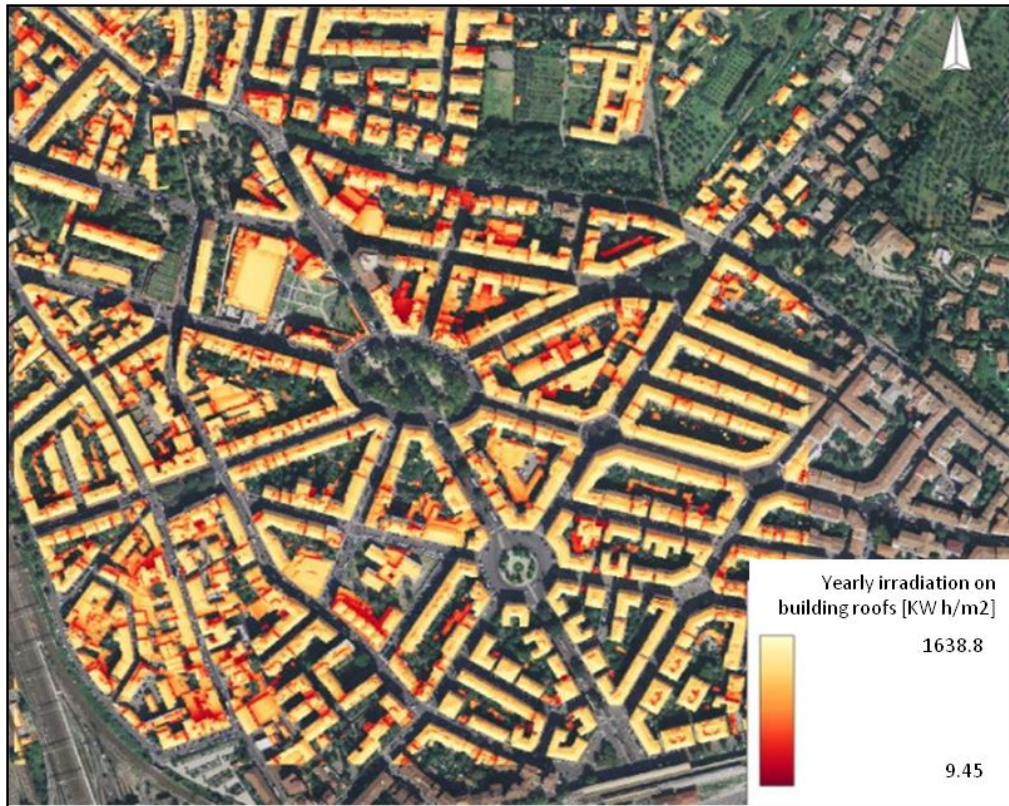


Figure 8.8. Yearly solar irradiation (kWh/m2) on building roofs: the representation (roofs are visualized in 2.5-D, above an orthophoto) of irradiation on a pixel basis for the Florence case-study area.

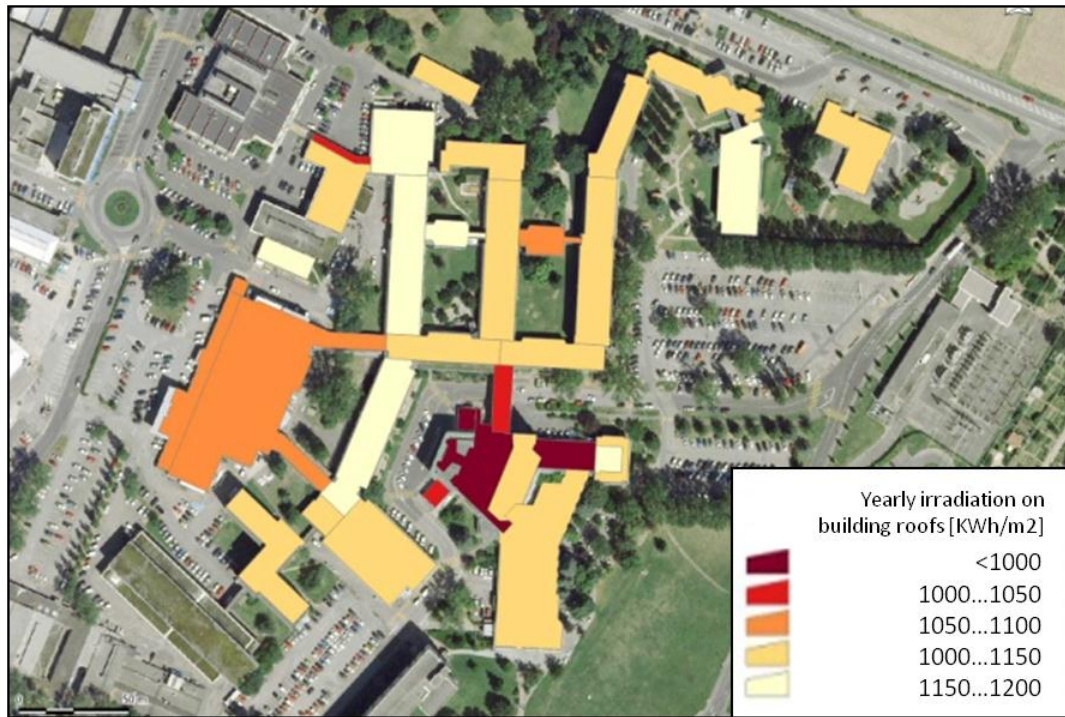


Figure 8.9. Yearly solar irradiation (kWh/m2): pixel values are aggregated by building roof (2-D visualization) on the CERN campus case-study area.

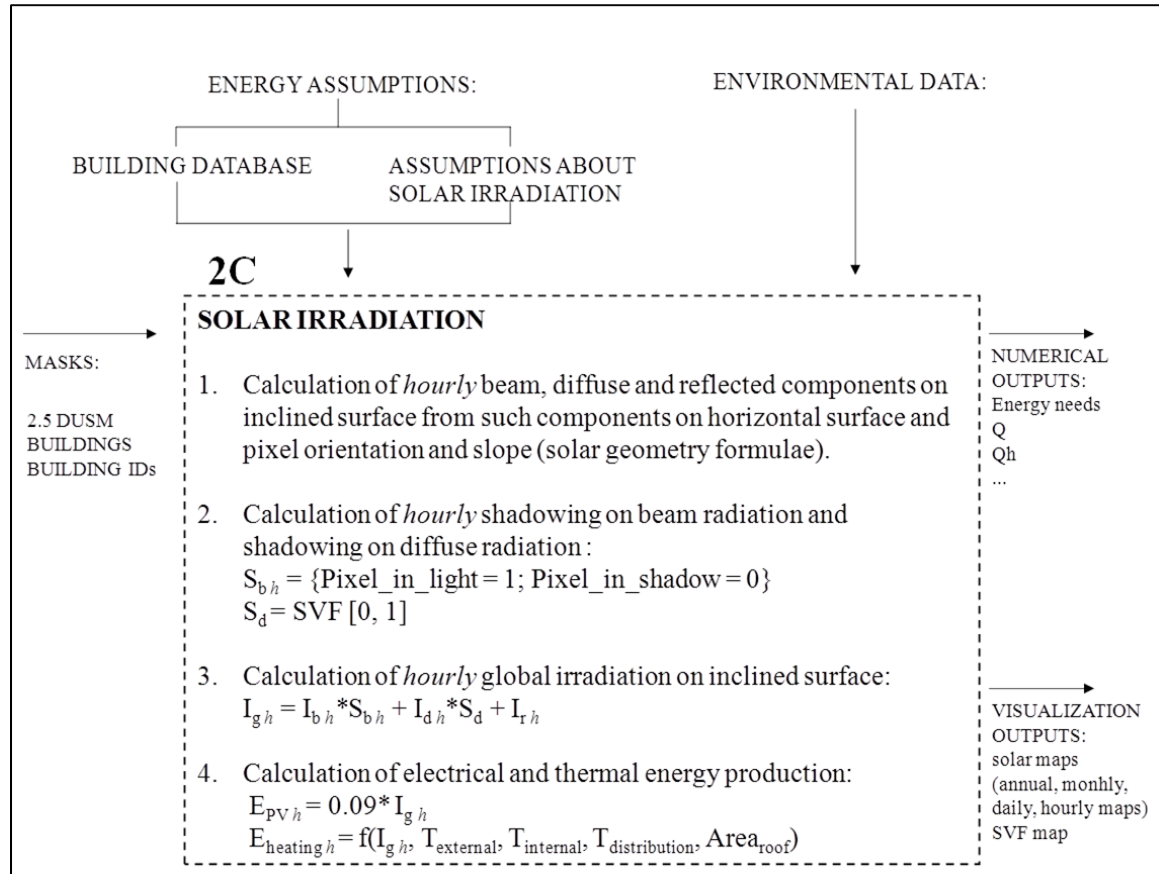


Figure 8.10. Solar irradiation calculation structure

8.3.8 Analysis of results

8.3.8.1 Direct outputs

Two types of outputs were produced: numerical data and visualizations. The latter is fundamental in order to communicate and to program interventions in the decision-making process, such being a novelty at an urban level. The vast flexibility of the proposed method of interactively classifying features in different ways allows the production of a great number of thematic maps covering the whole study area in order to highlight the distribution of building energy needs (thermal and lighting).

A series of 2-D and 3-D maps showing the energy needs and the energy needs per square meter for the case-study areas of both CERN and Florence are presented in Figures 8.11 to 8.14 respectively.

8.3 Case-study: evaluation of solar energy potential and energy needs for heating and lighting using 2.5-DUSM constructed from LiDAR data

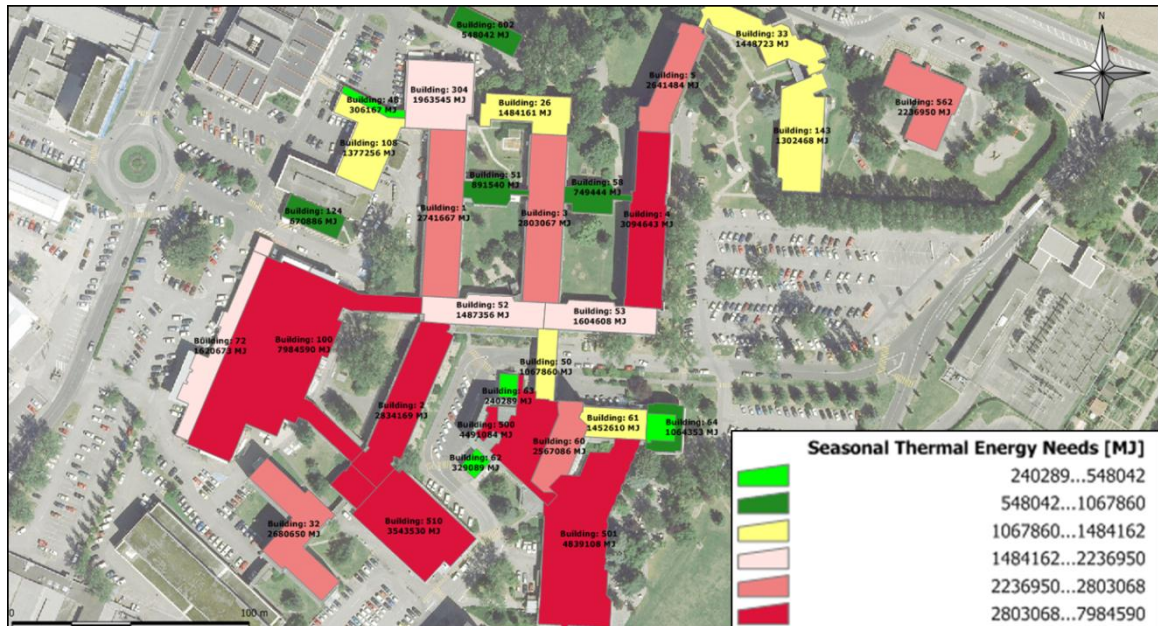


Figure 8.11. Seasonal energy needs for heating (MJ) visualized in 2-D for the case-study area of CERN.

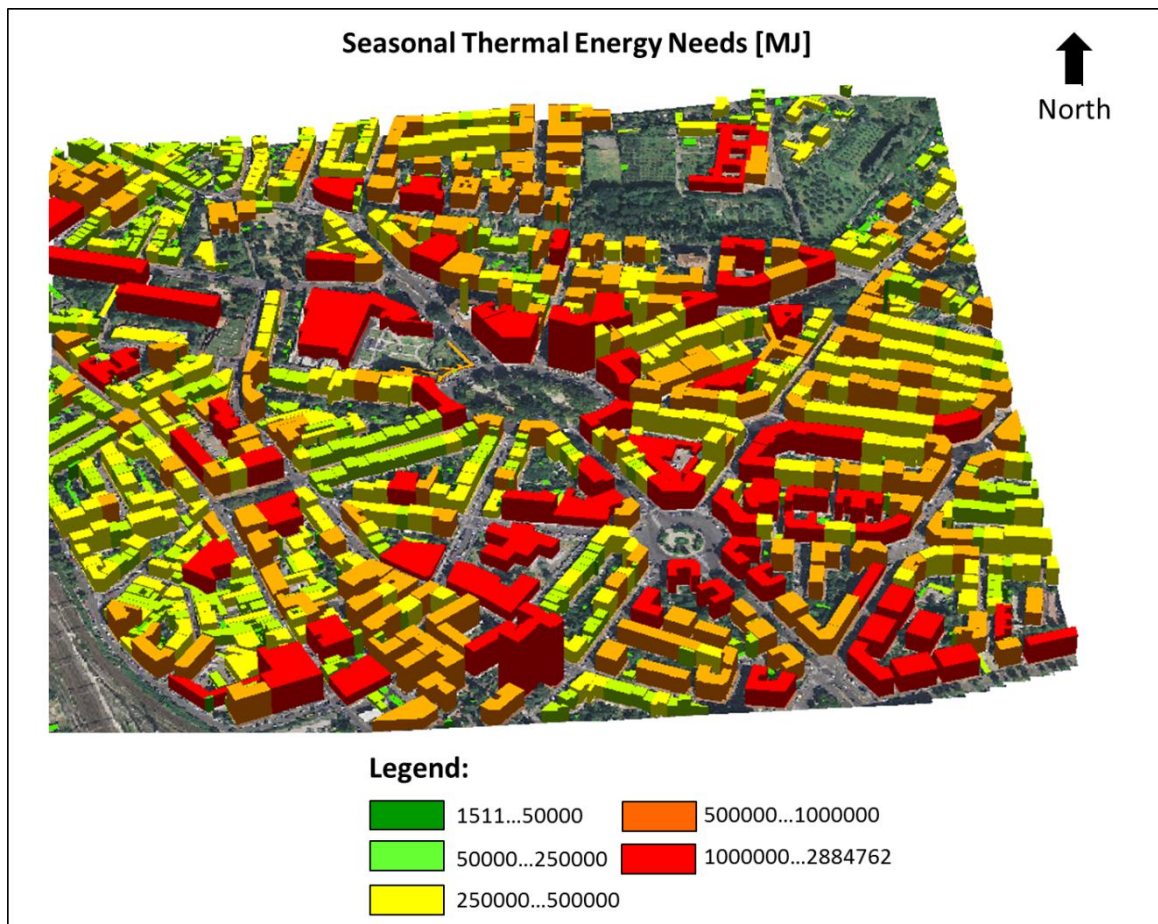


Figure 8.12. Seasonal energy needs for heating (MJ) visualized in 3-D for the case-study area of Florence.

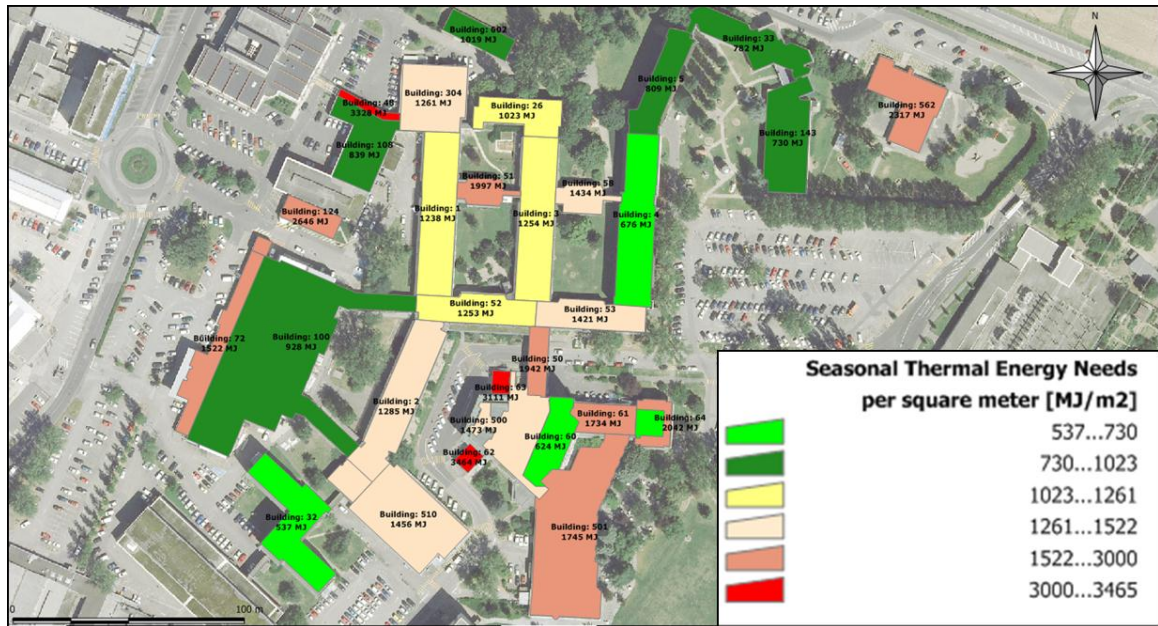


Figure 8.13. Seasonal thermal energy needs per square meter for heating (MJ/m²) visualized in 2-D for the case-study area of CERN.

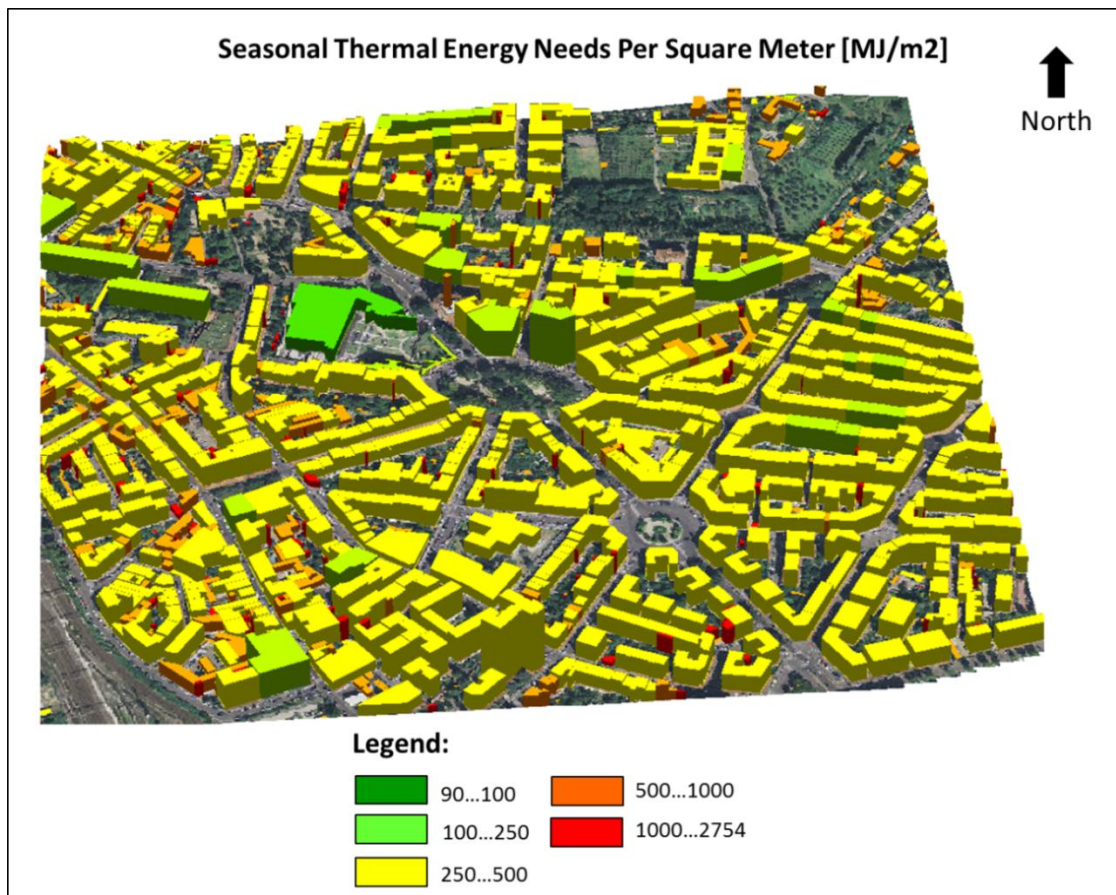


Figure 8.14. Seasonal thermal energy needs per square meter for heating (MJ/m²) visualized in 3-D for the case-study area of Florence.

8.3 Case-study: evaluation of solar energy potential and energy needs for heating and lighting using 2.5-DUSM constructed from LiDAR data

8.3.8.2 Different energy scenarios

As described in section 8.3.3 it is possible to construct different energy scenarios making two main comparisons:

- artificial lighting versus electrical energy production from sun collectors (energy scenario 1);
- heating versus thermal energy production from sun collectors (energy scenario 2): some statistical results and 2-D maps examples are presented in Figures 8.15 to 8.17.

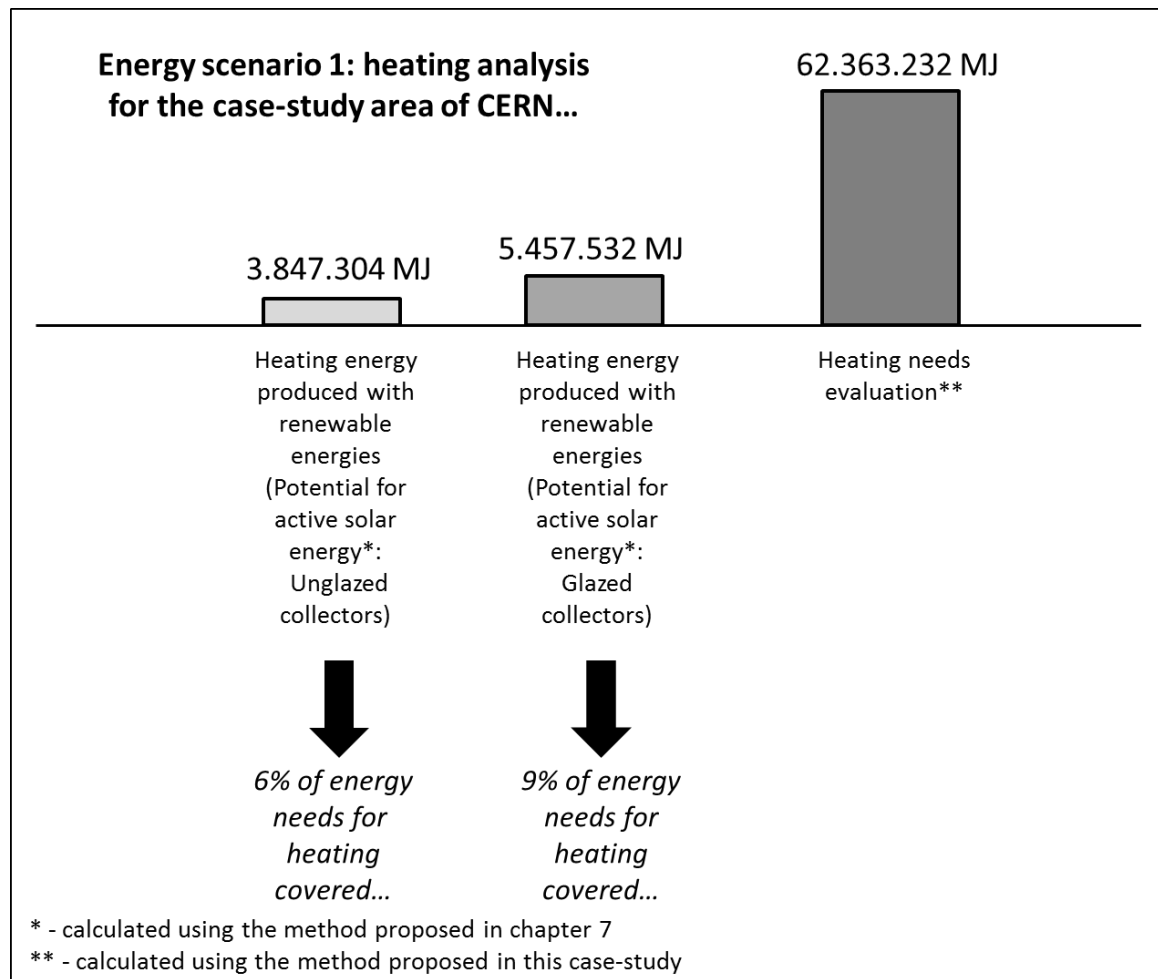


Figure 8.15. Energy scenario 2: statistical output showing the heating needs coverage using thermal collectors for the case-study area of CERN.

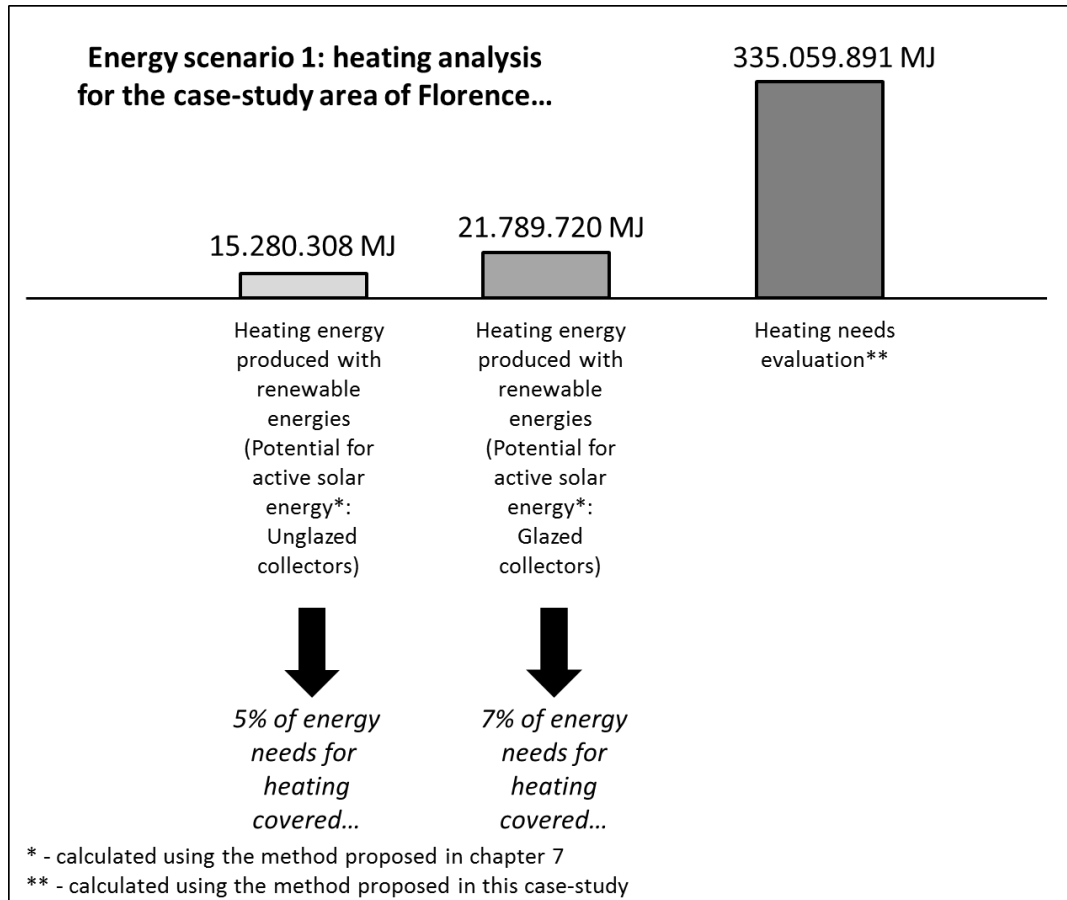


Figure 8.16. Energy scenario 2: statistical output showing the heating needs coverage using thermal collectors for the case-study area of Florence.



Figure 8.17. Energy scenario 2: 2-D visualization showing, building by building, the percentage of heating needs coverage using thermal collectors (in this case, glazed collectors) for the case-study area of CERN.

8.4 Validation and usefulness

The statistical analysis shown in Figures 8.15 and 8.16 is an interesting output for comparison between different groups of buildings or neighbourhoods of a single city or distinct cities, especially in order to check its performance regarding the installation of thermal collectors. For the two case-study areas studied in this chapter, CERN presents a slightly better performance than Florence. This may be due to the fact that the Florence case-study area presents a higher concentration of buildings with complex roofs and vegetation, which increases the shadowing effect inside the urban fabric, thus reducing the production of energy from thermal collectors.

With regards to the analysis of the map shown in Figure 8.17 a more detailed analysis can be undertaken. In fact, such allows the evaluation of which buildings demonstrate a better propensity for the installation of thermal collectors (in this case glazed) when compared to the energy needs of each building.

The lighting analysis method presented in section 8.3.6 is a task that is currently under development, implementation and validation. For this reason, outputs or energy scenarios considering this type of analysis are not still highlighted in this thesis.

8.4 Validation and usefulness

Since the proposed method implements a European Standard, there are mainly two levels of validation that have to be ensured:

- The first level of validation is to ensure that the Standard is well implemented and, for each building, it provides the correct result. This point was successfully certified by Gori (2010);
- The second level of validation is represented by the control of the deviation between simulated results (obtained from the implementation of the Standard) and the real values. Of course this would be an additional and important validation (if real data were available¹⁶) but, since the method is given by an effective Standard, it is not an aim of this thesis to verify it. The choice of implementing a standard and not to create an own method was taken into account to be sure that the method was ideally controlled and totally referenced.

8.5 Conclusions and chapter synthesis

This chapter focused on the extraction of complex indicators for the assessment of the energy demand on the urban fabric, belonging to the stake “estimation of the energy demand on the urban fabric”. The main emphasis was given to the analysis of heating and artificial lighting needs, which integrates the inputs derived from the morphological analysis of buildings. Moreover, by integrating electrical and thermal energy production from sun collectors (information derived from the assessment of solar irradiation on building roofs) it is also possible to define and analyse specific energy scenarios at different scales of the city, or eventually, between different cities. This innovative approach, using 2.5-DUSM automatically constructed from LiDAR data and digital image processing techniques, underlines the integration and articulation of different types of indicators for the extraction of more complex indicators (mixed scenarios). Such is rather useful and pertinent for the sustainable development of cities. Some important points related to the adaptability of this method that can be stressed are presented as follows:

¹⁶ It is not easy and quick to raise the information needed and the monitoring campaigns that have to be done would take years.

Chapter 8. Estimation of the energy demand on the urban fabric

- it is relatively easy to update the data: once new LiDAR data is available the construction of 2.5-DUSM is relatively easy and quick;
- simulations to update results are not time consuming: not very specialized technicians are needed;
- the display of outputs as simple 2-D and 3-D maps are easy to understand for specialized users;
- the database with the initial information about buildings does not necessary need to be very rich or analogue to the ones used in this study. Indeed, it is not mandatory to have a specific database structure in order to define the assumptions about building properties used for this study.

Finally, future work should allow to:

- accredit that the gain of using this method in terms of efficiency and reliability is not overbalanced by a loss of accuracy concerning the different outputs (extracted indicators);
- validate the integration of other building uses – not only residential, as applied in this study, but also commercial, offices, among others. This will allow to improve the results presented for the case-study area of CERN, where buildings' uses are mostly offices and laboratories ;
- expand the estimation of needs for cooling, which being highly dependent on urban geometry aspects that can be automatically extracted using the morphological analysis of buildings proposed in section 6.3, is a fundamental issue with regards to the overall energy balance of cities;
- verify whether the input data and the information used can differ from the input data and information used in the present case-study. For instance, further work may be concerned with the analysis of the impact of the quality and density of LiDAR data in the final results achieved, which, for the moment, was not the main purpose of this thesis research;
- instead of using 2-D and 3-D displays showing quantitative indicators (as proposed for the moment in this case-study) it would be undoubtedly useful to use this type of information to derive a set of relevant pseudo-qualitative indicators. Those are more easily understandable by users that are not highly specialized in this topic, such as public in general or politicians.

CHAPTER 9. UTILITY OF THE 3-D GEO-VISUALIZATIONS FOR URBAN ENVIRONMENTAL QUALITY INDICATORS

9.1 Introduction

As emphasized in the previous chapters of this thesis, the concept of indicator's *utility* is strongly related to its relevance (Desthieux, 2005). The set-up of an indicator system aiming to support visualization and decision making should be done following a double process (Maystre and Bollinger, 1999). The top-down process starts from the decision-makers' worldview which is generally based on qualitative or quantitative evaluations. The main question to answer is: *what* should be measured or valued and according to which goals? From this worldview, one goes down until the descriptive or predictive models of experts that select and organize data, and progressively aggregate them into indicators (bottom-up process). Or in other words, the set-up of an indicators' system consists, both on selecting relevant indicators according to issues and goals expressed by users, and proposing a method and tools to aggregated data and thus build and eventually visualize indicators.

Considering this target, it is rather important to scrutinize the right modalities in order to present results, both in terms of quantifiable indicators and, when needed, its 2-D, and 3-D (includes 2.5-D) visual representations. Thus, this chapter intends to contribute with a simple utility analysis among the 25 end-users of the State of Geneva involved in this study about the 3-D visualizations proposed for the urban environmental quality (UEQ) indicators highlighted in this thesis. A main focus is given to an evaluation of the added value of 3-D visualisations (mainly when compared to more common 2-D visualizations) of UEQ indicators for contributing to a better understanding of the information.

The following sections introduce information about:

- 9.2) – background and related work;
- 9.3) – geo-visualizations for UEQ indicators;
- 9.4) – evaluating the utility of the proposed 2-D and 3-D geo-visualizations;
- 9.5) – conclusions and chapter synthesis.

9.2 Background and related work

Scientific visualization is an interdisciplinary branch of science, primarily concerned with the visualization of three dimensional phenomena, such as architectural, meteorological, medical, and biological systems. The emphasis is on realistic rendering of volumes, surfaces, illumination sources, and with a dynamic (time) component. Scientific visualization focuses on the use of computer graphics to create visual images which aid in understanding of complex, often massive numerical representation of scientific concepts or results. In 1987, in a report to the United States National Science Foundation (NSF), the "Panel on Graphics, Image Processing, and Workstations" defined scientific visualization as "a method of computing (...) a tool both for interpreting image data into a computer, and for generating images from complex multi-dimensional data sets...". The goal of this discipline is "...to leverage existing scientific methods

by providing new insight through visual methods” (McCormick et al. 1987). On this basis, DiBiase *et al.* (1992) expanded that view by arguing that “visualization” is definitely not restricted to a method of computing but is first and foremost an act of cognition, a human ability to develop mental representations that allow us to identify patterns and create or impose order. And later they coined the term "Geo-visualization".

Thus, geo-visualization has been defined by MacEachren and Kraak (2001), as “the integration of visualization in scientific computing, cartography, image analysis, information visualization, exploratory data analysis and GIS, which all together provide theory, methods and tools for visual exploration, analysis, synthesis and presentation of spatial data”. 3-D geo-visualization can be applied at different phases, with distinct levels of detail (LoD), and according to user requirements and applications. However, professionals that could in principle be in a better position to use such technologies are often reluctant. Indeed, they regularly deal with unsuited visualization modes to their purpose; these modes are too complex, too detailed and dense, and hence, do not enable them to rapidly locate and interpret relevant 3-D urban geographic information to make presumptions.

By incorporating indicators, 3-D visualisations give the chance to connect all the dimensions, the visual and non-visual parts of the urban environment, and may well deliver new planning tools (Bishop and Lange, 2005). Nevertheless, very few studies exist that suggest possible designs of integrating indicators in 3-D visualisation tools (Hehl-Lange, 2001). Quantitative indicators are significant at the scale of the neighbourhood or at the scale of the city and should be used for comparative studies among different design schemes for specialized end-users; however, qualitative indicators are more often an easier approach in order to communicate with common end-users. Moreover, visualizations must be immediately comprehensive also to a wider audience, thus efficiently capturing and efficiently translating the indicators on the maps. Buziek *et al.* (2000) show that such representations intend to highlight explicit visualisation objects, in order to sustainance the perception of space and to simplify knowledge processes which are mainly elaborated for the enhancement of their potential for communicating specific information to end-users.

The procedure applied for the construction of the 3-D visualizations of the UEQ indicators proposed is based on the user-requirement analysis emphasized in chapters 4 and 5 and considers the following phases:

- results from psychological and media-pedagogical research on using images for information communication are applied in the design of 3-D visualisations with regards to human information processing. Indeed, the theoretical background of image reception, cognition and functions of images as an aid for learning can help to elucidate the effects of visual information on the recipient and to derive guidance for an effective design of the information in 3-D visualisations (Wissen *et al.*, 2005; Wissen, 2007).
- visualisations are used to assemble feedback from end-users according to thoughtful and utility.

The results reveal what qualities the respective designs and the mode of interactivity of the three types of integrated 3-D visualisations have for the end-users' information processing and for the planning process. In fact, the manner in which these indicators have to be three-dimensionally geo-visualized is still undefined, especially its integration (also semantic) into 3-D models using the different levels of details (LoD) defined by the CityGML standard and also by evaluating which constructed objects are cognitively perceived in a better way. Thus, they should provide a component for a standardised 3-D visualisation method for urban indicators, in this case, more specifically for environmental quality indicators (UEQ).

9.3. Geo-visualizations for urban environmental quality indicators

Hence, based on the new methods and tools highlighted in this study, which allow the derivation of UEQ indicators, a final survey was conducted with the 25 end-users of the State of Geneva engaged in this study. The main goal of this survey was to analyse the utility of the 3-D visualizations proposed (using LoD0 to LoD2), which were created according to the initial user requirements analysis highlighted in chapter 4, including a comparison to the traditional 2-D mapping.

9.3 Geo-visualizations for urban environmental quality indicators

9.3.1 Indicators related to the assessment of the morphological properties on the urban texture

Even though morphological indicators are not often visualized, the “surface to volume (S/V)” ratio (index) is calculated and visualized in 2-D and 3-D (LoD1) formats, as shown in Figures 9.1 and 9.2. This indicator is used in biology as well in architecture as one of the most relevant shape related property of objects. The more compact (low values of S/V) a shape is, the lower is its thermal loss to the environment. For instance, the sphere is the shape that optimizes the S/V ratio (refer to the igloo), since it contains the maximum volume within the minimum external surface. Hence, high values of S/V usually belong to short buildings, whereas low values of S/V are characteristic for tall buildings with bigger volumes and relatively small exterior surfaces.

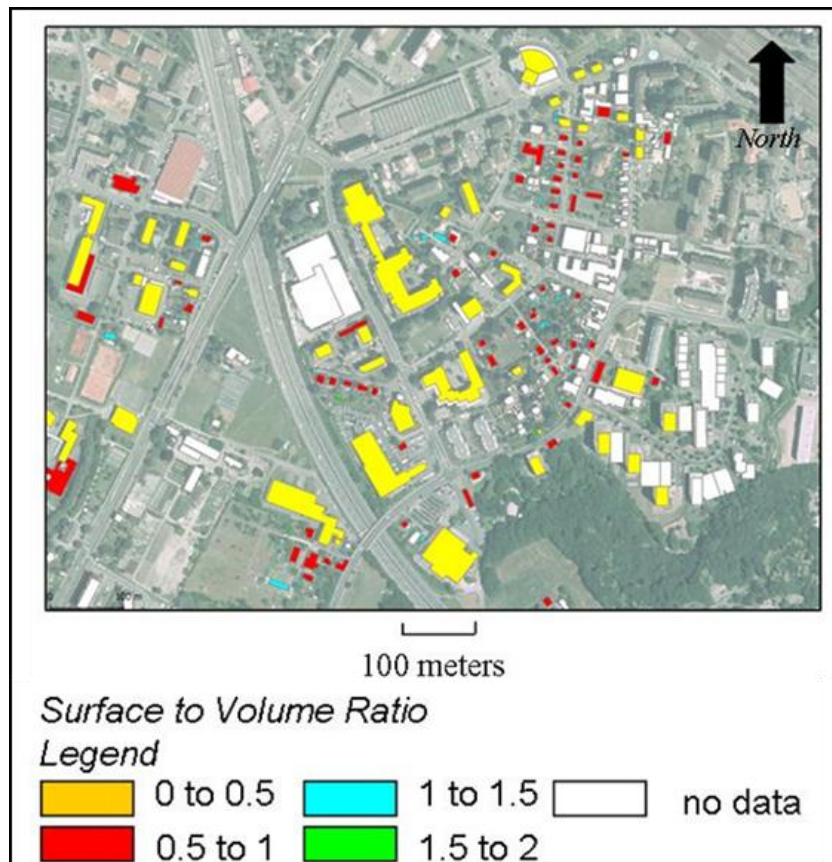


Figure 9.1. 2-D geo-visualization of the “Surface to volume” ratio (index) considering a neighbourhood scale for a neighbourhood (Chavannes pilot zone) of the City of Lausanne.

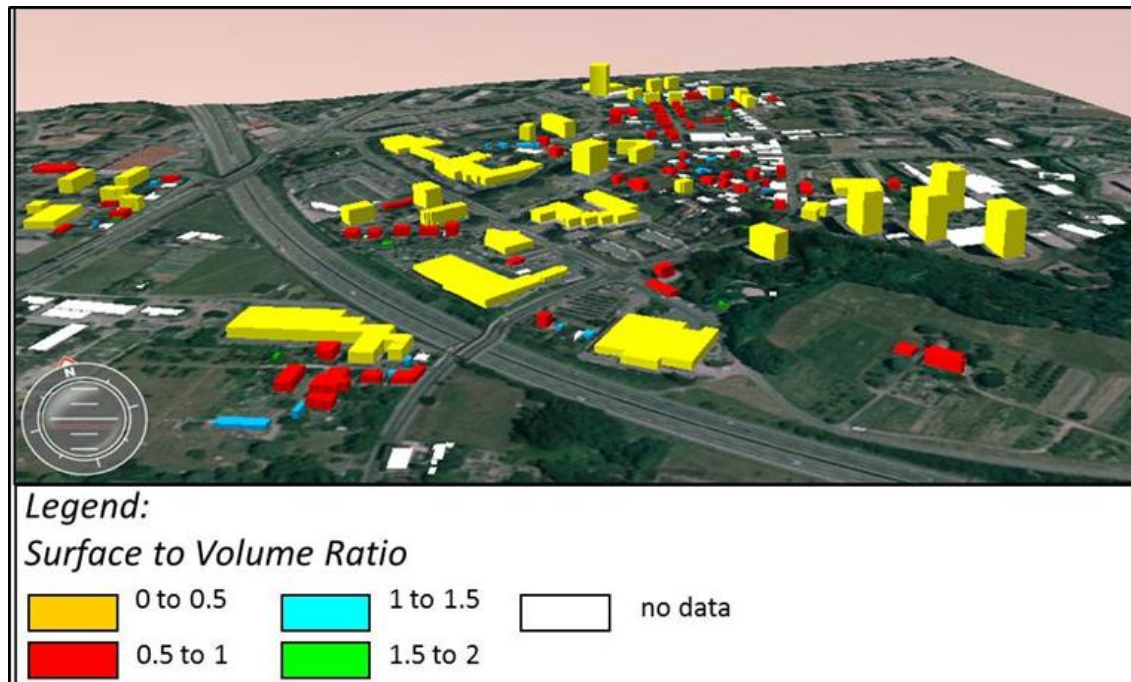


Figure 9.2. 3-D geo-visualization of the “Surface to volume” ratio (index) considering a neighbourhood scale for a neighbourhood (Chavannes pilot zone) of the City of Lausanne.

9.3.2 Indicators related to the exploration of the solar potential on the urban fabric

As highlighted in chapter 7, the indicators related to the exploration of the solar potential on the urban fabric, more particularly on buildings, can be sub-divided into two main topics: analysis on facades and analysis on roofs.

The indicators from solar irradiation analysis on facades can be represented in various forms:

- performances of the facades on a 2-D map: Figure 9.3 shows the mean irradiance (W/m²) falling on the second storey of vertical surfaces. Such map can be displayed for every storey, which may be useful for focused analysis but does not provide an overview. Alternatively, the average value of irradiation on the whole facade can be displayed in a single map;
- 3-D (LoD2) visualization: Figure 9.4 shows the average values per facade, however, due to the occlusion effect, this representation needs several maps considering various view origins in order to visualize the values of all the facades of a building. Therefore the 2-D form in a single map is more synthetic. The advantage of 3-D visualization is to refine the map by showing the results by storey and thus the vertical variation of irradiation with the elevation. A similar approach that emphasizes the vertical variation of residential quality in a 3-D visualization display was proposed by Lorenz and Döllner (2010);
- emergence of new and innovative ways of 3-D geo-visualization. For instance, the interviewed users perceived the added value of 3-D representation for some purposes such as displaying irradiation on facades. From this need results the 3-D view shown in Figure 9.5. It represents, for each building, the average irradiance values of its facades. One may wonder whether such a 3-D view could not be refined by showing the results by storey and thus the vertical variation of irradiation with the height of the building.

9.3. Geo-visualizations for urban environmental quality indicators

However, according to the previous survey (chapter 4) made with the same group of end-users, cognitively it would result in a complex representation. Alternatively, graphical profiles showing the percentage of vertical surfaces subjected to direct irradiation with increasing height [%] can be added to the 3-D geo-visualization proposed - thus highlighting both the global vertical irradiation in the analysed neighbourhood and the degree to which the top parts of buildings benefit from higher solar admittance, particularly during sunny hours. A similar approach showing the inclusion of graphical profiles to 3-D geo-visualization for the assessment of crime scene analysis was proposed by Wolff and Asche (2010). In fact, the new type of geo-visualization shown in this example resulted in a combined approach mixing 3-D representation with graphical and statistical data. An innovative method for the automated and dynamic placement of labels attached to objects of 3-D city models was proposed by Maass and Döllner (2008).

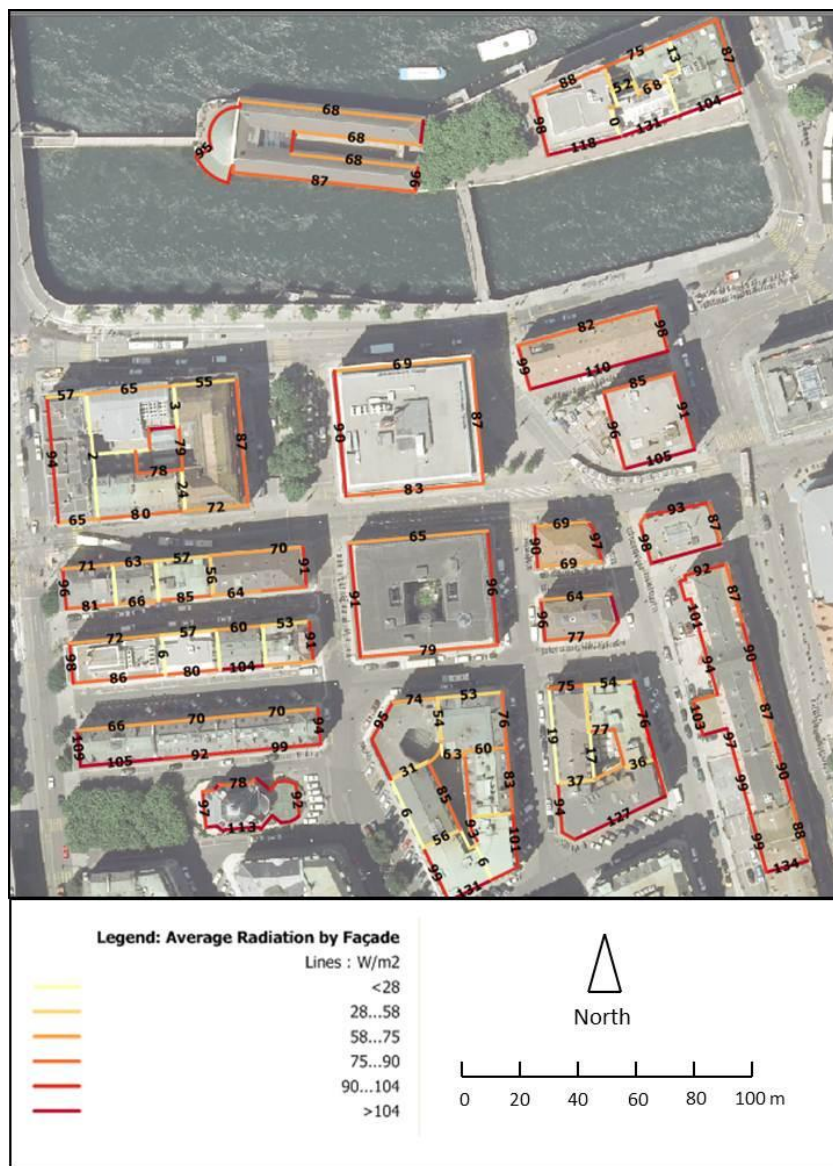


Figure 9.3. 2-D geo-visualization considering a neighbourhood scale: quantitative indicator inherent to the average irradiance values (considering both direct and diffuse contributions, expressed in W/m^2) collected by the second storey of each façade on the 10th of December at 12 PM, for a neighbourhood (business area) of the city of Geneva.

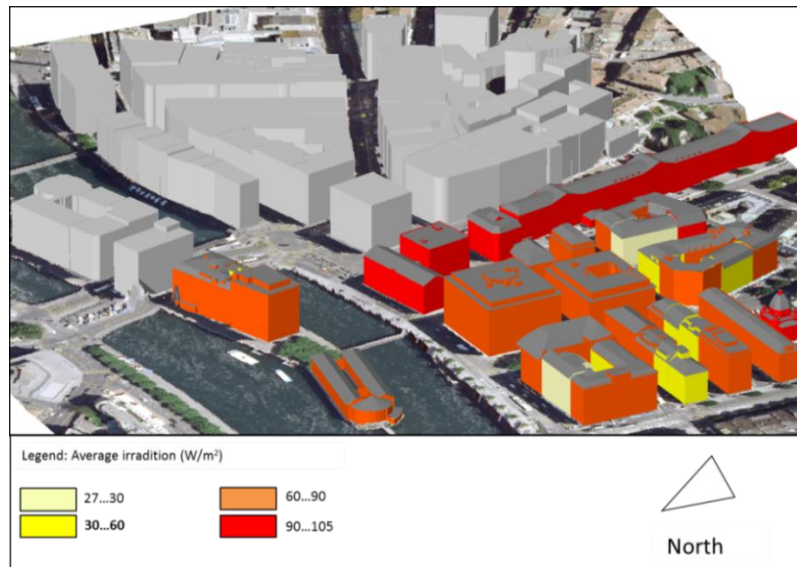


Figure 9.4. 3-D geo-visualization (LoD1 and LoD2) considering a neighbourhood scale: quantitative indicator inherent to the average irradiance values (considering both direct and diffuse contributions, expressed in W/m²) collected per building facades on the 10th of December at 12 PM for a neighbourhood (business area) of the city of Geneva.

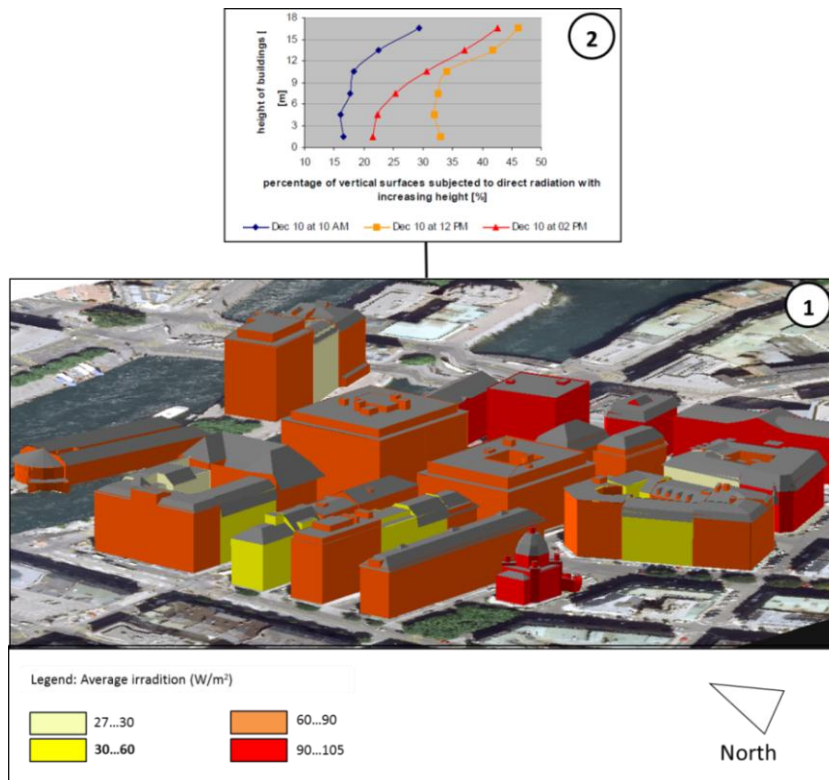


Figure 9.5. Hybrid approach of geo-visualization for urban indicators: (1) - 3-D visualization (LoD2) of a quantitative indicator inherent to the average irradiance values (considering both direct and diffuse contributions, expressed in W/m²) collected per building facades on the 10th of December at 12 PM for a neighbourhood (pilot zone) of the State of Geneva; (2) – graphical profile with statistical data that show the percentage of vertical surfaces subjected to direct irradiation with increasing height [%] (in this case, for a selected building) for the same day, at 10AM, 12PM and 2PM.

9.3. Geo-visualizations for urban environmental quality indicators

With regards to the indicators from solar irradiation analysis on roofs, the potential user would be in principle rather interested in assessing which section of the roofs would be suitable, or not, for solar panels collectors (for PV or thermal purpose) depending on the available solar admittance and roof area. When roof sections¹⁷ are available (for example, in the State of Geneva), yearly irradiation values (KWh/m²) are aggregated on each roof section as to highlight a synthetic representation of which surfaces are suitable for the installation of solar collectors. Thus, three examples of geo-visualization displays of the quantitative indicator inherent to the assessment of the yearly solar irradiation higher than 1.000 KWh/m² for all building roofs of the neighbourhood of Moillesulaz, State of Geneva are shown in Figures 9.6 (2-D representation), and Figures 9.7, 9.8 and 9.9 (3-D representation: LoD0, LoD1 and LoD2 respectively).

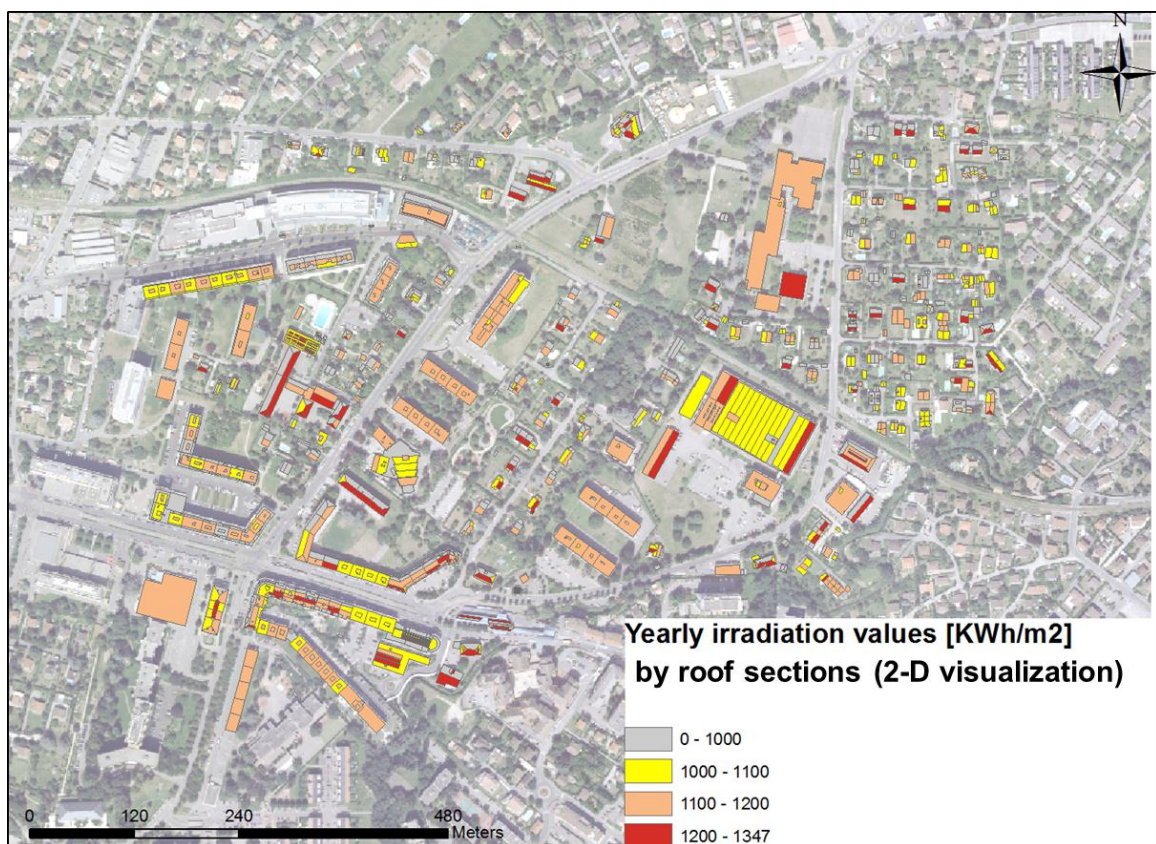


Figure 9.6. 2-D visualization considering a neighbourhood scale: quantitative indicator inherent to the annual solar irradiation (KWh/m²) by roof sections for a neighbourhood (Moillesulaz pilot zone) of the State of Geneva.

¹⁷ Usually, represents the 2-D projection of building roof sections existing in 3-D city models.

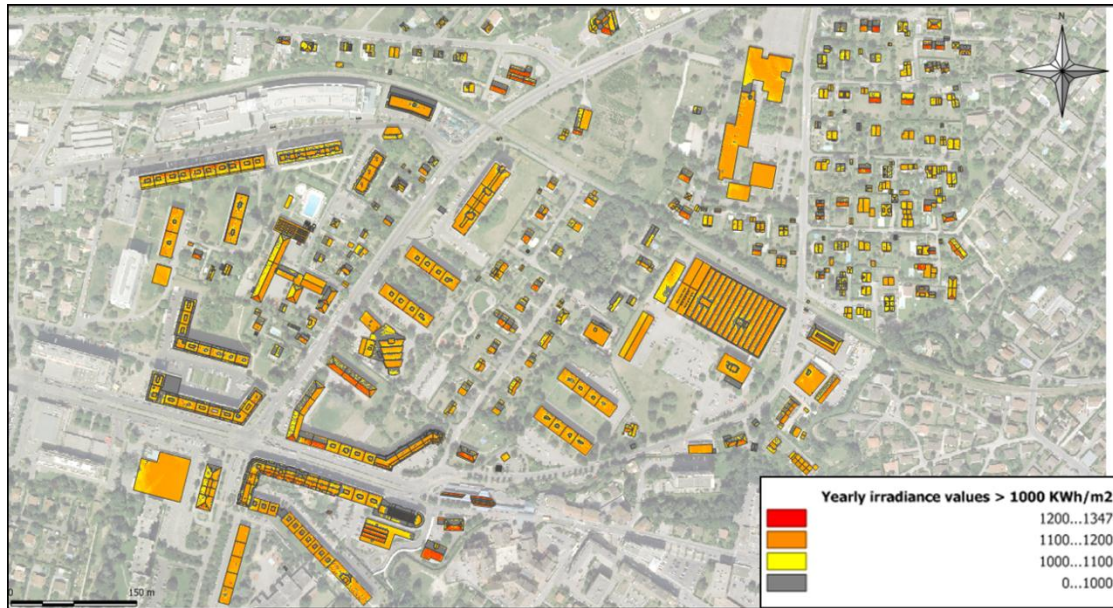


Figure 9.7. 2.5-D visualization (LoD0) considering a neighbourhood scale: quantitative indicator inherent to the annual solar irradiation (KWh/m²) by roof pixels for a neighbourhood (Moillesulaz pilot zone) of the State of Geneva.

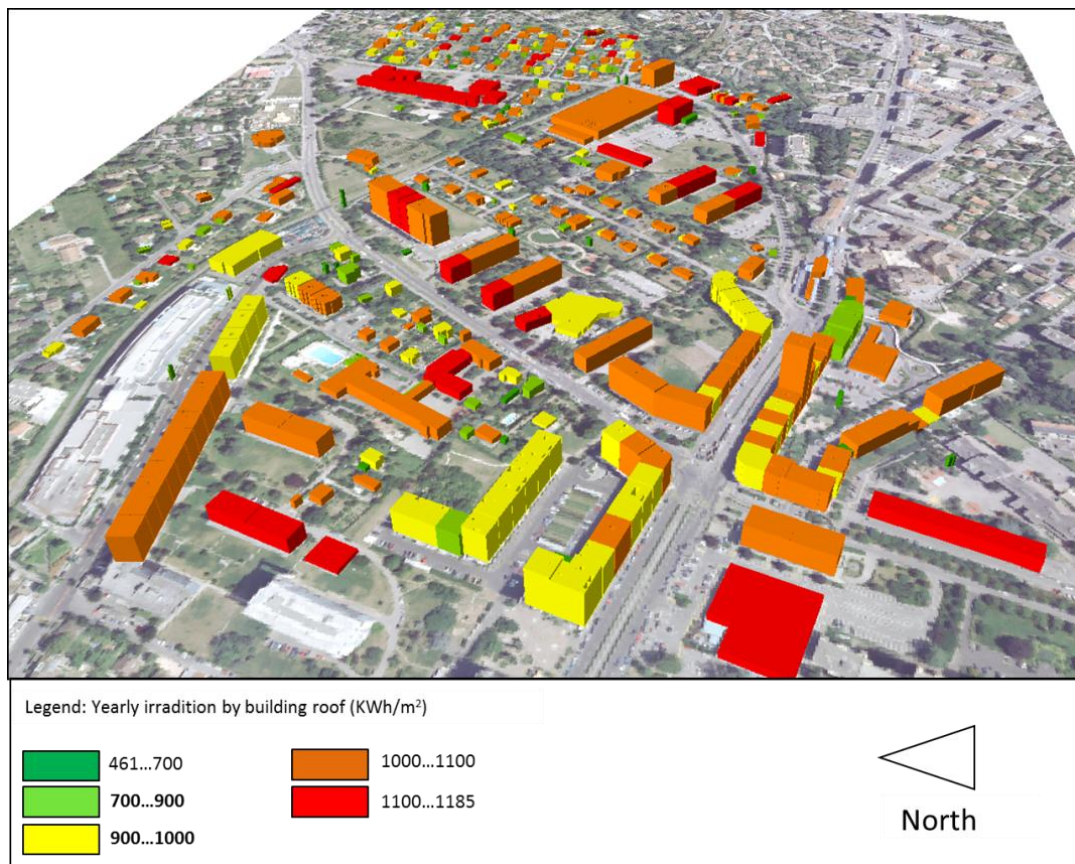


Figure 9.8. 3-D visualization (LoD1) considering a neighbourhood scale: quantitative indicator inherent to the annual solar irradiation (KWh/m²) by building for a neighbourhood (Moillesulaz pilot zone) of the State of Geneva.

9.3. Geo-visualizations for urban environmental quality indicators

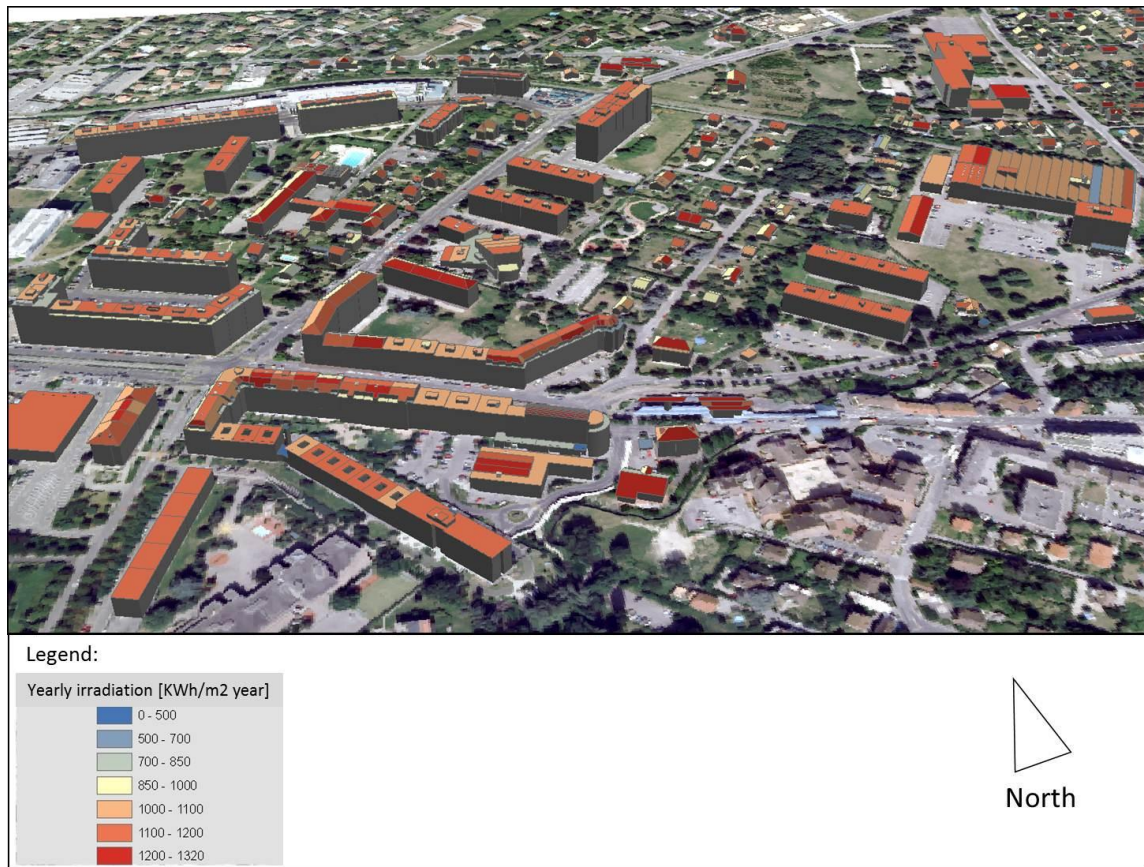


Figure 9.9. 3-D visualization (LoD2) considering a neighbourhood scale: quantitative indicator inherent to the annual solar irradiation (KWh/m²) by roof sections for a neighbourhood (Moillesulaz pilot zone) of the State of Geneva.

9.3.3 Indicators related to the estimation of the energy demand on the urban fabric

The potential user should be in principle rather interested in the indicators related to the estimation of the energy demand on the urban fabric. In the example presented in this section, values are aggregated on each building in order to highlight a synthetic representation of the seasonal thermal energy requirements. Thus, four examples of geo-visualizations: (1) 2-D, (2) 3-D using the same LoD, (3) 3-D using different LoD, and (4) 3-D using different LoD and the integration of labels, are shown in Figures 9.10, 9.11, 9.12 and 9.13 respectively, for the case-study area of CERN.

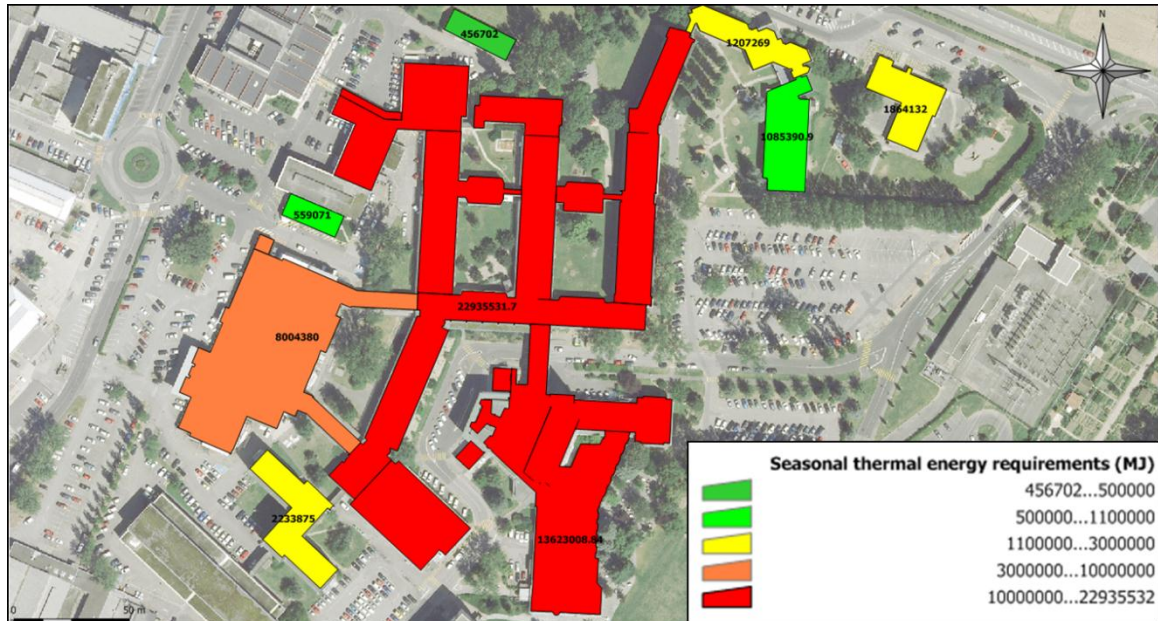


Figure 9.10. 2-D visualization considering a neighbourhood scale: quantitative indicator inherent to the seasonal thermal energy requirements (MJ) by building, for the case-study area of CERN.

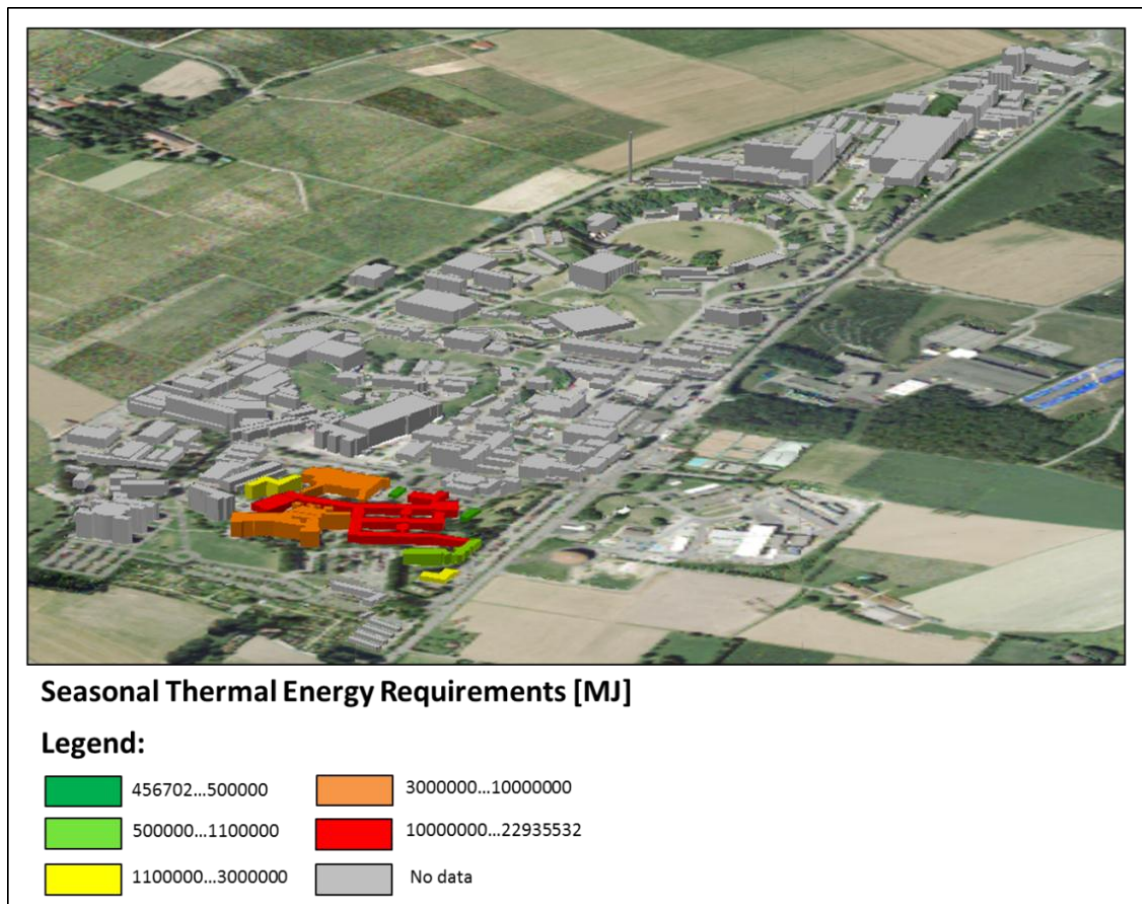


Figure 9.11. 3-D visualization (LoD1) considering a city scale: quantitative indicator inherent to the seasonal thermal energy requirements (MJ) by building, for the case-study area of CERN.

9.3. Geo-visualizations for urban environmental quality indicators

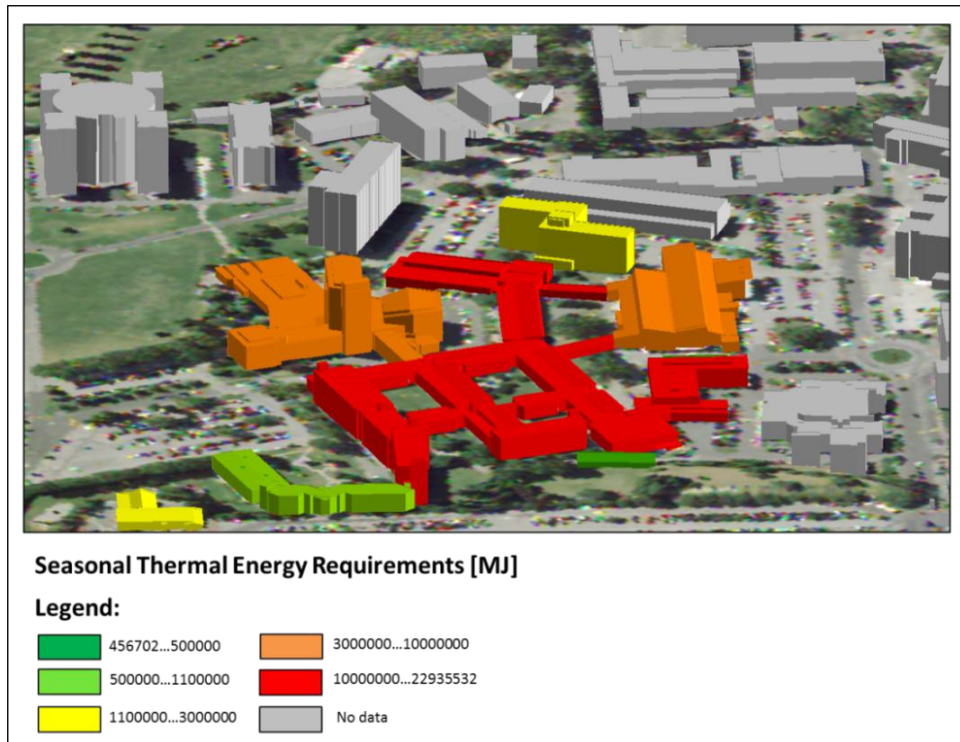


Figure 9.12. 3-D visualization considering a neighbourhood scale, using different LoD (LoD1 and LoD2): quantitative indicator inherent to the seasonal thermal energy requirements (MJ) by building, for the case-study area of CERN.

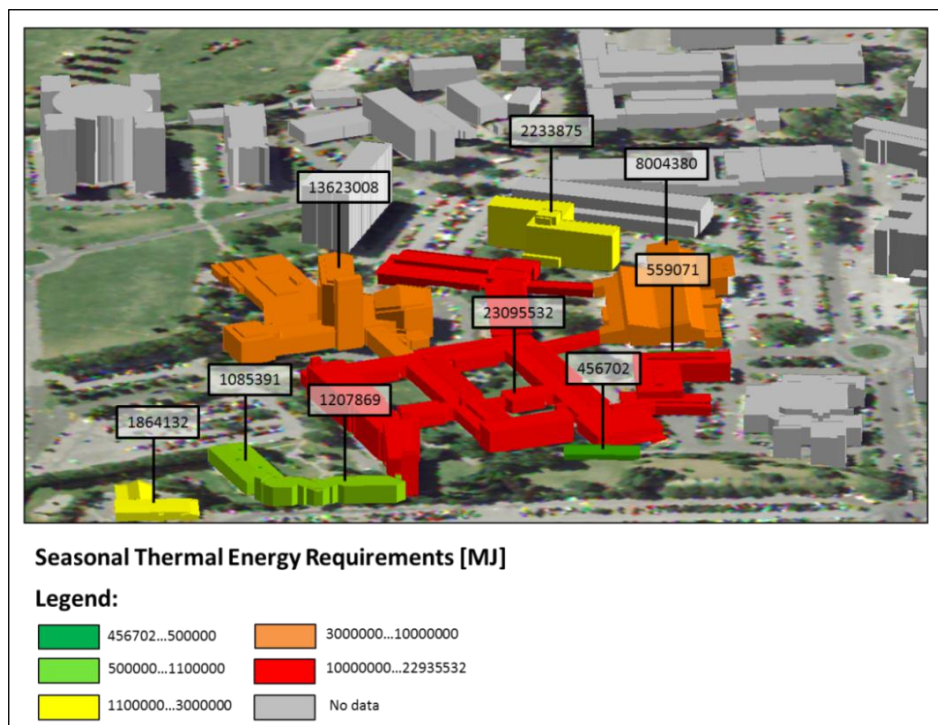


Figure 9.13. 3-D visualization considering a neighbourhood scale, using different LoD (LoD1 and LoD2) and building's labelling: quantitative indicator inherent to the seasonal thermal energy requirements (MJ) by building, for the case-study area of CERN.

9.4 Evaluating the utility of the proposed 2-D and 3-D geo-visualizations

9.4.1 Presentation of the survey conducted

In order to evaluate the utility and relevance of the 3-D (LoD0, LoD1 and LoD2) geo-visualizations proposed, especially when compared to traditional 2-D mapping, a survey was conducted with the same group of 25 end-users presented in section 3 of this paper. The experts' general opinion and trends concerning the utility of the visualizations proposed and application potential should be considered for further reflections and 3-D urban projects.

The survey was sub-divided into two main parts: (1) – general questions regarding professional expertise; (2) – questions directly related to the geo-visualizations presented. Within this thesis only the end-users' evaluations regarding the second group of questions are analysed and presented. The final results of the survey are highlighted in Table 9.1. Before giving out the survey to the users, the interactive versions of the 3-D geo-visualizations emphasized in this section were presented in form of a live-demo to the end-users.

The list of questions (Question 1 to Question 8) presented to end-users are described as follows:

Question 1 (Meaningfulness) – Are 3-D geo-visualizations of UEQ indicators meaningful in general?

Question 2 (Added value) – For the representation of UEQ indicators that can be represented in a “2-D world”, should 3-D geo-visualization be considered as an added value when compared to traditional 2-D mapping?

Question 3 (Vertical perception) – When the perception of the vertical component of an UEQ indicator cannot be ignored, should the use of this 3-D geo-visualization be considered relevant?

Question 4 (Different LoD) – Depending on the scale of visualization (city or neighbourhood) of the UEQ indicators under analysis, should different LoD be used?

Question 5 (Best LoD) – Depending on the scale of visualization (city or neighbourhood) of the UEQ indicators under analysis, which of the proposed LoD is considered to be the best option for 3-D geo-visualization?

Question 6 (User attention) – Is the use of 3-D geo-visualizations displays of UEQ indicators using simultaneously different LoD1 and LoD2 an added value when the attention of the user must be guided?

Question 7 (Complex visualizations) – Should the application of more complex and novel approaches using both 3-D geo-visualizations and graphical displays/labelling showing statistical data of UEQ indicators be considered an alternative for more simple and common 3-D geo-visualizations?

Question 8 (Day-to-day) – Finally, would you consider using 3-D geo-visualizations of this type of UEQ indicators in your day-to-day professional activities?

9.4. Evaluating the utility of the proposed 2-D and 3-D geo-visualizations

	Very high relevance	High relevance	Not relevant	Indifferent
Meaningfulness	6	17	2	0
Added value	3	3	16	3
Vertical perception	20	3	0	2
Different LoD	10	7	2	6
User attention	6	12	4	3
Complex visualizations	12	6	2	5
Day-to-day	3	3	13	6

Best LoD (city's scale)	Very high relevance	High relevance	Not relevant	Indifferent
<i>LOD0</i>	5	15	3	2
<i>LOD1</i>	3	12	7	3
<i>LOD2</i>	2	7	14	2

Best LoD (neighbourhood's scale)	Very high relevance	High relevance	Not relevant	Indifferent
<i>LOD0</i>	2	5	16	2
<i>LOD1</i>	13	8	3	1
<i>LOD2</i>	15	7	1	2

Table 9.1. Results of the final survey concerning the different geo-visualizations proposed for the UEQ indicators under analysis.

9.4.2 Analysis of results

Considering the UEQ indicators under evaluation, 23 end-users (92%) expressed that the proposed 3-D geo-visualizations (from LoD1 to LoD2) are in general meaningful. However, for 16 end-users (64%), the use of 3-D geo-visualization for representation of urban spatial indicators that can be interpreted in a “2-D world” is not an added value when compared to traditional 2-D mapping - exception is mainly for the cases where the perception of the altimetric component cannot be ignored, such as the perception of the surface to volume indicator of buildings. In this case 23 end-users (92%) considered the use of 3-D geo-visualization to be relevant. Depending on the scale of visualization, 17 end-users (68%) considered relevant the use of different LoD for 3-D geo-visualization. Hence, the relevance of each LoD varies according to the two classes of scales adopted for this survey. LoD0 is considered a better option for 3-D visualizations at the city scale, and LoD1 or LoD2 (users showed a slightly preference for LoD2) is considered a more suitable choice for 3-D visualizations at the neighbourhood scale. According to 18 end-users (72%), when the attention of the user must be guided, the employment of 3-D geo-visualization modes using simultaneously different LoD1 and LoD2 reveals itself to be essential. The use of innovative representations, combining 3-D geo-visualization and graphical displays/labelling is considered as being pertinent by most of the users (72%). Finally, end-users seem to be still renitent regarding the use of 3-D geo-visualizations in their day-to-day business activities – only 6 end-users (24%) demonstrated enthusiasm for this option, being the same that also stated that 3-D geo-visualization is an added value when compared to traditional 2-D mapping.

Following a final discussion with this group of 25 end-users of the State of Geneva, it is worth mentioning some important remarks regarding the survey emphasized in this study:

- from the comparison between Figures 9.1 and 9.2 (“surface to volume ratio”), it can be noticed that the 3-D representation reveals itself to be very important in cases where the

- perception of the building vertical component cannot be ignored. In other words, the 2-D representation does not allow the verification of the correctness of the map since a visual confirmation of the actual volumes of the represented objects cannot be assessed;
- depending on the manner in which the data is aggregated, a good example of 3-D geo-visualizations (city and neighbourhood scales) complemented by 2-D mapping is the analysis of solar irradiance along building facades. In this case, when data corresponding to all facades and storey of each building is aggregated by this type of object, results can be shown in a 3-D display (Figure 9.4). On the other hand, for a storey by storey analysis of each facade, 2-D mapping seems better adapted as it allows to have a general overview of the buildings under analysis (Figure 9.3). Moreover, the use of 2-D views avoids the occlusion effect of some facades when rendering this type of data in a 3-D model, which can be solved only by on-the-fly displays using the 3-D interfaces created;
 - the use of 3-D geo-visualizations with a lower level of detail (LoD0) seems more relevant at the scale of the city, allowing a continuous interpretation of the information displayed (Figure 9.11). However, according to the results presented for the UEQ indicators analysed, LoD0, as a continuous 3-D representation, seems only relevant for the evaluation of the phenomena that can be uninterruptedly and orthogonally measured and, thus, displayed, such as the assessment of solar irradiation along building roofs (Figure 9.7). Also, the representation of the assessment of solar irradiation over building facades, which is not orthogonally measured, is not possible using this type of 3-D visualization. For the neighbourhood scale, where the density of information shown is lower and the occlusion effect of 3-D models is less relevant, the use of 3-D geo-visualizations using LoD1 or LoD2 seems better adapted (Figure 9.8). Nevertheless, the 3-D geo-visualizations modes of the UEQ indicators presented always include a generalization degree: aggregation of data stored in raster images into a discrete vector format, which can affect the trustworthiness of the information shown in a 3-D model (vector-based);
 - for 3-D geo-visualizations of UEQ indicators at the neighbourhood scale, the creation of displays using different LoD1 and LoD2 is effectively considered to be an added value when the attention of the user must be guided (Figure 9.12). Hence, the buildings considered for analysis are shown using a LoD2, whereas all other buildings, which were not considered for analysis, are represented using a lower level of detail (LoD1);
 - it is important to mention that 3-D geo-visualization modes using LoD2 are extremely relevant for the display of the phenomena independently related to building facades or roofs. For instance, if the assessment of solar irradiation concerns only building facades and not roofs, 3-D geo-visualization displays should highlight building facades with different colours according to the phenomena evaluated, and therefore all building roofs should have associated a neutral colour, such as grey, which corresponds to a “no data” classification (Figure 9.4). On the other hand, if the assessment of solar irradiation concerns only building roofs and not facades, 3-D geo-visualization displays should be done in the opposite way (Figure 9.9). This is only possible when using LoD2, because the LoD1 representation of an object, such as a building, is defined as a “sugar block” (single entity). Moreover, the fact that in LoD1 representation each building is defined as a single entity also implies that its use is only suitable for the representation of urban environmental indicators that are aggregated by building and not by roof sections or facades. Hence, only when the UEQ indicator under analysis is aggregated by building, LoD1 or LoD2 can be freely used, otherwise only LoD2 should be chosen for 3-D visualization;
 - as shown in Figure 9.13, the use of labelling in 3-D geo-visualization modes seems more relevant at lower scales, such as neighbourhood. In fact, at the city scale too much information can result in a cognitively complex display. Moreover, as shown in Figure 9.5, the interactive linking of the UEQ indicators with diagrams on the 3-D geo-

9.5. Conclusions and chapter synthesis

visualizations proposed enables end-users to both animate and draw their attention to complementary relationships that otherwise would be impossible to detect. However, this point falls beyond the scope of this thesis because it involves complex thinking aspects. Thus, it should be more deeply studied in further analysis.

9.5 Conclusions and chapter synthesis

The objectives of all users of 3-D urban models for the geo-visualization of spatial indicators must be carefully identified - in fact, very detailed urban models, on its own, do not necessarily offer an effective solution for geo-visualization of the majority of 3-D UEQ indicators highlighted in this thesis. It is also interesting to note that nowadays most of end-users are not open to the generalization of use of 3-D city models for the visualization and analysis of this type of indicators.

The goal of this survey was to make a preliminary utility analysis of the geo-visualizations proposed to end-users, related to the UEQ indicators studied in this thesis. Many other aspects, such as analysing the impact related to the use of different degrees of transparency for selected displayed data or the integration of other urban objects (for instance, trees) on the 3-D interfaces created should also be taken into consideration for further utility and usability studies. Indeed, this is a very wide topic that exceeds the scope of this thesis and, for this reason, it was not more deeply considered. It could however be revealed that a great majority of the end-users engaged in this study appreciated the interactive 3-D interfaces and geo-visualizations proposed, considering it as a very useful complement to the more traditional 2-D mapping applied to their day-to-day professional activities.

Finally, for different participatory situations, other methods using simpler representations of this type of indicators into 3-D visualisations should be considered for wider collaborative end-users and stakeholder groups, such as interested citizens of different ages. In this case, the use of qualitative indicators, instead of quantitative indicators, seems to be a better approach because the communication process is simpler. Moreover, using heterogeneous groups of users with different experiences and ages allows the application of a more reliable usability analysis to the interactive 3-D geo-visualization displays proposed for this type of indicators.

This chapter closes the third part of this thesis, which focuses on several empirical case-studies implemented under the framework of this research. These case-studies are used for the extraction and assessment of the proposed UEQ indicators, established according to the analysis of requirements made with the end-users of the city of Geneva engaged in this study. Next section will close this thesis by presenting some conclusions, a final outcome and finally an overview of possible perspectives.

CHAPTER 10. CONCLUSIONS AND PERSPECTIVES

10.1 General overview

During the last two decades the main attention on the domain of 3-D modelling has been given to the construction of 3-D urban models, mainly related to the development of automatic procedures based on hybrid techniques using aerial photos, LiDAR data and 2-D cadastral data. However, little attention has been given to projects related to the use of 3-D models and data for the environmental analysis of cities, with the aim of delivering useful tools for: (1) territory management and planning, and (2) urban design. In order to fill this gap, this thesis, based in the end-user requirements provided by 25 end-users of the State of Geneva, set up a pertinent list of urban environmental quality (UEQ) indicators. Those were extracted using 2-D and 3-D information. The research is essentially empirical, therefore focusing on the development and testing of new methods and tools for several case-studies: mainly of the city of Geneva, but also of the cities of Lausanne and Florence.

Thus, this chapter summarizes the research highlighted in this thesis, focusing on: 10.2) - *review of the research goals*: the goals defined in the introduction (section 1.3) are now considered, reviewed, and commented with regards to the achievements of this thesis, 10.3) – *final outcome*: some final remarks are presented, and 10.4) – *perspectives*: several research, application and commercial perspectives for this study are exposed and discussed.

10.2 Review of the research goals

Definition of a list of pertinent 3-D urban indicators based on an analysis of user requirements

Nowadays, the use and utility of 3-D models and data for the study of urban development has not yet been deeply studied. Indeed, 3-D urban indicators for sustainable development are necessary and the best procedure to construct them remains widely open. Thus, in a context where the number of actors is important, in principle showing different profiles, experiences and visions of the urban phenomena, it was highly relevant to identify and to structure different groups of end-users showing similar affinities. Under this context, three main stakes related to the *state of the art* topic of UEQ have been retained: (1) assessment of the morphological properties of the urban texture, (2) exploration of the solar potential on the urban fabric, and (3) estimation of the energy demand on the urban fabric. For each stake, a set of significant UEQ indicators could be defined: geographical indicators (elementary or complex) and indexes that were considered sufficiently representative and relevant were defined according to the end-users' needs (summarized in Figure 10.1).

An important subject related to the extraction of indicators is to correctly define how those must be spread to specialized end-users, other stakeholder groups and general public. One powerful way of doing it is through the use of specific end-user oriented geo-visualization environments. For this reason, this preliminary analysis of requirements also included a wide-ranging overview related to the expectations of perceived usefulness by end-users for the proposed visualizations of urban indicators, mainly focusing on a preliminary evaluation of the different possibilities of

visualization for the elementary and complex indicators and indexes extracted: not visualized, 2-D visualization and 3-D visualization (includes 2.5-D visualization).

This goal was successfully achieved by implementing the *top-down* process proposed by Maystre and Bollinger (1999). It allowed to define a list of UEQ indicators and indexes to be extracted by selecting a list of appropriate 3-D urban indicators, based on an analysis of end-user requirements with a group of 25 end-users of the State of Geneva. However, these 3-D urban indicators do not present a universal nature, even if its use can be generalised to other cities presenting similar characteristics and typologies.

Stake	Input data	Urban environmental quality (UEQ) elementary indicator extracted	Urban environmental quality (UEQ) complex indicator extracted	Urban environmental quality (UEQ) indexes extracted	Domain
Assessment of the morphological properties of the urban texture	2-D and 3-D	Volume of building Area of roof Area of ground Area of facades Area of storey Area of site Number of faces of building Average height of building Type of roof		“Surface-to-volume” ratio “Envelope area-to-ground area” ratio “Urban built density” ratio “Volume-to-number of faces” ratio “Floor area” ratio “Vegetation coverage” ratio	Architecture, urbanism and territory planners Environment and energy
Exploration of the solar potential on the urban fabric	2-D and 3-D		Irradiation collected by roofs Irradiation collected by facades Photovoltaic energy production Thermal energy production	“Vegetation impact” ratio “Influence of shadowing and Sky View Factor (SVF)” ratio	Environment and energy
Estimation of the energy demand on the urban fabric	2-D and 3-D		Seasonal thermal energy requirements Seasonal thermal energy needs Seasonal heat losses Seasonal gains Lighting demand analysis		Environment and energy

Figure 10.1. Overview of the geographical indicators (elementary or complex) and indexes extracted in this study.

Outline of new methods and tools using different data and models in order to extract relevant UEQ indicators

As a whole, the methods suggested in this research study produced a large set of UEQ indicators which bring homogeneous and objective information concerning urban phenomena. An important innovation delivered by this thesis consists on the integration of UEQ indicators resulting from different stakes and domains (mixed scenarios), which allows to derive more precise results concerning the UEQ indicators to be extracted. For instance, the morphological properties of buildings and the solar irradiation collected by facades indicators can be used to complete and to improve the extraction of indicators related to energy demand (heating analysis) on the urban fabric (Figure 10.2). Furthermore, by integrating the indicator related to the potential for active

10.2 Review of the research goals

solar energy on roofs, this process also allows to build different energy scenarios towards the improvement of a more incorporated and ecological vision of the city.

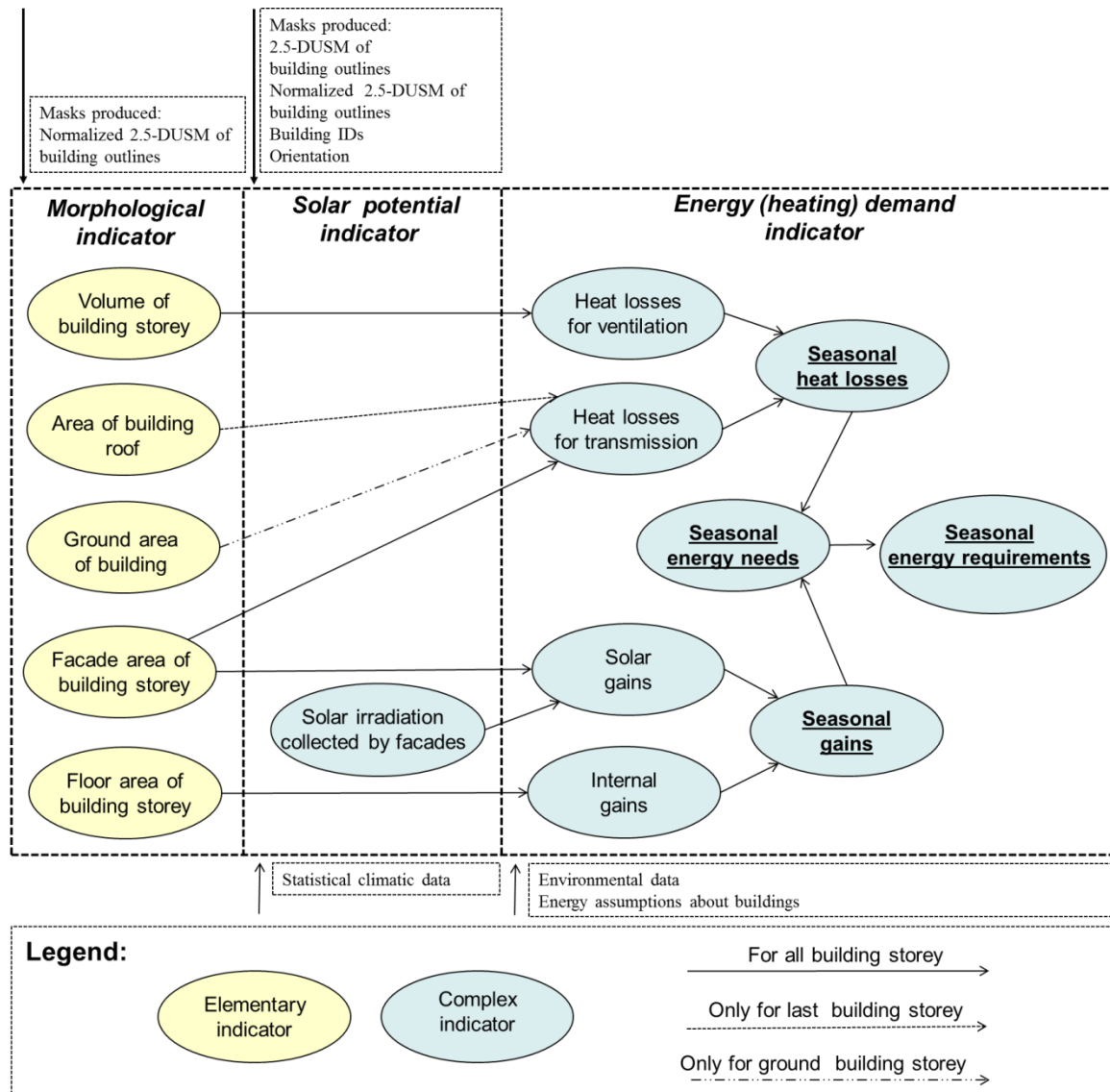


Figure 10.2. Integration of UEQ indicators inherent to different stakes and domains (mixed scenarios).

A main attention was given to LiDAR data, focusing on the development of new methods - based on a hybrid approach that uses this type of data with 2-D and 3-D vector data -, for an automatic and reliable step-by-step construction of different raster 2.5-DUSM and n2.5-DUSM. Those proved to be appropriate for the extraction of several UEQ indicators: the use of a raster format allowed to use a wide range of tools for complex analysis (e.g., solar analysis), at the neighbourhood and city scales, which otherwise would be too difficult to implement in such a fast way. The segmentation procedure for LiDAR data demonstrated to be: (1) an effective alternative to the use of the different 2.5-DUSM and n2.5-DUSM for the detection of independent roof planes in order to calculate its slope and orientation, and (2) essential in order to successfully achieve the innovative method proposed for the automatic and trustworthy classification of the type of roof of each building.

Finally, the enhancement method proposed for the used 2.5-DUSM and n2.5-DUSM demonstrated to be particularly important in order to improve the reliability of the extracted UEQ indicators, especially those related to particular analysis on building facades. A novel method based on the use of an enhanced n2.5-DUSM is the calculation of the areas of facades on an object-related (building) raster basis - results presented are extremely promising and highlight the potential of LiDAR data and derived 3-D models for the morphological analysis of cities.

This goal was successfully achieved by implementing the *bottom-up* process proposed by Maystre and Bollinger (1999), which allowed to define a list of 3-D urban models and data (using different 2-D and 3-D data sources) to be constructed in order to extract the UEQ indicators defined in the *top-down* process (already discussed in the review of the first goal of this section). Under this context, it is important to emphasize that the exploitation of LiDAR-based datasets and derived products (e.g., 2.5-DUSM and n2.5-DUSM) made it possible to enrich and improve the traditional data sources used (e.g., DEM and DHM). These correlated *top-down* and *bottom-up* processes were considered essential as a basis methodological framework for further development of empirical case-studies related to this research. Those aimed to develop and implement innovative methods and algorithms for a reliable extraction of a large set of UEQ indicators (including UEQ indexes).

Utility analysis about how end-users perceive and interpret the different exploratory 2-D, 2.5-D and 3-D geo-visualizations proposed

According to the preliminary end-users' requirements analysis presented in chapter 4, most of the UEQ indicators and some UEQ indexes should be visualized, however, the best way to represent them in a 3-D environment has not yet been defined. For this reason, a utility analysis about how the 25 end-users of the State of Geneva engaged in this study did perceive and interpret the different exploratory 2-D and 3-D geo-visualizations proposed for the extracted UEQ indicators was considered essential.

This goal was successfully achieved by analysing the relationship between a large set of 3-D UEQ indicators defined and extracted according to the correlated *top-down* and *bottom-up* processes proposed by Maystre and Bollinger (1999) and different hypothesis for 2-D and 3-D (includes 2.5-D) visualizations of this type of indicators. Thus, a final survey presenting a twofold objective was carried out: (1) to analyse the utility of the 3-D visualizations proposed for several quantitative UEQ indicators as an added-value for a better understanding of urban phenomena (Figure 10.3), and (2) to evaluate the acceptability of 3-D visualizations when compared to the long-established 2-D mapping. This final survey allowed to clearly outline that most end-users do not agree to generalize the use of 3-D city models for the representation of UEQ indicators. For these end-users, even if UEQ indicators have a 3-D dimension, the geo-visualization of most of them can be also done through the use of 2-D maps. In the case 3-D geo-visualizations environments are created, low levels of details (LoD1 and LoD2) should be used for the display of UEQ indicators. Indeed, very detailed urban models, on its own, do not offer a valuable clarification for geo-visualization of the greater part of UEQ indicators emphasized in this thesis.

10.3 Final outcome

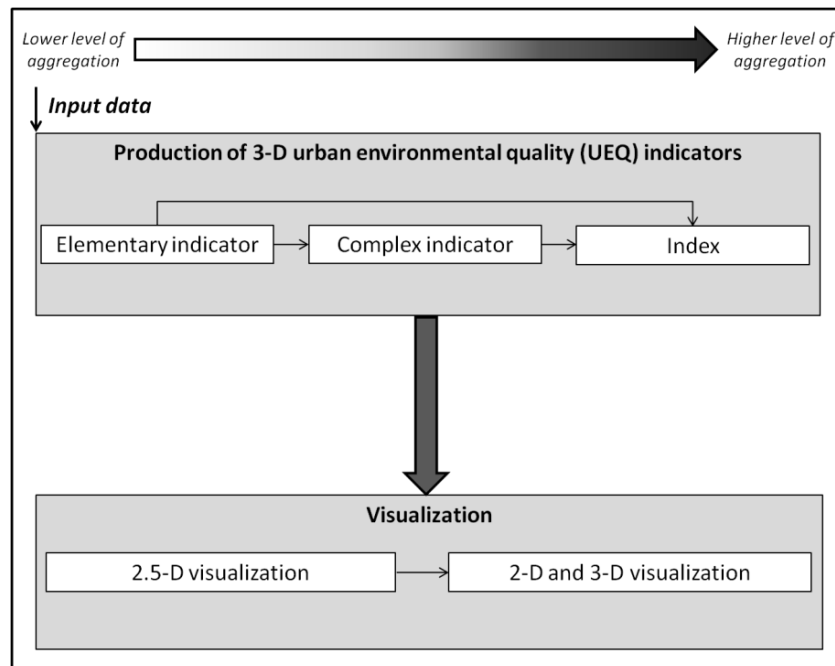


Figure 10.3. Synoptic view describing the method used for the extraction and visualization of UEQ indicators presenting a 3-D dimension: from lower to higher level of aggregation.

10.3 Final outcome

This thesis focused on the needs of specialized end-users that were interested in the extraction of UEQ indicators presenting a 3-D dimension. A double approach was implemented (Maystre and Bollinger, 1999): (1) *top-down* process, an analysis of the requirements among potential users of 3-D urban geo-referenced data, which allowed to define a list of UEQ indicators to be extracted (2) *bottom-up* process, the construction of 3-D urban models and data (using different 2-D and 3-D data sources) allowed to extract the UEQ indicators defined in point 1 in three main stakes. This was only feasible because several end-users (actors) were committed to the whole process, therefore facilitating the analysis of the different steps to be implemented. Moreover, the utility analysis related to the visualization of this type of indicators provided a general idea of how different modes of representation (2-D or 3-D, which includes 2.5-D) can be used and constructed in an urban environment. In fact, it was demonstrated that very detailed urban models apparently do not constitute an effective solution for the representation of this type of indicators. Thus, the tasks and the objectives of territory planners and urban designers must be carefully identified in order to be able to properly select a large set of indicators inherent to the urban development and the way in which they must be represented in a 3-D urban environment. Moreover, it should be highlighted that the case-studies studied proved to be extremely relevant inside the empirical research process of this thesis, therefore allowing to validate the significance and usefulness of the UEQ indicators extracted. The user requirements established for this study do not claim universality or completeness. Other cities, differing both in its nature and structure, will however imply different needs and therefore other indicators presenting a 3-D dimension. LiDAR technology proved to be a good option in order to automatically derive in a fast and accurate way the 2.5-DUSM and n2.5-DUSM used in this thesis, as it did not require to refer to the construction of complex models of the urban layout: mainly buildings and other urban objects that are reconstructed according to the LoD3 and LoD4 of the CityGML standard. Indeed, 2-D vector data of roofs resulting from the projection of 3-D roofs with a LoD1 and LoD2 (stored in a database of the city of Geneva) were used for the construction of the different 2.5-DUSM and

n2.5-DUSM emphasized in this thesis. It is also worth mentioning that if 3-D vector urban models are available, some indicators, e.g. morphological properties of buildings, are further easy and accurately computed using this type of representation. Thus, the use of methods and tools from digital image processing should not intend to substitute the usefulness and higher reliability of 3-D vector models for the extraction of many urban indicators. Nevertheless, as proposed and validated inside the framework of this thesis, the uniformity of the data structures allowing for a more easy combination and the applicability of methods and tools from digital image processing proved to be highly relevant for the analysis of cities.

In spite of several qualities, the airborne LiDAR systems are limited in the altimetric measurements (considering that the intensity of the return signal is not taken into account). If the use of an airborne platform facilitates a fast acquisition of the urban fabric, it however complicates the process of calibration of the data and the interpretation and construction of objects masked by other objects, mainly if an orthogonal perspective is considered, e.g. roofs covered by trees. Thus, LiDAR should not be taken into account as a competitor but as a complement to more traditional methods for the construction of more sophisticated 3-D urban models. Thus, the optimal solution to acquire a detailed and up to date knowledge of the urban fabric in the form of a 2.5-DUSM or a n2.5-DUSM is the combination of airborne LiDAR technology, photogrammetry and the inclusion of terrestrial inventories (which may be derived using terrestrial laser scanners). The high-resolution orthophoto can be very useful for the correct delimitation of vegetation, and the terrestrial laser scanners may allow the acquisition of more detailed information, for instance a more precise delimitation of the edges of buildings and existing elements of its facades (such as balconies). The data derived from terrestrial laser scanners can be also useful for the calibration of the data resulting from LiDAR technology.

Finally, an important question that may arise at the end of this thesis is: “*Could the analysis of 2.5-DUSM and n2.5-DUSM make a contribution to urban planning and related studies, which includes the extraction of relevant UEQ indicators presenting a 3-D dimension?*”. Considering the results emphasized in this thesis, it is possible to respond positively. Both 2.5-DUSM and n2.5-DUSM demonstrated to be a flexible support for storing, manipulating and analysing the geometry of the urban fabric, and also for the assessment of specific urban phenomena (aggregated in the form of UEQ indicators) occurring inside it. Furthermore, these methods are fast and easily reproducible and, according to the end-user’s requirements collected, the results achieved were considered sufficiently accurate if neighbourhood and city scales are considered for analysis.

10.4 Perspectives

10.4.1 Research perspectives

The question regarding the types of urban indicators that best synthesizes a significant UEQ assessment is still open. In fact, the variety as well as the amount of indicators proposed by environmental analysts to both urban planners and decision makers at the city scale may be counterproductive, whereby a selection of performance indicators should be identified to promote effective policies. In general, the current tendency of urban planning is to identify different typologies of urban textures and to promote context-specific environmental strategies in order to underline the peculiarity of each city or areas of the city under analysis - this last, as proposed inside the framework of this thesis, usually considering the neighbourhood scale of analysis. In this case, a range of indicators should be given, in order to guarantee that the objects (for instance, buildings) of the city under analysis refers to the proper strategy, which should be previously defined by an assessment of specific end-users' requirements. Furthermore, other

10.4 Perspectives

indicators (possibly also other indexes) not studied in this thesis may emerge and the best way to build them could eventually lead to novel research.

The selection of relevant and useful indicators should be done not only according to some goals, but in fact, also considering both utility and usability of a given indicators' system if it has to be visualized. Indeed, a given indicators' system cannot meet such requirements altogether, and therefore communication of 3-D geo-visualizations should be defined and adapted accordingly. This should be done by developing new interfaces, efficiently adapted for the interpretation of 3-D indicators by users more or less specialized. Indeed, during the last years, online geospatial systems have significantly evolved and thus, new interaction tools and functions are being put into operation (Ingensand, 2010). Today, a rising number of systems allow navigation in 3-D (e.g. Google Earth plug-in, porting 3-D-capabilities to web-browsers). Furthermore, new input devices arrived on the market (e.g. Logitech's 3-D Spatial Navigator device) and innovative tools for spatial navigation are being employed (e.g. "pinching" and "unpinching" for zooming in Apple's Iphone device). In order to keep up with these novel tendencies it is important to stress that new assessments will certainly be needed so as to validate both the usage and the usability of this type of indicators presenting a 3-D dimension within online geospatial systems.

The step-by-step based construction of the 2.5-DUSM and n2.5-DUSM used in this study, as well as the segmentation procedure for LiDAR data, were limited to the analysis and the exploitation of the altimetric nature of the LiDAR data used. However, spectral information - drawn from the imagery (orthophoto) colour or near infra-red - offers essential information (e.g., a better assessment of the urban zones covered by vegetation). The systematic integration of imagery in order to supplement or optimize the methods suggested in this study based on LiDAR data is undoubtedly a research axis that should be deepened. Similar approaches have been followed in the last years by some researchers (St-Onge *et al.*, 2008; Wang *et al.*, 2008). Moreover, taking into account the technologies that are currently under rapid development, it is very plausible that in the near future the extraction of indicators related to the morphological properties of buildings could be also performed through computer vision oriented photogrammetry which is currently presenting rather innovative methods for the automatic construction and interpretation of building facades.

The use of masks on an object-related raster basis - which is a new method that was proposed and applied in this thesis for the enhancement of the n2.5-DUSM used and for the extraction of the morphological properties of buildings - could certainly be an axis of research to be more deeply studied. In particular, it could be interesting to evaluate the relevance of applying such method for the extraction of other 3-D urban indicators not studied in this thesis.

It is also worth mentioning that the influence of the density of raw LiDAR points in the methods put into practice for the case-studies highlighted in this thesis is surely not insignificant. Although it was not the main intention of this research, it will certainly be pertinent for further studies to examine the impact of using lower or higher density of raw LiDAR points in the accuracy of the results attained, especially for all indicators related to the morphological properties of buildings.

Finally, it should be noted that a large number of new algorithms for the analysis of the 2.5-DUSM and n2.5-DUSM and therefore the extraction of other UEQ indicators could be imagined and implemented as a follow up of this work. However, despite not being possible to enumerate all of them here, a relevant example of an axis of research to be deepened could be the integration of these models in the assessment of urban pollutants dispersion.

10.4.2 Application perspectives

The methods and tools proposed in this thesis present a large margin of improvement with regards to the diffusion of this technique among professionals in the urban planning field. For instance, the procedure currently being used makes use of different GIS and raster images processing software and hence requires a deep specialization on several disciplines: 3-D urban models construction, GIS, environmental analysis, among others.

The UEQ indicators highlighted in this thesis form the basis of the development of further indicators and scenarios addressed to various urban applications:

- indicators related to the morphological analysis of buildings could lead to other interesting indicators (besides the ones highlighted in this thesis) that may be used by urban planners in order to predict the environmental behaviour of different urban textures;
- indicators related to the exploration of the solar potential on the urban fabric (mainly in buildings) can be applied in terms of urban energy planning and environmental policies devised at the level of community: inventory of well irradiated buildings, calculation of thermal and electrical potential for sun collectors, ratio to energy needs, among others (Figure 10.4);
- indicators related to the estimation of the energy demand on the urban fabric are important for the evaluation of different energy scenarios, and thus may provide valuable strategies to territory planners and urban designers in order to support integrated sustainable policies.

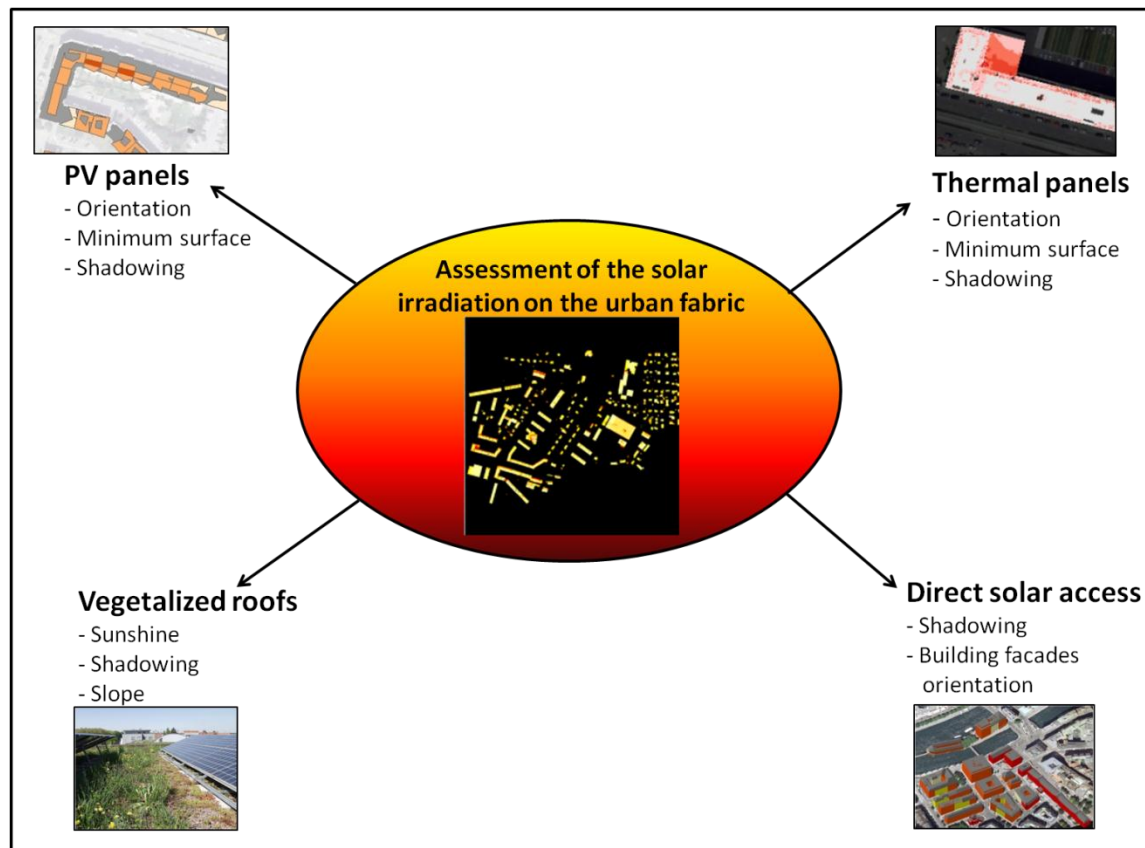


Figure 10.4. Different possibilities of application for the tool developed for the exploration of the solar potential on the urban fabric.

10.4 Perspectives

Future work should provide a common container with regards to managing different types of input data and to facilitate the computation of further indicators as those mentioned above.

10.4.3 Commercial perspectives

A better and more intuitive user interface as well as a reduction of steps among the software needed to run these tools would represent a relevant advantage concerning commercial perspectives. Indeed, the methods and tools emphasized in this thesis can be easily adapted to use free open source software, as they are friendly adaptable and they do not require high computation time or performance (a PC with 7– 9 GB RAM is sufficient). The case-studies developed in this thesis rely on the Matlab interface, which is rather user-unfriendly. Should this restriction be removed, this type of analysis may be more effectively diffused amongst potential end-users.

BIBLIOGRAPHY

- Aalders, H. (2002) The Registration of Quality in a GIS. In: Shi, W., Fisher, P. F., Goodchild, M. F. (Eds.), *Spatial Data Quality*, London, Taylor and Francis, pp. 186-199.
- Abdul-Rahman, A, Pilouk, M. (2008) *Spatial data modeling for 3-D GIS*. Springer, Berlin, Germany, 290 pp.
- Adriaanse, A. (1997) Environmental information management for use at the national level. In: Deelstra, T., Boyd, D. (Eds.), *Indicators for Sustainable Urban Development. The International Institute for the Urban Environment*, Delft, pp. 109-123.
- Alexander, C. (2005) *The nature of order: an essay on the art of building and the nature of the universe*. Center for Environmental Structure Publishing, Berkeley, California, USA, Vol.1, 476 pp.
- Alharthy, A., Bethel, J., Mikhail, E., M. (2004) Analysis and accuracy assessment of airborne laserscanning system. *The International Archives of the Photogrammetry, Remote Sensing and Spatial Information Sciences*, Vol. 35, part B2, pp. 144-149.
- Anderson, E. S., Thompson, J. A., Austin, R. E. (2005) LiDAR density and linear interpolator effects on elevation estimates. *International Journal of Remote Sensing*, Vol. 26, No. 18, pp. 3889-3900.
- Andrienko, N., Andrienko, G. (2003) Interactive maps for visual exploration of grid and vector geodata. *ISPRS Journal of Photogrammetry and Remote Sensing*. Vol. 57, No. 5-6, pp. 380-389.
- Andrienko, N., Andrienko, G. (2007) Intelligent visualization and information presentation for civil crisis management. *Transactions in GIS*. Vol. 11 (6), pp. 889-909.
- Appleton, K., Lovett, A. (2005) GIS-based visualisation of development proposals: reactions from planning and related professionals. *Computers, Environment and Urban Systems*. Vol. 29, pp. 321-339.
- Axelsson, P. (1992) Minimum description length as an estimator with robust properties. In: Foerstner, W., Ruwiedel, S. (Eds.), *Robust Computer Vision*, Wichmann, Verlag, Karlsruhe, Germany, pp. 137-150.
- Axelsson, P. (1999) Processing of laser scanner data - algorithms and applications. *The International Archives of the Photogrammetry, Remote Sensing and Spatial Information Sciences*, Vol. 54, Part 2, pp. 138-147.
- Baker, N., Steemers, K. (2000) *Energy and environment in architecture: a technical design guide*. Spon Press, London, UK, 240 pp.
- Balocco, C., Grazzini, G., Andreani, G. (2008) Rational Use and Energy Planning: A Thermodynamic and Geographical Approach. *Energy Efficiency Research Advances, Chapter "Research and Review Studies"*, NOVA Publ.Ed. D.M. Bergamann, New York, USA., pp.11-62.
- Baltsavias, E.P. (1999a) Airborne laser scanning: basic relations and formulas. *ISPRS Journal of Photogrammetry and Remote Sensing*, Vol. 54, Issue 2-3, pp.199-214.
- Baltsavias, E. (1999b) Airborne laser scanning: existing systems, firms and other resources. *ISPRS Journal of Photogrammetry & Remote Sensing*, Vol. 54, Issue 2-3, pp. 164-198.

Bibliography

- Barrenetxea, G., Ingelrest, F., Lu, Y. M., Vetterli., M. (2008) Assessing the challenges of environmental signal processing through the SensorScope project, *Proceedings of the 33rd IEEE International Conference on Acoustics, Speech, and Signal Processing (ICASSP)*, 30th March-4th April, Las Vegas, USA, pp. 5149-5152.
- Batara, A., Dave, B., Bishop, I. D. (2001) Translation between multiple representations of spatial data. *AURISA 2001*, Melbourne, Australia, pp. 1-10.
- Batty, M., Dodge, M., Jiang, B., Smith, A. (1999) Geographical information systems and urban design. In: Stillwell, J., Geertman, S., Openshaw, S. (Eds.), *Geographical Information and Planning*, Springer, Berlin, pp. 43-65.
- Batty, M., Longley, P. (1994) *Fractal cities: a geometry of form and function*, Academic Press, London, 394 pp.
- Bauler, T., Zaccai, E. (2004) *Indicateurs de développement durable*. In: Dictionnaire du Développement Durable Belge. Institut pour un Développement Durable – SSTC, 8 pp.
- Baxes G.A. (1994) *Digital image processing – Principles and applications*. John Wiley & Sons, New York, USA, 480 pp.
- Behan, A. (2000) On the matching accuracy of rasterized scanning laser altimeter data, *The International Archives of the Photogrammetry, Remote Sensing and Spatial Information Sciences*, Vol. 33, Part B2, pp. 75-82.
- Bell, S., Morse, S. (2000) *Sustainability Indicators: Measuring the Immeasurable?* Earthscan, London, UK, 240 pp.
- Berger, P., Nouhaud, J.-P. (2004) *Formes cachées, la ville*. Presses Polytechniques et Universitaires Romandes, Lausanne, Switzerland, 224 pp.
- Bishop, I., Lange, E. (2005) *Visualization in landscape and environmental planning. Technology and applications*. Taylor & Francis, London, UK, 320 pp.
- Biswas, S., Lohani, B. (2008) Development of high resolution 3-D sound model with LiDAR data and air photo. *The International Archives of the Photogrammetry, Remote Sensing and Spatial Information Sciences*, Vol. 37, pp. 1735-1740.
- Blanchet, C., November, A. (1998) *Indicateurs du développement durable appliqués à l'aménagement du territoire*, Publication of the CUEH and IUED, Genève, Switzerland.
- Borrego, C., Tchepel, O., Costa, A. M., Martins, H., Ferreira, J., Miranda, A. I. (2006) Traffic-related particulate air pollution exposure in urban areas. *Atmospheric Environment Journal*, Vol. 40 (37), pp. 7205-7214.
- Both J.F., Da Cunha, A., Mager, C. (2003) Evaluation du territoire, développement durable et indicateurs: un pragmatisme raisonné. In: Da Cunha, A., Ruegg, J. (Eds.), *Développement durable et aménagement du territoire*, PPUR, Lausanne, Switzerland.
- Brenner, C. (2004) Modelling 3-D objects using weak CSG primitives. *The International Archives of the Photogrammetry, Remote Sensing and Spatial Information Sciences*, Vol. 35, Part B3, pp. 1085-1090.
- Bretar, F. (2006) *Couplage de Données Laser Aéroporté et Photogrammétriques pour l'Analyse de Scènes Tridimensionnelles*. Unpublished Ph.D. thesis, Ecole Nationale Supérieure des Télécommunications, Paris, France.
- Burchell, R., Downs, A., McCann, B., Mukherji, S. (2005) *Sprawl Costs: Economic Impacts of Unchecked Development*. Island Press, London, UK, 208 pp.

Bibliography

- Burrough, P. A., McDonnell, R. A. (1998), *Principles of Geographical Information Systems*. Oxford University Press, 2nd Edition, 356 pp.
- Buziek, G., Dransch, D., Rase, W. D. (2000) *Dynamische Visualisierung—Grundlagen und Anwendungsbeispiele für kartographische Animationen*. Springer, Berlin, 235 pp.
- Canny, J. (1986) A Computational Approach To Edge Detection. *IEEE Transactions on Pattern Analysis and Machine Intelligence*, Vol. 8, pp. 679-714.
- Carneiro, C., Golay, F., Silva, V., Plazanet, C., Park, J. J. (2008) GIS and LiDAR data analysis for the integration of multidimensional indicators on urban morphogenesis multi-agent vector based geosimulation. In: Murgante, B., Borruoso, G., Lapucci, A. (Eds.) *Geocomputation and Urban Planning: Studies in Computational Intelligence*, Vol. 176, pp. 187-208.
- Chaplot, V., Darboux, F., Bourennane, H., Leguédou, S., Silvera, N., Phachomphon, K. (2006) Accuracy of interpolation techniques for the derivation of digital elevation models in relation to landform types and data density. *Geomorphology*, Vol. 77, Part 1-2, pp. 126-141.
- Charre, J., Maby, J., Martin, P., Dério, P., Laques, A.-E., Bachimon, P., Lajarge, R., Tanet, P. (2003) *Objects et indicateurs géographiques*. Edition des Actes d'Avignon (n°5), 316 pp.
- Chauve, A., Durrieu, S., Bretar, F., Pierrot-Deseilligny, M., Puech, W. (2007) Processing full-waveform LiDAR data to extract forest parameters and digital terrain model: validation in an alpine coniferous forest, *Proceedings of the ForestSat Conference*, Montpellier, France. (not paginated).
- Chen, Y., Su, W., Li, J., Sun, Z. (2009) Hierarchical object oriented classification using very high resolution imagery and LiDAR data over urban areas. *Advances in Space Research*, Vol. 43, pp. 1101-1110.
- Clode, S., Kootsookos, P., Rottensteiner, F. (2004). The Automatic Extraction of Roads from LiDAR Data. *The International Archives of the Photogrammetry, Remote Sensing and Spatial Information Sciences*, Vol. 35, Part B3, pp. 231-236.
- Cressie, N. (1993) *Statistics for Spatial Data*. John Wiley & Sons, New York, USA, 900 pp.
- Chrisman, N. R. (1998) Rethinking Levels of Measurement for Cartography. *Cartography and Geographic Information Science*. Vol. 25 (4), pp. 231-242.
- Chwieduk, D. A. (2009) Recommendation on modelling of solar energy incident on a building envelope. *Renewable Energy*. Vol. 34, No. 3, pp. 736-741.
- Compagnon, R. (1999) Evaluation du gisement solaire en milieu urbain. *Proceedings of the International Conference CISBAT*, Lausanne, Switzerland, pp. 137-142.
- Compagnon, R. (2004) Solar and daylight availability in the urban fabric. *Energy and building*, Vol. 36, pp. 321-328.
- Desthieux, G. (2005) *Approche systémique et participative du diagnostic urbain. Processus de représentation cognitive du système urbain en vue d'élaboration d'indicateurs géographiques*. Thesis n° 3216, Ecole Polytechnique Fédérale de Lausanne, Switzerland.
- Devillers, R., Bedard, Y., Jeansoulin, R. (2005) Multidimensional management of geospatial data quality information for its dynamic use within GIS. *Photogrammetric Engineering & Remote Sensing*, Vol. 71, N° 2, pp. 205-15
- DiBiase, D., MacEachren, A., Krygier, J. B., Reeves, C. (1992) Animation and the role of map design in scientific visualization. *Cartography and Geographic Information Systems*, Vol. 19 (4), pp. 201-214.

Bibliography

- Dong, F. (1996) *Three-dimensional models and applications in subsurface modeling*. Department of Geomatics Engineering Reports No. 20093, University of Calgary, Canada, 93 pp.
- Dubayah, R., Rich, P. M. (1996) GIS-based solar radiation modeling. In: Goodchild, M. F., Steyaert, L. T., Parks, B. O., Johnston, C., Maidment, D., Crane, M., Glendinning, S. (Eds.). *GIS and Environmental Modeling: Progress and Research Issues. Proceedings of the 2nd International Conference/Workshop on Integrating Geographic Information Systems and Environmental Modeling*, 26th-30th September, National Center for Geographic Information and Analysis, GIS World Books, Fort Collins, Breckenridge, Colorado, USA, pp. 129-134.
- Duffie, J. A., Beckman, W. A. (1991) *Solar engineering of thermal processes*. John Wiley & Sons, New York, 944 pp.
- Dumas, S., Redish, C. (1999) *A Practical Guide to Usability Testing*. Intellect Books, Exeter, United Kingdom, 404 pp.
- Durupt, M., Taillandier, F. (2006) Automatic building reconstruction from a digital elevation model and cadastral data: an operational approach. *The International Archives of the Photogrammetry, Remote Sensing and Spatial Information Sciences*, Vol. 36, Part 3, pp. 142-147.
- Eelberink, S. (2007) Re-using laser scanner data in applications on 3-D topography. *3-D Geoinfo07 Conference*, 12th-14th December, Delft University of Technology, Delft, Netherlands. (not paginated).
- Elberink, S. (2010) *Acquisition of 3-D topography. Automated 3D road and building reconstruction using airborne laser scanner data and topographic maps*. Unpublished Ph.D. thesis, International Institute for Geo-information Science and Earth Observation, Enschede, The Netherlands.
- Ellul, C., Haklay, M. (2006) Requirements for topology in 3-D GIS. *Transactions in GIS*, Vol. 10(2), pp. 157-175.
- EN prENV 1752 (1996) Ventilation of buildings. Design criteria for the indoor environment.
- Evseev, E. G., Avraham, I. K. (2009) The assessment of different models to predict the global solar radiation on a surface tilted to the south. *Solar Energy*. Vol. 83, No. 3, pp. 377-388.
- Fisher, P. F., Pyhtila, J. W. (2000) Timing quantization error in LiDAR-speed measurements devices. *IEEE Transactions on Vehicular Technology*, Vol. 49, Issue 1, pp. 276-280.
- Fisher, P. F., Tate, N. J. (2006) Causes and consequences of error in digital elevation models. *Progress in Physical Geography*, Vol. 30, No. 4, pp. 467-489.
- Franklin, W.R. (1973) *Triangulated irregular network program*. Downloadable from <ftp://ftp.cs.rpi.edu/pub/franklin/tin73.tar.gz>.
- Gachet, G. (2009) *Analyse et exploitation des données de LiDAR aéroportées pour la caractérisation des milieux boisés de la Suisse*. Thesis n° 3216, Ecole Polytechnique Fédérale de Lausanne, Switzerland.
- Gadsden, S., Rylatt, M., Lomas, K., Robinson, D., (2003) Predicting the urban solar fraction: a methodology for energy advisers and planners based on GIS. *Energy and Buildings*, Vol. 35, No. 1, pp.37-48
- Gallopin, G.C. (1997) Indicators and their use: information for decision-making. In: Moldan, B., Billharz, S. (Eds.). *Sustainability Indicators: Report of the Project on Indicators of Sustainable Development*. SCOPE 58, John Wiley & Sons, Chichester, pp.13-27.

Bibliography

- Givoni, B. (1998) *Climate considerations in building and urban design*. John Wiley & Sons, New York, USA, 480 pp.
- Glenn, T., Watson, I. (1984) The Determination of View-Factors in Urban Canyons. *Journal of Climate and Applied Meteorology*, Vol. 33, pp. 329-335.
- Glennie, C.L. (2007) Rigorous 3-D Error Analysis of Kinematic Scanning LiDAR Systems. *Journal of Applied Geodesy*, Vol. 1, pp. 147-157.
- Gonçalves, G. (2006) Analysis of interpolation errors in urban digital surface models created from LiDAR data. *Proceedings of the 7th International Symposium on Spatial Accuracy, Assessment in Resources and Environment Sciences*. pp. 160-168.
- Gonzalez, R. C., Woods, R. E., Eddins, S. L. (2009) *Digital Image Processing using Matlab*. Prentice Hall, 624 pp.
- Gori, V. (2010) *Metodi di valutazione dei fabbisogni energetici di aree diversamente edificate*. Not published Master Thesis, Università degli Studi di Firenze, Facoltà di Ingegneria, Corso di Laurea in Scienze dell' Ingegneria Edile.
- Guthe, M., Klein, R. (2003) Efficient NURBS Rendering using View-Dependent LoD and Normal Map. *Journal of WSCGs* (Int. Conf. in Central Europe on Computer Graphics, Visualization and Computer Vision), 3rd-7th February Plzen, Czech Republic. (not paginated).
- Haala, N., Kaada, M. (2010) "An update on automatic 3D building reconstruction". *ISPRS Journal of Photogrammetry and Remote Sensing*, Vol. 65, Issue 6, pp. 570-580.
- Haber, R. B., McNabb, D. A. (1990) Visualization idioms: a conceptual model for scientific visualization systems. In: Nielson, G., Shriver, B., Rosenblum, L. (Eds.), *Visualization in Scientific Computing*. IEEE Computer Society Press, Los Alamitos, California, pp. 74-93.
- Hall, P., Pfeiffer, U. (2000) *Urban future 21. A global agenda for 21st century cities*. Spon Press, New York, USA, 363 pp.
- Hay, J. E. (1979) Calculation of monthly mean solar radiation for horizontal and inclined surfaces. *Solar Energy*. Vol. 23, No. 4, pp. 301-330.
- Hehl-Lange, S. (2001) Structural elements of the visual landscape and their ecological functions. *Landscape and Urban Planning*. Vol. 54, pp. 105-113.
- Heißenhuber, A., Kantelhardt, J., Schaller, J., Magel, H. (2004) Visualisierung und Bewertung ausgewählter Landnutzungsentwicklungen. *Natur und Landschaft*. Vol. 79 (4), pp. 159-166.
- Hofmann, A. D., Maas, H. G., Streilein, A. (2003) Derivation of roof types by cluster analysis in parameter spaces of airborne laserscanner point clouds. *The International Archives of the Photogrammetry, Remote Sensing and Spatial Information Sciences*, Vol. 34, Part 3/W13, pp. 112-117.
- Hofmann, A. (2004) Analysis of TIN structure parameter spaces in airborne laser scanner data for 3-D building model generation. *The International Archives of the Photogrammetry, Remote Sensing and Spatial Information Sciences*, Vol. XXXV, Part B3, pp. 302-307.
- Hottel, H. C., Woertz, B.B. (1942) Performance of Flat-Plate Solar Heat Collectors. *American Society for Mechanical Engineer Journal*, Vol. 64, pp. 91-104.
- Incropera, F., DeWitt, D. (1960) *Introduction to heat transfer*. New York: John Wiley & Sons, 912 pp.
- Ingensand, J. (2010) *User interaction with online geospatial systems*. Thesis n° 4618, Ecole Polytechnique Fédérale de Lausanne, Switzerland.

Bibliography

- Innes, J.E. (1990) *Knowledge and Public Policy: The Search for Meaningful Indicators*. Transaction Publishers, New Brunswick, 375 pp.
- Iqbal, M. (1983) *An Introduction to Solar Radiation*, Academic Press, New York, 390 pp.
- Jähne, B. (2005) *Digital Image Processing*. Springer, Berlin, Germany, 650 pp.
- Jaynes, C., Riseman, E., Hanson, A. (2003) Recognition and reconstruction of buildings from multiple aerial images. *Computer Vision and Image Understanding*, Vol. 90, pp. 69-98.
- Jenks, M., Burton, E., Williams, K. (1996) *The Compact City: A Sustainable Urban Form?*, E & FN Spon, London, UK, 360 pp.
- Jenks, M., Burton, E., Williams, K. (2000) *Achieving Sustainable Urban Form*, E & FN Spon, London, UK, 408 pp.
- Jochem, A., Höfle, B., Rutzinger, M., Pfeifer, N. (2009) Automatic roof plane detection and analysis in airborne LiDAR point clouds for solar potential assessment. *Sensors*, Vol. 9 (7), pp. 5241-5262.
- Joerin, F. (1998) *Décider sur le territoire; proposition d'une approche par utilisation de SIG et de méthodes d'analyse multicritère*. Thesis n° 1755, Ecole Polytechnique Fédérale de Lausanne, Switzerland.
- Joerin, F., Nembrini, A., Billeau, S., Desthieux, G. (2005) Indicateurs spatialisés : un instrument de participation en aménagement du territoire. *Revue Internationale de Géomatique*. Vol. 15 (1), pp. 33-61.
- Kalbermatten, M. (2010) *Multiscale analysis of high resolution digital elevation models using the wavelet transform*. Thesis n° 4610, Ecole Polytechnique Fédérale de Lausanne, Switzerland.
- Kämpf, J. H., Montavon, M., Bunyesc, J., Bolliger, R., Robinson, D. (2009) Optimisation of buildings' solar irradiation availability. *Solar Energy*. Vol. 84 (4), pp. 596-603.
- Karzand, M. (2009) *Physics-based data analysis for the SensorScope project*. Unpublished MSc thesis, Ecole Polytechnique Fédérale de Lausanne, Switzerland.
- Kassner, R., Koppe, W., Schüttenberg, T., Bareth, G. (2008) Analysis of the Solar Potential of Roofs by Using Official LiDAR data. *The International Archives of the Photogrammetry, Remote Sensing and Spatial Information Sciences*, Vol. 37, Part B4, pp. 399-404.
- Kilian, J., Haala, N., Englich, M. (1996) Capture and evaluation of airborne laser scanner data. *The International Archives of the Photogrammetry, Remote Sensing and Spatial Information Sciences*, Vol. 31, Part 3, pp. 383-388.
- Knowles, R.L. (1978) *Energy and Form: an Ecological Approach to Urban Growth*. MIT Press, Cambridge, Massachusetts, USA, 208 pp.
- Knowles, R.L. (1985) *Sun Rhythm Form*. MIT Press, Cambridge, Massachusetts, USA, 303 pp.
- Kolbe T., Gröger G. (2004) Unified Representation of 3-D City Models. *Geoinformation Science Journal*. Vol.4, No. 1. (not paginated).
- Kolbe T., Gröger G., Plümer, L. (2005). CityGML - Interoperable Access to 3-D City Models. In: Van Oosterom, P., Zlatanova, S., Fendel, E. (Eds.): *Proceedings of the Int. Symposium on Geoinformation for Disaster Management*, 21st-23rd March, Delft, Netherlands, Springer. (not paginated).

Bibliography

- Koomen, E., Bação, F. (2005) Searching for the polycentric city: a spatio-temporal analysis of Dutch urban morphology. *Proceedings of the 8th AGILE Conference on GIS*, May 26th- 28th, Lisbon, Portugal. (not paginated).
- Krarti, M., Erickson, P. M., Hillman, T. C. (2005) A simplified method to estimate energy savings of artificial lighting. *Building and Environment*, Vol. 40, pp. 747–754.
- Kumar, L., Skidmore, A., Knowles, E. (1997) Modelling topographic variation in solar radiation in a GIS environment. *International Journal of Geographical Information Systems*, Vol. 11 (5), pp. 475-497.
- Kyriakidis, P. C., Goodchild, M. F. (2006) On the prediction of error variance of three common spatial interpolation schemes. *International Journal of Geographical Information Science*, Vol. 20, No. 8, pp. 823-855.
- Lachal, B. (2000) *ENERCAD, calcul de la production de chaleur de capteurs solaire sur une base mensuelle*. Rapport du CUEPE de l'Université de Genève, Switzerland.
- Lange, E. (1998) *Realität und Computergestützt Visuelle Simulation*. Unpublished PhD Thesis, ETHZ, Zurich, Switzerland.
- Larkham, P. J., Jones, A. N. (1991) *A glossary of urban form*. IBG Historical Geography Research Series 26, GeoBooks, Norwich, UK, 95 pp.
- Larkham, P. J. (2002) Missing 'morphology'? *Urban Morphology*, Vol. 6(2), pp. 95-98.
- Lemp, D., Weidner, U. (2005) Improvements of roof surface classification using hyperspectral and laser scanning data. *The International Archives of the Photogrammetry, Remote Sensing and Spatial Information Sciences*, Vol. 36, Part 8/W27. (not paginated).
- Li, R. (1994) Data structures and application issues in 3-D geographic information systems. *Geomatica*, Vol. 48, No. 3, pp. 209-224.
- Li, Z., Zhu, Q., Gold, C. (2005) *Digital Terrain Modeling, Principles and Methodology*. CRC Press, London, UK, 323 pp.
- Lim, C. (2007) *Estimation of Urban Tree Crown Volume based on Object-oriented approach and LiDAR Data*. Unpublished MSc thesis, International Institute for Geo-Information Science and Earth Observation, Enschede, The Netherlands.
- Littlefair, P. J., Santamouris, M., Alvarez, S., Dupagne, A., Hall, D., Teller, J., Coronel, J. F., Papanikolaou, N. (2000) *Environmental site layout planning: solar access, microclimate and passive cooling in urban areas*. BRE Publications, CRC Ltd, London, pp. 77-82.
- Liu, B. Y, Jordan, R. C. (1961) Daily insolation on surfaces tilted towards to equator. *ASHRAE Journal*, Vol. 3 (10), pp. 53-59.
- Liu, X., Zhang, Z., Peterson, J., Chandra, S. (2007) The effect of LiDAR data density on DEM accuracy. *Proceedings of the International congress on modelling and simulation (MODSIM07)*, Christchurch, New Zealand, pp. 1363-1369.
- Liu, X. (2008) Airborne LiDAR for DEM generation: some critical issues. *Progress in Physical Geography*, Vol. 32, No. 1. pp. 31-49.
- Liu, J. G., Mason, P. J. (2009) *Essential Image Processing and GIS for remote Sensing*. Wiley-Blackwell, John Wiley & Sons, Oxford, UK, 460 pp.
- Lloyd, C. D., Atkinson, P. M. (2006) Deriving ground surface digital elevation models from LiDAR data with geostatistics. *International Journal of Geographical Information Science*, Vol. 20, No. 5, pp. 535-563.

Bibliography

- Lorenz, H., Döllner, J. (2010) 3D feature surface properties and their application in geovisualization. *Computers, Environment and Urban Systems*, Vol. 34 (6), pp. 476-483.
- Luethy, J., Stengele, R. (2005) 3-D mapping of Switzerland challenges and experiences. *The International Archives of the Photogrammetry, Remote Sensing and Spatial Information Sciences*, Vol. 36, Part 3, pp. 42-47.
- Maas, S., Döllner, J. (2008) Seamless integration of labels into interactive virtual 3D environments using parameterized hulls. In: Brown, P., Cunningham, D. W., Interrante, V., MacCormack, J. (Eds.), *Proceedings of the 4th International Symposium on Computational Aesthetics in Graphics, Visualization, and Imaging*, The Eurographics Association, Lisbon, Portugal, pp. 33-40.
- MacEachren, A.M., Kraak, M.-J. (2001) Research challenges in geo-visualization. *Cartography and Geographic Information Science*. Vol.28 (1), pp. 3-12.
- Malczewski, J. (1999) *GIS and Multicriteria decision analysis*, Toronto, Johns Wiley & Sons, 408 pp.
- Martin, L., March, L., (1972) *Urban Space and Structures*. Cambridge University Press, Cambridge, UK, 279 pp.
- Maystre, L. Y., Bollinger, D. (1999) Aide à la Négociation Multicritère. *Presses Polytechniques et Universitaires Romandes*, Lausanne, Switzerland.
- McCormick, B. H., DeFanti, T. A., Brown, M. D. (1987) Visualization in scientific computing. *Computer graphics*, Vol. 21 (6), pp. 15-21.
- Mesev, V. (2010) Scale of analysis: Micro versus macro remote sensing. *Proceedings of the Sixth International Conference on Geographic Information Sciences*. 14th-17th September, Zurich. (not paginated).
- Miguet, F., Groleau, D. (2002) A daylight simulation tool for urban and architectural spaces: Application to transmitted direct and diffuse light through glazing. *Building and Environment*, Vol. 37 (8/9), pp. 833-843.
- Molines, N., Siret, D., Musy, M., Groleau, D., (2006) Benefits and limits of GIS for managing heterogeneous environmental data in sustainable urban design: example of the ADEQUA project. *Proceedings of the 9th International Conference on Geographic Information Science*, 20th-22th April, Visegrad, Hungary. (not paginated).
- Montavon, M. (2010) *Optimisation of Urban Form by the Evaluation of Solar Potential*. Thesis n° 4657, Ecole Polytechnique Fédérale de Lausanne, Switzerland.
- Moore, I. D., Greyson, R. B., Ladson, A. R. (1991) Digital terrain modelling: a review of hydrological, geomorphological and biological applications. *Hydrological Processes*, Vol. 5(1), pp. 3-30.
- Morello, E. (2006) *The urban morphology and the environmental quality: Tools to assess the strategies for the compact city at the scale of urban design*. Unpublished Ph.D. thesis, Politecnico di Milano, Italy.
- Morello, E., Ratti, C. (2007) Raster Cities: image processing techniques for environmental urban analysis. In: Thwaites, K., Porta, S., Romice, O., Greaves, M. (Eds.), *Urban Sustainability through Environmental Design: approaches to time, people and place responsive urban spaces*, Spon Press, London, UK, pp. 119-122.

Bibliography

- Morello, E., Gori, V., Balocco, C., Ratti, C. (2009) Sustainable Urban Block Design Through Passive Architecture: A Tool that Uses Urban Geometry Optimization to Compute Energy Savings. *Proceedings of the 26th International Conference on Passive and Low Energy Architecture (PLEA)*, 22nd-24th June 2009, Quebec City, Canada, pp. 146-151.
- Morello, E., Ratti, C. (2009a) SunScapes: 'solar envelopes' and the analysis of urban DEMs. *Computers, Environment and Urban Systems*, Vol. 33, pp. 26-34.
- Morello, E., Ratti, C. (2009b) A Digital Image of the City: 3-D isovists in Lynch's Urban Analysis. *Environment and Planning B: Planning and Design*, Vol. 36, pp. 837-853.
- Morin, K. (2002) *Calibration of airborne laser scanners*, The University of Calgary, Canada, 135 pp.
- Muneer, T. (1997) *Solar Radiation and Daylight Models for the Energy Efficient Design of Buildings*. Architectural Press, Oxford, UK, 224 pp.
- Neidhart, H., Sester, M. (2006) Creating a digital thermal map using laser scanning and GIS. *10th International Symposium on District Heating and Cooling*, Section 3 – Technology trends, the prospect of dispersed energy: CHP and DH/DC, Hanover University of Technology, Germany. (not paginated).
- Nielsen, A. (2005) Visual representations, usability and urban planning in real-time 3-D geovisualization. *Proceedings of the 8th International Conference on Geographic Information Science*, 26th-28th May, Estoril, Portugal. (not paginated).
- OCDE (1997) *Mieux comprendre nos villes. Le rôle des indicateurs urbains*. Collection Développement territorial. OCDE, Paris, France.
- OFS, ARE, Buwal (2003) Monitoring du développement durable. MONET. *Rapport final: Méthodes et résultats*. Neuchâtel, Switzerland.
- Osaragi, T., Otani, I. (2007) Effects of ground surface relief in 3-D spatial analysis on residential environment. In: Fabrikant, S., Wachowicz, M. (Eds.), *The European Information Society: Lecture notes in Geoinformation and Cartography*, Springer, Berlin, pp. 171-186.
- Pastille (2002) *Indicators into action: local sustainability indicators sets and their context*. Final report.
- Perez, R., Stewart, R., Arbogast, R., Seals, J., Scott, J. (1986) An anisotropic hourly diffuse radiation model for surfaces: description, performance validation, site dependency evaluation. *Solar Energy*, Vol. 36, No. 6, pp. 481-497.
- Perez, R., Seals, R., Ineichen, P., Stewart, R., Menicucci, D. (1987) A new simplified version of the perez diffuse irradiance model for tilted surfaces. *Solar Energy*, Vol. 39, No. 3, pp. 221-231.
- Perez, R., Ineichen, P., Seals, R., Michalsky, J. J., Stewart, R. (1990) Modelling daylight availability and irradiance components from direct and global irradiance. *Solar Energy*, Vol. 44, No. 5, pp. 271-289.
- Peucker, T.K. (1978) Data structures for digital terrain models: discussion and comparison. In: Dutton, G. (Ed.), *First International Advanced Study Symposium on Topological Data Structures for Geographical Information Systems*, Harvard paper on GIS, Vol. 5.
- Prélaç-Droux, R. (2001) *Planification territoriale*. Lecture notes.
- Quint, F., Landes, S. (1996) Colour aerial image segmentation using a Bayesian homogeneity predicate and map knowledge. *The International Archives of the Photogrammetry, Remote Sensing and Spatial Information Sciences*, Vol. 31, Part B3, pp. 663-668.

Bibliography

- Ratti, C. (2002) *Urban analysis for environmental prediction*. Unpublished Ph.D. thesis, University of Cambridge, UK.
- Ratti, C., Richens, P. (2004) Raster analysis of urban form. *Environment and Planning B: Planning and Design*, Vol. 31, pp. 297-309.
- Ratti, C., Baker, N., Steemers, K. (2005) Energy consumption and urban texture. *Energy and Buildings*, Vol. 37 (7), pp. 762-776.
- Ratti, C., Di Sabatino, S., Britter, R. (2006) Urban texture analysis with image processing techniques: winds and dispersion. *Theoretical and Applied Climatology*, Volume 84, pp. 77-90.
- Reichenbacher, T., Swienty, O. (2007) Attention-guiding geovisualization. *Proceedings of the 10th AGILE International Conference on Geographic Information Science*, 8th-11th May, Aalborg University, Denmark. (not paginated).
- Reitberger, J., Krzystek, P., Stilla, U. (2008) 3-D segmentation and classification of single trees with full waveform LiDAR data. *Proceedings of SilviLaser 2008, 8th International Conference on LiDAR Applications in Forest Assessment and Inventory*, Edinburgh, UK, pp. 216-226.
- Repetti, A., Desthieux, G. (2006) A relational indicator set model for urban land-use planning and management: Methodological approach and application in two case studies, *Landscape and Urban Planning*, Vol. 77, No1-2, pp. 196-215.
- Rissanen, J. (1983) A universal prior for integers and estimation by minimum description length. *The Annals of Statistics*, Vol. 11, No. 2, pp. 416-431.
- Robinson, G. J. (1994) The accuracy of digital elevation models derived from digitised contour data. *Photogrammetric Record*, Vol. 14, No. 83, pp. 805-814.
- Robinson, D., Stone, A. (2005) A simplified radiosity algorithm for general urban radiation exchange, *Building Services Engineering Research and Technology*, Vol. 36, No. 4, pp. 271-284.
- Robinson, D., Scartezzini, J., Montavon, M., Compagnon, R. (2005) *Solurban: Solar Utilisation Potential of Urban Sites*, Tech. Rep., Swiss Federal Office of Energy, June.
- Rogers, R. (1997) *Cities for a small planet*. Faber & Faber, London, UK, 196 pp.
- Roncayolo, M. (1988) *La ville et ses territoires*, Gallimard, Paris, France, 278 pp.
- Rotmans, J., de Vries, B. (1997) *Perspectives on Global Change: The TARGET Approach*. Cambridge University Press, Cambridge, UK, 479 pp.
- Rottensteiner, F., Briese, C. (2002) A new method for building extraction in urban areas from high-resolution LiDAR data. *The International Archives of the Photogrammetry, Remote Sensing and Spatial Information Sciences*, Vol. 34, Part 3A, pp. 295-301.
- Rottensteiner, F., Briese, C. (2003) Automatic generation of building models from LiDAR data and the integration of aerial images. *The International Archives of the Photogrammetry, Remote Sensing and Spatial Information Sciences*, Vol. 34, Part 3/W13. (pp. on CD-ROM).
- Rottensteiner, F., Trinder, J., Clode, S., Kubik, K. (2005) Automated delineation of roof planes from LiDAR data, *The International Archives of the Photogrammetry, Remote Sensing and Spatial Information Sciences*, Vol. 36, Part 3/W19, pp. 221-226.
- Rylatt, M., Gadsden, S., Lomas, K. (2001) GIS-based decision support for solar energy planning in urban environments, *Computers, Environment and Urban Systems*, Vol. 25, pp. 579-603.
- Samet, H. (1990) *The design and analysis of spatial data structures*. Addison-Wesley, Massachusetts, USA, 510 pp.

Bibliography

- Schwalbe, E., Maas, H.-G., Seidel, F. (2004) 3-D building model generation from airborne laser scanner data using 2-D GIS data and orthogonal point cloud projections. *The International Archives of the Photogrammetry, Remote Sensing and Spatial Information Sciences*, Vol. 36, Part 3/W19, pp. 209-214.
- Serra J. (1968) Les structures gigognes: morphologie mathématique et interprétation métallogénique. *Mineralium Deposita*, Vol. 3, pp. 135-154.
- Shepard, D. (1968) A two-dimensional interpolation function for irregularly-spaced data. In: R.B. Blue, Sr. and Rosenberg (Eds.), *Proceedings of the 1968 ACM National Conference*, ACM Press, New York, USA, pp. 517-524.
- Shi, W. Z., Tian, Y. (2006) A hybrid interpolation method for the refinement of a regular grid digital elevation model. *International Journal of Geographical Information Science*, Vol. 20, No. 1, pp. 53-67.
- Sillion, F. X., Puech, C. (1994) *Radiosity and global illumination*. Morgan Kaufmann Publishers, San Francisco, 251 pp.
- Silva, V. (2010) *Conception et évaluation d'un prototype de simulation de la morphogenèse urbaine par agents vecteurs multi-échelles*. Thesis n° 4761, Ecole Polytechnique Fédérale de Lausanne, Switzerland.
- Sithole, G., Vosselmann, G. (2003) Comparison of Filtering algorithms. *Proceedings of the ISPRS workgroupIII/3 workshop*, Dresden, Germany, pp. 71-78.
- Slocum, T. A., Clibum, D. C., Feddema, J. J., Miller, J. R. (2003) Evaluating the usability of a tool for visualizing the uncertainty of the future global water balance. *Cartography and Geographic Information Science*. Vol. 30, pp. 299-317.
- Smith, S.L, Holland, D.A., Longley, P.A. (2004) The Importance of Understanding Error in LiDAR Digital Elevation Models. *The International Archives of the Photogrammetry, Remote Sensing and Spatial Information Sciences*, Vol. 35, pp. 996-1001.
- Souza, L., Rodrigues, D., Mendes, J. (2003) A 3-D-GIS extension for sky view factors assessment in urban environment. *The 8th International Conference on Computers in Urban Planning and Urban Management "CUPUM '03 Sendai"*, 27-29 May, Japan. (not paginated).
- Stanilov, K. (2003) Sustainability and urban morphology, *Urban Morphology*, Vol. 7(1), pp. 43-45.
- Stemmers, K., Ratti, C. (1999) Informing Urban Bioclimatic Design. *Proceedings of the Architecture and Engineering Conference, European Association for Architectural Education (EAAE)*, University of Plymouth, Plymouth, UK. (not paginated).
- Stevens, S. S. (1946) On the theory of scales of measurement. *Science*. Vol. 103 (2684), pp. 677-680.
- St-Onge, B., Vega, C., Fournier, R. A., Hu, Y. (2008) Mapping canopy height using a combination of digital stereo-photogrammetry and lidar. *International Journal of Remote Sensing*, Vol. 29, pp. 3343-3364.
- Szokolay, S. V. (2004) *Introduction to architectural science: the basis of sustainable design*. Elsevier, Architectural Press, Amsterdam, Boston, 352 pp.
- Takase, Y., Sho, N., Sone, A., Shimiyama, K. (2003) Automatic generation of 3-D city models and related applications. *The International Archives of the Photogrammetry, Remote Sensing and Spatial Information Sciences*, Vol. 34 (5). (not paginated).

Bibliography

- Tao, V. (2006) 3-D data acquisition and object reconstruction for AEC/CAD. In: Zlatanova S. and Prospero, D. (Eds.), *Large-scale 3-D Data Integration*, Taylor & Francis, London, UK, pp. 39-56.
- Teller, J., Azar, S. (2001) TOWNSCOPE II—A computer system to support solar access decision making. *Solar Energy*, Vol. LXX, pp. 187-200.
- Theler, D., Reynard, E. (2008) Mapping sediment transfer processes using GIS applications. *Proceedings of the 6th ICA Mountain Cartography Workshop*, International Cartographic Association, 11th-15th February, Lenk, Switzerland, pp. 227-234.
- Tomlin C. D. (1983) A map algebra. *Proceedings of the 1983 Harvard Computer Graphics Conference*, Cambridge, Massachusetts, USA, Volume 2, pp. 127-150.
- Tomlin C.D. (1990) *Geographic Information Systems and Cartographic Modeling*. Prentice Hall, Englewood Cliffs, New Jersey, USA, 572 pp.
- Urban Task Force (1999) Towards an urban renaissance: final report of the Urban Task Force. Chaired by Lord Rogers of Riverside, E & FN Spon, London.
- UNI - TS 11300-1 (2008) Energy performance of buildings – Part 1: Evaluation of energy need for space heating and cooling.
- United Nations Centre for Human Settlements (UNCHS) (1995) *Indicators Programme*, Vol. 1, 2 and 3. UNCHS, Nairobi.
- Verbree, E., Van Maren, G., Germs, R., Jansen, F., Kraak, M. (1999) Interaction in virtual world views - Linking 3-D GIS with VR. *International Journal of Geographic Information Science*. Vol. 13 (4), pp. 385-396.
- Vieira de Mello, A. (2006) *Projet de levé de la troisième dimension dans la mensuration officielle*. Unpublished document. Direction Cantonale de la Mensuration Officielle (DCMO). Services des Systèmes d'Information et de Géomatique (SSIG).
- Vögtle, T., Steinle, E. (2000) 3-D modelling of buildings using laser scanning and spectral information. *The International Archives of the Photogrammetry, Remote Sensing and Spatial Information Sciences*, Vol. 33, Part B3, pp. 927-934.
- Vögtle, T., Steinle, E., Tóvári, D. (2005) Airborne laserscanning data for determination of suitable areas for photovoltaics. *The International Archives of the Photogrammetry, Remote Sensing and Spatial Information Sciences*, Vol. 36, Part 3, pp. 215-220.
- Von Stokar, T., Frick, R. *et al.* (2001) *Planification Directrice Cantonale et Développement Durable*. Publication interne, Office du Développement Territorial, Berne. 62 pp.
- Vosselman, G. (1999) Building reconstruction using planar faces in very high density height data. *The International Archives of the Photogrammetry, Remote Sensing and Spatial Information Sciences*, Vol. 32, pp. 87-92.
- Vosselman, G. (2000) Slope based filtering of laser altimetry data. *Proceedings of IAPRS*, Amsterdam, The Netherlands, Vol. 33, Part B3, pp. 935-942.
- Vosselmann, G., Dijkman, S. (2001) 3-D building model reconstruction from point clouds and ground plans. *The International Archives of the Photogrammetry, Remote Sensing and Spatial Information Sciences*, Vol. 34, Part 3/W4, pp. 37-44.
- Wang, Z., Boesch, R., Ginzler, C. (2008) Integration of high resolution aerial images and airborne LiDAR data for forest delineation. *The International Archives of the Photogrammetry, Remote Sensing and Spatial Information Sciences*, Vol. 37, Part B7, pp. 1203-1207.

Bibliography

- Ward, G. J. (1994) The RADIANCE Lighting Simulation and Rendering System, Proceedings of the 21st annual conference on Computer graphics and interactive techniques (SIGGRAPH), 24th-29th July, Orlando, USA, pp. 459-72.
- Wehr, A., Lohr, U. (1999) Airborne laser scanning - an introduction and overview. *ISPRS Journal of Photogrammetry and Remote Sensing*, Vol. 54, pp. 68-82.
- Wissen, U., Lange, E., Schmid, W.A. (2005) Optimizing the visualization of 3-D-information for participative planning. In: Buhmann, E., Paar, P., Bishop, I., Lange, E. (Eds.), *Proceedings of the Trends in Real-Time Landscape Visualization and Participation*. Anhalt University of Applied Sciences, Wichmann, Heidelberg, pp. 237-245.
- Wissen, U. (2007) *Virtuelle Landschaften zur partizipativen Planung: Optimierung von 3-D Landschaftsvisualisierungen zur Informationsvermittlung*. Thesis n° 17182, Eidgenössische Technische Hochschule ETH Zürich.
- Wolff, M., Asche, H. (2010) Towards spatio-temporal 3-D tactical intelligence assessments for crime scene analysis. *Lectures Notes in Computer Science, Computational Science and its Applications*, ICCSA 2010, Springer Berlin, pp. 346-360.
- Wood, J., Kirschenbauer, S., Döllner, J. (2005) Using 3-D in Visualization. In: Dykes, J., Maceachren, A. M., Kraak, M. (Eds.). *Exploring Geovisualization*. International Cartographic Association, London, UK, pp. 295-312.
- Yoshida, H., Omae, M. (2005) An approach for analysis of urban morphology: methods to derive morphological properties of city blocks by using an urban landscape model and their interpretations. *Computers, Environment and Urban Systems*, Vol. 29, pp. 223-47.
- Zimmerman, D., Pavlik, C., Ruggles, A., Armstrong, M. P. (1999) An experimental comparison of ordinary and universal Kriging and inverse distance weighting. *Mathematical Geology*, Vol. 31, No. 4, pp. 375-389.
- Zlatanova, S., Painstil, J., Tempfli, K. (1998) 3-D object reconstruction from aerial stereo images. *Proceedings of the WSCG '98: the 6th International Conference in Central Europe on Computer Graphics and Visualization*, Plzen-Bory, Czech Republic. (not paginated).
- Zlatanova, S., Bandrova, T. (1998) User requirements for the third dimensionality. *Proceedings of the E-mail Seminar of Cartography: Maps of the Future*, Vol. 1, Sofia, Bulgaria, pp. 61-72.
- Zwolak, K. (2008) *Extraction of morphological indicators from georeferenced data in urban areas*. Unpublished MSc thesis, Ecole Polytechnique Fédérale de Lausanne, Switzerland.

APPENDIX A. INQUIRY ABOUT 3-D NEEDS FOR THE STATE OF C

Nom	Prenom	Entreprise	Activité	Partenaire CFU	Interêt bâti 3D	Utilité modèle bâti 3D	Niveau de détails	Rendu	Landmarks	Modélisation d'autres classes	Ce
Lançon	Michel	SPBR	Bruit / Rayonnement EM	non	oui	les modèles de propagation du bruit utilisent les surface planes comme réflecteurs. Le niveau de détail doit être faible (surface > 10m2). La couche des bâtiments avec l'attribut hauteur est généralement suffisante.	simple	bicolore	non	lignes de crête, de cassure de pente, de fond de vallon du terrain. Assez facile à créer au besoin avec les rasters dérivés du MNT	no
Stussi	Andreas	DT/DAT	Aménagement du territoire	oui	oui	Intégration de projets d'aménagement/urbanisme dans le tissus existant afin d'améliorer la concertation et la communication.	simple	générique	non	Arbres, mobilier urbain, couverture du sol	ou
Viaccoz	Anne-Marie	Direction du patrimoine et des sites	études et protection du patrimoine	oui	oui	Très grande utilité dans le cadre du travail de gestion des autorisations de construire et de la réalisation des plans de protection: - visualisation de l'impact des projets de transformation de bâtiment sur le bâtiment lui-même et sur son environnement - étude de plan de protection (notamment, plan de sites, PLQ valant plan de sites) Utilité à vérifier dans les domaines suivants: - reconstitution historique et archéologique d'états anciens de bâtiments et de sites à partir de l'état actuel - valorisation des bâtiments anciens les plus remarquables	complet	réelle	oui	espaces publics remarquables (jardins, places, mobilier urbain)	no
Oehrl	Pascal	SSIG	Mobilité	oui	oui	L'intérêt n'est pas majeur, mais comme un complément éventuellement utile dans le domaine de la mobilité, notamment dans la communication ou l'aide à la décision autour des projets de mobilité. Donc les bâtiments et la couverture du sol du domaine routier en 3D seraient un plus sans être de loin indispensables ou prioritaires dans l'immédiat. Par contre des projets	complet	bicolore	oui	Graphe mobilité Couverture du sol du domaine routier	no
Pieron	Raphaël	SIG	PLANS RESEAUX	non	oui	Utile, mais pas prioritaire (pour illustrer des projets, dans le cadre de la communication avec des non-professionnels	complet	réelle	oui	Terrain naturel, forêts, arbres	no
Gubler	Daniel	Perreten & Milleret SA	Génie civil et environnement	non	oui		simple	réelle			

Table A.1. Inquiry about 3-D needs for the State of Geneva.

Appendix A. Inquiry about 3-D needs for the State of Geneva

Nom	Prenom	Entreprise	Activité	Partenaire CFU	Interêt bâti 3D	Utilité modèle bâti 3D	Niveau de détails	Rendu	Landmark	Modélisation d'autres classes	C
delorenzi	pascal	commune de troinex	responsable technique communal	non	oui	aide à la densification de la zone villa integration dans les sites construits de nvx bâtiments	simple		non	serres dans la zone agricole	n
Gobeli	André	SIG	Gaz et Environnement / DD	oui	oui	Connaitre le volume des bâtiments pour planifier la capacité des réseaux de gaz naturel pour le chauffage		réelle	non	L'altitude car elle influence la pression du gaz naturel.	n
Calame	Philippe	HCC	ing. géomètres	non	oui	renseignement pour nos clients architectes principalement	simple	bicolore	non		n
HOHL	Olivier	Aéroport	Architecture	oui	oui	Plan d'obstacle	complet	bicolore	non	Arbres et forêts	n
Spierer	Emile	Service cantonal énergie - ScanE	politique énergétique	oui	oui	outil au service de -décisions pour la politique énergétique -aménagement énergétique du territoire -vérification des dossiers d'autorisation -suivi du dossier Indices -développement du solaire Note: nous avons besoin de la représentation de base mais serions intéressés aux détails des parois et toitures	simple	bicolore	non		n
Dalang	Félix	STIPI, Etat de Genève	Pollution de l'environnement bâti	non	oui	En fait pas grande chose, mais ça sera chouette. Suite à des plaintes téléphoniques, on peut mieux s'imaginer la situation.		réelle	non	Sous-sol	n
Eperon	Pierre-Alain	Aéroport International de Genève	Aviation	oui	oui	Nous en avons un qui comprend: 1) un polyèdre régional issu des MNT, MNS et du cadastre (TIN) 2) le plafond de sécurité selon l'Annexe 14 de l'OACI (TIN et DWG)	superstructures		non	Nous avons modélisé la topographie du sol et les zones boisées	o
WISARD	JEAN-PAUL	retraité	intéressé	non	oui	Une perception du relief assortie de la représentation, même simplifiée, des bâtiments, est incontestablement un avantage. Dans l'état actuel des techniques, il ne semble pas (encore) opportun d'investir trop d'argent dans des représentations de détails, qui seront vraisemblablement accessibles à bien meilleur compte dans peu d'années. La texture "générique" ne me semble d'aucun avantage.	avant_toits	bicolore	oui	Les voies de circulations souterraines et certainement l'enveloppe des infrastructures. On arrivera peut-être un jour à représenter les réseaux de conduites en 3D!	n
Travaglini	Olivier	HES LULLIER	Architecture du Paysage	non	oui	Dans notre cas l'intérêt d'un modèle 3D est de pouvoir créer rapidement des maquettes virtuelles lors de projets d'aménagement paysager.	complet	réelle	oui	Ce qui nous a été présenté par Adrien à savoir les chaussées et objets divers tels que les escaliers nous intéressent également.	n

Table A.2. Inquiry about 3-D needs for the State of Geneva.

Appendix A. Inquiry about 3-D needs for the State of Geneva

Nom	Prenom	Entreprise	Activité	Partenaire CFU	Interêt bâti 3D	Utilité modèle bâti 3D	Niveau de détails	Rendu	Landmark	Modélisation d'autres classes	C
Lopes	Paulo-Miguel	SPBR	protection contre le bruit	non	oui	En transférant ces données sur Immi (modélisation des nuisances sonores), il serait possible de se rendre compte de l'effet d'obstacle de tel ou tel ouvrage ou bâtiment sur l'environnement sonore. Il est à remarquer que ce travail est déjà réalisé dans le cadre de notre service (par extrusion).	simple	bicolore	non	Ce qui pourrait nous apporter un réel bénéfice serait d'obtenir les lignes de crêtes (pied et sommet d'une bute,...) ainsi que dans la couche du domaine routier les niveaux des routes et autres chemins.	n
Vosicki	Gordan	ICS Computer Services	Informatique route + mens.	non	oui	Disposer du gabarit des façades dans les profils en travers routiers lors de l'aménagement et de la correction de routes existantes (dans le MNT). Les textures réelles pourraient amener, à terme, une touche réaliste dans des vues/animations 3D. Le type de rendu nécessaire serait donc soit minimal (bicolore) ou, à terme, texture réelle; dans ce cas, les avant-toits seraient aussi utiles.	simple	bicolore	non		n
KUNZLER	André	Urgences Santé 144	Urgences	non	oui	Visualisation des possibilités de pose d'hélicoptère. Evidemment cette notion 3D est moins intéressante en milieu purement urbain. Dans un milieu mixte, le fait d'avoir la notion de hauteur des bâtiments serait un valeur ajoutée bien que n'étant pas indispensable.	complet	réelle	oui	les ponts et peut-être les lignes à haute tension ou funiculaires etc...	o
Aysanoa	Pierrot	DT DAT	Aménagement	oui	oui	L'information publique. Partenaires SITG Prof.	complet	réelle	oui		n
chevalley	marc	commune de collonge	architecture, aménagement	oui	oui	maquette 3D village Vézenaz intégration de projet 3D de pariculier et projets routiers	complet	bicolore	non		o
Lilla	Martine	OCIRT / REG	Fichier d'entreprises	oui	oui	Etablir une cartographie des entreprises	simple	réelle	non		n
Probst	Jean	service d'architecture Ville de Genève	Atelier d'études	non	oui	Simulations d'insertion de bâtiments étudiés au niveau d'études de faisabilité.	simple	bicolore	non	Indication des étages des bâtiments -Emprise des sous-sols avec accès (rampes de parking) -Indication des altitudes (pied, corniche, falte) (possibilité) -Indication des zones - Végétation importante pour la définition de Alignements, éléments remarquables, etc.	

Table A.3. Inquiry about 3-D needs for the State of Geneva.

Appendix A. Inquiry about 3-D needs for the State of Geneva

Nom	Prenom	Entreprise	Activité	Partenaire CFU	Interêt bâti 3D	Utilité modèle bâti 3D	Niveau de détails	Rendu	Landmark	Modélisation d'autres classes
Gennai	Emanuele	ESRI Géoinformatique SA	Systèmes d'Informatiopn Géographique	non	oui	Divers clients de ESRI devraient être intéressés par une telle banque de données 3D, pour l'analyse et la représentation d'entités dans le cadre de leurs projets (tourisme, marketing, mobilité, visibilité...)	complet	réelle	non	chaussée, mobilier urbain, végétation
Fischer	Isabelle	Ville de Genève-Service des agents de ville et domaine public	Gestion de l'occupation du domaine public	oui	oui	Dans le cadre de la gestion de l'occupation du domaine public nous utilisons un logiciel de maquettage 3D et survol en temps réel (SpaceEyes). Mais nous ne disposons pas des données bâtiments nécessaires à une représentation 3D de qualité (ex. nous n'avons pas les données toitures). Disposer d'un modèle 3D des bâtiments nous permettrait de vérifier la pertinence, d'autoriser ou non, l'installation d'empiètement sur le domaine public.	complet	réelle	oui	le domaine routier (ex.: trottoirs, îlots, etc), les marquises des bâtiments
Zurbrügg	Bernard	TPG	Trafic	oui	non					
Bertola	Danielle	SSIG	information	non	oui	1) utilisation d'infographie dans intradt. 2) en faire bénéficier des personnes extérieures (par ex. maquetistes professionnels)	complet	réelle	oui	bâtiments classés et/ou à l'inventaire
VUILLERAT	CLAUDE-ALAIN	B+C INGENIEURS	environnemet & AT	oui	oui	Modelisations bruit , flux polluifs, cartes des dangers	simple		non	murs, obstacles permanents et mobiles,
van der Maas	jacobus	scane	énergie	oui	oui	Une meilleures appréciation du volume du bâtiment	simple	bicolore	non	
Verhoeven	Patrick	OCM	mobilité	non	non				non	
Beffa	Robert	Acousticien	environnement écoles	non	oui	Modélisation acoustique	superstructures	bicolore	non	courbes de niveaux ponts
Ehrat	Reto	AAE	architecture	non	oui	Modelisation partielle du territoire en 3d pour des études "urbaine" et plus particulièrement d'insertion de nouveaux éléments bâtis et l'étude de leurs impacts sur l'existant.	complet	réelle	non	Non. Etant donné l'actuel avancement des technologies de l'information, plus de détails impliquerait des ressources de calcul dépassant le simple cadre que les PME sont actuellement en mesure d'exploiter. Par contre ne pas oublier que les modèle doivent être évolutif de manière de pouvoir les compléter dans le temps.

Table A.4. Inquiry about 3-D needs for the State of Geneva.

Appendix A. Inquiry about 3-D needs for the State of Geneva

Nom	Prenom	Entreprise	Activité	Partenaire CFU	Interêt bâti 3D	Utilité modèle bâti 3D	Niveau de détails	Rendu	Landmarks	Modélisation d'au classes
Autullo	Angelo	Ville d'Onex	Génie civil	oui	oui	Pour les dossiers de présentation Pour visualiser les projets qui doivent être exposés à des gens qui ne sont pas du métier	avant_toits	bicolore	oui	Les ouvrages d'art Event. la végétation importante??
Hiltbrand	François	Analyses & dév immobiliers	architecture et expertises	non	oui	Notamment en zone 4 b, modélisation d'impact de nouveaux projets et surélévations	superstructures	générique	non	
Bodenmüller	Eric	Mairie Chêne-Bourg	Service technique communal	oui	oui	- Vision précise pour préaviser les demandes d'autorisation de construire. - Base pour la présentation de projets -	superstructures	réelle	oui	
chevalley	marc	commune de collonge	architecture	oui	oui	projet d'aménagement, plq	complet	bicolore	non	aménagement ro

Table A.5. Inquiry about 3-D needs for the State of Geneva.

APPENDIX B. MORPHOLOGICAL PROPERTIES OF BUILDINGS ANALYSIS

CERN + Centre of Geneva						
<i>Global volume analysis unenhanced n2.5-DUSM</i>				<i>Global volume analysis enhanced n2.5-DUSM</i>		
Type of building	Volume DIP techniques [m3]	Volume 3-D model [m3]	Global deviation error	Type of building	Volume DIP techniques [m3]	Volume 3-D model [m3]
Total	345887.50	338114.86	2.30%	Total	346105.48	338114.8
Simple	164666.78	158603.22	3.82%	Simple	164144.23	158603.2
Intermediate	108754.36	107689.42	0.99%	Intermediate	108734.80	107689.4
Multifaceted	72466.35	71822.22	0.90%	Multifaceted	73226.44	71822.2

Table B.1: Global analysis of volumes using DIP techniques. Left hand-side table: unenhanced model; right hand-side table: enhanced model.

CERN + Centre of Geneva					
<i>Building by building analysis unenhanced n2.5-DUSM</i>			<i>Building by building analysis enhanced n2.5-DUSM</i>		
Type of building	Volume [m3] Absolute building deviation error	Volume [m3] Standard deviation	Type of building	Volume [m3] Absolute building deviation error	Volume [m3] Standard deviation
Total	4.61%	3.16%	Total	4.09%	3.16%
Simple	3.55%	2.03%	Simple	4.15%	2.03%
Intermediate	4.82%	3.74%	Intermediate	4.25%	3.74%
Multifaceted	6.15%	2.96%	Multifaceted	5.49%	2.96%

Table B.2: Building by building analysis of volumes using DIP techniques. Left hand-side table: unenhanced model; right hand-side table: enhanced model.

Appendix B. Morphological properties of buildings: statistical analysis

CERN + Centre of Geneva							
Global area analysis							
Type of building	area 3-D model [m ²]	area case 1 (se1) [m ²]	area case 2 (se2) [m ²]	area case 3 (EM) [m ²]	area case 4 (OM) [m ²]	area case 5 (EM, se9) [m ²]	area case 6 (OM, se9) [m ²]
Total	101932.72	90431.09	93182.06	93783.39	93658.76	96079.59	94414.16
Simple	25101.98	22387.44	22943.92	23157.69	23092.32	23397.91	23178.98
Intermediate	31590.72	31095.59	31893.52	31890.47	31960.82	32333.79	32002.02
Multifaceted	45240.02	35918.56	37304.22	37694.93	37565.22	39303.39	38192.76
Global deviation error							
Type of building	area 3-D model [m ²]	area case 1 (se1) [m ²]	area case 2 (se2) [m ²]	area case 3 (EM) [m ²]	area case 4 (OM) [m ²]	area case 5 (EM, se9) [m ²]	area case 6 (OM, se9) [m ²]
Total	---	-11.28%	-8.58%	-7.99%	-8.12%	-5.74%	-7.38%
Simple	---	-10.81%	-8.60%	-7.75%	-8.01%	-6.79%	-7.66%
Intermediate	---	-1.57%	0.96%	0.95%	1.17%	2.35%	1.30%
Multifaceted	---	-20.60%	-17.54%	-16.68%	-16.96%	-13.12%	-15.58%

Table B.3: Global analysis of facade areas using DIP techniques. Legend of the acronyms used: se...: structural element, EM: En Model.

Appendix B. Morphological properties of buildings: statistical analysis

CERN + Centre of Geneva							
<i>Building by building analysis: absolute building deviation error</i>							
Type of building	area case 1 (se1)	area case 2 (se2)	area case 3 (EM)	area case 4 (OM)	area case 5 (EM, se9)	area case 6 (OM, se9)	area case 7 (EM)
	[m ²]	[m ²]	[m ²]	[m ²]	[m ²]	[m ²]	[m ²]
Total	9.46%	8.38%	8.85%	8.01%	8.12%	7.38%	
Simple	6.46%	6.00%	6.15%	5.63%	5.78%	5.39%	
Intermediate	4.52%	4.06%	4.53%	4.08%	5.37%	4.06%	
Multifaceted	17.24%	14.88%	15.62%	14.02%	12.36%	12.32%	
<i>Building by building analysis: standard deviation</i>							
Type of building	area case 1 (se1)	area case 2 (se2)	area case 3 (EM)	area case 4 (OM)	area case 5 (EM, se9)	area case 6 (OM, se9)	area case 7 (EM)
	[m ²]	[m ²]	[m ²]	[m ²]	[m ²]	[m ²]	[m ²]
Total	9.95%	9.14%	9.33%	8.70%	7.53%	7.76%	
Simple	5.53%	4.51%	3.65%	3.62%	3.63%	3.29%	
Intermediate	3.28%	4.01%	4.67%	4.07%	5.16%	4.11%	
Multifaceted	8.96%	8.42%	8.58%	8.58%	6.14%	7.86%	

Table B.4: Building by building analysis of facade areas using DIP techniques. Legend of the acronyms used: se: structural error; EM: Estimated Model; OM: Optimised Model.

Appendix B. Morphological properties of buildings: statistical analysis

CERN + Centre of Geneva						
DIP technique: reclassification of image pixel on the unenhanced n2.5-DUS						
Global area analysis						
Type of roof	Area 3-D model [m2]	Area all slopes [m2]	Area slopes > 15° set to 0° [m2]	Area slopes > 30° set to 0° [m2]	Area slopes > 45° set to 0° [m2]	Area slopes > 60° set to 0° [m2]
Total	35982.54	49584.42	34842.73	35270.39	36774.25	37421.18
Flat	3667.58	5972.75	3732.15	3755.51	3843.22	3931.89
Classic	2608.27	3190.40	2457.18	2592.92	2666.61	2698.44
Complex	29706.69	40421.27	28653.41	28921.96	30264.42	30860.35
Global deviation error						
Type of roof	Area 3-D model [m2]	Area all slopes [m2]	Area slopes > 15° set to 0° [m2]	Area slopes > 30° set to 0° [m2]	Area slopes > 45° set to 0° [m2]	Area slopes > 60° set to 0° [m2]
Total	---	37.80%	-3.17%	-1.98%	2.20%	3.12%
Flat	---	62.85%	1.76%	2.40%	4.79%	6.12%
Classic	---	22.32%	-5.79%	-0.59%	2.24%	2.96%
Complex	---	36.07%	-3.55%	-2.64%	1.88%	2.84%

Table B.5: Global analysis of roof areas using DIP techniques on the unenhanced model.

Appendix B. Morphological properties of buildings: statistical analysis

CERN + Centre of Geneva									
DIP technique: reclassification of image pixel on the enhanced n2.5-DUSM									
Global area analysis									
Type of roof	Area 3-D model [m ²]	Area all slopes [m ²]	Area slopes > 15° set to 0° [m ²]	Area slopes > 30° set to 0° [m ²]	Area slopes > 45° set to 0° [m ²]	Area slopes > 60° set to 0° [m ²]	Area slopes > 75° set to 0° [m ²]	Area slopes > 45° using a se diamond 9 [m ²]	Area slopes > 45° using a diamond 1 [m ²]
Total	35982.54	42353.39	34834.97	35238.59	35926.27	36911.09	38704.25	36452.85	36354
Flat	3667.58	4495.25	3731.53	3750.43	3802.47	3915.65	4179.21	3848.25	3838
Classic	2608.27	2973.36	2453.06	2569.18	2591.49	2615.01	2640.47	2610.79	2609
Complex	29706.69	34884.78	28650.39	28918.98	29532.32	30380.43	31884.57	29993.81	29906
Global deviation error									
Type of roof	Area 3-D model [m ²]	Area all slopes [m ²]	Area slopes > 15° set to 0° [m ²]	Area slopes > 30° set to 0° [m ²]	Area slopes > 45° set to 0° [m ²]	Area slopes > 60° set to 0° [m ²]	Area slopes > 75° set to 0° [m ²]	Area slopes > 45° using a se diamond 9 [m ²]	Area slopes > 45° using a diamond 1 [m ²]
Total	---	17.71%	-3.19%	-2.07%	-0.16%	2.58%	7.56%	1.31%	1.0
Flat	---	22.57%	1.74%	2.26%	3.68%	6.76%	13.95%	4.93%	4.6
Classic	---	14.00%	-5.95%	-1.50%	-0.64%	0.26%	1.23%	0.10%	0.0
Complex	---	17.43%	-3.56%	-2.65%	-0.59%	2.27%	7.33%	0.97%	0.6

Table B.6: Global analysis of roof areas using DIP techniques on the enhanced model.

Appendix B. Morphological properties of buildings: statistical analysis

CERN + Centre of Geneva Segmentation procedure Global area analysis			
Type of roof	Area image segmentation technique [m2]	Area 3D model [m2]	Global deviation error
Total	35533.95	35957.52	1.19%
Flat	3725.94	3667.58	-1.57%
Classic	2633.29	2608.27	-0.95%
Complex	29174.72	29681.67	1.74%

Table B.7: Global analysis of roof areas using the segmentation procedure.

Appendix B. Morphological properties of buildings: statistical analysis

CERN + Centre of Geneva						
DIP technique: reclassification of image pixel on the unenhanced n2.5-DUSM						
Building by Building analysis: absolute building deviation error						
Type of roof	Area all slopes [m2]	Area slopes > 15° set to 0° [m2]	Area slopes > 30° set to 0° [m2]	Area slopes > 45° set to 0° [m2]	Area slopes > 60° set to 0° [m2]	Area slopes > 75° [m2]
Total	38.84%	7.51%	6.12%	6.20%	6.26%	
Flat	38.92%	2.27%	2.93%	8.30%	9.20%	
Classic	21.76%	5.95%	1.27%	2.26%	2.92%	
Complex	45.65%	9.89%	9.13%	7.08%	6.62%	
Type of roof	Area all slopes [m2]	Area slopes > 15° set to 0° [m2]	Area slopes > 30° set to 0° [m2]	Area slopes > 45° set to 0° [m2]	Area slopes > 60° set to 0° [m2]	Area slopes > 75° [m2]
Total	32.32%	7.80%	7.82%	6.38%	4.74%	
Flat	34.26%	0.81%	0.92%	5.97%	5.51%	
Classic	24.59%	2.31%	1.82%	1.46%	1.42%	
Complex	33.75%	9.46%	9.19%	7.27%	4.77%	

Table B.8: Building by building analysis of roof areas using DIP techniques on the unenhanced mode

Appendix B. Morphological properties of buildings: statistical analysis

CERN + Centre of Geneva DIP technique: reclassification of image pixel on the enhanced n2.5-DUSM								
Building by Building analysis: absolute building deviation error								
Type of roof	Area all slopes [m2]	Area slopes > 15° set to 0° [m2]	Area slopes > 30° set to 0° [m2]	Area slopes > 45° set to 0° [m2]	Area slopes > 60° set to 0° [m2]	Area slopes > 75° set to 0° [m2]	Area slopes > 45° using a se diamond 9 [m2]	Area slopes > 45° using a se diamond 13 [m2]
Total	20.30%	7.44%	6.14%	4.84%	5.49%	7.32%	4.85%	4.80%
Flat	14.17%	1.80%	2.13%	2.98%	4.90%	9.08%	4.16%	4.00%
Classic	15.00%	7.08%	1.78%	0.41%	1.35%	2.89%	0.97%	0.78%
Complex	24.19%	9.71%	9.00%	6.90%	7.22%	8.61%	6.52%	6.46%
Building by Building analysis: standard deviation								
Type of roof	Area all slopes [m2]	Area slopes > 15° set to 0° [m2]	Area slopes > 30° set to 0° [m2]	Area slopes > 45° set to 0° [m2]	Area slopes > 60° set to 0° [m2]	Area slopes > 75° set to 0° [m2]	Area slopes > 45° using a se diamond 9 [m2]	Area slopes > 45° using a se diamond 13 [m2]
Total	22.73%	7.67%	7.57%	5.96%	4.50%	6.95%	4.45%	4.65%
Flat	13.84%	0.70%	0.65%	0.97%	2.88%	7.28%	1.23%	1.06%
Classic	24.04%	1.16%	2.14%	0.17%	2.17%	5.31%	0.89%	0.85%
Complex	24.73%	9.14%	8.76%	7.02%	4.68%	7.15%	4.95%	5.31%

Table B.9: Building by building analysis of roof areas using DIP techniques on the enhanced model.

Appendix B. Morphological properties of buildings: statistical analysis

CERN + Centre of Geneva Segmentation procedure Building by building analysis	
Type of roof	Area [m2] Absolute building deviation error
Total	3.47%
Flat	1.19%
Classic	2.79%
Complex	4.45%
Type of roof	Area [m2] Standard deviation
Total	4.09%
Flat	0.59%
Classic	3.43%
Complex	4.71%

Table B.10: Building by building analysis of roof areas using the segmentation procedure.

APPENDIX C. CALCULATION OF YEARLY AND MONTHLY IRRADIATION VALUES (2.5-D VISUALIZATION) USING THE ISOTROPIC MODEL

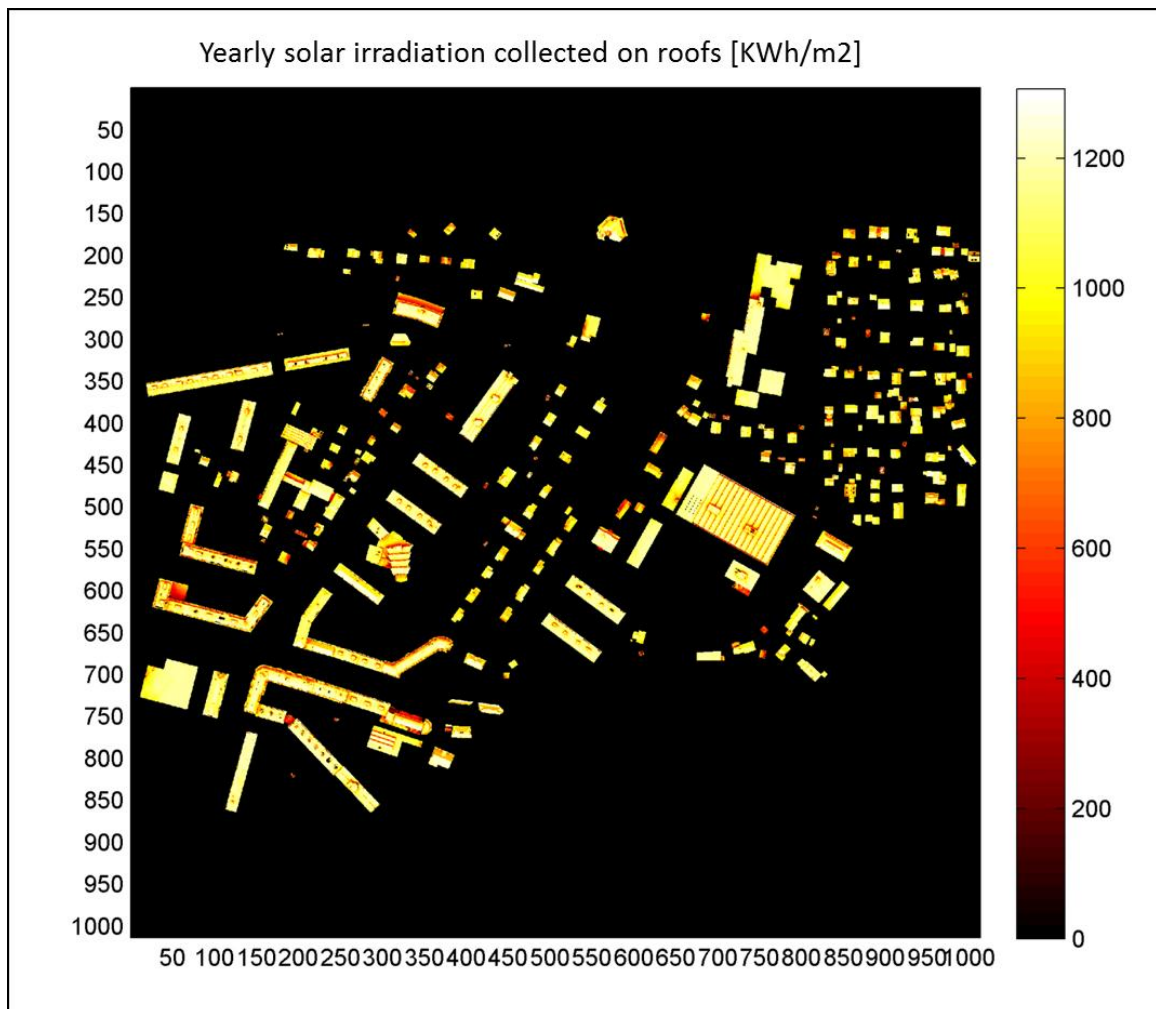


Figure C.1. Calculation of the yearly irradiation values (KWh/m²) applying the isotropic model for the case-study area of Moillesulaz, city of Geneva.

Appendix C. Calculation of yearly and monthly irradiation values (2.5-D visualization) using the isotropic model

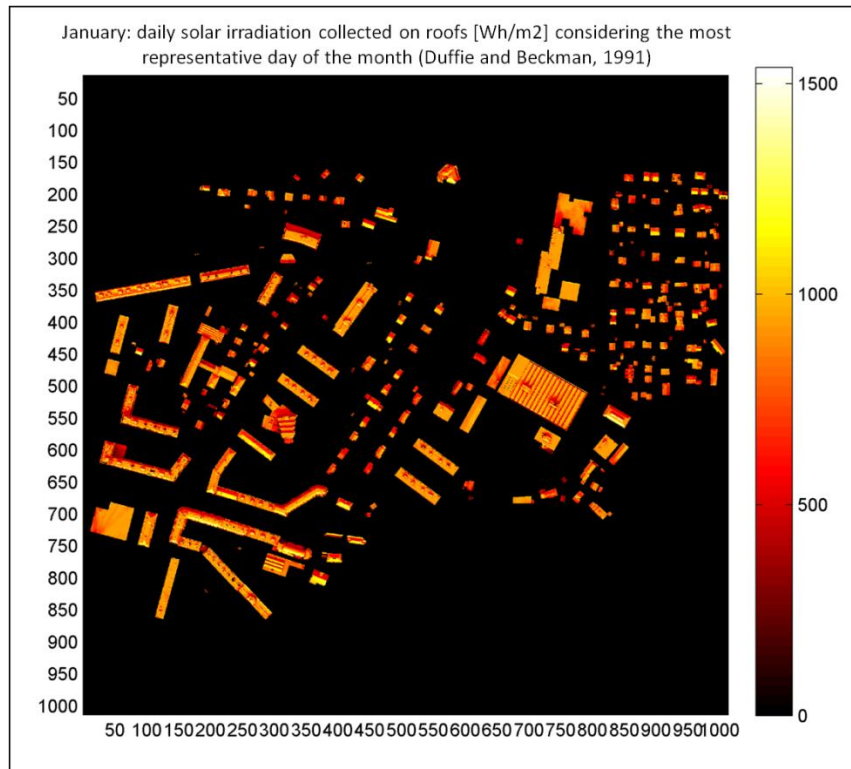


Figure C.2. Calculation of the daily (January) irradiation values (Wh/m²) applying the isotropic model for the case-study area of Moillesulaz, city of Geneva.

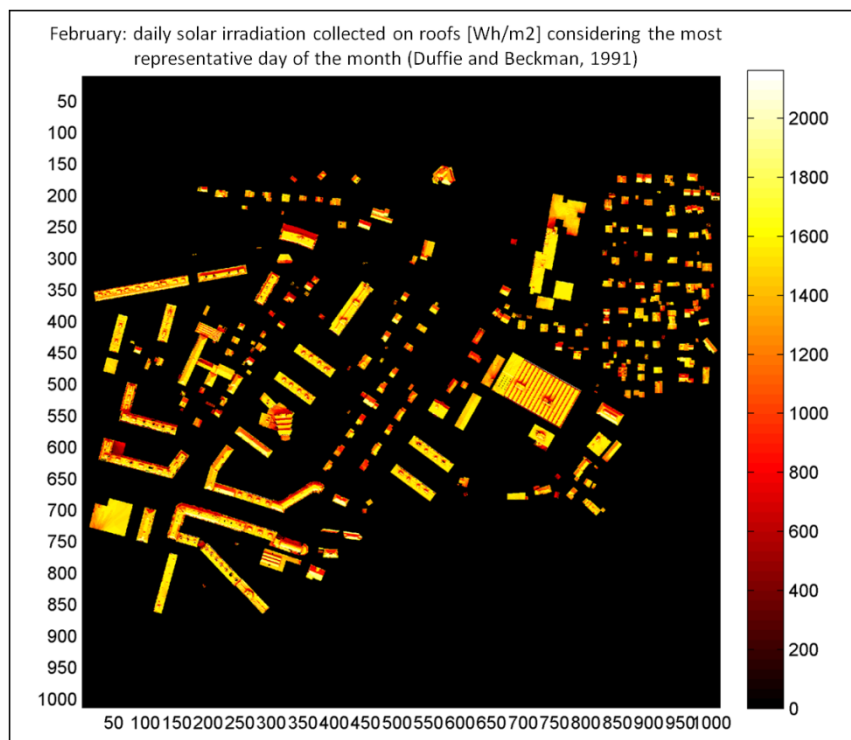


Figure C.3. Calculation of the daily (February) irradiation values (Wh/m²) applying the isotropic model for the case-study area of Moillesulaz, city of Geneva.

Appendix C. Calculation of yearly and monthly irradiation values (2.5-D visualization) using the isotropic model

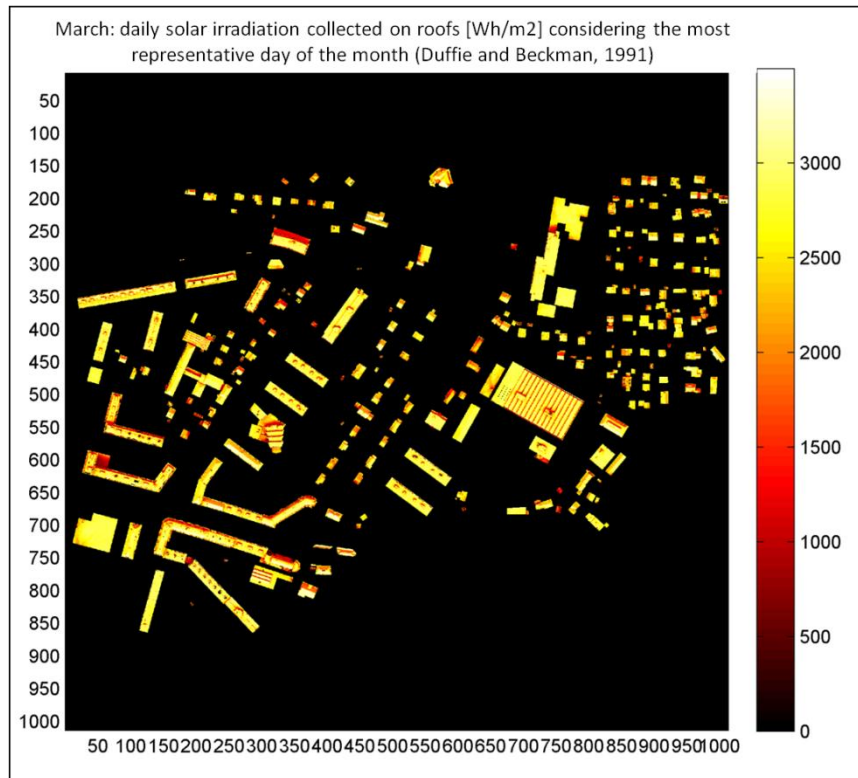


Figure C.4. Calculation of the daily (March) irradiation values (Wh/m^2) applying the isotropic model for the case-study area of Moillesulaz, city of Geneva.

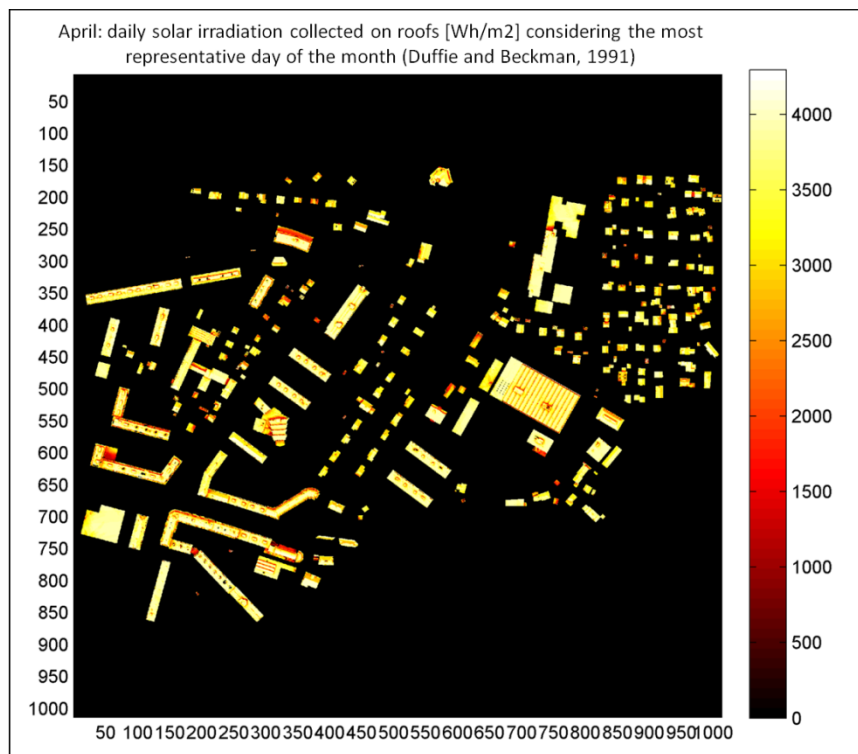


Figure C.5. Calculation of the daily (April) irradiation values (Wh/m^2) applying the isotropic model for the case-study area of Moillesulaz, city of Geneva.

Appendix C. Calculation of yearly and monthly irradiation values (2.5-D visualization) using the isotropic model

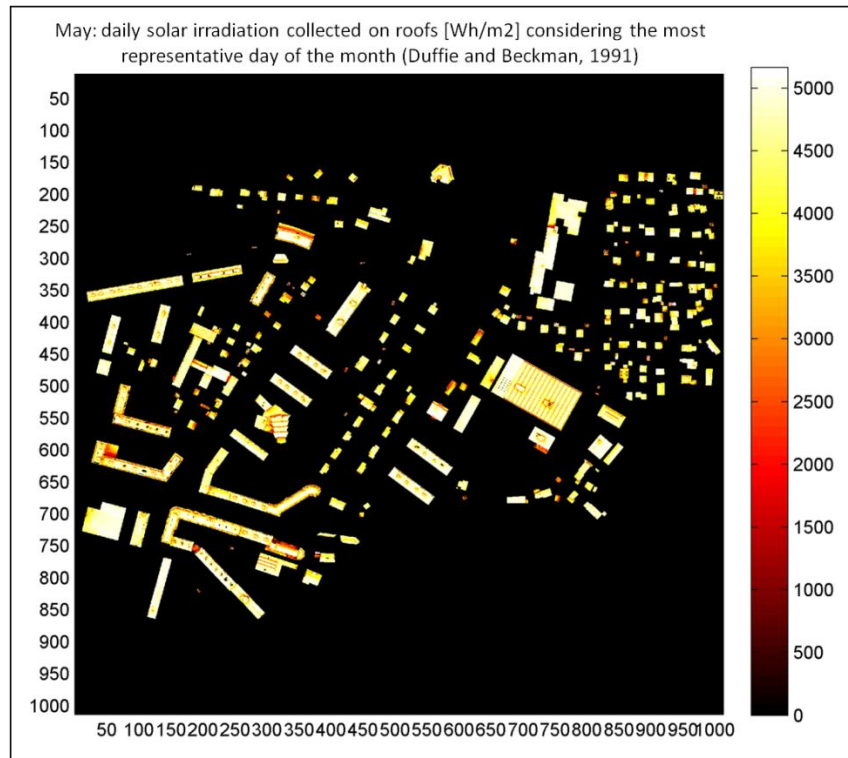


Figure C.6. Calculation of the daily (May) irradiation values (Wh/m^2) applying the isotropic model for the case-study area of Moillesulaz, city of Geneva.

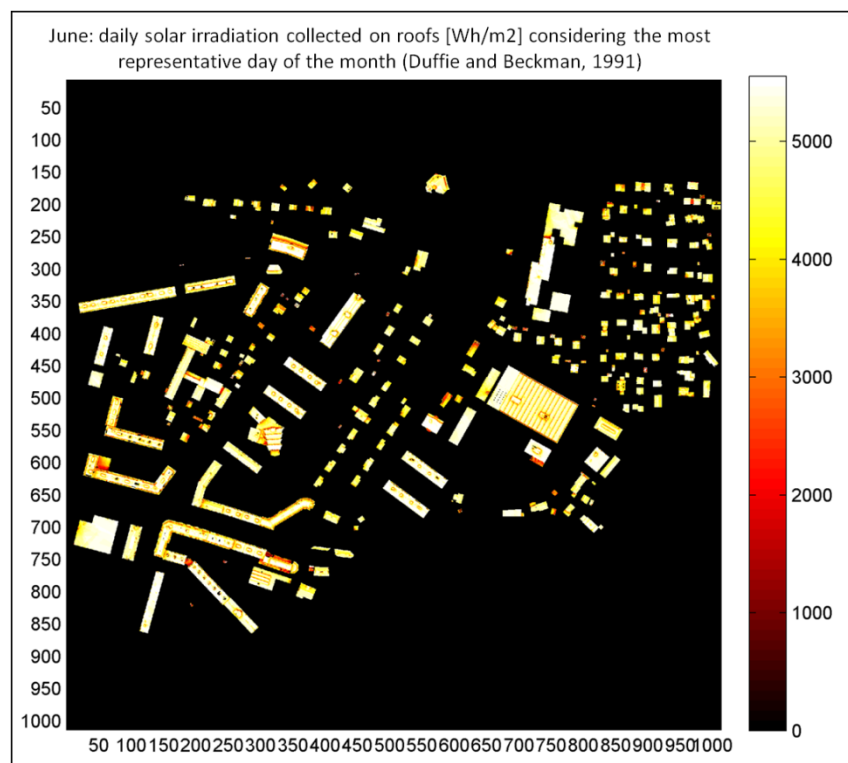


Figure C.7. Calculation of the daily (June) irradiation values (Wh/m^2) applying the isotropic model for the case-study area of Moillesulaz, city of Geneva.

Appendix C. Calculation of yearly and monthly irradiation values (2.5-D visualization) using the isotropic model

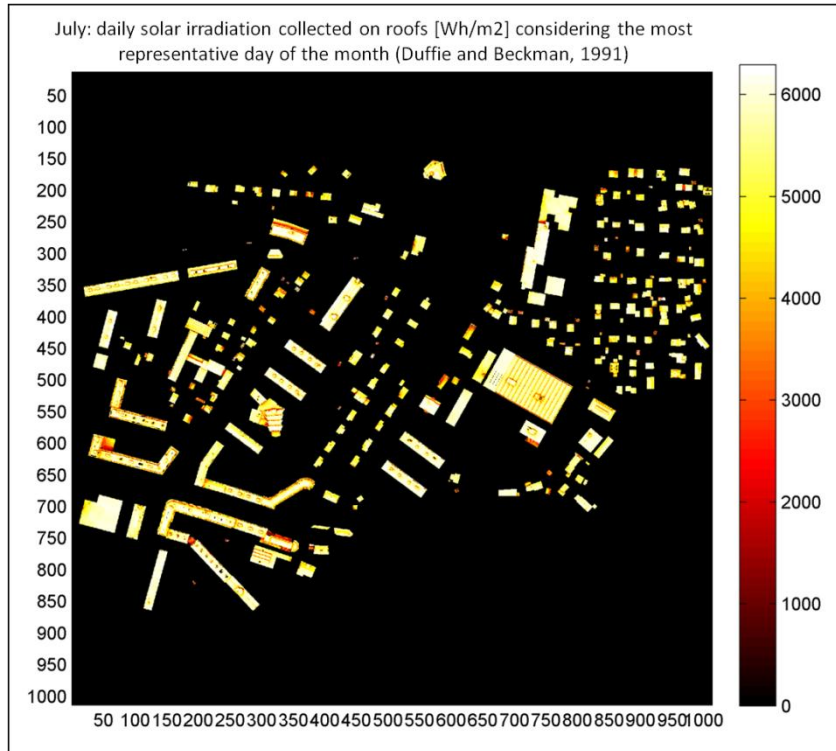


Figure C.8. Calculation of the daily (July) irradiation values (Wh/m^2) applying the isotropic model for the case-study area of Moillesulaz, city of Geneva.

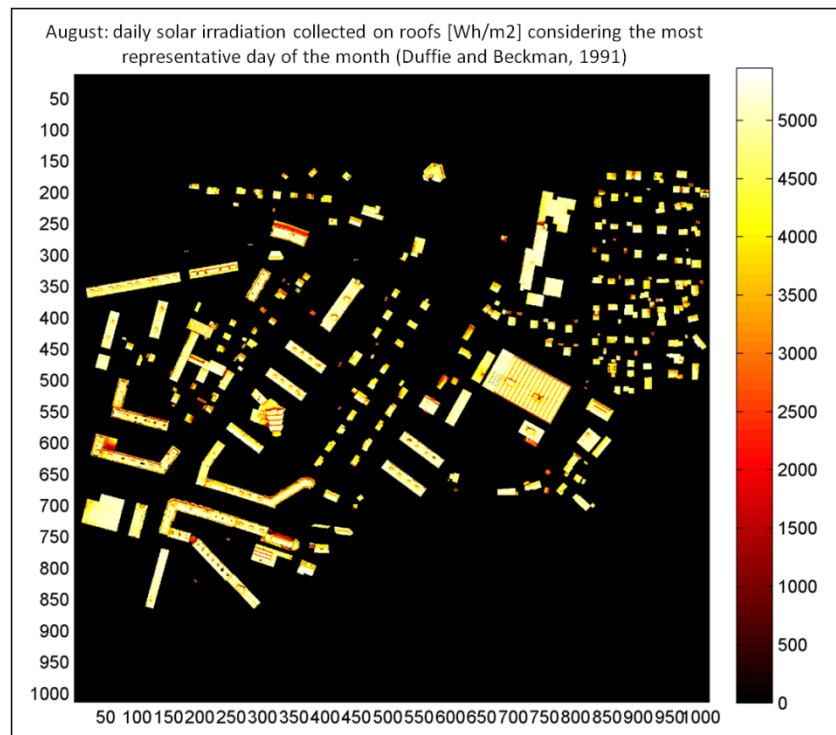


Figure C.9. Calculation of the daily (August) irradiation values (Wh/m^2) applying the isotropic model for the case-study area of Moillesulaz, city of Geneva.

Appendix C. Calculation of yearly and monthly irradiation values (2.5-D visualization) using the isotropic model

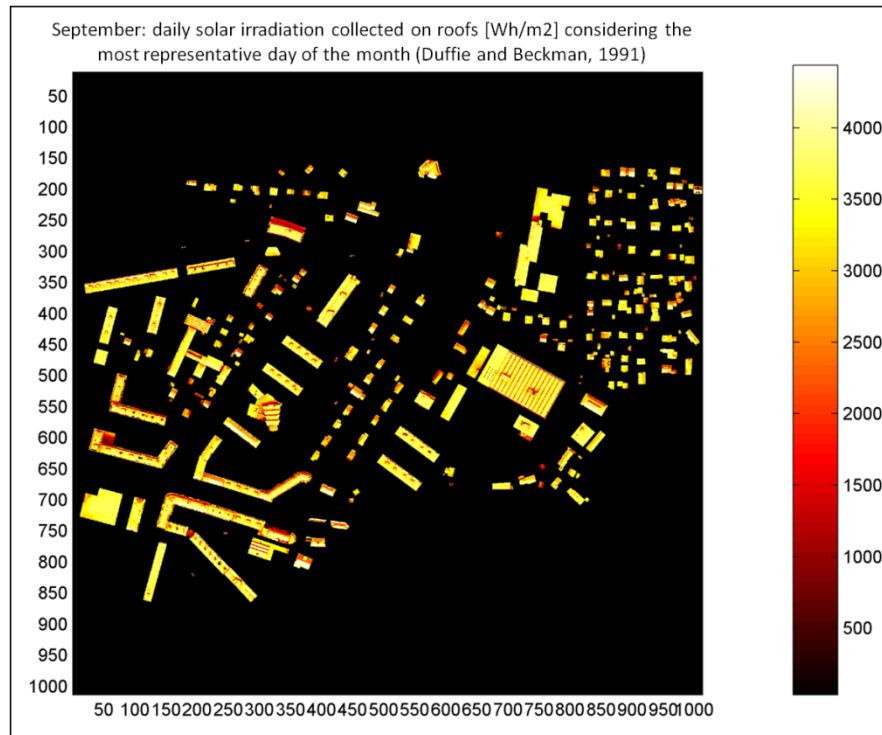


Figure C.10. Calculation of the daily (September) irradiation values (Wh/m²) applying the isotropic model for the case-study area of Moillesulaz, city of Geneva.

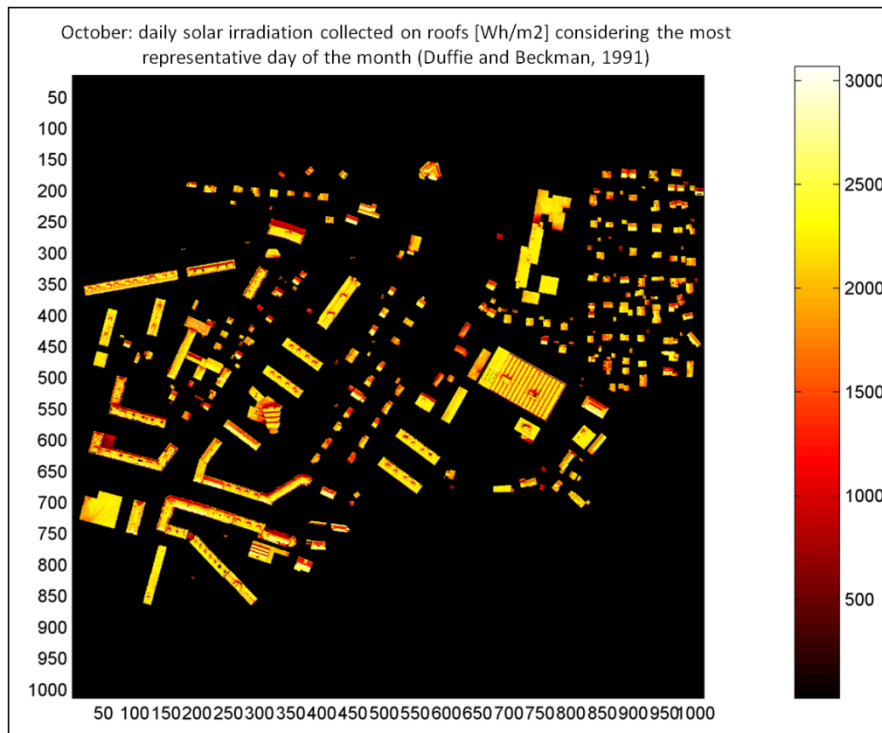


Figure C.11. Calculation of the daily (October) irradiation values (Wh/m²) applying the isotropic model for the case-study area of Moillesulaz, city of Geneva.

Appendix C. Calculation of yearly and monthly irradiation values (2.5-D visualization) using the isotropic model

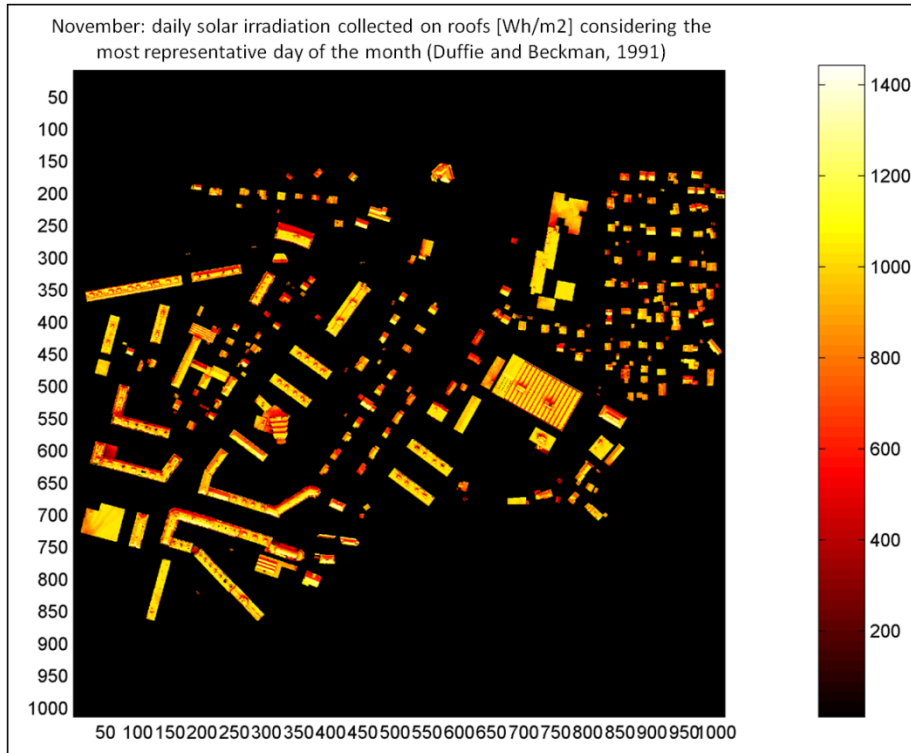


Figure C.12. Calculation of the daily (November) irradiation values (Wh/m²) applying the isotropic model for the case-study area of Moillesulaz, city of Geneva.

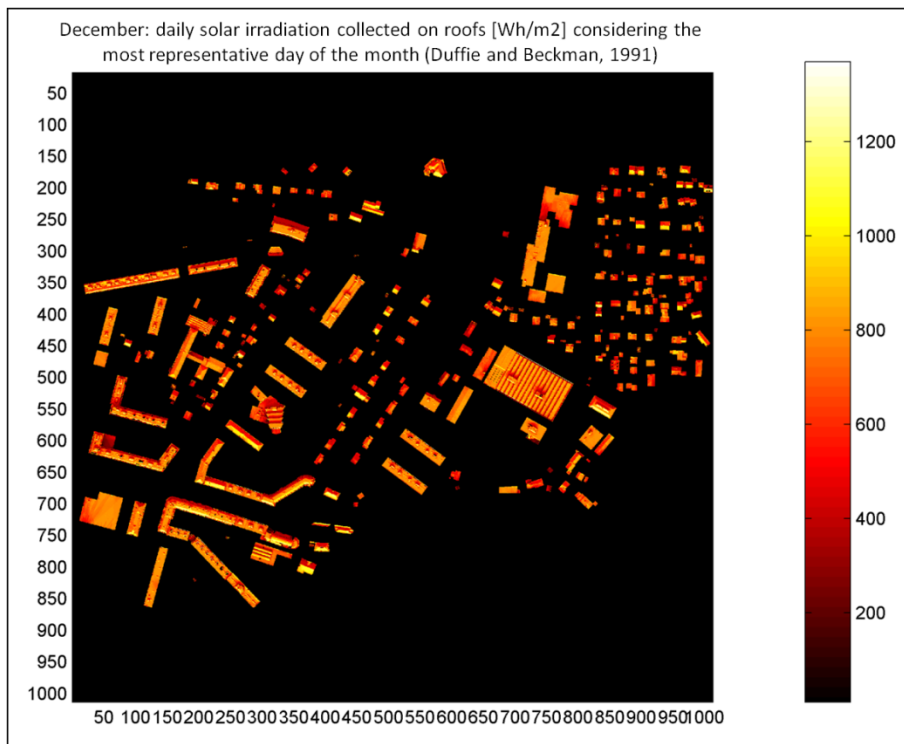


Figure C.13. Calculation of the daily (December) irradiation values (Wh/m²) applying the isotropic model for the case-study area of Moillesulaz, city of Geneva.

APPENDIX D. HEATING ANALYSIS: ASSUMPTIONS MADE FOR THE BUILDINGS OF FLORENCE AND CERN

Class of age		1	2	3	4	5	6	Legend:
Age		<1940	1940-1960	1960-1970	1970-1980	>1980	2010	
glass transmittance values (in W/(K*m2))	'P.Ug'	5.90	5.90	5.90	2.70	2.70	2.00	5.9 – single glazing 2.7 – double glazing 2.0 – triple glazing
opaque transmittance values (in W/(K*m2))	'P.Uo'	1.72	1.62	1.39	1.32	0.80	0.30	Mean global transmittance weighted on the real sample used in the PEAC
roof floor transmittance values respectively (in W/(K*m2))	'P.Ur'	1.72	1.62	1.39	1.32	0.80	0.30	Mean global transmittance weighted on the real sample used in the PEAC
column array with glazing ratio in the different orientation [s]	'P.GR'	21.00%	21.00%	21.00%	21.00%	21.00%	21.00%	
column array with glazing ratio in the different orientation [e]	'P.GR'	21.00%	21.00%	21.00%	21.00%	21.00%	21.00%	
column array with glazing ratio in the different orientation [n]	'P.GR'	21.00%	21.00%	21.00%	21.00%	21.00%	21.00%	
column array with glazing ratio in the different orientation [w]	'P.GR'	21.00%	21.00%	21.00%	21.00%	21.00%	21.00%	
external wall thickness (in m)	'P.w'	0.45	0.45	0.35	0.30	0.30	0.30	0.82 – single glazing 0.66 – selective single glazing 0.70 – double glazing
solar transfer coefficient of the glass chosen (to be chosen from "prospetto 4", UNI 10379:2005)	'P.g_p erp'	0.82	0.82	0.82	0.70	0.70	0.60	0.64 – selective double glazing 0.60 – triple glazing 0.55 – selective triple glazing
voluminal thermal capacity (to be chosen from the table "prospetto 3", UNI 10379) (in kJ/K*m3)	'P.Cv'	240	240	130	130	130	240	290 – stone and assimilables 240 – bricks and assimilables 130 – air bricks and assimilables 70 – internal insulation or light walls

Figure D.1 Assumptions made for the buildings belonging to the case-study area of the city of Florence.

Appendix D. Heating analysis: assumptions made for the buildings of Florence and CERN

Class of age		1	2	3	
Age		< 1965	1965–1970	> 1970	
glass transmittance values (in W/(K*m2))	'P.Ug'	5.90	5.90	2.70	5.9 – single glazing 2.7 – double glazing 2.0 – triple glazing Mean global transmittance weighted on the real sample used in the PEAC Mean global transmittance weighted on the real sample used in the PEAC
opaque transmittance values (in W/(K*m2))	'P.Uo'	3.65	2.50	2.01	
roof floor transmittance values respectively (in W/(K*m2))	'P.Ur'	3.44	2.32	1.86	
On ground floor transmittance (in W/(K*m2))	'P.Ugr'	0.41	0.41	0.41	
column array with glazing ratio in the different orientation [s]	'P.GR'	25.00%	25.00%	25.00%	
column array with glazing ratio in the different orientation [e]	'P.GR'	25.00%	25.00%	25.00%	
column array with glazing ratio in the different orientation [n]	'P.GR'	25.00%	25.00%	25.00%	
column array with glazing ratio in the different orientation [w]	'P.GR'	25.00%	25.00%	25.00%	
external wall thickness (in m)	'P.w'	0.40	0.35	0.30	
solar transfer coefficient of the glass chosen (to be chosen from "prospetto 4", UNI 10379:2005)	'P.g _{pe} r'	0.82	0.82	0.70	
voluminal thermal capacity (to be chosen from the table "prospetto 3", UNI 10379) (in kJ/K*m3)	'P.Cv'	240	240	240	290 – stone and assimilables 240 – bricks and assimilables 130 – air bricks and assimilables 70 – internal insulation or light walls

Figure D.2. Assumptions made for the buildings belonging to the case-study area of CERN campus.

CURRICULUM VITAE

I – PERSONAL DATA

NAME: Cláudio Magalhães Carneiro

ACTUAL ADDRESS: 15, Rue de Livron
1217 Meyrin, Switzerland

EMAIL: claudio.carneiro@epfl.ch

DATE OF BIRTH: 14th July of 1973 (37 years)

NATIONALITY: Portuguese

MARITAL STATUS: Married

II – LANGUAGES

Language	Spoken	Written
English	Fluent	Fluent
French	Fluent	Fluent
Italian	Average	Average
Spanish	Fluent	Average

III – ACADEMIC BACKGROUND

CATEGORY	UNIVERSITY	STUDIES	YEARS
1 – PhD	École Polytechnique Fédérale de Lausanne	Geographical Information Systems (GIS), urbanism and environment	Between January 2006 and April 2011
2 - Master of Science (Postgraduate Studies)	Instituto Superior Técnico of Lisbon	Geographical Information Systems (GIS)	Between 2002 and 2004 (1 st year of courses and 2 nd year to implement and write a master thesis)
3 - University Engineer (Graduation Studies)	Sciences University of Lisbon	Surveying and Geomatics Engineer	Between 1992 and 1997 (5 years of undergraduate studies)

1 – PhD thesis at the “École Polytechnique Fédérale de Lausanne” (EPFL - Switzerland) in the doctoral program “Environment”. The subject of the research work is:

“EXTRACTION OF URBAN ENVIRONMENTAL QUALITY INDICATORS USING LIDAR-BASED DIGITAL SURFACE MODELS”

This thesis anticipates the use of 2-D and 3-D models and data for the environmental analysis of cities, aiming to provide useful tools for urban planning and design. According to end-users requirements, the extraction of urban environmental quality (UEQ) indicators from 2-D and 3-D information using innovative methods is proposed and implemented, which is based on recent research on computational algorithms for the analysis, evaluation, management and design of the urban space. Moreover, results that can be obtained with different data sources and aggregation methods are compared. In particular, the main advantages of urban models generated from LiDAR data are highlighted.

2 - Master of Science (2 years of postgraduate studies) in Geographical Information Systems (GIS) at the Instituto Superior Técnico (Lisbon) finished the 5th of March 2004. The Curricular part (1st year of studies) of the Master of Science (MSc) in GIS (with the final result of 15.3 in 20), has incorporated the following courses:

- Data Bases;
- Digital Cartography (includes photogrammetry);
- Remote Sensing;
- Geodesy;
- Statistics;
- Artificial Intelligence;
- Digital Image Processing;

In the 2nd year of studies a master thesis with the final classification of “Very Good” and the following title has been implemented and approved:

“DEVELOPMENT PROJECT OF CERN GEOGRAPHICAL INFORMATION SYSTEM WITH AN EXAMPLE OF APPLICATION ON THE MANAGEMENT OF THE OPTICAL FIBER NET”

This master thesis was guided for geographic databases, over all its specifications having in consideration the European Norm ISO/TC 211 and also its applications in an Object Oriented Database using Unified Modeling Language (UML).

3 - University graduation (5 years of master studies) in Geographical (Surveying and Geomatical) Engineering made between the years of 1992 and 1997, by the Sciences University of Lisbon, with the final result of 13.3 in 20. Final work (to finish the graduation) made between March and September 1997 on the Geodesy Centre of the Institute of Scientific and Tropical Investigation, in Classical Geodesy (Triangulation and Least Mean Squares) and Spatial Geodesy (Cinematic Global Positioning System), by the Sciences University of Lisbon, with the final result of 17 in 20.

IV – SOCIAL SKILLS AND COMPETENCES

- Experience in working in an international environment such as the “Centre Européen pour la Recherche Nucléaire” (CERN);
- International social networking experience, mainly acquired during PhD research at the Ecole Polytechnique Fédérale de Lausanne (EPFL);
- Experience with project team work during past professional projects.

V – ORGANISATIONAL SKILLS AND COMPETENCES

- Good organizational skills, mainly acquired during projects developed at CERN and also during PhD research at EPFL;
- Supervision experience, mainly acquired by personal teaching experience with bachelor and master students at the EPFL;
- Experience with an organizational part of project management, mainly acquired with several projects developed at CERN;

VI – PROFESSIONAL EXPERIENCE

CATEGORY	ENTERPRISE	WORKING AREA	YEARS
1 – Assistant and researcher	Laboratoire de Systèmes d’Information Géographique (LASIG), EPFL	Geographical Information Systems (GIS)	From January 2006 until now
2 - Geomatics Engineer (GIS Senior Developer)	European Organization for Nuclear Research (CERN)	Geographical Information Systems (GIS) and ORACLE Database	Since June 2002 until December 2010
3 - Geomatics Engineer (GIS Junior Developer)	Regional Agriculture and Fishing Department of Azores (SRAPA)	Geographical Information Systems (GIS)	Between January 2001 and May 2002
4 - Geomatics Engineer (GIS Researcher)	Instituto Superior Técnico of Lisbon (IST)	Geographical Information Systems (GIS)	Between January 1999 and December 2000
5 - Environment Project Collaborator	Portuguese Ministry of Environment	Environment	During the year of 1998

1 – Since January 2006 until now assistant and researcher at the Laboratoire de Systèmes d’Information Géographique (LASIG), Ecole Polytechnique Fédérale de Lausanne (EPFL).

Main research projects developed at EPFL during the last years:

- Participation in a collaborative project between EPFL and Palestine for the implementation of advocacy tools using geo-referenced data and GIS. Urbanism is one of the main topics of the project;
- Responsible of the analysis of end-users requirements concerning its needs for the use of 3-D data of the State of Geneva;

Curriculum Vitae

- Responsible of many projects related to the use of the 3-D models and data for the State of Geneva, Switzerland. Under the supervision of ScanE, Geneva, currently engaged in the implementation of a new GIS layer and analysis of statistical data about the solar potential of building roofs belonging to the State of Geneva.

2 - Between June 2002 and December 2010, worked in the Information Site and Patrimony (ISP) Section of the Technical Support (TS) Department of the European Organization for Nuclear Research (CERN), hosted in Genève, Switzerland, developing its activities on the facilities management and spatial planning of the internal Geographical Information System of this International Organization, mainly in alphanumeric and geographical databases designing, implementation and updating (ORACLE environment: SQL and PL/SQL) and also in web GIS applications development (JAVA SCRIPT and HTML).

Main professional activities and projects developed at CERN during the last years:

- Migration of all data belonging to the GIS of CERN from “STAR” software to “ESRI” software and technologies: organization of data to be exported, development of “FME” scripts using several tools, such as “PLUG-IN’s” (“STAR” format), “DWG” files (“autocad” format) and “shapefiles” (“ESRI” format);
- Development of the “STAR_GIS” application “Space Managers” (“ORACLE” based) used for the consultation and “users oriented” maps production of all CERN’s offices;
- Development and updating of CERN’s ORACLE databases “STAR_UX” (GIS alphanumeric database), “GEOSIP” (infrastructures and facilities database) and “NETT” (cleaning of CERN’s offices database);
- Development of an ORACLE forms application for the data stored in the “NETT” database of CERN;
- Updating (web based application) of the ORACLE forms application used for the data stored in the “GEOSIP” database of CERN;
- Migration and updating of the application “Buildings and Roads”, available in the main web page of CERN: <http://building.web.cern.ch/building/>;
- Development of the web based GIS application “eNeXt NS”, used for the internal diffusion of the general GIS of CERN;
- Development of the web based GIS application “eNeXt PLANOTHEQUE”, used for the internal diffusion of specific information related to CERN’s offices;
- Development of a “STAR_GIS” application (“Gestionnaire de Thèmes”) for the maintenance of the huts of CERN;
- Participation in some topographical measures of the infrastructures and network of CERN.

3 - Between January 2001 and May 2002 was responsible for the management, development and application of a Geographical Information System on the Regional Agriculture and Fishing Department of Azores. The prosecution of these tasks took place according to two distinct ways: in the first place, implementing many Data Bases respecting to agriculture and maritime resources information, using SQLServer2000 and its tools; in the second place, geo-referencing and analysing this Data Bases with specific visualization software tools, developed by ESRI enterprise: ArcInfo, ArcSDE, ArcIMS, Spatial Analyst and MrSID Encoder.

4 - Between January 1999 and December 2000 collaborated as a full-time researcher in the Naval Engineering Department of the Instituto Superior Técnico of Lisbon, more specifically in the following scientific research fields:

Curriculum Vitae

- creation and implementation of a Geographical Information System associated to the thematic of the maritime pollution on the economic zone of the national territory belonging to Portugal;
- development of the SPAN (Safe Passage and Navigation), by measuring and analysing the dynamic of catamarans boats, using the Global Positioning System (GPS);

5 - During the year of 1998 collaborated in the elaboration of the National Plan of Environmental Politics, at the expense of the Ministry of Environmental.

VII - TEACHING EXPERIENCE

1 - During the first semester of the academic years of 2006/2007 to 2010/2011, lectured a “GIS” course (practical classes – 3 hours/week and also some theoretical courses of 1hour and a half each), on the ambit of the Bachelor in Environmental Engineer of the “Ecole Polytechnique Fédérale de Lausanne”.

2 - During the academic years of 2007/2008 to 2010/2011 has been responsible for the Master project of several students of the Master in Environmental Engineer of the “Ecole Polytechnique Fédérale de Lausanne”.

3 - During the second semester of the academic years of 2009/2010 and 2010/2011, lectured a “Design and project management of GIS” course (practical classes – 3 hours/week), on the ambit of the Master in Environmental Engineer of the “Ecole Polytechnique Fédérale de Lausanne”.

4 - Between July and September 2005 (3 months) has been responsible for the stage of a Portuguese university student in Informatics Systems Engineer (Braga / Portugal) - in the Information Site and Patrimony (ISP) Section of the Technical Support (TS) Department of CERN – developing different tasks related with the improvement of GIS metadata applications.

5 - During the second semester of the academic year of 1999/2000, lectured a “Topography” class (practical classes – 4 hours/week), on the ambit of the Graduation in Architecture, at the Instituto Superior Técnico of Lisbon.

VIII - MAIN PUBLICATIONS

Silva, F. M., Sebastião, P., Carneiro, C., Guedes Soares, C. (2000) Prediction System on the Expansion of Oil Spots as Far as Concern the Economical Zone of Portugal. *Proceedings of the VII Technical Journeys of Naval Engineering: The Sea and the Challenges of the Future*, In: Guedes Soares, C. (Ed.), Lisbon, 1-2 March 2000, pp. 371-385.

Carneiro, C., Ribeiro, F., Moniz, L., Sebastião, S. (2002) The GIS of Regional Agriculture and Fishing Department in Azores (SRAPA). *Proceedings of the 2nd Regional Meeting of Cartography and Geographic Information Systems*, In: Secção Regional dos Açores da Ordem dos Engenheiros (Eds.), Secondary School of Madalena Village, Pico Island - Azores, 9-10 October 2002, pp. 102-112.

Carneiro, C. (2003) Computational Methodology to Filter Raster Images in GIS Applications. *Proceedings of the FIG Working Week*, Ed. FIG, Ecole National des Sciences Géographiques, Champs-sur-Marne, Paris, France, 13-17 April 2003 (not paginated).

Carneiro, C., Gonçalves, L., Guyot, B. and Mayoud, M. (2004) Projet de Développement du SIG du CERN. Application à la Gestion du Réseau de Fibres Optiques. *Revue XYZ*, Numéro 98, pp. 45-52.

Carneiro, C. (2005) The GIS of CERN: Specification and Development. *Proceedings of the IV Conferência Nacional de Cartografia e Geodesia*, João Casaca and João Matos (Eds.), Laboratório Nacional de Engenharia Civil (LNEC), Lisbon, 10th and 11th March 2005 (not paginated).

Carneiro, C., Golay, F. (2007) Un modèle urbain numérique. Et puis? Vers une étude d'utilité. *Géogrès 2007: Histoire de voir le monde*, 2nd to 5th October, Québec, Canada (not paginated).

Neves, D. and C. Carneiro (2007) Semi-automatic use of High-Resolution Images and Digital Elevation Models for Counting and Identification of Forest Trees. *Geocomputation 2007 Conference*, 3rd to 5th September, Maynooth, Ireland (not paginated).

Carneiro, C., Alp, A., Macedo, J., Spaccapietra, S. (2008) Advanced Data Mining Method for Discovering Regions and Trajectories of Moving Objects: “Ciconia ciconia” Scenario”. *Lecture Notes in Geoinformation and Cartography*, In: Bernard, L., Friis-Christensen, A., Pundt, H. (Eds), Springer, Berlin, Germany, pp. 201-224.

Carneiro, C., Golay, F., Silva, V., Plazanet, C., Park, J.J. (2008) GIS and LIDAR data analysis for the integration of multidimensional indicators on urban morphogenesis multiagent vector based geosimulation. *Geocomputation and Urban Planning: Studies in Computational Intelligence*, In: Murgante, B., Borruoso, G., Lapucci, A. (Eds.), Springer, Berlin, Germany, Vol. 176, pp.187-208.

Silva, V., Plazanet, C., Carneiro, C., Golay, F. (2008) 3D LIDAR data application for urban morphogenesis multi-agent vector based geosimulation. *The 2008 International Conference on Computational Science and Its Applications: Third International Workshop on "Geographical Analysis, Urban Modeling, Spatial Statistics*, 30th June to 3rd July, University of Perugia, Italy (not paginated).

Carneiro, C., Morello, E., Ratti, C., Golay, F. (2008) Solar radiation over the urban texture: LiDAR data and image processing techniques for environmental analysis at city scale. *Lecture notes in geo-information and cartography. 3-D Geo-Information Sciences*, In: Zlatanova, S., Lee, J. (Eds.), Part II, Springer, Berlin, Germany, pp. 319-340.

Carneiro, C. (2008) Communication and visualization of 3-D urban spatial data according to user requirements: case study of Geneva. *The International Archives of the Photogrammetry, Remote Sensing and Spatial Information Sciences*, Vol. 37, Part B2, pp. 631-636.

Carneiro, C., Morello, E., Desthieux, G. (2009) Assessment of solar irradiance on the urban fabric for the production of renewable energy using LiDAR data and image processing techniques. *Advances in GIScience*, In: Sester, M., Bernard, L., Paelke, V. (Eds.), Springer, Berlin, Germany, pp. 83-120.

Carneiro, C., Silva, V., Golay, F. (2009) Incorporation of Morphological Properties of Buildings' Descriptors Computed from GIS and LiDAR Data on an Urban Multi-agent Vector Based Geo-simulator. In: Gervasi, O., Taniar, D., Murgante, B. (Eds.), *Lecture Notes in Computer Science: Computational Science and its Applications*, Springer, Berlin, Germany, Vol. 5592/2009, pp. 205-220.

Carneiro, C., Karzand, M., Golay, F., Lu, Y. M., Vetterli, M. (2009) Assessing Digital Surface Models by Verifying Shadows: A Sensor Network Approach. In: Devillers, R., Goodchild, H. (Eds.), *Spatial Data Quality: From Process to Decisions*. CRC Press, Boca Raton, Florida, USA, pp. 147-61.

Curriculum Vitae

Desthieux, G., Carneiro, C., Morello, E., Gallinelli, P., Camponovo, R. (2009) GIS-based assessment of solar irradiance on the urban fabric and potential for active solar technology. *Proceedings of the International Conference CISBAT: Renewables in a Changing Climate: from Nano to Urban Scale*, 2nd-3rd September, Lausanne, Switzerland, pp. 525-530.

Carneiro, C., Blunier, P. and Golay, F. (2009) Données et modèles urbains numériques 3-D en milieu urbain... à quoi cela peut-il bien servir ?, *Bulletin e-geo.ch*, July, Vol. 23, pp. 15-17.

Carneiro, C., Morello, E., Voegtle, T., Golay, F. (2010) Digital urban morphometrics: automatic extraction and assessment of morphological properties of buildings. *Transactions in GIS*, Vol. 14, Issue 4, pp. 497-531.

Carneiro, C., Morello, E., Desthieux, G., Golay, F. (2010) Urban environmental quality indicators: application to solar radiation and morphological analysis on built area. *Proceedings of the 3rd WSEAS Conference: Advances in Visualization, Imaging and Simulation*, 3rd and 4th November, Faro, Portugal, pp. 141-148. ISBN: 978-960-474-246-2.

Morello, E., Carneiro, C., Desthieux, G. (2010) The use of digital 3-D information to assess urban environmental quality indicators. *Proceedings of the 28th ECAADE Conference: Future Cities*, 15th-18th September, Zurich, Switzerland, pp. 499-505.

Gori, V., Balocco, C., Carneiro, C., Desthieux, G., Morello, E. (2011) The evaluation of solar energy potential and energy needs for heating and lighting using LiDAR data. *Proceedings of the 27th International Conference on Passive and Low Energy Architecture (PLEA)*, 13th-15th July, Louvain-la-Neuve, Belgium. (accepted, to publish).